25 Copies

NASA CONTRACTOR REPORT

NASA CR-66678-2

NASA CR-66678-2

MARS HARD LANDER CAPSULE STUDY

Volume II
Mission and Science Definition

Prepared by

GENERAL ELECTRIC
RE-ENTRY SYSTEMS

for Langley Research Center

31 JULY 1968

NATIONAL AERONAUTICS AND SPACE ADMINISTRATION–WASHINGTON, D. C.

MARS HARD LANDER
CAPSULE STUDY

Volume II

MISSION AND SCIENCE DEFINITION

NATIONAL AERONAUTICS & SPACE ADMINISTRATION

FOREWORD

The Mars "Hard Lander" Study Final Report is divided into four volumes and bound in eight books. The titles of the volumes and a brief description of the comtents of each book are presented below.

VOLUME I - SUMMARY (CR-66678-1)

Volume I contains a summary of the study activity, the conclusions reached, and a description of a possible design implementation suggested by the study results.

This study indicates that meaningful scientific payloads of approximately 1500 pounds can be placed on the Mars surface, survive for several months, and transmit more than a hundred million bits of data to Earth.

In addition, the study provided data which shows that a smaller Capsule of 700 to 900 pounds has the ability to transmit approximately 10 million bits of imagery and additional scientific surface data.

VOLUME II - MISSION AND SCIENCE DEFINITION (CR-66678-2)

Volume II contains a description of the 'reference' mission plans, both direct entry and out-of-entry, the mission analyses conducted to define the reference plans, the assumed Mars models considered, and the science definition tasks accomplished to select entry and surface science packages/measurement sequences specifically designed to satisfy LRC's scientific goals.

VOLUME III - CAPSULE PARAMETRIC STUDY (CR-66678-3, -4)

A discussion of the analysis and results derived in determining the Capsule subsystems' design characteristics parametrically is provided for the range of assumed Mars Models and the reference mission plans. The synthesis of these subsystems into complete Capsule systems is presented in terms of Capsule performance, total imagery data obtainable, and surface lifetime.

CR-66678-3 presents the Capsule System Parametric Synthesis and Entry and Retardation Subsystem Studies. CR-66678-4 presents both studies of the Lander and Re-entry Subsystems and Appendices associated with the Parametric Study.

VOLUME IV- CAPSULE POINT DESIGNS AND SUPPORTING ANALYSES
     (CR-66678-5, -6, -7, -8)

Volume IV contains a presentation of the detailed Capsule 'Point Designs', and their supporting analyses, derived to identify specific hardware approaches, weights, and system configurations; and confirm the correctness of the parametric results. In addition to the Capsule's engineering and design details, the results include development status. probability of success, and constraints imposed on the Orbiter by the Capsule mission.

CR-66678-5 contains a definition of the Capsule Point Design Requirements and descriptions of Point Designs 1 and 2. CR-66678-6 contains descriptions of Point Designs 3 and 4 and CR-66678-7 of Point Designs 5 and 6. CR-66678-8 provides additional information on Impact Attenuation, Surface Environment Definition, Effects on Point Designs due to Variations in Assumed Design Parameters as well as the Effects of a Lander on the Mariner Orbiter.

TABLE OF CONTENTS

TABLE OF CONTENTS (Continued)

LIST OF ILLUSTRATIONS

LIST OF TABLES

1. INTRODUCTION

1. INTRODUCTION

1.1 STUDY OBJECTIVES

As a continuing and scientifically important step in the US Planetary Exploration Program by the means of unmanned spacecraft, NASA has proposed a project which would send an Orbiter/Lander combination to Mars during the 1973 launch opportunity.

The primary objectives of this planned Mars '73 Orbiter/Lander mission would be to utilize the Lander to (1) characterize the composition and vertical structure of the planetary atmosphere by means of direct measurements during entry; and (2) obtain imagery and meteorological data while on the surface of the planet.

In order to determine the mission approach and spacecraft hardware concept which, within the constraints of allowable development time, hardware 'state-of-the-art', and available project resources, offers the maximum assurance of project success, the NASA is studying the various alternatives available for the subject project.

As a part of LRC's extensive study activity to assure adequate examination of these project alternatives, the General Electric Re-entry Systems is performing a Mars 'Hard Lander' Study for LRC under Contract No. NAS 1-8098. This document reports the results obtained during the first three months of the subject study.

The objectives of the Mars 'Hard Lander' Study, which are specifically directed toward the consideration of the aforementioned 1973 launch opportunity, are as follows:

1. Investigate mission and Capsule designs for Mars Hard Landers to provide (a) parametric design and performance data, and (b) several detailed Capsule point designs.

2. Consider two mission modes: direct entry and out-of-orbit entry.

3. Define Lander designs capable of (a) achieving a minimum lifetime on the planet surface of 1 diurnal cycle with a goal of up to several months; and (b) providing for the transmission of not less than 10^7 bits of surface imagery data with a design goal of 10^8 bits or greater.

The scope of the study performed to satisfy the aforementioned objectives is presented in tables 1.1-1 and 1.1-2. The information presented in table 1.1-2 was provided to the Study Contractor's Directive Letter - LRC, dated 20 May 1968. Table 1.1-1 lists the "Study Objectives" and the "Alternatives Studied in Parametric Analysis", while table 1.1-2 gives the system requirements for the six point designs which were studied in depth (i.e., design layouts and supporting analyses).

TABLE 1.1-1. PARAMETRIC ANALYSIS STUDY SCOPE

Study Objectives	Alternatives Studied in Parametric Analysis
1. Weight Consistent with: 1) Minimum Science & One Day Life Time 2) Minimum Science & Several Months Life Time 3) Increased Science & Several Months Life Time All must fit inside 16 ft shroud with goal of fitting inside 10 ft shroud.	**Direct Entry Mode** (A) Ballistic Entry + Parachute (B) Ballistic Entry + Inflatable Aft End or Flaps + Parachute (C) Lifting Entry + Parachute **Out-of-Orbit Entry Mode** (A) Ballistic Entry + Parachute
2. Impact Attenuation and Component Survivability:	• Lander Shape "Deep Ring" (Omnidirectional and Multidirectional) and Phenolic Glass Honeycomb Crushup. • Deceleration Level from 500 to 3000 G's. • 6 Touchdown Velocities Varied with Decelerator and Wind Model.
3. Imagery Data: 10^7 Bits Minimum Goal of 10^8 Bits of Greater	During Entry: (A) Relay Link to Spacecraft During Landed Operations: (A) Relay Link to Spacecraft at Periapsis and/or Apoapsis (B) Direct Link to Earth with a Steerable or Fixed Antenna
4. Surface Life: One day with a goal of several months	**Candidate Power Supply** **Candidate Thermal Control** • Batteries • Insulation + Thermal Storage + Local Electrical Heaters • Fuel Cells and Topping Batteries • Active Coolant Circulation + Local Electrical Heaters + Insulation • RTG and Topping Batteries • Active Coolant Circulation + Insulation • Solar Cells and Batteries (Ancilliary Power for Extended Life) • Insulation + Thermal Storage + Local Electrical Heaters

TABLE 1.1-2. SYSTEM REQUIREMENTS FOR THE SIX POINT DESIGNS

Out of Orbit Entry		Direct Entry	
Point Design Number	Capsule System	Point Design Number	Capsule System
1	Minimum science per objectives document of May 3, 1968. One diurnal cycle minimum. Battery only - relay communication only.	2	Same
3	Minimum science as above. 90-day life-time goal with battery plus solar cell. Imagery first day, meteorology data only afterward. S-band command link required. Initial imagery first day, meteorological data - low bit rate after.	4	Same
5	Increased science over above, S-band command, battery and solar cell for 90-day life. Relay and direct communication. Low total bit imagery periodically beyond the initial first day imagery.	6	Same
Note:	To expand somewhat on the above table, the following is offered: (a) Generally, designs which offer extended life should have S-band command capability; (b) for the two-point designs with minimum science, estimate any further gain from the elimination of the soil composition measurement; (c) a day or so after landing, the Orbiter will be made asychronous to allow maximum orbital photography. The picture data should thus be read out as soon after landing as possible. If it can be shown to be geometrically feasible with the asynchronous Orbiter to transmit the remaining data, no direct S-band link need be included. This remaining data would be low bit meteorological data and possibly low total bit pictures.		

1.2 SCOPE OF VOLUME II

In order to adequately define the spacecraft hardware system which satisfies the objectives of this scientific project, we must first define the requirements and interrelationships of the scientific measurements, the candidate mission modes, and the postulated physical environment of Mars. It was with that objective that this volume (Volume 2, Mission and Science Definition) was prepared and reports the results realized in the following study task areas:

1. Definition of the mission guidelines and constraints, including the postulated Mars models.

2. Analysis of the candidate mission modes, including the resultant subsystem design requirements (i.e., available communication times, entry parameters, aerodynamic loads, etc.).

3. Selection of scientific instrumentation and measurement mode.

The first of these tasks, reported in Section 2.0 of this volume, presents a discussion of the mission objectives in the light of some of the more significant mission operational and hardware implementation considerations; a summarization of the NASA-specified study constraints, the postulated Mars models, and the GE/RS-derived operational and design criteria/assumptions; and the mission profile and sequence of events employed to assure the successful accomplishment of the mission's science objectives within the constraints of the anticipated spacecraft hardware 'state-of-art'.

Utilizing the study constraints and guidelines, and the postulated Mars models presented in Section 2.0, a mission analysis was conducted whose results are presented in Section 3.0. This second task area, "Mission Analysis", is comprised of the following six work elements:

1. Definition of out-of-orbit entry and direct entry reference missions (Type I transit trajectories), including the resultant atmospheric entry trajectories, which set the subsystem design requirements (i.e., loads, etc.).

2. Examination of the possible entry path angle and downrange dispersions resulting from the reference mission conditions and the anticipated system tolerances.

3. The possible improvements that could be realized by revising the reference missions.

4. The relay link telecommunication problem for the direct entry mode wherein the Orbiter Lander geometry at the end of the first few days will be significantly affected by the probable orbital period errors.

5. Consideration of the possible advantages and disadvantages of employing Type II trajectories.

6. The Sun and Earth declinations and view times during the 1974 arrival period.

Section 4.0 presents the results of the third task area, "Science Definition". This task was accomplished by considering NASA/LRC's denoted science objectives, as specified to GE/RS at the initiation of the study, and the realizable mission conditions as derived in Section 3.0. GE/RS's science task, then, consisted of selecting the science instrumentation and the attendant measurement technique and mission sequence; determining the anticipated science accuracies for the selected system; and examining the special imagery considerations as related to a hard lander mission. While only one reference entry science package was defined and utilized throughout this subject study, two surface science packages were synthesized: a 'basic' package used in the major portion of the parametric study results and in Point Designs 1 through 4, and an 'increased' package considered in only a limited portion of the parametric data and in Point Designs 5 and 6.

2. MISSION REQUIREMENTS AND CONSTRAINTS

2. MISSION REQUIREMENTS AND CONSTRAINTS

2.1 MISSION OBJECTIVES

Building upon the mission techniques and spacecraft technology utilized so successfully in the Mariner IV Mars fly-by conducted in 1965, the NASA planned Mars Exploration Program (ref. 2-1) is as follows:

Lander Opportunity	Mission	Launch Vehicle
1969	Fly-by	Atlas–Centaur
1971	Orbiter	Atlas–Centaur
1973	Orbiter/Lander	Titan-class

The 1969 fly-by mission will be conducted employing basically the Mariner IV spacecraft modified to provide a significantly increased complement of science instruments and telecommunication capability. As noted in the Authorization Hearings, its primary objective is "to make exploratory investigations of Mars which will set the basis for future experiments, particularly those relevant to the search for extraterrestrial life. A secondary objective is to develop planetary mission technology."

The 1971 orbiter mission will again employ a Mariner-modified spacecraft. Due to the uniquely low launch energy requirements associated with the 1971 opportunity, it will be possible to conduct the planned orbiting mission with an Atlas–Centaur. Again quoting from the Authorization Hearings, the primary objective for the Mariner Mars '71 mission is "to conduct multiple scientific measurements and observations of the dynamic characteristics of the planet Mars on an orbiter mission with a designed operational lifetime in orbit of 3 months," while the secondary objective is "to develop technology required to conduct planetary orbital operations". The mission plan selected for the 1971 opportunity will have the Mariner spacecraft arrive at Mars during the spring season for the Southern Hemisphere, thus providing very favorable conditions for viewing the 'wave of darkening'.

With regard to the 1973 Orbiter/Lander project, the subject of the study reported herein, its mission objectives as stated by the NASA/LRC (ref. 2-2) are:

"1. Obtain from a landed vehicle imagery of the surrounding surface.

2. Obtain from a landed vehicle meteorological data consisting of pressure, temperature, wind velocity, wind direction, and specific humidity variations with time.

3. Obtain from a landed vehicle measurements that can be used to determine the surface soil composition.

4. Obtain from the Lander vehicle during entry direct measurements which will define the composition and vertical structure of the atmosphere.

5. Obtain from an Orbiter vehicle broad area imagery coverage of the planet to extend the coverage which may already exist at that time.

6. Obtain from an Orbiter vehicle site examination imagery of scientifically interesting areas at higher resolution than the broad area coverage.

7. Obtain from an Orbiter vehicle data which can be used to define the atmosphere and its diurnal and seasonal variation.

8. Obtain from an Orbiter vehicle data which provides information regarding the thermal distribution of the surface and its diurnal and seasonal variations.

9. Obtain data to improve the definition of Mars potential field and ephemeris by tracking of an Orbiter vehicle."

The subject three month study performed by GE/RS, then, was specifically directed towards defining mission approaches, the required scientific instrumentation, and the vehicle design approach which, within the study constraints defined in Section 2.2, would best satisfy these stated mission objectives.

2.2 MISSION GUIDELINES AND CONSTRAINTS

In performing the study reported herein, the study was guided and bounded by various criteria, constraints, and assumptions which can be considered as falling into three major categories:

1. Study Constraints - as specified by NASA/LRC in the study Work Statement and Technical Direction meetings.

2. Mars Models - the particular atmospheric and geophysical models of Mars that the Study Contractor was directed to use.

3. Criteria and Assumptions - those derived and utilized by the Study Contractor in such areas as program considerations, mission operations, and vehicle design.

This section of the report presents these subject guidelines and constraints.

2.2.1 NASA SPECIFIED STUDY CONSTRAINTS

The guidelines, assumptions, and constraints as specified by NASA/LRC may be grouped into mission objectives, mission planning, and vehicle design aspects. In the following tabulation, wherever feasible, the NASA phraseology, as quoted directly from their documentation, is used.

2.2.1.1 Mission Objectives

Mission objectives are as follows:

1. 10^7 bits minimum surface imagery required; design goal of 10^8.

2. Other required surface science measurements: pressure, temperature, wind velocity and direction, and moisture.

3. Required entry science measurements: see table 2.2-1. Minimum entry science shall consist of pressure, temperature, and composition measurements.

4. Minimum surface lifetime - one day.

5. Surface lifetime goal - several months.

II

TABLE 2.2-1. NASA/LRC SCIENCE PAYLOAD REQUIREMENTS

	Altitude Range	Accuracy
Entry Science		
Pressure	0 – 60 km	±5%
Temperature	0 – 60 km	±2%
Density	0 – 60 km	±5%
Atmos. Composition	< 50 km	±5% (if constituent is greater than 50% of total) ±10% (other constituents)
Atmos. Moisture	< 50 km	...
Surface Science		
Imagery of Surface		Low Resolution: 0.1% line High Resolution: 0.01% line
Temperature		±2%
Pressure		±5%
Wind Velocity		±5%
Wind Direction		±10°
Atmos. Moisture		Dew/Frost Pt. of ±2°C
Soil Composition		– – –

2.2.1.2 Mission Planning

Mission planning is as follows:

1. 1973 launch opportunity is considered prime.

2. Launch vehicle capability: consider Titan III D – Centaur (C_3 capability of 25 to 40 km^2/sec^2).

3. Both direct and out-of-orbit entry modes shall be considered.

4. Type I and Type II trajectories.

5. Spacecraft orbit: 1000 km periapsis "synchronous" orbit (24 hour, 37 minute period).

6. Spacecraft orbit: 60° inclination desired with mapping of Mars' Northern Hemisphere as part of Orbiter mission.

7. Landing site: for reference mission definition, the desired landing latitudes are 10°N and 20°N in conjunction with a Sun angle of 60° (i.e., 30° after the morning terminator or 30° ahead of the evening terminator).

8. Landing site: consider the implications of impacting at more northerly sites than those specified for the reference missions noted in item 7 above (i.e., evaluate landing latitudes of 25°N and 50°N).

9. Relay (via the Orbiter) or direct communication link from the Capsule or a mode combining both is acceptable.

10. Consider each of the following: (a) three 210-ft DSIF antennas available and (b) one 210-ft, two 85-ft antennas available.

11. Utilize the Mars orbital, physical, and astrodynamical data reproduced herein as para. 2.2.2.1.

2.2.1.3 Vehicle Design Aspects

Vehicle design aspects are:

1. Utilize the JPL VM-1 to VM-10 Mars atmospheric models as specified in JPL Project Document 606-4, "1973 Voyager Capsule Systems Constraints and requirements Document, Revision 1" dated 18 May 1967.

2. Utilize the Mars geophysical model as specified in NASA/OSSA Document, "Voyager Environmental Standards", dated 25 September 1967.

3. Capsule sterilization required (Note: ETO compatibility is not required.)

4. Maximum allowable shroud diameter is 16 feet. The minimum "hammerheading" from the launch vehicle's 10 foot diameter is desired.

5. Utilization of aeroshell/parachute decelerators.

6. Parachute deployment not exceeding Mach 2.0.

7. All Capsule support functions (power, communications, attitude control, etc.) except thermal control to be provided by the Spacecraft during transplanet cruise.

8. For the Capsule direct entry case, the Capsule will have to include propulsion capability to achieve the direct entry trajectory after separation from the support Spacecraft which must be targeted to miss the planet.

2.2.2 RANGE OF MARS MODELS

The Mars 'Hard Lander' Capsule systems derived in this study (see Vols. III and IV) were primarily influenced by three aspects of Mars and its environment: (1) the Mars orbital, physical, and astrodynamical data which significantly affects the interplanetary and near-Mars exoatmospheric trajectories; (2) the Mars atmospheric structure which designs the entry vehicle/retardation system with regard to loads, heating and aerodynamic performance characteristics; and (3) the Mars surface conditions which essentially sets the Lander's structural/impact attenuation design characteristics.

2.2.2.1 <u>Mars Orbital, Physical, and Astrodynamical Data</u>

The following information was specified by NASA/LRC to the Study Contractor (ref. 2-3) and is reproduced herein for ease of reference.

1. Orbit and Rotation

   a. Orbital Parameters

   The mean orbital elements of Mars for 1973 and 1974 are given in table 2.2-2 (ref. 2-4)

   b. Opposition

   Date of opposition: October 25, 1973

   Heliocentric longitude: $31.24°$

   Date of closest approach: October 17, 1973

   Distance at closest approach: 0.4360 A.U. (ref. 2-5)

   c. Seasons, Length of Year

   The Martian seasons are defined in table 2.2-3 (ref. 2-6)

   d. Rotation

   Sidereal period of rotation, $24^h 37^m 22.^s 6689$, (in ephemeris time)

   Location of North Pole:

   At beginning of year, t, right ascertion and declination:

   $$\alpha_o = 316.°55 + 0.°006533 \ (t-1905.0)$$

   $$\delta_o = 52.°85 + 0.°003542 \ (t-1905.0)$$

TABLE 2.2-2. MEAN ORBITAL ELEMENTS FOR MARS

Epoch		Mean distance from Sun a, astro- nomical units	Mean motion, deg/ ephemeris day	Eccen- tricity of orbit, e	Inclination of orbit to ecliptic, i, deg	Ascending node longitude, Ω, deg	Perihelion longitude, ω, deg
Gregorian Date	Julian Date						
1973 - April 8	2441800.5	1.523691	0.524033	0.093380	1.84985	49.35174	335.56793
1973 - Nov. 14	2442000.5	1.523691	0.524033	0.093381	1.84984	49.35596	335.57802
1974 - June 2	2442200.5	1.523691	0.524033	0.093381	1.84984	49.36018	355.58810

Mean elements are referred to mean equinox and ecliptic of date.
Values are calculated from data in the Explanatory Supplement to
the American Ephemeris and Nautical Almanac.

TABLE 2.2-3. THE MARTIAN SEASONS

Heliocentric Longitude, deg	Northern Hemisphere	Southern Hemisphere	Duration	
			Terrestrial days (24 h)	Martian days (24h37m)
87 to 177	Spring	Autumn	199 ⎫ 381	194 ⎫ 371
177 to 267	Summer	Winter	182 ⎭	177 ⎭
267 to 357	Autumn	Spring	146 ⎫ 306	142 ⎫ 298
357 to 87	Winter	Summer	160 ⎭	156 ⎭
87 to 87	Year		687	670

Central meridian, referred to zero meridian of 1909:

Longitude of central meridian: 344.°41;

1909 January 15, G. M. N. (J. D. 2418322. 0)

Daily motion: 350.°891962 (degrees per ephemeris day)

(Values as adoped in ref. 2-7)

Inclination of equator to Mars orbit: 24.°936 (ref. 2-6)

2.   Physical Properties

a.   Radius

Mean equatorial radius: 3393. 4 ± 4 km

Mean polar radius: 3375. 6 km

(Calculated from equatorial radius using dynamical flattening of f = 0.00525) (ref. 2-8)

These values are recommended for general use; however, for some purposes and for comparison, the optical values are also given:

Radius and flattening (optical)

Mean equatorial radius: 3395 ± 10 km

Mean polar radius: 3355 ± 10 km

Flattening: f = 0.0117 (ref. 2-9)

b. Mass, Density, and Surface Gravity

Mass = 6.423×10^{26} g (0.1074 mass of earth)

Density = 3.945 g-cm^{-3} (0.715 density of earth)

Surface gravity = 371 cm-sec^{-2} (ref. 2-8)

c. Satellites

Characteristics of the natural satellites of Mars are given in table 2.2-4. (ref. 2-8)

TABLE 2.2-4. SATELLITES OF MARS

	Phobos	Deimos
Distance from center of planet		
(km)	9,365	23,525
(mi)	5,820	14,615
Period (Sidereal)	$0^d.31891$	$1^d.26244$
or	$7^h39^m13^s.85$	$1^d6^h17^m54^s.87$
Period (Synodic)	$0^d.319$	$1^d.265$
Inclination of Orbit to Equator of Mars	0° 57'	1° 18'
Orbital Eccentricity	0.0210	0.0028
Apparent Visual Magnitude at Mean Opposition Distance	11.6	12.8
Estimated Diameter (km)	19	10
Estimated Diameter (mi)	12	6
Rate of Regression of Nodes	158°.0/year	6°.374/year

3. Astrodynamical Data

   a. Ephemerides

      1) The currently recommended ephemerides are those contained in the JPL Development Ephemeris Number 19 (Tape DE 19B), as described in ref. 2-10.

      2) Recommended constants for use with the ephemeris tapes are:

         Scale factor for "earth radius": 6378.1495 km

         Earth-moon mass ratio: 81.302 (ref. 2-11).

         Scale factor for Astronomical Unit

         A.U. = 149, 597, 892 ± 6 km (ref. 2-11)

         (E. T. - U. T.) time corrections from current issue of the American Ephemeris and Nautical Almanac.

   b. Gravitational Constants

      1) Gravitational potential function

         The following general form for the gravitational potential is recommended in order to provide for inclusion of non-zonal components for Mars when such information becomes available.

$$U = \frac{\mu}{r} \left\{ 1 + \sum_{n=2}^{\infty} \sum_{m=0}^{n} \left(\frac{R}{r}\right)^n \left[\bar{C}_{nm} \cos m\lambda + S_{n,m} \sin m\lambda\right] P_{nm}(\sin\varphi) \right\}$$

$$P_{nm}(x) = (1-x^2)^{m/2} \frac{d^m P_n(x)}{dx^m}$$

         (Form adopted by IAU (ref. 2-12)

where

   r = radial distance from center of mass

   λ = longitude, measured eastward from the central meridian

   φ = latitude, measured with respect to the equator.

In this form:

$$P_{2,0} = \frac{1}{2} (3 \sin^2 \varphi - 1)$$

$$P_{3,0} = \frac{1}{2} \sin\varphi (5 \sin^2 \varphi - 3)$$

$$P_{4,0} = \frac{1}{8} (35 \sin^4 \varphi - 30 \sin^2 \varphi + 3)$$

2) Constants for earth

$$\mu = GM = 398,600.9 \text{ km}^3/\text{sec}^2$$

$$C_{2,0} = -J_2 = -1082.61 \times 10^{-6}$$

$$C_{3,0} = -J_3 = +2.56 \times 10^{-6}$$

$$C_{4,0} = -J_4 = 1.63 \times 10^{-6}$$

with R = 6378.160 km (ref. 2-13)

3) Constants for Mars

$$\mu = 42,829.5 \pm 8 \text{ km}^3/\text{sec}^2 \text{ (ref. 2-9)}$$

$$C_{2,0} = -J_2 = -0.00195 \pm 0.0002 \text{ (ref. 2-14)}$$

Corresponds to dynamical flattening of f = 0.00525 (ref. 2-14)

c. Miscellaneous Constants

C = 299,792.5 m/sec (ref. 2-7)

2.2.2.2 Mars Atmospheric Structure

The Mars atmospheric models shown in table 2.2-5 and the atmospheric winds shown in table 2.2-6 were used in the design of the Capsule system. The data shown are reproduced from ref. 2-15. With regard to the interpretation of the wind data, the following explanation is given in the JPL reference document:

"The free stream continuous wind speed shown in table 2.2-5 corresponds to a height above the local surface of 100 meters. The surface boundary layer profile at any pressure level should be assumed to have the following characteristics:

TABLE 2.2-5. ATMOSPHERIC MODELS

Property	Symbol	Dimension	VM-1	VM-2	VM-3	VM-4	VM-5	VM-6	VM-7	VM-8	VM-9	VM-10
Surface Pressure	P_o	mb	7.0	7.0	10.0	10.0	14.0	14.0	5.0	5.0	20.0	20.0
Surface Density	ρ_o	lb/ft^2	14.6	14.6	20.9	20.9	29.2	29.2	10.4	10.4	41.7	41.7
		(gm/cm^3) 10^5	0.955	1.85	1.365	2.57	1.91	3.08	0.68	1.32	2.73	3.83
		(slugs/ft^3) 10^5	1.85	3.59	2.65	4.98	3.7	5.97	1.32	2.56	5.30	7.44
Surface Temperature	T_o	°K	275	200	275	200	275	200	275	200	275	200
		°R	495	360	495	360	495	360	495	360	495	360
Stratospheric Temperature	T_s	°K	200	100	200	100	200	100	200	100	200	100
		°R	360	180	360	180	360	180	360	180	360	180
Acceleration of Gravity at Surface	g	cm/sec^2	375	375	375	375	375	375	375	375	375	375
		ft/sec^2	12.3	12.3	12.3	12.3	12.3	12.3	12.3	12.3	12.3	12.3
Composition (percent)												
CO_2 (by mass)			28.2	100.0	28.2	70.0	28.2	35.7	28.2	100.0	28.2	13.0
CO_2 (by volume)			20.0	100.0	20.0	68.0	20.0	29.4	20.0	100.0	20.0	9.5
N_2 (by mass)			71.8	0.0	71.8	0.0	71.8	28.6	71.8	0.0	71.8	62.0
N_2 (by volume)			80.0	0.0	80.0	0.0	80.0	32.2	80.0	0.0	80.0	70.5
A (by mass)			0.0	0.0	0.0	30.0	0.0	35.7	0.0	0.0	0.0	25.0
A (by volume)			0.0	0.0	0.0	32.0	0.0	38.4	0.0	0.0	0.0	20.0
Molecular Weight	M	mol^{-1}	31.2	44.0	31.2	42.7	31.2	36.6	31.2	44.0	31.2	31.9
Specific Heat of Mixture	C_p	cal/gm°C	0.230	0.166	0.230	0.1530	0.23	0.174	0.230	0.166	0.230	0.207
Specific Heat Ratio	α		1.38	1.37	1.38	1.43	1.38	1.45	1.38	1.37	1.38	1.41
Adiabatic Lapse Rate	Γ	°K/km	-3.88	-5.39	-3.88	-5.85	-3.88	-5.14	-3.88	-5.39	-3.88	-4.33
		°R/1000 ft	-2.13	-2.96	-2.13	-3.21	-2.13	-2.82	-2.13	-2.96	-2.13	-2.38
Tropopause Altitude	h_T	km	19.3	18.6	19.3	17.1	19.3	19.4	19.3	18.6	19.3	23.1
		kilo ft	63.3	61.0	63.3	56.1	63.3	63.6	63.3	61.0	63.3	75.8
Inverse Scale Height (stratosphere)	β	km^{-1}	0.0705	0.199	0.070	0.193	0.0705	0.1655	0.0705	0.199	0.0705	0.145
		ft^{-1} ×10^5	2.15	6.07	2.15	5.89	2.15	5.05	2.15	6.07	2.15	4.41
Continuous Surface Wind Speed	$\bar{v}$	ft/sec	186.0	186.0	155.5	155.5	131.5	131.5	220.0	220.0	110.0	110.0
Maximum Surface Wind Speed	v_{max}	ft/sec	470.0	470.0	390.0	390.0	330.0	330.0	556.0	556.0	278.0	278.0
Design Vertical Wind Gradient	$\frac{dv}{dh}$	ft/sec/1000 ft	2	2	2	2	2	2	2	2	2	2
Design Gust Speed	v_g	ft/sec	200.0	200.0	150.0	150.0	150.0	150.0	200.0	200.0	100.0	100.0

TABLE 2.2-6. MEAN WIND AND WIND SHEAR MODELS FOR ATMOSPHERIC MODELS VM-1 & VM-2, VM-3 & VM-4, VM-5 & VM-6, VM-7 & VM-8, VM-9 & VM-10

Altitude feet	Wind Gradient	Shear Gradient	Horizontal Wind Speeds				
			VM-1,2	VM-3,4	VM-5,6	VM-7,8	VM-9,10
	fps/1000'	fps/1000'	fps	fps	fps	fps	fps
0	+2	±20	186.0	156.0	132.0	220.0	110.0
2,500			191.0	161.0	137.0	225.0	115.0
7,500			201.0	171.0	147.0	235.0	125.0
12,500			211.0	181.0	157.0	245.0	135.0
17,500			221.0	191.0	167.0	255.0	145.0
22,500			231.0	201.0	177.0	265.0	155.0
27,500			241.0	211.0	187.0	275.0	165.0
32,500			251.0	221.0	197.0	285.0	175.0
37,500			261.0	231.0	207.0	295.0	185.0
42,500			271.0	241.0	217.0	305.0	195.0
47,500	↓	↓	281.0	251.0	227.0	315.0	205.0
50,000	0	±40	286.0	256.0	232.0	320.0	210.0
52,500							
55,000							
57,500							
60,000							
62,500							
65,000							
67,500							
70,000							
72,500							
75,000							
77,500							
80,000							
82,500							
85,000							
87,500							
90,000	↓	↓	↓	↓	↓	↓	↓
790,000	0	0	0	0	0	0	0

TABLE 2.2-6.   MEAN WIND AND WIND SHEAR MODELS FOR ATMOSPHERIC
MODELS VM-1 & VM-2, VM-3 & VM-4, VM-5 & VM-6,
VM-7 & VM-8, VM-9 & VM-10 (CONT'D)

Altitude Feet	Wind Shear Speeds				
	VM-1,2	VM-3,4	VM-5,6	VM-7,8	VM-9,10
0	186.0	156.0	132.0	220.0	110.0
2,500	241.0	211.0	187.0	275.0	165.0
7,500	151.0	121.0	97.0	185.0	75.0
12,500	261.0	231.0	207.0	295.0	185.0
17,500	171.0	141.0	117.0	205.0	95.0
22,500	281.0	251.0	227.0	315.0	205.0
27,500	191.0	161.0	137.0	225.0	115.0
32,500	301.0	271.0	247.0	335.0	225.0
37,500	211.0	181.0	157.0	245.0	135.0
32,500	321.0	291.0	267.0	355.0	245.0
42,500	231.0	201.0	177.0	265.0	155.0
50,000	336.0	306.0	282.0	380.0	260.0
52,500	236.0	206.0	182.0	280.0	160.0
55,000	336.0	306.0	282.0	380.0	260.0
57,500	236.0	206.0	182.0	280.0	160.0
60,000	336.0	306.0	282.0	380.0	260.0
62,500	236.0	206.0	182.0	280.0	160.0
65,000	336.0	306.0	282.0	380.0	260.0
67,500	236.0	206.0	182.0	280.0	160.0
70,000	336.0	306.0	282.0	380.0	260.0
72,500	236.0	206.0	182.0	280.0	160.0
75,000	336.0	306.0	282.0	380.0	260.0
77,500	236.0	206.0	182.0	280.0	160.0
80,000	336.0	306.0	282.0	380.0	260.0
82,500	236.0	206.0	182.0	280.0	160.0
85,000	336.0	306.0	282.0	380.0	260.0
87,500	236.0	206.0	182.0	280.0	160.0
90,000	336.0	306.0	282.0	380.0	260.0
790,000	0	0	0	0	0

$\bar{v}$ at a height of 100 meters above the surface, $0.8\bar{v}$ at 10 meters, $0.67\bar{v}$ at 1 meter, and zero wind speed at the surface. Wind directions may be normal to the local vertical or parallel to the local terrain blowing upslope, downslope, or cross slope. For elevations above the surface greater than 1000 feet, the wind direction should be assumed normal to the local vertical.

The maximum surface wind speed is the maximum wind speed at 1 meter that a long life (greater than 30 days) landed vehicle must accommodate. The design must be capable of accommodating a gust speed as indicated in table 2.2-5 for all altitudes less than 90,000 feet. Removal of the gust at a critical stage of the induced motion shall also be evaluated. Superimposed on the near surface free stream continuous wind should be a mean vertical wind speed gradient of +2 ft/sec per 1000 feet to 50,000 feet. It is assumed that the mean continuous wind speed from 50,000 feet to 90,000 feet is equal to the value of 50,000 feet, and the mean continuous wind speed is zero above 90,000 feet. In addition to the mean vertical wind speed gradient, vertical wind shear may be present. The local mean horizontal wind speed, wind shear gradient, and maximum and minimum wind shear speeds are presented in table 2.2-6 for the atmospheric models shown in table 2.2-5."

2.2.2.3 Mars Surface Conditions

As specified by NASA/LRC, the Mars surface conditions, except for the atmospheric properties at the planet surface, were based on the model described in the NASA/OSSA Document, "Voyager Environmental Standards," dated 25 September 1967. Those planetary characteristics which most significantly affected the study results are reproduced from the reference document and presented herein:

1. Surface Atmosphere – The planetary atmospheric composition, pressure, temperature, wind velocity, and density properties used in the study are those presented in para. 2.2.2.2 herein. The solar energy at the surface can be determined by means of the computational procedures described in Sections IV C 1a and IV D 2a (4) of the reference NASA/OSSA document. That method utilizes the solar constants presented in table 2.2-7 and the results shown in figs. 2.2-1 and 2.2-2. In computing the anticipated solar irradiance at the Martian surface for the solar cell performance analysis, a reduction in the expected performance due to cloud coverage was used which was based on results of the type illustrated in fig. 2.2-3. This figure shows the position of large clouds (> 200 km) observed on Mars.

TABLE 2.2-7. SOLAR CONSTANT AT MARS ORBIT

Mars Position	Solar Constant (Watts/cm^2)
Perihelion (1.3814 AU)	0.0734 ± 0.009
Mean (1.5237 AU)	0.060 ± 0.009
Aphelion (1.6660 AU)	0.050 ± 0.009

2. <u>Surface Properties</u> – The estimated probability density distribution of such surface topography features as slopes, elevations, and craters on Mars are given in figs. 2.2-4, 2.2-5, and 2.2-6. For comparison, fig. 2.2-5 also presents the elevation probability density distribution on Earth.

The anticipated surface topography influences the Lander design in several ways. The slope angle significantly affects the Lander's impact characteristics and the post-impact telecommunication look angle between the Lander and Orbiter. For the study conducted herein, a reference maximum anticipated slope angle of up to $34°$ with the local horizontal was considered in the Lander's design. The expected elevation and/or crater depth affects the retardation system design. The higher the estimated landing site (i.e., the thinner the atmosphere), the larger and heavier will be the required parachute configuration to give a selected impact velocity. For these studies, the parachute system was designed for a 6000 foot (1.825 km) maximum altitude landing site.

With regard to the mechanical properties of the Martian surface, fig. 2.2-7 shows the probability density distribution of encountering various size particles on the surface of Mars, while fig. 2.2-8 presents the surface bearing strength for a 0.1 meter minimum width bearing pad. For this study, the Lander was designed specifically for maximum rock sizes of 5 inches (12.7 cm) in diameter and for landing on surfaces having a bearing capacity of 6 psi (42.2 gm/sq cm, log value of 2.63) to infinity.

The anticipated surface temperature is affected by latitude dependence, diurnal variations, and seasonal changes. Figure 2.2-9 presents the upper limits for the average surface temperatures for the 'light' areas of Mars at the equator and two Northern latitudes. The contours vary according to the time of day (ordinate) and the season (heliocentric longitude, η, as the abscissa). Between $87°$ and $177°$ heliocentric longitude, the northern hemisphere experiences its spring; between $177°$ and $267°$, its summer; between $267°$ and $357°$, its autunm; and between $357°$ and $87°$, its winter. Figure 2.2-10 shows the same information for the southern latitude of $-25°$ or along the axis of the main belt of dark areas.

Figure 2.2-11 gives the diurnal temperature variation with the bands on the figure indicating the uncertainty range of the temperature.

2.2.3 STUDY CRITERIA AND ASSUMPTIONS

At the initiation of the study and during its course, certain criteria were adopted and assumptions made on the basis of past entry vehicle hardware/program experience and planetary project studies. These criteria/assumptions were utilized so as to facilitate the conduct of the study and, in general, they can be considered as being in three general groupings: mission definition criteria, design criteria, and general program criteria.
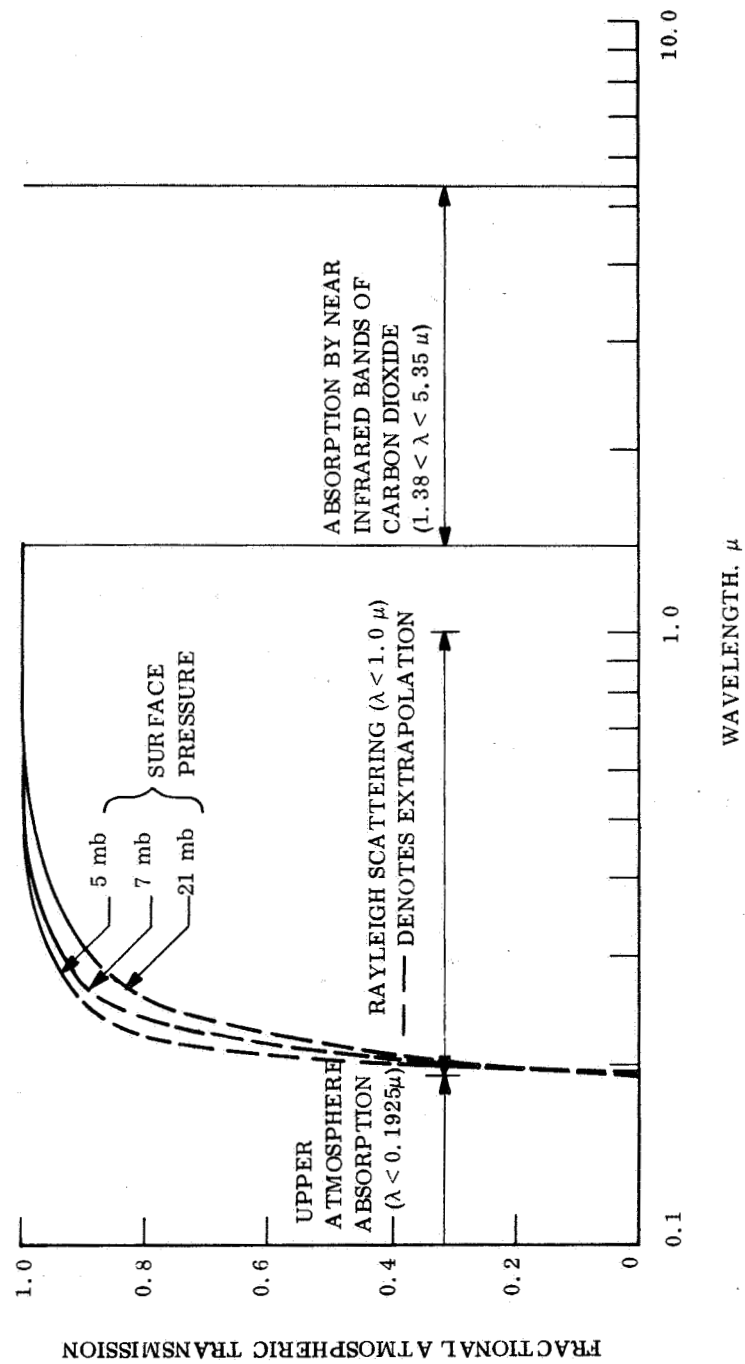
Figure 2.2-1. Fractional Transmission of the Martian Atmosphere – Clear Sky with Sun at Zenith
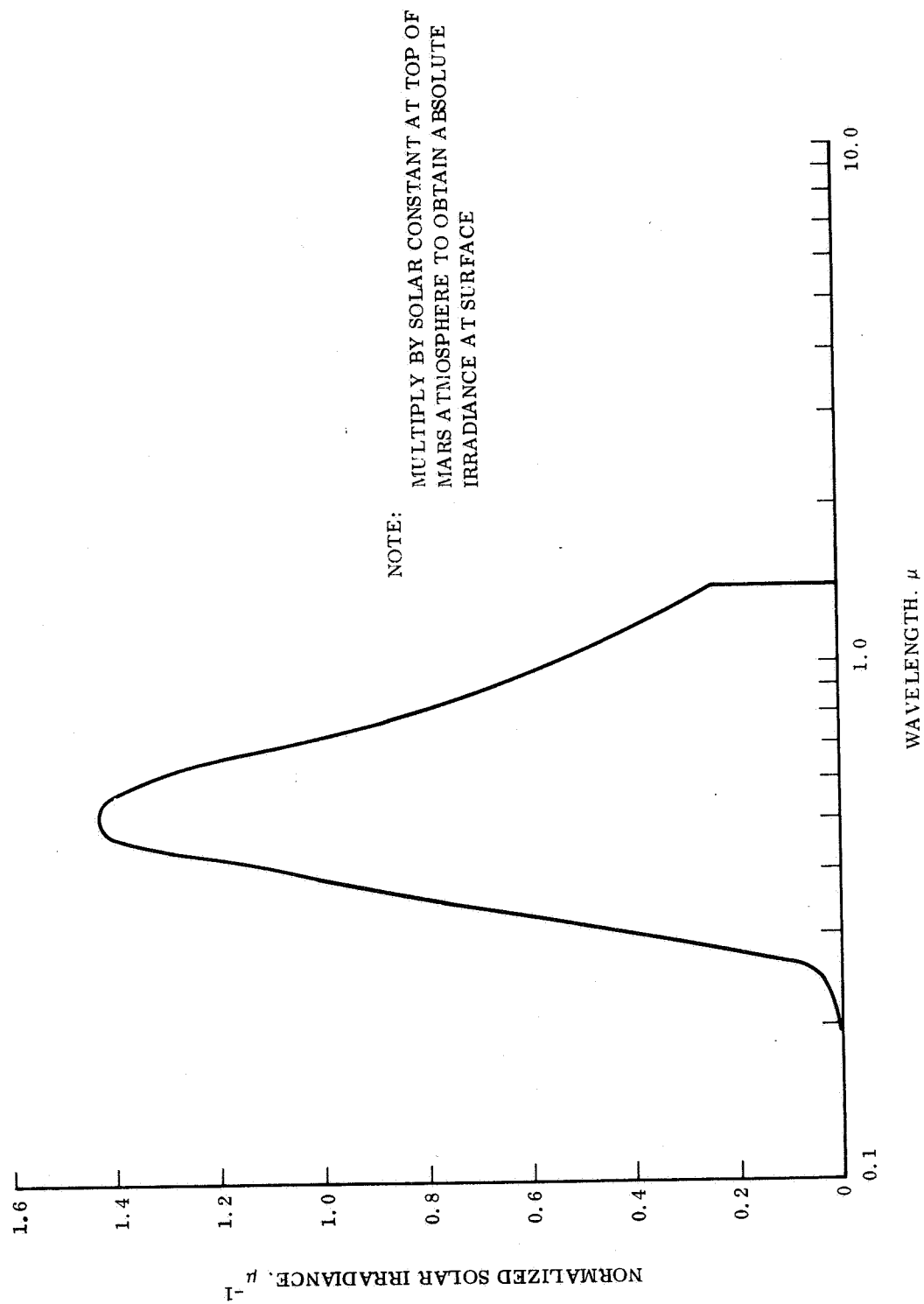
Figure 2.2-2. Normalized Solar Irradiance Spectra at the Martian Surface
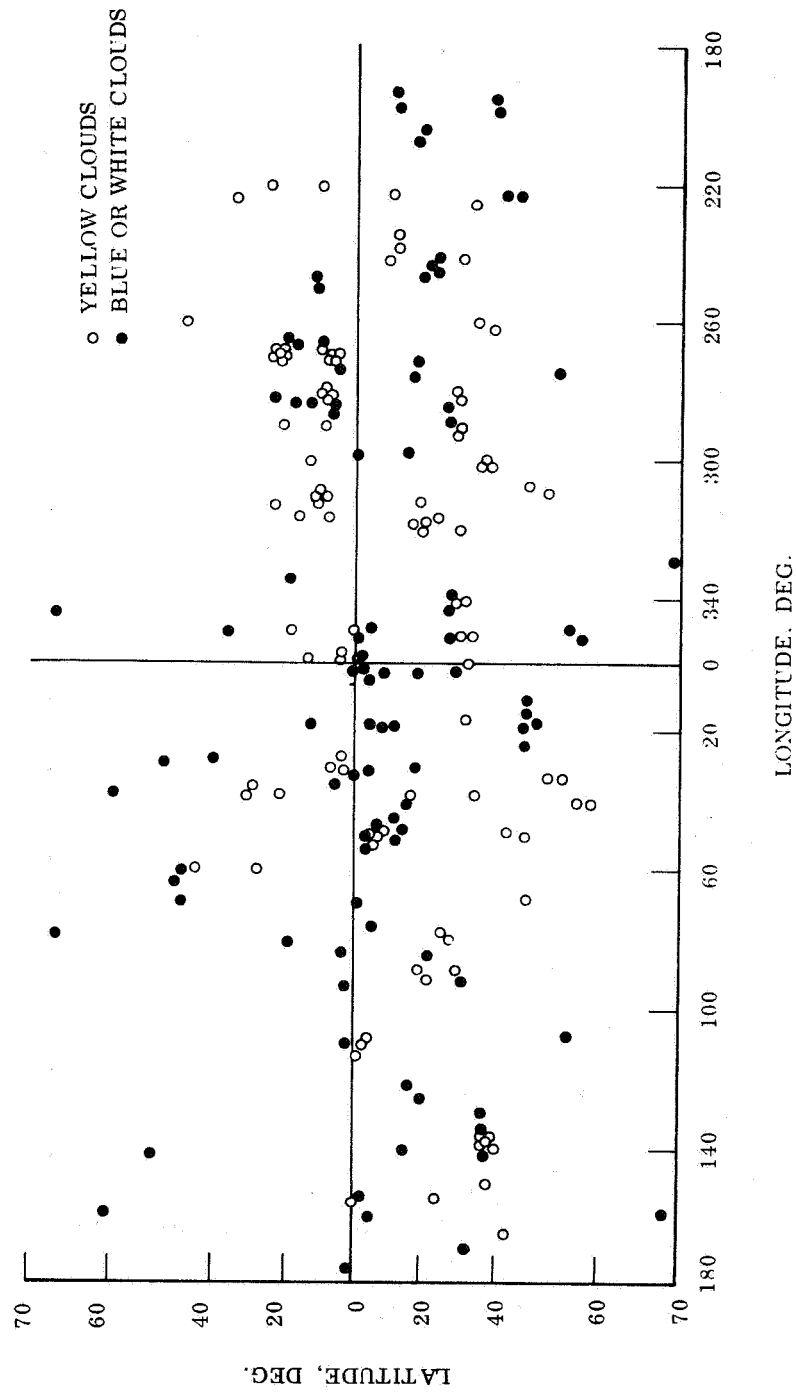
Figure 2.2-3. Position of Large Clouds Observed on Mars
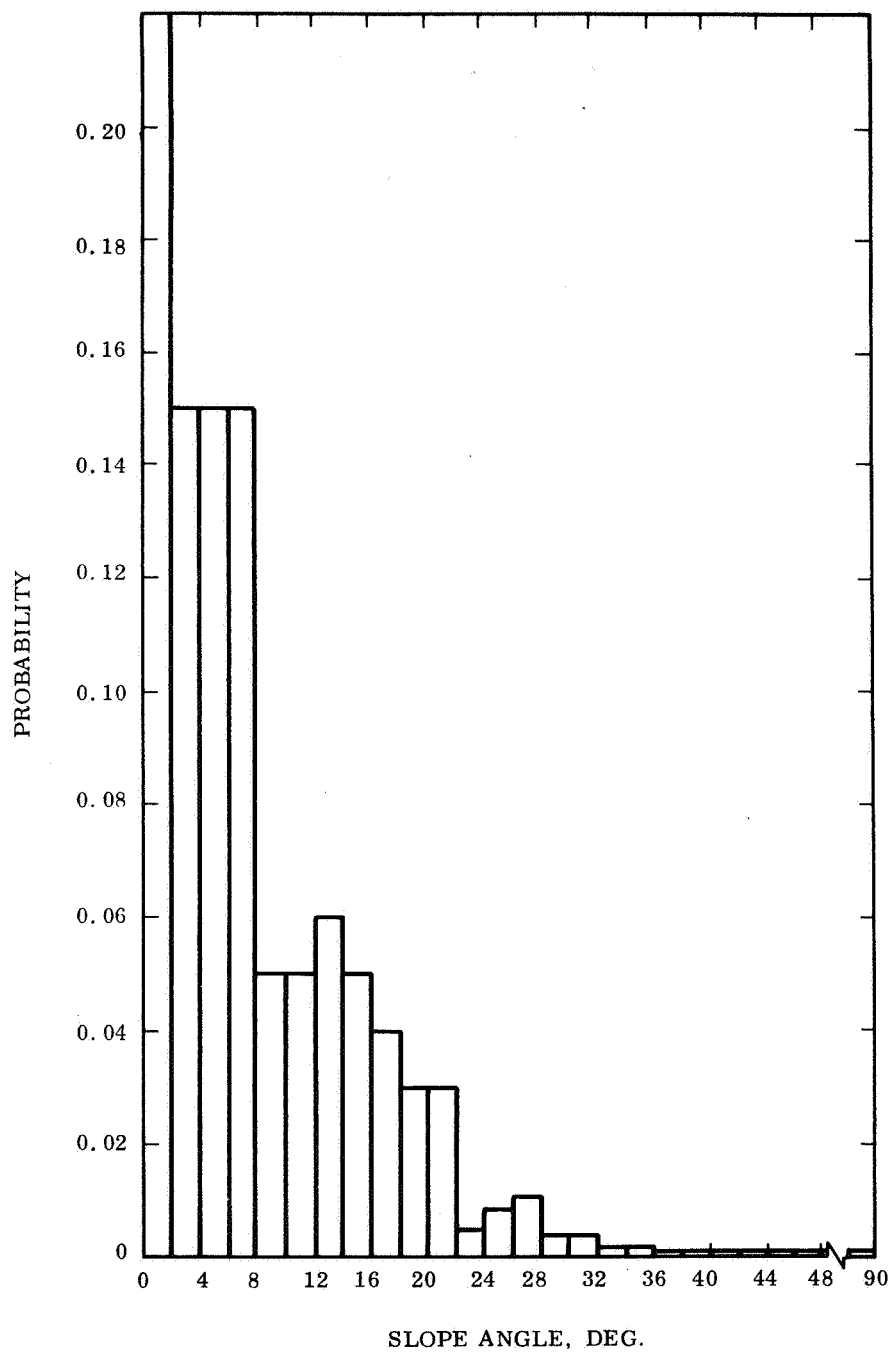
Figure 2.2-4. Probability Density Distribution for Slopes Between the
-60° to 60° Latitudes on Mars
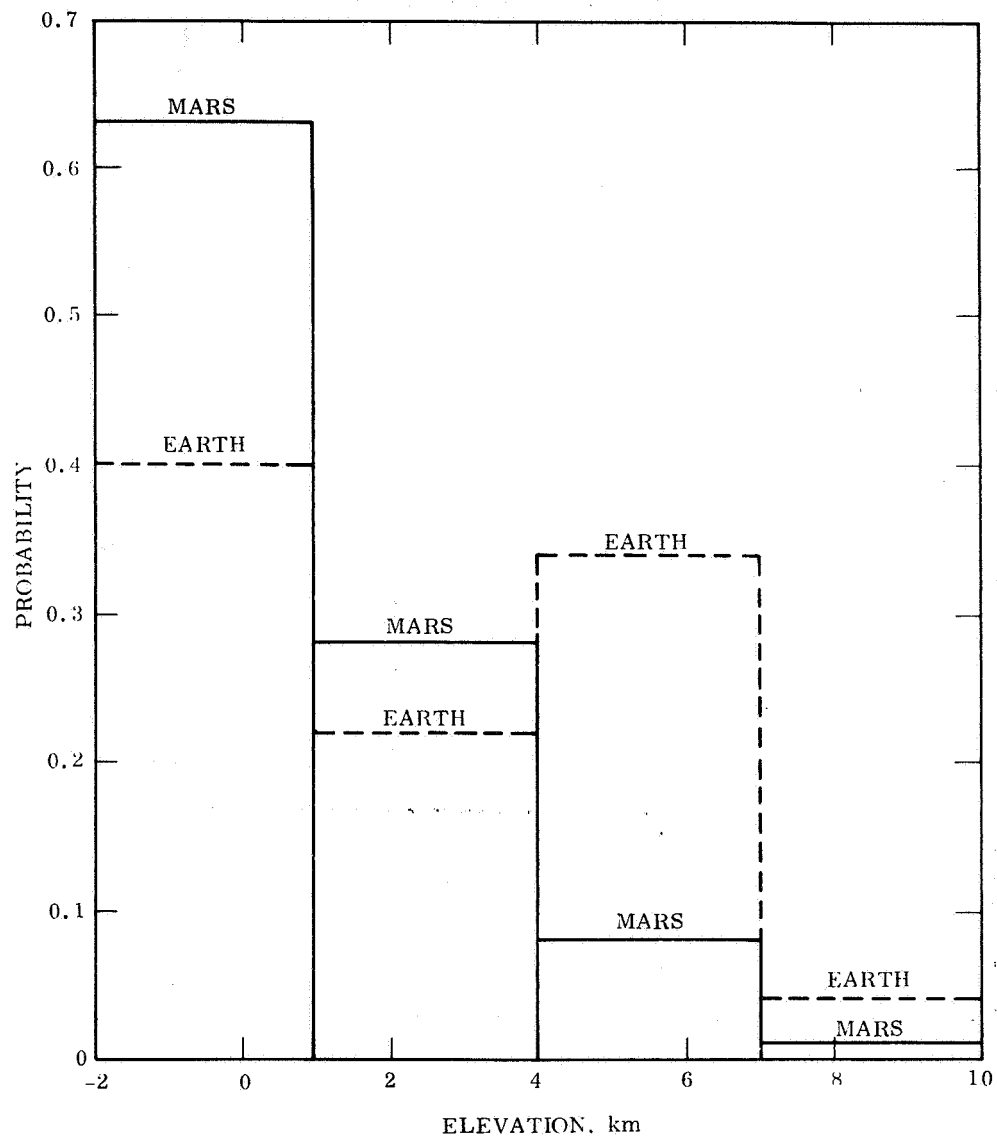
Figure 2.2-5. Probability Density Distribution for Surface Elevations
between the -60° to 60° Latitudes on Mars
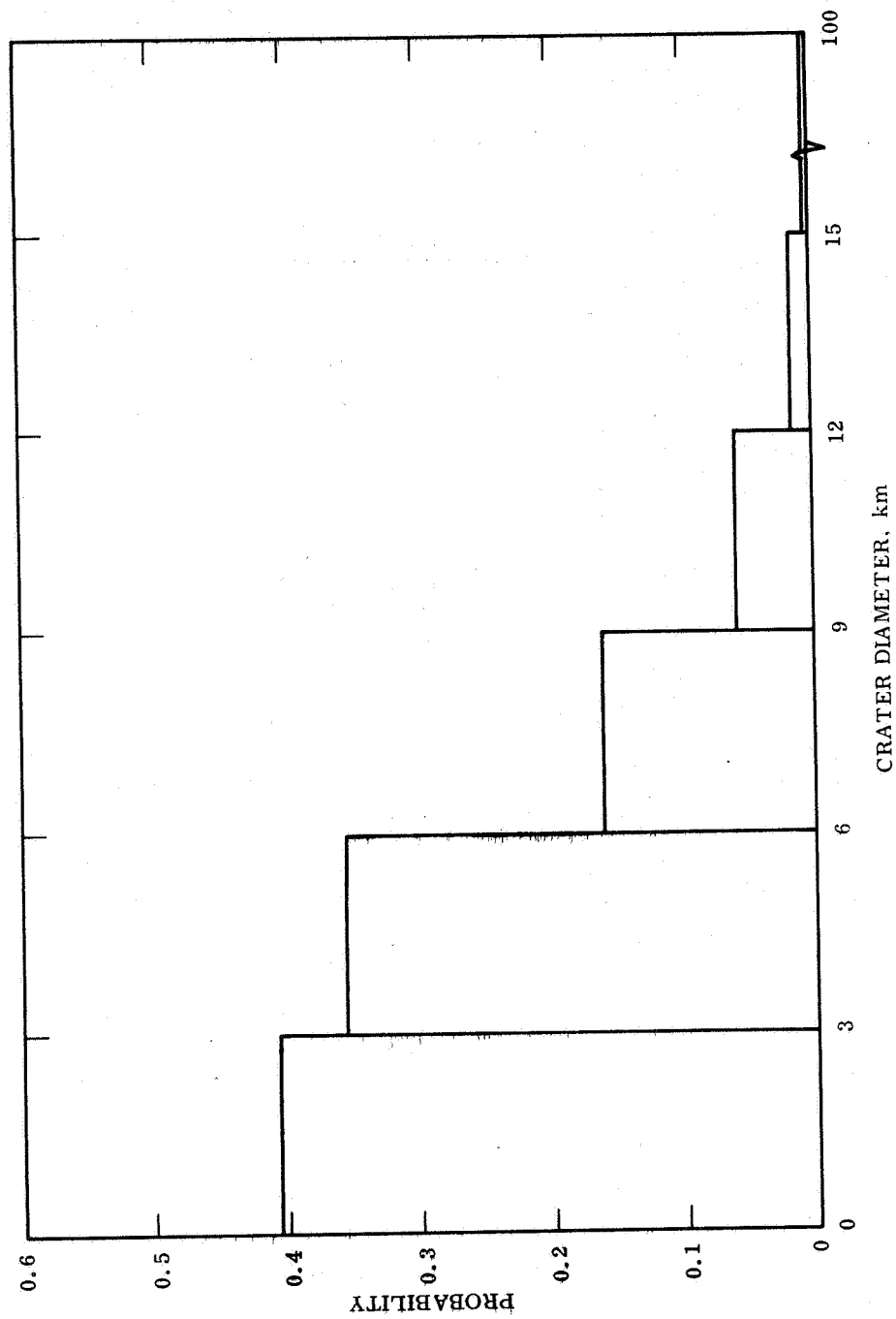
Figure 2.2-6. Probability Density Distribution of Landing on Mars in a Crater of a Given Diameter
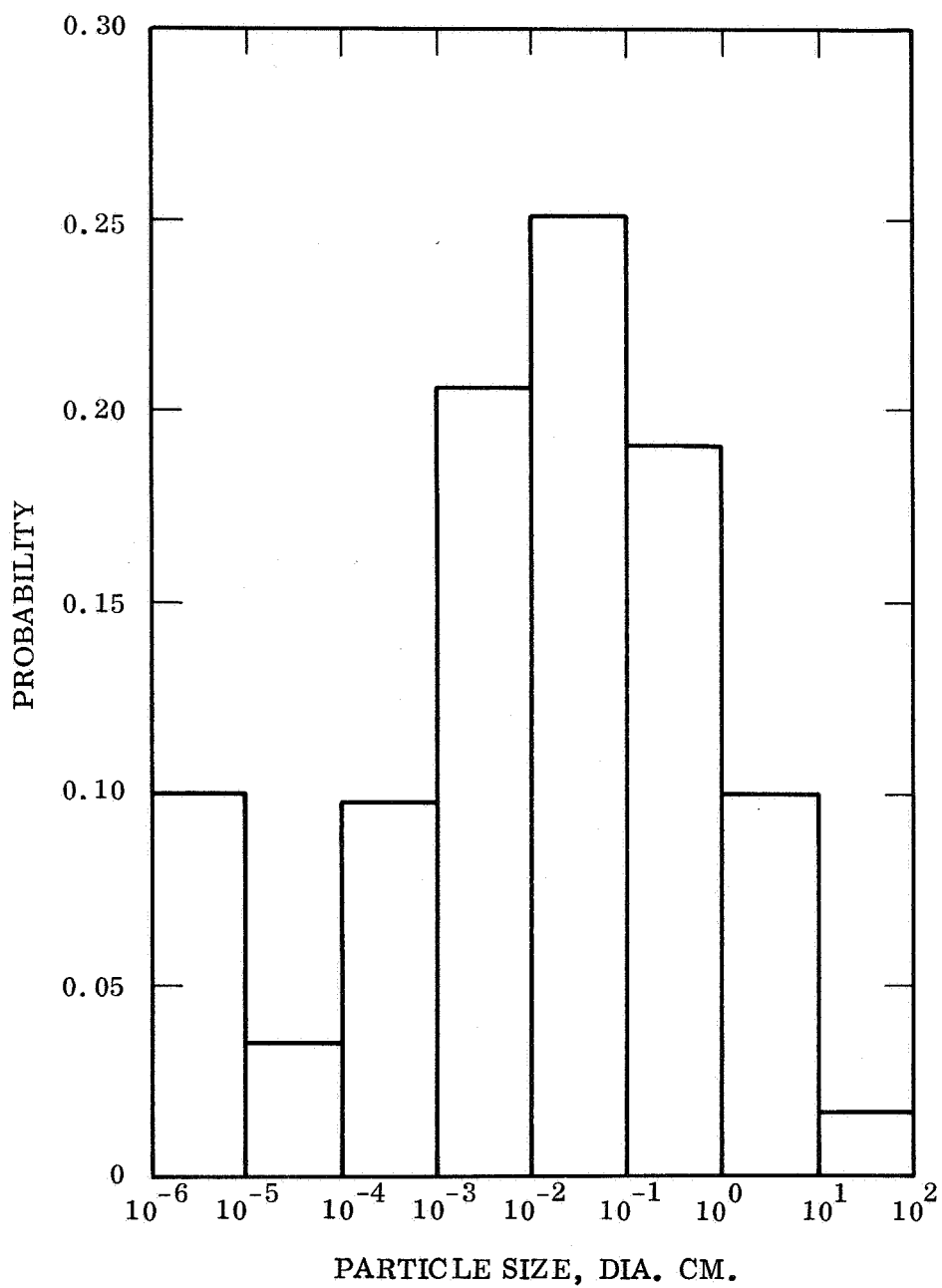
Figure 2.2-7. Probability Density Distribution of Particles on the
Surface of Mars
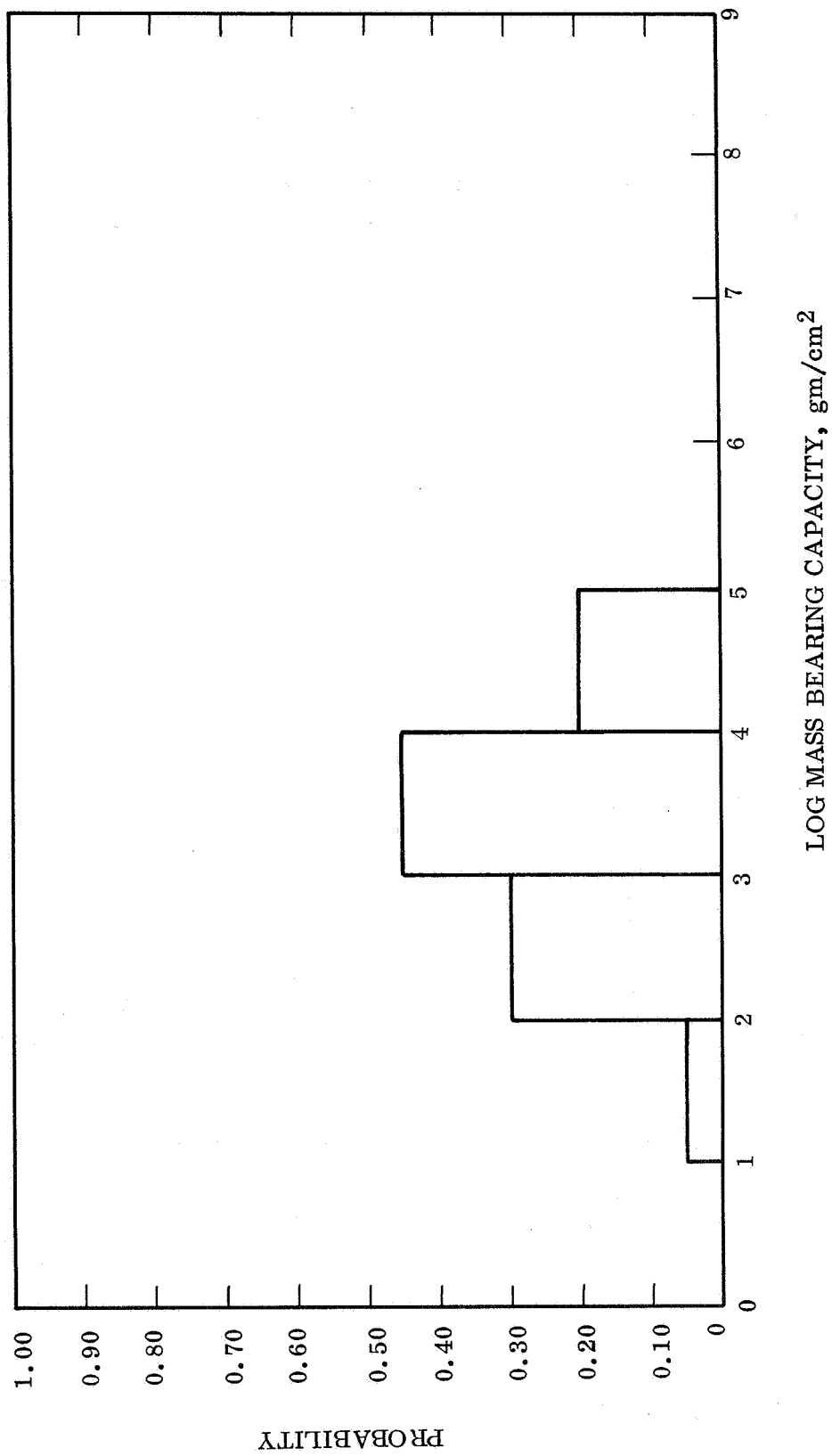
Figure 2.2-8. Probability Density Distribution for Logarithm of Mass Bearing Capacity

LATITUDE +25° LIGHT AREAS

LATITUDE +50° LIGHT AREAS

EQUATOR LIGHT AREAS
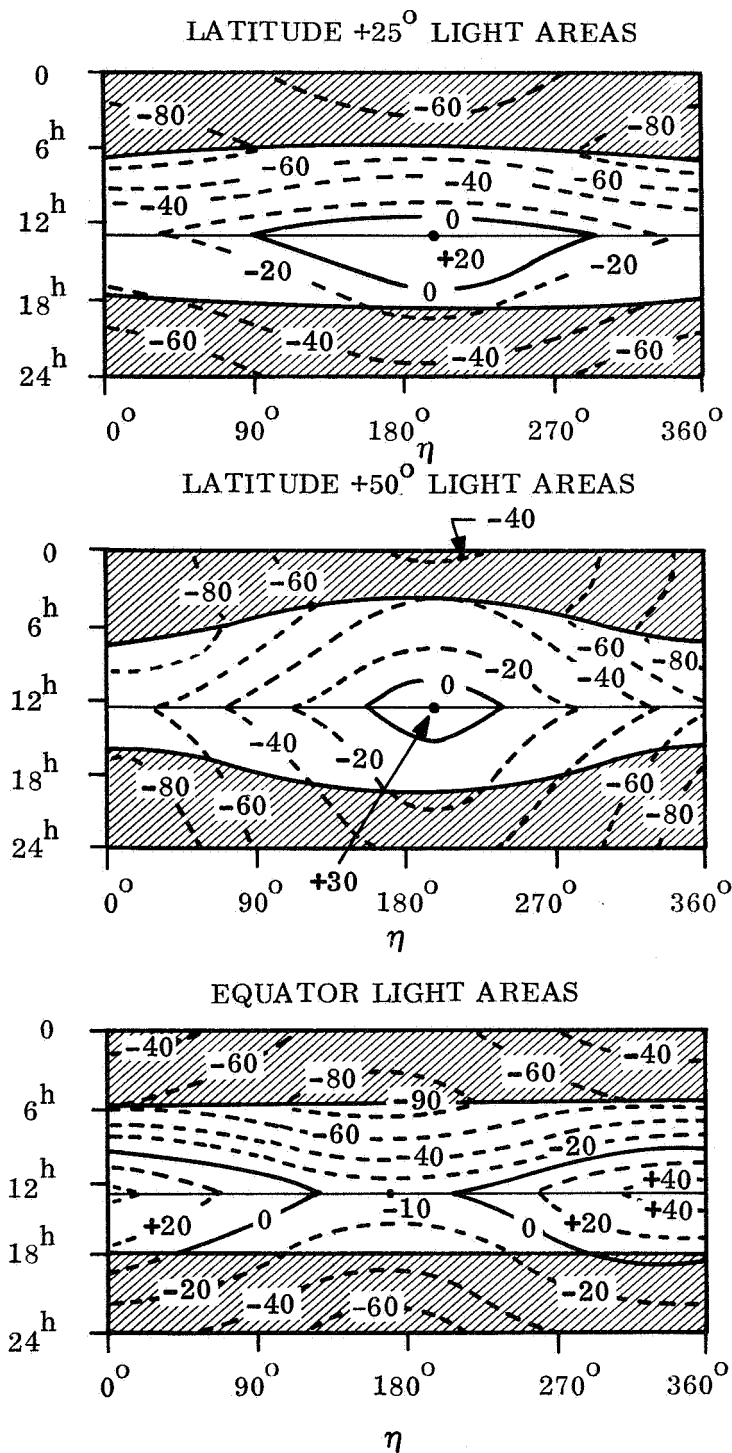
Figure 2.2-9. Mean Temperature of Light Areas in °C for Several
Latitudes as a Function of the Time of Day (Ordinate) and
the Heliocentric Longitude, η (Abscissa)

LATITUDE -25° DARK AREAS
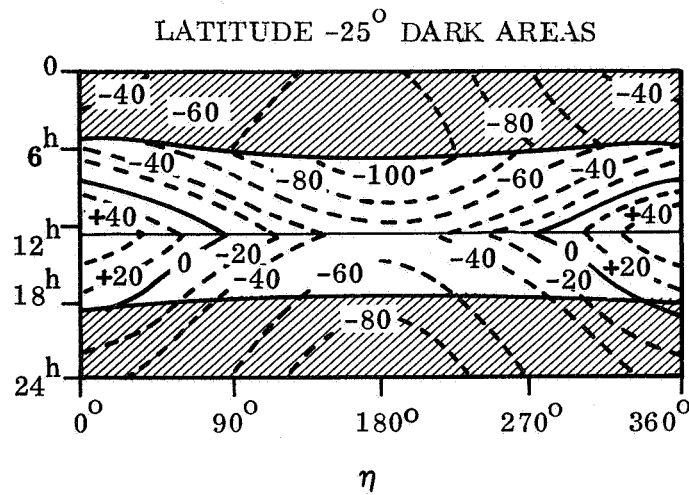
Figure 2.2-10. Average Isotherms in °C at -25° Mars
Latitude as a Function of the Time of Day
and the Heliocentric Longitude, η
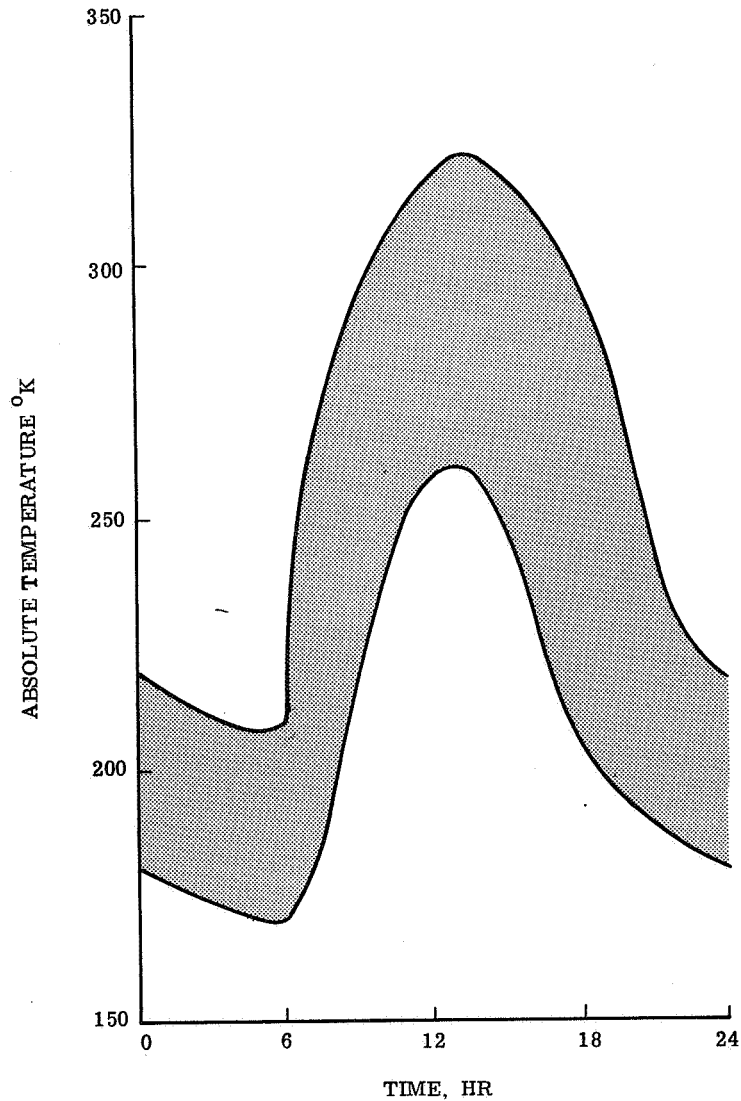
Figure 2.2-11. Daily Temperature Variation on Surface of Mars
at the Equator

II

2.2.3.1 Mission Definition Criteria

Mission definition criteria include:

1. Total launch period: 30 days, including two launches.

2. Range safety constraints at ETR: assume launch azimuths from 45° to 114° are permitted.

3. Separation distance between Capsule and Spacecraft before Capsule motor ignition (either deorbit motor or deflection motor depending upon mission mode): 1000 feet.

2.2.3.2 Design Criteria

Design criteria include:

1. Pre-entry Systems

   a. Environmental Control

      1) Capsule orientation relative to Sun during interplanetary cruise and in orbit: on shade side of Spacecraft.

   b. Canister

      1) Structural design criteria: the canister shall be designed for 1 psig internal pressure.

      2) Requirement for positive pressure maintenance during interplanetary cruise: none.

      3) Requirement for micrometeoroid protection: none.

2. Entry and Retardation Systems

   a. Aeroshell

      1) Aeroshell-Lander separation: delayed 10 seconds after parachute deployment (which can occur at MN as high as 2.0) to assure aeroshell-Lander separation at subsonic speeds.

   b. Parachute

      1) Parachute type: modified ring sail, disc gap band, or cross, are candidates. Modified ringsail selected for this study because of extensive data and previous experience (Mercury, Gemini, Apollo).

2) Parachute material: Nomex and Dacron are both candidates. Dacron selected for this study due to greater availability of material weaves and weights as compared to Nomex.

3) Deployment Mach Number: 2.0 (specified by study requirements).

4) Deployment dynamic pressure: 2 psf based on past tests and analysis.

5) Parachute size: in general, limited to 100 feet diameter, although no major problems are anticipated in deploying and opening chutes up to 200 feet diameter. In parametric studies, when size exceeds 100 feet D, a cluster is used with a limit of 3 canopies per cluster.

3. Landed Systems

a. Environmental Control

1) Lander radiation surface emissivity: 0.1

2) Heat transfer: negligible heat transferred by natural convection due to low atmospheric pressure and low gas density.

b. Power Supply

1) Batteries: must be heated above $+20°F$ to provide marginal performance.

2) Fuel Cells: minimum temperature must exceed $+30°F$. Product water stored in expanding polyethylene trap to prevent freezing or interference with science water detection experiments. Required interplanetary cruise eliminates use of cryogenics.

3) Solar Arrays: cell output efficiency affected by solar distance, dust, cloud cover, dust abrasion, temperature, and illumination time (landing latitude, landing angle).

4) RTG: radiation may affect science (alpha back-scatterer). Interplanetary cruise reduces effective half-life. Landing angle will affect thermocouple efficiency due to radiating view angle.

c. Telecommunication

1) Transmitted power limitation: 50 watts due to antenna performance 'breakdown' in Martian atmosphere.

2) Direct Link: based on one DSN station with 210-ft dish.

3) Command Link: based on 85-ft dish with 100 KW transmitter (under development by JPL).

2.2.3.3 General Program Criteria

The following criteria are applicable to all components and subsystems comprising the Capsule system.

2.2.3.3.1 Thermal Sterilization Requirements

NASA Planetary Quarantine policy requires that the Capsule System will be heat sterilized so that the probability that live microorganisms remain is 10^{-3} or less. This will be achieved by controlling the biological loading during assembly so that no more than 10^5 microorganisms will be present on the Capsule before terminal sterilization and by subjecting the Capsule to a thermal heat cycle to reduce the bioload by 10^8.

In accordance with this requirement, all components and subsystems have been selected on the basis of their compatibility with the NASA criteria shown in table 2.2-8 which has been reproduced from ref. 2-16.

2.2.3.3.2 Weight Calculations

The weight of all items in the Capsule system point designs shall be determined using the criteria shown in table 2.2-9.

2.2.3.3.3

The Capsule system structural criteria utilized in this study are presented herein. The structural requirements and criteria are derived from the launch vehicle characteristics, the interplanetary trajectory conditions, and the planetary environment for entry into the atmosphere and impact on the surface. The critical mission phases and environments for the design of the structural systems are presented in table 2.2-10. Table 2.2-11 tabularizes the structural requirements and criteria while table 2.2-12 gives the structural loading and environmental criteria. The data used for the launch vehicle characteristics was obtained from ref. 2-17.

TABLE 2.2-8. HEAT STERILIZATION CYCLE PARAMETERS

Item	Temp. °C	Chamber Nitrogen Concentration	Exposure Time hrs/cycle	No. of Cycles
Parts and Materials Qualification	135	**	92	6
Subsystem (Assy.) Testing				
FA	125	**	24.5	1
TA	135	**	92	6
System Testing				
FA	None (Performed at Subsystem Level)			
TA (PTM)	135	**	72	3
Terminal Sterilization	125	**	24.5	1
**Not available at this time				

TABLE 2.2-9. POINT DESIGN WEIGHT CRITERIA

Item	% Weight Allowance	
	Well-Defined Equipment	Advanced Design Equipment
Growth	5%	9%
Contingency	1%	15%
Incremental Weight	6%	6%
	12%	30%

TABLE 2.2-10. CRITICAL MISSION PHASES AND ENVIRONMENTS
FOR THE STRUCTURAL SYSTEMS DESIGN

Critical (x)   Secondary Criteria (●)

Mission Phase	System Component → Event ↓	Lander		Entry		Pre-entry	
		Landed Systems	Impact Attenuation & Structure	Heat Shield	Aeroshell Structure	Bio Canister	Spacecraft Adapter
Prelaunch	Manufacturing, Handling, Transportation, Sterilization, Prelaunch					● Shock ● Vibration x {Sterilization - Thermal & Pressure Cycles}	
Launch	Boost, Powered Flight, Stage Separation	x {Vibration ● & Inertia}			● Shock ● Vibration	x {Vibration & Inertia}	x {Vibration & Inertia}
Flight	Earth Orbit Insertion, Interplanetary, Mid Course Maneuver, Mars Orbit Insertion, Bio Separation, Deorbit Spin & Despin	● Vibration			● {Shock Vibration}	● {Thermal Meteoroid} ● Vibration	● Shock
Entry	Descent, Aeroshell Separation, Terminal Descent, Chute Separation			x Thermal	x {Inertia Thermal Vibration}		
Landing	Impact	x Shock ● {Wind Pressure Thermal}	x Shock				
	Deployment						
Post Landing	Operations	x {Wind Pressure Thermal}					

TABLE 2.2-11. STRUCTURAL REQUIREMENTS AND CRITERIA

Landed Systems:	• Survive impact shock and vibration, provide for damping • Martian and interplanetary environment • Sterilization
Lander Structure:	• Impact shock inertia and crush-up stresses • Vibration response and damping • Martian environment; pressure and temperature cycles • Sterilization
Impact Attenuation:	• Max. terminal and wind velocities • Max. deceleration • Ground slope, 34°, rock and protrusions • Directional capability and orientation • Sterilization • R. F. transparency
Heat Shield:	• Martian atmosphere: Critical models • Entry heating and thermal effects • Sterilization temperature cycles • Shield-structure bond and interface temperature
Aeroshell Structure:	• Aerodynamic loading: dynamic pressure, axial and lateral inertias • Shield structure interface temperature • Sterilization • Minimum gauge design
Canister:	• Sterilization cycle: pressure and temperature differentials • Launch environment: inertia, vibration, pressure and temperature • Meteoroid environment • Thermal environment/solar exposure • Minimum gauge design
Adapter and Systems Interfaces:	• Launch environment: inertia, vibration temperature • Separation response • Minimum gauge design

TABLE 2.2-12. STRUCTURAL LOADING AND ENVIRONMENTAL CRITERIA

TABLE 2.2-12. STRUCTURAL LOADING AND ENVIRONMENTAL CRITERIA

Phase	Mission Event	Load Factors and Inertias G_x (Earth g's)	G_n	Factor	Pressure lb/in²	Temperature °F	Vibration and Shock cps and Earth g's	Radiation, Meteoroid and Other Environments
Prelaunch	Manufacturing Handling Transportation	2g Pull-off Limit 1.0 1g Cantilevered Ultim. 1.5 Ground – MIL A8421B Air Transport if required			Ambient 50 lb, Hand-lean Load Ambient	Ambient		} Humidity and corrosion
	Sterilization Prelaunch				+1/2 lb/in² minimum differential Factors: Proof = 1.33 Burst = 1.67	6 cycles of +275° for 24 hrs +20 to 160°		Decontaminating chemicals
Launch	Boost and 1st stage Powered Flight 2nd stage Stage Separations	5.2 4.0 +6.0 –3.0	2.0 2.0 ±2.0	Limit 1.0 Ultim. 1.25	Ambient Pressure decay in minutes inside shroud	+20 to 160°	Low frequency 10–15 cps Dynamic factor on Inertias Acoustic 140 db.	
Flight	Earth Orbit Insert. Deorbit Interplanetary Mid Course Maneuver. Mars Orbit Insert. Bio-Separation Deorbit Spin and Despin	Low				–65 to 300° (External) 100° (Internal) to Canister	Low (covered by launch and powered flight conditions)	Cometary and Asteroidal Meteoroid Debris and Solar/Cosmic Radiation Particle and Energy Radiation (ref. 3) Also explosives – produced chemicals
Entry	Descent Aeroshell Separation Terminal Descent Chute Opening and Release	Ref. Vol. III, Sect. 3.1.2 Low Low 10.0	(Limit 1.0: Ultim. 1.25)		Ref. Vol. III Sect. 3.1.2	Ref. Vol. III Sect. 3.1.2		
Impact	Impact	> 1000g Ultim. 1.25			Wind Loads: Max 220 ft/sec.			
	Deployment							
Post Landing	Operation	1g Ultim. 1.25				Ambient Martial Surface		Martian Surface Model (Sect. 2.2.2.3)

2.3 MISSION PROFILE AND EVENTS

This section of the report presents the mission profiles and events for the 'reference' out-of-orbit entry and direct entry mission modes (both are Type I trajectories). Table 2.3-1 summarizes some of the more important characteristics for these two reference missions while Section 3.1 of this volume discusses the analysis conducted to define the two subject missions.

As previously noted in Section 1.1, Study Objectives, six point designs were derived during the course of this study and their system requirements are presented in table 1.1-2. In order to illustrate the interrelationship between the 'mission profile and events' and the Capsule system's operational and design features, these six point designs will be used as our discussion examples. Point Designs 1, 3, and 5 employ the out-of-orbit entry mode while Point Designs 2, 4, and 6 use the direct entry mission mode.

TABLE 2.3-1. SUMMARY TABLE OF THE REFERENCE MISSIONS
(TYPE I TRAJECTORIES)

Item	Out of Orbit	Direct Entry
Trajectory Type	I	I
Launch Date (Range of) [1]	Aug. 11 – Sep. 10, 1973	July 12 – Aug. 11, 1973
C_3 Reqd. km^2/sec^2	25	18
C_3 Avail., km^2/sec^2	40	40
Arrival Date (Range of)	April 20 – May 13, 1974	Jan. 4 – Jan. 14, 1974
Trip Time (Range of), days	245–253	156–176
V_∞ (Range of), km/sec	2.6–2.8	3.9–4.1
Deorbit Δ V, km/sec	.235	----
Deflection ΔV, km/sec	----	.045 (24 hrs before encounter)
Reference V_E, ft/sec	15,300	20,800
Capsule Impact Latitude, degs	10 N, 20 N	10 N
Orbiter Inclination, degs	60	10.7
Earth-Planet Distance at Arrival, km	294.7 x 10^6	137.5 x 10^6

Note: (1) This range is representative for a 30-day launch window.

The mission objectives are to achieve Capsule landing sites in the northern latitudes in conjunction with a highly inclined Orbiter orbit. The landings would be accomplished either approximately 30° ahead of the evening terminator or 30° after the morning terminator. The Orbiter orbit will be synchronous with a 1000 km periapsis and a 33,100 km apoapsis.

For the out-of-orbit case, orbital trims would be accomplished during the first few days after insertion of the Orbiter and Capsule (i.e., Spacecraft) into orbit. (This could require 5 days.) During this time, the Orbiter could photograph the candidate landing sites and the information would be used in the selection of the most suitable site. Immediately after impact, Lander imagery data would be obtained and read out real time.

For Point Design 1, the imagery acquisition (of new scenes) will be repeated at the return of the Orbiter (end of one day). For Point Designs 3 and 5, the imagery will be conducted during the first 3 days while the Orbiter's orbit is synchronous and the Orbiter supports the Lander mission.

The Orbiter would go asynchronous at the conclusion of the initial imagery mission in order to enhance its own planet mapping task. During the latter part of its mission, the Lander would serve as a 'weather station' and would obtain meteorological data which would be transmitted via a direct link to Earth.

In the Direct Entry case, Capsule separation from the Spacecraft and deflection of the Capsule trajectory to provide atmospheric entry will be effected from 1.0 day out from the planet. Transmission from the Capsule to the Orbiter during entry, and immediately after landing, would occur just prior to or during, orbital insertion of the Orbiter. After landing, the surface mission for the direct entry Point Designs will be exactly the same as that of their out-of-orbit entry counterparts.

During the first day on the surface of Mars, the Lander will store the meteorological data and the engineering diagnostic data. For Point Design 2, which is a Direct Entry mission, the Lander must cope with the fact that the Orbiter may have been inserted in a "sloppy" orbit which may have an orbital period of 24.6 ± 3 hrs. This affects both the communication range and the available time for transmission. In addition, it is desired to read out the imagery data in real time. Due to the selected landing sites (either two hours ahead of the evening terminator or two hours after the morning terminator), it is possible with the orbital period errors being considered, that the Orbiter would return at the end of the first day and find the Lander in darkness and thus unable to perform the imagery mission at the end of the first day. This imagery mission could be a repeat or an extension of the imagery previously performed just after impact.

For Point Designs 3 through 6, the long duration missions, the surface mission will consist of gathering soil composition data during only the first day. However, the meteorological data plus diagnostic data will be obtained daily and transmitted via the relay link for the first three days and via the direct link thereafter.

The following paragraphs describe the "Mission Profile and Events" in more detail. It should be noted that the time of initiation of the direction link (i.e., whether or not to use it during the first three days) is a trade-off for future study, and involves the deployment of the solar array for power support and the array's possible interference with the imagery mission.

2.3.1 LAUNCH TO CAPSULE/ORBITER SEPARATION

The Mars '73 missions studied herein are based on being launched from Cape Kennedy for a Titan III-class launch vehicle. The assumed launch energy level of available $C_3 \approx 40$ km^2/sec^2 (per LRC direction) is representative of that expected using a Titan IIID/Centaur. During the lift-off phase, through the atmosphere the canister is depressurized to assure that the pressure differential between canister internal pressure and the atmospheric pressure does not exceed 1 psi. No attempt is made, after the Spacecraft is out of the Earth's sensible atmosphere, to maintain any positive differential in the canister during the transit to Mars.

As described in Section 3.0, Mission Analysis, two Mars '73 reference missions were derived for use in the subsystem and system analyses performed during this study and which are reported in Volumes III and IV. The two reference missions selected represent the Out-of-Orbit Entry and the Direct Entry Mission modes, and both are Type I transit trajectories (helicentric transfer angles are less than 180°). Assuming that 30-day launch windows are representative, the launch periods for the two reference missions would be August 11 - September 10, 1973 for the out-of-orbit entry and July 12 - August 11, 1973 for the direct entry. These selected missions would have trip times and resulting arrival dates of 245-253 days (arrival dates of April 20 - May 13, 1974) for the out-of-orbit entry, and 156-176 days (arrival dates of January 4 - January 14, 1974) for the direct entry.

After launch, the Spacecraft (Orbiter and Capsule) is inserted into a near-Earth parking orbit and then into the trans-Mars trajectory. During the interplanetary cruise phase, the Capsule is carried on the shade side of the Spacecraft and is dependent upon the Spacecraft for all of its support functions (i.e., trickle-charge to batteries, diagnostic telecommunication, etc.) except for environmental control.

Up to the point in the mission profile of arrival in the vicinity of Mars, the Spacecraft mission is essentially the same whether the Capsule will employ an out-of-orbit entry or a direct entry. From this point on, however, the mission events differ significantly for the near-Mars exoatmospheric phase.

2.3.1.1 Out-of-Orbit Entry

The mission plan is that several days prior to Lander impact, the Spacecraft is inserted into a Mars orbit which has a synchronous period 24.6 hours, a periapsis of 1000 km, and an apoapsis of 33,100 km. The Spacecraft completes several orbits around the planet during which time the orbit is trimmed and the reconnaissance of candidate landing sites can be conducted. Approximately 22 hours before Capsule separation, the Capsule is interrogated as to its condition and the resulting diagnostic information is analyzed and evaluated on-board the Spacecraft. If all Capsule systems are in the 'go-condition', then the Spacecraft initiates the separation sequence of events which includes separation of the canister forebody and, subsequently, separation of the Capsule. It should be noted that both the orbit and the Orbiter's configuration (i.e., W/C_DA) are specifically selected to assure that the planetary quarantine guidelines are observed, that is, the Orbiter's orbit cannot decay in less than 12 years thereby assuring non-contamination of Mars prior to 1985. In similar fashion, the W/C_DA of the canister forebody has been specifically selected to assure that it too will not physically impact on Mars before the aforementioned date.

2.3.1.2 Direct Entry

The nomenclature employed herein should be clarified at this point to avoid confusion. While that portion of the Spacecraft remaining after Capsule separation is referred to as the Orbiter, it is actually performing a fly-by mission from the time the Capsule is separated until it is inserted into orbit after the Lander has impacted. The Capsule separation from the Spacecraft, in the direct entry mode, is effected one day prior to Capsule atmospheric entry. As in the case of the out-of-orbit entry, Capsule separation is preceded by separation of the canister forebody.

2.3.2 CAPSULE/ORBITER SEPARATION

For both mission modes, the detailed 'entry' sequence of events begins with the canister separation as shown in table 2.3-2.

2.3.2.1 Out-of-Orbit Entry

Approximately 10 minutes after canister separation, the Capsule system is separated from the Orbiter by the use of separation springs. The Capsule's resultant separation velocity effected by the springs is about 3/4 fps with any velocity increment imparted to the Orbiter being counteracted by the Orbiter's stabilization system. After

TABLE 2.3-2. SEQUENCE OF EVENTS FROM SEPARATION THROUGH ENTRY PHASE FOR OUT-OF-ORBIT ENTRY VS DIRECT ENTRY (BOTH WITHOUT RADAR ALTIMETER)

Event	Point Design 1 - Out-of-Orbit Entry Time		Point Design 2 - Direct Entry Time	
1. Start Final Capsule Diagnostic Checkout	To (Entry - 24 hrs)		To (Entry - 48 hrs)	
2. Complete Checkout	To +120 min		To +120 min	
3. Update Programmers Complete	To +20 hrs		To +20 hrs	
4. Turn on Lander Power, T/M and Sequencer	T1 (To +21.7 hrs)		T1 (To +23.8 hrs)	
5. Canister Separation	T2 (T1 +5 min)		T2 (T1 +5 min)	
6. S/C Maneuvers to Capsule Separation Attitude	T2 +10 min		T2 +10 min	
7. Capsule separates from S/C	T3 (T2 +10.1 min)		T3 (T2 +10.1 min)	
8. Spin Stabilization	T3 +0.5 sec		T3 +0.5 sec	
9. Ignite Deorbit (Deflection) Propulsion	T3 +30 min		T3 +30 min	
10. Terminate Deorbit (Deflection) Propulsion	T3 +30.3 min		T3 +30.3 min	
11. Initiate Despin	T3 +30.5 min		T3 +30.5 min	
12. Separate Thrust Cone	T3 +30.6 min		T3 +30.6 min	
13. Turn Power and T/M Off	T3 +30.7 min		T3 +30.7 min	
14. Turn On Mass Spectrometer for Warm-Up	T4 -15 min		T4 -15 min	
15. Turn on T/M, Initiate Accel., Stag. Temp. and Press. Sensors	T4 -60 sec		T4 -60 sec	
16. Entry	T4 (T3 +119 min)		T4 (T3 +24 hrs 8.3 min)	
	VM-8	VM-9	VM-8	VM-9
17. Mach 5 - Initiate Mass Spec., Water Vapor, Base Temp. Sensors	T4 +255 sec	T4 +217 sec	T4 +107 sec	T4 +97 sec
18. Mach 2 - Deploy Chute	T4 +285 sec	T4 +259 sec	T4 +121 sec	T4 +118 sec
19. Aeroshell Separation	T4 +295 sec	T4 +269 sec	T4 +131 sec	T4 +128 sec
20. Release Parachute	T4 +459 sec	T4 +1250 sec	T4 +350 sec	T4 +1216 sec
21. Impact	T5 (T4 +460 sec)	T5 (T4 +1251 sec)	T5 (T4 +851 sec)	T5 (T4 +1217 sec)

about 30 minutes (1800 seconds), a separation distance between the Capsule and the Orbiter of at least 1000 feet will have been achieved and the Capsule deorbit motor can be fired. Past experience would indicate that a separation distance of 1000 feet would be sufficient to prevent impingement of the deorbit motor plume on the Orbiter. The deorbit motor provides the Capsule with a ΔV of 235 mps.

On the basis of the 'Down Range Dispersion' analysis discussed in Section 3.2 of this volume and the 'Attitude Control Subsystem' description in Section 5.2 of Volume III, it would appear that the required thrust alinement during the deorbit motor firing can be satisfied with spin stabilization. Spinup will occur about 4 seconds after the Capsule separates from the Orbiter with despin being initiated about 12 seconds after deorbit motor fire.

Approximately 18 seconds after deorbit motor fire, the thrust cone would be jettisoned in order to minimize the Capsule's weight at entry. With the completion of the separation of the thrust cone, the Capsule's telemetry system is turned off until about 1-1/2 hours later when atmospheric entry starts. Using a timing signal (the time from deorbit motor firing until an altitude of 244 kilometers is reached, essentially the start of atmospheric entry, is a readily calculable increment), the telemetry and the entry science instrumentation except for the mass spectrometer, base region temperature and water vapor detector, would be turned on. The time from deorbit motor fire to the start of entry is 5330 seconds for the reference mission.

2.3.2.2 Direct Entry

As in the case of the out-of-orbit entry, the direct entry sequence of events includes the Capsule separation (again by means of separation springs), the attainment of a 1000 foot separation distance between the Capsule and the Orbiter (actually on a Mars fly-by trajectory), the firing of the deflection motor (it provides a ΔV of 45 mps and puts the Capsule on a ballistic impact trajectory with the planet), the jettisoning of the thrust cone, and the start of atmospheric entry.

2.3.3 CAPSULE ATMOSPHERIC ENTRY

To this point in the mission profile, the events occurring generally fell into two categories; those corresponding to the out-of-orbit entry mode and those corresponding to the direct entry mission mode. In the atmospheric entry phase and the subsequent landed operations phase, the events are more nearly dependent on the deceleration system sensing method and the designed for surface lifetime than they are on the entry mission mode. As previously noted in Section 1.1, "Study Objectives", six Point Designs were synthesized and analyzed as a part of this study, and their varying design characteristics significantly affected their atmospheric entry and landed operations events. Table 2.3-3 summarizes the vehicle design features of the Point Designs which

TABLE 2.3-3. VEHICLE DESIGN FEATURES OF POINT DESIGNS WHICH INFLUENCE THEIR MISSION PROFILE AND SEQUENCE OF EVENTS CHARACTERISTICS

Point Design No.	1	3	5	2A	2B	4	6
Mission Mode	Out-of-Orbit Entry			Direct Entry			
Parachute Deployment Sensing	Sense MN 2.0	Radar Altimeter		Sense MN 2.0	Radar Altimeter		
Entry Science	Basic Pkg.			Basic Pkg.			
Lander Configuration	Omni-Directional	Uni-Directional		Omni-Directional	Uni-Directional		
Surface Lifetime	25 Hrs. +	90 Days or More		25 Hrs.		90 Days or more	
(1) Imagery Read-Out (R-O)	2 R-O Periods @ Relay Link	4 R-O Periods @ Relay Link	4 R-O Prds. @ Relay Link Plus Several @ Direct	2 R-O Periods @ Relay Link	2 R-O Periods @ Relay Link	4 R-O Periods @ Relay Link	4 R-O Prds. @ Relay Link Plus Several @ Direct
Surface Science	Minimum Pkg.		Increased Pkg.	Minimum Pkg.			Increased Pkg.
Telecommunication	Relay Only	Relay and/or Direct		Relay Only		Relay and/or Direct	
Power Source	Batteries	Batteries Plus Solar Cells		Batteries		Batteries Plus Solar Cells	
Command Link	No	Yes		No		Yes	

Note: (1) When using relay link, the first read-out period occurs immediately after impact and subsequent periods are spaced 24.6 hours apart.

II

influenced their mission profile and sequence of events characteristics. For the Capsule atmospheric entry phase, the mission/design aspect which categorizes the Capsule's performance is the use or non-use of a radar altimeter. Table 2.3-4 lists the events during the atmospheric entry phase and illustrates the influence of the radar altimeter on the timing of events in the VM-8 and VM-9 atmosphere models.

The main effect of the type of entry mode (direct versus out-of-orbit) is that the Capsule system employing the out-of-orbit entry mode experiences lower entry velocities (15,300 fps vs 20,800 fps) and lower entry path angles ($13.5°$ to $20°$ vs $16°$ to $32°$) than the direct entry cases. This, of course, means that to achieve vehicle designs compatible with the same parachute subsystem capability, the direct entry vehicles (Point Designs 2, 4, and 6) must provide better upper-altitude deceleration characteristics, i.e., lower $W/C_D A$, than the out-of-orbit entry configurations (Point Designs 1, 3, and 5).

2.3.3.1 Without Radar Altimeter

If the Capsule design being considered does not utilize a radar altimeter (such as Point Designs 1 and 2), then the Capsule must depend upon 'g' measurements plus a base pressure reading to sense MN 2.0 (the parachute deployment velocity). Since the entry configuration ($W/C_D A$) is designed to achieve MN 2.0 at a low parachute deployment altitude (~ 6.7 km for the out-of-orbit reference mission) in the thinnest atmosphere, VM-8, the selected $W/C_D A$ will result in MN 2.0 being reached at a high altitude (~ 32.4 km) if the densest atmosphere, VM-9, is encountered. This differential in parachute deployment altitudes, with the subsequent difference is descent time, results in a very significant difference in total time for entry between VM-8 and VM-9 of 791 seconds for the out-of-orbit reference mission. This difference in Capsule entry time naturally affects the resultant Lander/Orbiter telecommunication relay link geometry as discussed in detail in Section 3.0 of this volume. A nominal entry profile must be employed whose resultant Lander/Orbiter geometry at Lander impact is such as to assure that whether the Capsule system encounters the thin VM-8 atmosphere (in which case the Orbiter will be somewhere near its ascending horizon with respect to the Lander's line of sight at impact) or the dense VM-9 atmosphere (in this case the Orbiter will be close to its descending horizon), the Lander will always have sufficient communication time to read out the necessary post-impact data before the Orbiter disappears from communication view.

As indicated in table 2.3-2, there are three main events which must be sensed and acted upon during the atmospheric entry phase (i.e., between entry at 244 km and impact). These events are the attainment of MN 5.0 (the point at which certain entry science measurements are initiated), of MN 2.0 (the point at which the parachute is deployed), and of an altitude ≈ 100 feet (the point at which the parachute is released and the Lander free falls to the surface). Study of a large number of entry trajectories for various combinations of $V_E - \gamma_E$ and VM- models has revealed that MN 5.0 always

TABLE 2.3-4. COMPARISON OF ENTRY TIMES WITH AND WITHOUT A RADAR ALTIMETER FOR THE VM-8 AND VM-9 MODEL ATMOSPHERES, AND FOR THE REFERENCE OUT-OF-ORBIT ENTRY AND DIRECT ENTRY MISSIONS

Event	VM-8 Without Radar Altimeter			VM-8 With Radar Altimeter			VM-9 Without Radar Altimeter			VM-9 With Radar Altimeter		
	Time	MN	Alt	Time	MN	Alt	Time	MN	Alt	Time	MN	Alt
Out-of-Orbit												
1. Start of Entry	0	29	244 km	0	29	244 km	0	17	244 km	0	17	244 km
2. Initiate Mass Spec., Water Vapor, and Base Temp. Sensors	255 sec	5	11.5 km	255 sec	5	11.5 km	217 sec	5	43 km	217 sec	5	43 km
3. Deploy Parachute	285 sec	2	6.7 km	288 sec	1.86	6.1 km	259 sec	2	32.1 km	394 sec	.6	6.1 km
4. Impact	460 sec	-	0	452.5 sec	-	0	1251 sec	-	0	630 sec	-	0
Direct Entry												
1. Start of Entry	0	39.5	244 km	0	39.5	244 km	0	23.3	244 km	0	23.3	244 km
2. Initiate Mass Spec., Water Vapor, and Base Temp. Sensors	107 sec	5	12.1 km	107 sec	5	12.1 km	97 sec	5	46.1 km	97 sec	5	46.1 km
3. Deploy Parachute	121 sec	2	9.2 km	142 sec	1	6.1 km	118 sec	2	38.7 km	325 sec	.38	6.1 km
4. Impact	351 sec	-	0	302 sec	-	0	1217 sec	-	0	566 sec	-	0

Entry Conditions

Parameter	Out-of-Orbit	Direct Entry
$M/C_D A$ (slugs/ft^2)	.445	.16
V_E (fps)	15,300	20,788
γ_E (deg.)	16	25

Difference between VM-8 and VM-9 Entry times:

	Without Radar Altimeter	With Radar Altimeter
Out-of-Orbit	791 sec	177.5 sec
Direct Entry	866 sec	264 sec

occurs approximately 30 seconds after peak 'g' has been reached. Thus, this event can be sensed by using a timer in combination with 'g' sensing. At MN 5.0, those entry science measurements which were not initiated at the start of entry at 244 km (namely, the base region temperature, the mass spectrometer and the water vapor detector) will be turned on.

MN 2.0 will be sensed, as previously noted, by means of 'g' sensing in combination with base pressure. At this signal, the parachute is deployed with subsequent separation of the parachute plus Lander from the aeroshell 10 seconds later. This 10 second delay is utilized to assure that the extraction of the Lander from the aeroshell occurs at a subsonic speed.

By the use of a trailing line and weight, the near-presence of the ground can be sensed and used as the signal for release of the parachute from the Lander at the desired altitude of about 100 feet above local marain. The Lander is then allowed to free fall to the surface while some technique, such as spilling the canopy by lengthening one of two risers, is employed to assure that the parachute does not fall on top of the Lander during the impact sequence. The methods being considered to avoid the possible draping of the parachute on the Lander are discussed more fully in Section 3.2, 'Parachute Deceleration', of Volume III.

During the atmospheric entry phase, the Capsule utilizes its relay link to transmit to the Orbiter at a bit rate of 1350 bps. The read out data consists of real-time data interleaved with data delayed by 70 seconds to account for the maximum anticipated blackout period. In addition, 100,000 bits of entry data will be stored and read out after the Lander has impacted - first, during the transmission period immediately after impact and then again at the end of the first day of surface operation.

2.3.3.2 With Radar Altimeter

As previously discussed, the Orbiter/Lander joint mission profile and relay link geometry are severely constrained by being required to cope with a large possible spread in entry time -- a spread which is primarily caused by the differences in parachute deployment altitude for the various VM-models when Mach number is used as the deployment signal. By using a radar altimeter and thereby always having the same deployment altitude (i.e., height above local marain), regardless of the atmosphere encountered by the Capsule, this possible disparity in entry times is considerably reduced (see table 2.3-4) and the Orbiter/Lander relay problem is significantly eased as discussed in Section 3.5 of this volume. This effect of the radar altimeter on the relay link operation is illustrated in table 2.3-5 for the out-of-orbit reference mission.

TABLE 2.3-5. SEQUENCE OF EVENTS FOR LANDED OPERATIONS

MEASUREMENT

ENTRY DATA — REAL TIME + 70 SEC DELAY — STORED

ENGRG. DIAGNOSTIC — REAL TIME + 70 SEC DELAY — REAL TIME & STORED DURING ENTRY

IMPACT DATA — (MEASURED & STORED) — STORED

SURFACE METEOR. DATA — REAL TIME

IMAGERY DATA — REAL TIME

[DATA RATE] — 1350 BPS — 160,000 BPS

IMPACT

SETTLING & BOOM DEPLOY. COMPLETED

−1400 −1200 −1000 −800 −600 −400 −200 0 200 400 600 800 1000 1200 1400

ENTRY TIME PRIOR TO IMPACT, SECS — LANDED TIME AFTER IMPACT, SECS

Δt = 460 SECS — Δt = 430 SECS — VM-8; NO ALTIMETER

Δt = 1251 SECS — Δt = 0 — VM-9; NO ALTIMETER

Δt = 452.5 SECS — Δt = 450 SECS — VM-8; WITH ALTIMETER

Δt = 630 SECS — Δt = 200 SECS — VM-9; WITH ALTIMETER

— ENTRY TIME

— ORBITER IS BETWEEN 45° RISE & SET

The radar altimeter under consideration utilizes a frequency of 1 GHz and has a peak power of 50 watts. With the radar altimeter in the Capsule system, the atmospheric entry sequence is conducted in the following manner. Mach number 5.0 is sensed as previously noted and is used as the signal to initiate the operation of the radar altimeter. In the VM-8 atmosphere, and for the out-of-orbit reference mission, this event will occur at 11.5 km (37,800 ft), while in the VM-9 atmosphere, it will occur at 43 km (141,000 ft). Parachute deployment will be initiated at 6.1 km (20,000 ft) upon a radar altimeter signal. It should be noted that the lowest minimum desired altitude for parachute deployment is determined from the requirement to decelerate to terminal velocity by 6000 ft. In order to satisfy that criteria, it is necessary to deploy the parachute at an altitude of at least 18,000 ft in the VM-7 model (critical atmosphere model for the subject deceleration requirement). Since the Capsule will not reach MN 2.0 until an altitude of 22,000 ft for the out-of-orbit reference mission case in the VM-8 atmosphere, a nominal deployment altitude of 20,000 ft would appear to be a good compromise.

The radar altimeter utilizes two antennas: an antenna on the aeroshell which is employed during entry until aeroshell separation and an antenna on the bottom of the Lander for use during parachute descent. Switch over from one antenna to the other occurs at aeroshell separation. At this event, the radar altimeter transmitter is shut down and the radar, using the Lander antenna, begins functioning again about 4 to 6 seconds after aeroshell separation. The altimeter's pulse length depends upon altitude and the altimeter is in the 'long range' mode until about 5000 ft, whereupon it changes to the 'short range' mode. At about 20,000 ft, in the 'long range' mode, the radar altimeter's accuracy is approximately ±175 ft, while below an altitude of 5000 ft, its accuracy will be about ±45 ft. At a nominal altitude of 150 ft ±45, the radar altimeter's mark is used as the signal for parachute release. It should be pointed out that the previously noted trailing line could be employed instead of utilizing the radar altimeter's signal (with its possible tolerances) for parachute release.

It should be noted that in addition to simplifying the Orbiter/Lander relay link situation and to serving as the sensing system for parachute deployment and release, the radar altimeter serves as a valuable adjunct to the entry science package by providing a direct measurement of altitude for correlation with the entry science measurements.

2.3.4 LANDER OPERATION ON PLANET SURFACE

The Lander's operation on the planet surface can be considered as being comprised of three phases. The first phase is that time period starting with impact of the Lander and ending with the completion of the initial required data transfer period from the Lander to the Orbiter via the relay link. It should be noted that in the case of the direct entry mode, the Orbiter is actually on a fly-by trajectory and it is not inserted into orbit until after this first phase of the Lander's ground operation is essentially

completed. During the initial part of this first phase, as during the atmospheric entry phase, the Lander will be transmitting to the Orbiter by means of the 400 MHz, 50 watt relay link at the relay link's low bit rate (1350 bps). This data transmission sequencing is shown in table 2.3-5.

Note that table 2.3-5 reflects the results derived in Section 3.2 and indicates the gains that can be realized in the landed-phase relay communication period, for the out-of-orbit reference mission, by the use of a radar altimeter during entry. To illustrate this possible gain, the duration of the time period which satisfies two criteria: (1) the Orbiter is between its 45° horizons with respect to the Lander, and (2) the Lander is in a position to transmit at its high data rate and perform its imagery mission (i.e., it has completely come to rest and deployed its cameras) is used as the basis of comparison. This time period when the Orbiter is between its 45° horizons represents a time when the relay link data quality should be exceptionally high. As shown in table 2.3-5, without the radar altimeter there was no '45° horizon time' available if the Lander had encountered a VM-9 atmosphere during entry whereas, with the radar altimeter, 200 seconds of '45° horizon time' was available for a VM-9 entry. It should be noted that in the case of the actual vehicle/mission implementation, sufficient communication time will be made available by the trajectory and deorbit techniques discussed in Section 3.3, Revised Reference Missions.

The first phase of landed operation starts with the Lander obtaining and storing the ground impact data; then, after coming to rest, it senses "up-direction", opens the hatch covers and deploys its camera and wind detector booms. (Note: It is estimated that it takes about two minutes for the Lander to come to rest and about 30 seconds for it to deploy its booms, thereby requiring approximately 2.5 minutes for the settling and boom deployment sequence.) Until this settling and boom deployment sequence is completed, the Lander continues to transmit to the Orbiter, at the low bit rate, the entry science and diagnostic data. When the Lander has come to rest, a timing sequence is initiated and 30 seconds later (in essence at the end of the boom deployment), the timer signals for the switchover from the low to the high data rate. (Note: for the out-of-orbit entry case, a nominal value for the high data rate is 160,000 bps; for the direct entry case it is 31,000 bps.) At this point, the Lander initiates its imaging mission, and the real-time imaging data plus real-time surface meteorological data plus the stored entry and impact data are now communicated repetitively to the Orbiter. Upon a timing signal, the Lander communication is terminated and the first phase of the Lander's ground operation ends.

The second phase of the Lander's operation begins after the initial Lander-to-Orbiter data transfer has been accomplished and covers that period during which the Orbiter is in a synchronous orbit and is supporting the Lander's communication requirements. This results, of course, in the relay link data read out periods being spaced 24.6 hours (one Mars day) apart. While the imaging will be accomplished whenever the Orbiter is at the proper location for relay link transmission, and thus

TABLE 2.3-6. REPRESENTATIVE LANDED OPERATIONS SEQUENCE
FOR FIRST DAY AFTER LANDING; OUT-OF-ORBIT
REFERENCE MISSION

Landed Operations - First Day	
Reference Mission: Out-of-Orbit Entry Entry Atmosphere: VM-8 Radar Altimeter: Utilized during Entry	
Event	Time
1. Impact force sensed and stored - Lander relay link on low data rate (Orbiter at 34° rise)	0
2. Lander comes to rest - clinometer reading stored - hatch covers ejected and booms deployed - data rate changed from low rate to high rate - imaging and surface meteorology initiated (Note: Orbiter at 45° rise at 110 sec.)	150 sec (2.5 min)
3. Orbiter at 45° set	600 sec (10.0 min)
4. Orbiter at 34° set	685 sec (11.4 min)
5. Orbiter at 10° set	1015 sec (16.9 min)
6. Wind, temperature, pressure, moisture readings and clinometer taken and store data - 3 times/hr.	
7. Read alpha-scatter soil sample (internal) and store data	60 min (1 hr)
8. Deploy alpha-scatter sensor to 'background' position, read 'background' and store data	180 min (3 hrs)
9. Deploy alpha-scatter sensor to surface	3.1 hrs
10. Read surface composition and store data	6 hrs
11. Repeat surface composition reading every 3 hours	9 hrs
12. Lander beacon receiver antenna signals that Orbiter is returning to range (Note: timing signal is also used and either beacon or timer may initiate transmission.)	24.5 hrs
13. Lander relay transmission begins - initiate imaging - readout stored data	24.6 hrs
14. Timing signal used to terminate transmission	Approx. 25 hrs

the imaging data is only transmitted in real time, it is planned to obtain surface meteorological plus surface composition measurements between the 24.6 hour-spaced data readout periods and to store the resulting data in a 180,000 bit capacity core storage. The surface composition measurements are only performed the first day, and then this experiment is shut down. During the first day, this core storage contains 100,000 bits of previously stored entry data. The storaged entry data is read out during the period immediately after impact and again at the end of the first day. After the second read out, the memory core is wiped of the entry data. Table 2.3-6 tabularizes these first-day, landed operations for an example case — the out-of-orbit reference mission based on the VM-8 atmosphere and the use of a radar altimeter during entry.

Table 2.3-3 summarizes some of the main design features and mission requirements of the point designs and indicates that for Point Designs 1 and 2, their entire landed mission is only one diurnal cycle long. For Point Designs 3 through 6, however, this second phase of the Lander's operations is conducted for three days. At the end of that time, the Orbiter goes asynchronous, in order to improve its own planet-mapping mission, and the Lander's ground operations now move into the third phase.

In the third phase of Lander operations, the Orbiter is not available as a relay station and the Lander now must utilize a direct link as its communication mode to Earth. The selected direct link system has a 20 watt transmitter operating at 2295 MHz and uses a vertically-oriented antenna deployed from the Lander.

If it is assumed that the communication ground station on Earth is one DSN station with a 210-ft diameter receiving dish, a daily transmission period of approximately 1.6 hours is available for the Lander design and reference mission under consideration. For the point designs studied herein, the transmission time utilized is less than 1.6 hours and is limited by the power capability provided by the Lander's solar array. As indicated in table 2.3-3, Point Designs 3 through 6 are designed to survive on the planet and function as 'weather stations' for 90 days or more. The surface meteorological data will be accumulated over a diurnal cycle and then read out during the daily transmission period at a data rate of 15 bps. Point Designs 3 and 4, which contain the 'basic' landed science package described in Section 4.2.3 of this volume, only require a read out time of 16 minutes.

In Point Designs 5 and 6, the Lander's science payloads have been increased (see Section 4.2.3) over those considered in Point Designs 1 to 4 and this additional surface science will be measured, in conjunction with the meteorological data, during the 90+ days that these subject Lander point designs survive on the surface of Mars.

The extended lifetime Point Designs 3 through 6 incorporate a command receiver which will provide direct link - access from Earth to the Lander's programmer, thus permitting changes to be made to the Lander's activities as deemed desirable. Based on an 85-ft diameter DSN antenna and a 100 KW transmitter (under development by JPL), a command rate of 0.5 bps will be obtained utilizing a 2115 MHz command link.

2.4 REFERENCES

2.1   "1969 NASA Authorization Hearings"

2.2   Mars Mission Objectives Langley Research Center Planning Document, dated 3 May 1968.

2.3   Mars Engineering Model Parameters for Mission and Design Studies, 1968 (Preliminary Draft), Langley Research Center, May 1968.

2.4   Explanatory Supplement to the American Ephemeric and Nautical Almanac.

2.5   Meeus, J.: Oppositions of Mars, 1960 to 1980. J. Brit. Astron. Association, Vol. 20, No. 3, March, 1960.

2.6   Michaux, C. M.: Handbook of the Physical Properties of Mars. NASA SP-3030, 1967.

2.7   American Ephemeris and Nautical Almanac, 1968.

2.8   Mars Scientific Model. JPL Document 606-1, 1968.

2.9   Dollfus, A.; Optical Diameter and Ellipticity of the Globe of Mars; In Mantles of the Earth and the Terrestial Planets; Ed. by S. K. Runcorn. Interscience Publisher, New York, 1967.

2.10   JPL Development Ephemeris Number 19. JPL Technical Report 32-1181. Nov. 15, 1967.

2.11   Ash, M. E.; Shapiro, I. I.; and Smith, W. B.: Astronomical Constants and Planetary Ephemerides Deduced from Radar and Optical Observations. Astronautical Journal, Vol. 72, No. 3, April, 1967.

2.12   Transactions International Astronomical Union, Vol. XIIA, Reports on Astronomy, 1964. Academic Press, New York, 1965.

2.13   Kozai, Y.: The Earth Gravitational Potential Derived from Satellite Motion. Space Science Reviews 5, pp. 818-879, 1966.

2.14   Wilkins, G. A.: The Determination of the mass and Oblateness of Mars. In Mantles of the Earth and the Terrestial Planets; Ed. by S. K. Runcorn. Interscience Publishers, New York, 1967.

2.15   1973 Voyager Capsule Systems Constraints and Requirements Document, Revision 1. JPL Document 606-4, dated 18 May 1967.

2.16   1973 Voyager Capsule Systems Constraints and Requirements Document. JPL Document, dated 1 Jan. 1967.

2.17   Titan IIIC Payload Users Guide. Martin-Marietta Corp. Report IR 68-3, dated Jan, 1968.

3. MISSION ANALYSIS

3. MISSION ANALYSIS

Reference missions for out-of-orbit entry and for direct entry are defined in Section 3.1 and their resultant downrange dispersions in Section 3.2 The definition of a reference mission depends on two steps. First, launch and arrival dates are selected such that the arrival configuration will satisfy the requirements on orbit inclination, landing latitude and sun angle. In the case of the direct entry mission the entry path angle is an additional constraint to be considered, because of its direct relation to the central angle between approach asymptote and landing site. Second, a separation maneuver (or deorbit in the out-of-orbit entry case, deflection in the direct entry case) is defined which results in achieving the desired entry path angle and in satisfying certain relay communication requirements. These relay communication requirements and their effect on the definition of separation maneuvers are the subject of Section 3.3, but in the first definition of reference missions the requirement used is; the Lander must see the Orbiter above a $34°$ elevation at the time of landing, after entry through any of the VM atmospheres. With the parachute deployed at Mach 2 (regardless of atmosphere), it is shown that this requirement cannot be completely satisfied in the out-of-orbit entry mission. This was the major reason for introducing the concept of deploying the parachute at a fixed altitude, using an altimeter. Thereby, the difference in entry times between the VM-8 and VM-9 is reduced considerably so that the landing may be seen in all cases and some post-landing communication time is obtained. Both missions defined in Section 3.1 employ Type I transfer trajectories. For the direct entry mission the required geometric conditions at arrival cannot all be met with a Type I trajectory; the inclination constraint (high inclination orbit) is therefore freed, and the inclination comes out as approximately equal to the latitude of the landing site. It is shown in Section 3.5 that by using Type II transits, the geometric conditions can all be met approximately in the sense that, for the $20° N$ landing latitude, high inclination orbits are possible.

Entry trajectories with parachute deployment at a fixed altitude are introduced in Section 3.2. This section discusses the path angle and downrange dispersions which may be expected in the out-of-orbit entry and direct entry missions. The effects of dispersions on the post-landing relay communication are displayed in diagrams which offer a convenient means of considering how the trajectory should be changed to meet different relay communication requirements.

The selection of the relay communication requirement is the subject of Section 3.3. It is shown that the maximum number of bits may be transmitted in a pass which is designed to have a half cone angle of about $45°$, measured from zenith at the Lander. Adopting such a criterion would result in designing the separation maneuver such that the Lander will see the Orbiter not higher than at a $45°$ elevation (rising), some 150 seconds after landing (assuming that 150 seconds are needed to settle and deploy equipment). Results are also shown for still a different criterion, namely that of obtaining the maximun possible communication time after landing. With this requirement satisfied it would be impossible to observe the landing event, and some of the final portion of the entry trajectory would also be missed.

Since in the direct entry mission the orbital relay communication must take place with an orbit which has not yet been trimmed, it is important to consider the effect of orbit period errors. This is done in Section 3.4. It is seen that in the presently defined direct entry mission (with low inclination orbit), the relay communication is not entirely lost with period errors of several hours, although the communication range may increase considerably. In high inclination orbits, any orbit period error would soon move the Lander site so far away from the orbital plane that there may be no communication at all.

The possibility of using Type II transfer trajectories is discussed in Section 3.5. Type II trajectories offer no particular advantage for the out-of-orbit entry mission. For the direct entry mission, on the other hand, Type II transfers are attractive in that high inclination orbits may be obtained with a 20° landing latitude, while satisfying the sun angle and entry path angle requirements.

In the study of direct to Earth communication for an extended lifetime mission, the position of the Earth with respect to the landing site must be known. Section 3.6 presents data on the Sun and Earth declinations, and Sun and Earth visibility periods at different latitudes.

3.1 REFERENCE MISSIONS

This section presents the analysis employed and results obtained in defining the out-of-orbit entry and direct entry reference missions. It was not the intent of this study that these reference missions be optimum, but only that their mission characteristics and resultant entry conditions be sufficiently representative of the 1973 Mars mission that these subject reference missions could serve as nominals in the design of the Capsule subsystems.

3.1.1 OUT-OF-ORBIT ENTRY REFERENCE MISSION

This section discusses the derivation of the out-of-orbit entry reference mission. Basic mission requirements which were agreed on with NASA/LRC early in the study are used paras 3.1.1.1 and 3.1.1.2 to define the arrival and deorbit configurations. Para 3.1.1.3 gives a summary of the reference mission as it is defined by combining the results of paras 3.1.1.1 and 3.1.1.2.

Para 3.1.1.4 presents six parameters related to communication and power subsystems as functions of time during the first orbit after landing. Three different trajactory times from entry to impact (400; 700; 1000 seconds) are considered.

Entry trajectory data and communication parameters during entry are presented in para 3.1.1.5 for four atmospheres (VM-3, -7, -8 and -9).

3.1.1.1 Launch and Arrival Dates, Launch Energy and Arrival Configuration

The transfer trajectory is selected to satisfy the following requirements:

1. Orbit inclination: 60 degrees

2. Landing latitudes: 10 and 20° N latitude

3. Surface imagery: 30 degrees from evening terminator

With the requirement that the imagery data is to be transmitted to the Orbiter in real time, the requirement "surface imagery: 30° from evening terminator" is equivalent to: landing 30° from evening terminator.

Combinations of launch and arrival dates for which these requirements are fulfilled are shown on the basic mission planning chart, fig. 3.1-1 (this figure was obtained from NASA/LRC during discussions at the beginning of the study). The orbit insertion impulses indicated in fig. 3.1-1 are according to the apsidal rotations which are required for a landing true anomaly of minus 5°. As shown in para 3.1.1.3, the landing true anomaly of the reference mission defined here is minus 14.4°; the corresponding apsidal rotation and orbit insertion velocities are shown in table 3.1-2. The two lines marked "g = 60°" mark the missions for landing latitude 10° (upper line) and for landing latitude 20° (lower line) where the sun angle is 60° (this is the complement of the angle at which the Sun is seen over the horizon at the landing point). It is seen that a
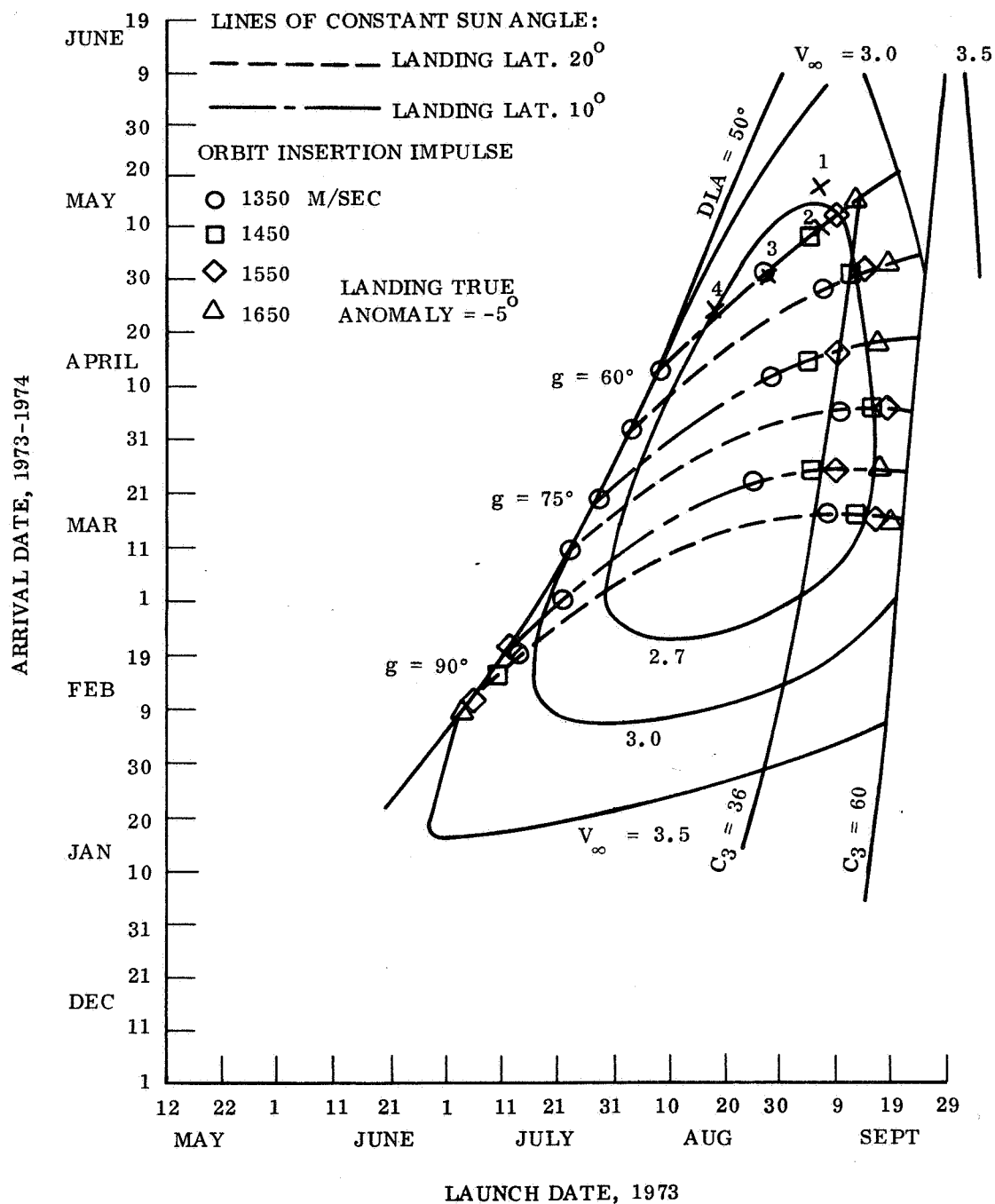
Figure 3.1-1. Basic Mission Planning Chart, Mars '73 Out-of-Orbit Reference
Mission

30 day launch window is easily available between the constraints of DLA < 50° and C_3 < 40 km^2/sec^2. The points marked 1, 2, 3 and 4 were investigated in some detail and point 3 was chosen to be the basis for the out-of-orbit reference mission. Table 3.1-1 lists several pertinent parameters for these four mission points. The nomenclature is defined in detail in para 3.1.1.6.

The arrival configuration for the reference mission (i.e., point 3 in fig. 3.1-1) is illustrated in figs. 3.1-2 and 3.1-3. The directions of Sun, Earth, Canopus, North Pole and aimpoint are shown as projected on the RT plane in fig. 3.1-2. The terminator and equator are also indicated. Fig. 3.1-3 shows the same configuration as projected in the Mars equatorial plane. The landing points at 10° and 20° north latitude are also marked.

3.1.1.2 Deorbit Analysis

The positions of Earth, Sun and the orbital plane with respect to the landing site at the time of landing have now been defined. For the Lander trajectory and the Lander-Orbiter geometry to be defined completely, the orbit periapse position must be defined in relation to the landing point, and a deorbit maneuver must be determined by which the Lander departs from the orbit. The orbit maneuver is defined in this section, in accordance with certain requirements on the relative positions of the Lander and Orbiter during entry; it will be seen that the position of the orbit periapse is then known in relation to the landing site, so that, if a specified landing site is to be reached, the position of the orbit in inertial space is also known. The requirement on the relative Lander-Orbiter geometry during entry is related to the relay communication; various requirements could be stated, the most desirable requirement not being known a priori (for any requirement to be useful for defining a mission, there must be a way in which it can be satisfied). However, in order to be specific, the requirement used here is: there must be relay communication throughout the entry phase, including the landing event, in order to achieve greatest likelihood that all the entry data and the landing signal are transmitted. The success of meeting this condition is highly dependent on the atmosphere, since the Orbiter continues in its path while the Lander takes an unknown amount of time for ascent. It is shown in what follows that this requirement can only be nearly satisfied when the parachute is deployed at Mach 2. Therefore, the effects of stating the relay communication requirement differently, in combination with a later parachute deployment, (i.e., at a specific altitude, using an altimeter) are discussed in Section 3.3.

The deorbit maneuver must be defined according to the following mission requirements:

1. Synchronous orbit

2. Orbit periapse altitude = 1000 km

3. Entry path angle = 16°

4. Lander trajectory coplanar with the orbit.

TABLE 3.1-1. ARRIVAL CONFIGURATIONS - OUT-OF-ORBIT ENTRY REFERENCE MISSION

		1	2	3	4
	Launch Date	9-8-73	9-8-73	8-29-73	8-19-73
	Arrival Date	5-18-74	5-10-74	4-30-74	4-24-74
	C_3 (km^2/sec^2)	32.191	32.269	25.477	22.760
	V_∞ (km/sec.)	2.740	2.659	2.594	2.76?
	T_F (days)	252	244	244	248
	R_C (km x 10^6)	316.151	302.863	294.682	276.079
RST Coordinate System	ZAP	65.68	68.56	75.45	80.29
	ETS	- 10.10	- 7.77	- 6.65	- 5.74
	ZAE	91.05	95.46	102.05	104.75
	ETE	2.10	4.03	9.06	14.60
	ZAC	64.51	66.10	58.93	49.99
	ETC	105.71	105.51	106.52	108.45
	ZPA	91.64	90.01	97.13	106.13
	EPA	- 80.49	- 80.52	- 79.50	- 78.31
Equatorial Coordinate System	RAS	46.43	42.90	38.51	35.90
	DES	17.10	16.02	14.59	13.69
	RAE	19.49	15.07	9.62	6.39
	DEE	7.44	5.43	2.88	1.34
	RAC	123.88	123.88	123.88	123.88
	DEC	- 65.41	- 65.41	- 65.41	- 65.41
	RAA	110.33	110.55	111.41	111.35
	DEA	- 1.64	- 0.01	- 7.13	- 16.13
	ETT	- 50.46	- 50.52	- 49.24	- 46.95
	OMEGA	126.33	125.47	134.54	142.83
	RA for 10°N. Lat.	56.60	57.46	48.29	40.10
	RA for 20°N. Lat.	44.91	45.77	36.60	28.41

For definition of symbols, see para 3.1.1.6.

LAUNCH: AUG 29, 1973
ENCOUNTER: APRIL 30, 1974
LAUNCH ENERGY: $C_3 = 25.477 \ KM^2/SEC^2$

APPROACH VELOCITY: $V_\infty = 2.594 \ KM/SEC$
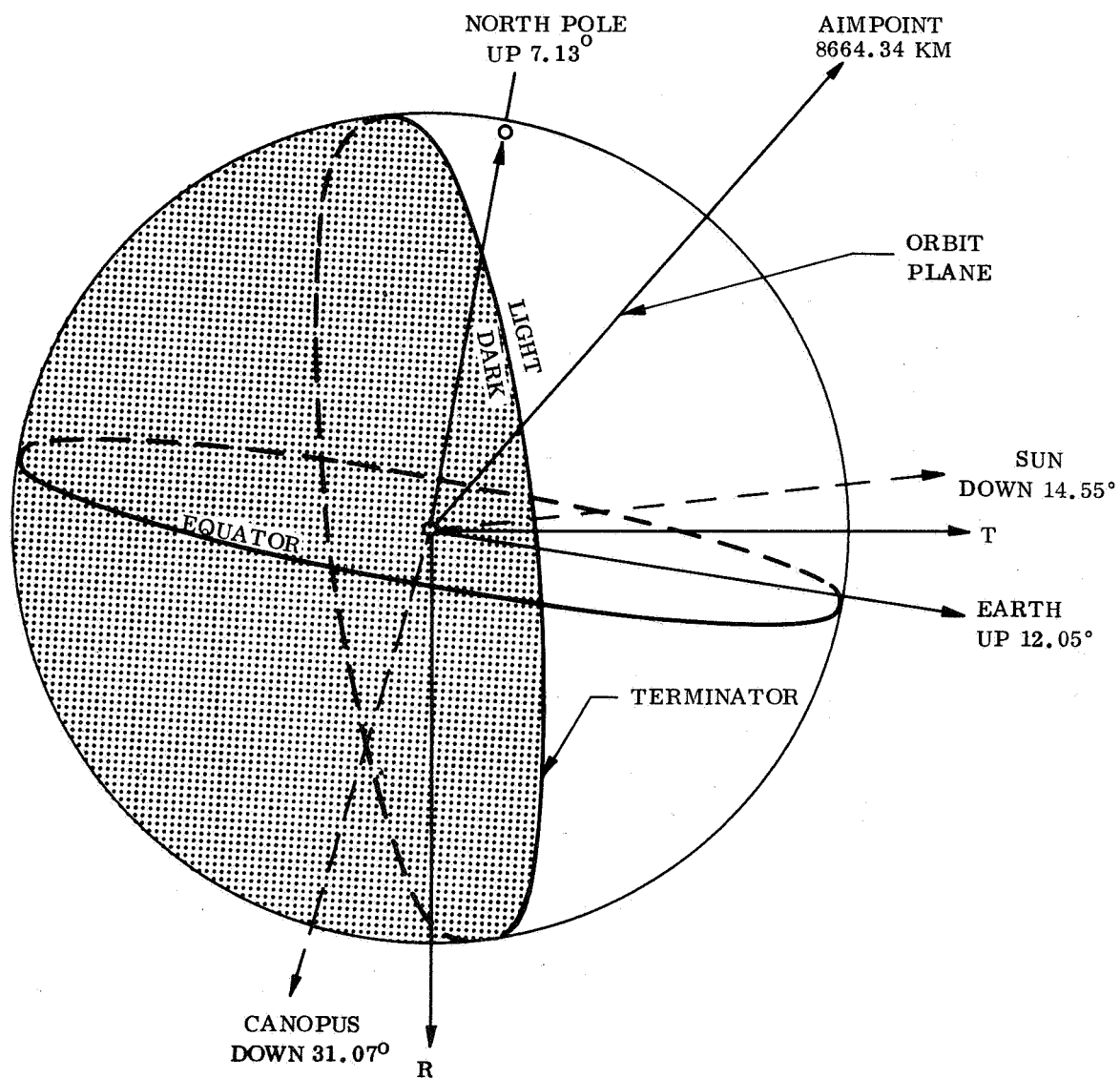
Figure 3.1-2. Arrival Configuration (Mars Impact Parameter Plane) Out-of-
Orbit Reference Mission

ARRIVAL CONFIGURATION (MARS EQUATORIAL PLANE)

LAUNCH: AUG. 29, 1973
ENCOUNTER: APRIL 30, 1974
LAUNCH ENERGY: $C_3 = 25.477$ KM^2/SEC
APPROACH VELOCITY: $V_\infty = 2.594$ KM/SEC

APPROACH DIRECTION
7.13° BELOW EQUATOR

LANDING 10° N. LATITUDE
LANDING 20° N. LATITUDE

CANOPUS 65.41° BELOW EQUATOR

SUN 14.59° ABOVE EQUATOR

EARTH 2.88° ABOVE EQUATOR

ORBIT

NORTH POLE

LIGHT
DARK

TERMINATOR

EQUATOR

EARTH AT HORIZON

LINE OF NODES
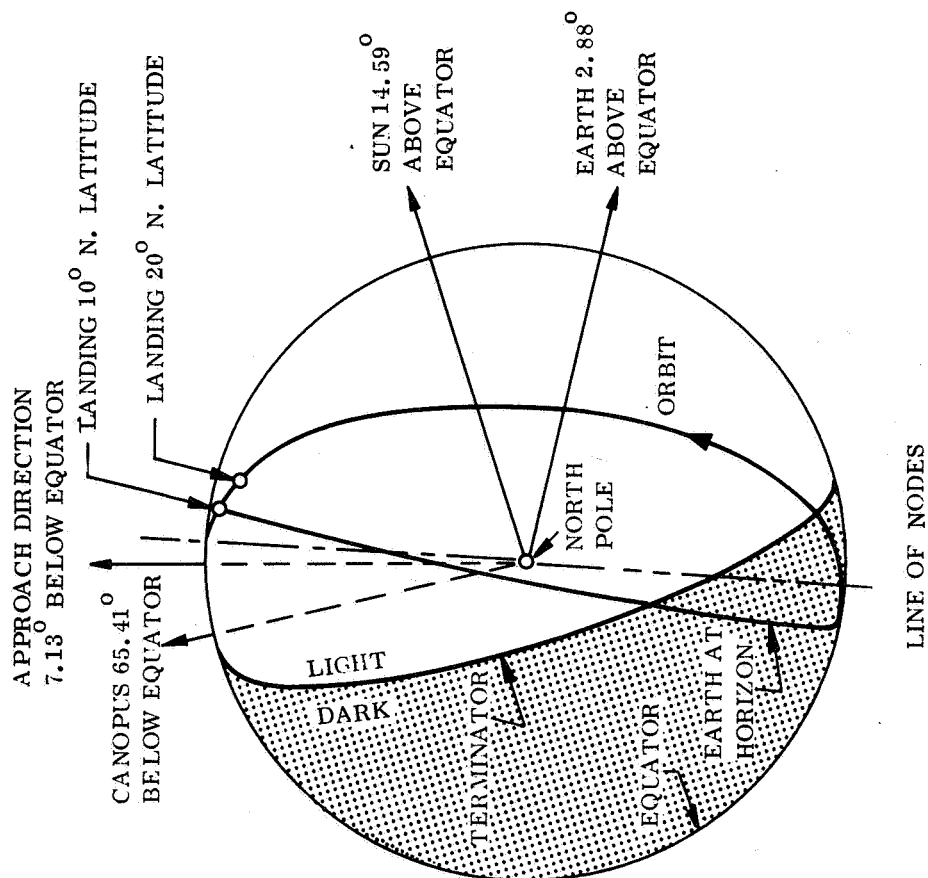
Figure 3.1-3. Arrival Configuration (Mars Equatorial Plane) Out-of-Orbit Reference Mission

Strictly speaking, only the first two of these are mission requirements. The entry path angle is fixed at 16°, because previous studies have shown that this value is reasonable in relation to the aeroshell design (which favors path angles as close as possible to the skip-out limit) and in relation to the trajectory dispersion (which favors larger path angles). In the subsequent analysis nothing is found to contradict fixing the entry path angle at this point in the mission analysis. The fourth of the above basic requirements is determined by the desire for obtaining the longest possible relay communication time. The coplanarity makes the determination of the Lander trajectory a planar problem, requiring four parameters for a complete trajectory definition. Two of these parameters are the given entry path angle and the radius from the planet center to the entry point, known by definition. Thus, only two more parameters need to be determined; this problem lends itself to a convenient presentation if the entry velocity and the deorbit true anomaly are chosen to be these two parameters.

Fig. 3.1-4 shows the geometry of the orbit, the Lander trajectory and the entry configuration. (This figure is approximately in scale for the deorbit configuration which results from this analysis.) With the orbit, and the entry radius and path angle known, the Lander trajectory is determined when the deorbit true anomaly (i.e., the angle F_{OD} in fig. 3.1-4) and the entry velocity are known; the deorbit velocity vector (magnitude and direction) follows simply from the difference between the Orbiter and Lander velocities at the deorbit point.

A criterion is now needed which will lead to a specific deorbit maneuver, or, equivalently to a specific set of values for the entry velocity and the deorbit true anomaly. This criterion may be sought in the relay communication between Orbiter and Lander. Specifically, the criterion to be used here is: there must be relay communication during the entire duration of atmospheric entry, including the landing event, for entry into any of the VM range of atmospheres.* As illustrated in fig. 3.1-4, this is a geometric problem of which the outcome is determined by: 1) the central angle, β_{EI}, between the points of entry and landing, and 2) the entry time T_{EI}, which determines the distance traveled by the Orbiter during entry.

The communication parameter which is critical for the requirement stated above is the angle at which the Lander sees the Orbiter above the horizon at the time of landing. This angle, E_I, is plotted in figs. 3.1-5 through 3.1-9, against the variables of this problem in their ranges of interest:

1. F_{OD}, deorbit true anomaly, 220 to 260°

2. V_E, entry velocity, 15,200 to 15,300 ft/sec

3. T_{EI}, entry time, 300 to 1200 seconds.

---

*Other requirements, also related to relay communication, are discussed in Section 3.3. The purpose here is 1) to show precisely how the reference trajectory was selected, and 2) to illustrate the principle of the method which was used, so that generalization and specialization follow easily.
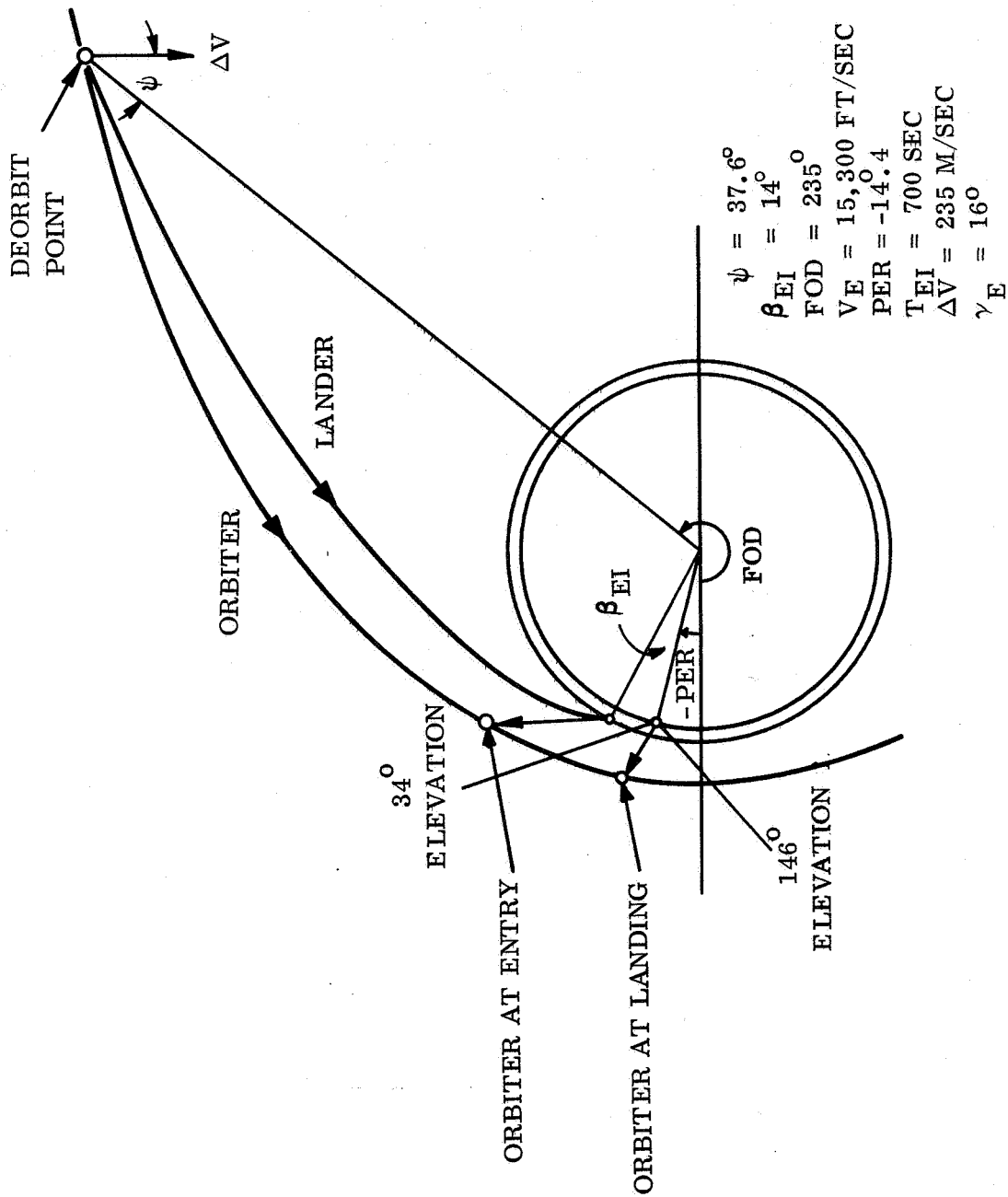
Figure 3.1-4. Deorbit Analysis Configuration

DEORBIT POINT

ΔV

ψ

LANDER

ORBITER

34° ELEVATION

146° ELEVATION

ORBITER AT ENTRY

ORBITER AT LANDING

β_{EI}

FOD

- PER

ψ = 37.6°
β_{EI} = 14°
FOD = 235°
V_E = 15,300 FT/SEC
PER = -14.4°
T_{EI} = 700 SEC
ΔV = 235 M/SEC
γ_E = 16°

The computations were performed with the following constants:

1. Entry path angle   = 16°

2. Mars radius   =   3386 km

3. Entry radius   =   3630 km

4. Gravitation constant   = $42829.5 \ km^3/sec^2$

5. Central angle from entry to landing = 14°.

The central angle, β_{EI}, from entry to landing should also be treated as a variable, since it depends on the atmosphere. However, for the purpose of this analysis, it was assumed to be constant. Actually, within the range of the VM atmospheres, this angle may have a range of about three degrees. The value of 14° is the average value of β_{EI}, corresponding to entry of a 60° sphere-cone with ballistic coefficient equal to $7.71 \ lb/ft^2$, with a parachute designed for 150 ft/sec terminal velocity in the VM-7 atmosphere and deployed at Mach 2. This ballistic coefficient was adopted in the early phase of this study; later, the ballistic coefficient was set at $14 \ lb/ft^2$. The central angles and times from entry to landing for both ballistic coefficients are listed in the following table, for the limiting atmospheres (VM-8 and VM-9).

	VM-8		VM-9	
	β_{EI} (deg)	T_{EI} (sec)	β_{EI} (deg)	T_{EI} (sec)
$7.71 \ lb/ft^2$, used in early phase of study and for definition of orbit maneuver	15.5	425	12.5	1160
$14.0 \ lb/ft^2$, finally adopted for reference purposes and used for computing entry trajectories	18.2	460	14.8	1251

Although the $7.71 \ lb/ft^2$ ballistic coefficient (resulting in $\beta = 14^\circ$) was used in the definition of the orbit manuever, the newer value ($14 \ lb/ft^2$, resulting in $\beta_{EI} = 16.5^\circ$, average) was used for the computation of the actual entry trajectories (see para 3.1.1.5). A deorbit maneuver was not specifically computed for the newer ballistic coefficient because it was found that 1) only a small readjustment would be required, which would not alter the entry trajectories and the communication parameters significantly, and 2) the relay communication requirement as stated above cannot quite be satisfied, so that different requirements need to be discussed; this is done in Section 3.3.

Using the information contained in figs. 3.1-5 to 3.1-9, the deorbit maneuver can now be determined by assigning a specific value to the elevation angle E_I, such that when the Orbiter is at a higher elevation, the Lander will certainly see it. This critical value of E_I was chosen to be 34°, corresponding to the maximum slopes that may be expected. It

must be noted that in figs. 3.1-5 to 3.1-9 the elevation angles range from 20 to 180°; although usually the maximum elevation is 90°; i.e., at zenith. This is done for the convience of plotting; angles smaller than 90° are directly elevation angles, specifically such that the Orbiter is behind the Lander (above the "backward" horizon), angles between 90 and 180° are the supplement of elevation angles, specifically for the situation in which the Orbiter is ahead of the Lander (above the "forward" horizon). Correspondingly, two lines are drawn in each of the figs. 3.1-5 to 3.1-9, at $E_I = 34°$ and $E_I = 146°$. In general, the lower line is seen to intersect the curves for the smaller T_{EI} values, indicating that (as expected) the Orbiter is seen above the backward horizon at time of landing after entry through the less dense atmosphere; similarly, the higher line intersects the curves for longer T_{EI} times, indicating that the Orbiter is seen above the forward horizon after entry through the denser atmospheres. The points of intersection of the 34° and 146° lines with the T_{EI} lines are plotted on a deorbit true anomaly -- entry velocity "map", in fig. 3.1-10. Each point on this map defines completely a specific deorbit maneuver and thereby a specific entry trajectory. It is now seen that a unique decision on the deorbit maneuver cannot be made: all the lines of constant entry time, T_{EI}, are nearly parallel. The point indicated at $V_E = 15,300$ ft/sec and $F_{OD} = 235°$ was chosen as the reference result; it accommodates entry times from about 350 secs (Orbiter rising at backward horizon) to 1050 secs (Orbiter setting at forward horizon). At this phase of the study the precise reasons for this choice were still somewhat vague, although the principle of the analysis method was understood. The reasons were mainly: 1) it was felt that an entry time still a little shorter than the 425 secs for the VM-8 atmosphere should be considered, in case a different parachute or deployment would be chosen; 2) since the entire range from 425 to 1160 secs could not be accommodated in any case, the longer entry times should be emphasized because of the small likelihood that the Mars atmosphere is really as dense as the VM-9 model; 3) if reasons 1) and 2) are accepted, several combinations of V_E and F_{OD} offer solutions, such as $V_E = 15,500$ $F_{OD} = 235°$ (point 1 in fig. 3.1-10), $V_E = 15,250$, $F_{OD} = 230°$ (point 2) or $V_E = 15,400$, $F_{OD} = 240°$ (point 3). (There are no deorbit conditions with V_E smaller than 15,195 ft/sec.) Although it was understood that a smaller entry velocity is advantageous for aeroshell design, the case was settled by choosing the first of these sets of values, with V_E about 100 ft/sec more than the minimum possible, in order to avoid being overly optimistic about the entry velocity. It was found later in the study that the entry path angle dispersion is smaller with smaller entry velocity and smaller deorbit true anomaly (this is mainly due to the fact that the required deorbit velocity is smaller); this would have lead, in the present case, to choosing a solution nearer to point 2 in fig. 3.1-10. This matter is discussed in Section 3.3 as part of a more rigorous application of the same analysis technique, applied to a different relay communication criterion.

For the definition of the reference mission, the chosen solution was $V_E = 15,300$ ft/sec, and $F_{OD} = 235°$. Hereby the entire Lander trajectory is known; in particular, the deorbit velocity is 234.8 m/sec (see fig. 3.1-11), directed at an angle of 37.6° with the deorbit location radius. Furthermore, it follows that the true anomaly of the landing point (the "PER angle") is -14.4°, based on the fixed average value of 14° for the central angle from entry to landing. The significance of the PER angle lies in that it locates the landing point with respect to the orbit periapse point; thus it enables the orbit to be located in inertial space, such that the landing point coincides with a desired location. The way in which this is done is to perform the orbit insertion such that an "apsidal rotation" is obtained. The apsidal rotation is the difference in the positions of the periapses of the approach hyperbola and the orbit.
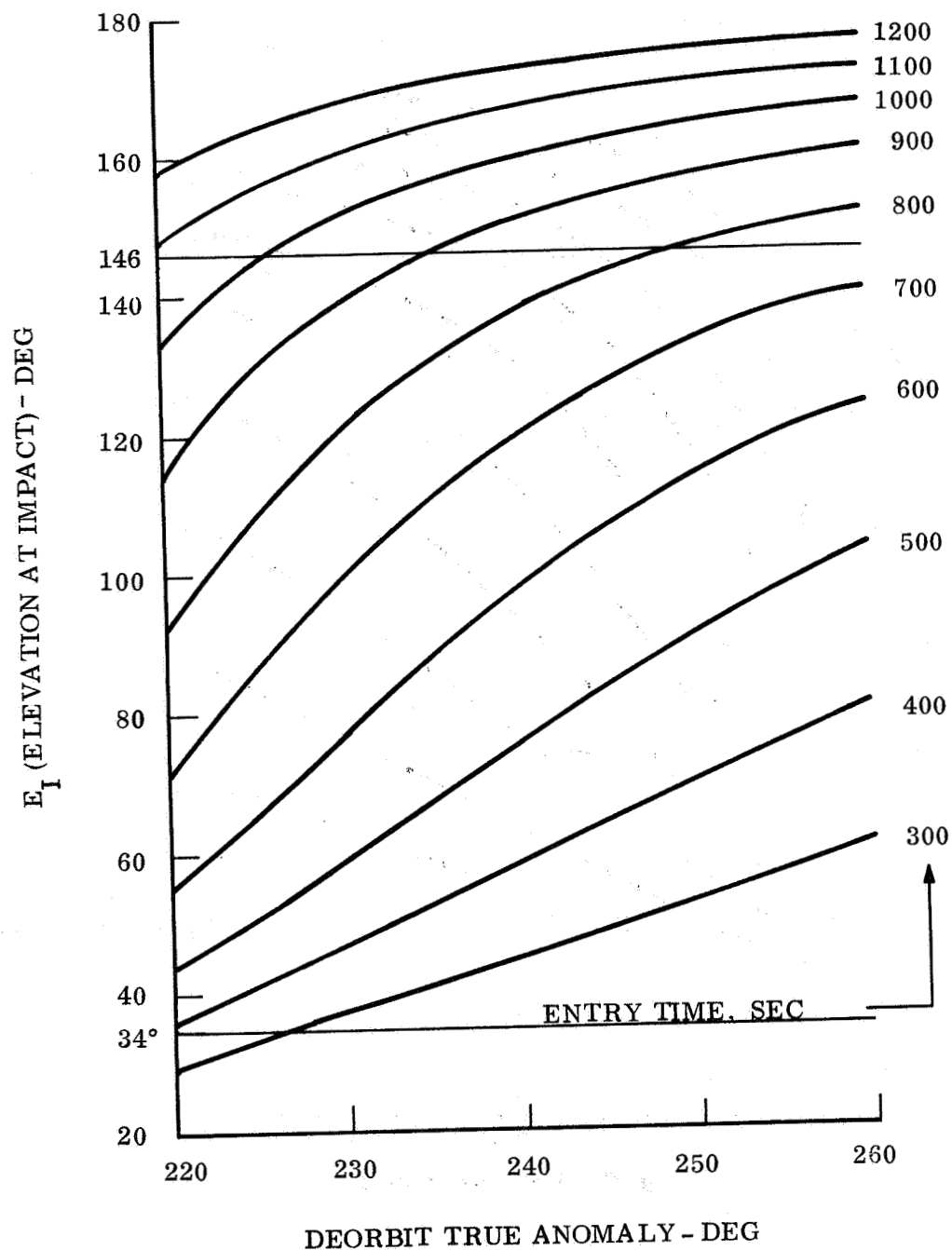
Figure 3.1-5. Deorbit Analysis (Synchronous Orbit),
$V_e = 15,200$ fps

$V_e = 15,250$ FPS

$\gamma_e = 16^o$

$\beta_{EI} = 14^o$
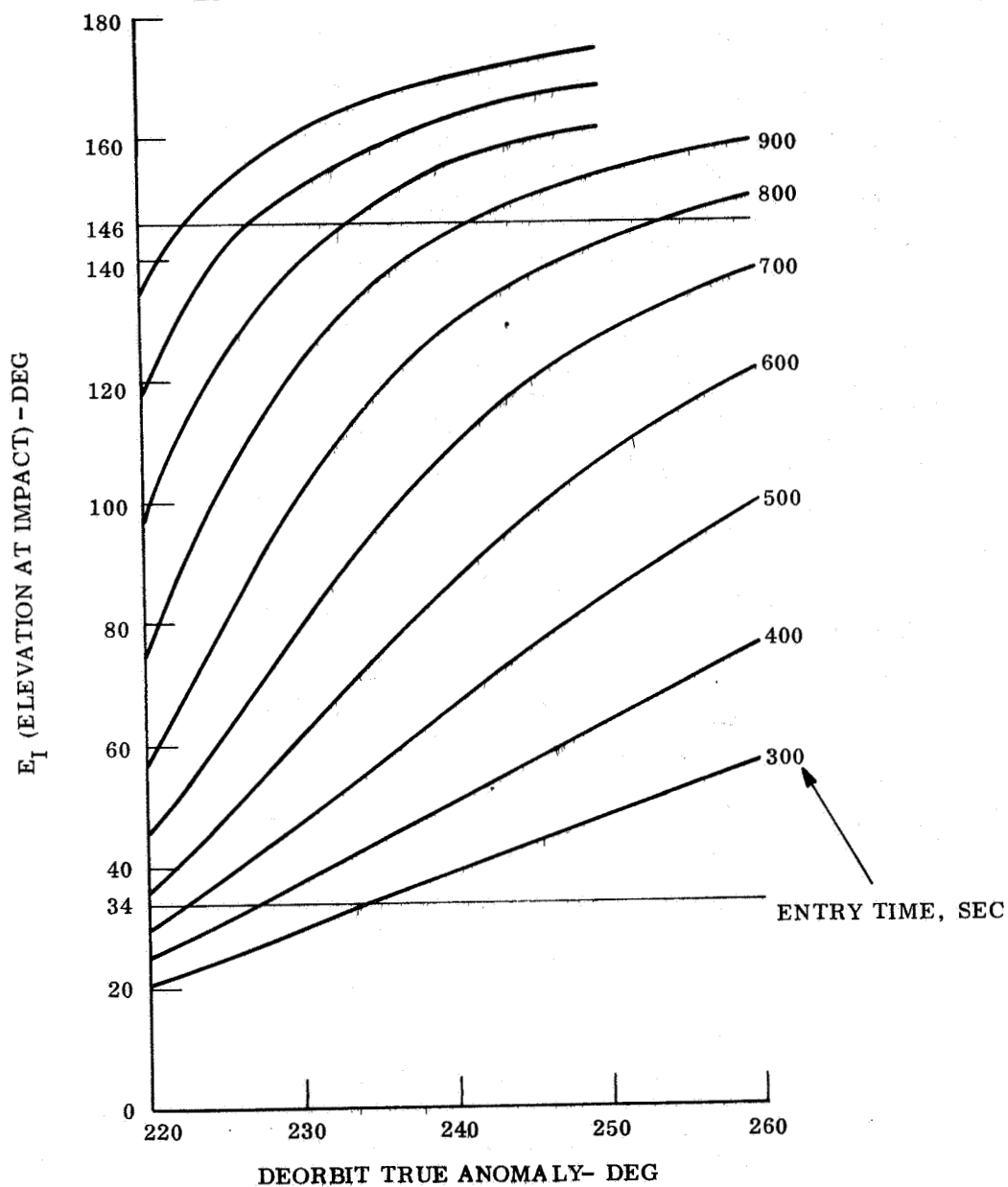
Figure 3.1-6. Deorbit Analysis (Synchronous Orbit),
$V_e = 15,250$ fps

$V_e = 15,300$ FPS

$\gamma_e = 16^\circ$

$\beta_{EI} = 14^\circ$
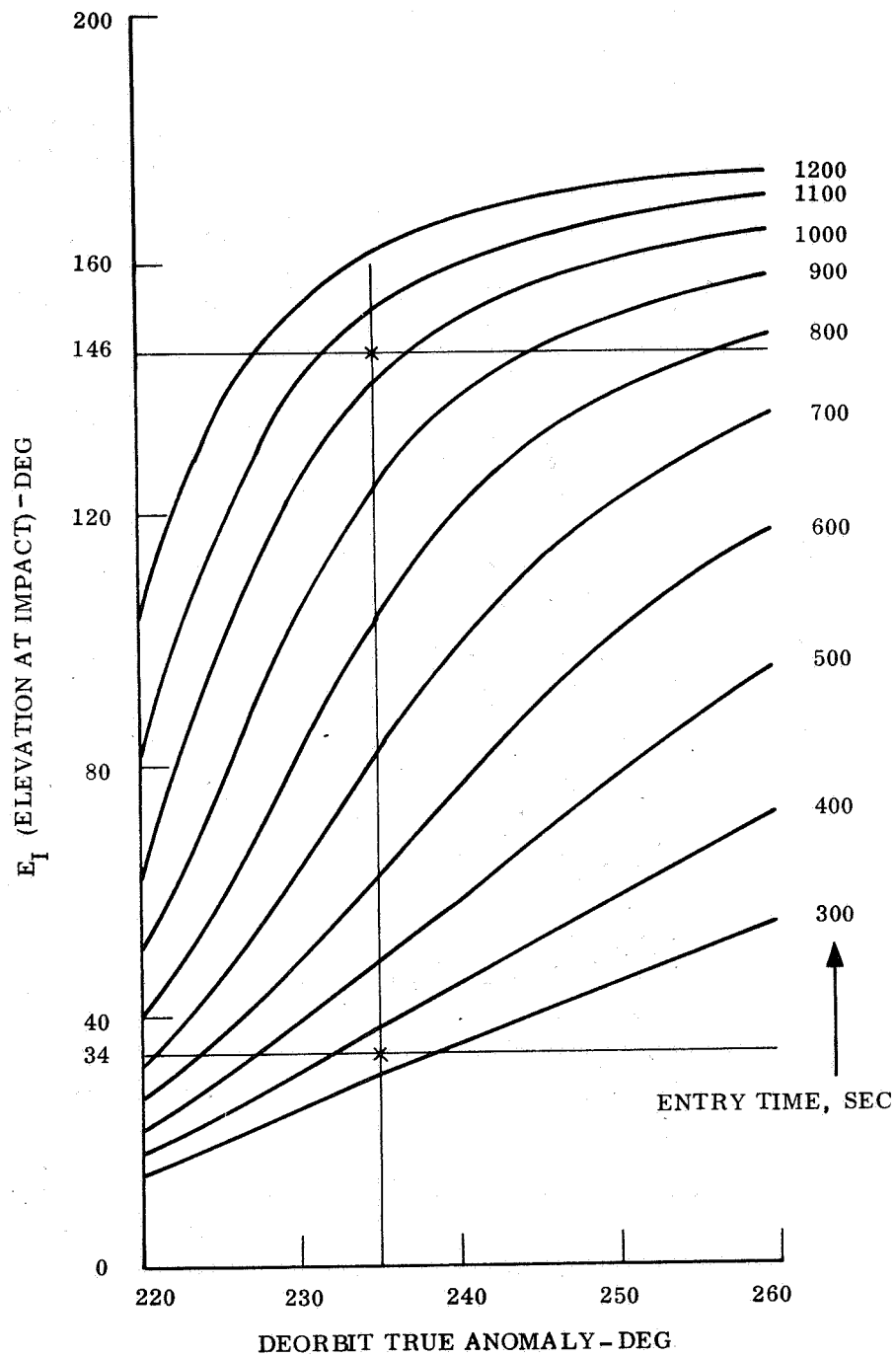
Figure 3.1-7. Deorbit Analysis (Synchronous Orbit),
$V_e = 15,300$ fps
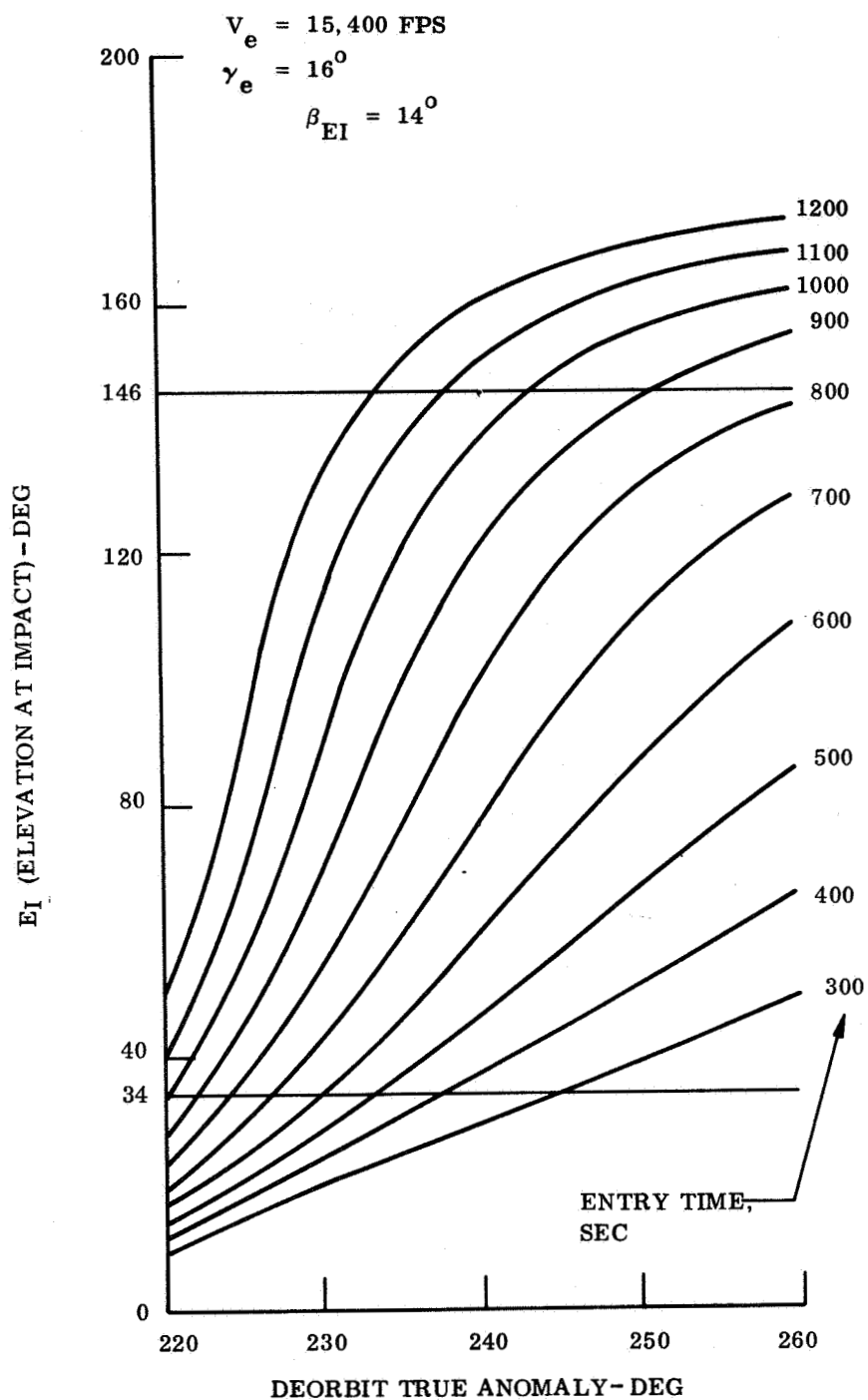
Figure 3.1-8. Deorbit Analysis (Synchronous Orbit), V_e = 15,400 fps
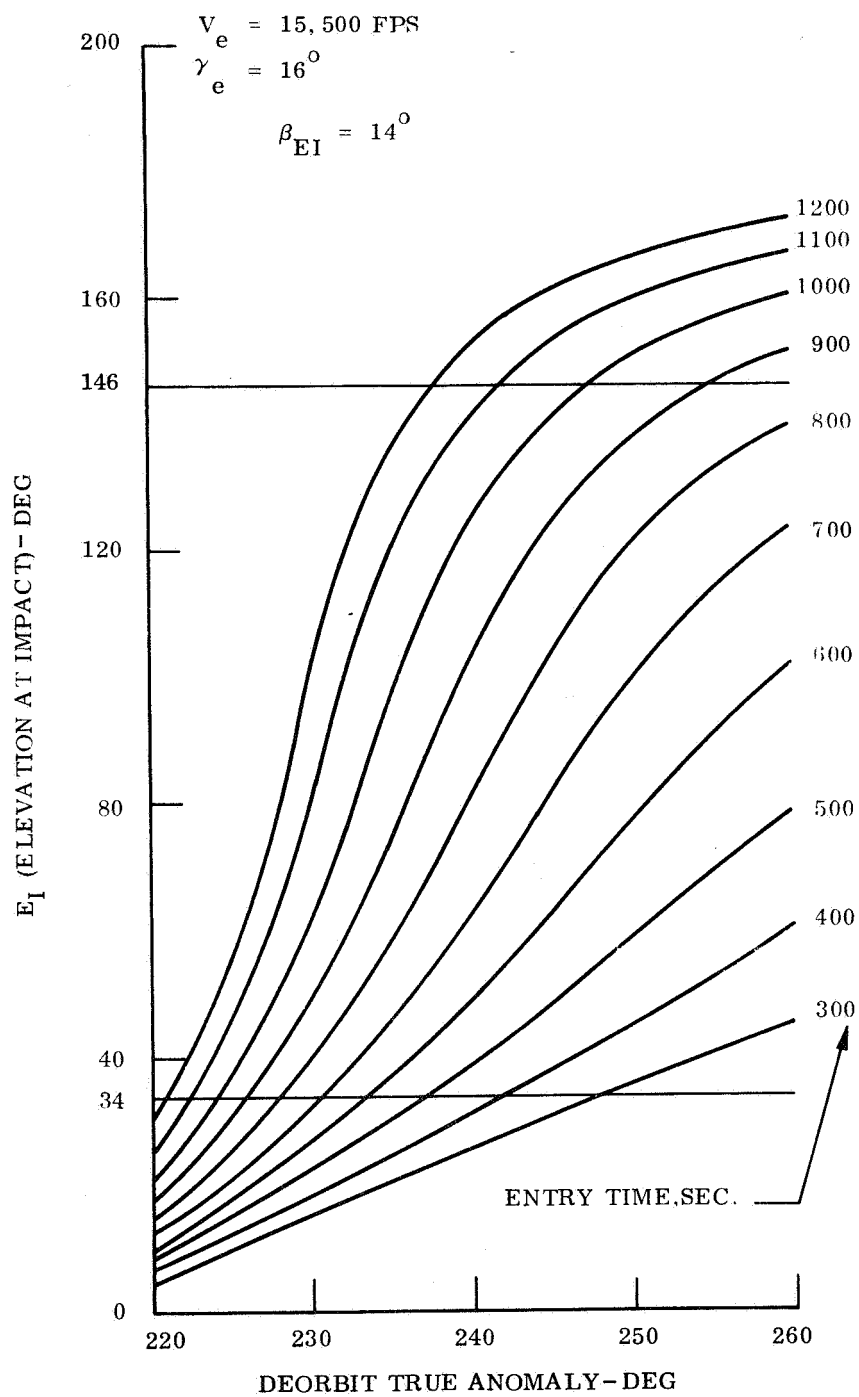
Figure 3.1-9. Deorbit Analysis (Synchronous Orbit),
V_e = 15,500 fps
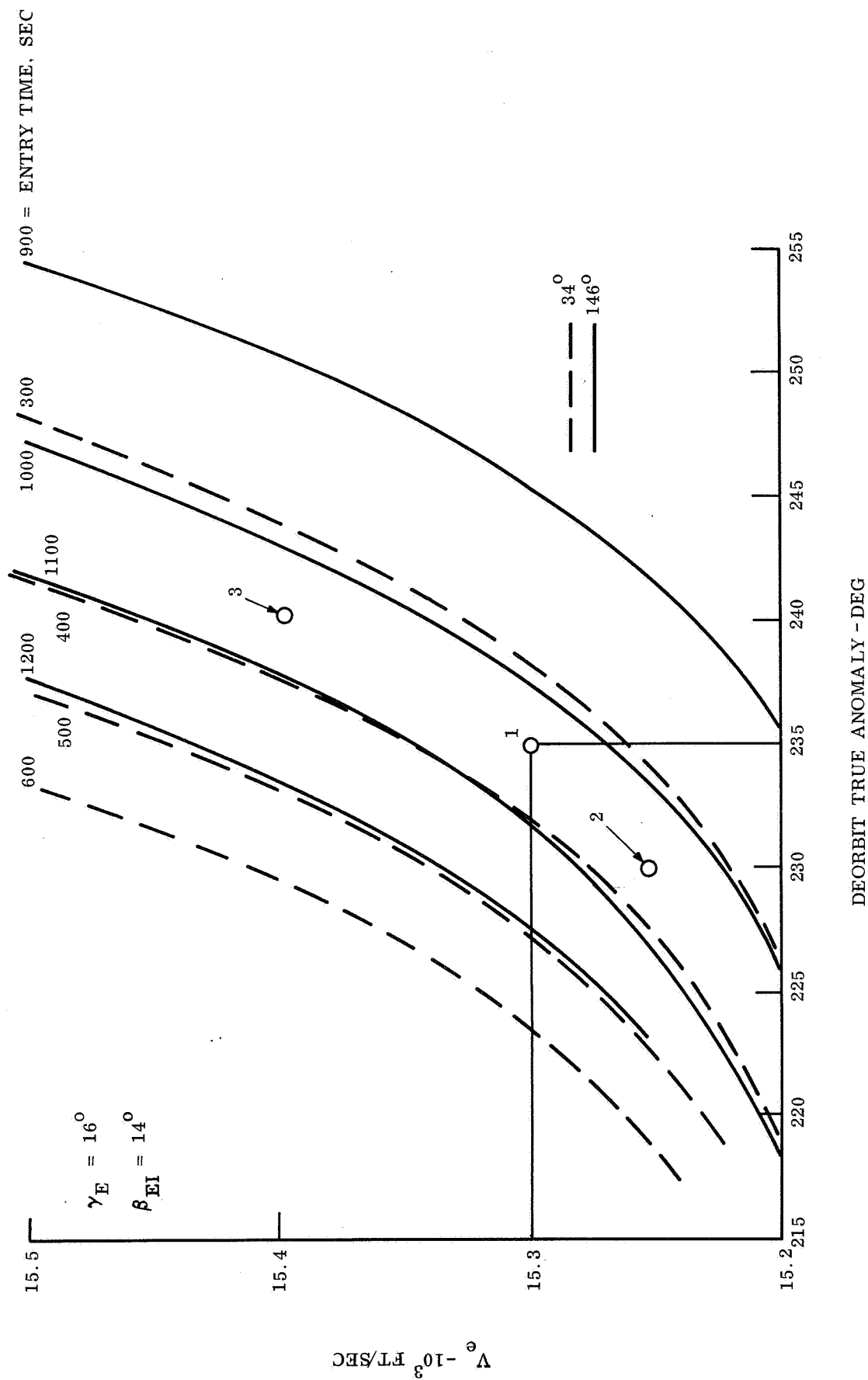
Figure 3.1-10. Deorbit Analysis (Synchronous Orbit)
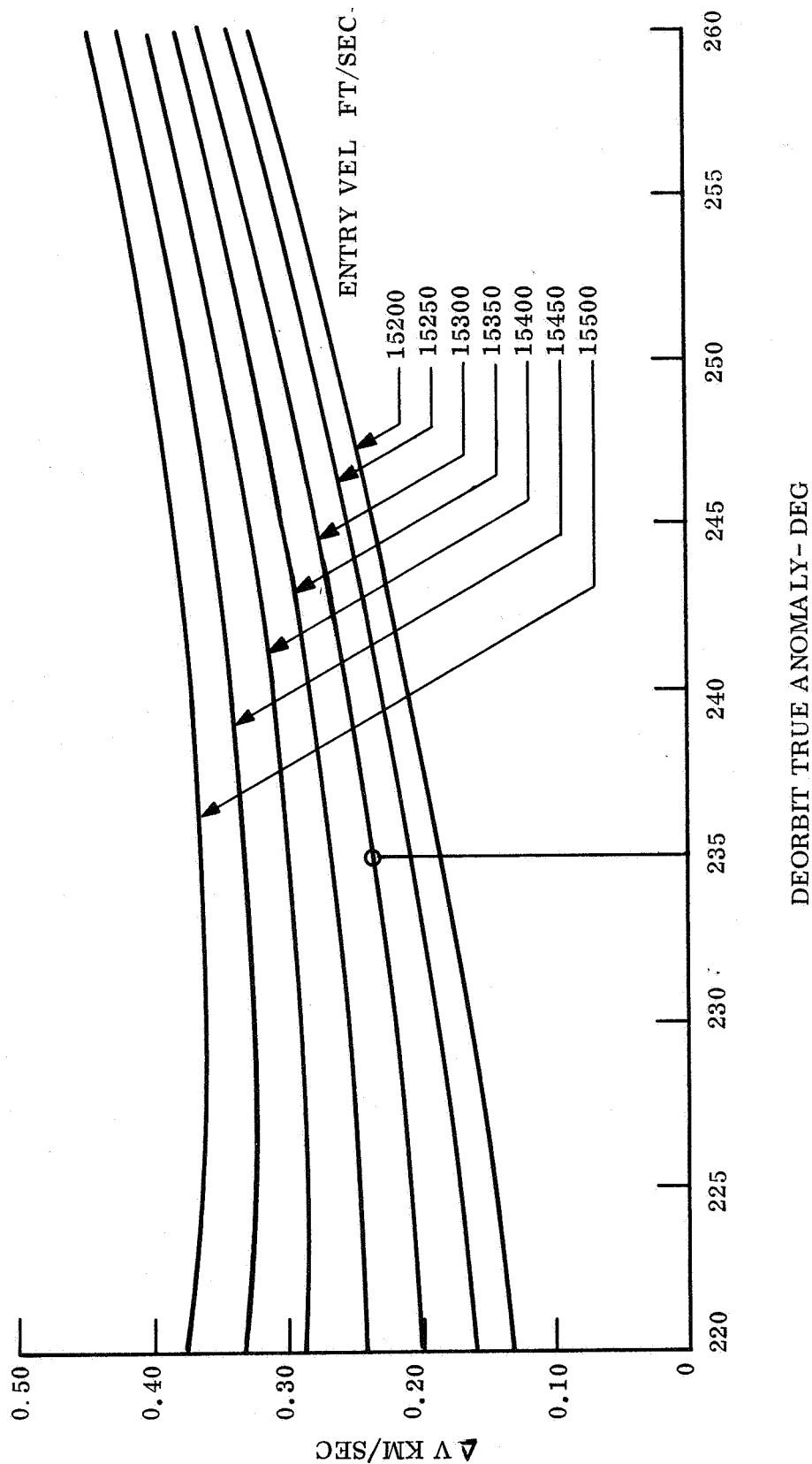
Figure 3.1-11. Deorbit Analysis (Synchronous Orbit)

3.1.1.3 Reference Mission Summary

With the transfer trajectory and arrival configuration determined at the beginning of the mission and the deorbit configuration determined at the end, there remains only an apsidal rotation to be found such that the required orbit can be fitted into the arrival configuration. Considering the positions of the line of nodes and the landing point in fig. 3.1-3, the required apsidal rotation follows from

$$RA = \pi - \sin^{-1} \left(\frac{\sin l}{\sin i} \right) - \omega - PER$$

where

RA = apsidal rotation, positive in orbit direction

l = landing latitude

i = orbit inclination

ω = angle from line of nodes (ascending node) to periapse of approach hyperbola, without apsidal rotation

PER = true anomaly of landing point.

It is here assumed that both landing points are obtained from the same approach. This approach is designed to satisfy the sun angle requirement of $g = 60°$ at the lower latitude landing. The sun angle will therefore be a little too small at the other landing point; to satisfy the sun angle at both landing points, two different approaches should be designed, but this was not deemed necessary since this study pertains to the Lander: the entry trajectory and communication parameters are not very sensitive to the precise value of 'g' when 'g' is at least approximately satisfied.

The required apsidal rotations are listed in table 3.1-2, which also lists the required orbit insertion velocity (ΔV), the true anomaly on the actual approach hyperbola where ΔV is applied (f_H), the true anomaly of ΔV application in the orbit of (f_E) and the periapse altitude of the actual apprach hyperbola (h). The numbers listed in table 3.1-2 are based on a minimum ΔV calculation.

TABLE 3.1-2. APSIDAL ROTATION FOR OUT-OF-ORBIT ENTRY REFERENCE MISSION

Landing Latitude	RA (deg)	f_H (deg)	f_E (deg)	h (km)	ΔV (m/sec)
10° N	48.3	-49	-105	4300	1480
20° N	36.6	-46	-88.4	2700	1290

RA: apsidal rotation
ΔV: orbit insertion velocity
h : periapse altitude of approach hyperbola

f_H : true anomaly of ΔV in hyperbola
f_E : true anomaly of ΔV in orbit
Synchronous orbit, 60° inclination
Approach: Case 3 of table 3.1-1

The reference mission which is obtained by combining the transfer trajectory (para 3.1.1.1) with the deorbit configuration (para 3.1.1.2), by means of the apsidal rotations listed here, is summarized in table 3.1-3.

3.1.1.4 Communication After Landing

In this section information is provided which is related to the design of Lander communication and power subsystems. The basis for computations is the deorbit condition specified in para 3.1.1.2. Since the Lander trajectory time from entry to landing is not a priori known, three sets of data are given, for entry times (T_{EI}) of 400, 700 and 1000 secs. However, in each of these cases the central angle from entry to landing has been held constant, equal to the 14° used in para 3.1.1.2. Therefore, the PER angle is also the same in all cases (-14.4°).

Curves are given for six parameters as functions of time during the first orbit after landing. The six parameters are:

1. EIS   =   elevation of Sun at the landing site

2. EIB   =   elevation of Orbiter at the landing site

3. EIE   =   elevation of Earth at the landing site

4. R   =   relay communication range

5. COA   =   cone angle of Lander at Orbiter

6. CLA   =   clock angle of Lander at Orbiter

The definition of the variables EIS, EIB, EIE and R is illustrated in fig. 3.1-12. The variables COA and CLA are defined in fig. 3.1-13.

The graphs are arranged as listed in table 3.1-4.

According to the "guidelines and Constraints", it is expected that the orbit is established with a period so close to being synchronous with the daily rotation of Mars, that the information presented here may safely be applied to any of the orbits during the first several days after landing. Eventually, the combined effects of residual period error and oblateness perturbation will change the relay communication. (The rates at which this happens are approximately: 0.04° per day due to the residual period error, 0.4° per day due to periapse motion, 0.2° per day due to motion of line of modes, and 0.5° per day due to motion of Sun and Earth.) The time zero in all plots corresponds to the time of landing, or an integral number of Martian days after that time.

TABLE 3.1-3. SUMMARY OF OUT-OF-ORBIT ENTRY REFERENCE MISSION

launch date	8-29-73	
arrival date	4-30-74	
flight time (days)	244	
launch energy (km^2/sec^2)	25.48	
communication distance (km)	294,700,000	
approach velocity (km/sec)	2.594	
ZAP angle (deg)	75.45	
approach	posigrade, Northern	
orbit inclination (deg)	60	
synchronous orbit (km)	1000 x 33,084	
Landing Latitude:	$10°N$	$20°N$
apsidal rotation (deg)	48.3	36.6
orbit insertion velocity (km/sec)	1480	1290
sun angle (deg)	61.5	54.1
angle, landing to terminator (deg)	27.1	33.4
deorbit true anomaly (deg)	235	
deorbit velocity increment (m/sec)	234.8	
landing true anomaly (deg)	-14.4	
entry path angle (deg)	16	
entry velocity (ft/sec)	15,300	
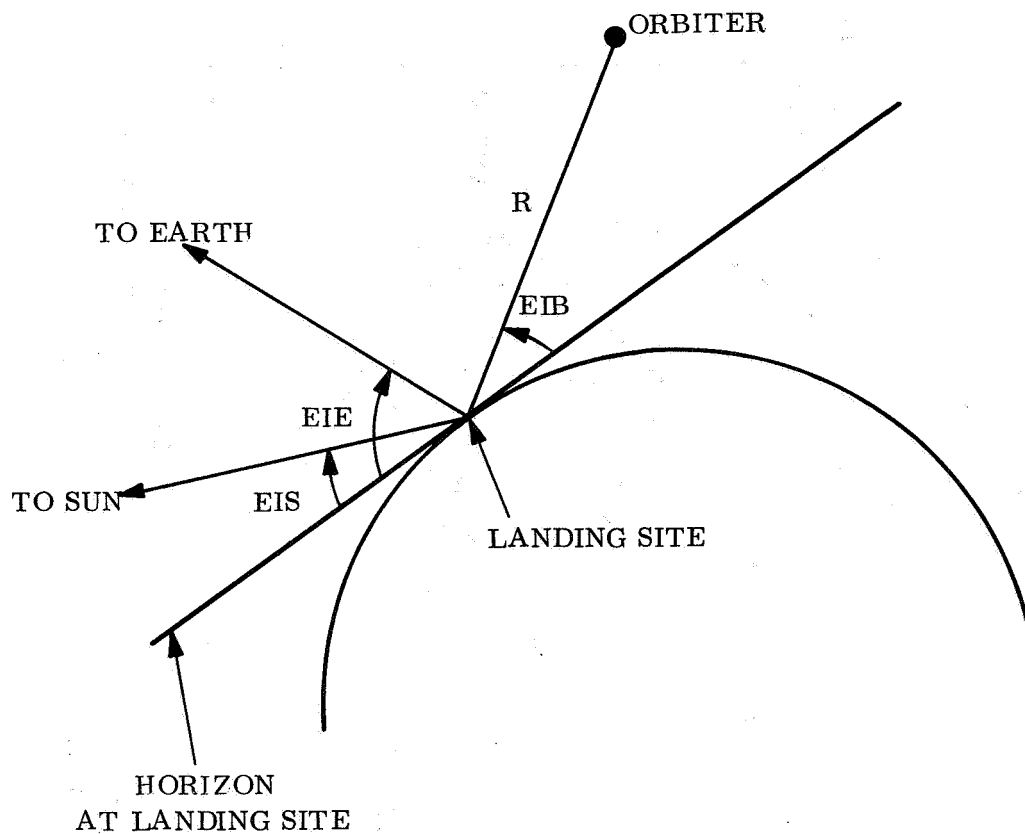
EIS = Elevation of Sun at Landing Site

EIE = Elevation of Earth at Landing Site

EIB = Elevation of Orbiter at Landing Site

R = Relay Communication Range

("Elevation = Angle at which Lander sees object above the horizon.)

Figure 3.1-12. Definition of Communication Parameters
After Landing

S

TO SUN

B
(LANDER)

CLA

O

D

COA

A

(ORBITER)

C

TO CANOPUS

PLANE THROUGH AS,
CONTAINING CANOPUS

PLANE THROUGH B,
PERPENDICULAR TO AS

COA, CONE ANGLE OF B AT A = < OAB

CLA, CLOCK ANGLE OF B AT A = < DOB,
(COUNTERCLOCKWISE FROM OD)
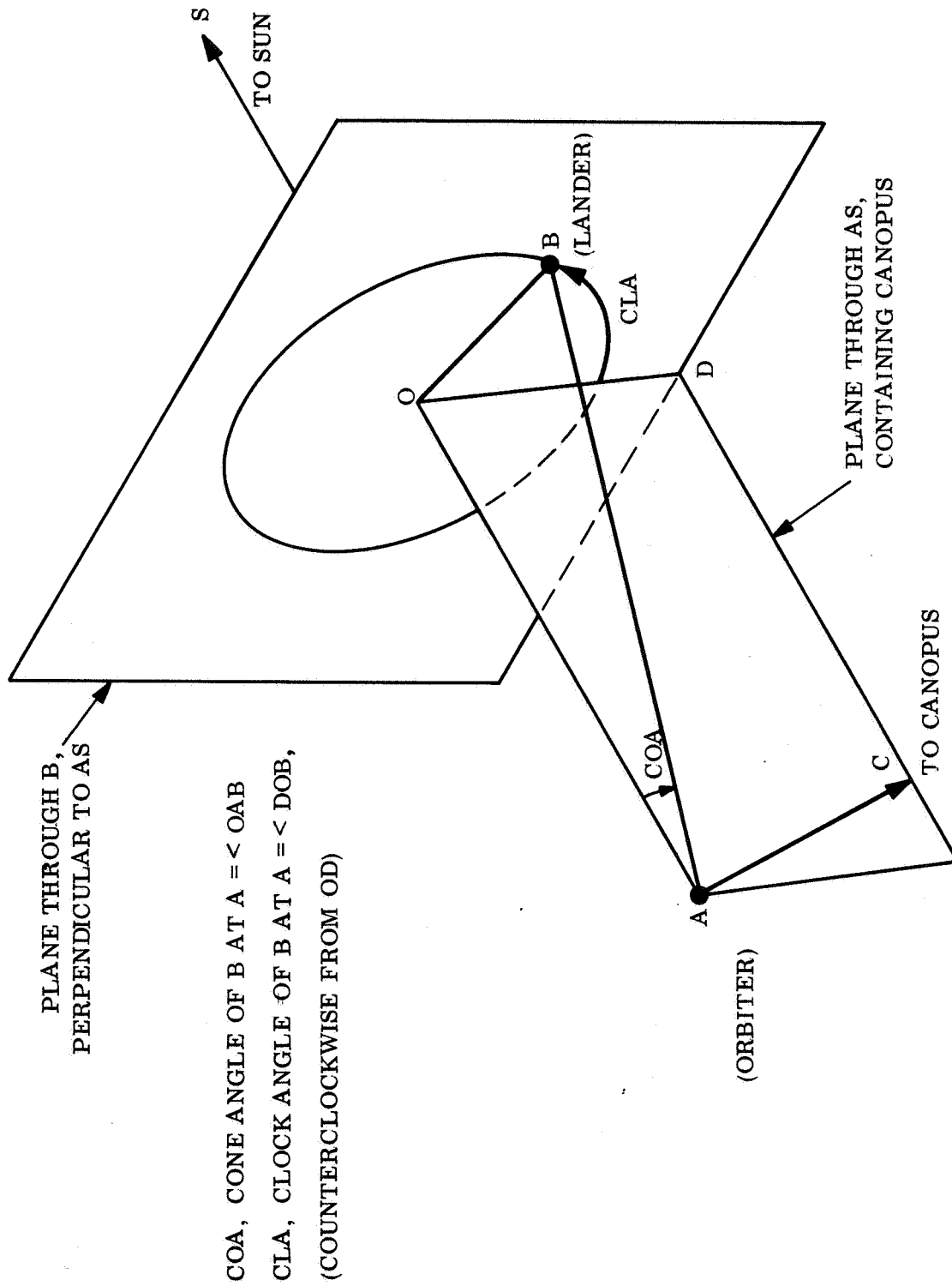
Figure 3.1-13. Definition of Clock and Cone Angles

TABLE 3.1-4. ORBITAL RELAY COMMUNICATION PARAMETERS, OUT-OF-ORBIT ENTRY REFERENCE MISSION

Time, Entry to Landing	700		400		1000	
Landing Latitude (deg)	10	20	10	20	10	20
Figure Numbers For: EIS / EIE	3.1-14	3.1-17	A-1	A-4	A-7	A-10
R / EIB	3.1-15	3.1-18	A-2	A-5	A-8	A-11
COA / CLA	3.1-16	3.1-19	A-3	A-6	A-9	A-12

Deorbit: synchronous orbit
deorbit true anomaly = 235°
deorbit velocity = 234.8 m/sec
entry velocity = 15,300 ft/sec
entry path angle = 16°
PER angle = -14.4°
central angle, entry to landing = 14°

Note: figs. 3.1-14 through 3.1-19 are in this section.
figs. A-1 through A-12 are in the Appendix

PER = -14.4° β EI = 14°

TEI = 700 SEC   LANDING LATITUDE = 10° N.

SYNCHRONOUS ORBIT, I = 60°

EIS = SUN ELEVATION ABOVE HORIZON
EIE = EARTH ELEVATION ABOVE HORIZON

TIME, SEC. x 10^4
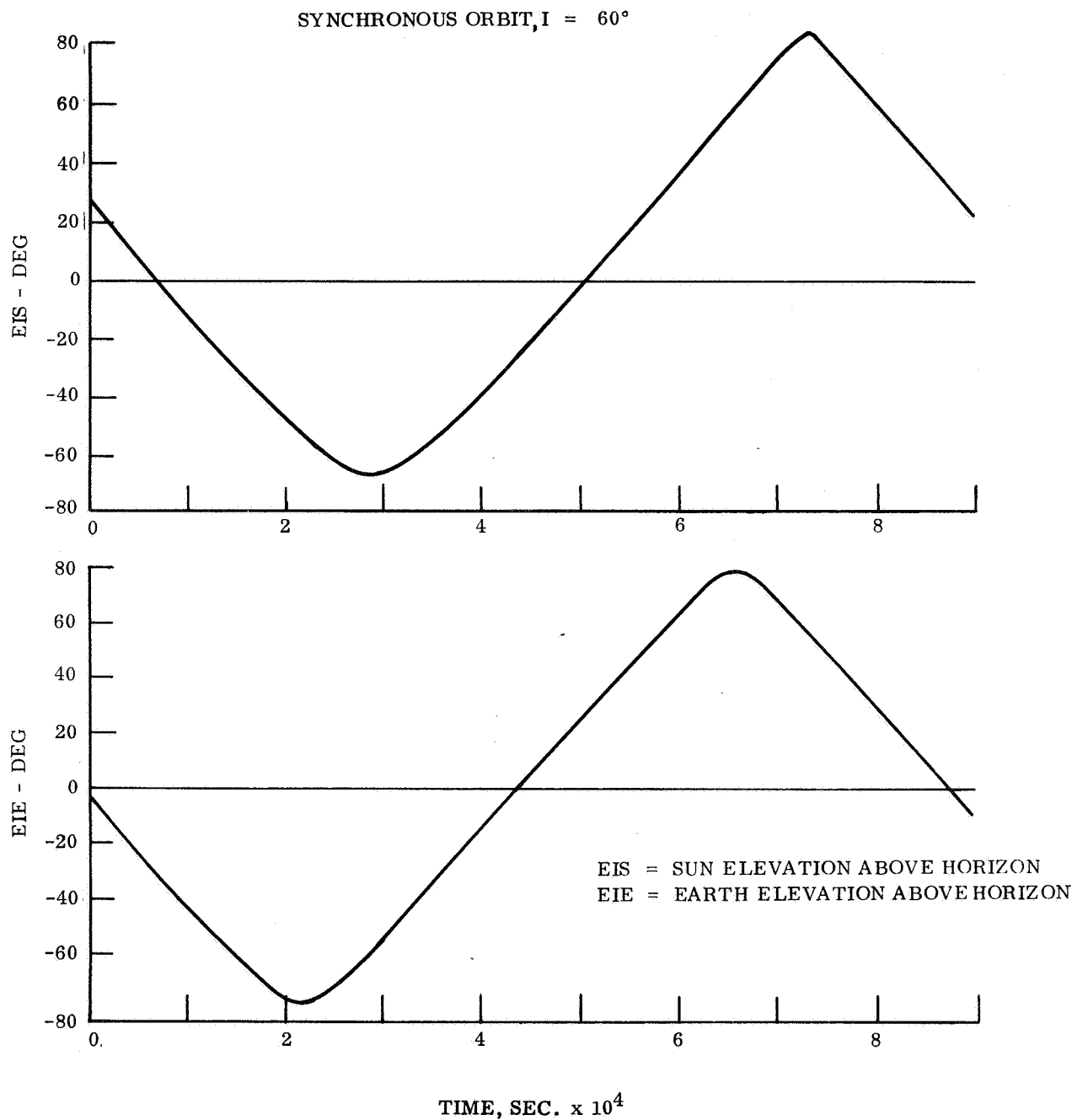
Figure 3.1-14.   Earth and Sun Elevations at Landing Site During First
Orbit After Landing

PER = -14.4° $\beta_{EI} = 14^{\circ}$

TEI = 700 SEC   LANDING LATITUDE = 10°N
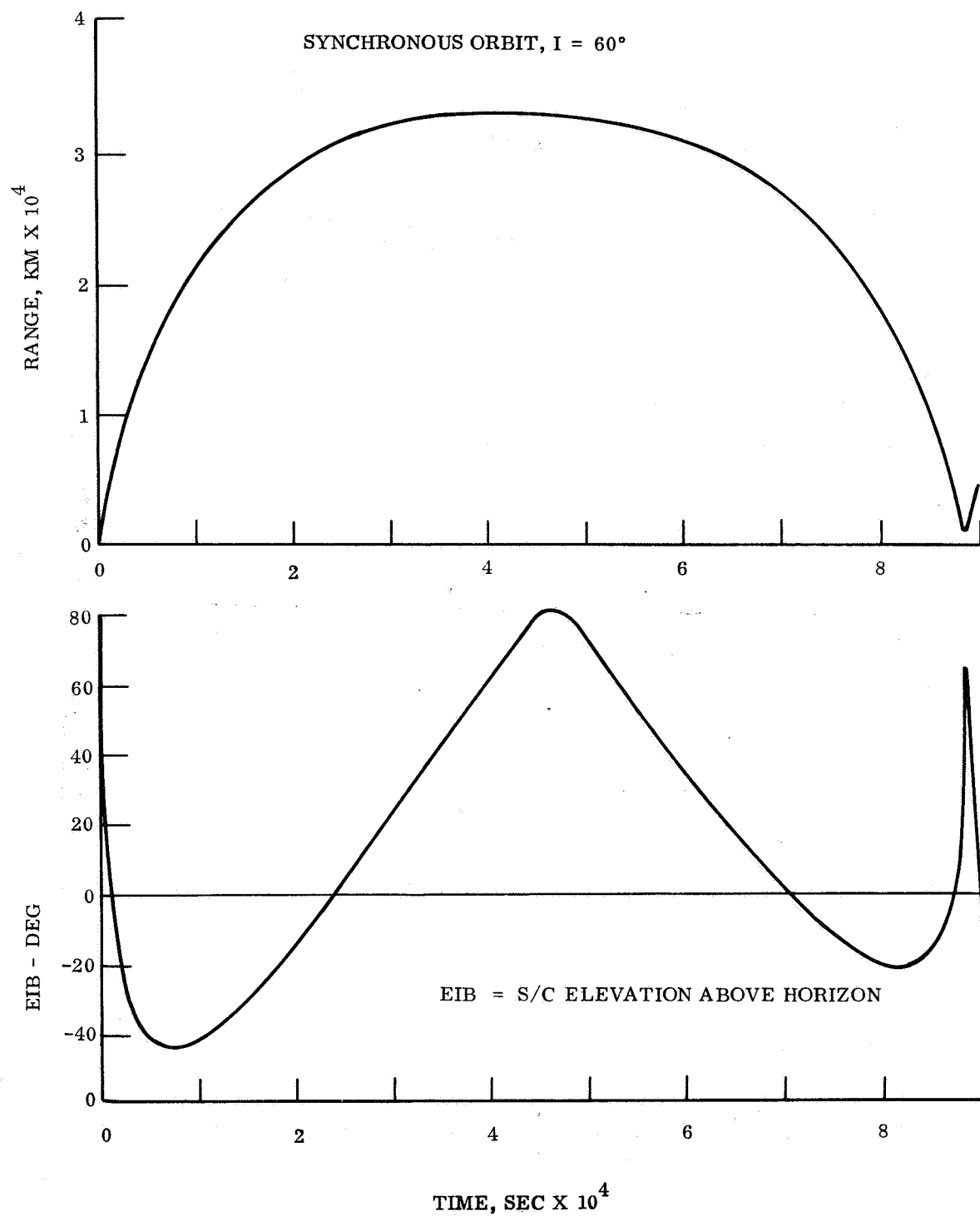
Figure 3.1-15. Relay Communication Range and Orbiter Elevation at Landing Site, During First Orbit After Landing

PER = -14.4° β_{EI} = 14°

TEI = 700 SEC   LANDING LATITUDE = 10°N
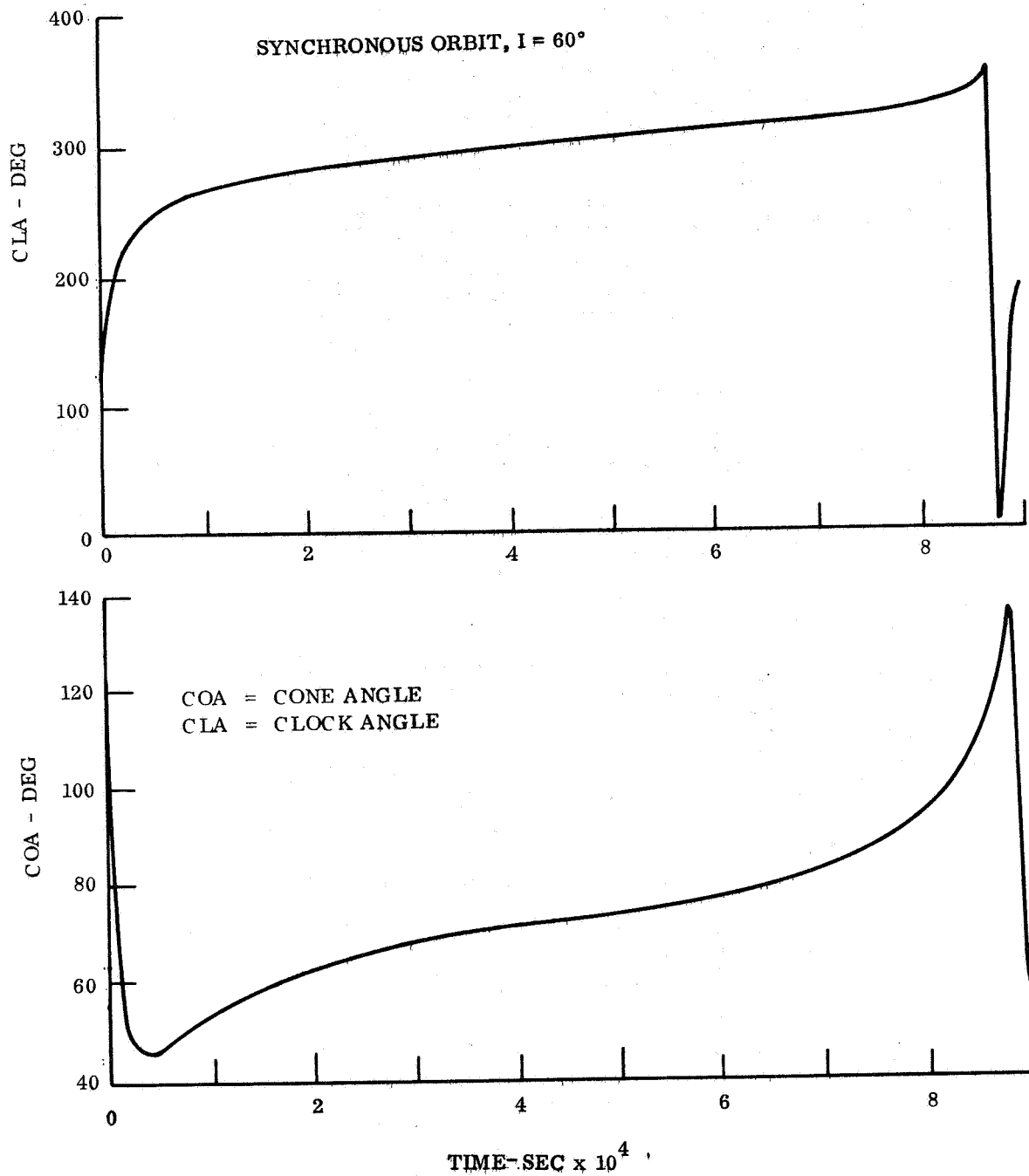
Figure 3.1-16. Lander Clock and Cone Angle at Orbiter During First Orbit After Landing

PER = -14.4°   β   EI = 14°
TEI = 700 SEC   LANDING LATITUDE = 20°N

SYNCHRONOUS ORBIT, I = 60°

EIS = SUN ELEVATION ABOVE HORIZON
EIE = EARTH ELEVATION ABOVE
              HROIZON

TIME, SEC x 10⁴
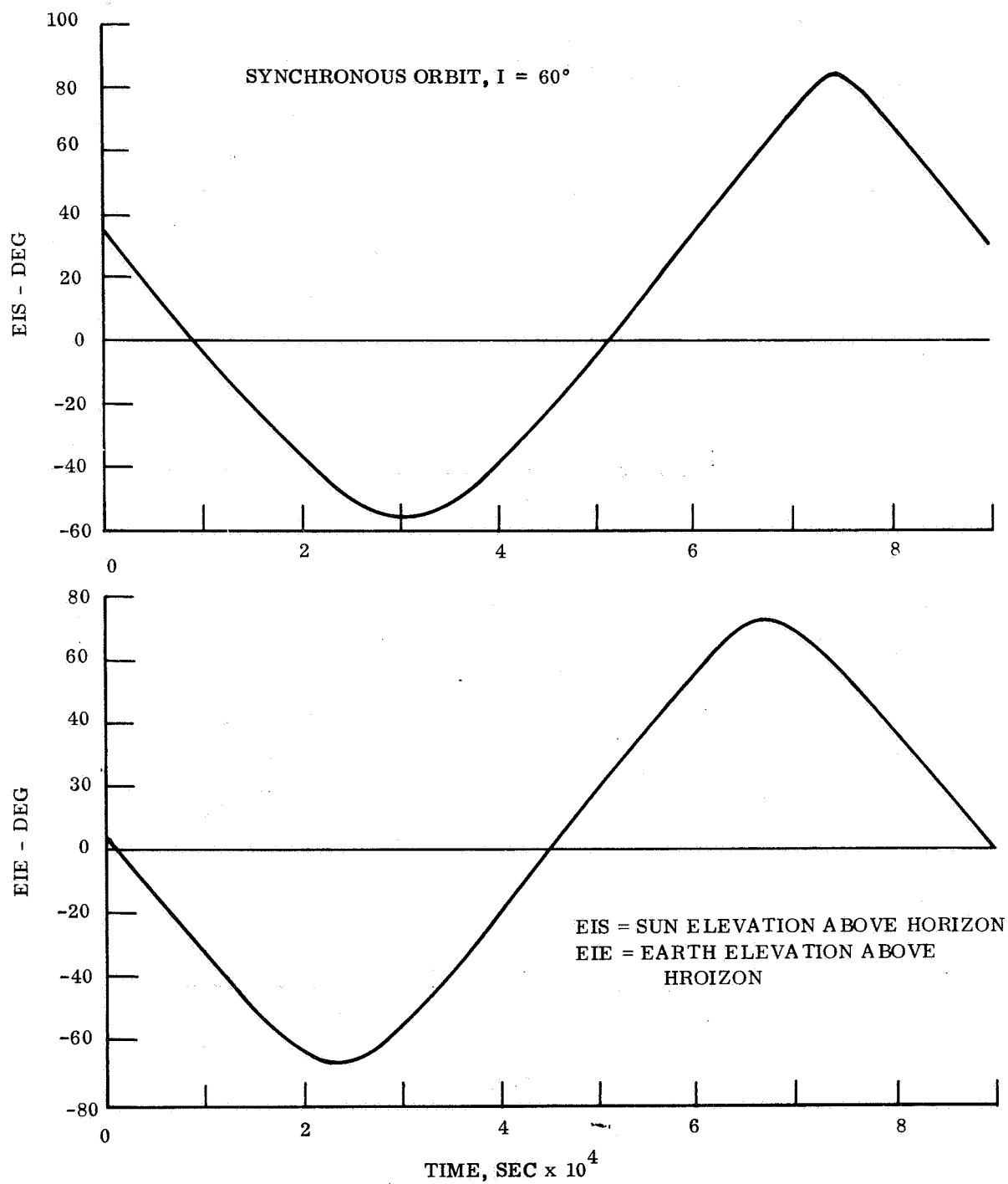
Figure 3.1-17.   Earth and Sun Elevations at Landing Site During First
Orbit After Landing

II

PER = 14.4°   β EI = 14°
TEI = 700 SEC   LANDING LATITUDE = 20°N

SYCHRONOUS ORBIT I = 60°
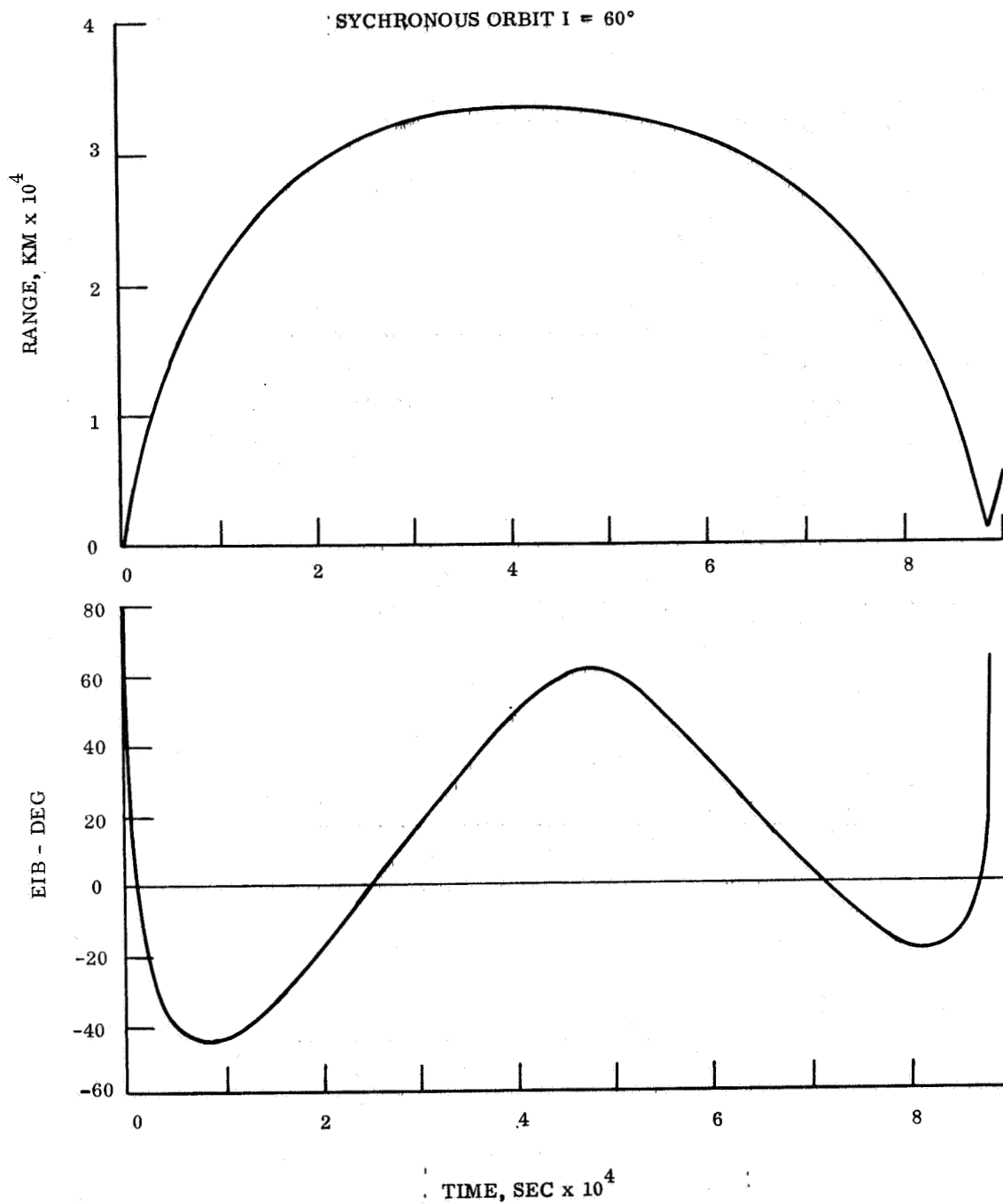
EIB = S/C ELEVATION ABOVE HORIZON

Figure 3.1-18. Relay Communication Range and Orbiter Elevation at Landing
Site During First Orbit After Landing

iI
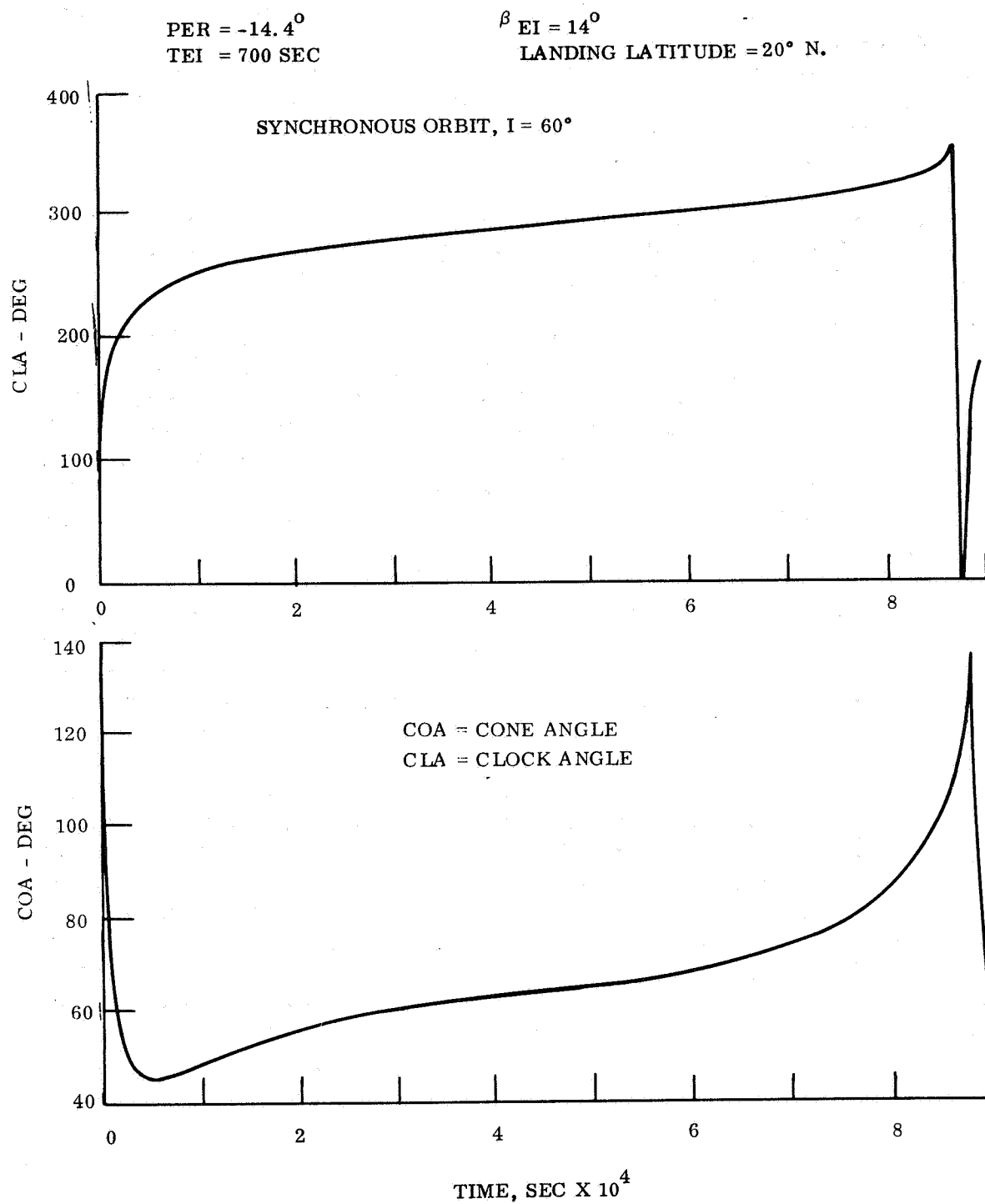
Figure 3.1-19. Lander Clock and Cone Angle at Orbiter During First
Orbit After Landing

3.1.1.5 Entry Trajectories

Reference mission data for the entry trajectories is presented in figs. 3.1-21 through 3.1-30 and A-13 through A-42. Some pertinent parameters are summarized in table 3.1-5. The entry trajectories have been computed according to the deorbit condition specified in para 3.1.1.2 for four VM atmospheres: VM-3, VM-7, VM-8 and VM-9. The atmosphere specifications are given in table 2.2-5 of Section 2.0 of this volume. The particular four atmospheres used here were selected to cover the range of various design parameters, such as time from entry to impact, heating rate, total heating and deceleration.

The aeroshell is a 60° sphere-cone configuration with a ballistic coefficient $(W/C_D A)$ of 14 lb/ft^2; the parachute is designed to provide a terminal velocity of 150 ft/sec in the VM-7 atmosphere. This terminal velocity was shown in previous studies to be near optimum for the design of the combined parachute plus crush-up structure arrangement. Parachute deployment is at Mach 2. In the computation of entry trajectories, this is provided for by using the C_D versus Mach number of the aeroshell when the Mach number is greater than 2. For that portion of the trajectory where the Mach number is smaller than 2, an artifical drag coefficient is used which, in combination with the aeroshell reference area, will give the proper drag; this drag number is 52.0 and, with the vehicle weight to reference area ratio (W/A) of 20.44 lb/ft^2 the ballistic coefficient is therefore 0.393 lb/ft^2. The resulting drag curve is shown in fig. 3.1-20.

Table 3.1-5 lists some of the entry trajectory parameters. More detail is provided in figs. 3.1-21 through 3.1-30 for the VM-3 trajectory, A-13 through A-22 for VM-7, A-23 through A-32 for VM-8 and A-33 through A-42 for VM-9. The parameters which are shown as functions of time from entry to landing in these graphs are arranged as listed in table 3.1-6.

The angle at which the Lander sees the Orbiter above the Lander's horizon, the Lander look angle, and the clock and cone angles have been computed in accordance with the arrival configuration of Mars, Earth and Sun as defined in para 3.1.1.1, for the landing site at 10 degree North latitude. The Lander look angle, i.e., the angle between the Lander's velocity vector and the direction to the Sun, provides some information concerning the Lander's antenna requirements for relay communication to the Orbiter; to obtain complete information for antenna design, the attitude motion of the Lander should be superimposed on this Lander look angle. The Lander clock and cone angles at the Orbiter identify the direction in which the Orbiter sees the Lander relative to the Sun and Canopus; these angles provide information for the Orbiter's relay communication antenna design. The Lander look angle and Orbiter elevation angle are defined in fig. 3.1-31.

$$\frac{W}{C_D A} = 14.0 \text{ LB/FT}^2$$

60° SPHERE CONE WITH PARACHUTE

$$V_{TERM} = 150 \text{ FT/SEC IN VM-7}$$
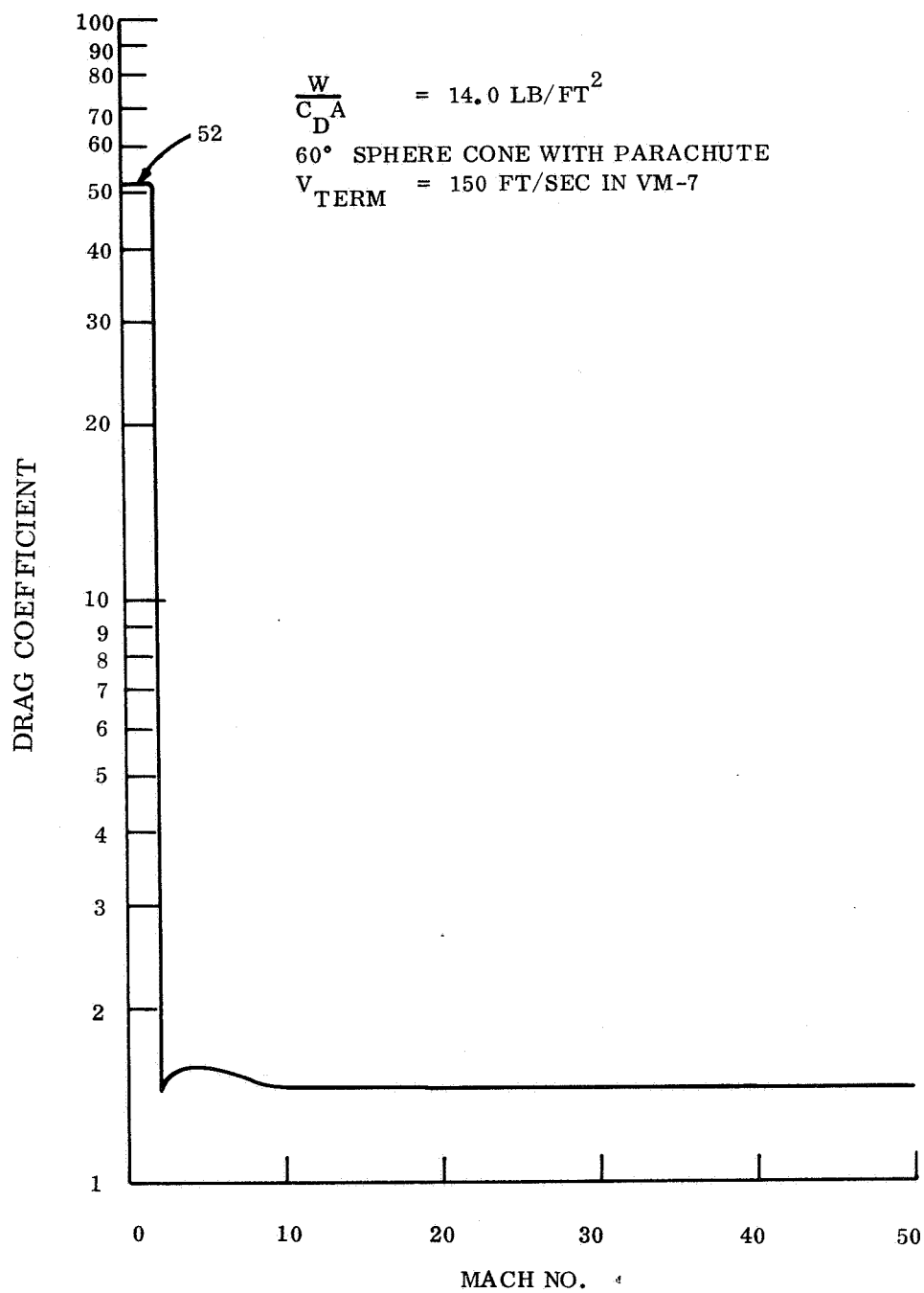
Figure 3.1-20.   Drag Coefficient vs Mach Number

ENTRY VELOCITY — 15,300 FT/SEC
ENTRY PATH ANGLE — 16°
ENTRY ALTITUDE — 244 KM
DRAG, SEE FIG. 3.1-20
VM-3
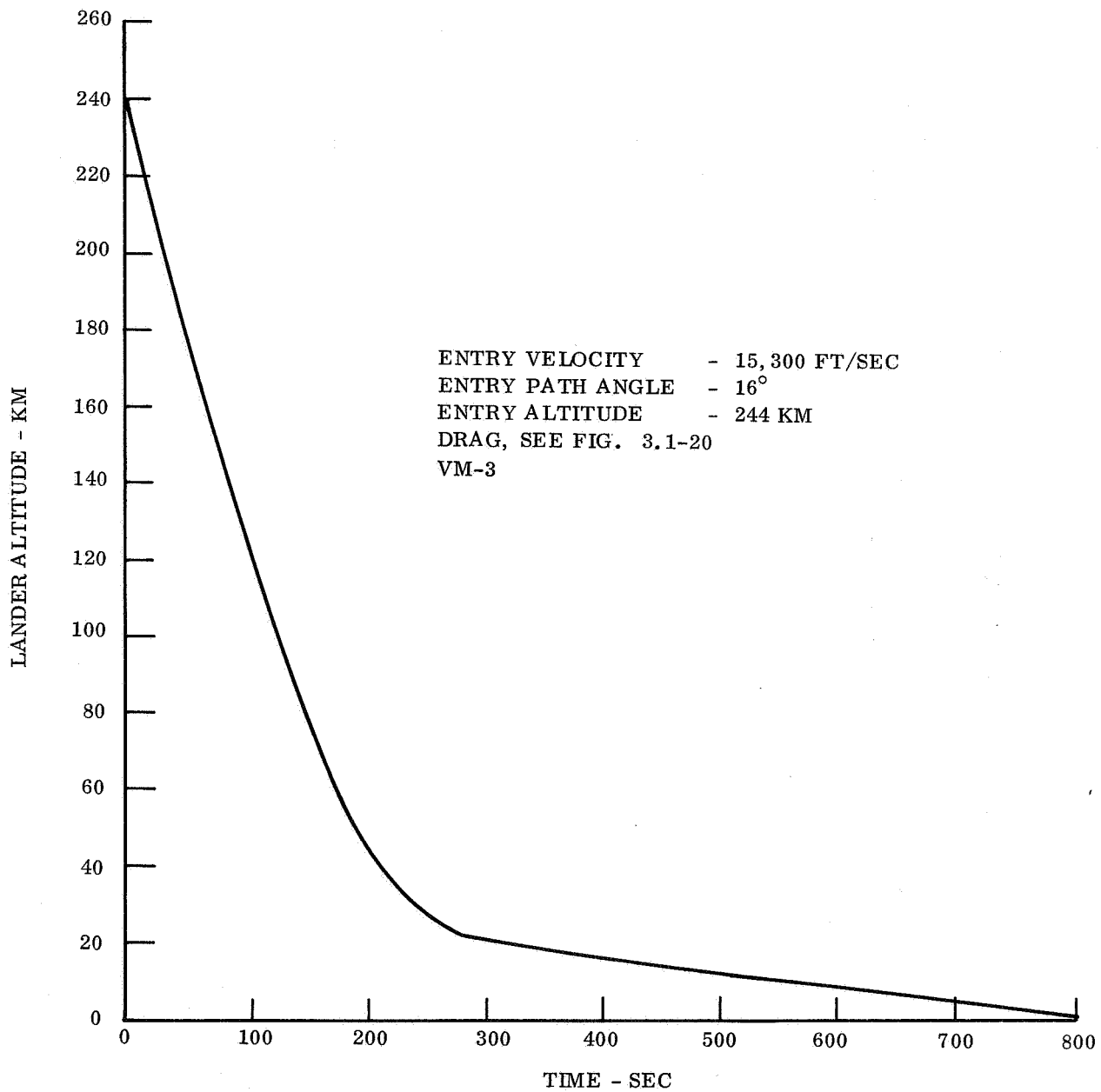
Figure 3.1-21. Lander Altitude vs Time

ENTRY VELOCITY   -   15,300 FT/SEC
ENTRY PATH ANGLE   -   16°
ENTRY ALTITUDE   -   244 KM
DRAG, SEE FIG. 3.1-20
VM-3
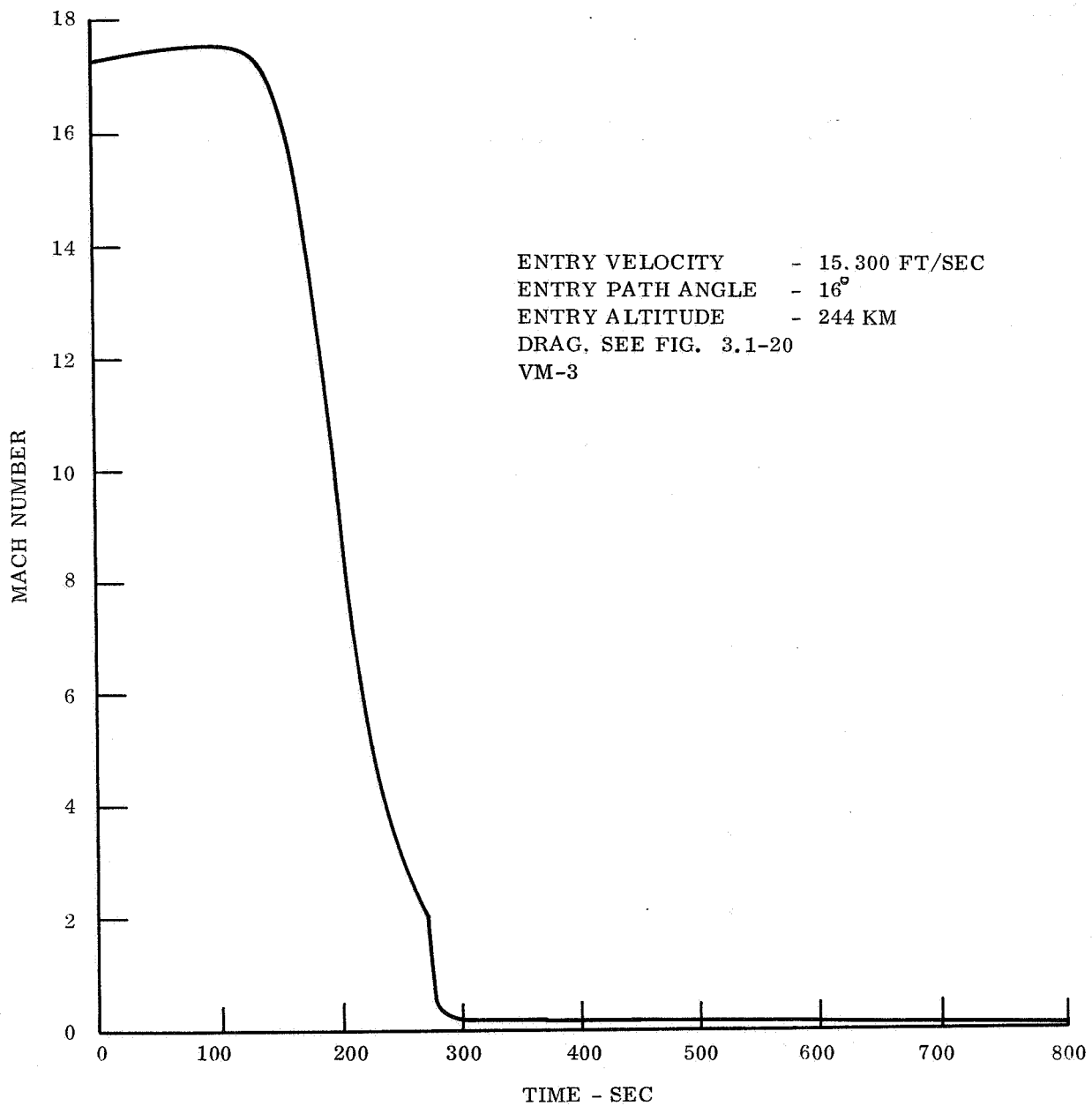
Figure 3.1-22.   Mach Number vs Time

ENTRY VELOCITY   - 15,300 FT/SEC

ENTRY PATH ANGLE - 16°

ENTRY ALTITUDE   - 244 KM

DRAG, SEE FIG. 3.1-20

VM-3
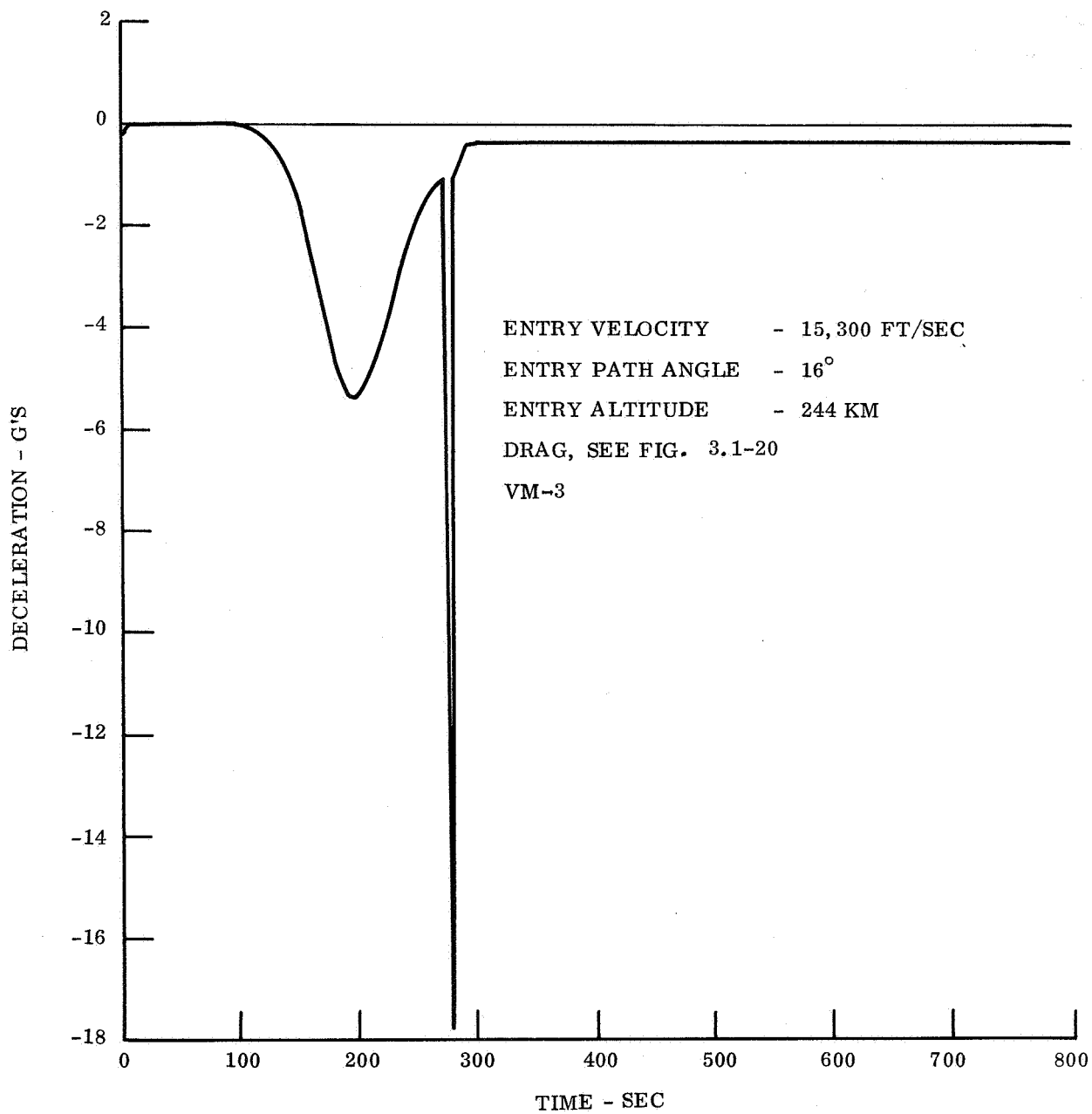
Figure 3.1-23. Lander Deceleration vs Time

ENTRY VELOCITY   = 15,300 FT/SEC

ENTRY PATH ANGLE   = 16°

ENTRY ALTITUDE   = 244 KM

DRAG, SEE FIG. 3.1-20

VM-3
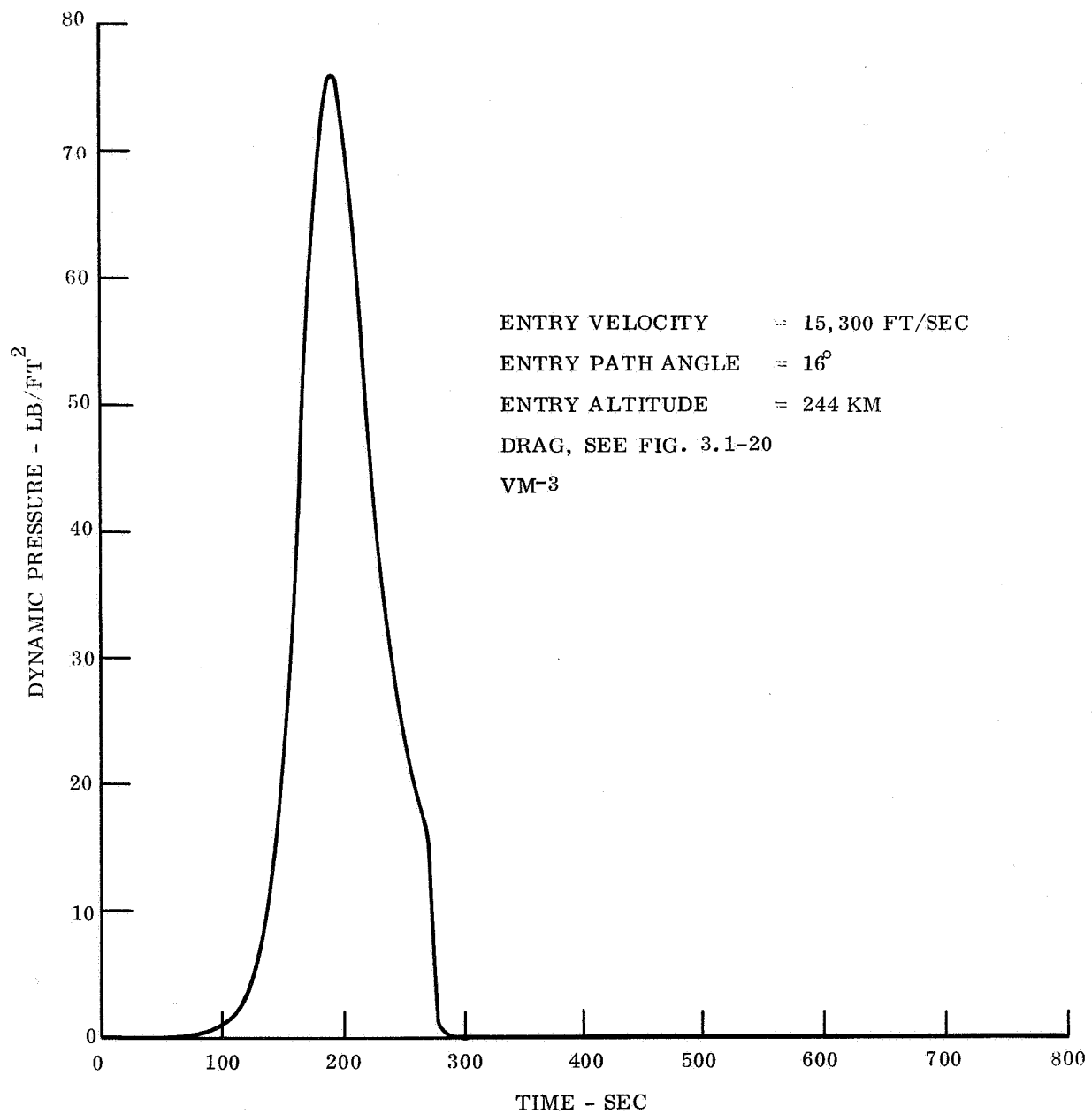
Figure 3.1-24. Dynamic Pressure vs Time
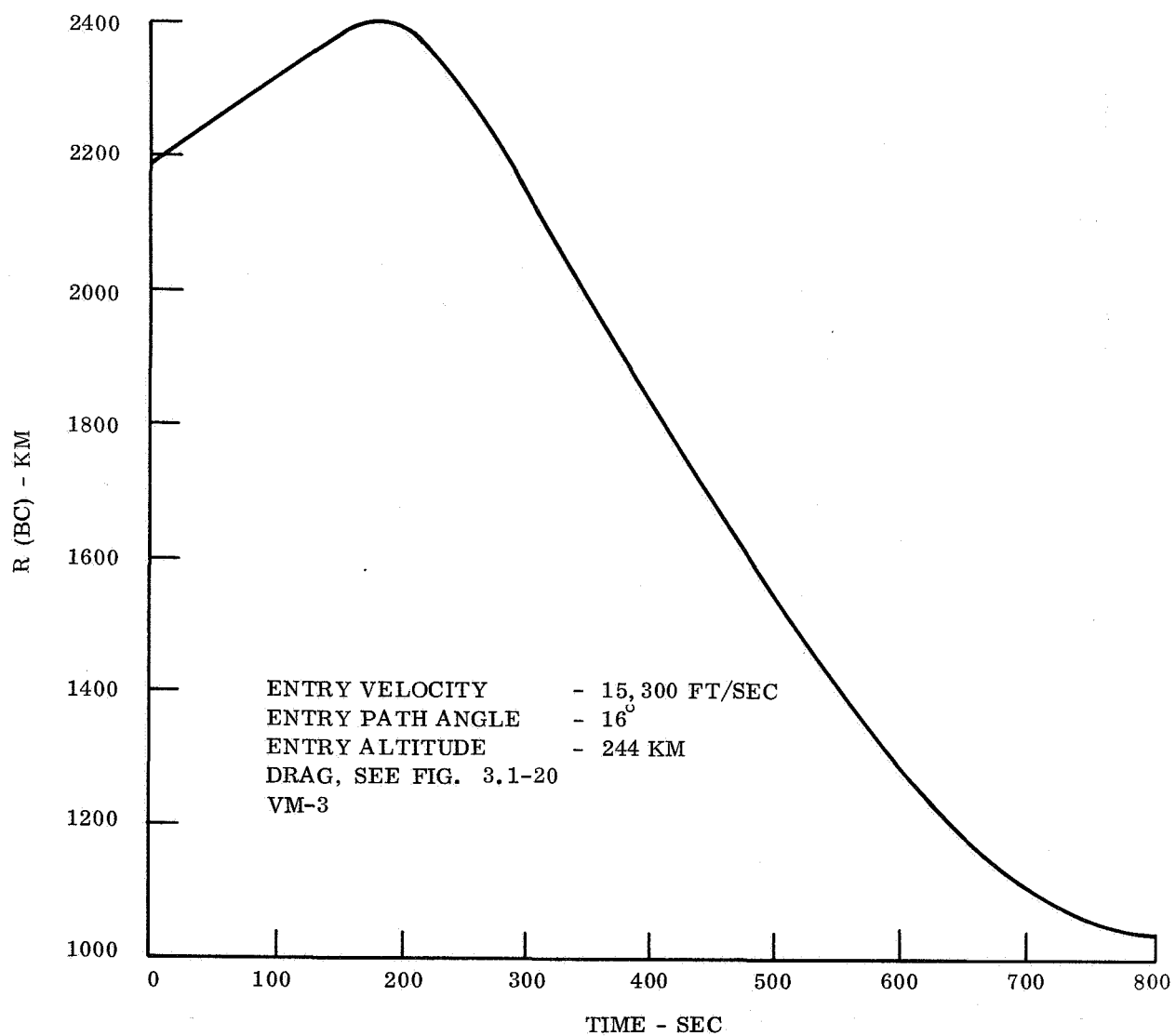
Figure 3.1-25. Communication Distance R(BC) vs Time

The chart displays R (BC) - KM on the vertical axis (from 1000 to 2400) versus TIME - SEC on the horizontal axis (from 0 to 800).

Annotations within the chart:

ENTRY VELOCITY   – 15,300 FT/SEC
ENTRY PATH ANGLE   – 16°
ENTRY ALTITUDE   – 244 KM
DRAG, SEE FIG. 3.1-20
VM-3

ENTRY VELOCITY — 15,300 FT/SEC
ENTRY PATH ANGLE — 16°
ENTRY ALTITUDE — 244 KM
DRAG, SEE FIG. 3.1-20
VM-3
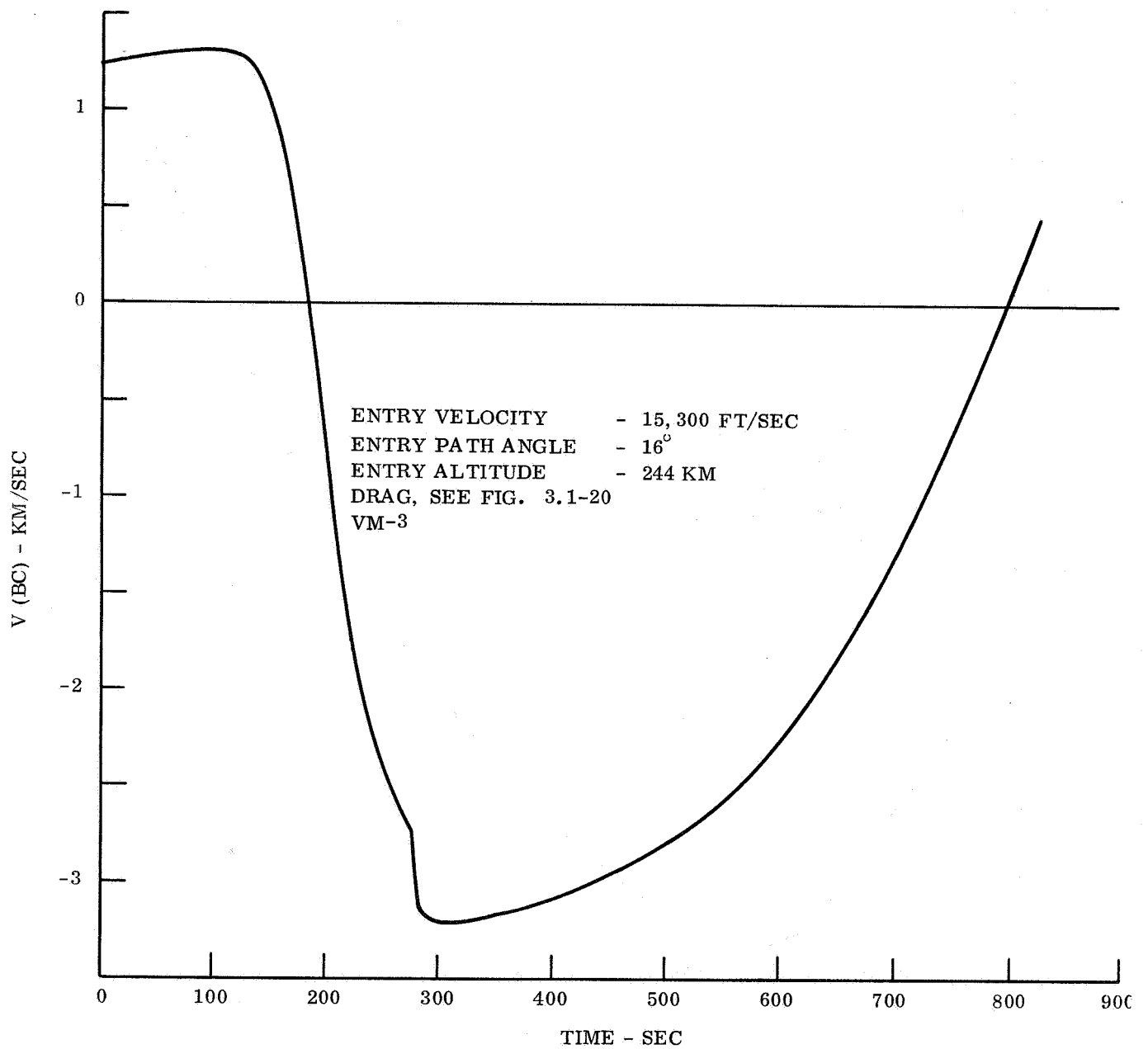
Figure 3.1-26. Range Rate vs Time

ENTRY VELOCITY   - 15,300 FT/SEC
ENTRY PATH ANGLE   - 16°
ENTRY ALTITUDE   - 244 KM
DRAG, SEE FIG. 3.1-20
VM-3
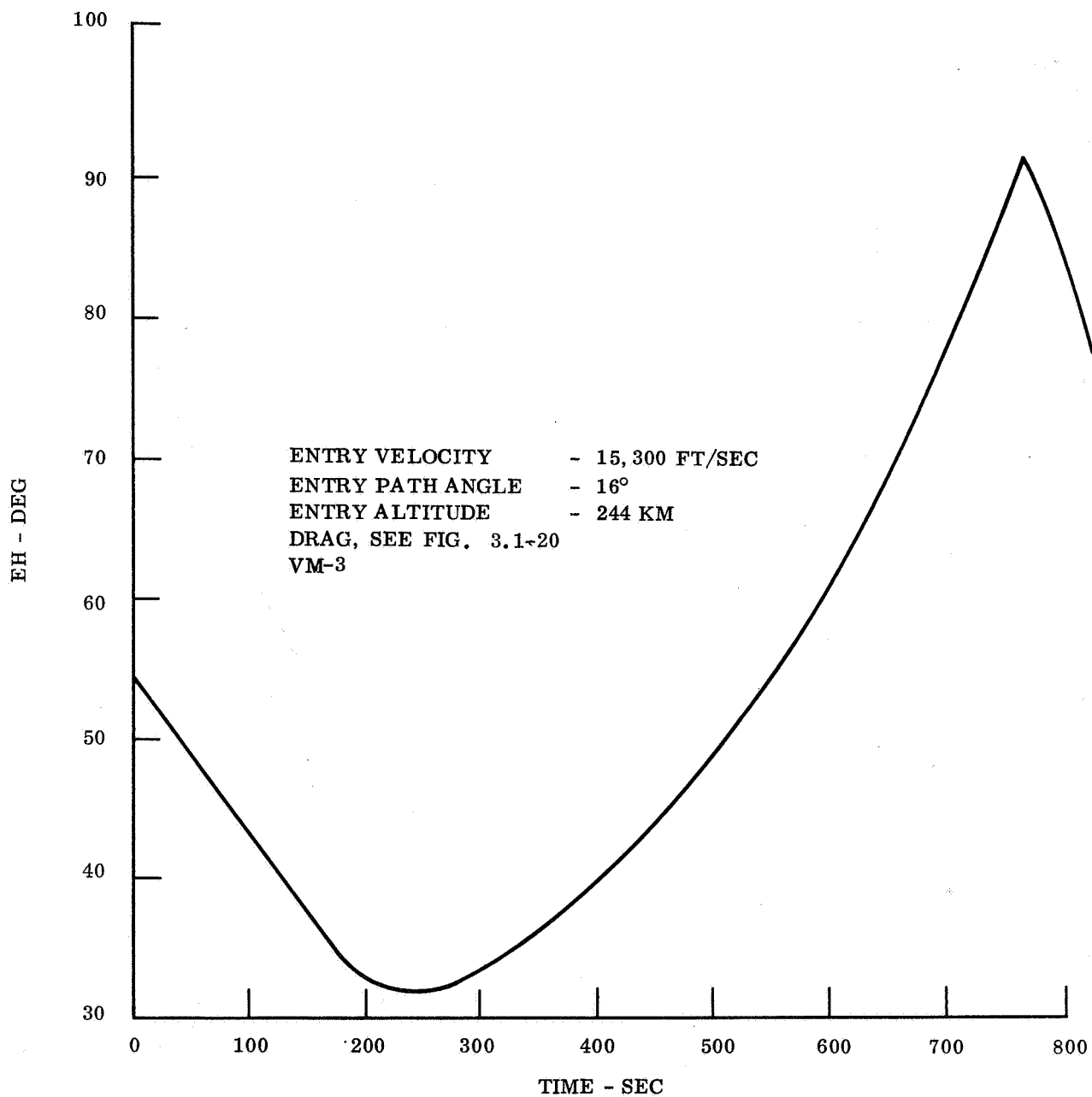
Figure 3.1-27. Angle at which Lander Sees Orbiter above Horizon

ENTRY VELOCITY — 15.300 FT/SEC
ENTRY PATH ANGLE — 16°
ENTRY ALTITUDE — 244 KM
DRAG, SEE FIG. 3.1-20
VM-3
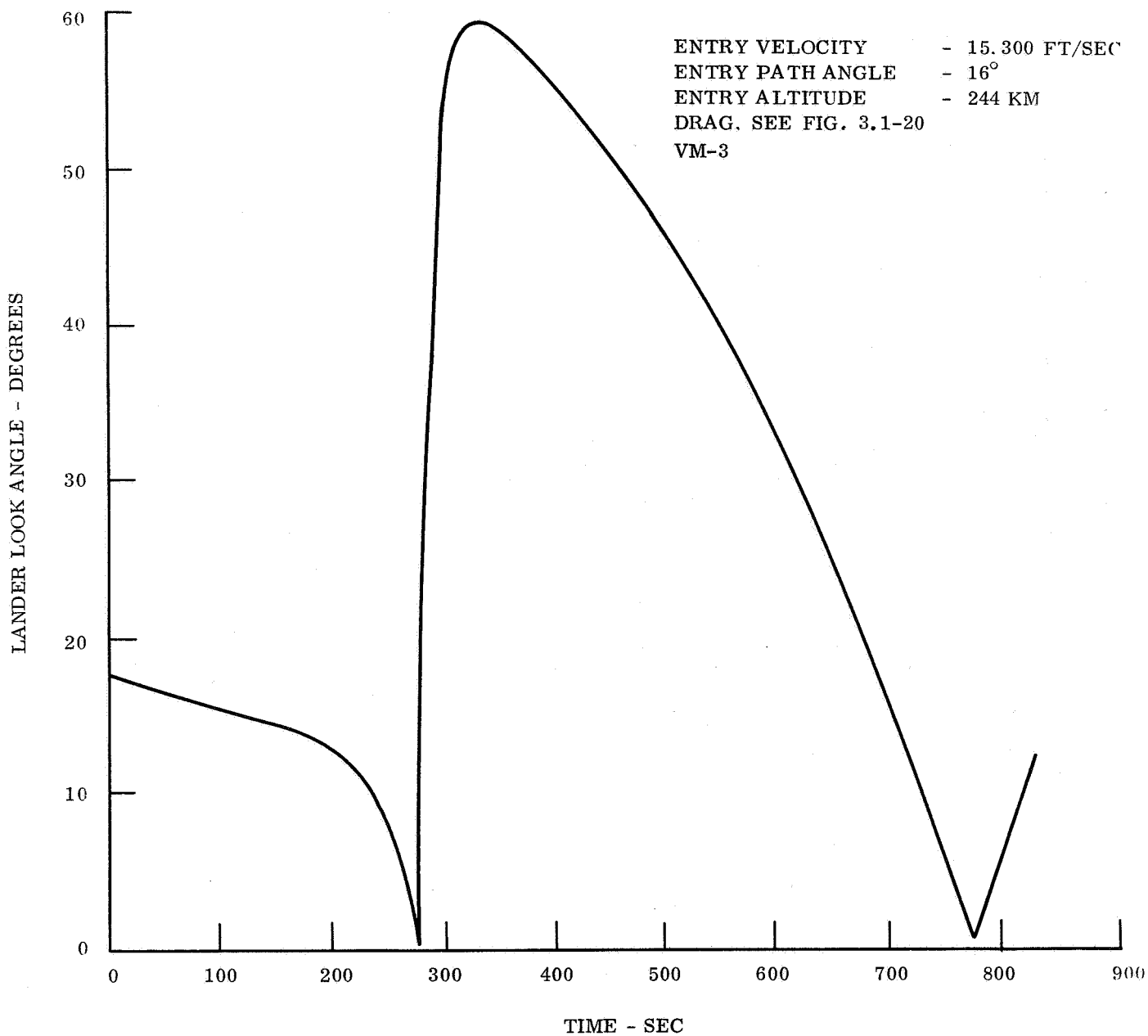
Figure 3.1-28. Lander Look Angle vs Time
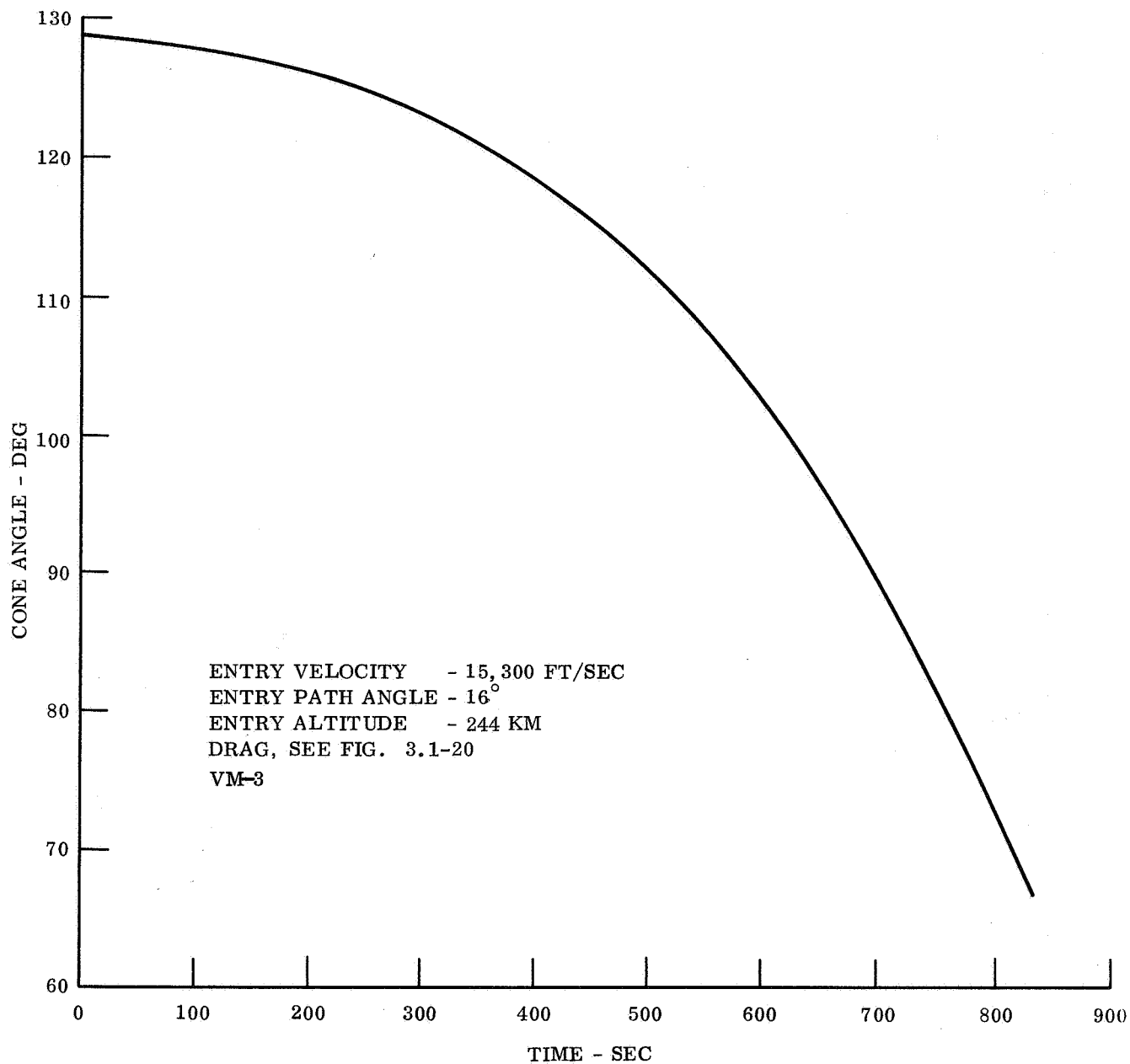
Figure 3.1-29. Cone Angle vs Time

The graph plots CONE ANGLE - DEG (vertical axis, 60 to 130) against TIME - SEC (horizontal axis, 0 to 900).

ENTRY VELOCITY   - 15,300 FT/SEC
ENTRY PATH ANGLE - 16°
ENTRY ALTITUDE   - 244 KM
DRAG, SEE FIG. 3.1-20
VM-3

ENTRY VELOCITY   – 15,300 FT/SEC
ENTRY PATH ANGLE – 16°
ENTRY ALTITUDE   – 244 KM
DRAG, SEE FIG. 3.1-20
VM-3
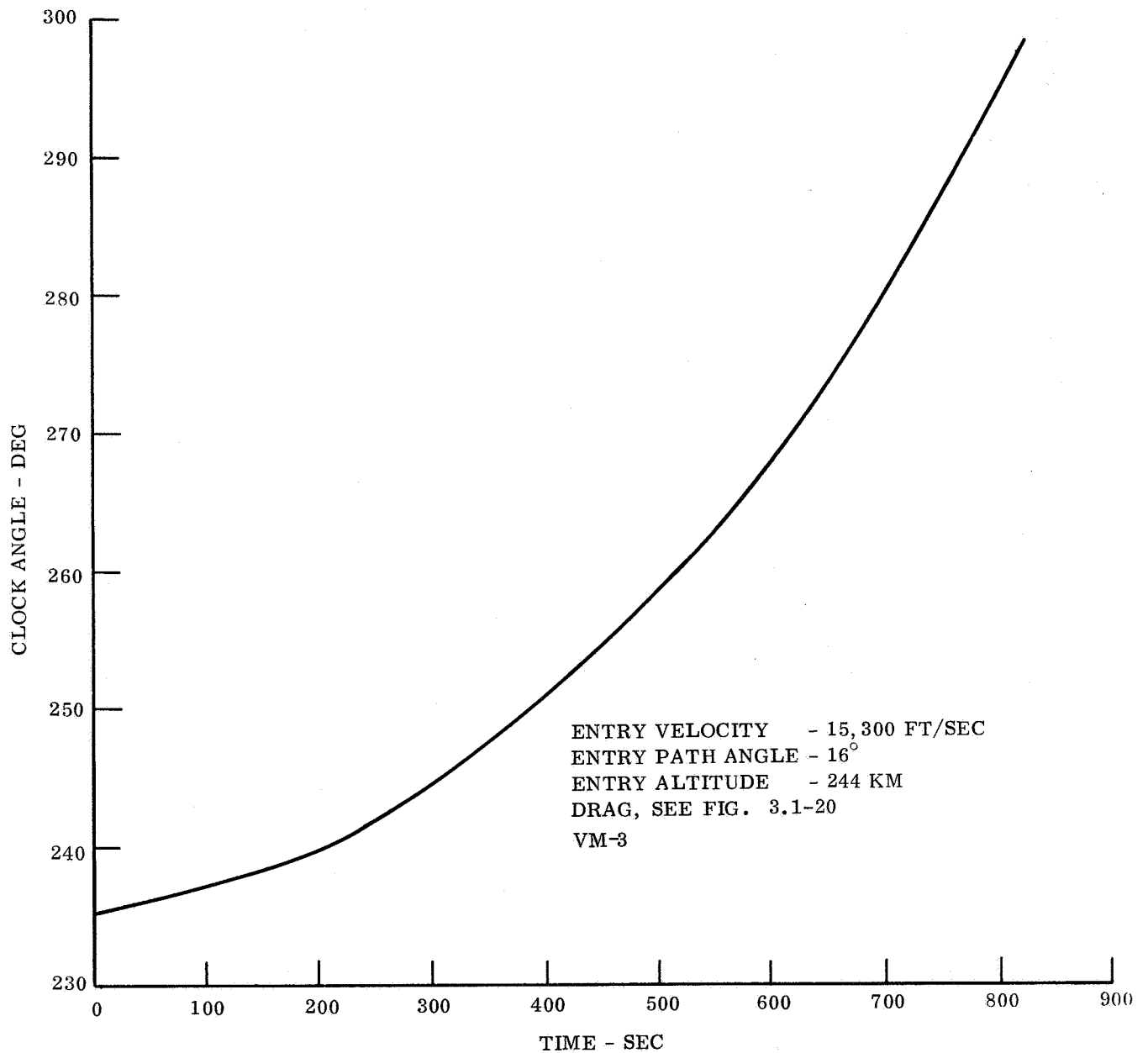
Figure 3.1-30.   Clock Angle vs Time

TABLE 3.1-5. SUMMARY OF ENTRY TRAJECTORY PARAMETERS FOR OUT-OF-ORBIT ENTRY REFERENCE MISSION

60° Sphere cone $W/C_D A = 0.445$ slug/ft²	VM-3		VM-7		VM-8		VM-9	
Entry time (sec)	830		530		460		1251	
Range at entry (km)	2190		2190		2190		2190	
Range at landing (km)	1047		1520		1792		2077	
Elevation at entry (deg)	33.4		33.4		33.4		33.4	
Elevation at landing (deg)	77.6		44.4		34.3		16.1	
Central angle entry to landing (deg)	15.7		16.8		18.2		14.8	
	Seconds to Impact	Alt km	Seconds to Impact	Alt km	Seconds to Impact	Alt km	Seconds to Impact	Alt km
Mach 5	601	33.7	288	23.8	205	11.5	1034	42.9
Mach 2 Parachute Deployment	557	22.7	244	12.9	175	6.7	992	32.4
Mach 1	553	22.2	242	12.5	173	6.4	988	31.8
Max. deceleration (g)	5.43 / 635	47.5	5.28 / 324	37.9	12.70 / 231	18.9	5.59 / 1068	57.1
Max dynamic pressure (psf)	451.6 / 635	47.5	459.8 / 324	37.9	306.8 / 231	18.9	444.0 / 1068	57.1

LLA = the angle between the Lander's velocity vector and the direction to the Orbiter, or "Lander look angle"

E_H = the angle at which the Lander sees the Orbiter above the Lander's horizon

R(BC) = relay communication distance, the distance between Lander Lander and Orbiter

Figure 3.1-31. Definition of Communication Parameters during Entry

TABLE 3.1-6. ENTRY TRAJECTORY PARAMETERS FOR OUT-OF-ORBIT ENTRY REFERENCE MISSION

	Figure Number			
	VM-3	VM-7	VM-8	VM-9
Altitude	3.1-21	A-13	A-23	A-33
Mach Number	-22	-14	-24	-34
Deceleration	-23	-15	-25	-35
Dynamic Pressure	-24	-16	-26	-36
Relay Communication Distance	-25	-17	-27	-37
Relay Communication Range Rate	-26	-18	-28	-38
Angle at which Lander see Orbiter Above Horizon	-27	-19	-29	-39
Lander Look Angle	-28	-20	-30	-40
Cone Angle of Lander at Orbiter	-29	-21	-31	-41
Clock Angle of Lander at Orbiter	-30	-22	-32	-42

3.1.1.6 Definition of Parameters in Table 3.1-1

3.1.1.6.1 Angles in RST Coordinate System

The RT plane is the impact parameter plane, with the T axis parallel to the ecliptic; the S axis is in the direction of the approach asymptote. Angles η and ξ are used to refer any direction to this coordinate sytem as follows. The angle ξ is the angle to the positive S axis; the angle η is the angle between the projection on the RT plane and the T axis, measured positive from the T axis in the direction of a right hand screw along the S axis. This is illustrated below.
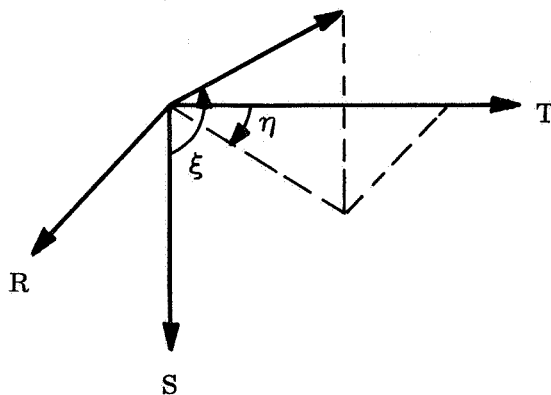
Definition of angles in the RST system.

The nomenclature in table 3.1-1 is as follows:

ZAP	$= \xi_S$	ETS	$= \eta_S$
ZAE	$= \xi_E$	ETE	$= \eta_E$
ZAC	$= \xi_C$	ETC	$= \eta_C$
ZPA	$= \xi_N$	EPA	$= \eta_N$
		ETT	$= \eta_T$

where the subscripts S, E, C and N refer to the Sun, Earth, Canopus and North Pole. The angle η_T defines the position of the aimpoint (located in the RT plane). All directions are positive as seen from the center of the RST system to the object.

3.1.1.6.2 Angles in the Equatorial Coordinate System

In the Mars equatorial coordinate system directions are identified by the "right ascension", α, and the "decelination", δ. The right ascension is measured eastward from the ascending node on the line of nodes, which is the intersection of the Mars equator with the approach trajectory plane. The nomenclature is as follows:

RAS	$= \alpha_S$	DES	$= \delta_S$
RAE	$= \alpha_E$	DEE	$= \delta_E$
RAC	$= \alpha_C$	DEC	$= \delta_C$
RAA	$= \alpha_A$	DEA	$= \delta_A$

where, S, E, C indicate the Sun, Earth and Canopus, as before, and A refers to the positive direction of the approach asymptote.

The angle Omega $(= \omega)$ is the angle from the ascending node, measured in the approach trajectory plane to the periapse of the approach hyperbola (before apsidal rotation); the value listed corresponds to a periapse altitude of 1000 kms.

The angle RA is the apsidal rotation required to achieve the landing latitudes. The values listed here are based on a landing true anomaly of $-14.4°$ (the PER angle). Other nomenclature is as follows:

C_3 = twice the launch energy per unit mass

V_∞ = approach velocity

T_F = flight time on heliocentric transfer

R_C = Earth-Mars distance at arrival

3.1.2 DIRECT ENTRY REFERENCE MISSION

This section defines the direct entry mission which is the basis for the Mars Hard Lander study. The basic mission requirements are the same as for the out-of-orbit missions, but it is seen that the conditions of landing latitude (10, 20° North), orbit inclination (60°) and sun angle (60°) cannot all be satisfied if the entry path angle is to be small (25°). It was therefore agreed with NASA/LRC to relax the orbit inclination. A Type I mission is defined accordingly.

The arrival configuration is defined in para 3.1.2.1; the separation condition and near-approach geometry are defined in para 3.1.2.2. Para 3.1.2.3 summarizes the basic mission parameters.

Para 3.1.2.4 presents six parameters related to communication and power subsystems as functions of time near the end of the first orbit after landing. Data are presented for three different times from entry to landing (400, 800 and 1200 seconds) but the results are very nearly indpendent of this entry time because of the low orbit inclination (10.74° for the 10° landing latitude).

Entry trajectory data and communication parameters during entry are presented in para 3.1.2.5 for four atmospheres (VM-3, -7, -8 and -9).

3.1.2.1 Launch and Arrival Dates, Launch Energy and Arrival Configuration

The selection of the transfer trajectory depends on the following requirements:

1. Landing latitude: 10 and 20° N

2. Orbit inclination: 60°

3. Surface imagery: 30° from a terminator (or: Sun angle, 60°).

In order to have relay communication throughout the entry phase, the Lander trajectory must be coplanar with the approach trajectory. Furthermore, a small path angle is desired for aeroshell design considerations. It follows from data about the entry corridor that the nominal entry path angle may safely be chosen as 25°. The central angle between the approach asymptote and the landing site is then about 90° (i.e., 81° to the entry point and 9° from entry to landing) for approach velocities near 4 km/sec and periapse altitude equal to 1000 km. This central angle, combined with the 60° orbit inclination and the 10 or 20° landing latitude requires LVI angles which are far outside the range of LVI for the 1973 (Type I and Type II) missions. (The LVI angle is the Mars latitude of the negative approach direction.) It was therefore decided, in concurrence with NASA/LRC, to relax the requirement on orbit inclination.

Combinations of launch and arrival dates for which the Sun angle is 60° and the entry path angle is 25° at 10° and 20° Northern latitudes are shown on the basic mission planning chart, fig. 3.1-32. The mission point chosen for the direct entry reference

mission is indicated by a cross. The launch date is July 30, 1973, the arrival date is January 10, 1974; the launch energy is 16 km^2/sec^2 and the approach velocity is about 4 km/sec. It is seen that a 30 day launch window is easily available, requiring launch energies not reater than 18 km^2/sec^2. The approach velocity remains close to 4 km/ sec throughout the launch window. The direct entry mission is defined only for the 10°N. latitude landing site, because the Capsule design is not very sensitive to the small changes which will be required to reach the 20° latitude. The orbit inclination for this mission is 10.7°. Other pertinent mission parameters are listed in table 3.1.7.

The configurations of Sun, Earth, Canopus, north polar axis and approach direction are shown in figs. 3.1-33 and 3.1-34. Fig. 3.1-33 shows the projection on the impact parameter plane; the projection on the Mars equatorial plane is shown in fig. 3.1-34, where the landing point is also indicated.
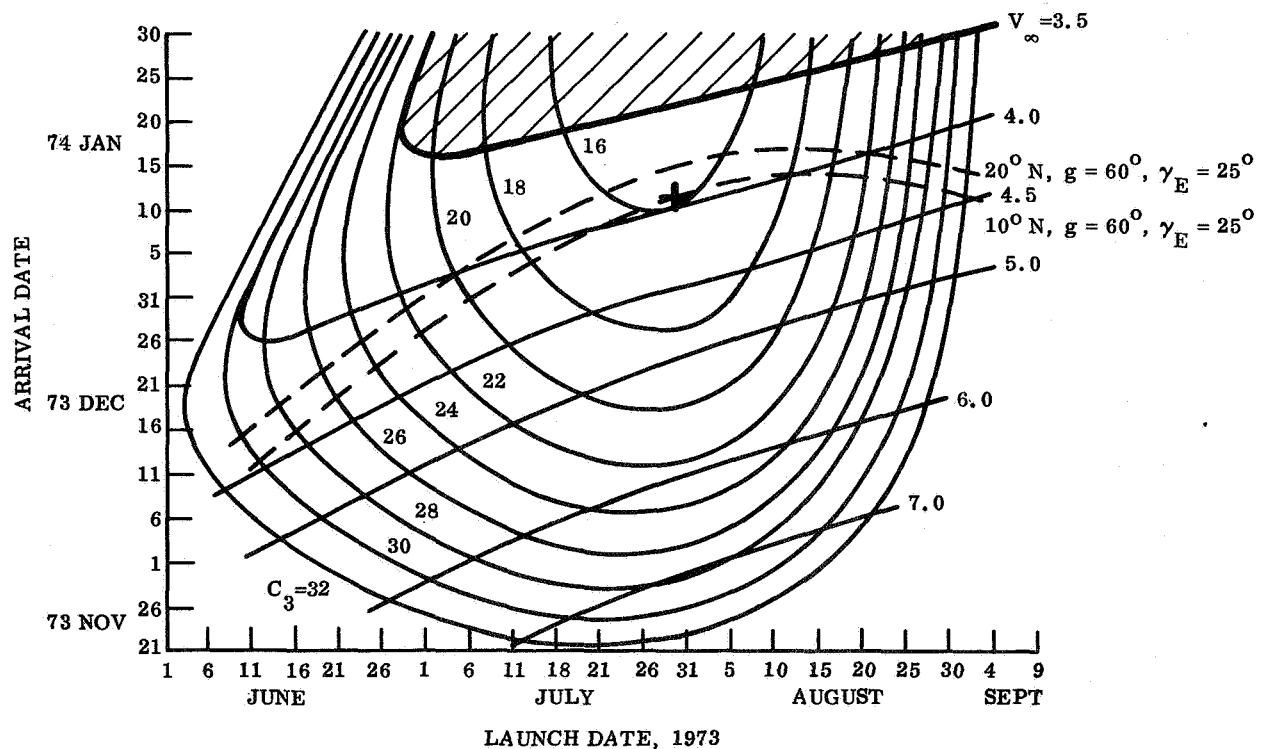
Figure 3.1-32. Direct Entry Mission Basic Mission Planning Chart, Mars 1973, Type 1

TABLE 3.1-7. SUMMARY OF DIRECT ENTRY REFERENCE MISSION

Transfer	
Launch	July 30, 1973
Arrival	January 10, 1974
Flight Time	164 days
Launch Energy	16 km^2/sec^2
Communication Distance	137.52 x 10^6 km
Approach Velocity	4.028 km/sec
Zap Angle	149.6 deg
Approach, Entry and Orbit	
Approach	Southern Posigrade
Orbit Inclination	10.74 deg
Synchronous Orbit	1,000 x 33,084 km
Landing Latitude	10 deg N
Separation Velocity	45 m/sec (24 hrs before encounter)
Apsidal Rotation	-22 deg
Approach Hyperbola Periapse Alt.	1400 km
Orbit Insertion Velocity	1905 m/sec
Sun Angle	60 deg
Entry Path Angle	25 deg
Entry Velocity	20,788 ft/sec

LAUNCH JULY 30, 1973
ARRIVAL JAN. 10, 1974
$V_\infty = 4.028$ KM/SEC
$C_3^\infty = 16$ KM^2/SEC^2

NORTH POLE
DOWN 3.89^o

TERMINATOR

EQUATOR

EARTH AT HORIZON

APPROACH
TRAJ. PLANE

DARK

LIGHT

T

9.45^o

AIMPOINT

SUN
UP 59.59°

EARTH
UP 72.69^o

CANOPUS
DOWN 19.8^o

R
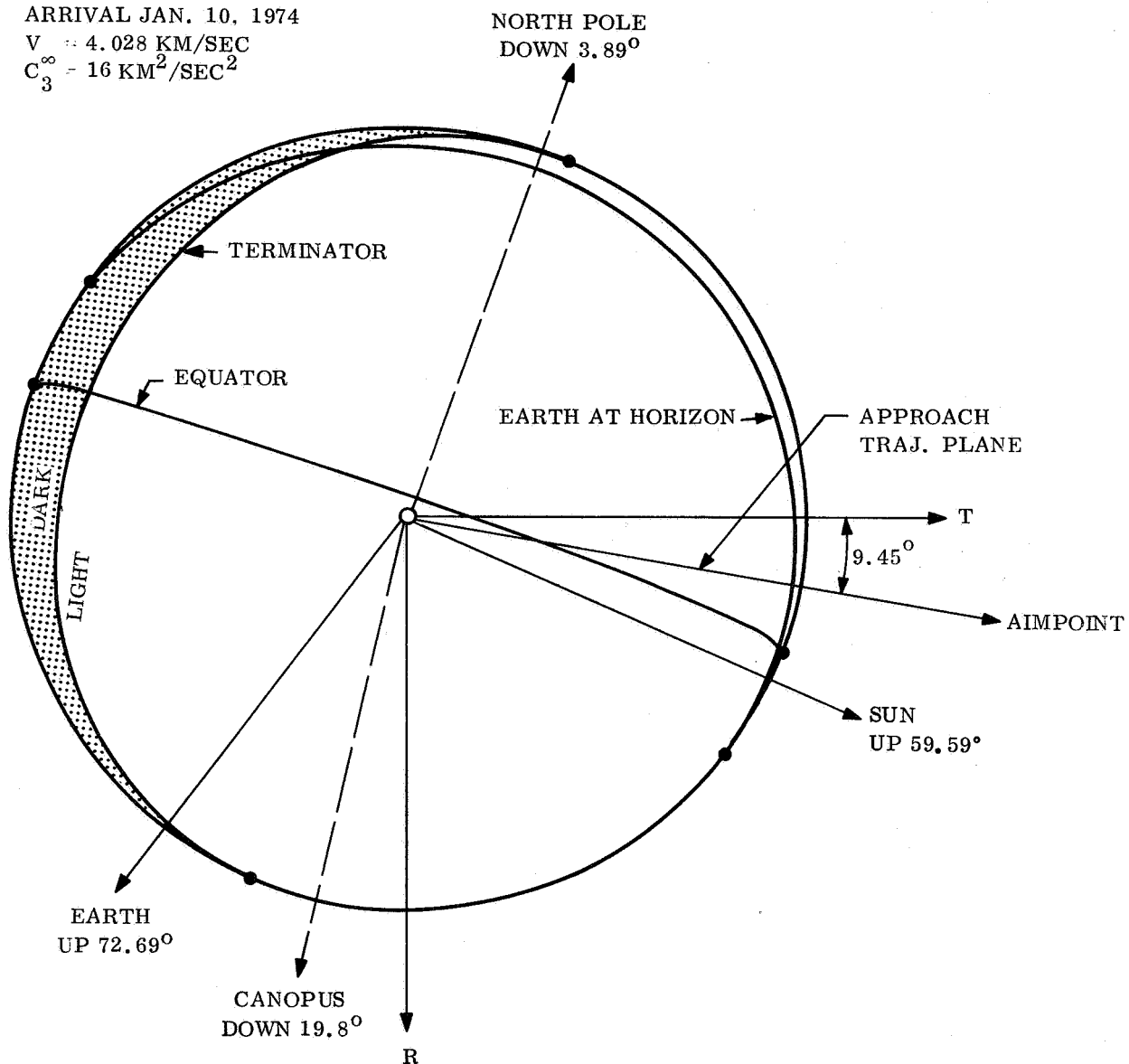
Figure 3.1-33. Direct Entry Mission Arrival Configuration
(Mars Impact Parameter Plane)

LAUNCH: JULY 30, 1973
ENCOUNTER: JAN. 10, 1974
LAUNCH ENERGY:
  $C_3 = 16$ KM^2/SEC^2
APPROACH
VELOCITY:
  $V_\infty = 4.028$ KM/SEC

APPROACH
ASYMPTOTE
UP 3.89°

CANOPUS
DOWN 65.41°

ORBIT INSERTION

ΔV

APPROACH PERIAPSE

EARTH AT
HORIZON

NORTH POLE

TERMINATOR

LANDING SITE

ORBITER PERIAPSE

DARK

LIGHT

EQUATOR

SUN
DOWN 5.72°

EARTH
DOWN 20.34°

ORBITER   SPACECRAFT
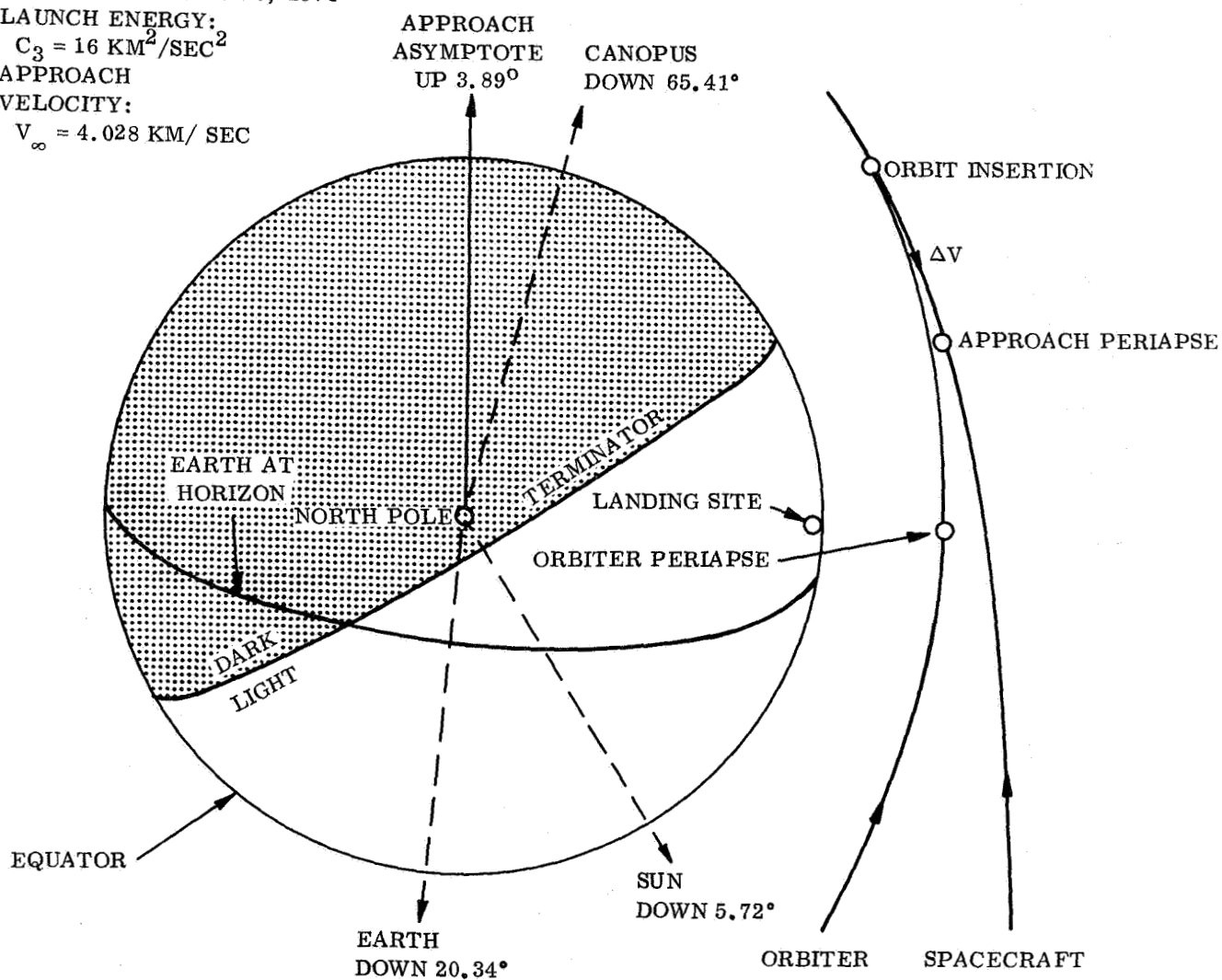
Figure 3.1-34. Direct Entry Mission Arrival Configuration
(Mars Equatorial Plane)

3.1.2.2 Determination of the Deflection Velocity

The central angle between the approach asymptote and the periapse is 112° for an approach velocity of 4 km/sec and periapse altitude of 1000 km. The true anomaly of the landing site (on an entry trajectory with entry path angle of 25°) is thus 22°. In order to obtain the best possible periapse communication, the orbit insertion is performed to obtain an apsidal rotation of -22°. Fig. 3.1-35 shows that this required orbit insertion at true anomaly 20° and an orbit insertion velocity of 1905 m/sec. The periapse altitude of the approach hyperbola is 1310 km. (The entry trajectory data exhibited in para 3.1.2.4 has been computed with h_p = 1400 km, before the required altitude was exactly known. For the purpose of obtaining reference data for Lander design the differences are insignificant.)

The definition of the deflection maneuver, which determines the Lander trajectory, is in principle quite similar to the definition of the deorbit maneuver as discussed in great detail in para 3.1.1.2. That discussion applies here as well, with the following differences. As is the case with the deorbit maneuver, the definition of the deflection is also a two parameter problem; one of these parameters may be taken as the time to encounter at which the deflection is to take place, the other as the tangetial component of deflection velocity. The time to encounter is here taken as 24 hours; if any other time is desired, the corresponding results are easily determined because the deflection velocity components are very nearly inversely proportional to the time to encounter. Thus, only tangential components of the deflection maneuver still need to be found, the normal component being directly determined by the required entry path angle (the normal component for a given entry path angle is slightly dependent on the tangential velocity, but a simple iteration establishes that). The tangential deflection velocity, then, is selected in accordance with the relay communication requirement; in effect, it is adjusted to cause the Orbiter to pass over the Lander at just the right time. The information which is required for this adjustment is in fig. 3.1-37; this figure has the same function here as fig. 3.1-10 had in the out-of-orbit mission analysis.

The approach geometry is shown approximately to scale in fig. 3.1-36. In the particular case illustrated, the Lander is given a tangential velocity of 40 m/sec at separation in addition to the 20.7 m/sec normal component which is required to obtain the 25° entry path angle. Separation is taken to occur 24 hours before the Orbiter's periapse passage. The position of the Orbiter is indicated for the case in which the entry time (i.e., from entry to landing) is 800 sec. As will be seen in detail in para 3.1.2.4, entry times between 460 and 1220 sec are to be expected throughout the range of VM atmospheres. In order to have relay communication throughout the entry phase, the Orbiter position at the time of landing must be on that part of the approach hyperbola which lies between the 34° "horizons" at the landing point (see fig. 3.1-36). Fig. 3.1-37 shows that this is accomplished by a tangential velocity component of 40 m/sec applied at separation, 24 hours before the Orbiter periapse passage. The range of entry times which is accommodated within the 34° limit on elevation is 400 to 1200 sec. (For separation at different times to encounter the velocity components are very nearly inversely proportional to the time to periapse for the same entry conditions.)
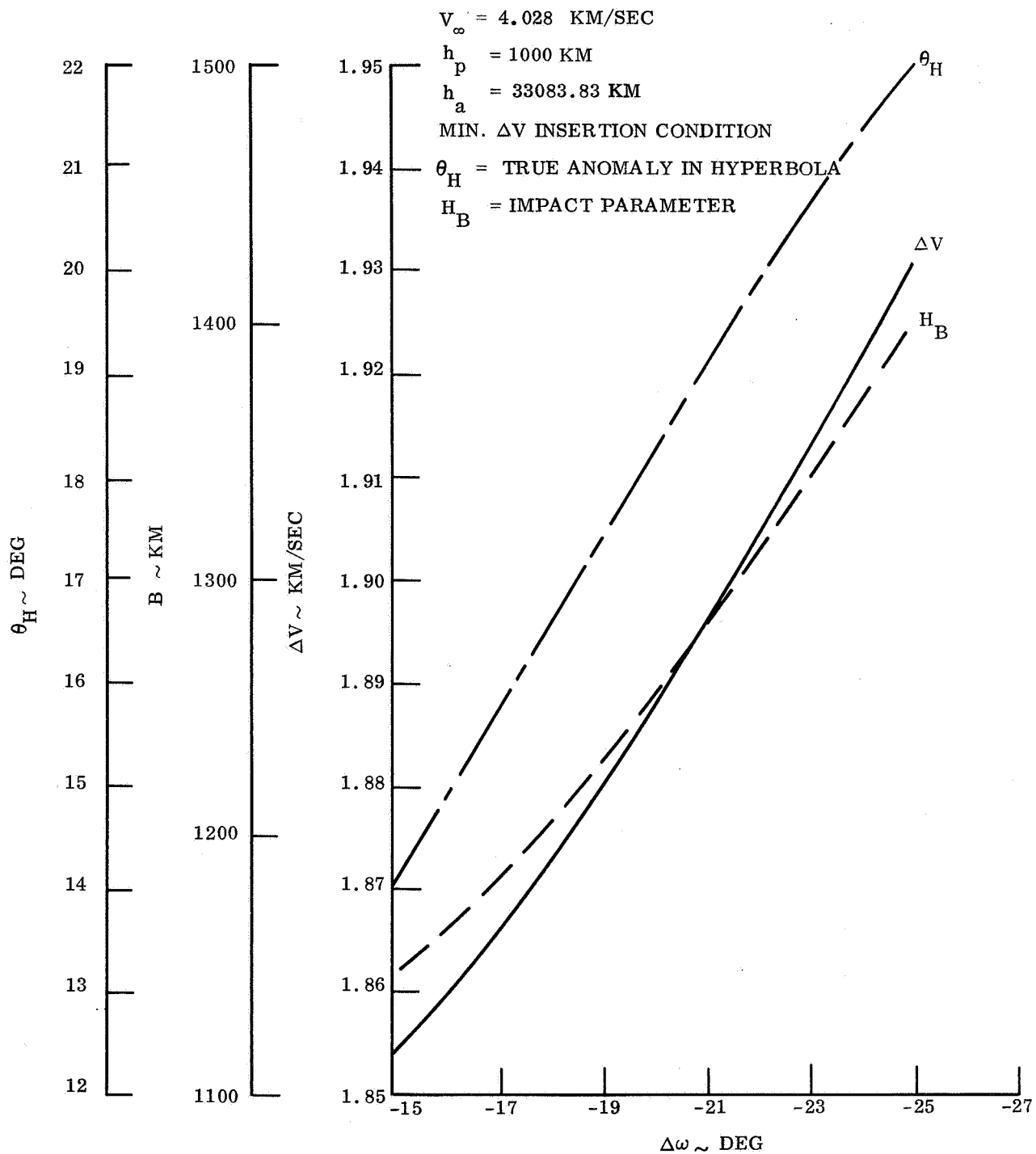
Figure 3.1-35. Apsidal Rotation
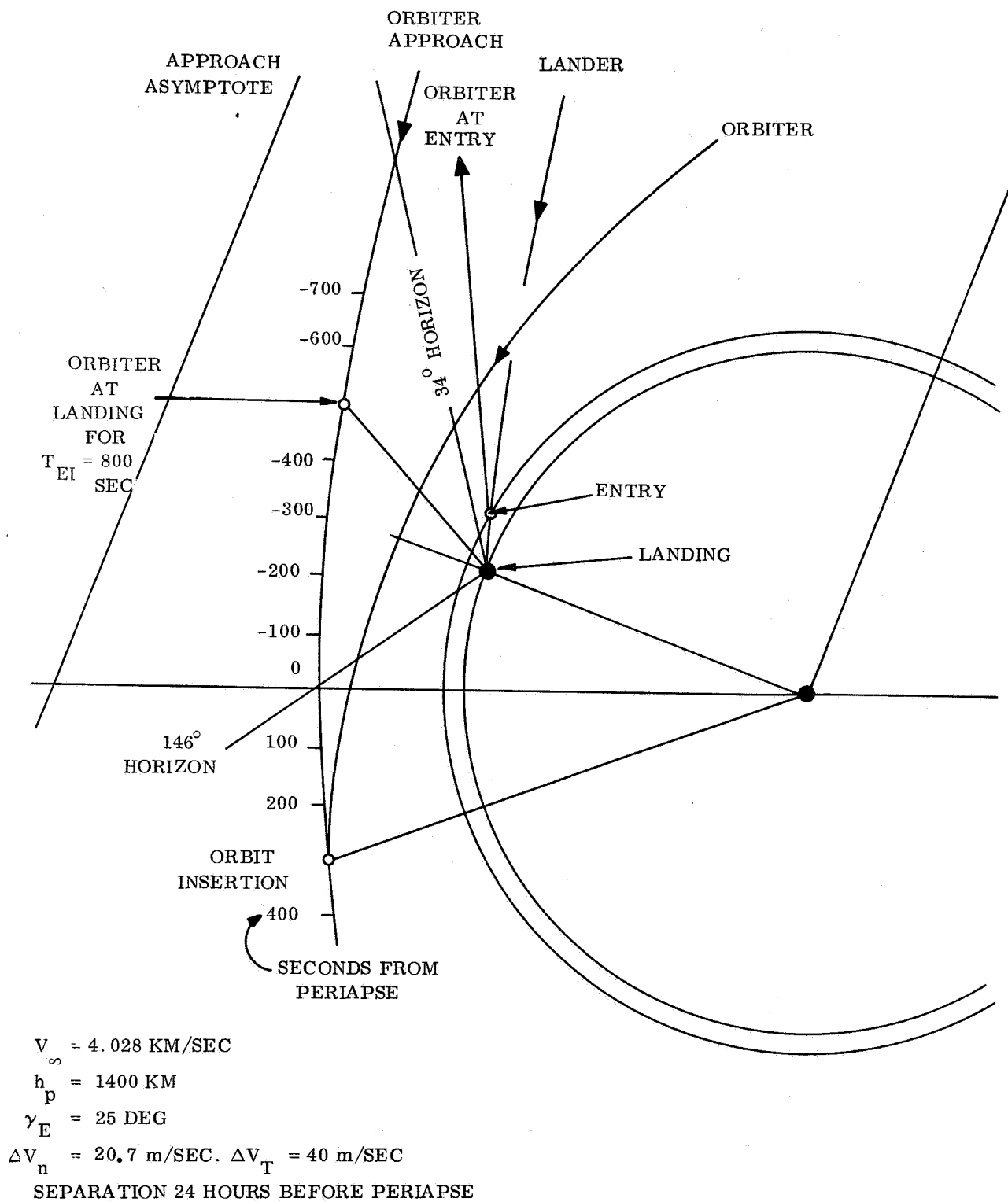
Figure 3.1-36. Approach and Orbit Insertion

$V_\infty = 4.028$ KM/SEC

$h_p = 1400$ KM

$\gamma_E = 25$ DEG

$\Delta V_n = 20.7$ m/SEC, $\Delta V_T = 40$ m/SEC

SEPARATION 24 HOURS BEFORE PERIAPSE
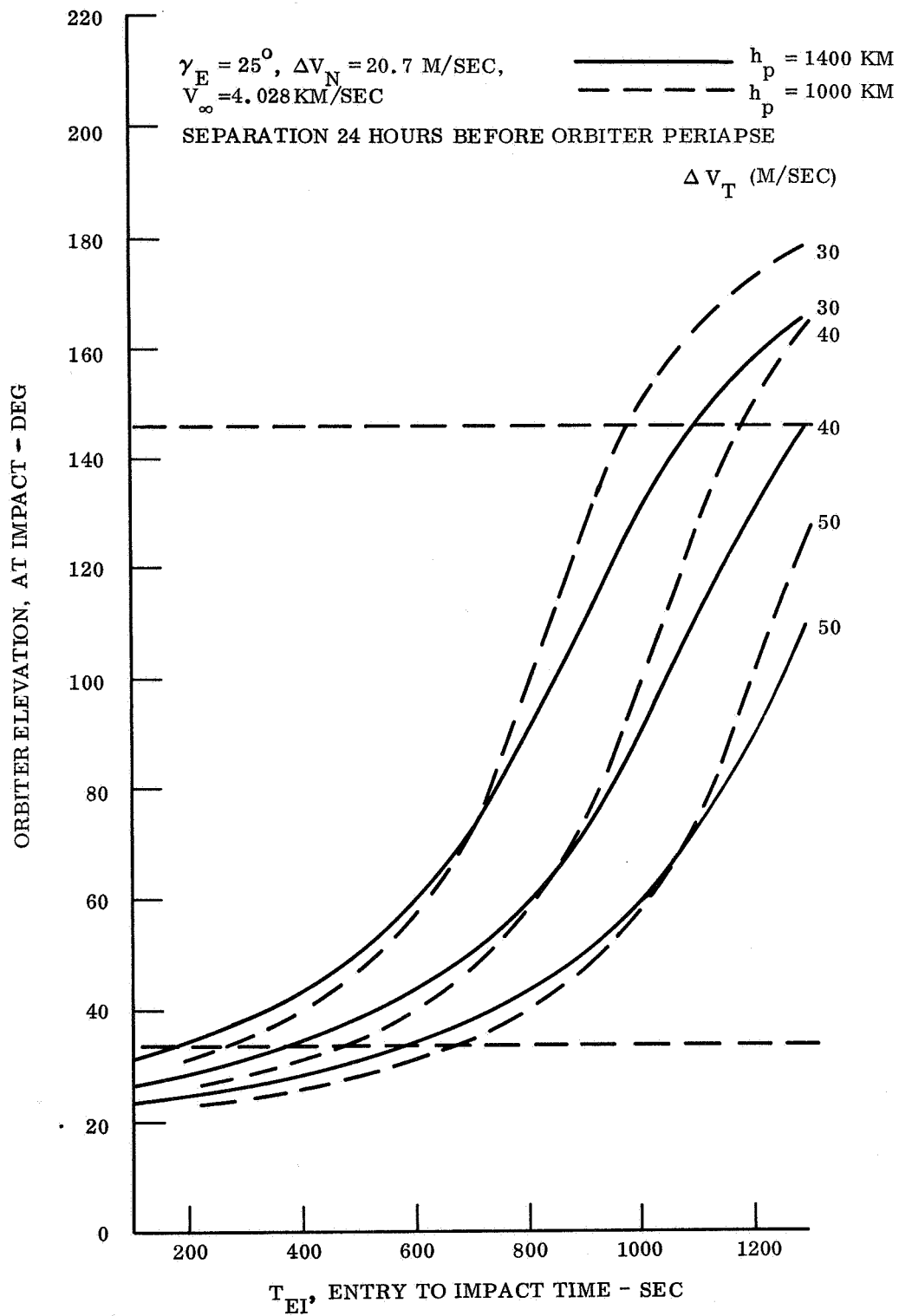
Figure 3.1-37. Determination of Tangential Separation Velocity

3.1.2.3 Reference Mission Summary

The complete reference mission for direct entry is obtained by combining the results of paras 3.1.2.1 and 3.1.2.2. To obtain the required orbit inclination of 10.74° the aimpoint is chosen at a point 6190 km from the planet center, 9.45° below the T-axis (see fig. 3.1-33). If separation is to occur 24 hours before the Orbiter periapse passage the required velocity increment has a component normal to the spacecraft velocity of 20.7 m/sec, and a tangential component of 40 m/sec.

The pertinent mission parameters are listed in table 3.1-7.

3.1.2.4 Communication After Landing

Information related to the design of communication and power subsystems is presented in this section. Since the trajectory time from entry to landing is not a priori known, the data is presented for entry times of 400, 800 and 1200 sec. In each case the separation condition, and therefore the entry condition, is the same. Six parameters are shown as functions of time near the end of the first orbit after landing in figs. 3.1-38 through 3.1-40 and A-43 through A-48. The information is slightly in error during the first few minutes of these plots, because at the time of landing the S/C has not yet been inserted into orbit. The computations which resulted in these plots, on the other hand, treated the S/C as if it were already in orbit at the time of landing. The same parameters are also computed for the entry phase, up to landing, with the S/C properly in its hyperbolic trajectory (see para 3.1.2.5). If precise information is required, the inconsistency could be removed by a simple interpolation between the two sets of data.

The six parameters (illustrated in figs. 3.1-12 and 3.1-13) are:

EIS = elevation of Sun at the landing site

EIE = elevation of Earth at the landing site

EIB = elevation of Orbiter at the landing site

R   = relay communication range

COA = cone angle of Lander at Orbiter

CLA = clock angle of Lander at Orbiter.

The graphs are arranged as listed in table 3.1-8.

Viewtimes during which the Lander can see the Orbiter above the 34 and 0° horizons and maximum communication ranges are listed in table 3.1-9. This table lists also the view times immediately after landing and the elevation of Sun and Earth at the instant of landing. The Earth is below the horizon, as is to be expected at any landing during 1974, which occurs 30° from the evening terminator.

SYNCHRONOUS ORBIT
TEI = 800 SEC
LANDING LATITUDE = 10° N.
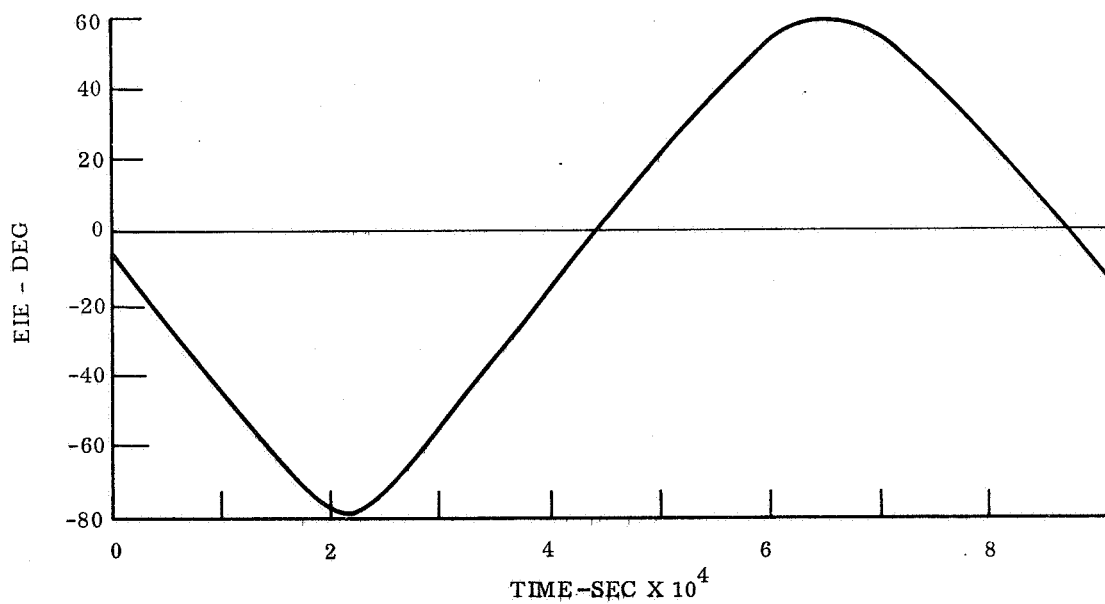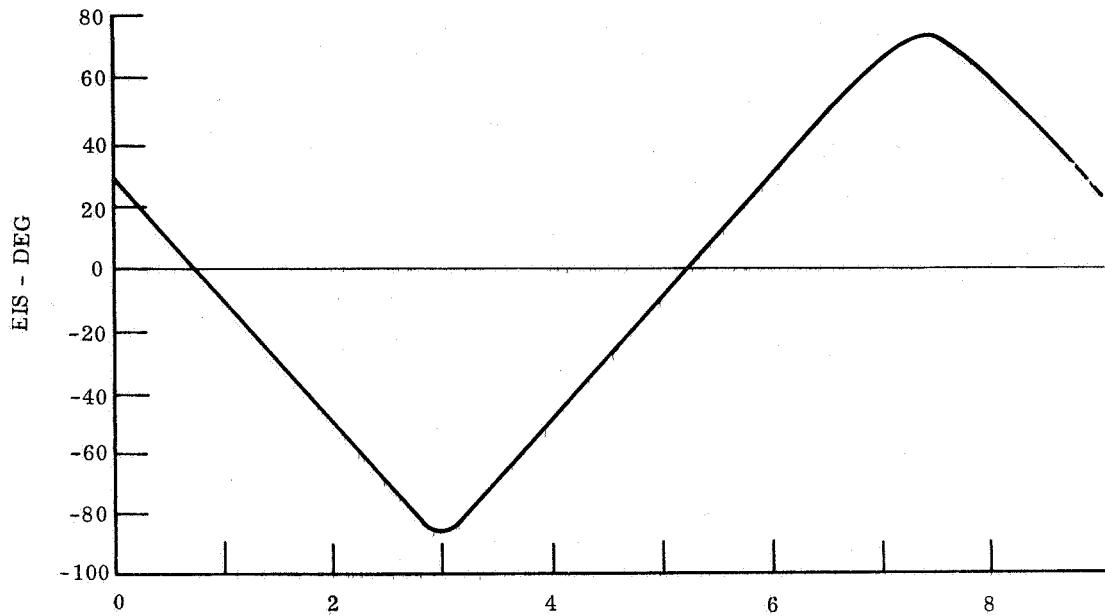
EIS = SUN ELEVATION ABOVE HORIZON
EIE = EARTH ELEVATION ABOVE HORIZON

Figure 3.1-38.   Earth and Sun Elevations at Landing Site During First
Orbit After Landing
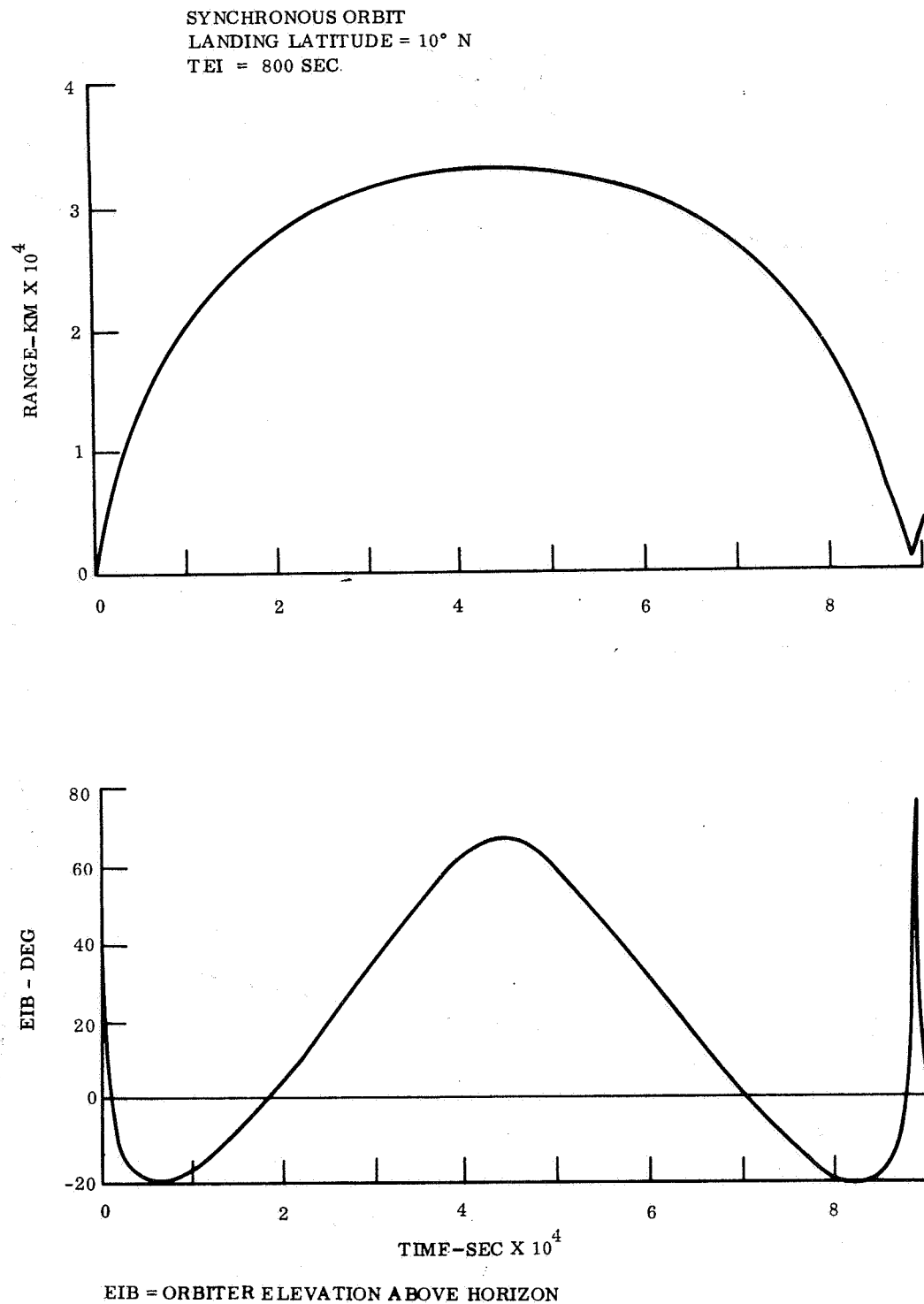
Figure 3.1-39. Relay Communication Range and Orbiter Elevation at Landing
Site During First Orbit After Landing
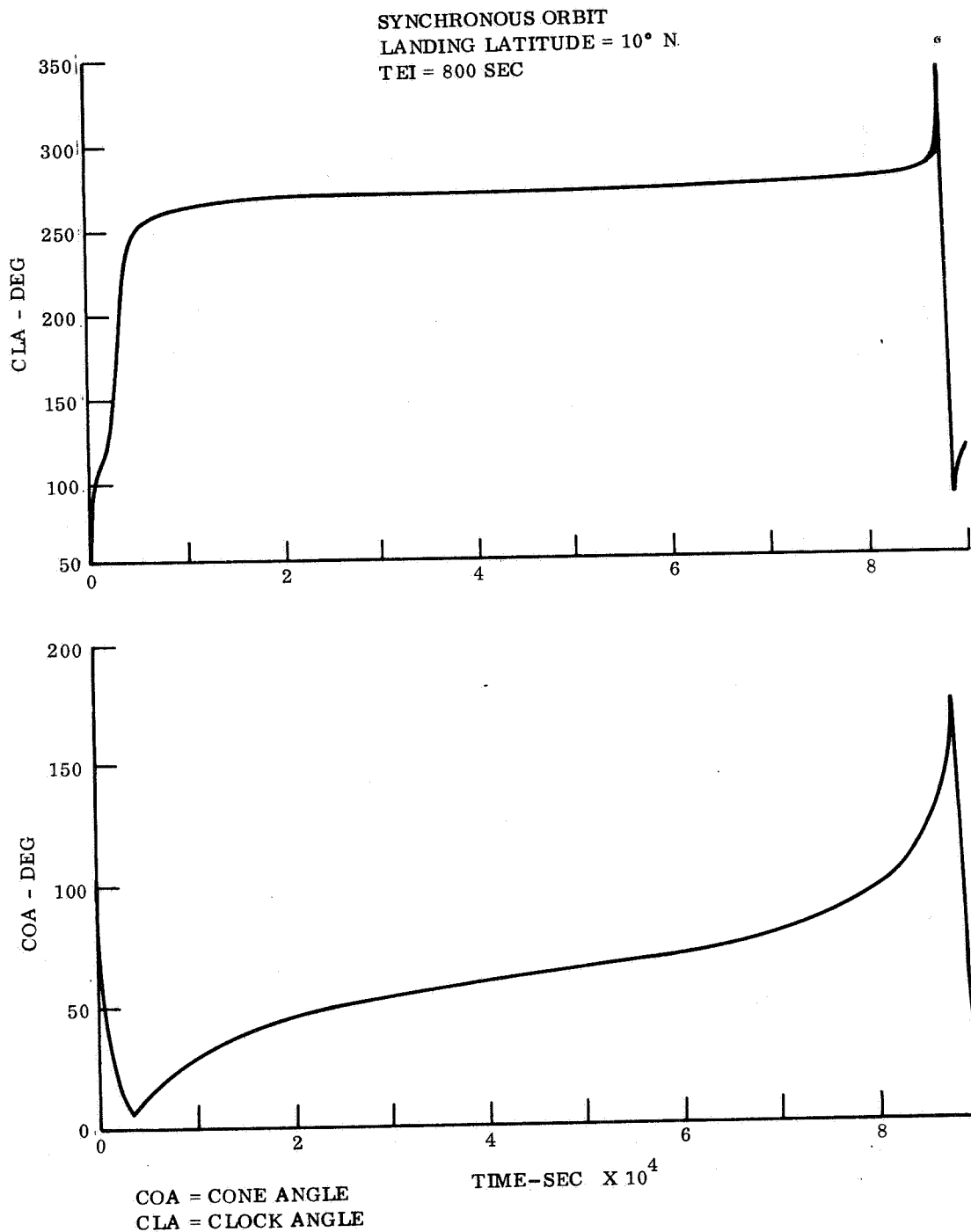
Figure 3.1-40. Lander Clock and Cone Angle at Orbiter During First Orbit After Landing

TABLE 3.1-8. POST LANDING PARAMETERS

Time, Entry to Landing (sec)		400	800	1200
Figure Numbers For:	EIS EIE	A-43	3.1-38	A-46
	R EIB	A-44	3.1-39	A-47
	COA CLA	A-45	3.1-40	A-48

TABLE 3.1-9. DIRECT REFERENCE MISSION
10° North Latitude Landing Site

Post Landing Viewing Times				
Entry Time (sec)		400	800	1200
View Time (min) Orbiter Elevation 0 deg		22.5	16.3	9.2
View Time (min) Orbiter Elevation 34 deg		15.0	8.8	1.5
Periapsis Communication Parameters				
Entry Time		400	800	1200
View Time (min) Orbiter Elevation 0 deg		40.5	40.3	42.1
View Time (min) Orbiter Elevation 34 deg		12.7	12.8	12.2
Periapsis Communication Parameters				
Maximum Range (km) Orbiter	0 deg	4000	4100	4200
Maximum Range (km) Orbiter	34 deg	1700	1700	1700
Earth Elevation at Landing	-8.03 deg			
Sun Elevation at Landing	29.25 deg			

Note: Entry path angle = 25°
Normal deflection velocity = 20.7 m/sec ⎫
Tangential deflection velocity = 40 m/sec ⎭ at 24 hrs before encounter

3.1.2.5 Entry Trajectories

For the computation of entry trajectory and communication parameters during entry, the entry vehicle is assumed to be a 60° sphere-cone with parachute. The entry vehicle W/C_DA is 5.2 lb/ft^2 and the parachute is sized to provide a terminal velocity of 150 ft/sec in the VM-7 atmosphere. In the VM-8 atmosphere deployment is to occur at Mach 2; by monitoring the ratio of base pressure to acceleration, deployment can be made to occur at Mach 2 in the other atmospheres as well. In the computation of entry trajectories, this is provided for by using the C_D vs Mach number of the aeroshell when the Mach number is greater than 2. For that portion of the trajectory where the Mach number is smaller than 2, an artifical drag coefficient is used which, in combination with the aeroshell reference area, will give the proper drag; this drag number is 19.3 and, with the vehicle weight to reference area ratio (W/A) of 7.59 lb/ft^2, the ballistic coefficient is therefore 0.393 lb/ft^2. The resulting drag curve is shown in fig. 3.1-41. Some of the most interesting entry trajectory parameters are listed in table 3.1-10 as computed for the VM-3, -7, -8 and -9 atmospheres. In all cases the entry conditions and the position of Orbiter, Sun, Earth and Canopus at the time of entry are according to the direct entry mission definition in paras 3.1.2.1 and 3.1.2.2. More detailed information is provided in figs. 3.1-42 throug 3.1-51 and A-49 through A-78 which show ten entry parameters as functions of time from entry to landing. The graphs are arranged as listed in table 3.1-11. The Lander look angle is the angle between the negative Lander velocity vector and the direction from the Lander to the Orbiter. The cone and clock angles identify the direction in which the Orbiter sees the Lander with respect to the Sun and Canopus. The communication parameters are the same as were given for the out-of-orbit reference mission; their definition is illustrated in figs. 3.1-13 and 3.1-32.
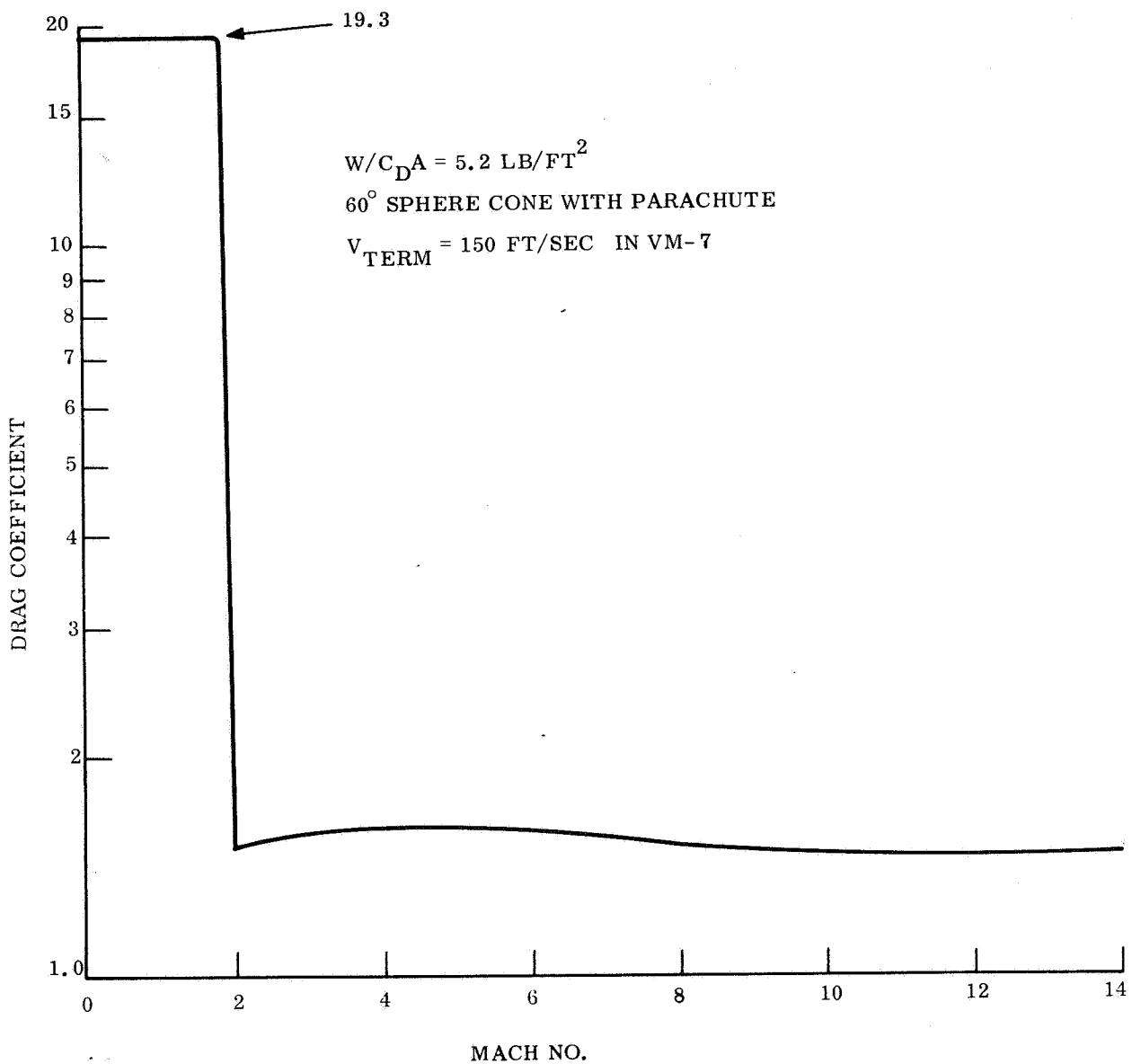
Figure 3.1-41. Drag Coefficient vs Mach Number

The chart shows:
- Y-axis: DRAG COEFFICIENT (1.0 to 20)
- X-axis: MACH NO. (0 to 14)
- Arrow pointing to value: 19.3
- $W/C_D A = 5.2 \text{ LB/FT}^2$
- 60° SPHERE CONE WITH PARACHUTE
- $V_{TERM} = 150 \text{ FT/SEC}$ IN VM-7

#3

TABLE 3.1-10. DIRECT ENTRY MISSION ENTRY PHASE

60° Sphere Cone W/C_DA = 0.16 slug/ft²	VM-3	Seconds to Impact/ (Alt km)	VM-7	Seconds to Impact/ (Alt km)	VM-8	Seconds to Impact/ (Alt km)	VM-9	Seconds to Impact/ (Alt km)
Entry Time (sec)	784		466		351		1217	
Range at Entry (km)	5320		5320		5320		5320	
Range at Landing (km)	2226		3656		4236		1810	
Elevation at Entry (deg)	35.2		35.2		35.2		35.2	
Elevation at Landing (deg)	50.2		37.8		32.8		42.8	
Central Angle Entry to Landing (deg)	8.59		9.04		9.61		8.12	
Mach 2 Parachute Deployment		660/29.0		338/19.1		231/9.3		1099/38.9
Mach 1		658/28.6		334/18.4		229/9.0		1095/38.2
Max. Deceleration (g)	18.30	702/52.9	18.2	380/43.6	48.2	255/19.0	18.5	1139/62.0
Max. Dynamic Pressure (psf)	95.1	702/52.9	94.6	380/43.6	250.6	255/19.0	96.0	1139/62.0

Parachute sized for

V_{term} = 150 ft/sec in VM-7

II

ENTRY VELOCITY   –   20,788 FT/SEC
ENTRY PATH ANGLE   –   25°
ENTRY ALTITUDE   –   244 KM
DRAG, SEE FIG. 3.1–41
VM–3
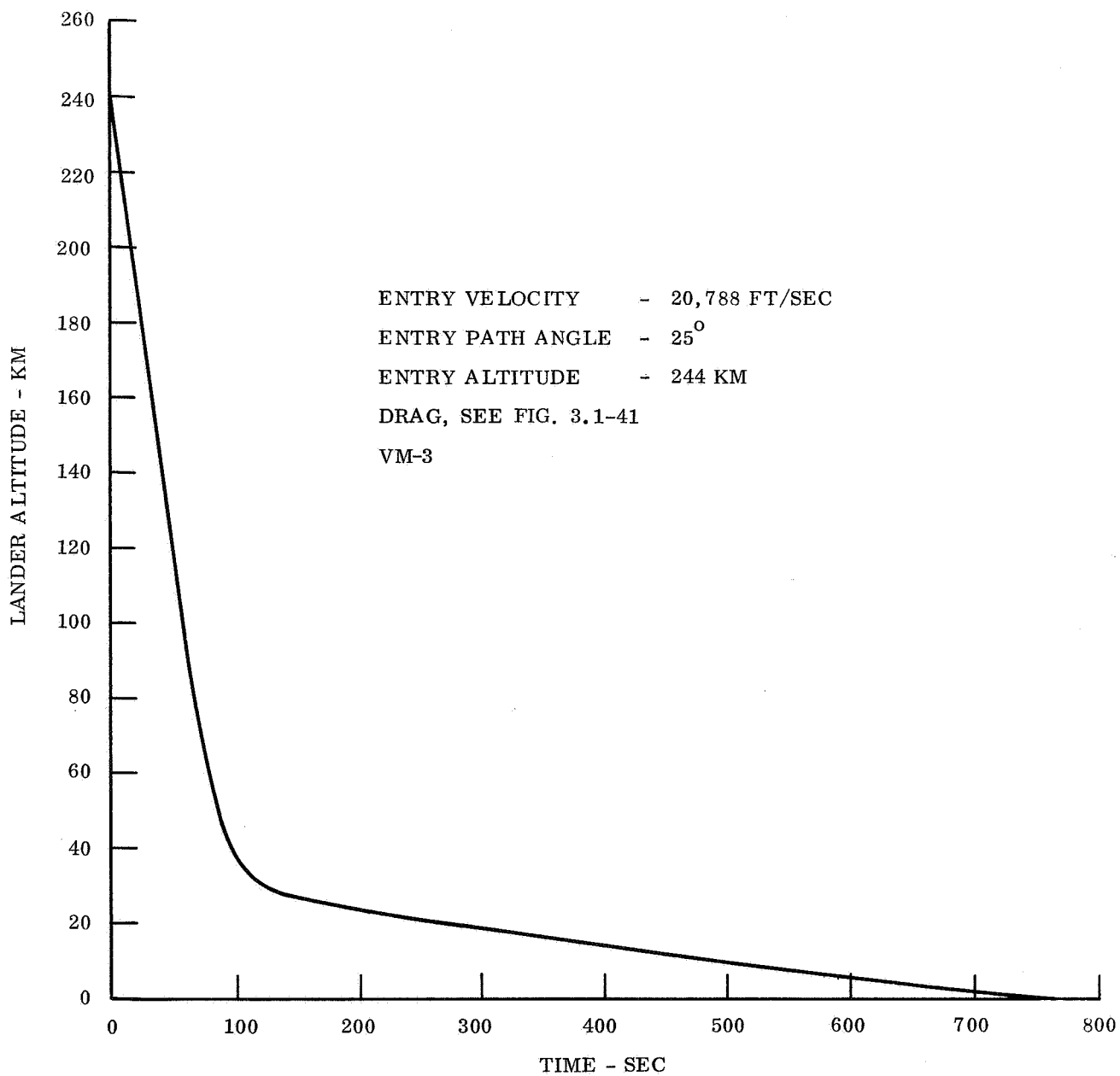
Figure 3.1-42.   Lander Altitude vs Time
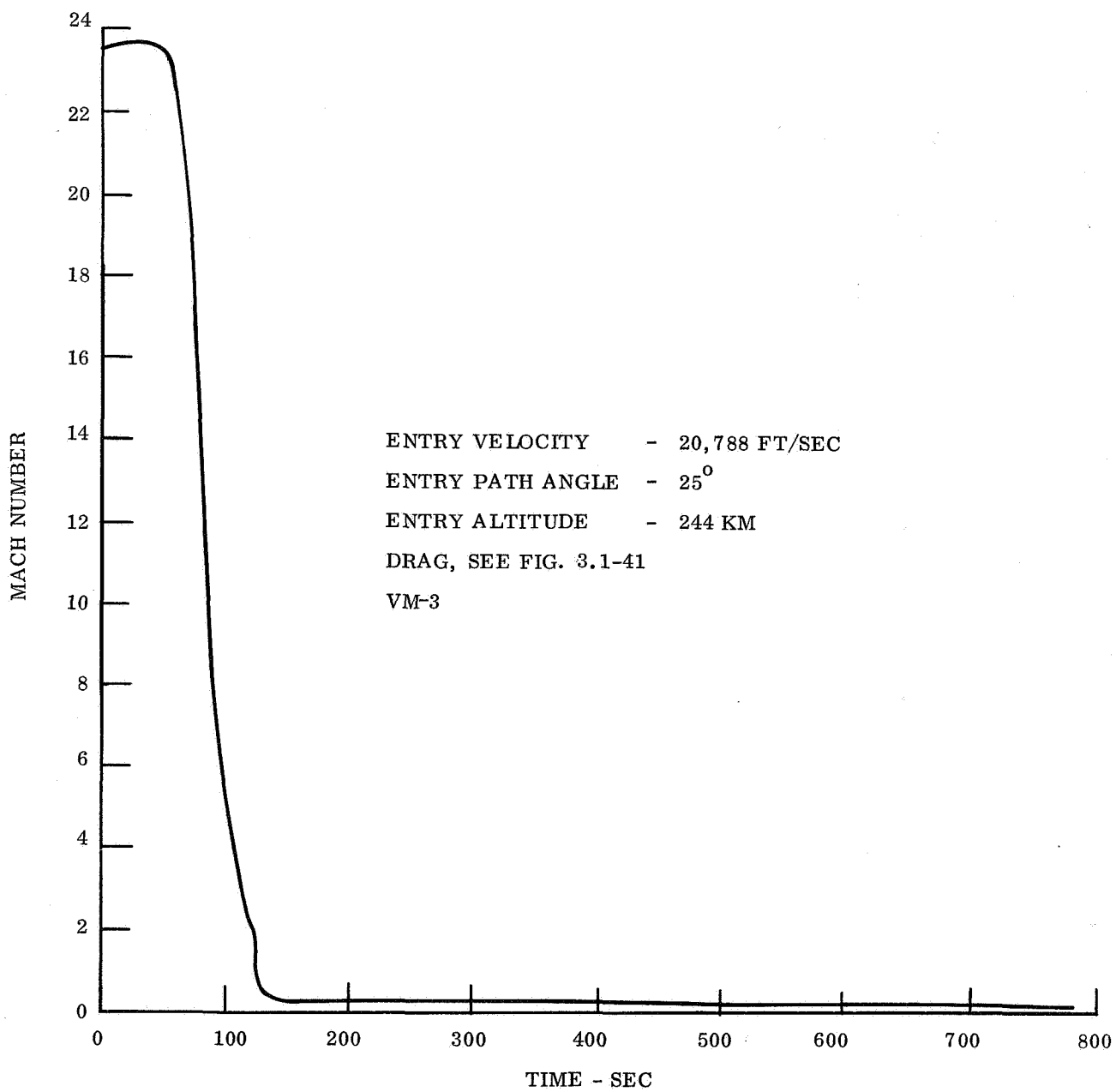
Figure 3.1-43.   Mach Number vs Time

ENTRY VELOCITY   — 20,788 FT/SEC

ENTRY PATH ANGLE   — 25°

ENTRY ALTITUDE   — 244 KM

DRAG, SEE FIG. 3.1-41

VM-3
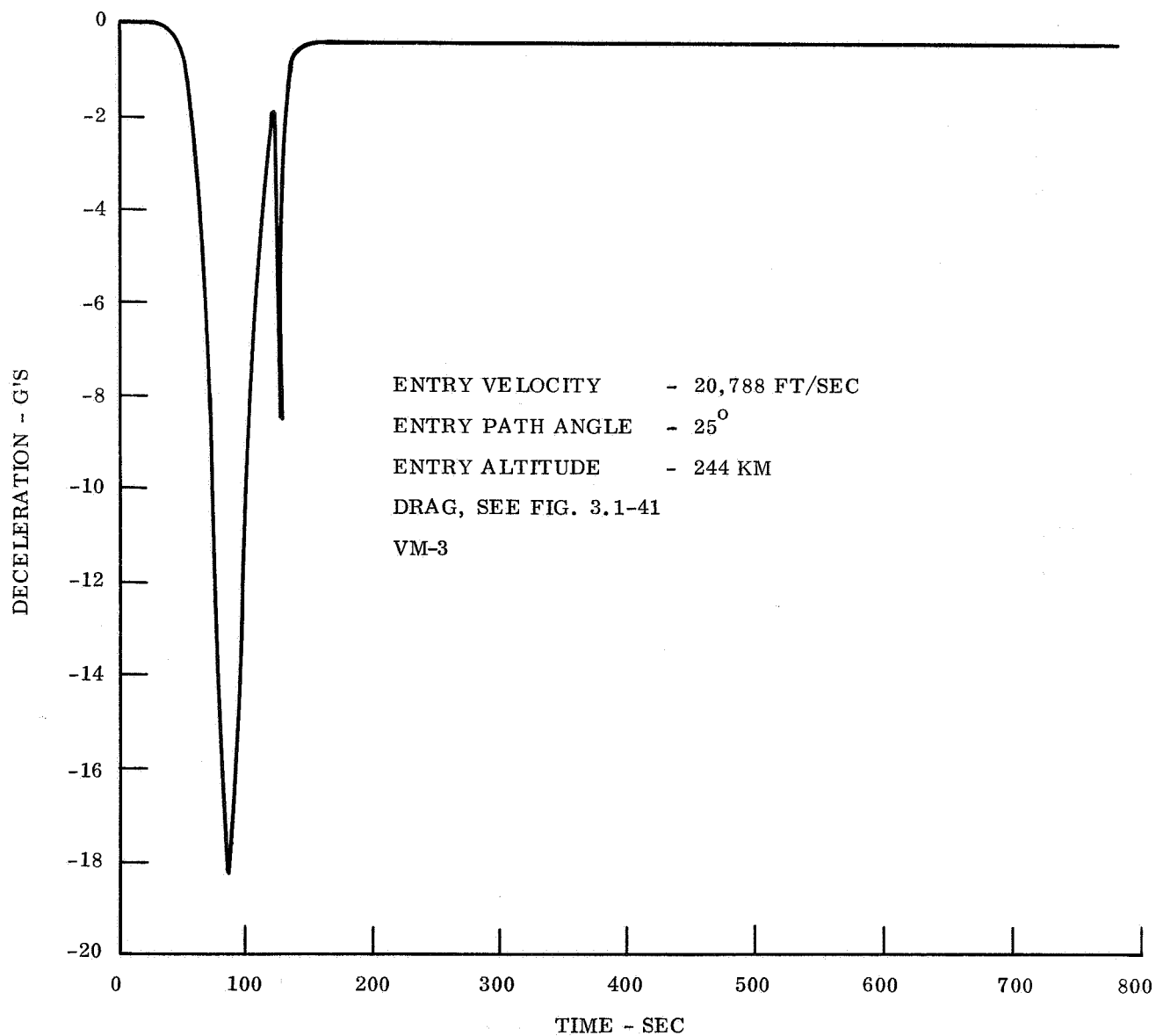
Figure 3.1-44.   Lander Deceleration vs Time

ENTRY VELOCITY   – 20,788 FT/SEC.
ENTRY PATH ANGLE – 25°
ENTRY ALTITUDE   – 244 KM.
DRAG, SEE FIG. 3.1-41
VM-3
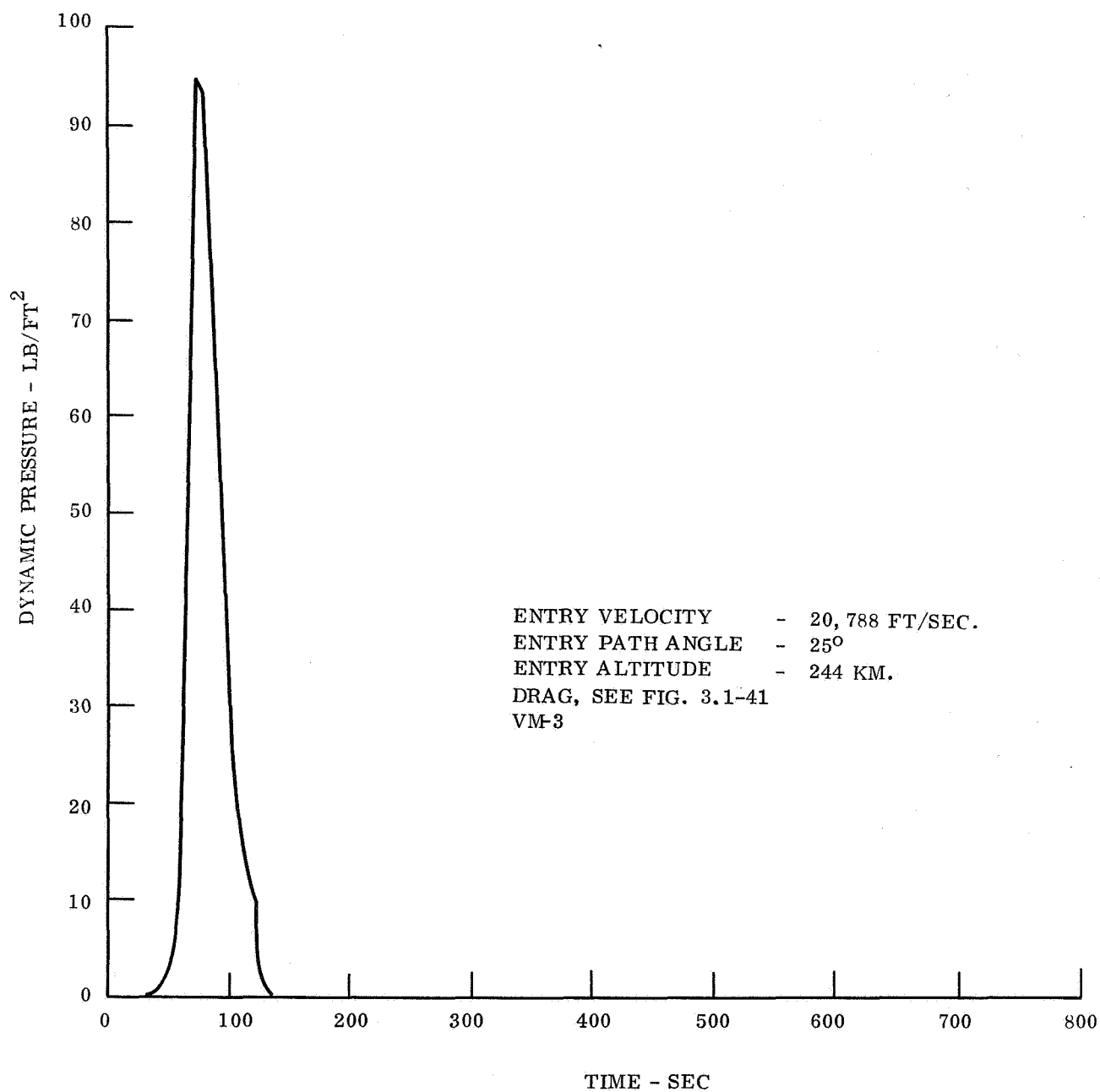
Figure 3.1-45. Dynamic Pressure vs Time

ENTRY VELOCITY   – 20,788 FT/SEC
ENTRY PATH ANGLE – 25°
ENTRY ALTITUDE   – 244 KM
DRAG, SEE FIG. 3.1-41
VM-3
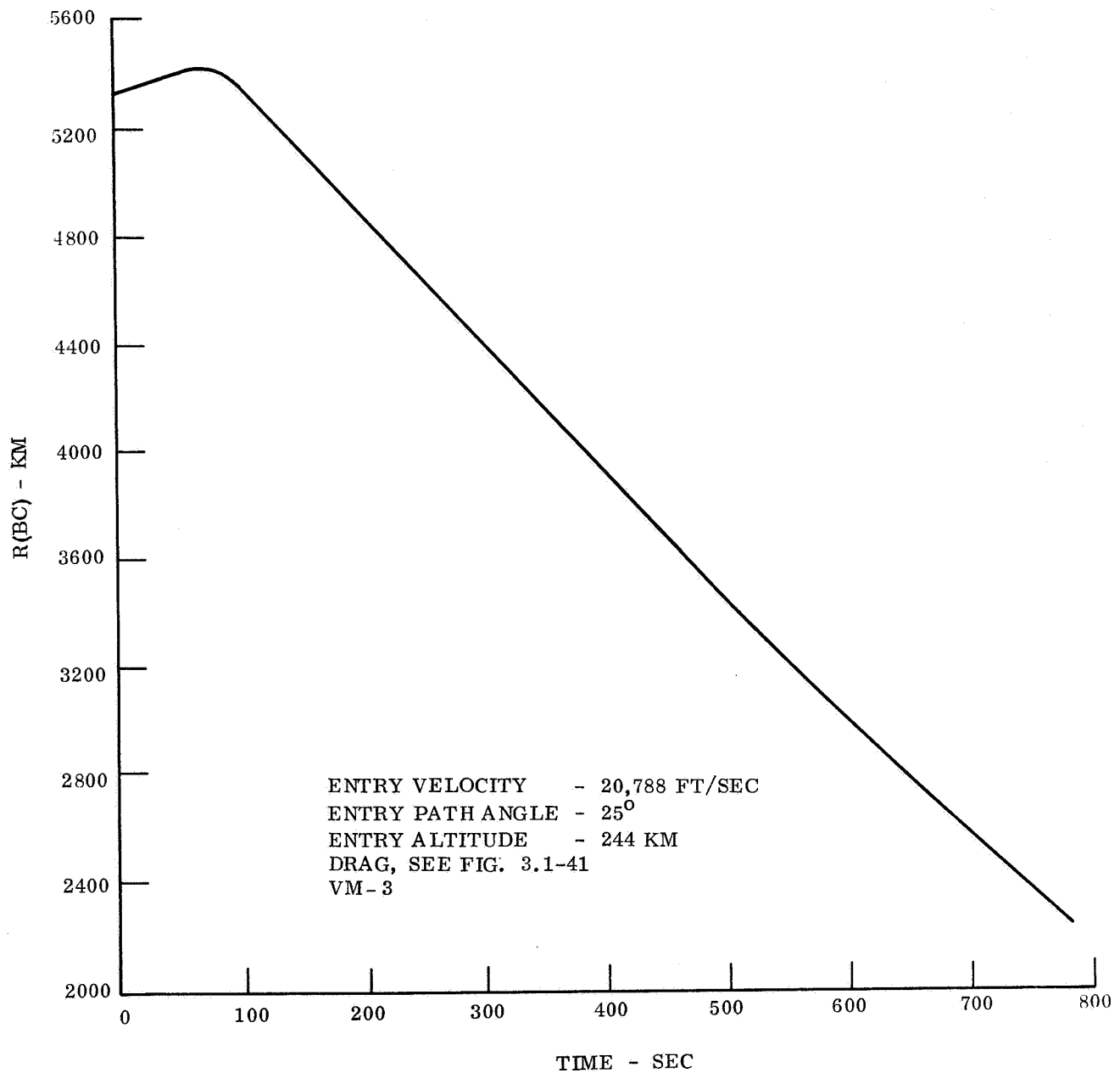
Figure 3.1-46. Communication Distance R (BC) vs Time

The figure shows a plot of V(BC) - KM/SEC versus TIME - SEC, with the vertical axis labeled from 1. at top to -5. at bottom and the horizontal axis from 0 to 800.

ENTRY VELOCITY   - 20,788 FT/SEC
ENTRY PATH ANGLE   - 25°
ENTRY ALTITUDE   - 244 KM
DRAG, SEE FIG. 3.1-41
VM-3
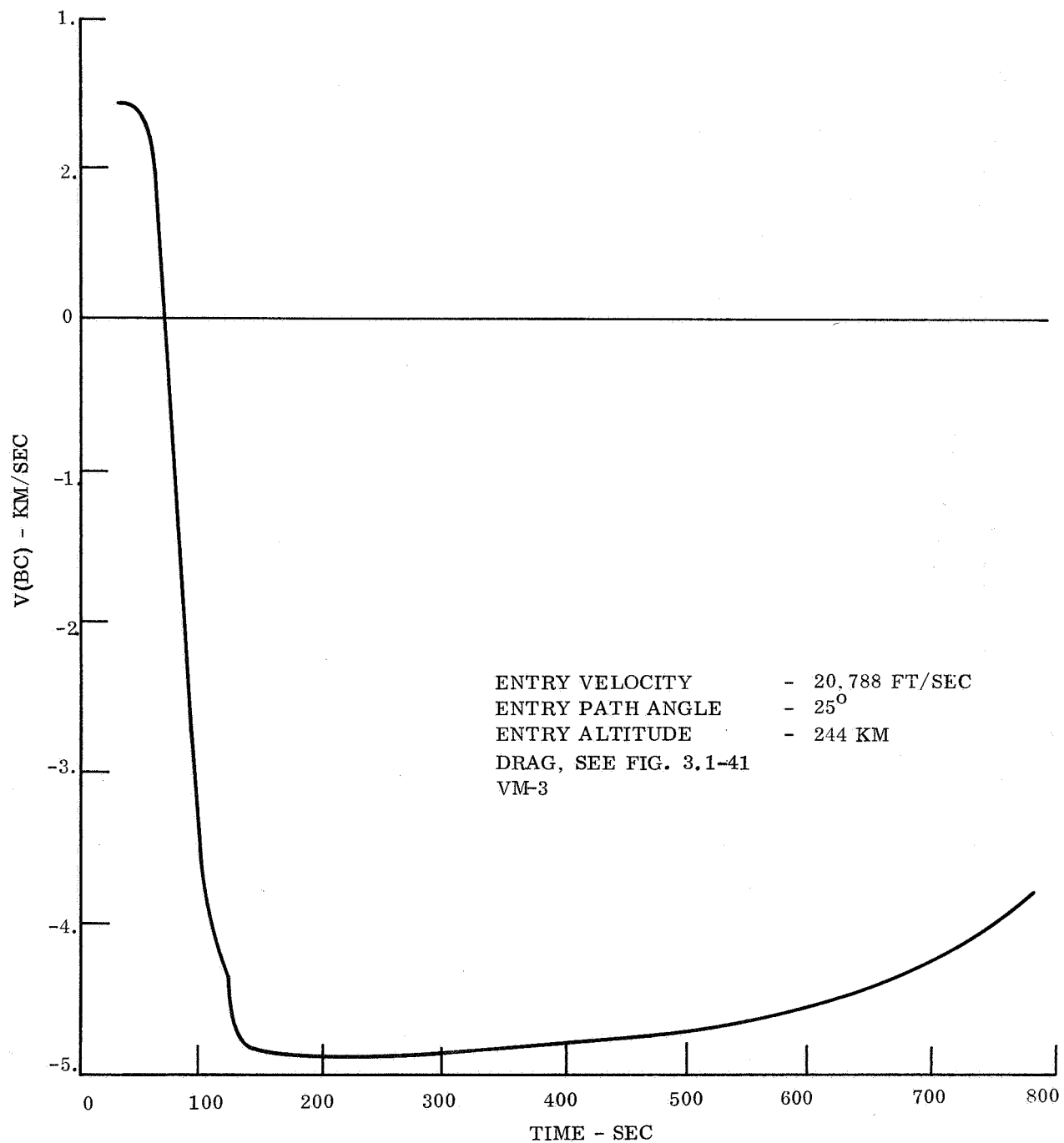
Figure 3.1-47. Range Rate vs Time
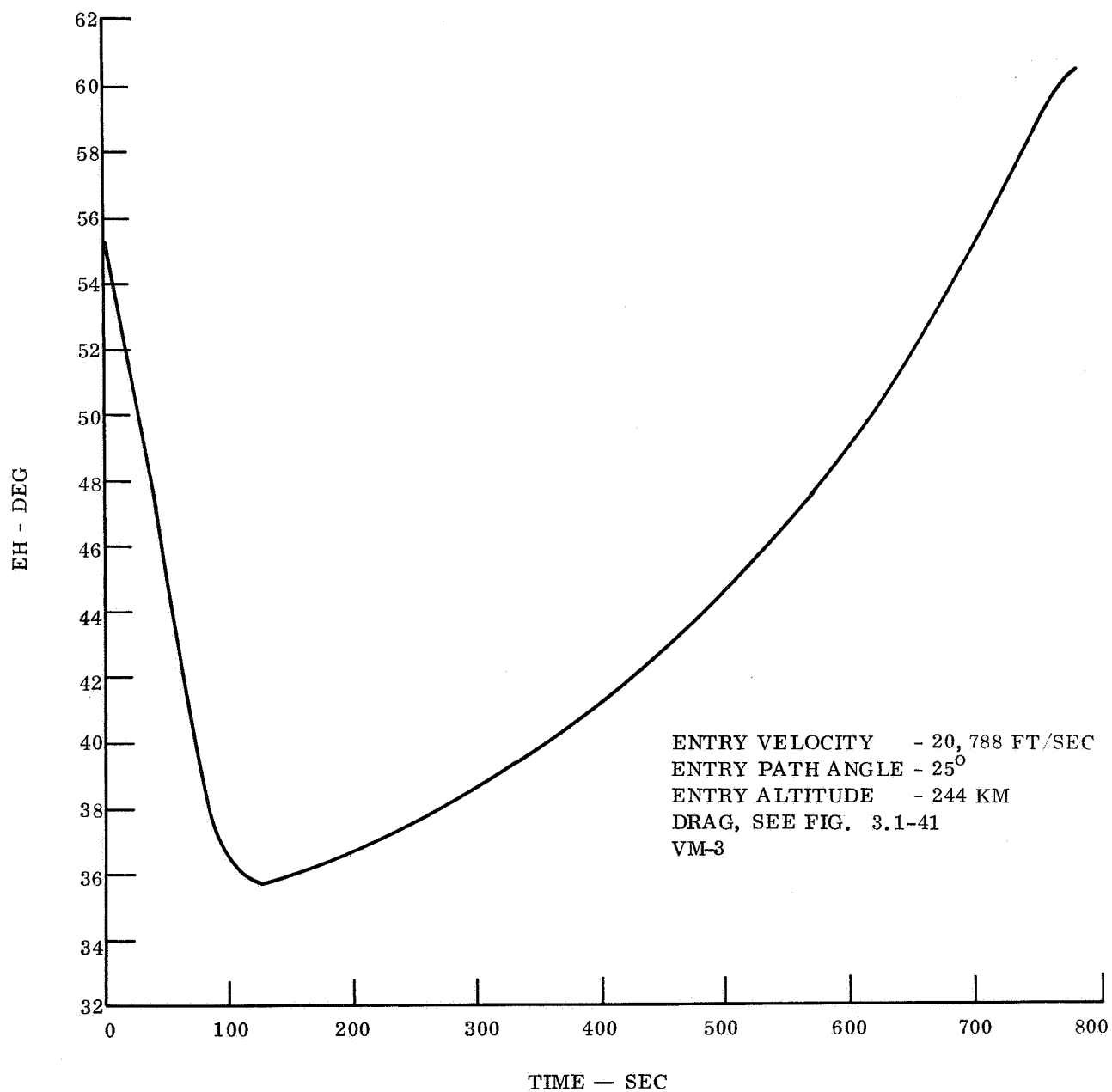
Figure 3.1-48. Angle at which Lander Sees Orbiter Above Horizon

The figure plots EH – DEG (vertical axis, ranging from 32 to 62) versus TIME – SEC (horizontal axis, ranging from 0 to 800). The curve starts near 55 degrees at time 0, drops to a minimum of about 36 degrees near 130 seconds, then rises steadily to about 60.5 degrees at 780 seconds.

ENTRY VELOCITY   – 20,788 FT/SEC
ENTRY PATH ANGLE – 25°
ENTRY ALTITUDE   – 244 KM
DRAG, SEE FIG. 3.1-41
VM-3
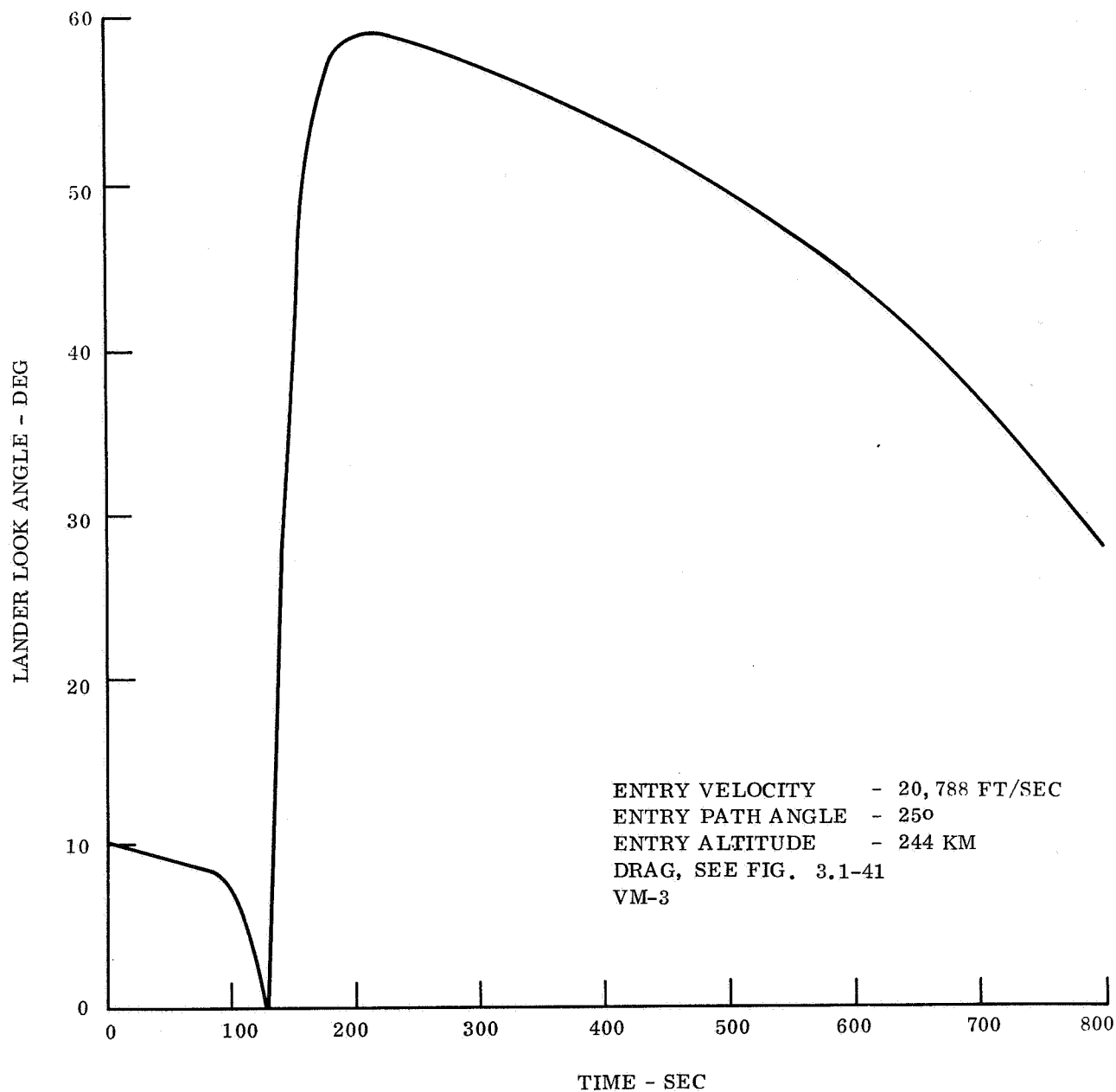
Figure 3.1-49. Lander Look Angle vs Time
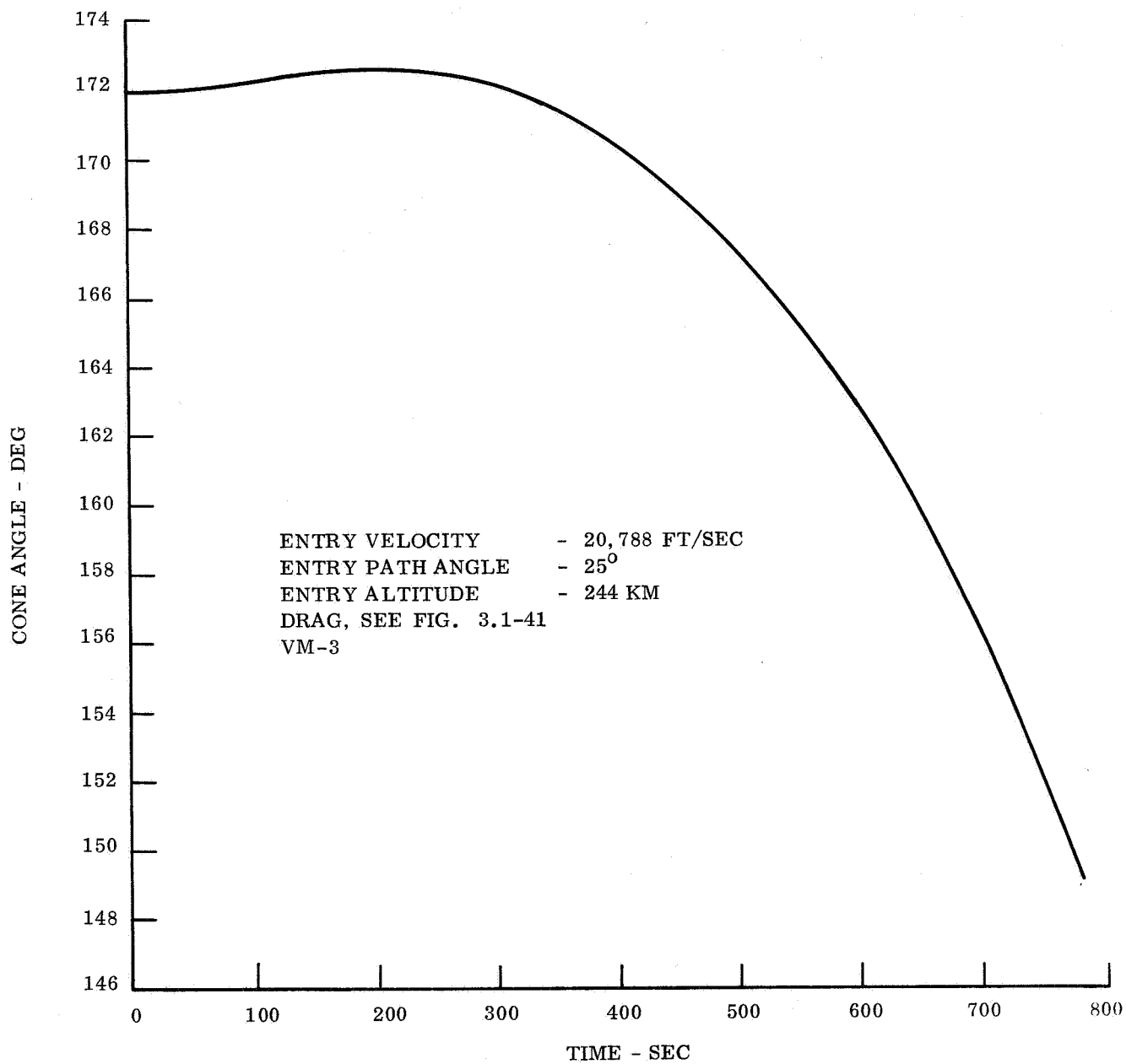
Figure 3.1-50. Cone Angle vs Time

The chart shows CONE ANGLE - DEG (y-axis, 146 to 174) versus TIME - SEC (x-axis, 0 to 800).

Annotation on chart:

ENTRY VELOCITY — 20,788 FT/SEC
ENTRY PATH ANGLE — 25°
ENTRY ALTITUDE — 244 KM
DRAG, SEE FIG. 3.1-41
VM-3

ENTRY VELOCITY   – 20,788 FT/SEC.
ENTRY PATH ANGLE   – 25°
ENTRY ALTITUDE   – 244 KM
DRAG. SEE FIG. 3.1-41
VM 3
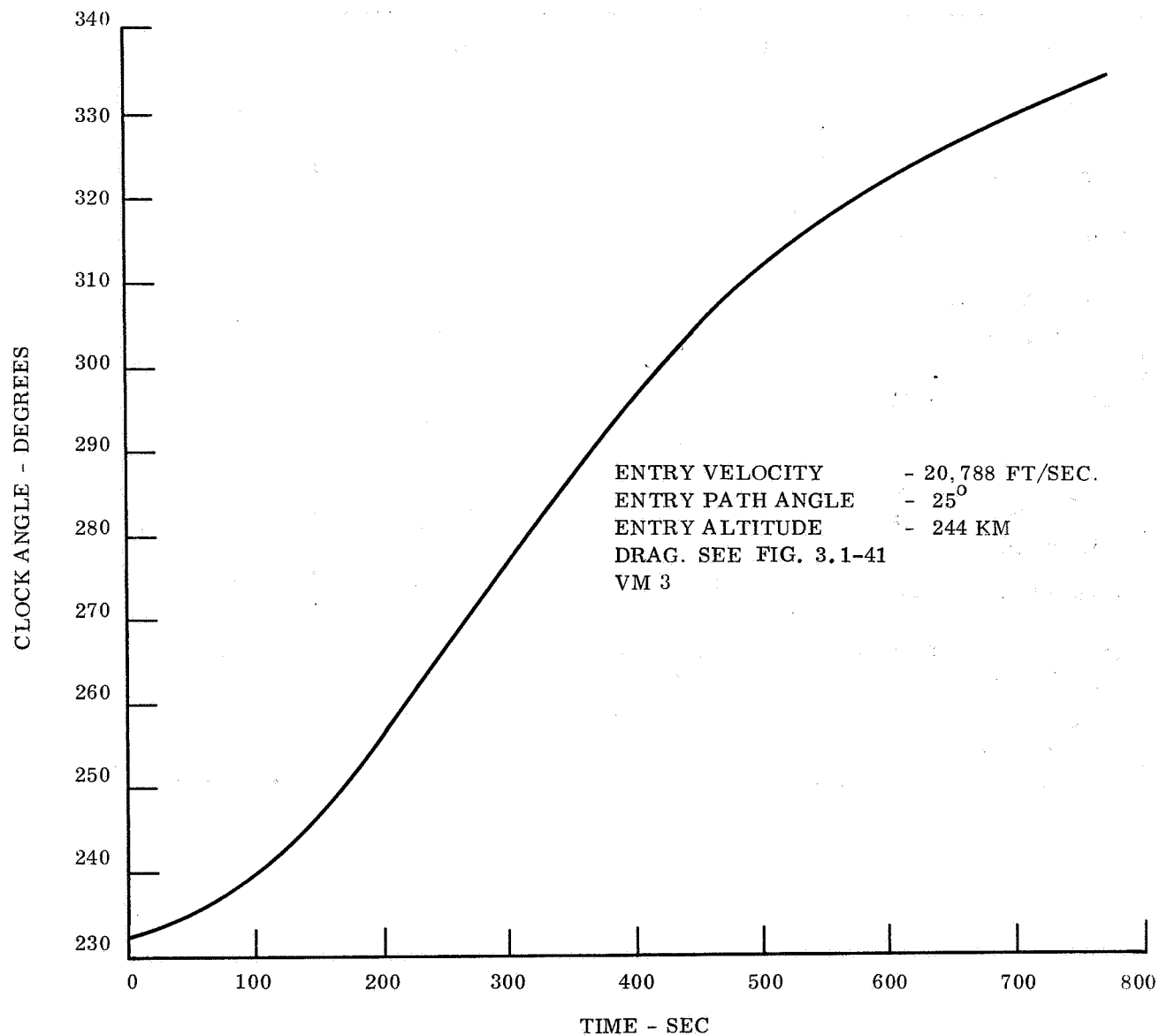
Figure 3.1-51. Clock Angle vs Time

TABLE 3.1-11. ENTRY TRAJECTORY PARAMETERS

Atmospheres	Figure Numbers			
	VM 3	VM 7	VM 8	VM 9
Altitude	3.1-42	A-49	A-59	A-69
Mach No.	-43	-50	-60	-70
Deceleration	-44	-51	-61	-71
Dynamic Pressure	-45	-52	-62	-72
Relay Communication Distance	-46	-53	-63	-73
Relay Communication Range Rate	-47	-54	-64	-74
Angle at which Lander Sees Orbiter Above Horizon	-48	-55	-65	-75
Lander Look Angle	-49	-56	-66	-76
Cone Angle of Lander at Orbiter	-50	-57	-67	-77
Clock Angle of Lander at Orbiter	-51	-58	-68	-78

3.2 PATH ANGLE AND DOWNRANGE DISPERSIONS

In this section the previously defined out-of-orbit entry and direct entry reference missions are subjected to a simple dispersion analysis. The parameter of prime interest is the downrange dispersion, or length of landing footprint. The downrange dispersion is made up of two parts: the dispersion due to the range of atmospheres from VM-8 to VM-9 and the dispersion of entry path angle. In general, errors in entry trajectories are due to errors in entry path angle, entry velocity, and out-of-plane displacement of the entry point. However, the entry velocity is in all cases subject to only very small errors, and the out-of-plane error can be considered separately from in-plane errors. Therefore, the downrange dispersion may be considered to be directly dependent on only the entry path angle.

The error in entry path angle, in turn, has two causes: the errors in Lander separation velocity (magnitude and direction), and the errors in either the approach trajectory or the spacecraft orbit.

The downrange dispersion goes along with differences in flight time from entry to impact, and the downrange dispersion, together with the entry time, influence the relay communication between Lander and Orbiter. The entry path angle and downrange dispersions for the out-of-orbit entry and direct entry reference missions are determined in the following two sections. Their effect on the relay communication is shown for the two extremes in atmospheres, VM-8 and VM-9.

3.2.1 DISPERSIONS OF OUT-OF-ORBIT ENTRY REFERENCE MISSION

Because of the accuracy with which the orbit is expected to be established, the contributions of orbit errors on the path angle dispersion are small compared to the contributions of errors in separation velocity, magnitude, and direction. Therefore, only separation velocity errors are considered in what follows.

A numerical error analysis of the reference mission results in the following expressions for path angle and downrange dispersion (at entry):

$$\delta \gamma_E = -26.00 \, \frac{\delta \Delta V}{\Delta V} - 0.506 \, \delta \varphi$$

$$\delta \beta_E = 50.8 \, \frac{\delta \Delta V}{\Delta V} + 0.869 \, \delta \varphi$$

where:

$\delta \gamma_E$ = error in path angle

$\delta \beta_E$ = error in central angle from separation to entry

$\delta \Delta V$ = error in separation velocity magnitude

$\delta \varphi$ = error in separation velocity direction (with respect to direction of orbit major axis).

All angles are expressed in degrees.

The reference mission is defined by:

1. Synchronous orbit

2. Entry velocity = 15,300 ft/sec

3. Entry path angle = 16°

4. Deorbit true anomaly = 235°

5. Deorbit velocity = 234.8 m/sec; deorbit velocity direction = 37.6°.

Based on root-sum-squaring the two error sources, fig. 3.2-1 shows the dependence of the entry path angle error on the magnitude and direction of separation velocity. It is seen that, if 0.5 percent is taken as a reasonable assumption for the one sigma error of velocity magnitude, a three sigma error of one degree is obtained in the path angle if the one sigma error in velocity direction is 0.6 degree. The effect of a $\pm 1^{\circ}$ change in path angle is about 610 km in downrange dispersion at landing, including the effect of the range of atmospheres from VM-8 to VM-9. This compares well with the 700 km diameter of Syrtis Major, and the following dispersion results are therfore based on the three sigma error of 1° in entry path angle.

The dispersion analysis of the out-of-orbit entry reference mission was performed by choosing combinations of velocity errors which result in entry path angles of 15 and 17°. Corresponding trajectories were run in the VM-8 and VM-9 atmospheres for the vehicle as defined in Section 3.1.1, but with parachute deployed at altitude = 6.66 km. This different parachute deployment was introduced at this point in the mission analysis because in establishing the reference mission (Section 3.1), it was found that the entry time differential between VM-8 and VM-9 atmospheres was too great for the landing event to be observed in all cases. Deploying the parachute at the VM-8 Mach 2 altitude (this requires an altimeter) reduces the entry time differential from about 800 sec to about 250 sec. The results are shown in tabular form in table 3.2-1. Of particular interest in these results are the various entry times and the downrange dispersion which is shown as an error in the downrange central angle β_{EI}. Note that each degree difference in error of this angle corresponds to 59 km on the planet surface. A pictorial presentation of the dispersions is shown in fig. 3.2-2 which indicates the positions of the Orbiter at the time of landing for the four cases which result from combining the two atmospheres and the two path angles.

The effect of these dispersions on the post landing relay communication is shown in fig. 3.2-3. This figure shows at which time (referred to the time of landing) the spacecraft is seen at 10, 15, 34 and 45° elevations. The first four lines are for the reference mission with parachute deployed at Mach 2. This was the case for which the deorbit conditions were designed, according to the condition that, in any atmosphere, the Orbiter should be seen above the 34° elevation at the time of landing; as explained before (see Section 3.1) this condition is not quite met. The next six lines are for the dispersion cases defined in this section; the same deorbit condition is used (subject to

separation velocity errors), but the parachute is deployed at VM-8 Mach 2 altitude.*
The last three lines are for a redesigned deorbit condition (see Section 3.3) according
to the condition the maximum available relay communication time is obtained.

3.2.2 DISPERSION OF DIRECT ENTRY REFERENCE MISSION

In the case of the direct entry mission it cannot be simply assumed that the
entry path angle error depends only on the separation velocity errors. In fact, the
dominant error source is the error in impact parameter of the approach trajectory.
Other error sources do exist, but they are insignificant in comparison to errors in
impact parameter and velocity magnitude and direction (at least in a root-sum-square
sense). A simple analytical error analysis on the cosine of the entry path angle re-
sults in the following numerical expressions, when applied to the reference trajectory:

$$\delta\,(\cos\gamma_E) = 1.22\,\frac{\delta B}{B} - 0.304\,\frac{\delta\Delta V}{\Delta V} + 0.612\,\delta\varphi$$

$$\delta\,(\cos\beta_E) = 3.04\,\delta\,(\cos\gamma_E),$$

where:

γ_E = the path angle

β_E = the central angle from separation to entry

B = impact parameter

ΔV = separation velocity magnitude

$\delta\varphi$ = separation velocity direction error (in radians).

---

* In the initial phases of this study when considering the influence of a radar
altimeter on the entry trajectory, it was decided to use, as the altimeter 'mark'
altitude for parachute deployment, the value corresponding to MN 2.0 for
parachute deployment, the value corresponding to MN 2.0 for the VM-8 atmos-
phere (i.e., the lowest 'MN 2.0 altitude' of all the VM models). This meant
that while each set of entry V_e/γ_e combinations had a different design mark
altitude setting, for any particular set of entry conditions the mark altitude
setting could never result in parachute deployment at a MN greater than 2.0
regardless of the atmosphere model encountered. For the two selected refer-
ence missions, the mark altitude setting were 6.7 km for the out-of-orbit entry
case and 9.3 km for the direct entry case.

During the latter phases of the study, however, it became evident that it was
desirable to delay parachute deployment to the lowest allowable altitude in order
to minimize the parachute descent time and thereby provide the longest possible
time for relaying data during the period after landing. With this objective and
as discussed in para 2.3.3.2, a mark altitude of 6.1 km (20,000 ft) was later
selected for use with all entry conditions and VM model atmospheres. The re-
sults shown in figs. 3.2-3 and 3.2-6 were based on the earlier ground rules but
are indicative of the mission improvements that can be achieved through the use
of a radar altimeter.

REFERENCE MISSION:

γ_E = 16 DEG

ΔV = 234.8 M/SEC

f_{OD} = 235 DEG ϕ = 37.6^o

V_E = 15,300 FT/SEC

$\delta \gamma_E = -26.60 \dfrac{\delta \Delta V}{\Delta V} -0.506 \, \delta \phi$

PATH ANGLE DISPERSION:

$\dfrac{\delta \Delta V}{\Delta V}$ (1 σ)

1.0%

0.5%

0.3%

$\delta \gamma_E$, DEG (3σ)

2.5
2.0
1.5
1.0
0.5
0

$\delta \phi$, DEG (1 σ)

0.5   1.0   1.5
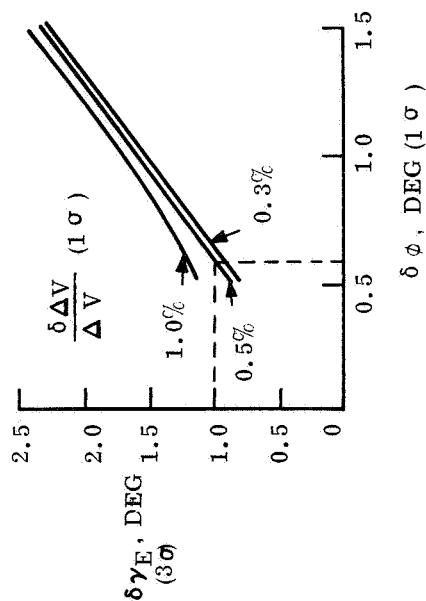
DOWN RANGE DISPERSION: $\delta \beta_E = 50.8 \dfrac{\delta \Delta V}{\Delta V} +0.869 \, \delta \phi$

$\dfrac{\delta \Delta V}{\Delta V}$ = .5% (1 σ)

$\delta \phi$ = .6° (1 σ)

$\delta \gamma_E = 1^o$ (3 σ)

$\delta \beta_E = 1.74^o$ (3 σ)

ϕ

ΔV

γ_E

β_E

f_{OD}
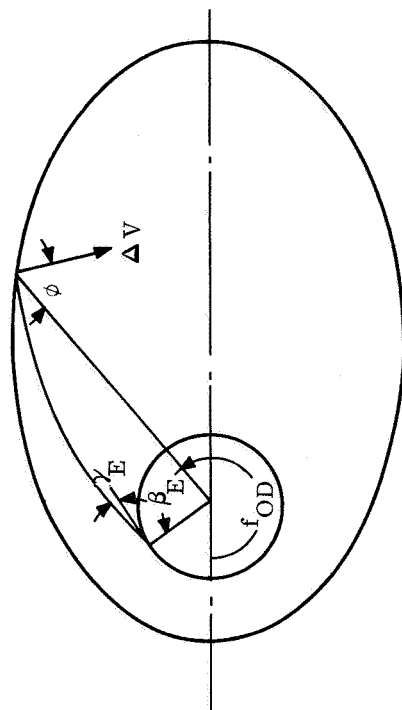
Figure 3.2-1. Out-of-Orbit Entry, Dispersion

II

TABLE 3.2-1. OUT-OF-ORBIT ENTRY DISPERSIONS

Atmosphere	VM-8	VM-8	VM-8	VM-9	VM-9	VM-9
Entry Path Angle (deg)	15	16	17	15	16	17
Entry Velocity (ft/sec)	15312	15300	15293	15312	15300	15293
Time, Separation to Entry (sec)	5376	5349	5324	5376	5349	5324
Time, Entry to Landing (sec)	511	463	430	680	649	625
Range at Entry, Lander to Orbiter (km)	2202	2191	2183	2202	2191	2183
Elevation at Entry, Lander to Orbiter (deg)	31.4	33.4	35.3	31.4	33.4	35.3
Entry True Anomaly (deg)	-26.48	-28.40	-30.05	-26.48	-28.40	-30.05
Central Angle, Entry to Landing (deg)	20.78	18.17	16.33	16.58	15.16	13.98
δ Central Angle, Entry to Landing (deg)	2.61	0	-1.84	1.42	0	-1.18
Range at Landing (km)	1774	1784	1791	1162	1186	1209
Elevation at Landing (deg)	31.7	34.5	37.1	54.8	66.3	67.9
Per Angle (deg)	-5.70	-10.23	-13.72	-9.90	-13.24	-16.07

Downrange Dispersion: One degree of central angle entry to landing equals 59 km on Mars surface.

Parachute Deployment at h = 6.66 km

Reference Mission: $f_{o_D} = 235^o$, $\Delta V = 234.8$ m/sec, $\gamma_E = 16^o \pm 1^o$, $V_E = 15300$ ft/sec

DISPERSION: $\delta\gamma_E$ = ±1 DEG (3σ)

PARACHUTE DEPLOYED AT 6.66 KM

β = 14 PSF; V_{TERM} = 150 FPS IN VM-7
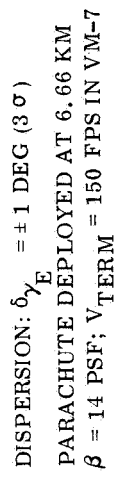
ENTRY PATH ANGLE	VM8			VM9		
	15	16	17	15	16	17
TIME, ENTRY TO LANDING, (SEC)	511	463	430	680	649	625
LANDING TRUE ANOMALY, (DEG)	5.7	10.2	13.7	9.9	13.2	16.1
TIME, LANDING TO 34° (SET)	699	657	620	450	411	385

TOTAL DOWNRANGE DISPERSION: 613 KM

X   LANDING POINT, VM-8 ATMOSPHERE

△   LANDING POINT, VM-9 ATMOSPHERE

Figure 3.2-2. Out-Of-Orbit, Relay Communication

ELEVATION

LANDING

TIME FOR SETTLING, DEPLOYMENT

TIME, SEC

-400 -200 -100 0 100 200 400 600 800 1000 1200 1400 1600 1800 2000 2200

○ 10° RISE, 10° SET
□ 15° RISE, 15° SET
◇ 34° RISE, 34° SET
△ 45° RISE, 45° SET
(RANGE, KM)

*R/A - RADAR ALTIMETER

ALT. = 6.66 KM

REFERENCE MISSION SECTION 3.1.1

ATM	ENTRY PATH ANGLE	PARACHUTE DEPLOYMENT	DEORBIT TRUE ANOMALY	ELEVATION
VM-3	16°	M = 2	235°	60.6°
VM-7	16°	M = 2	235°	27.4°
VM-8	16°	M = 2	235°	21.6°
VM-9	16°	M = 2	235°	34.5°

(1230) (1490) (2160) (2450)
(1845) (1506) (1286) (1493) (2198) (2499)
(1800) (1460) (1290) (1500) (2930) (2550)
(1470) (2150) (2430)

ENTRY PATH ANGLE DISPERSION SECTION 3.2.1

VM-8	15°	R/A*	235°	18.7°
VM-8	16°	R/A	235°	21.7°
VM-8	17°	R/A	235°	24.2°
VM-9	15°	R/A	235°	37.7°
VM-9	16°	R/A	235°	39.7°
VM-9	17°	R/A	235°	41.6°

(1698) (1401) (1478)(1573) (2334) (2692)
(1804) (1477) (1285)(1504) (2224) (2540)
(1913) (1552) (1203)(1552) (2156) (2455)
(1467) (1399) (1521) (2220) (2537)
(1535) (1284) (1486) (2157) (2455)
(1603) (1288) (1479) (1997) (2394)

REVISED REF. MISSION SECTION 3.3

VM-8	16°	R/A	204°	2.4°
VM-3	16°	R/A	204°	0.5°
VM-9	16°	R/A	204°	3.2°

(3804) (3208) (1897) (1531) (1284) (1483) (2148) (2438)
(4032) (3390) (1981) (1589) (1290) (1482) (2119) (2396)
(4156) (3490) (2032) (1624) (1290) (1482) (2103) (2358)

Figure 3.2-3. First Relay Communication (Out-of-Orbit Entry)

As defined in Section 3.1.2, the reference trajectory is characterized by:

approach velocity = 4.03 km/sec

approach periapse altitude = 1400 km

separation time before encounter = 24 hours

entry path angle = 25$^{\text{o}}$

separation velocity components:

tangential = 40 m/sec

normal = 20.7 m/sec

Fig. 3.2-4 shows the dependence of the entry path angle error on impact parameter error and separation velocity direction error for a constant separation velocity magnitude error of one percent (one sigma). (This one percent error may be judged too large, but, as the error coefficients show, the result is not very sensitive to this error.) It is seen that, if a reasonable assumption for the one sigma impact parameter error is 100 km, the skip-out limit can be avoided if the direction error is less than 0.5$^{\text{o}}$ (one sigma). This is taken as the basis for what follows.

If the minimum path angle in the three sigma range is 16$^{\text{o}}$ (skip-out limit), the maximum angle is approximately 32$^{\text{o}}$. (For such large errors the dependence is quite nonlinear; that is why the error analysis was performed in terms of the cosine of the path angle, in which the dependence is very nearly linear.) The dispersion analysis of the direct entry reference mission was performed by choosing a combination of errors which results in the above defined range of entry path angles (actually the range came out to be from 16.5 to 31.4$^{\text{o}}$). Corresponding trajectories were run in the VM-8 and VM-9 atmospheres for the vehicle as defined in Section 3.1.2, but with parachute deployed at altitude = 9.32 km. This different parachute deployment was introduced at this point in the mission analysis to see how deployment at the VM-8 Mach 2 altitude (requiring an altimeter) may improve the probability of observing the landing event; the reduction of the entry time differential between the VM-8 and VM-9 atmospheres from about 800 sec to 300 sec not only assures that the landing event can always be seen, but also makes some post-landing communication time becomes available. The results are shown in table 3.2-2 and in fig. 3.2-5. Of particular interest is to see that the total range of downrange travel from separation to landing is 40$^{\text{o}}$, which corresponds to a landing footprint length of 2400 km. About 75 percent of this is due to the entry path angle dispersion, which in turn is mostly due to the impact parameter error.

The effect of these dispersions on the post landing relay communication is shown in fig. 3.2-6. This diagram shows the time, referred to the instant of landing, at which the Orbiter is seen at 10, 15, 34 and 45$^{\text{o}}$ elevations. The first four lines are for the reference mission as defined in Section 3.1.2, with parachute deployed at Mach 2. This was the case for which this trajectory was designed, according to the

condition that the Orbiter should be seen above a 34° elevation for landing in any atmosphere, at the time of landing. It is seen that this condition is very nearly met. The next six lines are for the dispersion as defined in this section. The same separation conditions are used, subject to the errors defined above, but the parachute is deployed at altitude = 9.32 km (the Mach 2 altitude in VM-8 for $\gamma_E = 25^{\circ}$).
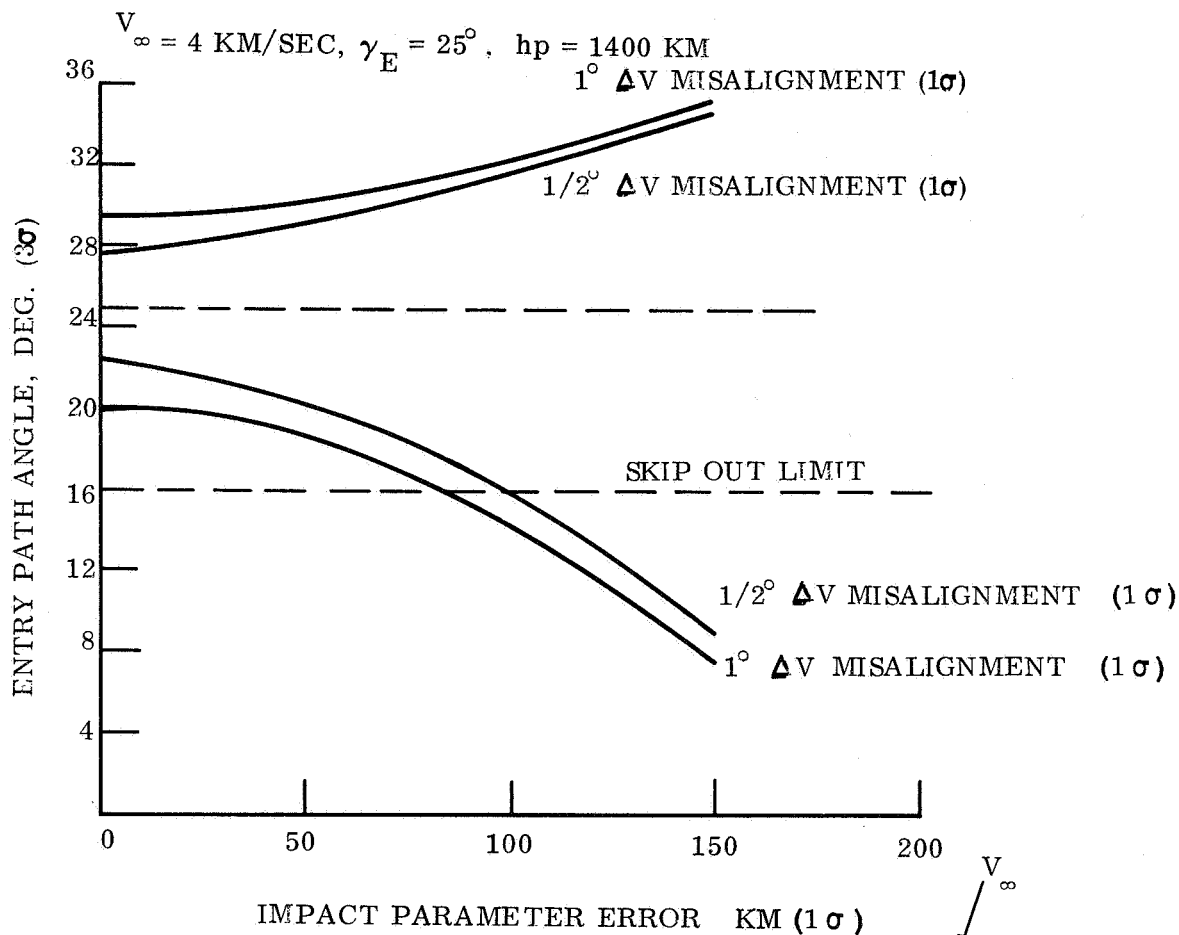
PATH ANGLE:

$$\delta\,(\cos\gamma_E) = 1.22\,\frac{\delta B}{B} - 0.304\,\frac{\delta \Delta V}{V} + 0.612\,\delta\phi$$

DOWN RANGE:

$$\delta\,(\cos\beta_E) = 3.04\,\delta(\cos\gamma_E)$$
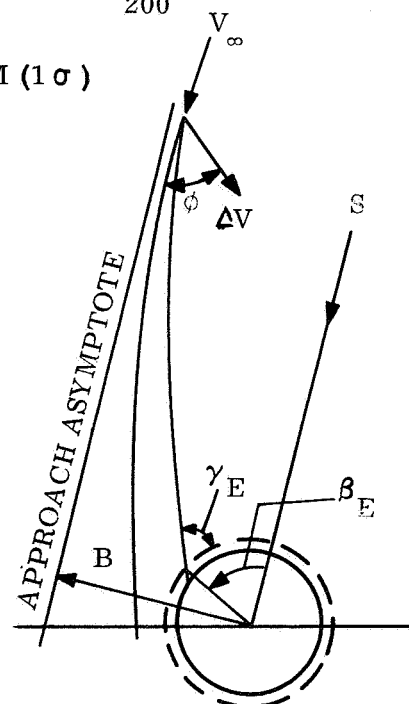
Figure 3.2-4. Direct Entry Mission, Entry Path Angle Dispersion

TABLE 3.2-2. DIRECT ENTRY DISPERSIONS

Atmosphere	VM-8	VM-8	VM-8	VM-9	VM-9	VM-9
Entry Path Angle (deg)	16.5	25	31.4	16.5	25	31.4
Impact Parameter (km)	7211	6941	6671	7211	6941	6671
Orbiter Periapse Radius (km)	5039	4786	4535	5039	4786	4535
Entry Velocity (ft/sec)	20791	20788	20786	20791	20788	20786
Range at Entry, Lander to Orbiter (km)	5537	5320	5142	5537	5320	5142
Elevation at Entry, Lander to Orbiter (deg)	24.6	35.2	43.2	24.6	35.2	43.2
Central Angle, Separation to Entry (deg)	91.05	79.90	71.79	91.05	79.90	71.79
Central Angle, Entry to Landing (deg)	26.64	9.61	6.94	15.60	8.39	6.28
Time, Entry to Landing (sec)	633	354	313	807	661	613
Elevation at Landing (sec)	12.0	32.9	43.0	37.4	49.7	58.9
Range at Landing (km)	4049	4221	4103	2650	2727	2681
PER Angle (deg)	8.7	-20.2	-31.8	-2.3	-21.4	-32.5

Downrange Dispersion: One degree of central angle from entry to landing equals 59 km on Mars surface.

Parachute Deployment at h = 9.32 km

Reference Mission: $\Delta V_T = 40$ m/sec $h_p = 1400$ km $T_S = 24$ hr $\gamma_{max} = 31.4°$

$\Delta V_N = 20.7$ m/sec $\gamma_E = 25$ deg $\gamma_{min} = 16.5°$
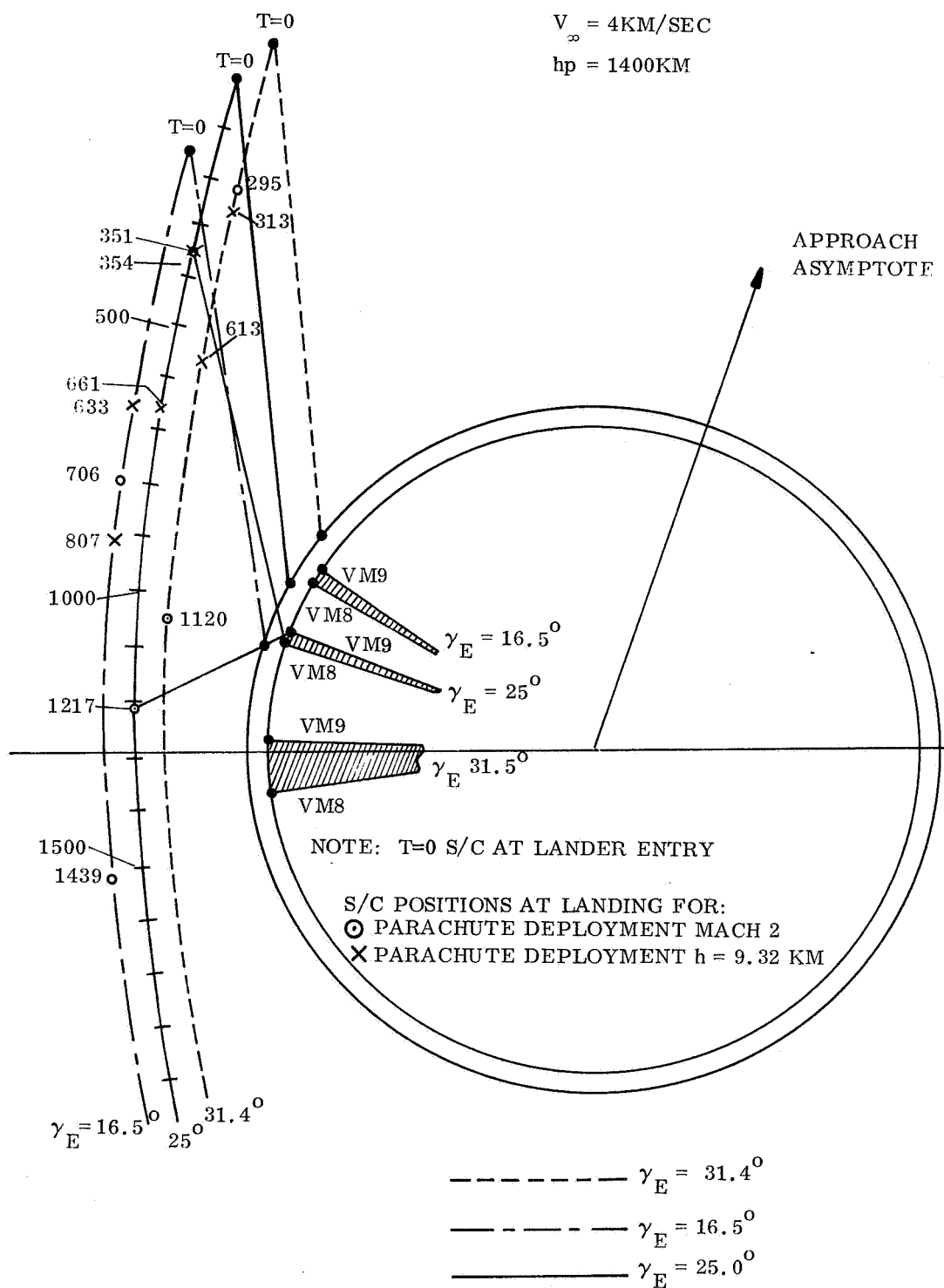
Figure 3.2-5. Direct Entry Dispersions
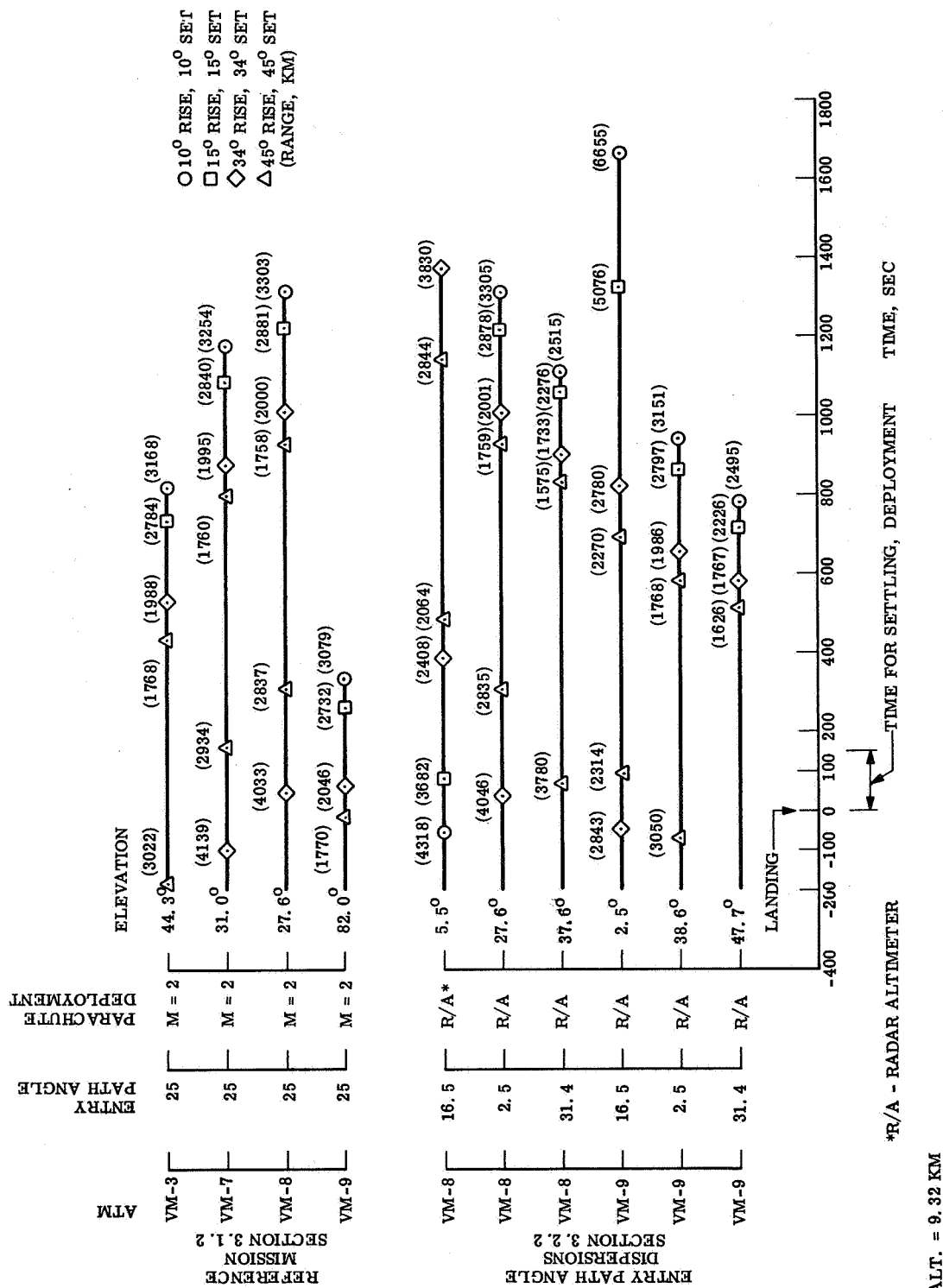
Figure 3.2-6. First Relay Communication (Direct Entry)

3.3 REVISED REFERENCE MISSIONS

As discussed in Section 3.2, the Lander separation in the out-of-orbit entry and direct entry reference missions was designed to have relay communication at the time of landing for entry into any of the VM atmospheres. The visibility horizons were assumed to be 34° and the parachute was deployed at Mach 2. Since the adjustment of the separation condition depends on the trajectory time from landing to impact, only two atmospheres need be considered: the VM-8 atmosphere to get the shortest entry time and the VM-9 atmosphere to get the longest entry time. It was seen that in the direct entry mission the requirement of seeing the landing event in all cases could be met, but also that in the out-of-orbit entry mission this requirement could not quite be met because the Orbiter time between 34° horizons is only 700 sec, while the entry time difference between the VM-8 and VM-9 atmospheres is 800 sec. This situation was greatly improved by assuming the parachute to be deployed at the Mach 2 altitude in VM-8 (this requires the availability of an altimeter); the entry time difference was hereby reduced by about 600 sec. The results, in terms of the time after landing at which the Orbiter is at certain elevations are shown in fig. 3.2-3 for the out-of-orbit entry mission and in fig. 3.2-6 for the direct entry mission. The effect of entry path angles is also shown for the case of parachute deployment at altitude.

It is seen in these figures that, with the parchute deployed at a certain altitude, some relay communication time is obtained after landing. (A minimum of 430 sec in the out-of-orbit entry case, VM-9 with $\gamma_E = 17^{\circ}$, and 580 sec in the direct entry case, VM-9, $\gamma_E = 31.4^{\circ}$). Note that this is without changing the separation conditions as first defined on the basis of seeing only entry, with parachute deployed at Mach 2. At this point, the natural question is can the separation conditions be revised to provide even better relay communication?

It is clear that the separation conditions can be adjusted on the basis of a relay communication requirement. Some requirements can be met and some can be met only partially so that a compromise is required. In order to achieve the exact opposite of the requirement of the first paragraph of this section (which may be thought of as asking for no communication time in order to be sure to see the landing event), a separation condition was defined for the out-of-orbit entry mission to give the maximum possible communication time. The result is shown in the last three lines of fig. 3.2-3. The Orbiter is seen to be rising at the 10° horizon a little after landing, after entry in the VM-9 atmosphere. By extrapolating the effect of path angle dispersions it is seen that in the worst case the Orbiter will just rise at the 10° horizon at the time of landing. The separation condition which will produce this result is obtained by the deorbit analysis method described in para 3.1.1.2. The result is shown in fig. 3.3-1. Any combination of true anomaly and entry velocity on the line in the left part of the figure will produce the desired result. It is clear that a much earlier deorbit is required (in the reference mission defined before, the deorbit true anomaly is 235°). A particular point on the curve is chosen by considering the sensitivity of the entry path angle to separation errors. This is shown in the right portion of the figure. This sensitivity decreases with decreasing true anomaly. The deorbit condition is thus: deorbit true anomaly = 204°, entry velocity = 15,250 ft/sec,

MAXIMUM POST-LANDING COMMUNICATION; ORBITER AT 10° HORIZON AT T_{EI}

MAXIMUM ENTRY TIME	650 SEC
SETTLING, DEPLOYMENT	150 SEC
$T_{EI} =$	800 SEC
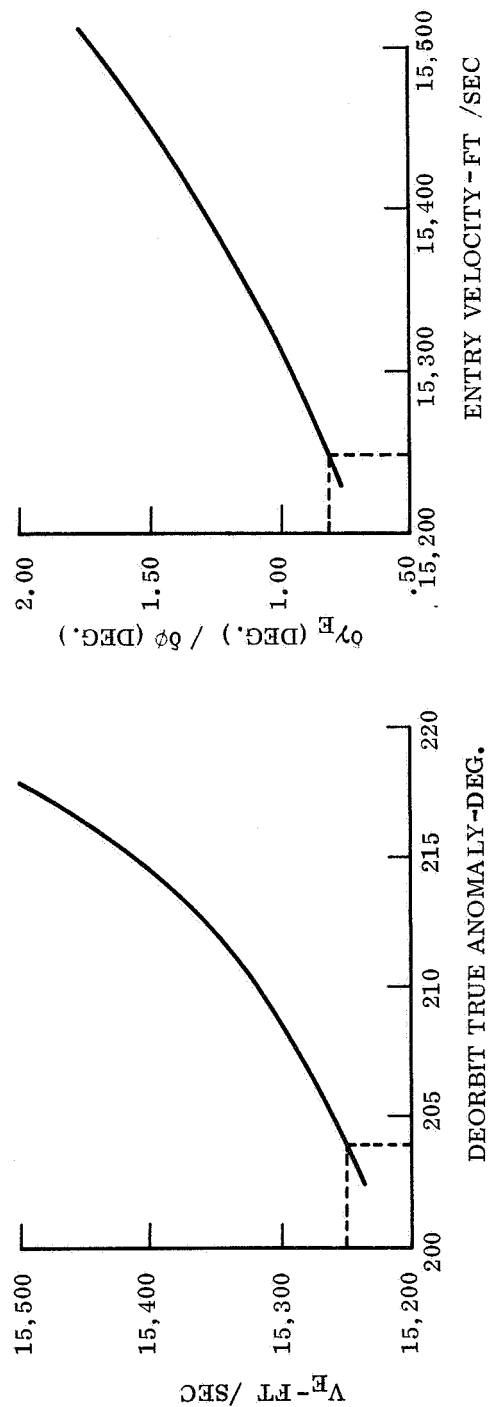
RESULTS: 1) INCREASED COMMUNICATION TIME: 500 700 300 SEC

FOR HORIZON: $10° \rightarrow 34°$ $34° \rightarrow 34°$ $34° \rightarrow 10°$

2) INCREASED DISPERSION:

$$\delta\gamma_E = 26 \frac{\delta\Delta V}{\Delta V} + .94\delta\phi \rightarrow \delta\gamma_E = 1.70° \ (3\sigma)$$

ENTRY VELOCITY - FT /SEC

$\delta\gamma_E$ (DEG.) / $\delta\phi$ (DEG.)

DEORBIT TRUE ANOMALY-DEG.

V_E - FT /SEC

Figure 3.3-1. Revised Out-of-Orbit Lander Trajectory

II

separation velocity = 144.4 m/sec. Even though the point of smallest path angle sensitivity was chosen, this sensitivity is still almost twice as large as in the earlier reference mission, $\pm 1.7^{\circ}$ in this case versus $\pm 1^{\circ}$ in the earlier case; with this goes a longerfootprint. Another result of asking for the maximum communication time is, of course, that the landing event is not seen. This means that the landing data and the data of the last part of entry must be recorded and transmitted later.

Instead of asking for communication time, it may be more reasonable to ask for the maximum number of bits that can be transmitted. Considering that for a given transmitter power the bit rate is determined by the maximum range during a pass, there is a trade-off; a long pass has a long maximum range, a short pass has a short range, and the number of bits is proportional to the time, inversely proportional to the square of the distance. This leads to a very simple result, illustrated by the following, much simplified analysis
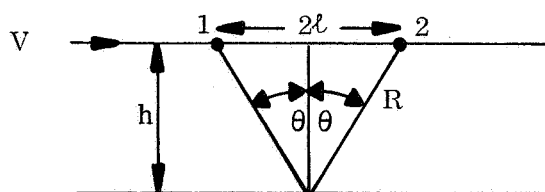
Assume the Orbiter to pass with velocity V, along a horizontal straight line, at altitude h. Optimize the half angle, θ, of the communication coverage. Let the number of bits be

$$B = k\ \frac{T}{R^2}$$

where

T is the time from 1 to 2.

Clearly,

$$T = \frac{2\ell}{V} = \frac{2h}{V}\ \tan\theta$$

and,

$$R = \frac{h}{\cos}$$

therefore:

$$B = k\ \frac{\sin 2\theta}{2V}$$

This is maximum for $\theta = 45^{\circ}$,

and

$$B_{max} = \frac{k}{hV}$$

This is shown for the actual out-of-orbit entry and direct entry passes in fig. 3.3-2. In each case the very best coverage is obtained if the landing site is at periapse, that is, at true anomaly f = 0. It is seen that in this case the result is very nearly as indicated by the simplified analysis above: the maximum number of bits is obtained for $\theta = 45^{\circ}$, and the variation with Θ is approximately according to sine 2θ. The deviation from this function (in particular that B does not vanish for $\theta = 90^{\circ}$) is caused by the curvature of the S/C and Orbiter tracks: for $\theta = 90^{\circ}$, the distance is still finite. The position of landing site at zero true anomaly cannot be obtained practically. In the out-of-orbit entry this would require exorbitantly high separation velocity and entry velocity; in the direct entry mission this position is obtained only at the low end of path angle dispersion (see fig. 3.2-5). Results for more realistic landing site true anomalies are also shown in fig. 3.3-2. (Note: The significance of the four curves in this figure does not lie in the absolute values of the number of bits but in the relative comparison. The numbers are evaluated for a system that transmits 50,000 bits per second at a distance of 2000 km.)

For fig. 3.3-2 it was assumed that the antenna gain is spherically symmetric. Figure 3.3-3 shows again the number of bits as a function of coverage half angle for the out-of-orbit entry case and for a more reasonable assumption on antenna gain; the effect of landing in a tilted position is also indicated. With the antenna gain not sperically symmetric, the angle of tilt must be considered. The antenna pattern has about 140° width but considerably greater sensitivity near the axis. The effect of this is seen in the distortion of the curves in fig. 3.3-3 as compared to the almost sine function in fig. 3.3-2.

The conclusions are now clear:

1. From figs. 3.2-3 and 3.2-6 it follows that the smaller the coverage half angle for which the pass is designed the better is the likelihood of seeing the landing event in addition to getting the desired communication.

2. From fig. 3.3-2 it follows that the coverage half angle need not be greater than 45° in order to obtain the maximum number of bits.

3. From fig. 3.3-3 it follows that, if antenna gain and tilt angle are considered, the optimum coverage half angle is about 35 to 40°.

4. It is also seen that the minimum required number of bits (10^{7}) is easily obtained in passes much smaller than the optimum passes indicated in figs. 3.3-2 and 3.3-3. This may be used to further relax the relay communication problem.

This may now be applied to the design of separation conditions as follows. The Orbiter is to be positioned such that the Lander sees it rising at the 45° horizon (or at an even higher elevation, if the maximum available number of bits is not required) at a time after landing sufficient for settling and deployment of equipment. As a first approximation, this time is estimated to be 150 sec. By observing the six lines related to the VM-8 and VM-9 path angle dispersion results in figs. 3.2-3 and 3.2-6, in particular by observing the diagrams for VM-9 and the steepest path angle in each case, it is seen that this requires the Orbiter to be delayed by about 325 sec in the out-of-orbit entry case, and about 400 sec in the direct entry case. This may easily be obtained by an adjustment of the separation conditions (velocity and deorbit true anomaly), using the methods discussed in paras 3.1.1.2 and 3.1.2.2. It may also be seen that, in the out-of-orbit entry case, the Lander will see the Orbiter near the 34° horizon at the time of landing, regardless of the path angle dispersions, if the condition is designed for a particular atmosphere. If, on the other hand, the condition is to be considered in the range of VM atmospheres, the pass is designed for the VM-9 atmosphere, but then the Orbiter is well below the 34° horizon at time of landing after entering through the VM-8 atmosphere. In the direct entry case (fig. 3.2-6) it is seen that a 45-45° pass cannot be obtained in addition to always seeing the landing event if only a specific atmosphere is considered. This is because of the large entry path angle dispersion.
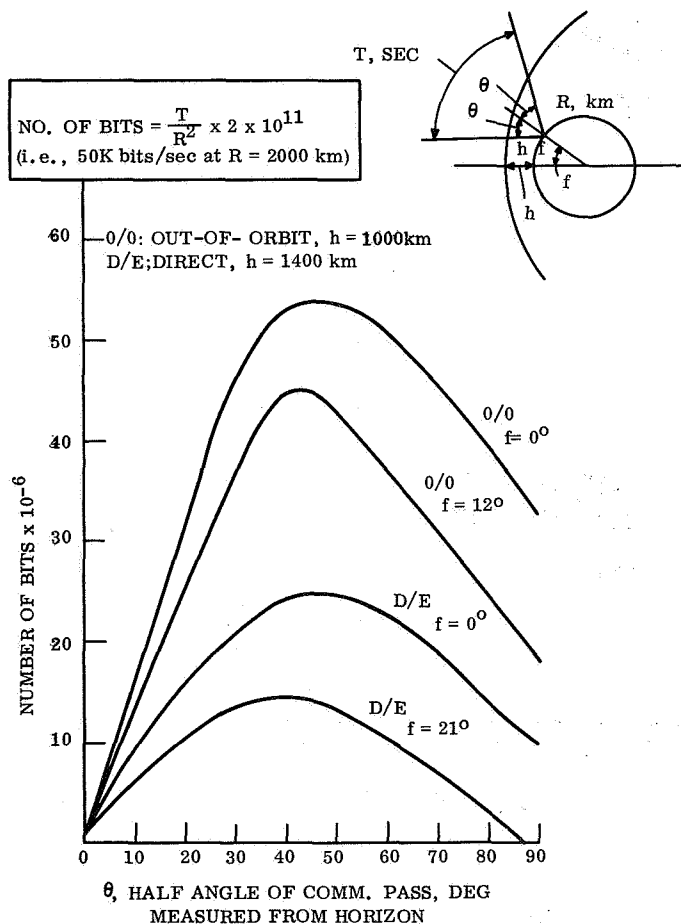
Figure 3.3-2. Post-Landing Relay Communication
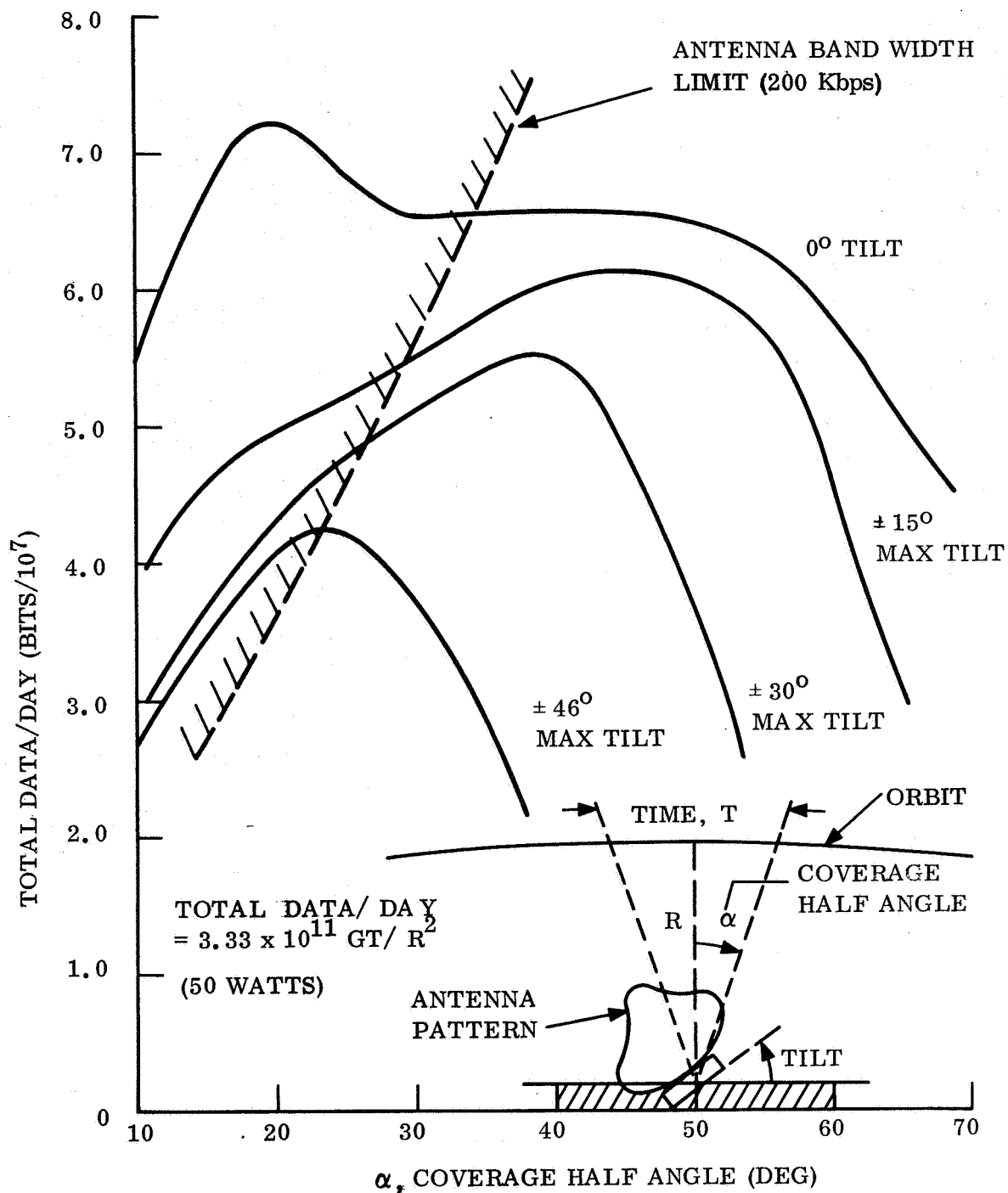
Figure 3.3-3. Total Data/Day vs Coverage Half Angle

3.4 RELAY COMMUNICATION IN DIRECT ENTRY MISSION WITH PERIOD ERRORS

3.4.1 SPECIFIC RESULTS FOR PERIOD ERRORS OF 1 AND 2 HOURS

Relay communication distance and Orbiter elevation have been computed for the first orbit in the direct entry mission, including the effect of errors in orbit period.

The reference case is according to Section 3.1.2: arrival 10 January, 1974, landing latitude 10°N, Sun angle 60°, and orbit inclination 10.74°. The communication distance and Orbiter elevation are shown as functions of time in figs. 3.4-1 through 3.4-12. Figs. 3.4-1 through 3.4-3 repeat the information contained in fig. 3.1-13 but the figure is now presented in three parts: fig. 3.4-1 from -5400 sec to 9000 sec, fig. 3.4-2 from 9000 sec to 80,000 sec, and fig. 3.4-3 from 80,000 sec to 104,000 sec. As defined before, the time zero is the time of landing, in this case with time from entry to landing equal to 800 sec. Similarly, figs. 3.4-4 through 3.4-6, figs. 3.4-7 through 3.4-9, and figs. 3.4-10 through 3.4-12 show the same parameters when the orbit period error is, respectively, -1 hour, +1 hour and 2 hours.

The time interval during which the Lander sees the Orbiter higher than 10° above the horizon is listed in table 3.4-1 for the first and second periapse passage and for the first apoapse passage; this table lists also the communication distance at rise and set, and the maximum or minimum distance as well as the maximum elevation.

In this case, where both the landing latitude and the orbit inclination are small, the periapse relay communication is not lost; it will just occur at an earlier or later time, with somewhat increased distances and with a maximum elevation away from zenith. In the case of a direct entry mission with a high inclination orbit, the probability that the periapse passage communication would be lost is great, because the landing site would be carried too far away from the orbital plane.

3.4.2 A SIMPLE ORBIT PERIOD ERROR ANALYSIS

Errors in orbit period are caused mostly by errors in the impact parameter of the approach hyperbola and in the magnitude of the orbit insertion velocity. If the orbit insertion is performed at the approach periapse, the period errors can be expressed simply as:

$$\frac{dP}{P} = \frac{2}{3e_h}\left[\frac{2(e_h - e_o)}{1 - e_o} - 2\frac{1 + e_o}{1 - e_o}\frac{\Delta V}{V_{op}}\right]\frac{dB}{B} - \left(2\frac{1 + e_o}{1 - e_o}\frac{\Delta V}{V_{op}}\right)\frac{d\Delta V}{\Delta V}$$

where:

B =   impact parameter

V =   orbit insertion velocity

$$e_h = \text{eccentricity of approach hyperbola}$$

$$e_o = \text{eccentricity of orbit}$$

$$V_{op} = \text{orbit velocity at periapse}$$

In the reference trajectory the orbit insertion is not performed at the approach periapse, but at a later time in order to get an apsidal rotation of $22°$; the approach periapse altitude is 1400 km, and the orbit periapse altitude is 1000 km. However, a reasonable stimate of period errors can still be obtained easily by assuming insertion at periapse, and at approach altitude equal to 1000 km. The corresponding impact parameter is then 6511 km and $\Delta V = 1806$ m/sec and the period error is:

$$\frac{dP}{P} = 5.78 \frac{dB}{B} - 10.83 \frac{d\Delta V}{\Delta V}$$

Some numerical results for period errors which may be expected are shown in fig. 3.4-13 as a function of B, for velocity errors at 0.1 and 0.5 percent.

TABLE 3.4-1. RELAY COMMUNICATION IN DIRECT ENTRY
MISSION WITH ORBIT PERIOD ERRORS

			Reference	dP= -1 hr	dP= +1 hr	dP=+2 hr
1st periapse passage	Time*	(sec)	1620	1880	1890	3410
	R_{BC} { rise		3100	4250	2600	2300
	min	(km)	1000	1050	1100	1300
	set		3000	2480	4300	8050
	E max	(deg)	85	81	80	85
1st apoapse passage	Time*	(sec)	45300	47650	45300	46600
	R_{BC} { rise		28750	31150	24970	18300
	max	(km)	33300	32700	34900	37200
	set		28800	19050	33950	37180
	E max	(deg)	68	69	68.5	67.5
2nd periapse passage	Time*	(sec)	1600	3250	3340	- -
	R_{BC} { rise		3050	7800	2300	2500
	min	(km)	1080	1250	1250	2000
	set		2970	2300	7900	- -
	E max	(deg)	70	82	69	- -
	see fig. No.		3.4-1 through 3.4-3	3.4-4 through 3.4-6	3.4-7 through 3.4-9	3.4-10 through 3.4-12

*time between $10°$ horizons

DIRECT ENTRY
SYNCHRONOUS ORBIT, P = 24.6 HRS
TEI = 800 SEC
LANDING LATITUDE = 10° N

Figure 3.4-1. Synchronous Orbit Period TEI = 800 Sec

DIRECT ENTRY
SYNCHRONOUS ORBIT, P = 24.6 HRS
TEI = 800 SEC
LANDING LATITUDE = 10° N

Figure 3.4-2.   Synchronous Orbit TEI = 800 Sec

DIRECT ENTRY
SYNCHRONOUS ORBIT, P = 24.6 HRS
TEI = 800 SEC
LANDING LATITUDE = 10° N

TIME-SEC X 10^5

Figure 3.4-3.   Synchronous Orbit TEI = 800 Sec

DIRECT ENTRY
SYNCHRONOUS ORBIT, P = 23.6 HRS
TEI = 800 SEC
LANDING LATITUDE = 10° N

Figure 3.4-4.   Synchronous Orbit Period -1 Hr

DIRECT ENTRY
SYNCHRONOUS ORBIT, P = 23.6 HRS
TEI = 800 SEC
LANDING LATITUDE = 10° N

Figure 3.4-5. Synchronous Orbit Period -1 Hr

DIRECT ENTRY
SYNCHRONOUS ORBIT, P = 23.6 HRS
TEI = 800 SEC
LANDING LATITUDE = 10° N

Figure 3.4-6. Synchronous Orbit Period -1 Hr

DIRECT ENTRY
SYNCHRONOUS ORBIT, P = 25.6 HRS
TEI = 800 SEC
LANDING LATITUDE = 10° N

Figure 3.4-7.   Synchronous Orbit Period +1 Hr

Figure 3.4-8. Synchronous Orbit Period +1 Hr

Figure 3.4-9. Synchronous Orbit Period +1 Hr

DIRECT ENTRY
SYNCHRONOUS ORBIT, P = 26.6 HRS
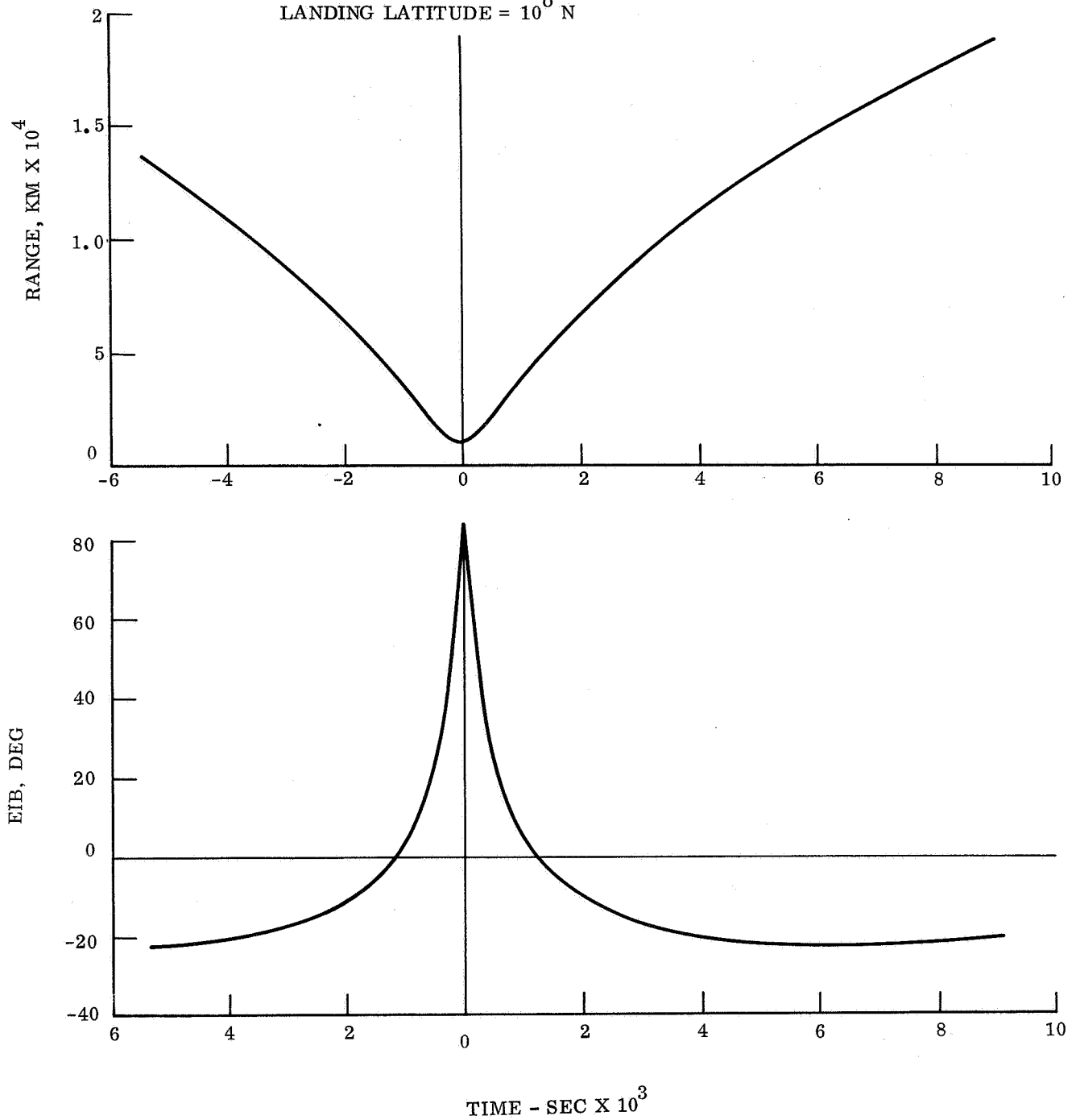TEI = 800 SEC
LANDING LATITUDE = 10° N

Figure 3.4-10.   Synchronous Orbit Period +2 Hr

DIRECT ENTRY
SYNCHRONOUS ORBIT, P = 26.6 HRS
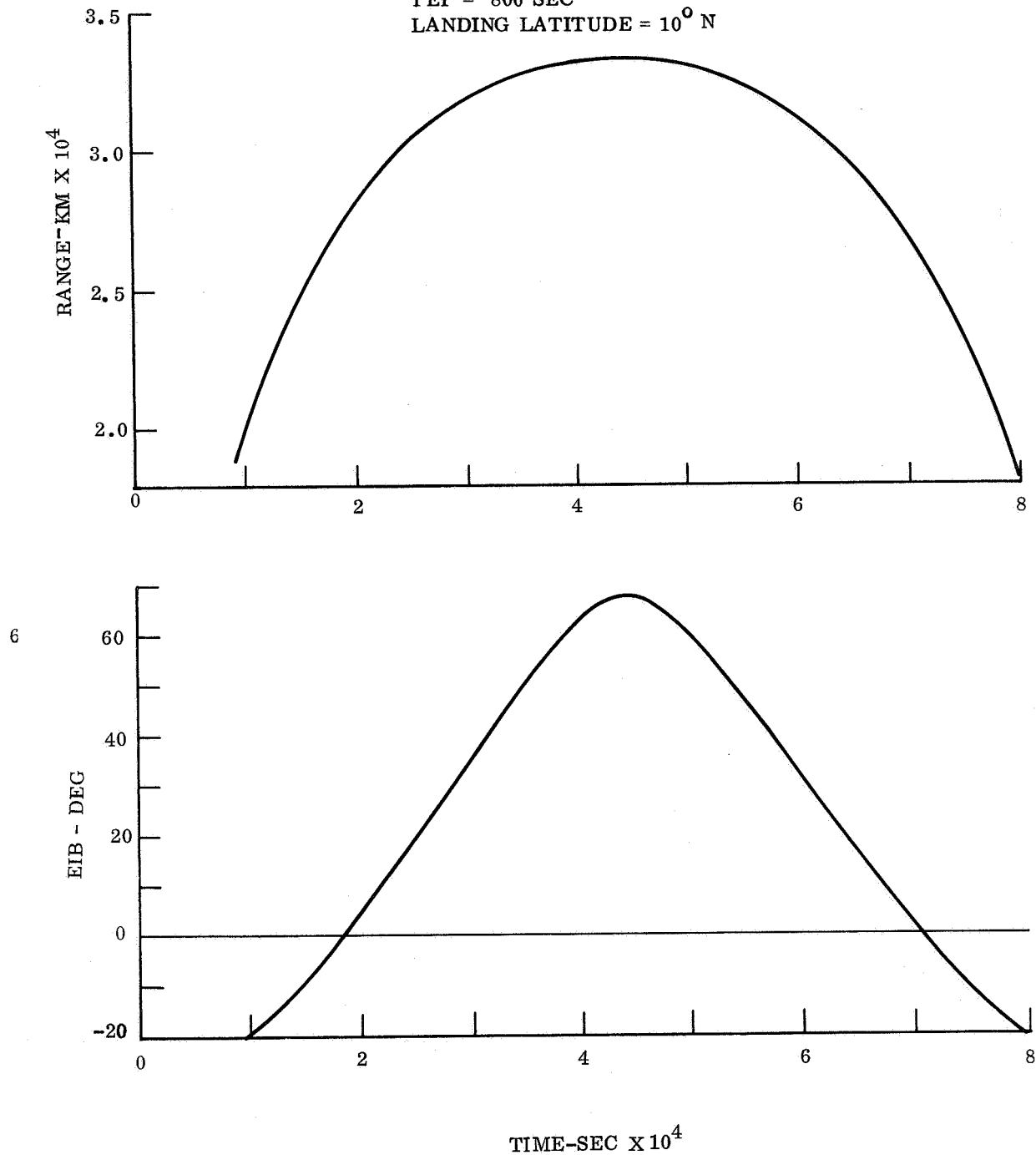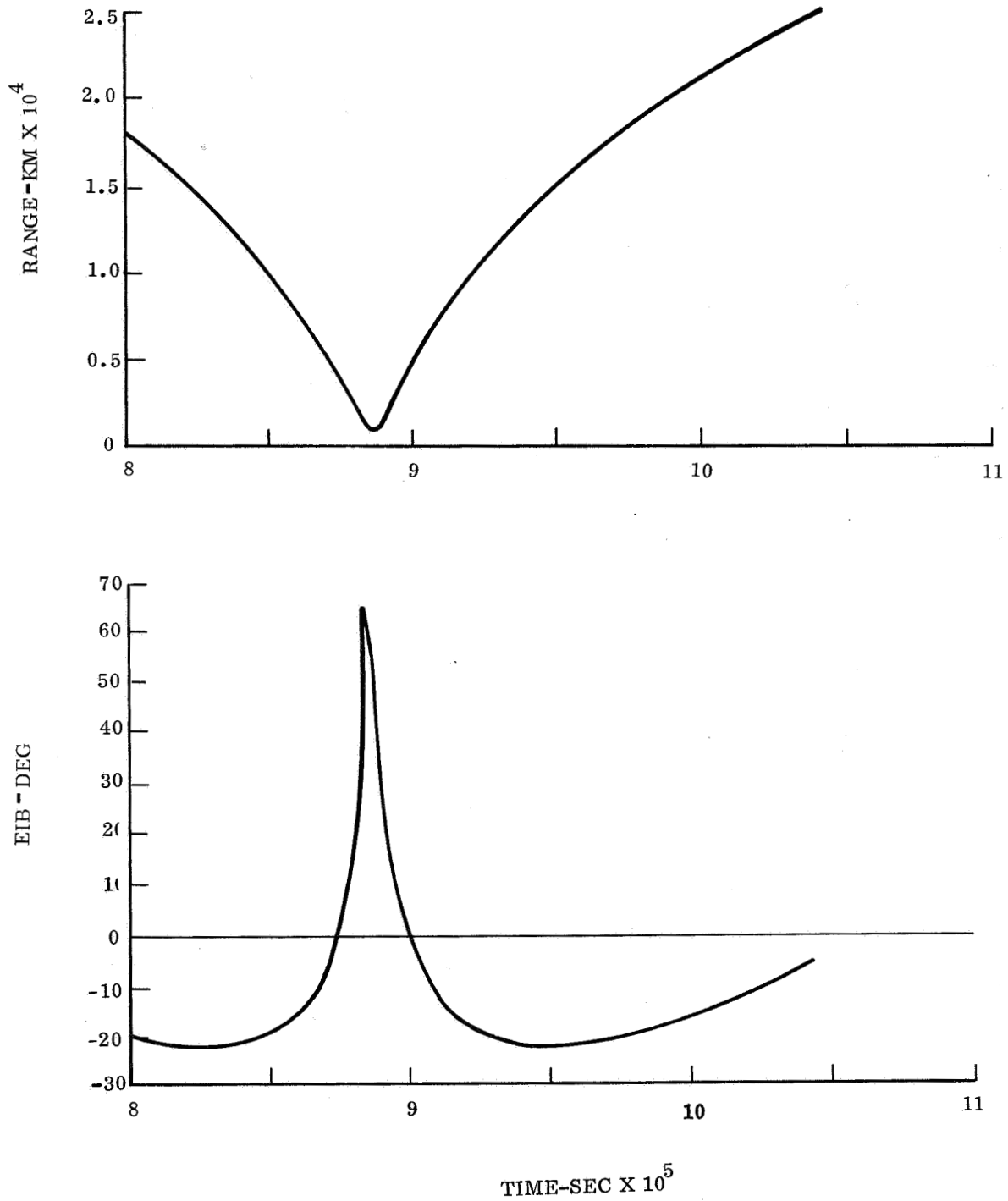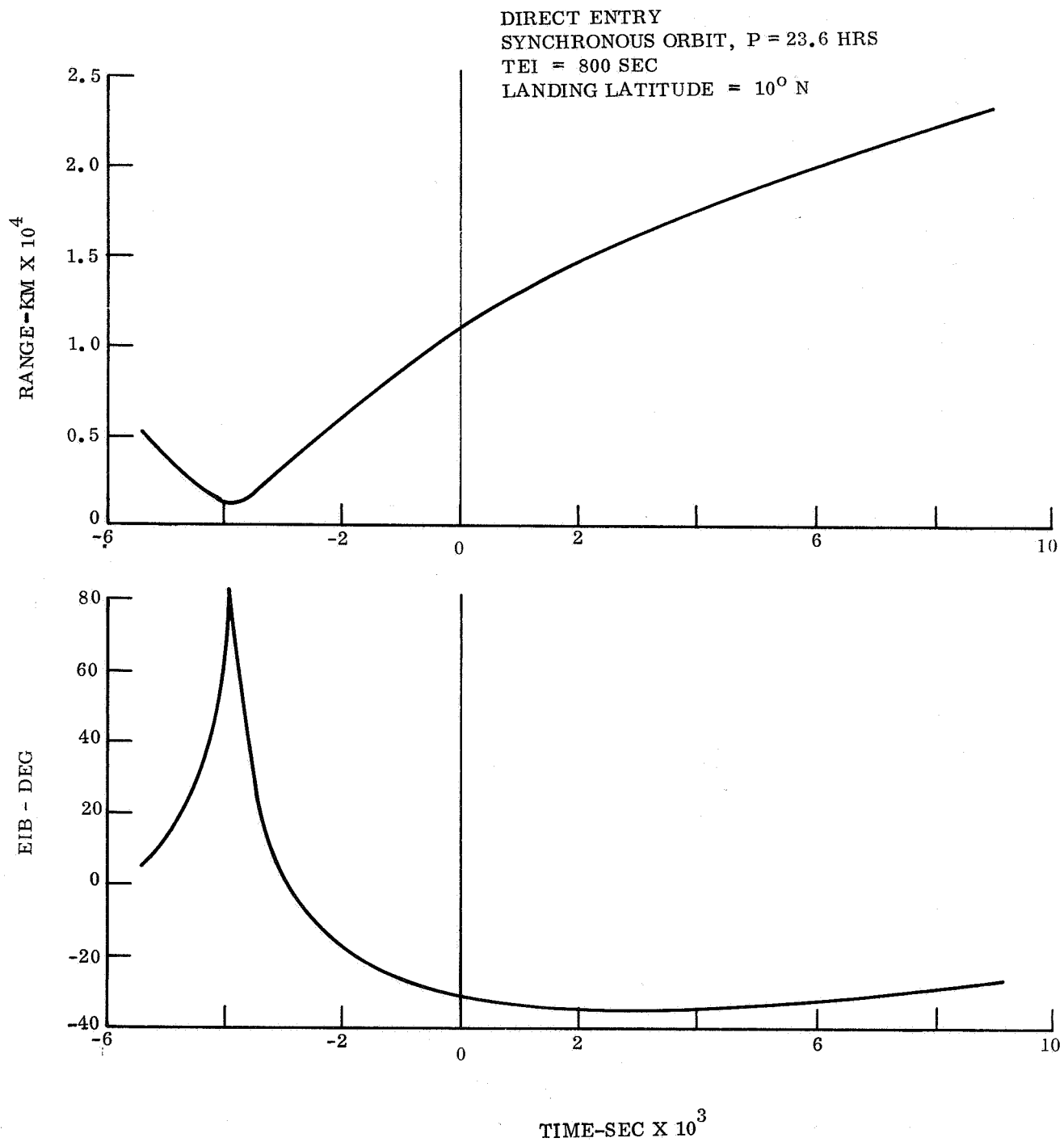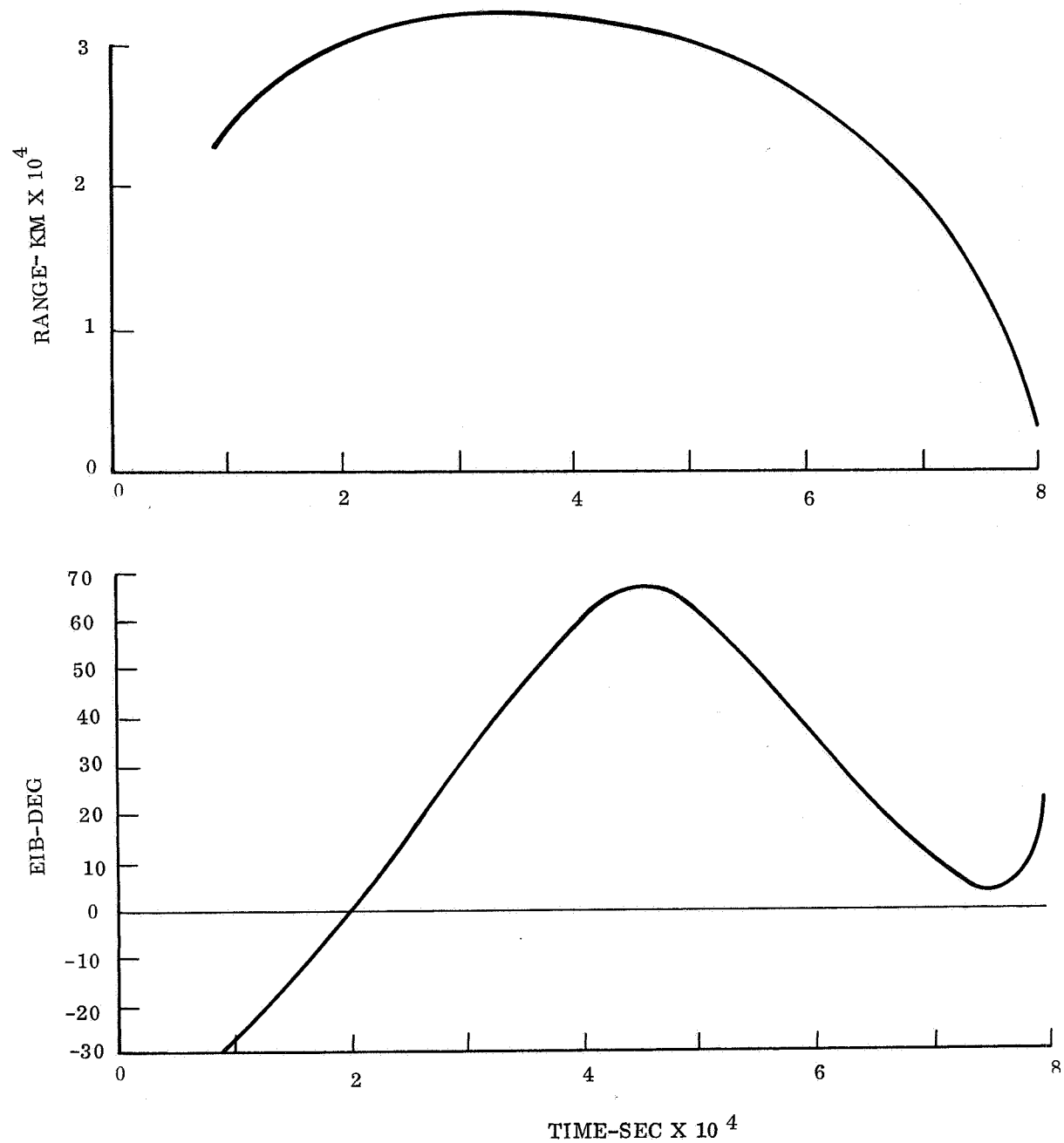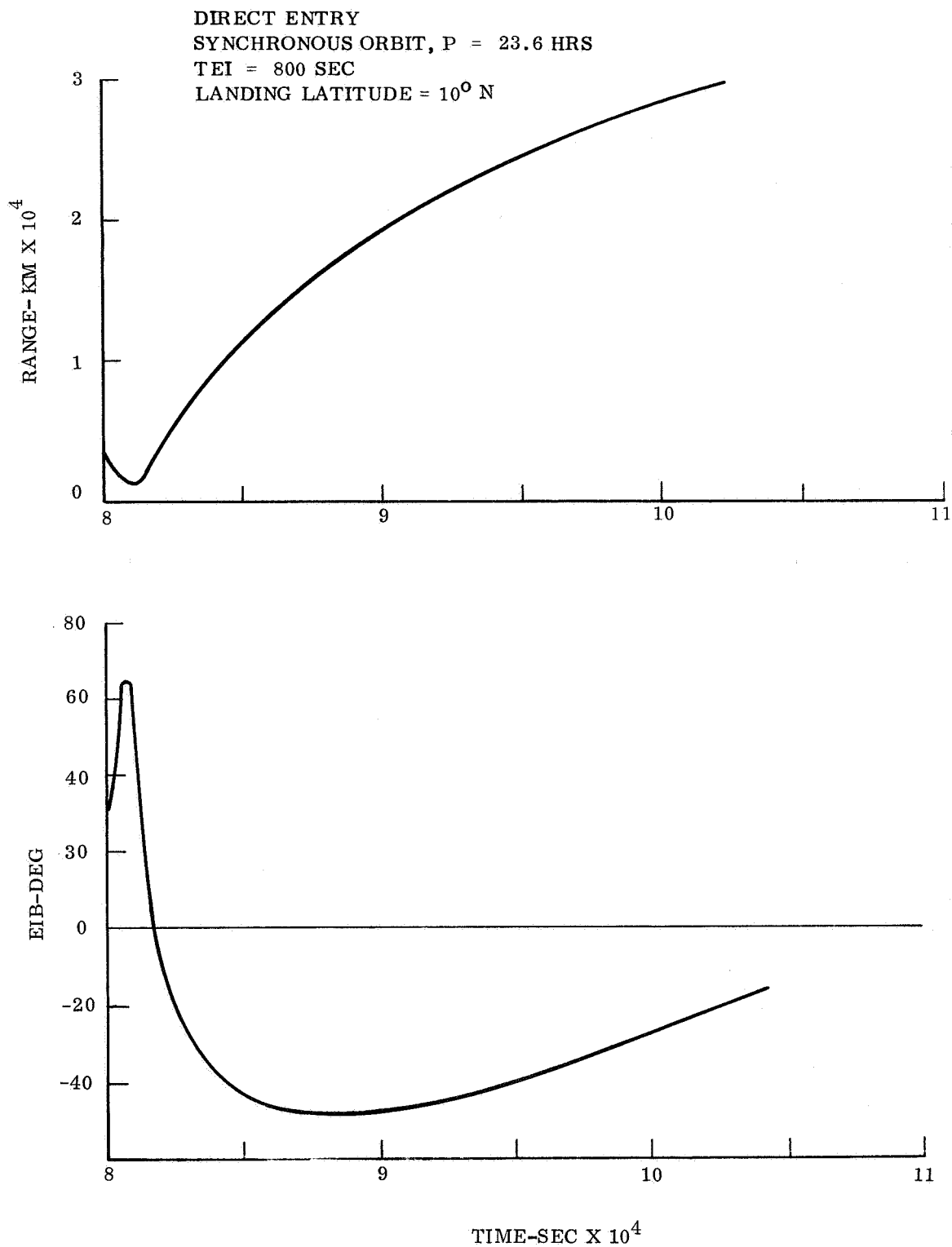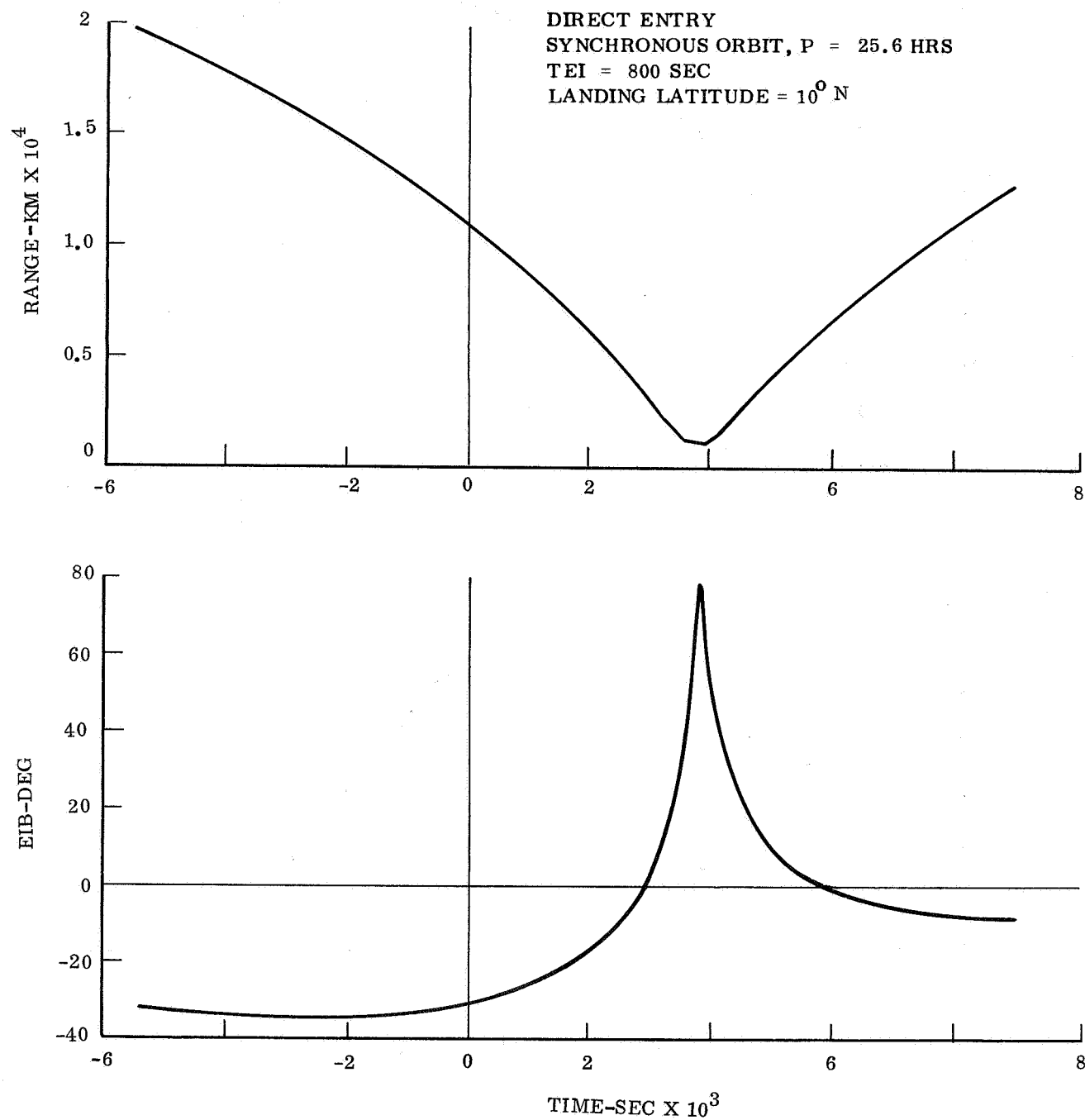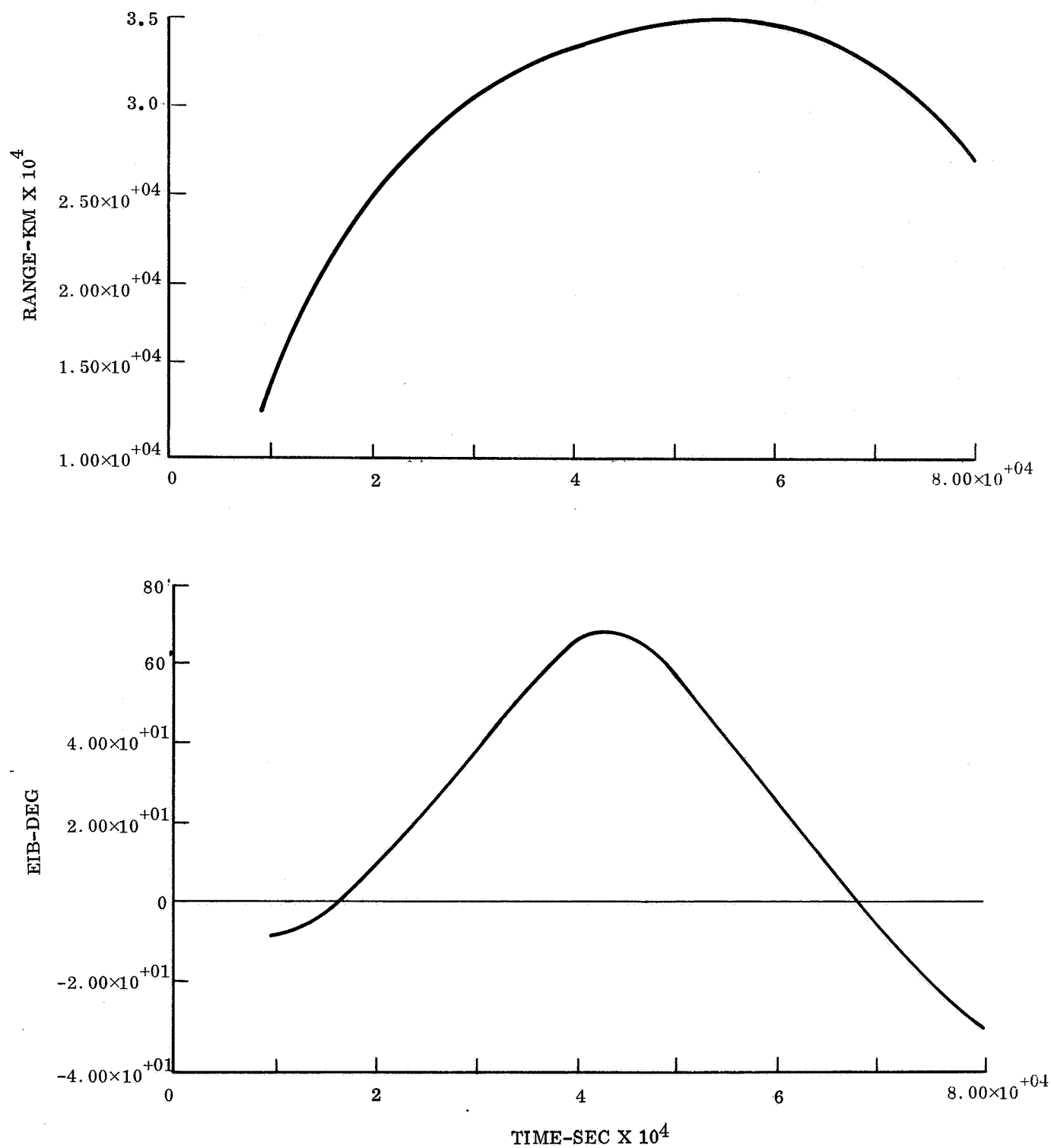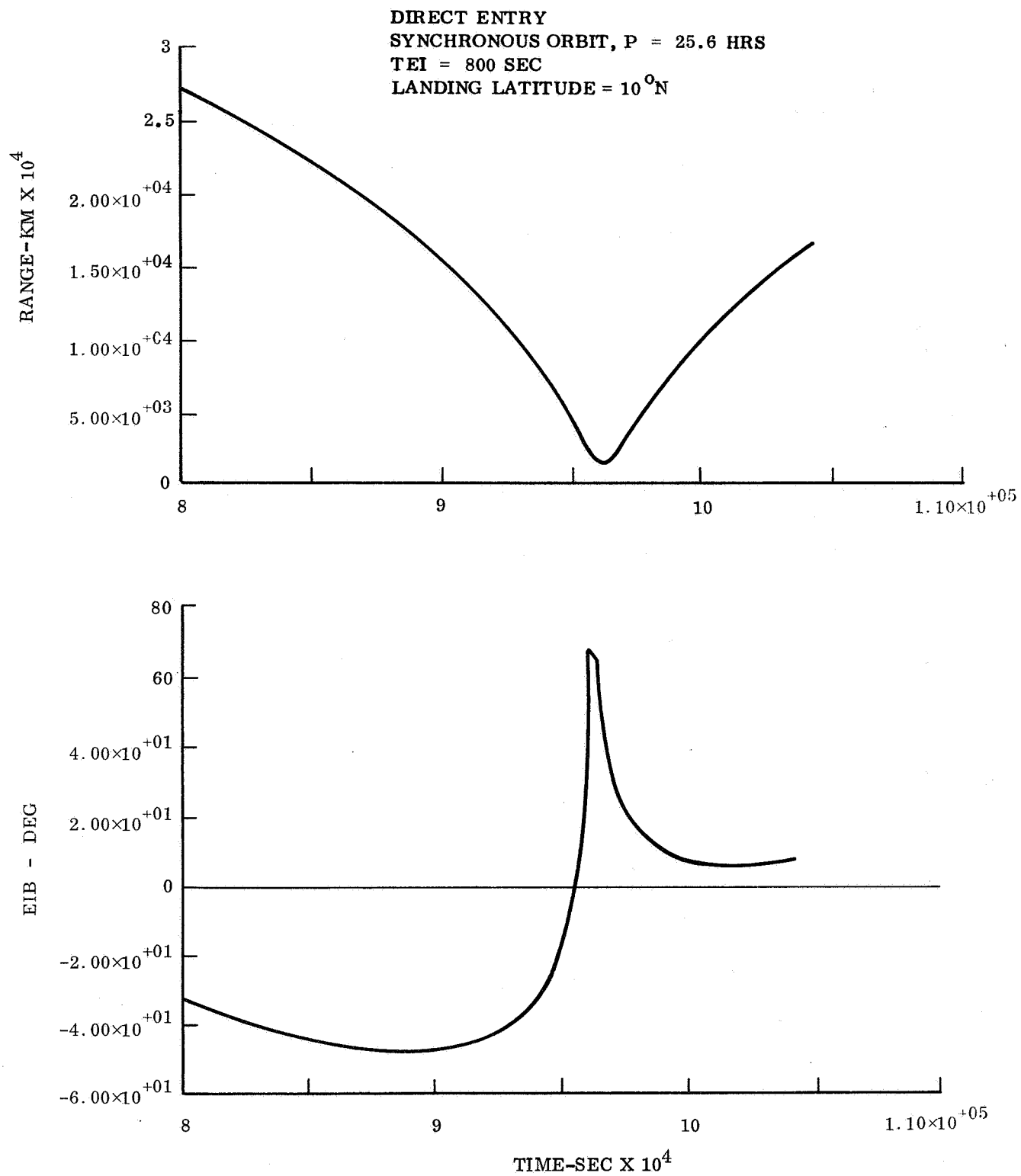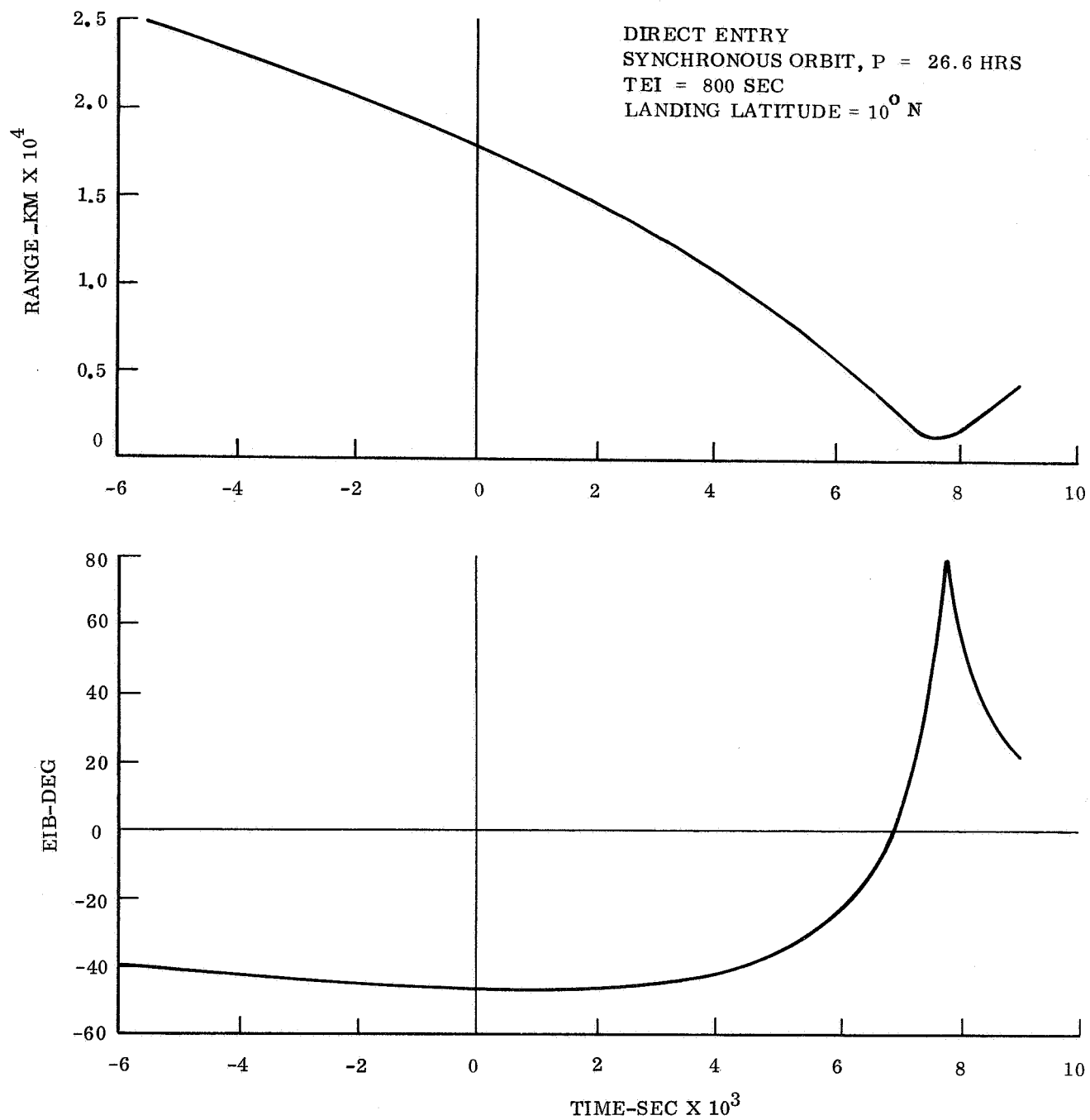TEI = 800 SEC
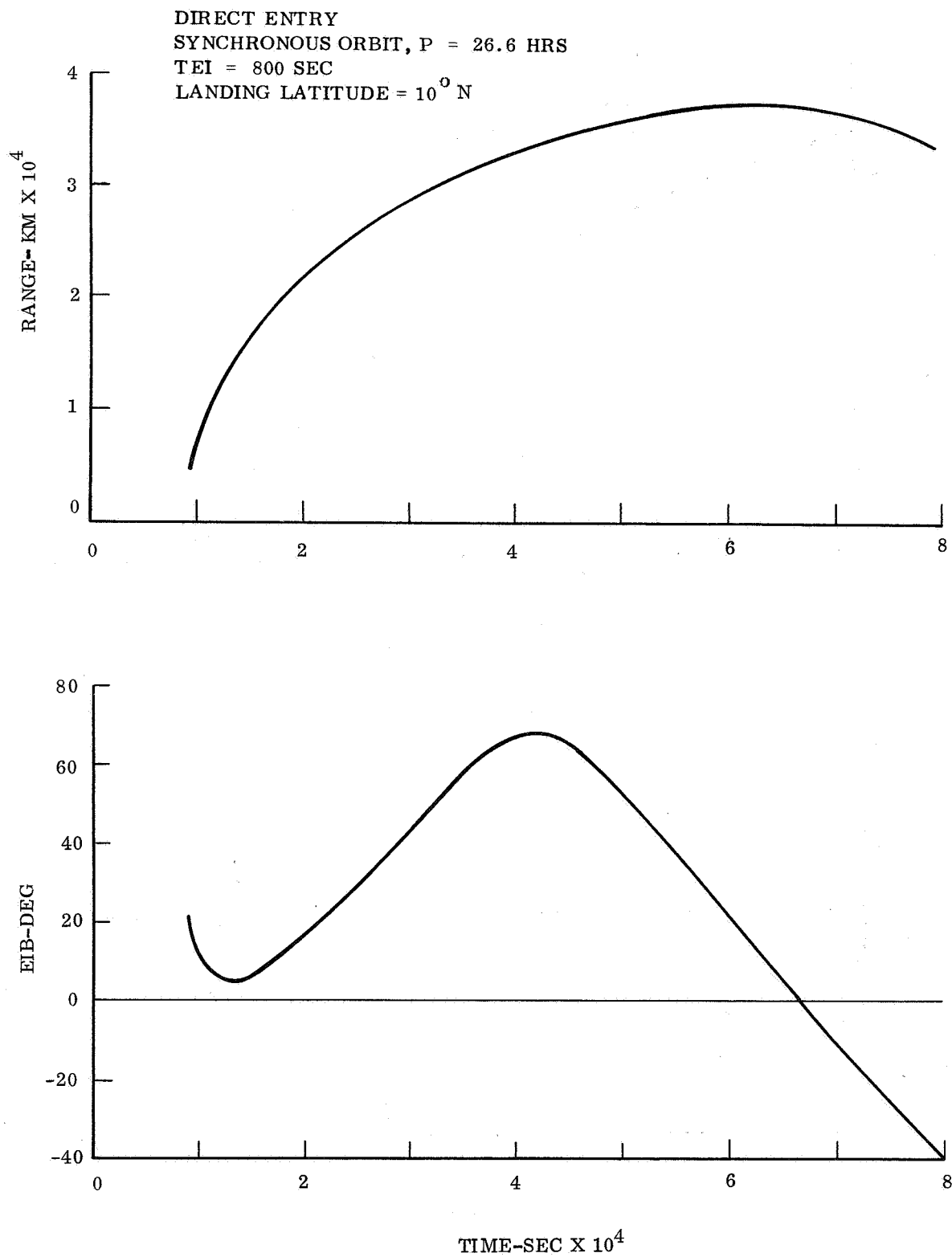LANDING LATITUDE = 10° N

TIME-SEC X 10^4

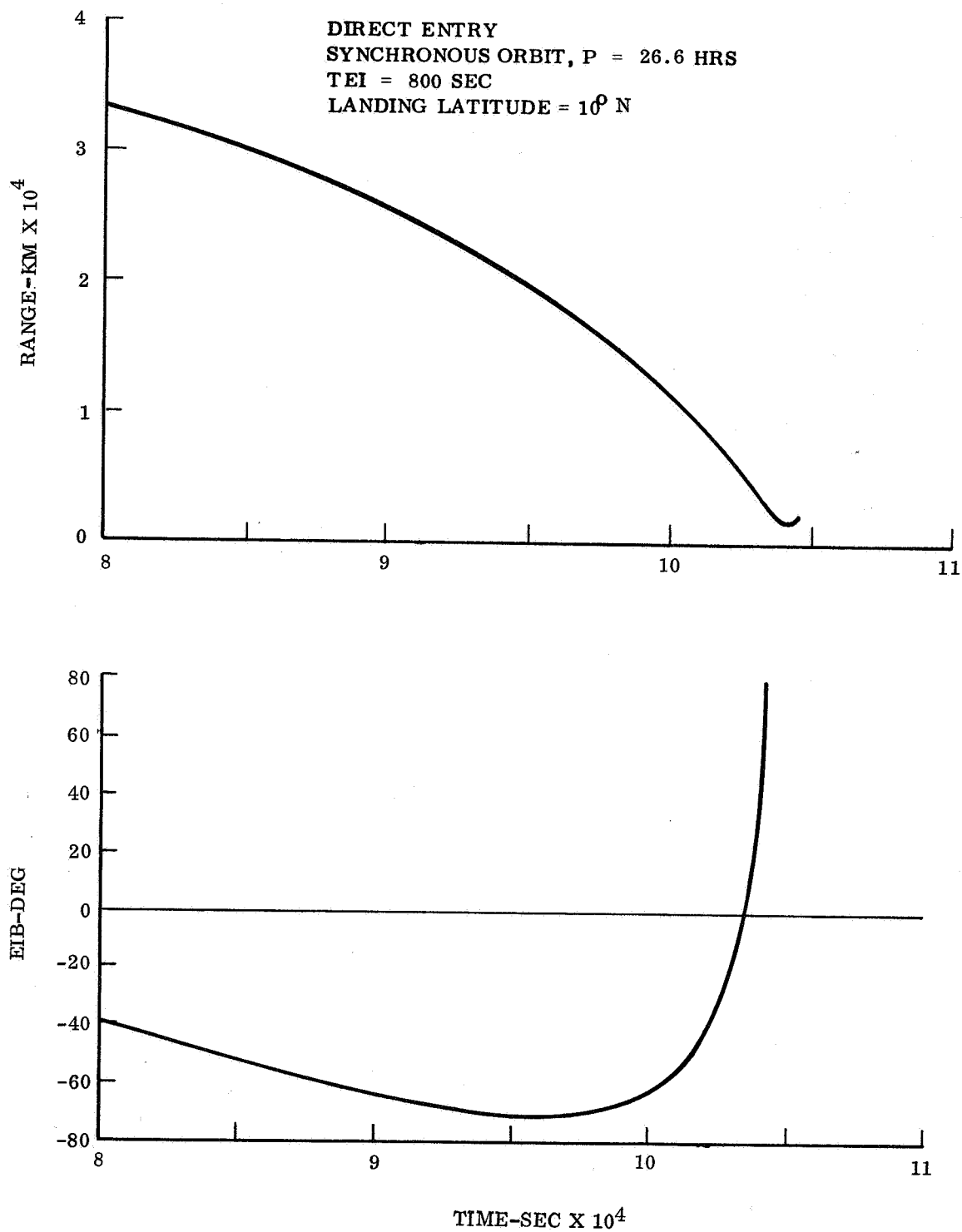Figure 3.4-11.   Synchronous Orbit Period +2 Hr
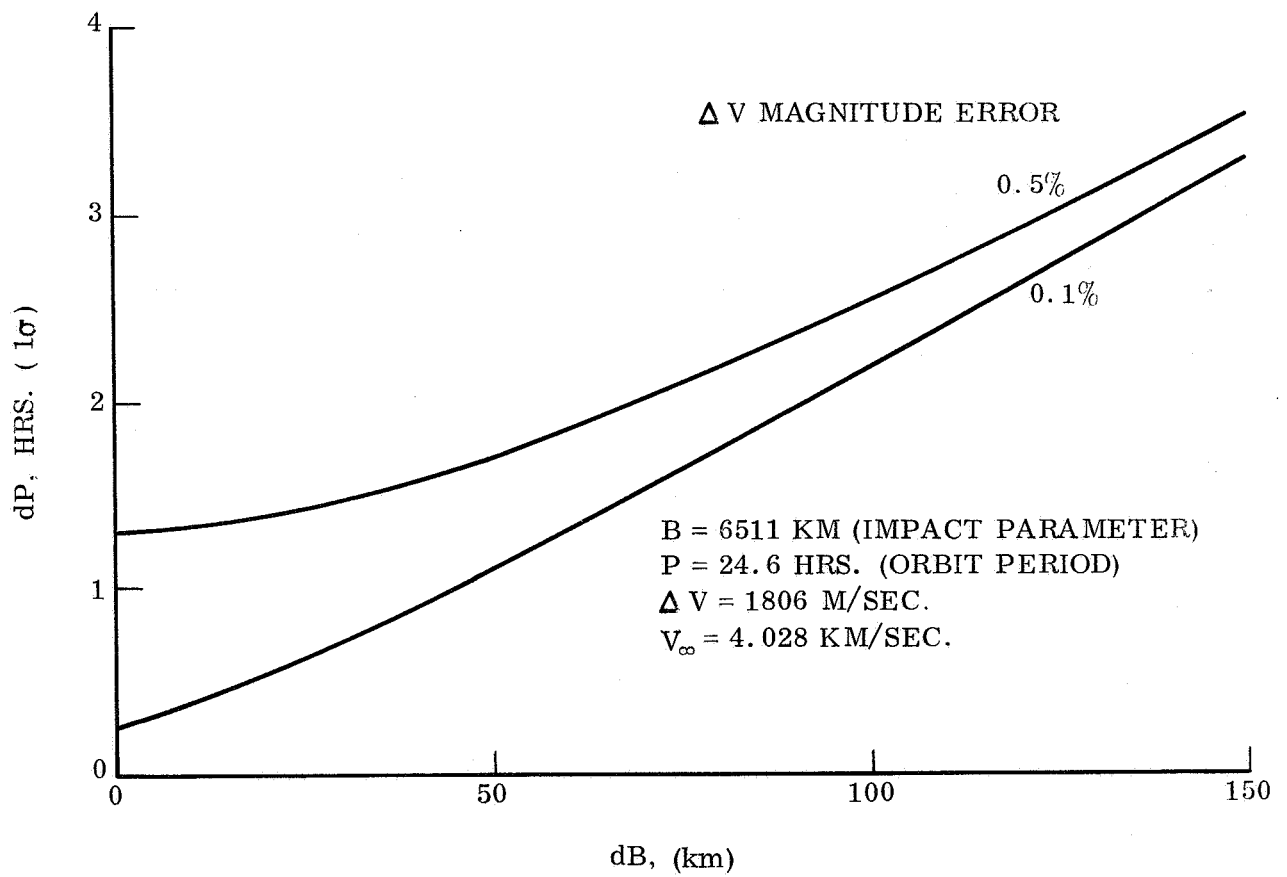
Figure 3.4-12. Synchronous Orbit Period +2 Hr

Figure 3.4-13. Orbit Period Dispersion, 1σ

3.5 TYPE I VS. TYPE II TRANSFERS

The out-of-orbit entry and direct entry missions, as defined in Section 3.1, are based on Type I transfers. In this section it is shown how Type II transfers can also be used, and some comparisons are made.

The definition of any mission begins with the identification of launch and arrival dates, using the "basic planning charts", such that the mission requirements are fulfilled. It is here that a basic difference between out-of-orbit entry and direct entry missions is of great significance. In the out-of-orbit entry mission the Lander is separated after an orbit is established; any requirements on landing site latitude can therefore be met by establishing the orbit with the proper apsidal rotation regardless of requirements on the Capsule trajectory (in particular, the entry path angle). In the direct entry mission the Lander is separated before the orbit is established, and the same flexibility in meeting a landing latitude requirement is not available unless the entry path angle is free. This because the entry path angle is directly related to the central angle between the approach asymptote and the landing site. Because a small path angle is important for the aeroshell design, the approach taken here is to make the entry path angle a mission requirement; for the direct entry mission as 25° path angle was chosen (in relation to the path angle dispersion and the need for avoiding skip-out (see Sections 3.1 and 3.2). The result is that, with landing latitude and entry path angle fixed, the orbit inclination is determined by the declination of the approach asymptote. For any particular combination of launch and arrival dates the declination of the approach asymptote and the ZAP angle (angle between the approach asymptote and the Sun) are fixed. Thus, if the Sun angle is to be equal to a given value, whatever orbit inclination follows from landing latitude, entry path angle, and declination of approach asymptote, this orbit inclination must be accepted. In this manner it was found that with Type I transfers the 60° orbit inclination cannot be satisfied if landing latitude, entry path angle and Sun angle requirements are to be met. (Of course, it follows also that any desired inclination can be obtained if either the landing latitude or the entry path angle are free).

The characteristic flexibility of meeting out-of-orbit entry mission requirements makes it possible to choose out-of-orbit entry missions using either type of transfer. Also, landing sites may be near either terminator, thus satisfying the Sun angle requirements with either type of transfer. Fig. 3.5-1 and 3.5-2* show the launch and arrival date combinations for which the orbit inclination is 60°, the Sun angle is 60° and the landing latitude is 10° North; the first figure is for Type I transfers, the second for Type II transfers and landing sites near either terminator are considered. However, the flexibility of mission selection is not quite complete: for a desired entry path angle, there is a fixed relation between the landing site and orbit periapse locations. This leads to the necessity of establishing the orbit with an apsidal rotation, i.e., the angle between the approach trajectory and orbit periapses. This apsidal rotation may be very large in some cases, leading to impractically large orbit insertion velocities. The apsidal rotations required for an entry path angle of 16° are indicated on the curves in fig. 3.5-1 and 3.5-2; they are very large for the case of Type I transfers with landing site near the morning terminator.

* These figures are to be thought of as superimposed on the basic mission planning chart (fig. 3.1-1) the bottom part of which is shown in more detail in fig. 3.1-34.

SUN ANGLE = 60°
LANDING LATITUDE = 10°
PERIAPSE ALTITUDE = 1000 KM

OUT OF ORBIT ENTRY:
    RA = APSIDAL ROTATION
    FOR PER = -14°.4
    AND ENTRY PATH ANGLE = 16°

RA = 48°.3

OUT-OF-ORBIT ENTRY
NEAR EVENING
         TERMINATOR
INCLINATION = 60°

−98° −102° −107° −108° −105° −103° −48°

OUT-OF-ORBIT ENTRY
NEAR MORNING TERMINATOR
INCLINATION = 60°

RA = -91°

DIRECT ENTRY
NEAR EVENING TERMINATOR
ENTRY PATH ANGLE = 25°
INCLINATION ≈ 10°

ARRIVAL DATE
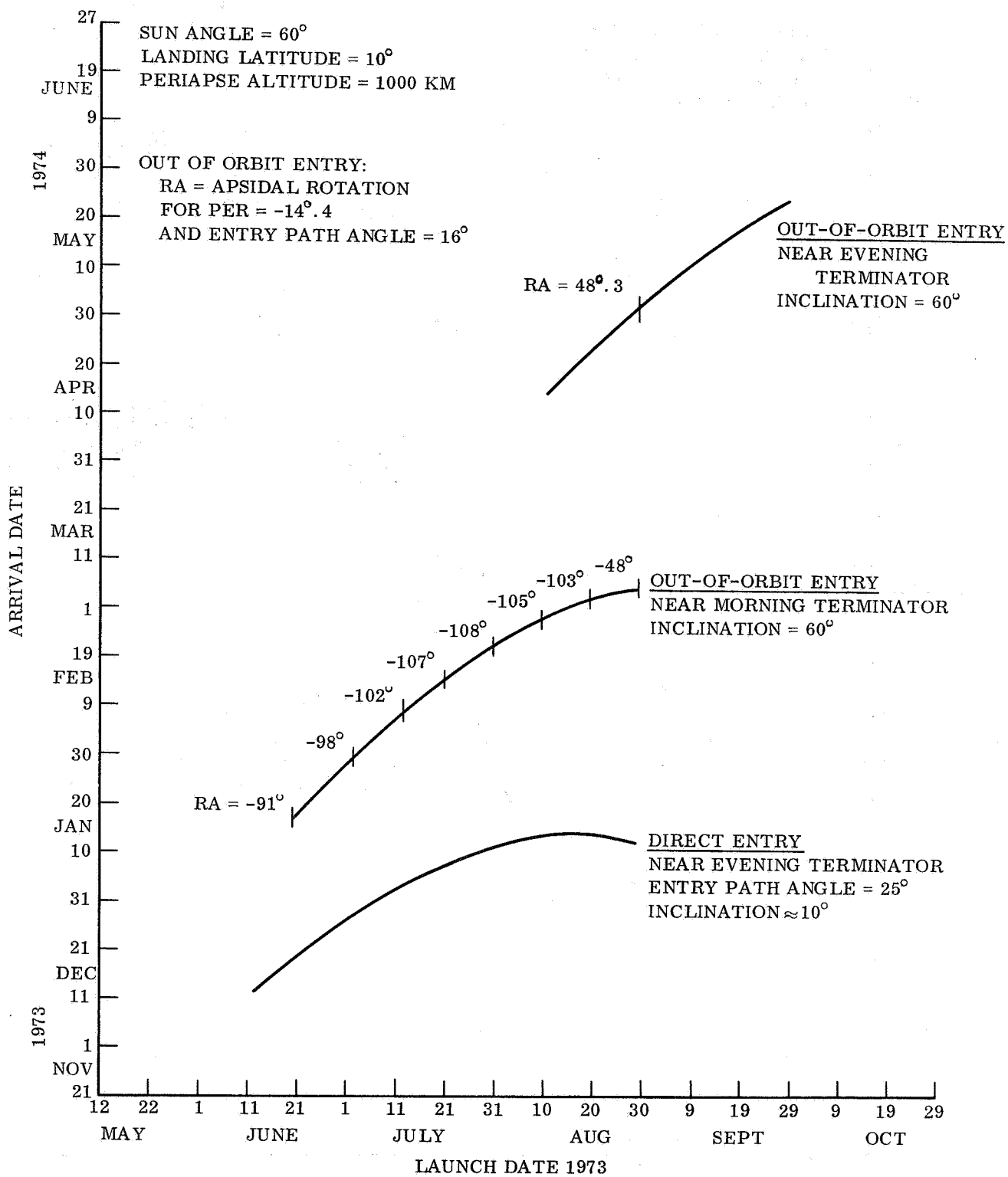
1974

1973

LAUNCH DATE 1973

Figure 3.5-1.   1973 Earth - Mars Trajectories, Type I

II

3-109
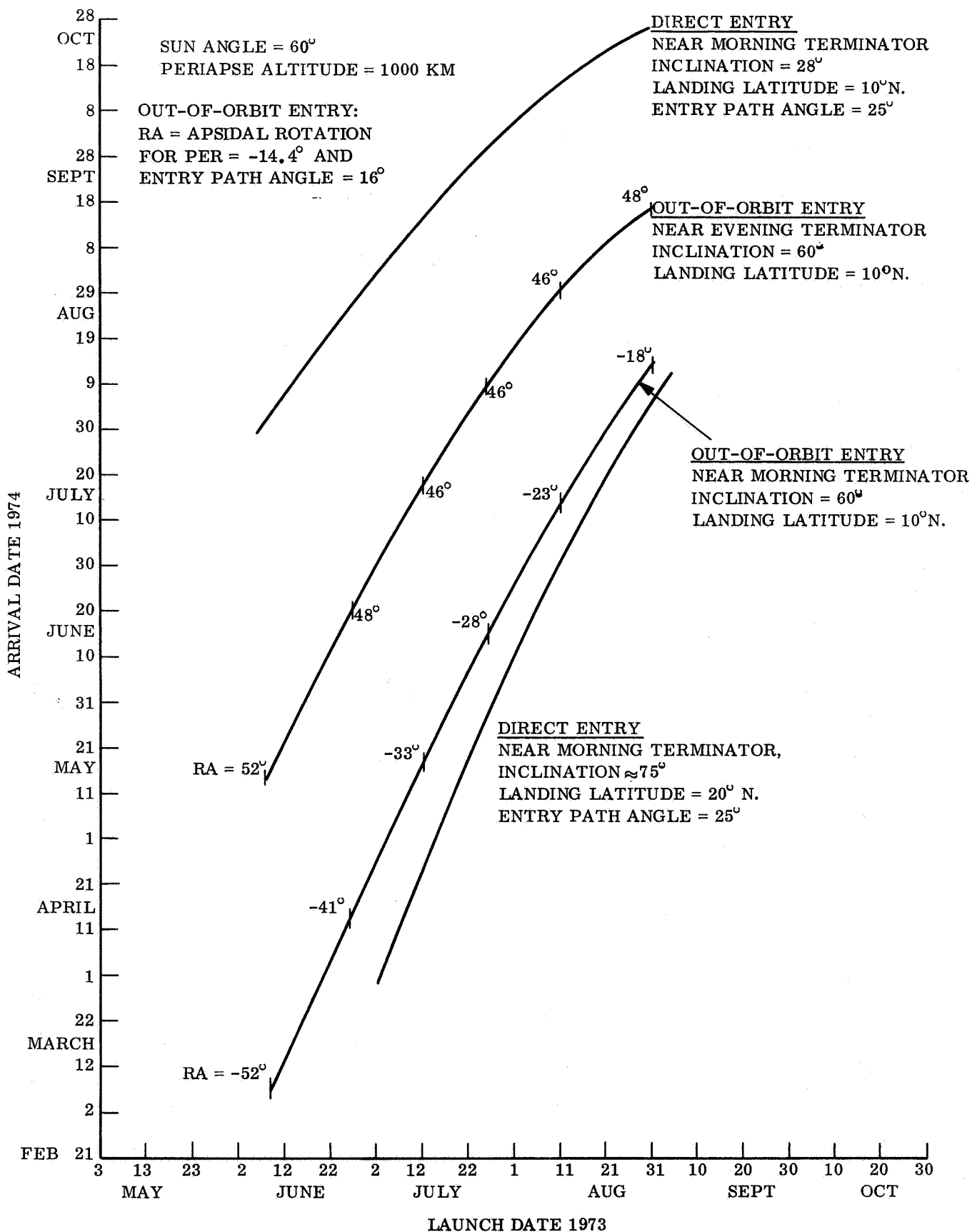
Figure 3.5-2. 1973 Earth - Mars Trajectories, Type II

With respect to the out-of-orbit entry missions it can thus be stated, in relation to the Type I versus Type II question, that out-of-orbit entry missions can be defined using either transfer. However, Type II transfers offer no particular advantage over Type I transfers, while on the other hand Type II transfers generally have longer trip times, later arrival dates, and much longer Mars-to-Earth distances.

Since it was found early in this study that, in direct entry missions using Type I transfers, all of the mission requirement cannot be satisfied, it was decided, in concurrence with NASA/LRC, to free the orbit inclination requirement. The launch and arrival date combinations for which the other requirements are satisfied (i.e., Sun angle 60°, path angle 25°, and landing latitude 10°) are shown in fig. 3.5-1. (This is the same as shown in fig. 3.1-34 where the dates for 20° landing latitude are also indicated). It should be noted here that the approach velocities are not less than approximately 4 km/sec. Using Type II transfers it is possible to obtain the 25° path angle and the 60° Sun angle on two sets of launch and arrival date combinations. These are shown on fig. 2.5-2; this figure should be thought of as superimposed on the Type II basic mission planning chart (fig. 3.5-3) which shows lines of constant approach velocity, launch energy, and ZAP angle. Landing sites at 10° latitude and near the morning terminator can be obtained at very late arrival dates and long flight times; the orbit inclination is approximately 28° and the approach velocity approximately 4 km/sec. Landing site with latitude of 20°, also near the morning terminator, can also be obtained at earlier arrival dates with an orbit inclination of about 75°. This inclination is higher than the required 60°, but it does more nearly satisfy the requirements of a northern hemisphere imaging mission by the Orbiter than the very low inclinations to which the direct entry Type I missions are limited. Of particular interest in this last defined mission case is the approach velocity: it is less than 3.4 km/sec and the corresponding orbit insertion velocity for a synchronous orbit is therefore less than 1400 m/sec. This corresponds to the capability of the Mariner 1971 Spacecraft orbit-insertion engine with minimum modifications. Orbit insertion velocity as a function of approach velocity is shown in fig. 3.5-4. For the direct entry reference mission as previously defined in Section 3.1, the insertion velocity is about 1800 m/sec without apsidal rotation, and about 1900 m/sec with the apsidal rotation that puts the orbit periapse over the landing site.

A typical mission definition for direct entry with high orbital inclination, using a Type II transfer is the following:

Launch date	24 July 1973
Arrival date	24 May 1974
Landing latitude	20° North
Orbit inclination	75°
Sun angle	60°
Approach velocity	3.25 km/sec
Launch energy, C_3	26.74 km^2/sec^2
Orbit Insertion	1310 m/sec

Based on errors of 50 km (1 σ) in impact parameter, 1 percent (1 σ) in separation velocity and 0.7$^{\rm o}$ (1 σ) in separation velocity direction, 3 σ entry path angle dispersion for this mission is about from 20 to 29$^{\rm o}$ (if the nominal path angle is 25$^{\rm o}$) and downrange dispersion is about 900 km (3 σ). The error in the orbit period is about 2.6 hours. These errors are much smaller than those which are found in the direct entry reference mission defined in Section 3.1-2; this is caused mainly by the smaller assumed impact parameter error. The period error is also decreased by a smaller approach velocity (because the orbit insertion velocity is smaller).
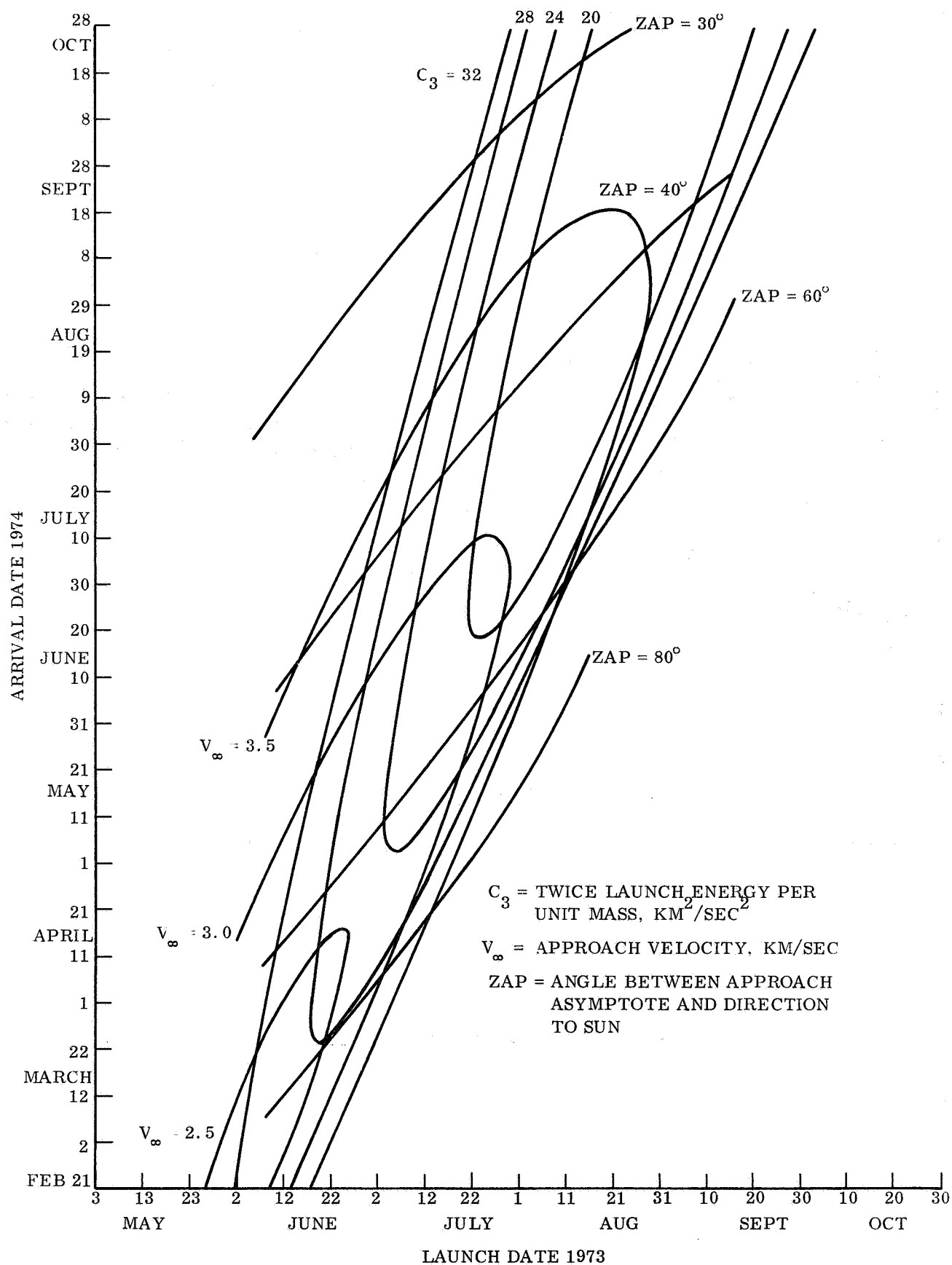
Figure 3.5-3. 1973 Earth - Mars Trajectories, Type I

GRAVITATIONAL CONST. $= \mu = 42829.5$ KM^3/SEC^2

MARS RADIUS $= 3386$ KM

ORBIT PERIOD $=$ SYNCHRONOUS (24 HRS 37 MIN)

$R_A =$ ORBIT APOAPSE RADIUS

$R_P =$ ORBIT PERIAPSE RADIUS

$V\infty =$ APPROACH VELOCITY

$\Delta V =$ ORBIT INSERTION VELOCITY

$h_p =$ PERIAPSE ALTITUDE

$R_A = 35470$ KM, $R_P = 5386$ KM
$R_A = 35970$ KM, $R_F = 4886$ KM
$R_A = 36470$ KM, $R_P = 4386$ KM

ΔV (KM/SEC)

V_∞ (KM/SEC)

MARINER S/C LIMIT
FOR $h_p = 1000$ KM
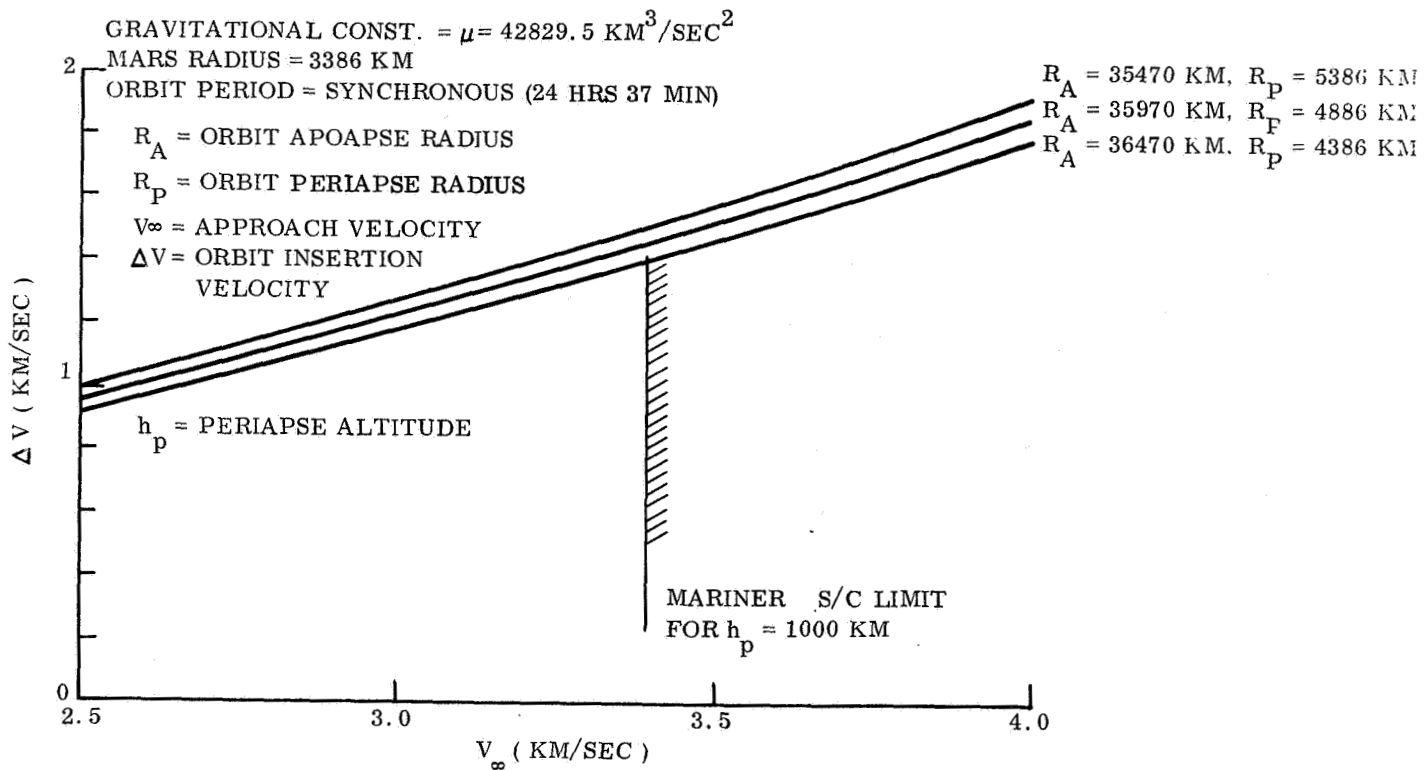
Figure 3.5-4. Insertion Into Mars Orbit

3.6 SUN AND EARTH DECLINATION AND VIEW TIMES IN 1974

In considering direct communication between Earth and a landing site on Mars it is necessary to know the distance between Mars and Earth, the elevation at which the Earth is seen above the horizon, and the time interval in any Martian day during which the Earth can be seen. The elevation of the Sun and the periods of its visibility vetween specified elecations are of importance in considering solar cell design for the power subsystem.

Fig. 3.6-1 shows the declination of the Sun and Earth and the distance to Earth during 1974. Figs. 3.6-2 through 3.6-5 show the visibility periods for 0, 10, 15 and 34° "masks" as functions of declination and latitudes from 0 to 60°.

The highest elevation at which an object with declination δ is seen at a landing latitude λ is:

$$E_{max} = (90^{\circ} - \lambda) + \delta$$

As an example of the use of these graphs, let the latitude of the landing site be 50° and consider communication early in May. The declination of Earth is then 3° and the distance is 300×10^{6} km; the declination of the Sun is 14.5° according to fig. 3.6-1. The maximum elevations are thus 43° for the Earth and 54.5° for the Sun according to the above formula. The visibility periods are listed in the table below as they follow from figs. 3.6-2 through 3.6-5.

VISIBILITY PERIODS (HR)

May 1, 1974	Elevation Limits			
	0°	10°	15°	34°
Earth	12.8	10.6	9.6	4.9
Sun	14.8	12.6	11.5	7.3
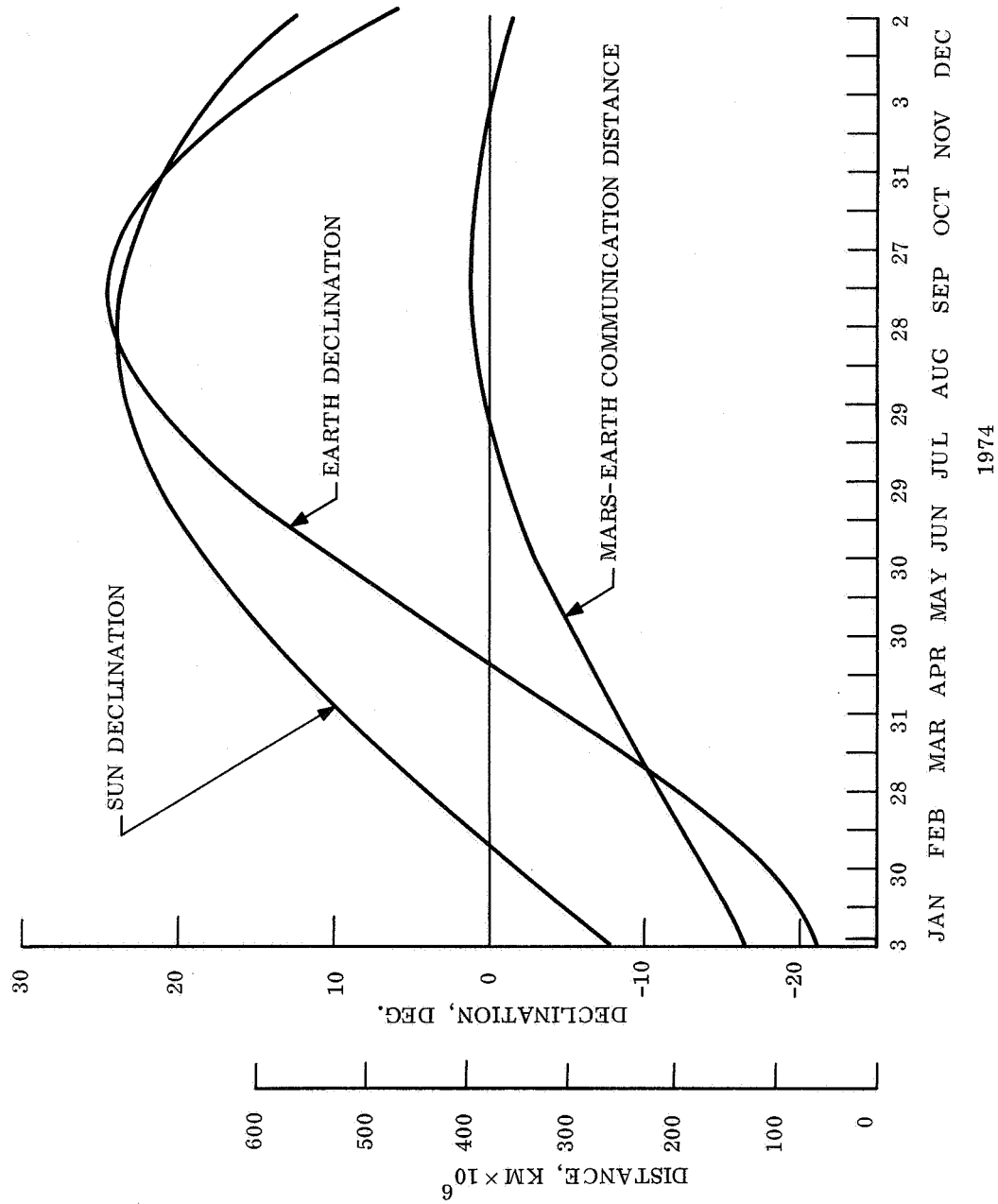
Figure 3.6-1. Earth and Sun Positions, 1974
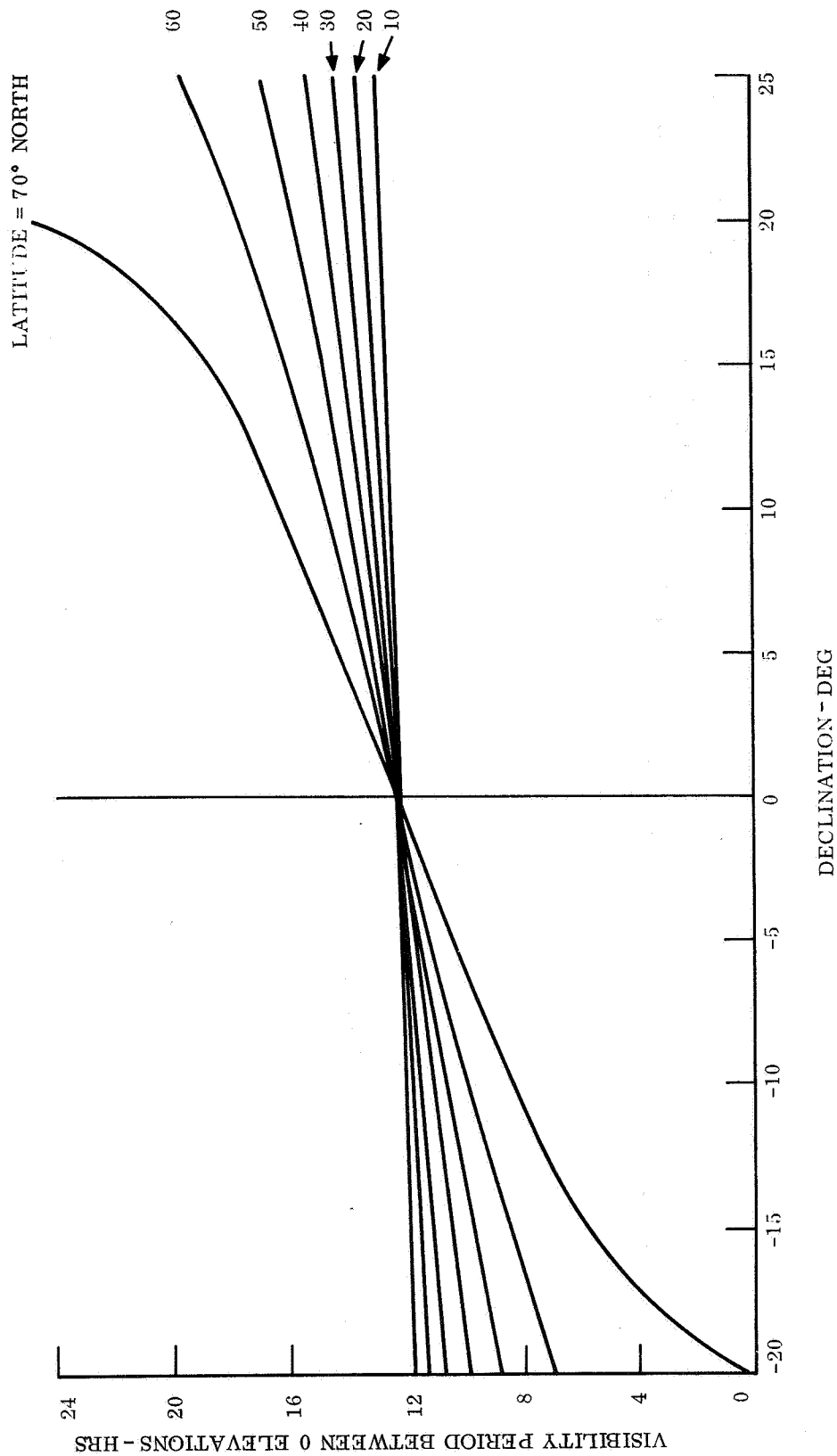
Figure 3.6-2. Visibility Period Between 0° Elevations
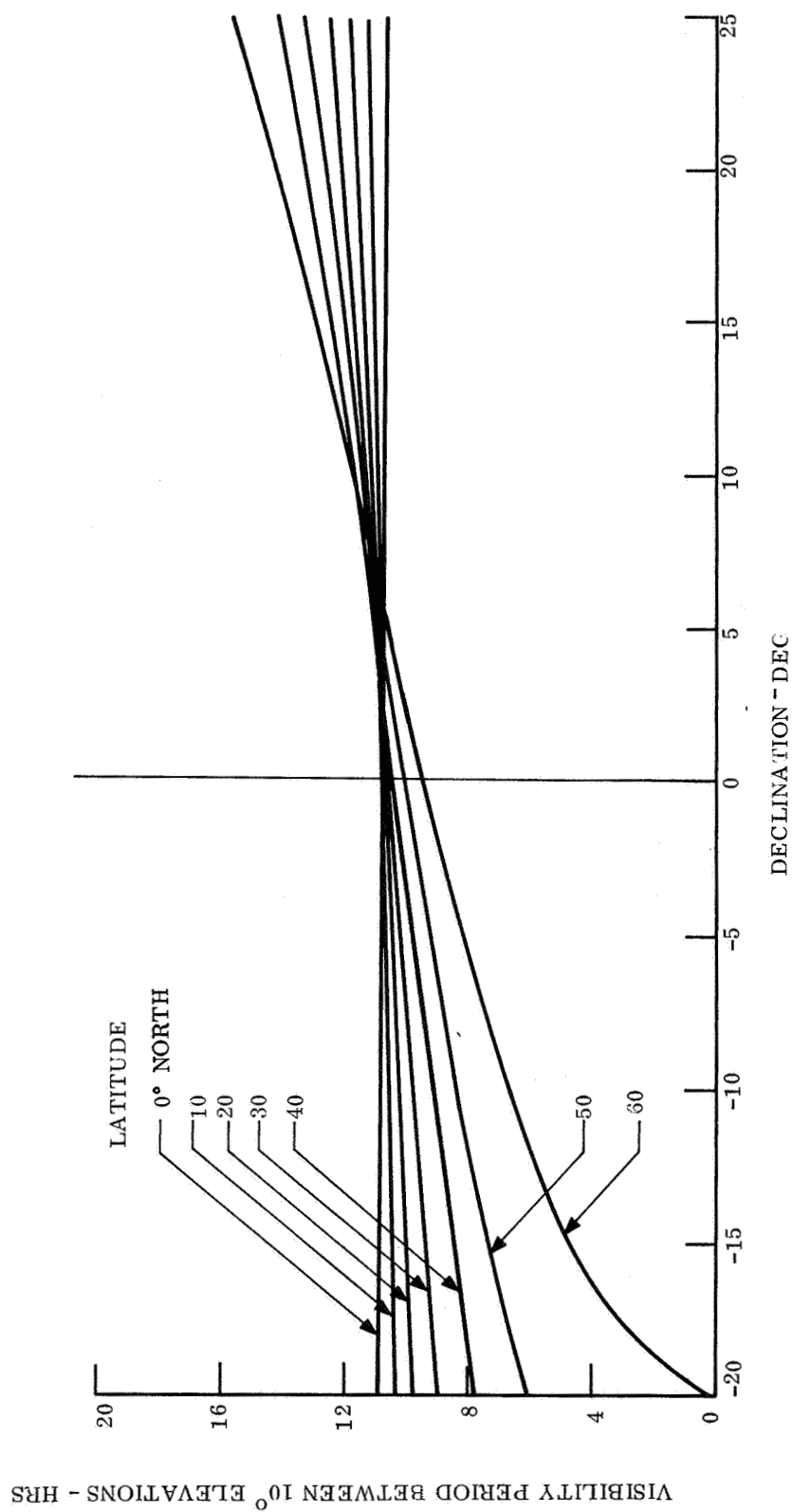
Figure 3.6-3. Visibility Period Between 10° Elevations
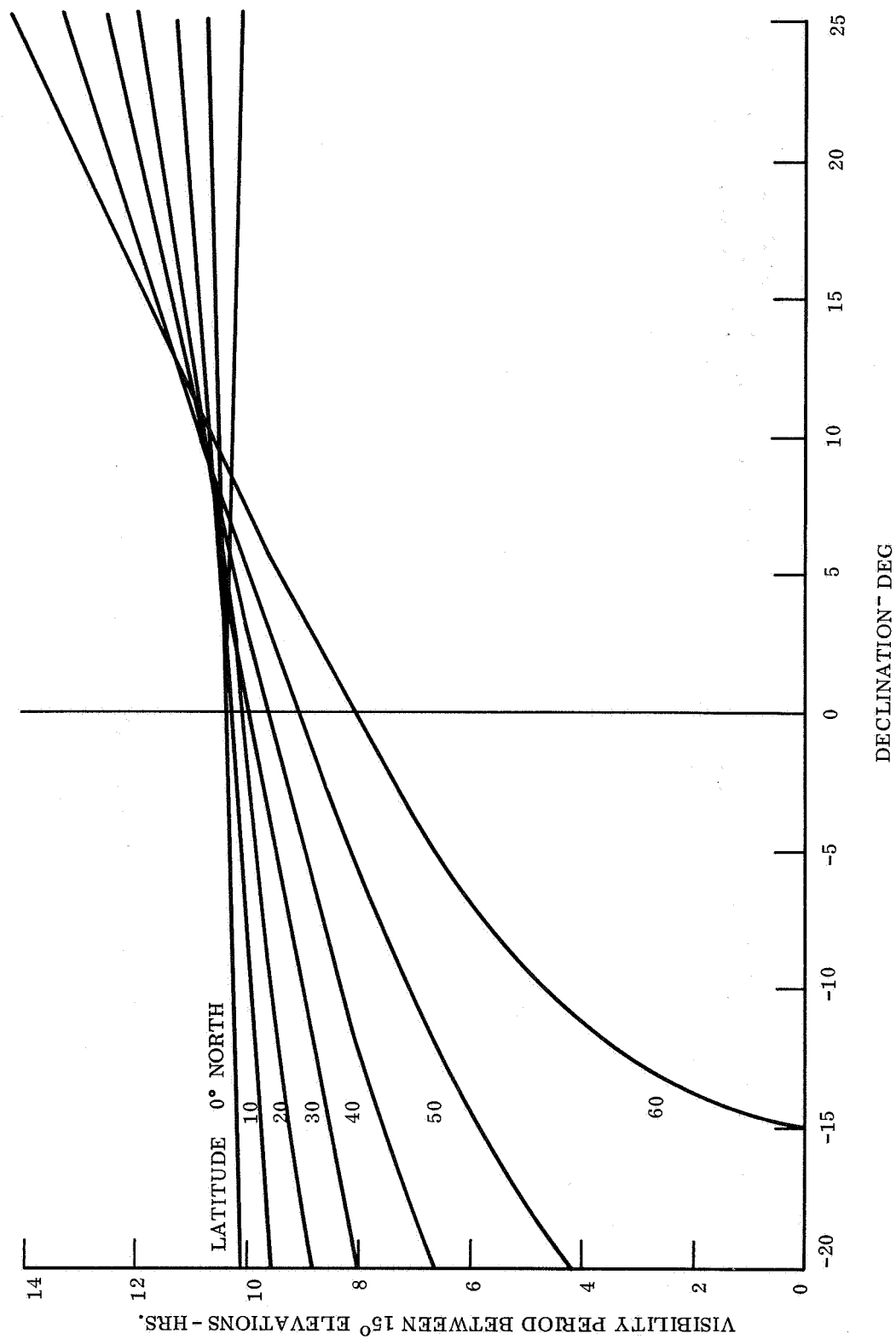
Figure 3.6-4. Visibility Period Between 15° Elevations
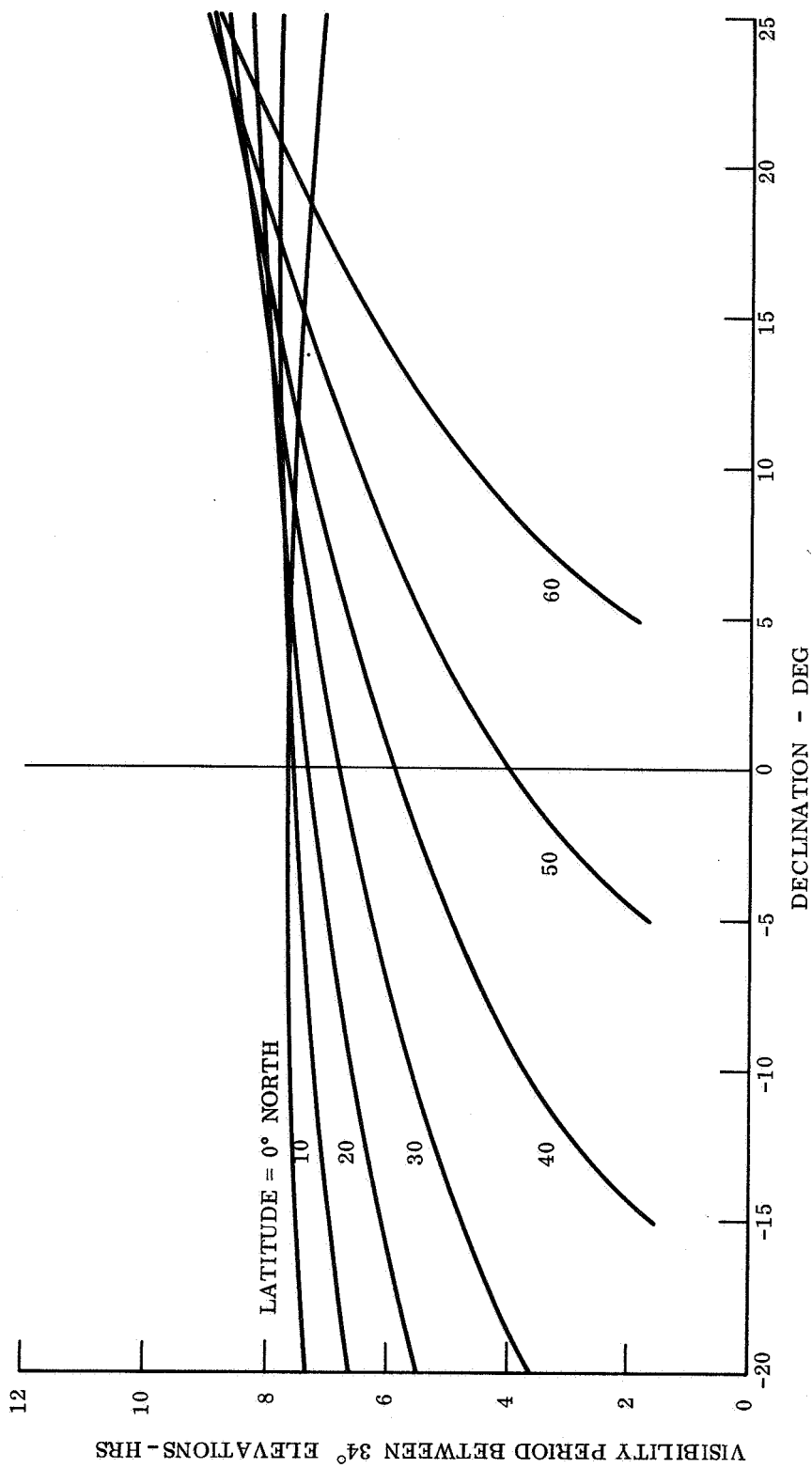
Figure 3.6-5. Visibility Period Between 34° Elevations

4. SCIENCE DEFINITION

4. SCIENCE DEFINITION

At the initiation of this study, the study contractor was given NASA/LRC's science requirements which covered the desired measurements and accuracy goals for both the entry and surface (including imagery) science. These science requirements are presented in table 2.2-1 in Section 2.2, "Mission Guideline and Constraints". During the course of this study, the study contractor translated these science requirements into instrument selections and defined the mission profile during which the science measurements would be made. On the basis of the available information concerning the characteristics of these instruments, and the environment in which the measurements would be taken, anticipated accuracies were determined and compared with the NASA/LRC goals. Entry science sampling rates and expected atmospheric reconstruction characteristics were determined utilizing the study contractor's Experiment Simulation Technique, a computerized analytical modeling method. In addition science studies were conducted concerning: 1) the parametric aspects of the science package (e.g., influence of entry conditions on required entry science sampling rates, effect of camera boom height on desired photographic quality versus resultant installation weight, etc.) and 2) the detailed instrument requirements (e.g., power, thermal, weight, etc.) as they influence the point designs.

It should be noted that three science packages were defined in the study; namely, an entry science package, a minimum surface science package, and an expanded surface science package. The minimum surface science package is based on the NASA/LRC requirements specified in table 2.2-1. The expanded package considers the case of acquiring additional information, beyond the capability of the minimum package, primarily in the area of the physical properties of the planet with particular emphasis on obtaining indications of the past or present existance of life. While the same entry science package was employed for all of the parametric studies and point designs, there are two classes of parametric vehicles corresponding to the minimum and expanded surface science packages. The minimum package has been incorporated into Point Designs 1 to 4 whiie Point Designs 5 and 6 are based on the use of the expanded surface science package. (Note: A description of the system requirements and the design aspects of the point designs are given in tables 1.1-2 and 2.3-3, respectively.).

The studies performed on the scientific payloads may be grouped into four major categories: 1) science measurement requirements; 2) general implementation considerations; 3) parametric studies of the more significant payload quantities; and 4) scientific instrument operation and packaging. The first two categories appear in this section of Volume II, the parametric studies in Volume III, and the operation and packaging studies in Volume IV.

The discussions on measurement requirements and implementation considerations are subdivided into the areas of entry, Lander with a minimum payload, and Lander with an expanded payload. Special attention is given to the conditions required for proper photoimaging, the sequence of scientific measurements during the mission, and the measurement accuracies anticipated in the various mission phases. The implementation considerations are limited primarily in this volume to the instrument's general characteristics but are extended to the vehicle installation aspects in the point design work given in Volume IV.

The parametric studies given in Volume III on the scientific payload are constrained to quantities of importance to Capsule subsystem and system design. Parametric studies that attempt to evaluate one class of measurement against another in terms of their relative scientific information, instrument parameters, and data loads have not been considered as the objective of the science task of this overall study. Information on the effect of alterations in the payload/instrument physical description and data requirements on the Capsule system is provided, however and included in the mission maps of Volume III. The parametric studies directly involving the scientific payload include: 1) camera viewing conditions versus boom height, location, and vibrations; and 2) anticipated measurement accuracies during entry as a function of atmosphere, entry conditions, ballistic coefficient, sampling rates, and random errors. The discussion and graphical results are presented in Volume III.

The details of instrument design, packaging, and operation are discussed in Volume IV where envelope drawings, installation points in the vehicle, and instrument status are included. Discussions are provided also on the candidate instruments for each class of measurement and on the rationale for selecting a given instrument for the point designs.

4.1 SCIENTIFIC REQUIREMENTS

4.1.1 GENERAL

The environment of interest for measurements by the Capsule system (entry/landing) starts at the beginning of measurable atmospheric effects on the Capsule and continues down to and including the surface of the planet. Above this altitude regime, data on the near-planet environment is of primary importance to orbiting systems and is best collected by them. The planetary environment characteristics of interest to the Capsule system include the atmospheric thermodynamic parameters of temperature, pressure, and density; the atmospheric gaseous and particulate compositions; the winds; and the subsurface planetary composition. In addition, these characteristics along with the knowledge of the surface topography form the bulk of information of significance for the initial scientific missions.

Most of the available knowledge about the Martian environment has come from the Earth based observations and the experiments of Mariner IV. The most significant results of the past few years have come from the Mariner IV flight and have included the limitation of surface pressures to the range of 5 to 25 millibars, the increase in evidence for a CO_2 rich atmosphere, and the first data on existence of a heavily cratered surface which apparently shows little erosion from water. Information on the planet's surface temperatures, dust clouds, surface composition, and the polar caps have existed essentially unaltered for a number of years. The overall tolerance in our knowledge about the Martian atmosphere is such that ten different VM atmospheres (Hess and Pounder) have been postulated. These models, summarized in table 2.2-5, clearly show the relatively wide range of uncertainties in our knowledge. Not included in table 2.2-5 are other factors also requiring better definition such as the polar cap composition (water versus carbon dioxide), the surface soil composition, the altitude profiles of the thermodynamic parameters, their seasonal and latitude variations, and the planetary gas circulation patterns. Several studies have been conducted to collect, evaluate, and summarize the current knowledge (refs. 4-1, -2, -3, -4); but reduction in the uncertainties must await future exploratory missions.

Improvement in our understanding of the atmospheric and surface structures is important and necessary both for the optimization of entry vehicle designs and to enhance the sophistication of our future biological and geological experiments. Some of the more important quantities to be measured are:

1. The Martian wind fields because of their influence on erosion rates by particle transport, landing system touchdown dynamics and design, and deployment mechanism design;

2. The altitude, latitude, and seasonal profiles of the atmospheric thermodynamic parameters and composition since they not only significantly effect entry/landed vehicle design but have a strong influence on the surface environment (including incident radiation, thermal balance, etc.) which has a profound effect on the evolution and maintenance of biological systems;

3. The concentration of water vapor in both the atmosphere and soil because of its importance to the existence of living systems.

4. The surface topography and geological structure which are important for Lander design, geological history (including erosion phenomena), and evidence of biological activity.

Failure to properly investigate such quantities can limit unnecessarily the capability of future missions and the scope of scientific investigations.

Therefore, the scientific objectives for the Mars Hard Lander system center on the reduction of the current uncertainties of the Martian environment and the acquisition of data that will increase significantly our knowledge of Mars and provide new insight into the design of future experiments.

4.1.2 ATMOSPHERE PROFILE

The entry measurements to be made by the Capsule system will include the altitude profiles of temperature, pressure, and density and the gas composition in the well-mixed atmosphere. In order to explicitly determine the accuracy and resolution requirements of the entry instrumentation it is first required to define the specific use intended for the data to be obtained.

If the data, for example, are only to discriminate among the surface temperatures called for in the VM models of table 2.2-5, then a resolution 20°K with an accuracy of $\pm15^{\circ}$K would be adequate. However, the measurement of the thermal lapse rate requires a resolution of typically 2°K/km, and an accuracy of $\pm5^{\circ}$K in order to apply to any of the 10 VM models. Similarly the discrimination among the models for pressure at the surface requires a resolution of 2 millibars with an accuracy of ±1 millibar while the measurement of the pressure profile with altitude leads to highly altitude-dependent resolution and accuracy requirements.

A conversion has been made of the NASA/LRC requirements presented in table 2.2-1 which are typically expressed as percentages of the reading at a given altitude or time. The conversion to magnitudes rather than relative percentages is necessary to explicitly identify the requirements that are valid for all the atmospheres and to facilitate the translation of these requirements into instrument requirements. The converted requirements are summarized in table 4.1-1 where use has been made not only of the NASA/LRC objectives but also of currently available knowledge about the Martian atmospheric variations and the biological significance of the measurements.

The primary guideline in establishing the requirements has been to select values that are adequate for all the atmosphere models. In particular the requirements for the altitude profile measurements have been taken from the VM-8 model and, as such, are much better on a relative percentage basis for the VM-9 model than required by the NASA/LRC objectives. However, a compromise has been made for the VM-8 model and all models similar to it. In establishing the magnitudes for the required

TABLE 4.1-1. ATMOSPHERIC MEASUREMENT REQUIREMENTS

Measurement	Resolution	Accuracy	Minimum Reqd. Mission Approx.
1.0 Temperature			
1.1 Altitude Profile:			
0-20 km	$2°K/km$	$±5°K$	Single Probe
20-60 km	$2°K/km$	$±5°K$	Single Probe
1.2 Diural Variation Near Surface at Equator	$2°K/hr$	$±5°K$	One diurnal cycle Lander
1.3 Seasonal Variation at Surface	$2°K$	$±5°K$	Six month Lander
1.4 Latitude Variation at Surface	$2°K$	$±5°K$	Multiple Probes
2.0 Pressure			
2.1 Altitude Profile:			
0-20 km	$5 \times 10^{-1} mb/5km$	$±5 \times 10^{-2} mb$	Single Probe
20-40 km	$1 \times 10^{-2} mb/5km$	$±1 \times 10^{-3} mb$	Single Probe
40-60 km	$2 \times 10^{-4} mb/5km$	$±2 \times 10^{-5} mb$	Single Probe
2.2 Diurnal Variation at Surface	$2 \times 10^{-1} mb$	$±2 \times 10^{-1} mb$	One diurnal cycle Lander
2.3 Seasonal Variation at Surface	0.5 mb	$±2 \times 10^{-1} mb$	Six month Lander
2.4 Latitude Variation at Surface	0.5 mb	$±2 \times 10^{-1} mb$	Multiple Probes
3.0 Density			
3.1 Altitude Profile:			
0-20 km	$2 \times 10^{-6} g/cm^3/5$ km	$±2 \times 10^{-7} g/cm^3$	Single Probe
20-40 km	$6 \times 10^{-8} g/cm^3/5$ km	$±6 \times 10^{-9} g/cm^3$	Single Probe
40-60 km	$1 \times 10^{-9} g/cm^3/5$ km	$±1 \times 10^{-10} g/cm^3$	Single Probe
3.2 Diurnal Variation at Surface	- - - - - -	$±1 \times 10^{-7} g/cm^3$	One diurnal cycle Lander
3.3 Seasonal Variation at Surface	- - - - - -	$±1 \times 10^{-7} g/cm^3$	Six month Lander
3.4 Latitude Variation at Surface	- - - - - -	$±1 \times 10^{-7} g/cm^3$	Multiple Probes
4.0 Composition (including water vapor)	1 Mass Unit (Water 1 part per billion)	$±5\%$ if 50% of total $±10\%$ if 50% of total	Single Probe
5.0 Winds			
5.1 Altitude Profile	2 m/sec/km	$±5$ m/sec	Multiple Probes
5.2 Surface Magnitude	- - -	$±5$ m/sec	Extended life Landers
5.3 Surface Direction	- - -	$±10°$	Extended life Landers
6.0 Particle Transport			
6.1 Impacts	10^2 impacts/cm^2/sec	$±10\%$ of total number	Extended life Landers
6.2 Mass Distribution	1 microgram	$±1$ microgram	Extended life Landers

accuracy, sensor performance has been taken into consideration. Sensors typically have errors that are constant and not proportional to their measurement. This characteristic does not permit sensors to meet, in general, accuracies expressed as constant percentages relative to the measured values. Therefore an order of magnitude change in the measured quantity results in an order of magnitude change in the relative accuracy. To minimize this problem, the altitude profiles have been divided into several altitude regimes where the quoted accuracies do not exceed 20 percent of the smallest measurement that will occur for the VM-8 model.

The requirements for composition measurements in table 4.1-1 are identical to the NASA/LRC objectives with the one addition that the resolution requirement for water detection is set at 1 part per billion. The high sensitivity for water detection is dictated by the seemingly low concentration of water in the Martian atmosphere and represents the best capability that probably could be made available for the 1973 mission.

The extreme right hand column in table 4.1-1 indicates the minimum mission approach required to obtain statistically adequate measurements on the atmospheric quantities. The measurements requiring a single probe and a one diurnal cycle Lander are included in the minimum science-minimum lifetime payloads of the study. The measurements requiring an extended life Lander are included as part of the candidate experiments for the expanded payloads. The one exception in this latter category is the wind experiment which is included in the minimum lifetime mission. Although statistically adequate data cannot be obtained in a 24 to 48 hour period, the engineering value of providing preliminary data on the apparent magnitude of steady-state wind conditions and their variability is very high. The detection of steady or gust wind conditions in the vicinity of 150 to 200 ft/sec (table 2.2-5) would help verify the necessity for concern on the gust-loading problem for touch-down dynamics of future Landers.

4.1.3 SURFACE METEOROLOGY

4.1.3.1 Diurnal Variations

The requirements for observing the diurnal variations of the atmospheric parameters can be set with the least speculation for temperature measurements. On the basis of the more recent observational data and theoretical analyses, the most probable variation to be observed at the surface of Mars near its equator, is given in fig. 4.1-1 (ref. 4-5). The prediction of this variation is assumed valid for all the VM models and a measurement resolution of 2°K/hour with a ±5°K accuracy should be adequate to verify the actual variation. It must also be pointed out that several investigators (ref. 4-6) anticipate the near-surface diurnal variation in temperature to differ markedly from the surface variations. In fact, recent theoretical studies on the subject (ref. 4-6) indicate the maximum near-surface (0.5 meters altitude) temperature will be 30°K to 50°K less than the maximum surface temperature. The situation is summarized in fig. 4.1-2 where it can be noted also that the temperature resolution and accuracy requirements in table 4.1-1 are adequate to detect the near-surface diurnal variation.
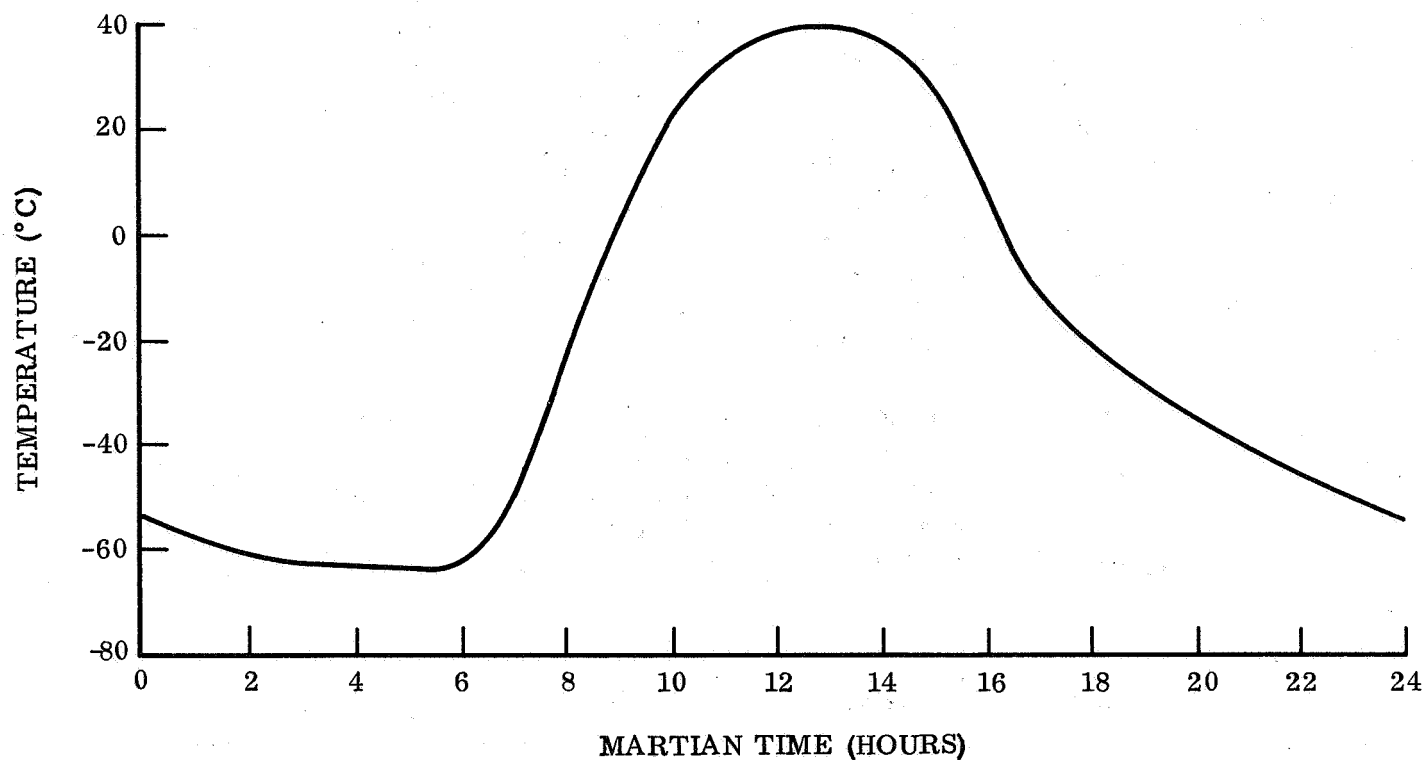
Figure 4.1-1. Diurnal Variation of Surface Temperature on the
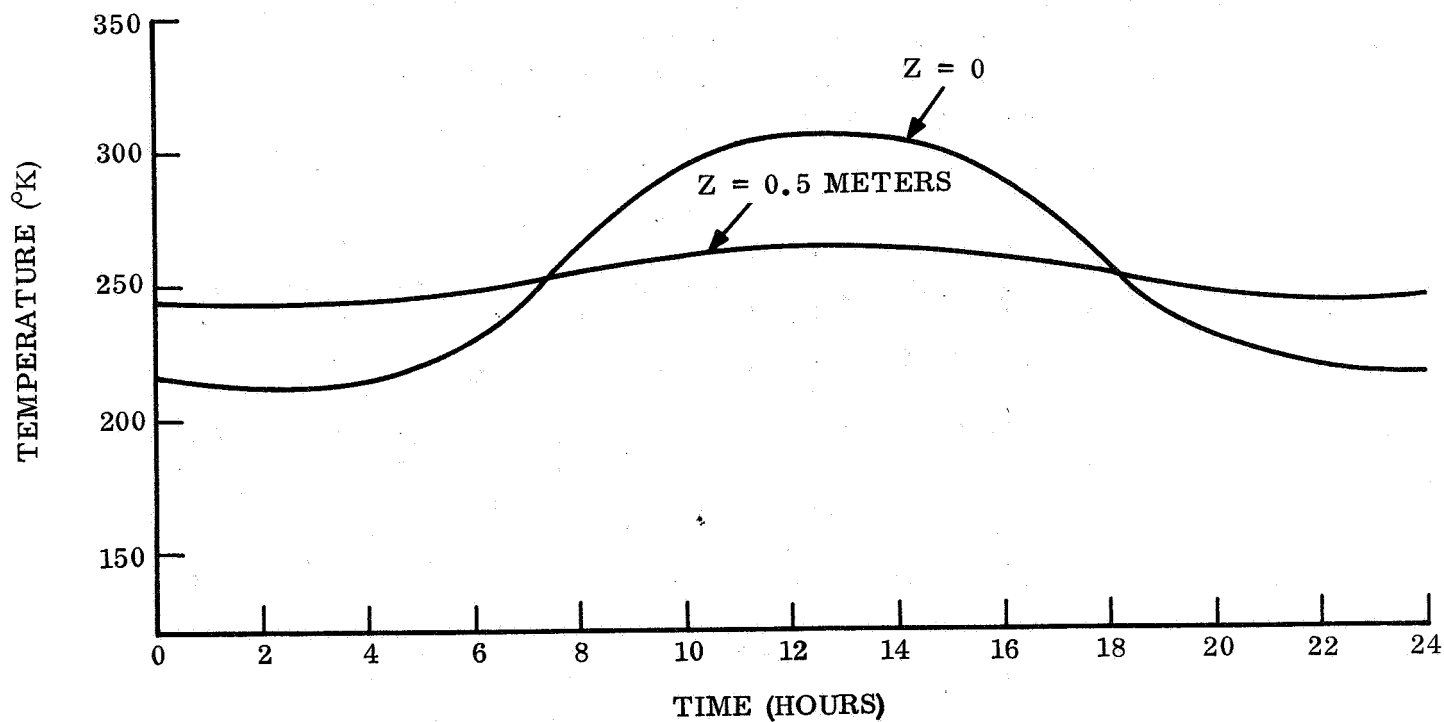Martian Equator at Perihelion

Figure 4.1-2. Temperature Versus Time at the Equator of Mars at
the Surface and at Z-0.5 Meters (Neubauer - 1966)

The lack of observational data on pressure and density variations makes the establishment of their resolution requirements very speculative. The diurnal variation for pressure has been estimated to be on the order of 0.2 millibar which for VM-8 is a 4 percent change and VM-9 is a 1 percent change. This type of variation is not uncommon on Earth and while its relationship to the actual variations on Mars is uncertain, it does not seem an unreasonable design goal. No attempt has been made to estimate the diurnal variation of density since its variation should be quite small (<1 percent) and no direct density measurement is currently planned. The accuracy requirement on pressure is consistent with NASA/LRC objective (±5 percent of value at known time) if the requirement is to be met for the lowest surface pressure models.

The only other atmospheric parameter that could show distinct diurnal characteristics is the local wind field which could be significantly affected by the solar thermal flux. The lack of observational data makes all estimates highly speculative therefore the NASA/LRC objectives for accuracy have been directly used in table 4.1-1 while the resolution requirement comes from the vertical wind gradient of 2 ft/sec/1000 ft in table 2.2-5.

4.1.3.2 Long Term Variations

The variation of surface temperature as a function of season and latitude has been determined by theoretical analyses based on considerations of radiative and conductive equilibrium conditions for the atmosphere and surface (refs. 4-7 through 4-10). An investigation into the merits of the various studies has established that considerable differences exist in their results but that a reasonable reference for temperature variability is given by Gifford's (1956) work shown in table 4.1-2. An examination of the model shows the measurement of the seasonal variability at any latitude should have the 2°K resolution and ± 5°K accuracy shown in table 4.1-1.

TABLE 4.1-2. MEAN TEMPERATURE (°K) AS A FUNCTION OF LATITUDE AND SEASON ON MARS

Season	Latitude (degrees)													
	-70	-60	-50	-40	-30	-20	-10	0	10	20	30	40	50	60
Southern summer	235	250	261	266	273	277	280	277	272	266	258	251	241	232
Southern winter	245	252	254	262	268	272	275	278	280	283	284	283	278	269
Δ T	10	2	7	4	5	5	5	1	8	17	26	32	37	37
Southern summer	235	250	261	266	273	277	280	277	272	266	258	251	241	232
Northern summer (reverse of southern winter)	–	269	278	283	284	283	280	278	275	272	268	262	254	252
Δ T	–	19	17	17	11	6	0	1	3	6	10	11	13	20

The latitudinal and seasonal variation of surface pressure is expected to be quite small. The maximum seasonal variation is estimated to be 1 mb by (ref. 4.11) who show such a variation could arise from CO_2 precipitation over the polar caps. Therefore a measurement resolution of 0.5 mb with an accuracy of ± 0.2 mb as shown in table 4.1-1 are required to detect such significant changes. The requirements to detect latitudinal changes are identical but are based on the expectation that the changes will come from the surface elevation changes relative to the mean planet radius and not "true" latitude changes. With elevations of up to 7 km possible and a pressure lapse rate of about 1 mb/km, a resolution of 0.5 mb and an accuracy of ± 0.2 mb is reasonable.

Studies on the possible density variations with season and latitude have also shown that small changes are to be expected at the surface (ref. 4-12). In fig. 4.1-3, it can be seen that density changes are essentially indistinguishable in time and latitude until altitudes of about 20 km are reached. Therefore density accuracies of $\pm 1 \times 10^{-7}$ g/cm^3, which are about ± 3 percent of the surface values in all of the models, are required to detect any possible changes.
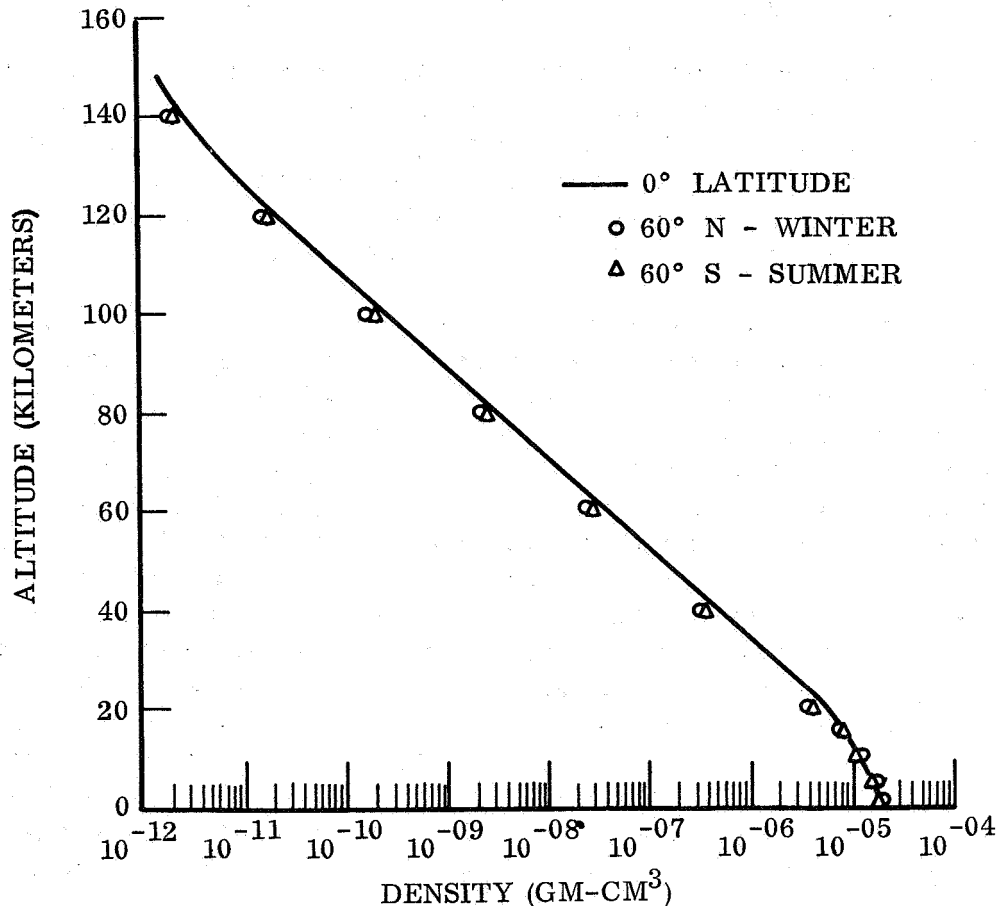

Figure 4.1-3. Density Profile Variation with Season and Latitude

The last two items which must be examined for long term variations are winds and their resulting particle transport. Long term observations may be required before a reliable statistical description can be established. Current data on low altitude winds is limited to only 53 observations in an 87 year period of the motion of low level dust clouds. The paucity of data has placed serious limitations on our understanding of the circulations patterns and has forced extreme wind values for design reference to be used (table 2.2-5). The design values lead to the measurement requirements shown in table 4.1-1. Studies on the particle transport that can accompany steady 60 m/sec winds have shown that particles from 1 to 100 microns in diameter can be carried over considerable distances (ref. 4-13). If the yellow dust storms on Mars are likened to terrestrial storms, then particle impact measurements must be able to resolve 10^2 impacts/cm^2/sec with an overall accuracy of ± 10 percent of the total count. The assumption that the particles are iron oxides with densities of 5.7 g/cm^3 leads to mass resolution of microgram for 1 micron diameter particles. An accuracy of ± 1 microgram is assumed reasonable.

4.1.4 SURFACE OBSERVATIONS

4.1.4.1 Photographic Observations

Initial imaging missions of the Martian surface will most likely be concerned with Lander site topography and geomorphology. Imaging requirements therefore, consist of panoramic sweeps at moderate spatial resolutions supplemented by periods of acquisition at higher spatial resolutions with attendant reduced fields of view. Additional pictures should also be acquired at this higher spatial resolution by depressing the line-of-sight so that the field of view encompasses the surface near the Lander.

By combining this total set of pictures it should be possible to establish the geological model. Images produced by an suitable means are without peer in their ability to indicate visible landforms, relative roles of land building and destructive process (e.g., tectonic versus erosional processes), to define sizes, shapes and relative positions of objects of interest. To be useful geologically, the images must cover a substantial spatial resolution range, preferably with nested fields. Field experience gained indicates that the highest resolution ought to correspond to that of the human eye at a distance of about 2 meters; i.e., a ground resolution of 1 mm. The lowest resolution will be dictated by the necessity of acquiring panoramic views at a reasonably rapid rate (operational lifetime constraints). Since the geologist and geographer obtain a large proportion of their information by visual processes it is highly desirable to obtain pictures that simulate as closely as possible what a human observer would see. Thus more advanced instrumentation with a larger bit budget will undoubtedly portray the planetary scence in stereo-monochrome, color, and possibly both. Not only these two disciplines benefit from these advantages but the biologist and botanist would also benefit enormously from viewing the particular subjects they are interested in on the planet.

Although the contribution of imaging reconnaissance to life detection on Mars is likely to be of an indirect nature, the results will undoubtedly center on the establishment of the role certain unusual environmental conditions play in the development of

life forms. Such unusual conditions are thought to exist in the areas of high reflectivity at the boundaries of the Martian polar caps and especially within the dark areas, maria such as Syrtis Major (a likely candidate for a Lander site on the first mission) which exhibit seasonal changes. Currently these changes (known as the wave of darkening) can be interpreted either as a biological phenomena or as a seasonal transport of dust between the highlands and the lowlands. On the basis of available evidence no preference can be attached to either theory. An imaging reconnaissance may resolve this problem and we note that the spatial resolution requirements indicated for geological purposes (figs. 4.1-4 and -5) will adequately serve for the detection of primitive plants, such as lichens, should they be encountered in the immediate vicinity of the Lander.

4.1.4.2 Surface Composition

The soil sampler that is used on Mars is likely to be a specially modified version of the Surveyor model. The objective of the instrument will be precisely the same as that of Surveyor, namely, to detect as many elements as possible on the surface of Mars. The most likely constituent to detect is generally agreed to be Limonite $[(Fe_2O_3)(FeO)^n H_2O]$. The mass range needed to detect this constituent extends from 1 to 55 mass units and according to current opinion it is unlikely that other constituents will be outside this range. Other constituents that are highly probable such as Hematite (Fe_2O_3) Manganese (MnO_2), Quartz (SiO_2) and possibly Felspars $[K Al Si_3 O_8$ and $(N_a C_a) Al_2 Si_3 O_8]$ have atomic weights lying roughly around the middle of the range necessary to detect Limonite.

The minimum requirement for the soil sampler is to record the elements lying beneath it on the part of the surface which it covers. Ultimately, however, more is desired; it is clearly more advantageous to record the soil composition in as many places around the Lander as is engineeringly possible. There are several reasons for wanting this; first there is a distinct possibility that with a proportionately large percentage of Limonite at the sample site, other constituents can be masked. It is well known that Limonite, by virtue of its finely divided state in dry atmospheres, can form a surface film over other materials such as Quartz. The low penetration depth of the soil sampler (circa 25μ) may well be insufficient to prevent this masking effect from being detected. This undesirable feature may not be completely obviated, but possibly minimized, by having a movable sampler. This feature also has the added attraction that it may enable the sampling of materials at some distance from the Lander and again minimize a probable undesirable occurrence -- that of recording only crush-up material from the Lander.

4.1.4.3 Expanded Payloads

When power, volume and weight considerations permit, the scientific payload can be increased to accomodate additional experiments. These experiments have been specifically selected to provide new information that will not be obtained with the minimum science payload. Additional information may also be obtained by extending the capability of some of the minimum science instrumentation. The primary goal of the minimum and expanded payloads is to acquire information that will reveal the physical properties of the planet, its suitability to support life, and, in particular, to indicate

Unit	Centimeters	Mineral Composition	Crystal Structure	Rock Fragments	Lineation	Rock Exposure	Rock Unit	Major Global Unit	Terrestrial Planet	Typical Investigative Techniques
	10^{-2}									Polarized
MM	10^{-1}									Photomicrog.
CM	1									Hand Lens
DM	10									Visual Inspect.
M	10^{2}									Photography
	10^{3}									
	10^{4}									Mapping
KM	10^{5}									Aerial Photog.
	10^{6}									
	10^{7}									Satellite Photog.
	10^{8}									
	10^{9}									Telescope
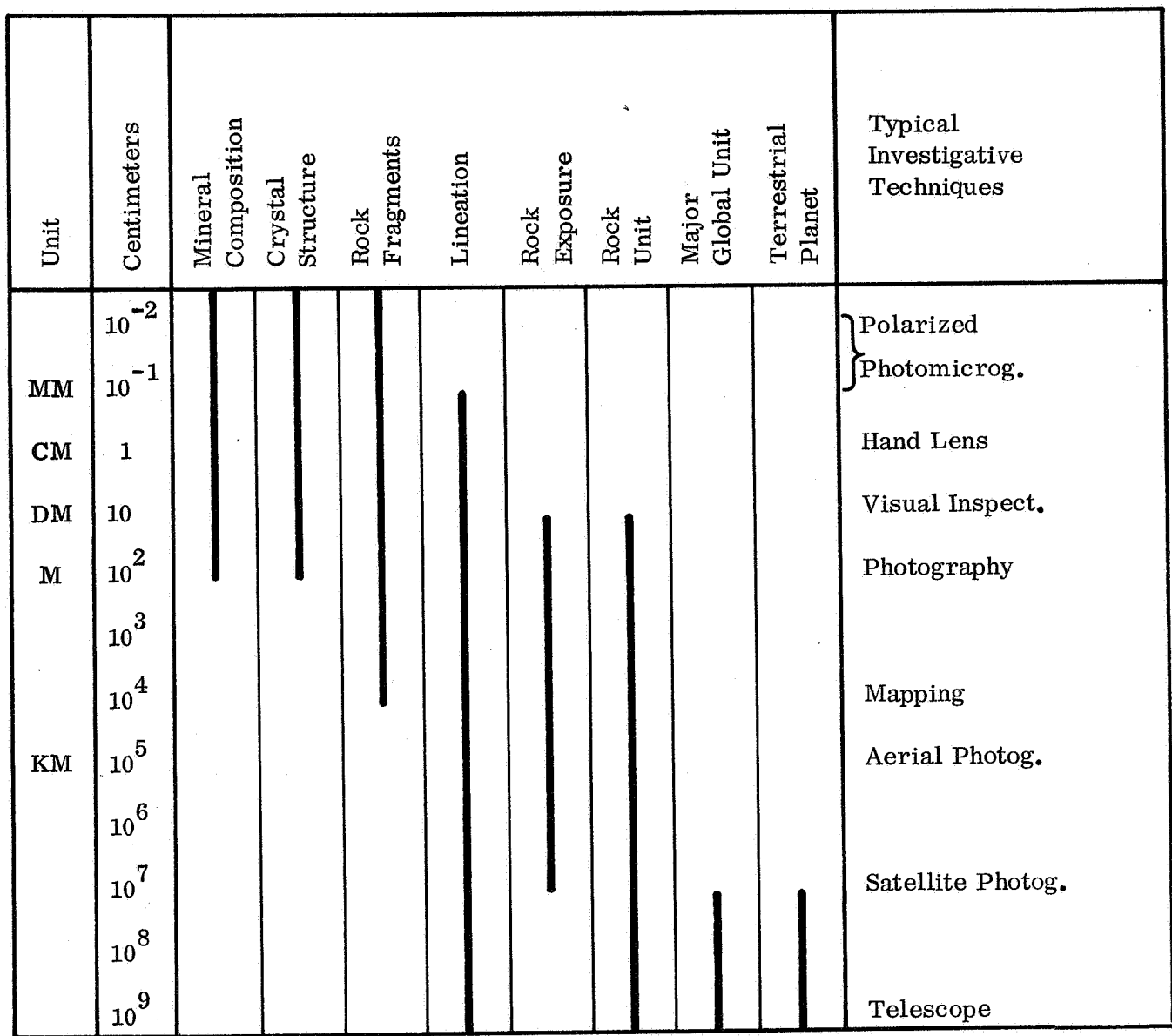
Figure 4.1-4.   Dimensions of Visible Geological Phenomena

4

Order of Magnitude													
Centimeters													
	10^{-5}	10^{-4}	10^{-3}	10^{-2}	10^{-1}	1	10^{1}	10^{2}	10^{3}	10^{4}	10^{5}	10^{6}	10^{7}
Clay	▬												
Silt		▬											
Sand			▬▬▬										
Gravel					▬								
Boulders						▬▬▬							
Basalt Grains			▬▬▬										
Granite Grains				▬									
Pore Spaces		▬▬▬▬											
Lava Bubbles					▬▬▬▬▬▬▬								
Snow					▬								
Ice Floes								▬▬▬▬▬▬▬					
Icebergs									▬▬▬▬				
Glaciers										▬▬▬			
Ice Caps											▬▬▬		
Delta									▬▬▬▬				
Alluvial Fan								▬▬▬▬					
Land Slide									▬▬▬				
Sand Dune								▬▬▬					
Fault						▬▬▬▬▬▬▬▬▬							
Lava Flow										▬▬▬			
Volcano										▬▬▬			
Impact Crater										▬▬▬			

Figure 4.1-5. Some Common Geological Phenomena Order of Magnitude

the past or present existance of life. In discussing the requirements of the experiments, no attempt has been made to grade the experiments in order of importance or desirability.

4.1.4.3.1 Photoimaging

The photoimaging program in the minimum science payload is constrained to 1.02×10^7 bits. This constraint not only limits the scope of the scene coverage but also limits the information retrieved from the re-constituted images. An extension of the number of allocated bits could permit the inclusion of color, multi-spectral and stereo techniques. The purpose in considering these features is the many-fold gain in information that could be obtained with their use. Color pictures would greatly enhance the ability of the geologist to identify minerals, rock formations, erosion processes and land building processes by providing him with information in the form with which he is most familiar. The probability of distinguishing simple plant life such as lichens is also enhanced by color discrimination. The ultimate in optical discrimination would be to employ multi-spectral techniques extending into the infrared part of the spectrum for certain cases where color discrimination is not sensitive enough. Stereo techniques require only the rearrangement of the formats of the two cameras so that they overlap in the region of the normal to the lander axis between the two cameras -- the gain in information by the use of stereo though is less pronounced than that brought about by color. The inclusion of color will probably involve a heavy increase in the amount of data to be accumulated and also in the weight of the data-sensitive subsystems, i.e., telecommunications and power.

4.1.4.3.2 Subsurface Moisture

Astronomical observations supported by laboratory experiments point strongly to the predominance of Limonite and other iron oxides containing water of crystallization, as the main surface constituent. Water available in this or some other form within the soil may provide the necessary support for some form of life of the planet. Its existance would also indicate the existance of environmental conditions similar to those existing on Earth at some earlier period. It is necessary for the moisture sensor to detect the presence of water at some depth below the surface. Opinions differ as to how deep the device should penetrate but an existing instrument capable of boring to a depth of 1 foot may be adequate. It is also possible that this instrument, if used, could provide evidence to explain the 'wave of darkening' if this phenomena, as it is thought to be, is associated with the melting of the polar caps.

The quantity of water to be found is highly uncertain since direct measurements indicate only small quantities of water vapor in the atmosphere and the existence of water of crystallization in the soil is highly speculative. The requirement for detecting subsurface moisture must be at least as demanding as that for atmospheric measurements in order to insure a reasonable capability being available for landed operation. A sensitivity of 1 part per billion is therefore required and would demand a measurement technique identical to that used in atmospheric measurements.

4.1.4.3.3 Large Molecule Detection

The aim of this experiment would be to show the existance of a long chain, heavy molecule of the carbon cycle. Evidence of the CH bond has occurred in some astronomical spectrographic observations of Mars. The objective of the instrument on the Lander would be to identify the complexity of these molecules through a gas and mass number analysis. These long chain molecules are most likely to be found on or below the soil surface since they will be too heavy to exist in the atmosphere.

Since the likelihood of finding heavy molecules in the Martian atmosphere is extremely small their detection will require the use of auxiliary equipment to provide soil samples and to extract the molecules from the samples for analysis. Early exploration missions are anticipated to be sufficiently simple as to exclude the use of sophisticated wet chemistry techniques in favor of more rugged and reliable approaches such as pyrolysis for molecular extraction. Although the latter approach limits molecular extraction to the more volatile compounds, there exist a sufficient number of biologically interesting volatile compounds to warrant that serious consideration be given to the pyrolysis technique.

Analyses for the detection of large, complex organic molecules typically requires sophisticated and carefully controlled procedures in order to avoid undesired molecular breakdowns and amibiguities. It is not unreasonable therefore to limit, on early Lander missions, the investigation of large molecules to molecular masses of less than 200 mass units where such problems are minimal.

4.1.4.3.4 Ultra-Violet Penetration

The nature of the short wave radiation reaching the planetary surface can markedly affect the form of life located there if any exists. The inclusion of an ultra-violet radiometer in the payload will again be an indirect indicator for the likelihood of life forms existing and in addition will provide information about atmospheric constituents. The UV radiometer must cover the range from $2000\overset{\circ}{A}$ to $4000\overset{\circ}{A}$ in several discrete bands, preferably those in which the absorption bands for DNA, 0 and 0_3 occur. The significant peril that UV radiation can have on biological systems is well established. Direct solar UV radiation can cause the death of bacteria in several minutes and its influence on mutation processes is still important even when the direct radiation levels are reduced several orders of magnitude. The impact of UV radiation on surface life forms on Mars therefore can not be underestimated if insufficient atmospheric attenuation exists.

In addition, knowledge of UV scattering in the atmosphere is of interest to evaluating atmospheric structure. Determination of the scattered component will require either sophisticated experimental techniques to separate out the direct radiation or extensive post flight analysis using such data, as total intensity levels and the relative Sun-to-sensor angular orientations. The latter approach is consistent with the intent of the expanded surface science payload and would require only the addition of an immobile solid state sun angle sensor to the basic radiometer used for total intensity measurements.

4.1.4.3.5 Life Detection

Several of the experiments given above have the capability to detect life, but it is highly desirable to have an experiment to directly measure the life process. Such experiments utilize processes involving microbiological growth or metabolism with the inherent assumption that the chemistry involved is carbon-water based. The experimental devices that may be used for the life detection function also have other similar requirements which involve sample acquisition, nutrient definition, environmental conditions for growth, and data interpretation for minimum amibiguities. Two of the most highly developed devices, Gulliver and Wolf Trap, have been demonstrated to provide adequate solutions for the requirements under a wide variety of operating conditions. The prediction of success for these units when placed on Mars is uncertain since the identification of the proper nutrients, the anticipated bacterial concentrations, and the proper depth for sampling are extremely difficult, if not impossible, to establish. These requirements for the proper conduction of life detection experiments therefore will remain unresolved until Lander missions provide sufficient data on the physical and chemical structures of the Martian atmosphere and surface.

4.1.4.3.6 Airborne Dust Detection

The occurrence of persistent dust transport in the Martian atmosphere could present significant design problems for future Landers that will use moving parts and extensive optical equipment. Pitting and dogging of their surfaces and joints by the particle impacts could jeopardize the longevity of many experiments. Collection of data to characterize the transport phenomena therefore represents a significant experiment for inclusion on an expanded payload.

The determination of the experiment requirements relies on knowledge of the wind fields, surface composition surface roughness, and particle size distribution. In general, there exists only a small amount of direct data which after careful evaluation does not permit the establishment of definite requirements. The paucity of data has placed serious limitations on our understanding of low altitude winds and has forced the use of extreme wind values for design reference (table 2.2-5). These wind values are based on the direct observations of large yellow dust storms and on assumption of surface roughness and particle size and mass distributions. As such, the reference winds are speculative and the only reliable statement is that their magnitude seldom exceeds the 60 m/sec value.

Definition of the experiment requirement given in table 4.1-1 was therefore based solely on theoretical studies (ref. 4-13). Studies on the particle transport that can be expected in the Martian atmosphere show that sizes from 1 to 100 microns in diameter can be expected. With the assumption that the Martian yellow dust storms are similar to terrestrial storms, the particle impact rates can be in the vicinity of 100 impacts/cm^2-sec. Finally, the particles on Mars are believed to be most likely in the iron oxide group which has a typical density of 5.7 g/cm^3. This density corresponds to about a 1 microgram particle that has 1 micron diameter. Particles of smaller diameter are expected to be highly unlikely (if the natural occurrence on Earth of particle sizes is assumed to hold). Moreover if the granules are more like sand, the density and hence mass change is still within a factor of two for that of iron oxide. Hence the requirements of a ± 1 microgram resolution appears reasonable.

4.2 SELECTED SCIENCE IMPLEMENTATION

4.2.1 GENERAL

The implementation of payloads to meet the mission scientific requirements falls into the four categories of supersonic entry, subsonic entry, minimum landed, and expanded landed payloads. Each of the categories involves unique implementation problems that involve data analysis and interpretation, instrument packaging and deployment, and lifetime. One of the primary objectives of the parametric and point design studies is the identification of the reasonable solutions to these problems. The studies are concerned not only with the selection of candidate sensors, and measurement techniques but also with the most promising analysis methods that can reliably extract the maximum possible information from the data.

The flight regime in which the payloads for the entry probe must operate are supersonic flight and subsonic flight. Attempts to directly measure the ambient atmospheric properties while the vehicle is well above Mach 1 are hampered seriously by flow field heating and ram effects, by heat shield ablation products, and by the short time spent in any one altitude regime. The overall results stemming from consideration of the problems is to: 1) favor the use of acceleration data with our knowledge of the vehicle aerodynamic properties to construct a density-altitude profile; and 2) attempt to use stagnation temperature and pressure data with our knowledge of flow field phenomena to unfold ambient temperature and pressure information versus time. Atmospheric composition measurements during supersonic flight are limited to low Mach numbers (typically below Mach 5) where both heat shield outgassing and dissociation of the atmospheric gases in crossing the shock front are ignorable.

Atmospheric measurements during subsonic flight are only slightly perturbed by the above problems. As a result, it is possible to consider a minimum payload as consisting of temperature and pressure sensors mounted on the Capsule base and to use their data (which can be reliably corrected to give ambient values) with our knowledge of vehicle dynamics to: 1) determine temperature, pressure, and density altitude profiles; 2) determine mean molecular weight; and 3) grossly estimate the most probable major atmospheric constituents. The use of mass spectrometers, and possibly radar altimeters, not only improve our confidence level in the derived atmospheric model but also will aid the removal of biases in the subsonic data and ease the matching of this data with the data obtained in supersonic flight.

Landed measurements during one complete diurnal cycle are characterized by their intent to: 1) refine the data on surface atmospheric temperature, pressure, and composition (particularly water content); 2) evaluate atmospheric variability; and 3) provide initial data on surface topography and composition. The implementation of the science payload must provide for the selection of deployment or sampling schemes to insure monitoring of the ambient conditions with minimum vehicle-induced perturbations and by sensor sensitivities and stabilities.

Measurements that are most likely to be made for Landers with expanded capability might not only include acquisition of more atmospheric and photographic data but might involve attempts at life detection and at increasing the detail of data on surface and sub-surface composition and environments. In general, the implementation will again be dominated by the selection of deployment or sampling mechanisms but the level of sophistication will be higher since whole sensors with their most important subsystems must be precisely deployed and the capability to re-deploy certain sensors (including changing camera viewing format) is significant.

The following sections will amplify on the candidate approaches selected for implementing the specific measurements and will discuss the experiment simulation technique developed to identify the optimum measurement and analysis methods for reconstructing the atmospheric profile from entry data. Tables 4.2-1 and -2 show the physical, electrical and communication requirements of selected instruments for entry and surface science measurements.

4.2.2 ENTRY SCIENCE

4.2.2.1 Temperature

Two candidates for temperature profile measurements were considered for the 1973 Hard Lander. They were the platinum resistance thermometer and the thermistor.

The platinum resistance thermometer was selected for use in the entry science payload since it has superior performance characteristics in the temperature regime ($100-300°K$) of interest. Additionally its excellent calibration stability provides a high confidence level in the ultimate measurement accuracy.

Temperature measurements during supersonic flight will be limited to stagnation point readings and will be made from the beginning of entry to the deployment of the parachute and separation of the aeroshell. The use of only stagnation readings in the higher Mach number altitude regime stems primarily from the extreme difficulty in reliably interpreting temperature data at other points when extensive aeroshell heating and ablation occurs. In addition to the effort required to design a sensor for optimum performance during Martian entry, extensive pre-flight testing will be required to evaluate and establish calibration curves for the sensor performance under the anticipated flow field conditions. The data is necessary for the post-flight analysis to determine ambient temperatures.

Measurements in the subsonic regime will be made at the base of the vehicle since available data indicates that the correspondence between the measured base temperatures and the ambient values can be reliably predicted. The resolution and accuracy for the temperature measurement system in order to meet the scientific requirements is being evaluated by the Experiment Simulation Technique discussed below. The results of the evaluation are discussed in Section 3.4.2 of Volume III.

TABLE 4.2-1. ENTRY SCIENCE PAYLOAD

Instrument	Weight	Volume	Thermal Req'mts.	Power Req'mts.	Location	Deployment/ Orientation	Sampling Schedule	Data Format
Mass Spectrometer	8 lbs.	2 x 7 x 14 inches	N.A.	7 watts	Internal near surface Requires port through heat shield. (See Note 1)	N.A.	Initiates near Mach 5. Terminates at impact.	50 (8) bit words per sample (2 sec. scan, 8 sec. readout) 50 bits/second readout
Resistance Thermometer	0.5 lbs. each	1 inch dia. x 2 inches long	N.A.	1 watt each	Two on base of Capsule	N.A.	Initiates near Mach 5. Terminates at impact.	One 0.25% analog channel each. 9 bits/sample 1 sample/sec. 18 bits/sec. total throughout, post-chute deployment period
Variable Capacitor Pressure Transducer	0.5 lbs. each	2 inch dia. x 2 inches long	N.A.	1 watt each	Two on base of Capsule	N.A.	Initiates at beginning of entry. Terminates at impact.	One 0.25% analog channel each. 9 bits/sample 1 sample/sec. 18 bits/sec. total throughout post-chute deployment period

NOTE 1: This penetration may be through the heat shield if out-gassing of heat shield materials can be avoided at velocities below Mach 5. Placement of this port at the base of the vehicle will necessitate the inclusion of a pump in the gas line.

TABLE 4.2-1. ENTRY SCIENCE PAYLOAD (CONT'D)

Instrument	Weight	Volume	Thermal Req'mts.	Power Req'mts.	Location	Deployment/ Orientation	Sampling Schedule	Data Format
Tri-Axial Accelerometer (Dual Scale)	2 lbs.	2.8 x 1.8 x 2 inches	N.A.	4 watts	Located at body C.G. with one axis aligned to Capsule vertical axis	N.A.	Initiates at beginning of entry. Terminates at impact.	8 bits/sample/axis. 10 samples/sec. 72 bits/sec. total. Automatic scale switching
Water Vapor	1 lb. (ducting only)	Detector located in surface science package	N.A.	N.A.	Ducting located same as mass spectrometer ducting	N.A.	Initiates near Mach 5. Terminates at impact.	One sample/15 sec. 2 seven bit (parallel) channels. 1 eleven bit (parallel) channel
Stagnation Temperature Transducer (1)	0.5 lb.	1 inch dia. x 2 inches long	N.A.	1 watt	See text	N.A.	Initiates at beginning of entry. Terminates at aeroshell ejection.	1 analog channel. 0.25% accuracy. 1 sample/sec.
Stagnation Region Pressure Transducers (4)	0.5 lbs. each	2 inch dia. x 2 inches long each	N.A.	1 watt each	Behind nose of aero-shell (See text)	N.A.	Same as above	4 analog channels. 0.25% accuracy. 1 sample/sec.

TABLE 4.2-2. SURFACE SCIENCE PAYLOAD

Instrument	Weight	Volume	Power	Location	Deployment/Orientation	Mission Profile	Data Format/Requirements	Point Design
Pressure Transducer (2)	0.7 lbs. each	2 in. dia. 2 in. long each	1 watt each	Internal near skin of Lander	Port through skin to ambient environment either top or bottom. No deployment	Operates continuously after impact	3 samples/hr. each 1% accuracy. Two channels total	1 through 6
Resistance Thermometer (4)	0.5 lbs. each	1 in. dia. 2 in. long. each	1 watt each	One on each camera boom	Deployed above Lander on camera booms. One on each boom.	Same as above	3 samples/hr. each 1% accuracy. Four channels total	1 through 6
Wind Velocity Transducer (2)	2.5 lbs. each	25 cubic inches prior to deployment each	3 watts each	One on each of two camera booms	Boom deployment above vehicle on camera booms	Same as above	3 samples/hr. 6 channels. Each channel consisting of 11 parallel bits. Total of 66 bits/sample	1 through 6
Moisture Detector (1)	10 lbs.	60 cubic inches	5 watts	Mounted internal to Lander	Pneumatic tubes deployed as part of camera booms	Same as above	3 samples/hr. 2 seven bit (parallel) channels. 1 eleven bit (parallel) channel	1 through 6
Surface Composition (Alpha-Scatter) (1)	9.5 lbs.	5.5 in. x 7.5 in. x 4.5 in.	5 watts	Internal to Lander	Must be deployed so that sensor head rests on surface of planet. Top or bottom deployment controlled by clinometer	Deploy 3 hours after impact. First readout 1 hour after impact. Second readout 3 hours after impact, then readouts every 3 hours thereafter	1 sample/3 hrs. 130 channels 14 bits (parallel) each, 130 channels 12 bits (parallel) each, 3 channels 7 bits (parallel) each	1 through 6
Photo Imaging (4)	4.8 lbs total	1 in. - 2 in. dia. 9 in. - 12 in. long each	6-10 watts total	One on each of four booms deployed above Lander	Boom deployment 36"> Height > 18", One boom/camera	4 frame sweeps on high resolution and 4 frame sweeps on low resolution in sequence. Operation time coincident with transmissions	Flexible to meet maximum transmission capability of Lander. Period from one second to eight hours per picture. Total bits between 107 and 108	1 through 6

TABLE 4.2-2. SURFACE SCIENCE PAYLOAD (CONT'D)

Instrument	Weight	Volume	Power	Location	Deployment/Orientation	Mission Profile	Data Format/Requirements	Point Design
Clinometer (2)	1.3 lbs. each	2 in. dia. x 3 in. long	3 watts	Two internal to Lander mounted with long dimension parallel to vertical axis of Lander	N/A	Sampled immediately after impact. Then once every six hours.	1 sample/6 hrs. 2 channels 7 bits (parallel) per channel	1 through 6
Sub-Surface Water Detector (2)	0.5 lbs. (Borer), 3 lbs. (Deployment), 1 lb. (flexible ducting) each	0.25 in. dia. x 18 in. + 2 in. x 2 in. x 2 in. + deployment mechanism	40 watts each	One borer assy on top and one on bottom of Lander. Water detector inside Lander.	Bellows or pneumatic deployment with 10 lbs. vertical force required	One sample taken – 10 minutes for drilling – 45 minutes for sampling	3 seven bit words 1 eleven bit word one sample	5 and 6
Airborne Dust Detector (1)	4.0 lbs.	125 in³ (5 in. x 5 in. x 5 in.)	0.5 watts	Sounding Box on Top of Lander	Deployed by camera boom	Operates full time. Records impacts and is read out 1/4 hours. Resets at read out	8 bits/sample 1 sample/4 hrs.	5 and 6
Ultra-Violet Radiometer (2)	5.0 lbs. each	60 in³	2.5 watts each	One on top and one on bottom of Lander	Oriented to look upward	Operates during daylight only	2 1% analog channels per sample, 4 0.25% analog channels per sample, 1 sample/hr.	5 and 6
Large Molecule Detector (Mass spectrograph/gas chromatograph) (1)	17.0 lbs.	600 in³	16 watt + 40 watt (Pyrolizer)	Internal to Lander	N/A	Subsurface borer collects sample (10 min.) Standby (1 hr.) for H₂O detection – Transfer sample to pyrolizer (1 min.) – Heat (20 min.) – Sample gas (30 min)	Mass Spectrometer 2 channels – 8 bits each work 175 serial words/sample 2800 bits/sample Gas Chromatograph 1 channel, 8 bits/word 1 channel 9 bits/word 30 words/sample 510 bits/sample	5 and 6

4.2.2.2 Pressure

Various types of pressure transducers including variable reluctance, potentiometer, variable capacitance, and Dimeff Viscosity transducers were evaluated for application to pressure measurement in the Martian atmosphere.

Based upon its demonstrated reliability, independence from other measurements, and the accuracy requirements of the measurement the variable capacitance transducer was selected for point design evaluation. A controlled leak rate differential transducer being developed by General Electric has not been flight tested as yet but is a prime contender for this application when it is fully developed.

Pressure measurements will be made at two sites on the entry vehicle while it is in supersonic flight. The primary measurements for determining the ambient values of pressure will be made at the vehicle base since correlation studies (ref. 4-14) indicate that a reliable correction curve can be obtained. The second site will be the stagnation region where four pressure transducers will provide data primarily for determining vehicle angle-of-attack and will serve as back up devices for the base pressure transducer. Pre-flight testing will be employed for establishing the measurement requirements and post-flight analysis.

The subsonic pressure measurements will also be made at the base of the vehicle and will be used with the corresponding temperature measurements to determine the altitude-time profile to impact. The resolutions and accuracies needed to meet the scientific requirements are discussed in Volume III, Section 3.4.2.

4.2.2.3 Density

Two methods of atmospheric density profile were considered for the 1973 Hard Lander. They were density determination by radiation backscatter from the atmosphere and density determination through the analysis of entry capsule deceleration.

The measurement approach chosen for point design evaluation is the body acceleration interpretation approach. The choice is based upon consideration of weight, volume, and system compatibility. Backscatter devices for this purpose would weigh upwards to 15 lbs. and seriously limit the design flexibility due to their shielding and orientation requirements. By sampling the accelerometer at high rates the body dynamics sensitivity of the evaluation is minimized and bias errors are significantly reduced by virtue of the fact that pressure and temperature profiles are measured during the low velocity portion of the entry.

The utilization of triaxial accelerometers at high Mach numbers provides a capability for the indirect determination of density as a function of time. The use of a single set mounted at the Capsule's center of gravity is adequate for this function if the body motion undergoes small angle-of-attack oscillations. The determination of the Capsule's altitude-time profile using the same basic data imposes more stringent requirements and forces the use of at least two measurement ranges on the triaxial accelerometers. In addition, the existence of large angles-of-attack, if they occur, will demand the use of off-axis rate gyros to establish angle-of-attack histories which would be needed to account for the variation of the drag coefficient with angle-of-attack.

The primary operating regime will be from the beginning of entry down to parachute deployment. Below this point, the acceleration data will have primary importance for engineering performance and only a secondary scientific value.

4.2.2.4 Composition

Mass spectrometry, gas chromatography and specific chemical reaction/detection experiments have been proposed to identify the major constituents of the Martian atmosphere. The ability of the mass spectrometer to operate at velocities as high as Mach 5, withstand sterilization environments, and accommodate all of the potential atmospheric constituents with equal facility in measurement coupled with its relatively advanced state of development for this application have led to its selection as the composition measurement experiment for the Hard Lander. Further, the three classes of spectrometers that have been designed as prototype flight hardware and are applicable to measurements during Martian entry are: 1) R-F quadrapule, 2) double focusing, and 3) monopole analyzer. For reasons of magnetic cleanliness and state of development, the R-F Quadrapule Mass Spectrometer was selected for point design evaluation. In addition to the above, the R-F Quadrapule has the desirable feature of requiring only one detector telemetry channel.

The direct measurement of atmospheric composition at supersonic speeds presents an extremely difficult analysis problem with the presence of ablation products and gas dissociation. Past studies have produced no ready solutions. The problems can be circumvented by delaying the measurements to low supersonic and subsonic speeds where dissociation and ablation processes are considerably reduced and where the use of a non-ablative cap in the area of gas sampling eliminates their remaining influences. Gas sampling can be most easily accomplished with a port in the stagnation area since use can then be made of the ram pressure to provide a positive pressurehead. The gas will be collected at specific altitudes and analyzed using a mass spectrometer to provide absolute quantities of the major and more abundant minor constituents (including CO_2, N_2, A). The use of a mass spectrometer equipped with a molecular leak inlet permits direct readout of the absolute quantities. The number of gas samples need not be high since all the measurements will be made in a well mixed atmosphere where no altitude dependence will be evident.

II

The detection of water vapor during descent will be extremely difficult with the mass spectrometer. The maximum water vapor detection sensitivity for these devices is about 100 parts per million which is inadequate for the low concentrations (<10 ppb) that are anticipated. The importance of water to biological systems warrants sensing devices specifically designed for ultra sensitivity and selectivity. It is planned to employ such a water vapor detector for the landed phase and the same device (located in the Lander) can be used for the entry measurements by using special ducting from the Capsule stagnation region for gas sample transport to the detector.

The presence of a mass spectrometer provides a direct means of determining composition and mean molecular weight with little ambiguity. In the event of equipment failure, the subsonic temperature and pressure data serve as a back-up since they can lead to a determination of mean molecular weight with the proper data analysis.

4.2.2.5 Data Analysis and Interpretation

The measurements made throughout entry are all made on a time base where conversion to altitude can be performed by either of two methods. The direct method relies on the use of a radar altimeter which can provide altitude information with little uncertainty. The indirect method relies on deceleration, or temperature and pressure data to calculate the altitude profile using knowledge of the Capsule's mass and dynamic properties. The indirect method is attractive since it uses atmospheric data which may be obtained by any minimum payload and does not require additional hardware to derive altitude information.

The indirect method forms a basic part of the Experiment Simulation Technique used in this study. Experiment Simulation is a method by which the data from an experiment is mathematically simulated, analyzed, and interpreted before the experiment is actually conducted. By observing the effect, on the simulated results, of various changes in the type of data considered, the experiment design, instrumentation properties, and analysis techniques used, it is possible to make decisions regarding the optimization of these factors for the actual experiment. The technique is used to parametrically evaluate the achievable experiment accuracy as a function of ballistic coefficient, sampling rate, sensor accuracy, atmospheric model, and subsystem errors. The results are given in Section 3.4.1 of Volume III. The study is limited primarily to the subsonic regime and clearly demonstrates that mean molecular weight and density can be obtained independent of a spectrometer and direct density measurements.

Figure 4.2-1 shows a flow diagram illustrating the steps involved in the Experiment Simulation Technique under discussion. As given quantities, we have: the Capsule parameters, namely mass m, cross-sectional area A, and the drag curve, giving drag coefficient C_D as a function of Mach number M_∞; an atmospheric model giving temperature T, pressure P, and density ρ, as a function of altitude h, as well as molecular weight M; the Capsule entry conditions of position (altitude h_E) and velocity V_E (in the
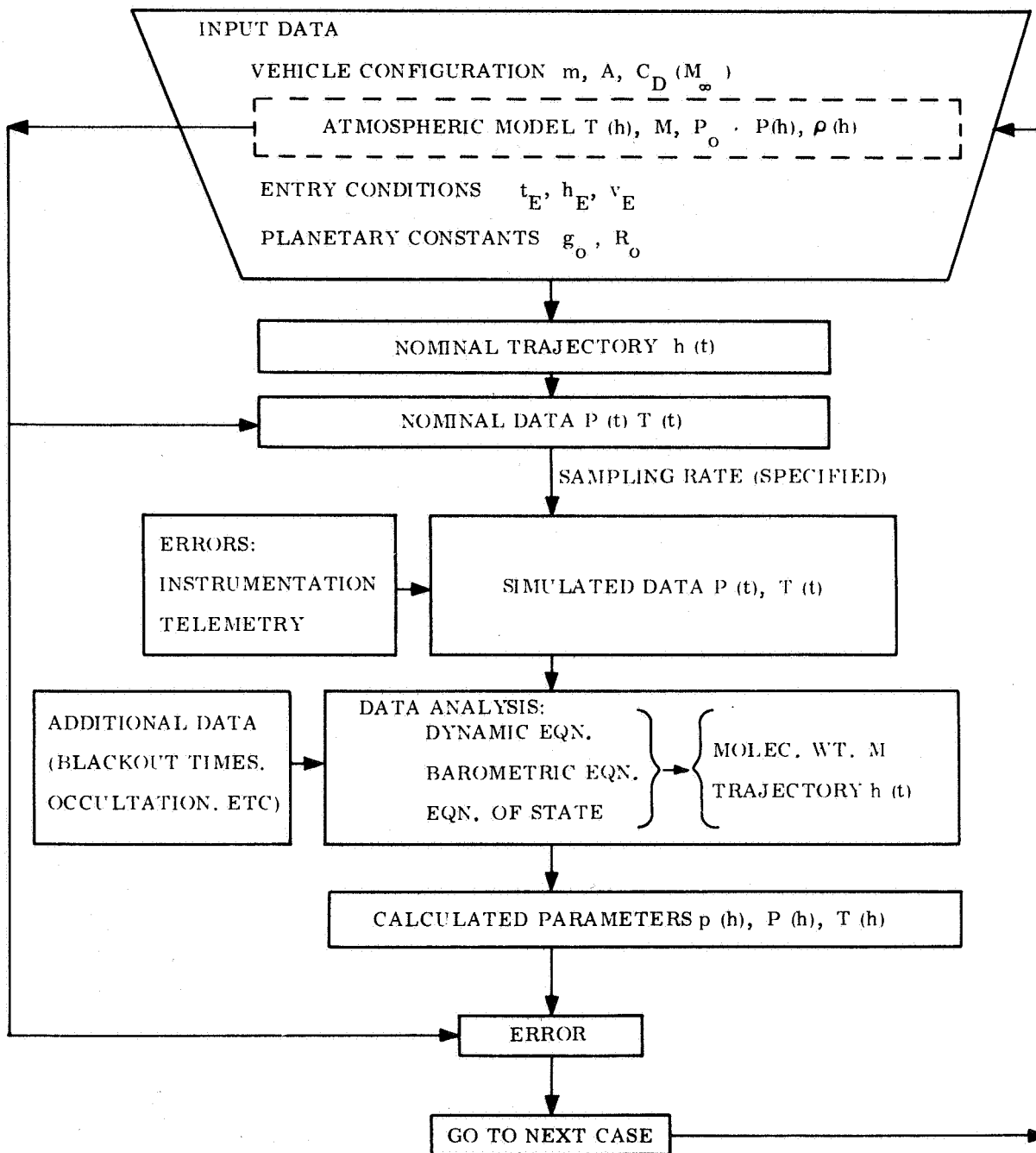
Figure 4.2-1.   Flow of Experiment Simulation for Atmosphere
Reconstruction

terminal velocity case a vertical (90°) descent is assumed); and the planetary physical constants, surface acceleration of gravity g_0, and planet radius R_0. This data is used to generate the nominal trajectory (altitude versus time) from which the nominal pressure and temperature history is derived. When instrumentation, telemetry, and flow-induced errors are added, and the results taken at a specified sampling rate, this time history becomes the simulated raw data to be analyzed. The data analysis, which is described in detail below, basically uses the dynamic equation (equation of motion), the barometric equation, and the equation of state, supplemented by other available data, to obtain the molecular weight and trajectory from the input pressure and temperature data. From the trajectory, the altitude profiles of the desired atmospheric parameters, density, pressure, and temperature are obtained. These calculated profiles are then compared with the nominal atmospheric model to determine the accuracy of the technique.

The data analysis method is summarized in Figure 4.2-2. In the analysis, zero time corresponds to the planet's surface and increasing time corresponds to increasing altitude. That is, the calculations proceed backward timewise from impact. Basically the input consists of the simulated pressure and temperature history (with errors), together with the data on the planet and the Capsule, and the other available data. The pressure and temperature data is smoothed and estimates are made for initial molecular weight M_0, initial velocity V_0, and ratio of specific heats γ .

Each run-through of the method involves three separate trajectory calculations, based on three values of molecular weight (a chosen nominal value M_0 plus and minus some tolerance ΔM). For a given molecular weight, altitude-versus-time profiles are calculated by two separate routes, dynamic and barometric. The first involves integrating the equation of motion (in this case the one for terminal velocity), and the second integrating the barometic equation. The difference between the two routes is measured by the fraction $\delta h/h = (h_D - h_B)/h_B$, where h_D is the dynamic altitude, and h_B the barometric altitude. Using the values for $\delta h/h$ found at the end of the first time step for the two extreme molecular weights, interpolate to find the value of M for which there is a matching of the two routes, that is, $\delta h/h = 0$ (the "cross-over" point). This value is then the M_0 used to compute the entire "mean" trajectory with $M_0 \pm \Delta M$ used for the "extremes". Although the molecular weight for a given trajectory is held constant throughout, an interpolation (or extrapolation) is performed at each time step to obtain the cross-over point (M_1) at that time. At the end of the trajectory calculation the average M_1 is computed (M_{1AV}) together with the corresponding standard deviation σ_M. These quantities are then taken as a new M_0 and ΔM and the entire procedure is repeated. The iterations continue until successive results are within a desired tolerance. Usually one or two iterations suffice.

Each run-through of the method produces an average molecular weight, a trajectory (altitude versus time), and density, pressure, and temperature profiles.
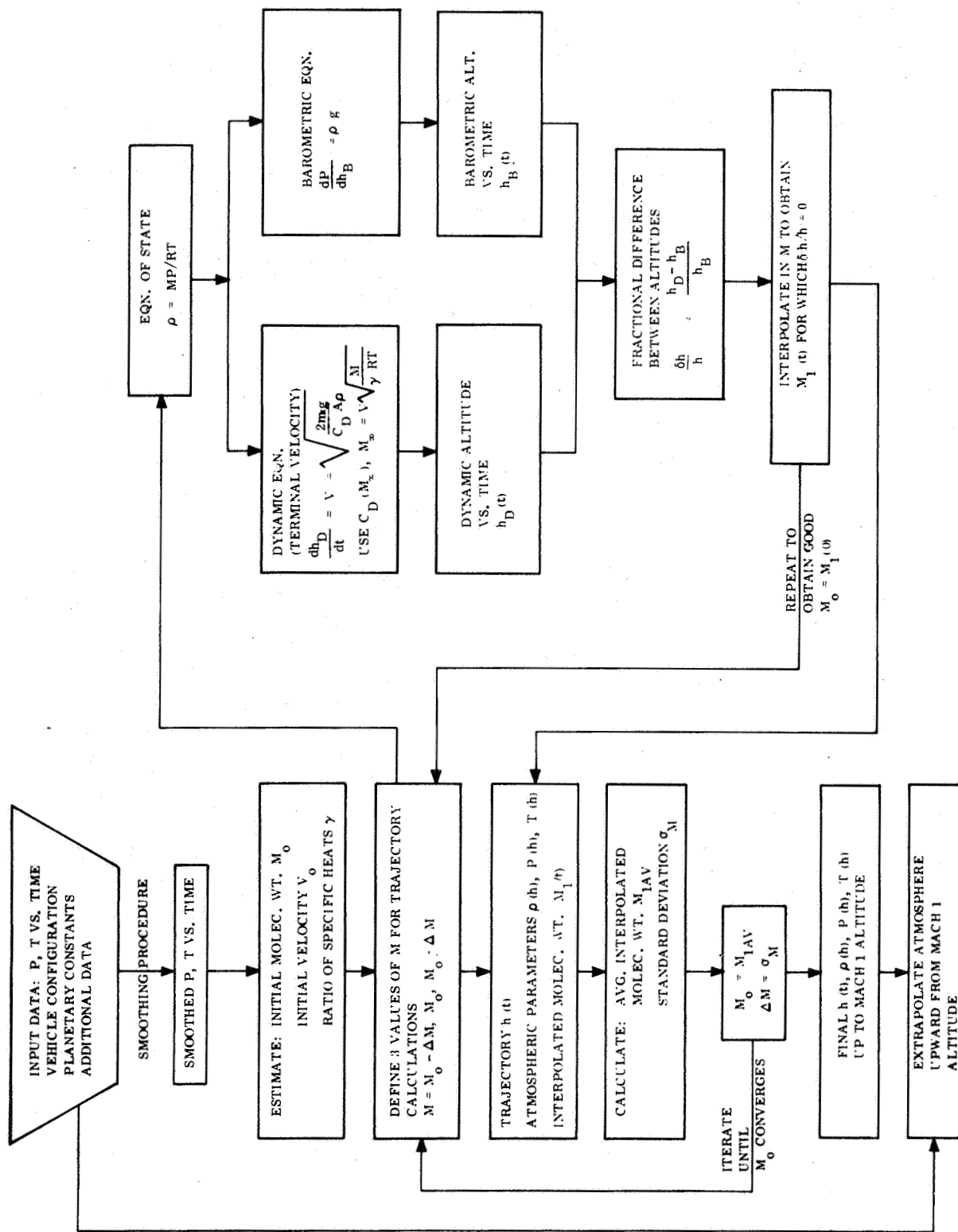
Figure 4.2-2. Flow of Data Analysis for Atmosphere Reconstruction

Above Mach 1 where the real data becomes more difficult to correct because of flow effects, a mating of the results is made with the density-altitude profiles derived from the acceleration data.

Density is determined by integrating the trajectory from entry downward using measured deceleration and gravitational attraction. The density is obtained from the velocity and drag characteristics of the entry configuration. The same integration is used to calculate altitude and pressure.

From the measured acceleration components in three axes and the angle of attack history, the drag acceleration, a_d, and the lift acceleration, a_ℓ, are determined. Entry conditions are defined and the trajectory is computed according to the following trajectory equations:

$$\frac{d^2 r}{dt^2} = -\frac{\mu}{r^2} + r\left(\frac{d\theta}{dt}\right)^2 + a_d \sin \gamma + a_\ell \cos \gamma \qquad (1)$$

and

$$r\frac{d^2 \theta}{dt^2} = -a_d \cos \gamma - 2\frac{dr}{dt} \cdot \frac{d\theta}{dt} + a_\ell \sin \gamma \qquad (2)$$

where

γ is the entry flight path angle.

At any point on the trajectory, the density follows from

$$\rho = \frac{2a_d m}{C_D(M)AV_\infty^2}$$

where

M is Mach number, m is vehicle mass and A is vehicle area.

The drag coefficient, $C_D(M, \alpha)$, is a function of Mach number and angle-of-attack. The angle of attack history is known but the Mach number is as yet unknown. In the high speed portion of the trajectory (above Mach 4), the drag coefficient is very nearly independent of Mach number. Below Mach 5 a preliminary estimate of speed of sound is used representing a nominal profile between the postulated extreme Voyager Mars (VM) atmospheres.

II

The exercise of both the supersonic and subsonic experiment simulation can in general, be repeated for various model atmospheres, sampling rates, instrumentation errors, data analysis methods, etc., in order to obtain criteria for mission analysis, instrumentation selection, and experiment design.

4.2.3 SURFACE SCIENCE

Scientific measurements of the surface, subsurface, and meteorological character-istics of Mars will be performed during a one to 90 day period following a successful landing. In general, the geological characteristics along with nominal identification of the meteorological condition at the surface will be measured during the first 24 hours on the planet. The more sophisticated measurement or identification of life on the planet's surface or in the subsurface along with the variability of the metorological conditions at the surface will require a longer period of operation. The following discussions of the scientific measurements that will be performed on the surface will identify some of the difficulties anticipated with measurement of the various significant parameters.

4.2.3.1 Pressure

Section 4.1.2 discussed the various models of the Martian atmosphere. Further it was pointed out that pressure variations of as much as 0.5 millibar from the nominal may occur during the Martian year. The nominal value itself is in question and appears to lie somewhere between 5 and 20 millibars (0.073 to 0.29 psi). Diurnal pressure variations on the order of 2×10^{-1} millibars are likely to occur. Thus, some form of pressure transducer, probably of the referenced flexible diaphragm type will be required to measure absolute pressure in the range from 0.06 to 0.3 pounds per square inch. The resolution of this device must be sufficient to discern the small diurnal variations and yet withstand the severe shock encountered during landing. The location of the actual transducer itself on the vehicle is of little importance except that large thermal fluctuations must be avoided if precise measurements are desired. The location, orientation and design of the entrance port will be critical in that it can seriously affect the accuracy of pressure measurements in the presence of winds. The possibility of obtaining stagnation of the wind at the entrance port or the formation of vortices in the immediate vicinity of the entrance port should be eliminated by design.

4.2.3.2 Temperature

The measurement of atmospheric temperature and its time dependent fluctuations at the surface of the planet will be accomplished by direct measurement with a resis-tance thermometer. The actual temperature of the resistance element in the thermometer and the temperature of the atmosphere will differ by an amount dependent upon several variables. The most significant of these variables is the radiant heating of the element by direct solar radiation. This can materially increase the temperature of the element, thus inducing large errors in the measurement. Radiation shields employing specially

treated surfaces that minimize the absorption of energy from the Sun can help in reducing this effect.

The low density of the atmosphere on Mars introduces a problem in measurement of its temperature since the amount of energy that can be transferred from the atmosphere to the temperature sensitive element in the thermometer is quite small. It thus becomes imperative that the thermal mass of the detector element be as small as practical in order that this process of energy transfer take place as quickly as possible. In essence, the time constant of the system is increased by the low density of the heat transfer medium. Additionally, the thermal conductivity of the structure upon which the heat sensing element is wound or deposited must be low enough so that the thermal path from the structure to the element (or vice versa) is significantly poorer than the path from the element to the atmosphere.

Interference with the measurement caused by energy leakage (radiated or convected) from the Lander proper should be significantly smaller than that from the Sun. Care must be taken, however to minimize the likelihood of exposure to this energy by placing the sensors as far from Lander surfaces as possible and providing for adequate thermal decoupling in the form of thermally reflective surfaces on the sensor.

4.2.3.3 Winds

The measurement of surface winds in an atmosphere as tenuous as that of Mars is best accomplished by employing non-mechanical techniques. The approach selected is that of measuring the propagation velocity, in each of three mutually orthogonal paths, of an ultrasonic acoustic wave traveling in a given direction. A second measurement of these orthogonal components with the wavefront moving in the opposite direction provides sufficient information to measure both the velocity of the wind and the propagation velocity of sound in that medium. The details of this concept are described in greater detail in Section 2.3.4 and Section 3.5.2 in Volume IV and the anticipated configuration shown in fig. 4.2-3. It appears that wind velocity determination down to a resolution of about 1 meter per second is feasible with the existing state of the art. The only difficulties anticipated in this measurement are associated with the stability of the deployment mechanism and the local disturbances in the flow generated by the presence of the Lander. In the case of very large wind velocities the Reynolds number may become critical and turbulence will occur. The area affected will be a function of the Lander configuration as well as the wind velocity and atmosphere dynamic properties, and thus the location of the sensor must be based upon these factors.

4.2.3.4 Atmospheric Water Vapor

To date, attempts to measure the concentration of water vapor in the Martian atmosphere by radiometric techniques from the Earth have been rather unsuccessful.
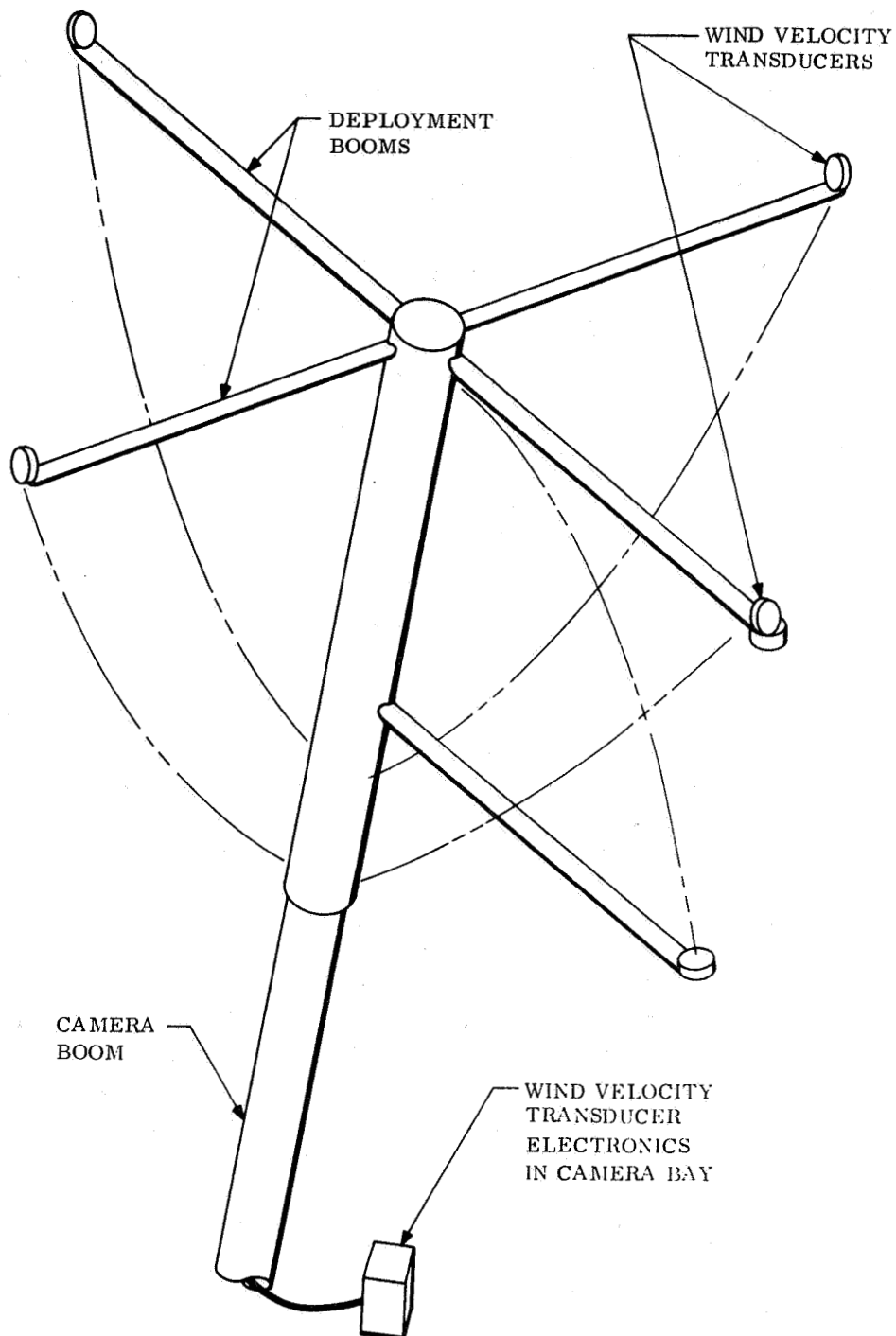
Figure 4.2-3.   Wind Velocity Transducers as Located on the Camera Boom

II

One explanation for this situation is that Mars has little or no water vapor in its atmosphere. Since water is basic to all life forms as we know them, there is a strong driving force to quantitatively measure the concentration of water vapor in the atmosphere of Mars. The difficulty in measuring extremely low water concentrations (on the order of a few tens of parts per billion (ppb)) cannot be overstressed. Here on Earth where water can be found in practically all substances, it is very difficult to reproduce the environment expected on Mars. Measurements down to the low part per million (ppm) range have been accomplished under laboratory conditions. Extension of these measurements down to the ppb range will require development of techniques and apparatus for producing calibrated samples to measure. Water vapor sorption -- desorption by conventional material is another area of development that must be pursued if successful measurement of water concentration in the Martian atmosphere is desired.

The chemical/radiological technique (see fig. 4.2-4) of water detection selected for implementation in the 1973 Hard Lander has been under investigation at General Electric for the past 18 months. The significant results of this investigation to date are;

1. An acceptable procedure for generating known water vapor-gas mixtures in the 1 to 30,000 parts per million range has been established.

2. The feasibility of quantitatively determining water vapor in gases in the part per billion range based on work in the low part per million range has been demonstrated.

3. Satisfactory design and materials for the reactor bed have been identified.

4. The feasibility of using avalanche semiconductor radiation detectors for tritium gas detection has been demonstrated.

In summary, the basic problem in measuring water vapor in the atmosphere of Mars is the development of a suitably sensitive device and calibration technique applicable to the low part per billion concentration range.

4.2.3.5 Surface Composition

The selection of a radiological spectrometer for measurement of the composition of the Martian surface is based primarily on the size, weight, and complexity of competing techniques. The design concept employed in Point Designs 1 through 6 is discussed in Section 2.3.4 and Section 3.5.2 of Volume IV. The instrument is a modification of an alpha scatter spectrometer designed for the Surveyor program (fig. 4.2-5). As such, it is sensitive to the same influences as the Surveyor device

II
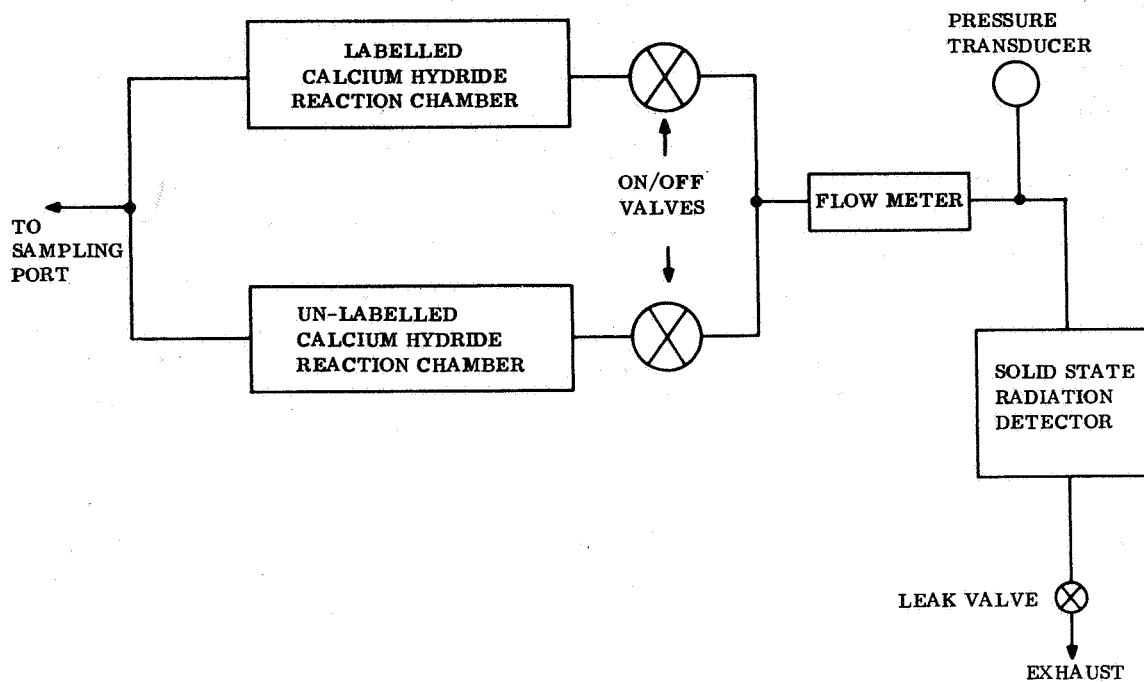
Figure 4.2-4.   Block Diagram of Water Vapor Detector
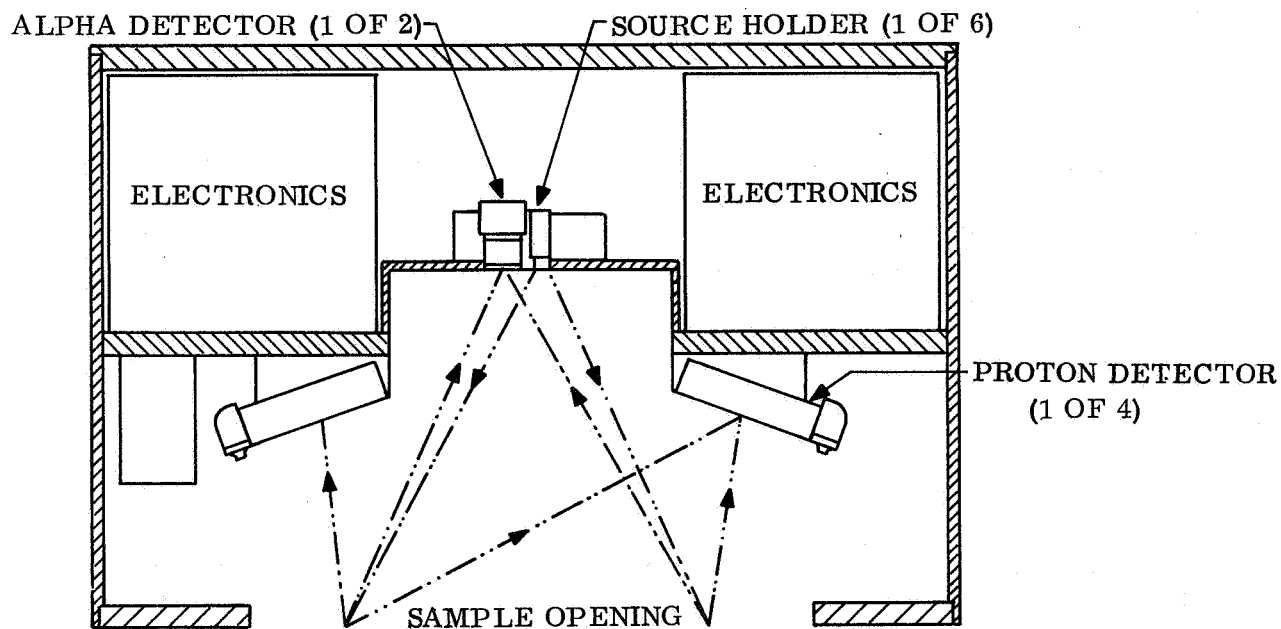
VERTICAL SECTION THROUGH THE CENTER

Figure 4.2-5.   Alpha Back-Scatter Sensor

with the possible addition of atmospheric scattering and its resultant energy distribution smearing. The basic difficulty encountered with the Surveyor device is its requirement for closely controlled deployment on a flat (smooth) surface. Local protrusions in the surface under the sensor tend to change the scattering angles and paths. This results in erroneous interpretation of the accumulated data. Additionally the alpha-scattering and alpha-proton reactions do not provide adequate energy sensitivity to atomic mass number for mass numbers above 40. Thus a new source will be needed that provides gamma radiation that can be used in X-ray fluorescence experiment to achieve good resolution of the larger atoms.

4.2.3.6 Photoimaging

The severe g-loads imposed on the Hard Lander instrumentation and the desire to minimize weight limit the choice of photoimaging system to one of two alternatives. They are the facsimile camera made by Philco-Ford and a camera system built around the RCA ceramic vidicon.

4.2.3.6.1 The Facsimile System

In the facsimile camera a simple lens system is used with a pinhole located at the first focal plane and behind this is a solid state sensor. The objective field is scanned by a mechanically driven mirror in a vertical plane during a synchronized azimuthal movement of the whole camera body. The image of the objective field is swept across the pinhole aperture, and the emerging radiant energy forms the objective field in a solid angle formed by the pinhole aperture and focal length of the imaging lens, and falls on the detector. The most common detector used is a photovoltaic silicon cell, though others can be used, and it is used in the short circuit mode, for reasons given later in this section. The advantage of the single silicon cell is that the total field of view is sensed by the one sensor whose characterisitics can be very well known. A disadvantage of the mechanical scanning technique is that mechanical vibrations can be transmitted to the optics which may result in deleterious effect on the quality of the rendered image, particularly if the pinhole – focal length distance results in an instantaneous field of view (IFOV) which is less than $0.1°$ wide. Cameras have been made by Philco-Ford that weigh 1 pound for the complete unit, withstand 3000 g's and full sterilization cycles. The weight of the camera depends on the specification to which it is designed and currently a range of cameras are being built from 1/2 pound to 6-1/2 pounds in weight.

4.2.3.6.2 The Ceramic Vidicon

This is a specially designed ceramic vidicon tube hardened to withstand up to 3000 g's. To date only the vidicon has been made and tested environmentally. A breakboard electronics model has been assembled but a phototype model using state-of-the-art electronics has not yet been made. The vidicon is a typical slow scan vidicon design employing electrostatic focussing and magnetic deflection. It requires a shuttered exposure and the image information is electronically stored and electronically read off. Scan times from 1 to 40 seconds are available and the vidicon has an RCA-ASOS cathode sensitive in the visible part of the spectrum.

The performance of both systems is similar and past space experiments have utilized vidicon techniques successfully. The advantage of the facsimile techniques lies mainly in its single detector, simple optics and the capability to change the format easily. The most versatile rugged detector is the photo-voltaic silicon cell which is most commonly used in the facsimile. Its wide spectral range and dynamic response admirably suit the Hard Lander requirements particularly in the mode lacking command capability. The flexibility available in changing the format by extending the azimuthal coverage for example (if the full panoramic cannot be accommodated) allow for incremental changes in the bit budget to be accepted without any difficulties. The vidicon on the other hand can only take set formats of large bit content and small changes in the bit content per frame can only be accommodated easily by altering the gray scale.

In terms of resolution the facsimile is capable of matching that of the conventional vidicons with less optics -- a significant feature. Finally the weight of the facsimile, interchangeability of detectors and format flexibility and state of development make it the prime candidate.

4.2.3.7 Expanded Payloads

The landed scientific payloads of Point Designs 5 and 6 differ from the payloads of designs 1 through 4 in that additional equipments (beyond the minimum) are carried for the purpose of collecting valuable data about the planets surface, subsurface, and atmosphere. Since the extension of the science payload beyond the minimum identified in paras 4.2.3.1 through 4.2.3.6 entails the selection of a relatively limited number of experiments from a much larger group of scientifically desirable candidates, and at present there is no well defined set of criteria by which the selection can be made, the selection is the result of qualitative analysis of the probability of success of the experiment and consideration of the state of development of the hardware necessary for its implementation. The experiments chosen for consideration in Point Designs 5 and 6 are:

1. Subsurface water detection

2. Airborne dust detection

3. Ultraviolet radiometry

4. Large molecule detection

5. Life detection

4.2.3.7.1 Subsurface Water Detection

In addition to the significant problems peculiar to the detection of low concentrations of water vapor (para 4.2.3.4), the detection of water vapor in the surface of Mars involves the collection and processing of some finite quantity of the surface. Small, lightweight boring devices have been under investigation by JPL and the design con-

cept described in Volume IV of this report makes use of such a device. The possibility does exist, however, that the Lander will come to rest over a portion of the surface that will possess sufficient hardness to deny the collection of a sample. The probability of such an occurrence is difficult to predict, however, it was assumed to be relatively small for Mars. There have been some field tests of the boring device and other than some difficulties encountered in boring through surfaces possessing the consistency of a rather "wet" mud, no problems have been uncovered. This borer can drill through materials as hard as adobe at rates up to one inch per minute. The deployment mechanism may prove to be the most difficult to fabricate and most space consuming among the several deployment systems carried in the expanded science payload.

4.2.3.7.2 Airborne Dust Detection

Detection of airborne particles by acoustic techniques presupposes the following conditions:

1. Particles of sufficiently small mass to become airborne exist on Mars.

2. Winds of sufficient velocity to impart the minimum detectable energy to those dust particles occur on Mars.

3. The frequency of occurrence of high velocity winds on Mars is sufficiently high to provide a reasonable probability of their occurrence during the lifetime of the Lander on the surface.

The probability of very finely structured particles on Mars is rather high if the planet is as devoid of water as it appears to be. In addition, particulate matter of meteoric origin is likely to be present on the surface in reasonably large quantities because of the low efficiency of Mars tenuous atmosphere in screening out small meteorite particles.

The impulse sensitivity of existing micrometeoroid detectors of the microphone type lies in the range of 10^{-3} to 10^{-5} dyne-seconds. At the greatest anticipated wind velocity (61×10^2 cm/sec), assuming airborne particles reach this velocity, the smallest detectable particle could have a mass of approximately 1.6×10^{-9} grams. Whether or not these particles can become airborne in such a tenuous atmosphere is dependent on a number of variables including particle shape, wind velocity, particle density, atmospheric density, atmospheric temperature, and marain configuration. Analytic approaches to answering this question fall short because of the lack of information about the planet.

It is not likely that peak wind gusts of 200 fps (61×10^2 cm/sec) will occur during a short term mission, however the probability increases with increasing time on the surface (ref. 4-15). It appears reasonable to assume that for missions lasting as long as 90 days, winds in excess of 50 fps will be encountered.

The acoustic detection device described in Section 2.3.4, Volume IV, appears to meet the requirements for particle detection but some doubt exists concerning the compatibility of ultra-sensitive microphones and the extreme deceleration loads encountered during a rough landing.

4.2.3.7.3 Ultraviolet Radiometry

The ultraviolet radiometer experiment carried in Point Designs 5 and 6 employs current state-of-the-art devices to measure the ultraviolet flux reaching the surface of Mars. The measurements will not include suntracking capability in order to minimize complexity and analysis of the data will therefore include extraction of scattered light intensities from the total measured values. To facilitate the analysis, the radiometer experiment will include, in the total package, a sun angle sensor to provide data on the Sun's azimuth and elevation angles. This data used in conjunction with the Lander inclination information will enable the determination of an adequate sun angle history at the landing site. Complete analysis of the atmosphere scattering will require not only angular information but data on atmospheric composition and thermodynamic parameter altitude profiles.

The primary intent of the ultraviolet radiometry will be to investigate the atmospheric radiation attenuation properties in the radiation regimes of particularly significance to biological systems. Large intensities of UV radiation could significantly alter the potential life forms of the planet or they could make impossible the existence of life on the planet's surface and force subsurface investigations for life. The measurements will be made in relatively large bandwidths that cover the wavelength regions of interest and provide a reasonable intensity profile. The relative simplicity of UV radiometry as an experiment, when compared to UV spectroscopy, favors its use in the expanded payload.

4.2.3.7.4 Large Molecule Detection

The large molecule detector in Point Designs 5 and 6 is a mass spectrometer – gas chromatograph combination. A sample of the surface is collected by the same boring device used in the subsurface water detection experiment. After transferral of this sample to a small pyrolizer located in the MSGC, analysis commences. This transferral process is one of the more difficult mechanical manipulations accomplished by the expanded science payload. The problems of interfacing the mass spectrometer and gas chromatograph have been studied and solutions in time for a 1973 flight are expected. The ability of a MSGC to survice > 1000 g shocks is in question and thus appears to present a design problem for the Lander.

4.2.3.7.5 Life Detection

The two major candidates approaches to this experiment are Gulliver and Wolf Trap. Both suffer the universal problem of all life detection schemes identified to date: that of not being able to answer the question of whether life exists on Mars

without ambiguity. This stems from the fact that the nutrients carried by the experiment may not properly support the growth of the life forms encountered. Indeed the fact is that certain life forms thrive on nutritive materials that are toxic to other life forms. The result is that the conclusion "Life does not exist at this place at this time" cannot be drawn until a universal nutrient is developed or some practical method of detecting life is discovered that does not require biological multiplication.

The present status of the two candidate experiments indicates that mechanical redesign is necessary if exposure to > 1000 g shocks is anticipated.

The ambiguity of the data returned by a life detection experiment and the fact that indirect means of identifying whether or not life has or can exist on Mars and the apparent incompatibility of the existing designs with the high level shocks of a rough landing have led to the exclusion of this experiment from Point Designs 5 and 6.

4.3 SPECIAL IMAGERY CONSIDERATIONS

4.3.1 PHOTOGRAPHIC COVERAGE

The prime task of the photoimaging equipment is to take pictures of the surface of the planet. The ability of the photoimaging system to do this successfully depends on a number of factors some of which can be determined and others which can only be estimated. The two most important factors – camera position and the height of the camera above the crushup can be controlled by engineering design. The shape of the crushup around the camera, the inclination of the vehicle and the position of the cameras relative to the lowest point on the Lander are functions of the way in which the Lander lands and can only be treated through probability techniques. Accordingly a parametric study has been done (see Section 4.1.1, Vol. III) on the influence of all these factors on the amount of surface likely to appear in the recorded pictures. The shape of the picture formats have been chosen to cover the widest possible range in resolution that, depending on the location of the landing, will extend from sub-millimeters to meters. The location of the Lander is dominant in determining the far field scene since, owing to the weight penalties imposed by strengthening a high camera boom, the camera is likely to be very close to the planet's surface, of the order of four feet. Thus, in order to see over a range of a few miles, the location of the Lander must be on a high point of the planet's surface.

4.3.2 ILLUMINATION

The illumination requirements for the scene in the neighborhood of the Lander must try to satisfy two disciplines having diverging requirements – that of science and engineering. From scientific considerations the illumination from the Sun at a large zenith angle in a low scattering atmosphere is ideal. This results in a large range in phase angle (angle between source, subject, and camera), and enables the illuminated subject to be more easily identified through its photometric properties. Concurrently, from the standpoint of the engineering requirements, this presents to the photoimaging sensor a wide signal dynamic range, a requirement that is not easily accommodated in all detectors. For this study the arrival time on the planet has been restricted to correspond to 30° from the terminator and the Sun is therefore at a zenith angle of 60°. In this situation the illumination in the absence of scattering is, in the main, ideal for determining local topography from the shadows cast, creates a wide signal dynamic range and a large difference in phase angle. In addition it throws long shadows of the Lander which may reduce the information content in the high resolution domain. If alternatively there is a strongly scattering region in the atmosphere, better photographic illumination is obtained when the Sun is at zenith angles of between thirty degrees and sixty degrees. A detailed study is necessary to determine which zenith angle is the most appropriate for Mars surface-imaging.

4.3.3 OBSCURATION BY DUST

The photographic coverage determined in the parametric section, (Section 4.1 of Vol. III), assumed a clear atmosphere. A probability exists for the occlusion of a large percentage of the photographable scene by a dust cloud generated by the Lander. This is particularly pertinent to the initial imaging sequence that begins a few minutes after impact. If the planetary surface is dusty, even in the presence of a light wind, the dust cloud generated will take considerably longer to settle on Mars than an equivalent cloud on Earth. Exactly how long is not known. Protection of the optical components is relatively simple, but the intrusion of the cloud into the imaging formats, cannot be obviated. There is, in addition, the probability of naturally occurring dust storms but unless they are particularly severe they will not interfere with the photo-imaging program as much as a vehicle-generated dust cloud.

4.3.4 CAMERA DEPLOYMENT

There are many techniques by which the cameras can be deployed after impact. The technique chosen must have certain qualities that satisfy the photoimaging criteria in addition to the obvious mechanical ones. The most important feature of the deployment is that, in the erected position, there must be sufficient rigidity in the support to prevent significant camera movement in the worst wind environments anticipated on Mars. These criteria are particularly severe and as shown in Section 4.1.1., Volume III, result in wide guage heavy tubing for heights as low as two feet.

4.3.5 RESOLUTION LIMITATIONS

The cameras are designed to have fixed angular resolutions of $0.1°$ and $0.01°$ respectively. The ground resolution achievable is therefore determined by the optical arm, i.e., the distance between object and camera. The effect of camera height and position on the ground resolution is shown in the parametric curves of Section 4.1.1. of Volume III: the degradation of this resolution by the telemetry and reconstruction processes is also discussed in the same section. The requirements for the best surface coverage and those for the highest ground resolution are in opposition so that it is not possible to have the optimum conditions for both simultaneously. The maximum ground resolution achievable with the $0.1°$ instrument will be of the order of 2.5 mms and 0.25 mms for the $0.01°$ camera, but in order to have this resolution the Lander must be tilted with its low point along one of the camera taking axes. The probability of this situation occurring is not expected to be high so that on the average a poorer ground resolution may be anticipated, as the curves in Section 4.11.3, Vol. III show.

4.4 SCIENCE MISSION SEQUENCE

The mission sequence includes not only a description of the schedule of events but encompasses the logic used to define the schedule, an evaluation of the variability in measurement conditions for different entry conditions, and a comparison of the selected sequence with the NASA/LRC requirements. The logic used to define the schedule is based primarily on the measurement requirements and the limitations posed by entry conditions or design constraints. During entry, the primary limitation is heating and its associated effects. The landed sequence is affected most by data storage and handling constraints. The influence of these factors on scheduling is discussed for each experiment.

The variability in measurement conditions is to be expected since there exists a range of possible atmospheres in which the usual parameters used to initiate events will occur at different altitudes, times, and flow conditions. The variations are significant only for the entry phase of the mission and their effect on meeting the measurement requirements is delineated.

4.4.1 ENTRY SCIENCE

The entry science measurement goals have been specified by NASA/LRC and, in particular, include the altitude range over which the atmospheric parameters are to be obtained and the accuracy of the measurements. The selection of the entry experiment sequencing must take into account the regions of the entry flight where the flow and heating phenomena are anticipated to excessively degrade measurement accuracies. In addition, the initiation and conduction of experiments over the desired altitude ranges must be examined for their implementation requirements and for the compatibility of these requirements with design constraints. For comparison with the results on implementing the entry sequence, the NASA/LRC goals are summarized:

Measurements	Altitude Range	Accuracy
Pressure	0 – 60 KM	±5%
Temperature	0 – 60 KM	±2%
Density	0 – 60 KM	±5%
Composition	0 – 50 KM	±5%(if constituent is greater than 50% of total) ±10%(other constituents)
Moisture	0 – 50 KM	---

Before outlining the proposed time sequence, some of the difficulties that will be encountered in arranging the sequencing will be identified.

It is anticipated that the real Martian atmosphere lies within the range of possible Martian atmospheres simulated by the VM Models 1 through 10.

The extreme atmospheres, VM-8 and -9 have been selected to demonstrate the variable features of the entry phase that depend on the atmospheric properties. For the out-of-orbit case, the total time to impact from 244 kms is 460 sec VM-8 and 1251 sec. (VM9) without the radar altimeter, and 452 sec VM-8 and 630 sec VM-9 with the altimeter. (See section 2.3 for a discussion of the altimeter.) Similar variations occur for the direct entry mode. In general, the atmosphere model differences affect entry conditions sufficiently so that neither a g-load measurement nor a time interval can indicate a particuliar desired height accurately. The alternative is to include a high powered radar altimeter that has the capability to measure altitudes up to 60 kms. The radar altimeter referred to above is only effective up to about a height of 6 kms and is used primarily to initiate parachute deployment. It is possible to obtain a usable indication of Mach 5 by measuring a fixed time interval (about 30 seconds)from the time of maximum retardation. To obtain a Mach 5 indicator is important because it is the phase of flight below which dissociation of the atmospheric gases ceases to occur. It is also the point at which ablative nose cones are no longer significantly contributing ablative products to the shock wave. If no damage occurs to the water vapor sensor by exposing it to the hot stagnation point gases then a way of overcoming the problem of switching this instrument to sampling at the approximate time is to switch it on with the mass spectrometer. However, the possibility of contaminating the s ensor is not insignificant so that a later activation time is preferable.

These problems exist for both the direct and out-of-orbit missions. Also applicable to both missions is the sensing of the entry phase by means of a sensitive accelerometer or timing device which drives by means of suitable logic circuitry the approximate sampling circuits for the temperature, pressure and accelerometer transduces. Prior to this time all the entry instruments and sampling circuit have power supplied.

The selected sequence of events for the entry mission without an altimeter for parachute deployment are given in tables 4.4.-1 and 4.4.-2.

4.4.1.1 Supersonic Entry

The first event in the science measurement sequence, after instrument checkout, is the initiation of the stagnation temperature, the four stagnation pressure, the base pressure and the triaxial acceleration sensors. In reviewing the possible mechanisms (g-switch, altimeter, timers) for initating these sensors near the desired 60 km altitude, the simplest scheme applicable to all missions was found to be initiation of the readings well in advance of the 60 km altitude. The data obtained at altitudes well above the regime of significant entry phenomena will be of little value since the sensors are to be optimized for data collection during entry. As a means of comparing the altitude regimes where useful atmospheric sensing will begin, a threshold deceleration of 0.2g has been selected and the conditions at this value are shown in tables 4.4-1 and 4.4-2. It can be seen that the VM-8 atmospheric entries fall short of the altitude goal while the VM-9 entries are well in excess of the 60 km goal. The 15 km difference in the VM-8 out-of-orbit mission is not serious since the sensors shall be operating well above this altitude.

TABLE 4.4-1.   ENTRY MISSION SEQUENCE, OUT-OF-ORBIT, (Sheet 1 of 2)

Event	Seconds to Impact	Altitude (km)	Heating Rate (BTU/ft²-sec) (Note 1)	Mach No.	Ambient Temp. (°K)	Ambient Press (mb)	Ambient Density (gm/cm³)
				VM-8			
1. Stagnation T&P Sensors, Base P Sensor, and Accelerometer Using 0.2 g Reading	270	45	22.5	29.7	100	2.2×10^{-3}	1.2×10^{-8}
2. Peak Heating Rate	240	24	103	24.5	100	1.4×10^{-1}	7.2×10^{-7}
3. Peak Acceleration	232	18	66.3	18.5	103	4.4×10^{-1}	2.3×10^{-6}
4. Initiate Base Temp., Mass Spectrometer and Water Detector at Mach 5	205	12	Negligible	5.0	135	1.2×10^{0}	4.7×10^{-6}
5. Chute Deployment Near Mach 2	175	67	Same	2.0	163	2.4×10^{0}	7.8×10^{-6}
6. Impact	0	0	Same	---	200	5.0×10^{0}	1.3×10^{-5}

Note 1:   Heating rates based on a three foot nose radius.

Note 2:   Radar altimeter not included.

TABLE 4.4-1. ENTRY MISSION SEQUENCE, OUT-OF-ORBIT, (Sheet 2 of 2)

Event	Seconds to Impact	Altitude (km)	Heating Rate (BTU/ft2-sec) (Note 1)	VM-9 Mach No.	Ambient Temp. ($^\circ$K)	Ambient Press (mb)	Ambient Density (gm/cm^3)
1. Stagnation T&P Sensors, Base P Sensor, and Accelerometer Using 0.2 g Reading	1151	128	13.8	17.3	200	4.2×10^{-3}	7.9×10^{-9}
2. Peak Heating Rate	1091	72	51.7	14.6	200	1.7×10^{-1}	3.2×10^{-7}
3. Peak Acceleration	1071	58	37.8	11.2	200	4.4×10^{-1}	8.3×10^{-7}
4. Initiate Base Temp.,	1031	42	Negligible	5.0	200	1.3×10^{0}	2.5×10^{-6}
5. Chute Deployment Near Mach 2	991	32	Same	2.0	200	2.6×10^{0}	5.0×10^{-5}
6. Impact	0	0	Same	---	275	2.0×10^{-1}	2.7×10^{-5}

Note 1: Heating rates based on a three foot nose radius.

Note 2: Radar altimeter not included.

II

TABLE 4.4-2. ENTRY SEQUENCE – DIRECT (Sheet 1 of 2)

Event	Seconds to Impact	Altitude (km)	Heating Rate (BTU/ft²-sec) (Note 1)	Mach No.	Ambient Temp. (°K)	Ambient Press (mb)	Ambient Density (gm/cm³)
VM-8							
1. Stagnation T&P Sensors, Base P Sensor and Accelerometer Using 0.2 g Reading	275	58	15.4	40	100	1.8×10^{-4}	1.0×10^{-9}
2. Peak Heating Rate	260	27	218	35	100	7.7×10^{-2}	4.0×10^{-7}
3. Peak Acceleration	256	20	130	23	100		
4. Initiate Base Temp., Mass Spectrometer and Water Detector at Mach 5	248	12	35	5	135	1.2×10^{0}	4.7×10^{-6}
5. Chute Deployment Near Mach 2	231	9	Negligible	2	151	1.7×10^{0}	6.3×10^{-6}
6. Impact	0	0	Negligible	--	200	5.0×10^{0}	1.3×10^{-5}

Note 1: Heating rates based on a three foot nose radius.

Note 2: Radar altimeter not included.

TABLE 4.4-2. ENTRY SEQUENCE – DIRECT (Sheet 2 of 2)

Event	Seconds to Impact	Altitude (km)	Heating Rate (BTU/ft^2-sec) (Note 1)	VM-9 Mach No.	Ambient Temp. ($^\circ$K)	Ambient Press (mb)	Ambient Density (gm/cm^3)
1. Stagnation T&P Sensors, Base P Sensor and Accelerometer Using 0.2 g Reading	1187	165	9.3	23	200	3.9×10^{-4}	7.2×10^{-10}
2. Peak Heating Rate	1147	75	103	20	200	1.4×10^{-1}	2.6×10^{-7}
3. Peak Acceleration	1138	62	66.5	14	200	3.4×10^{-1}	6.4×10^{-7}
4. Initiate Base Temp., Mass Spectrometer and Water Detector at Mach 5	1119	46	5.5	5	200	1.00×10^{0}	1.9×10^{-6}
5. Chute Deployment Near Mach 2	1097	39	Negligible	2	200	1.6×10^{0}	3.0×10^{-6}
6. Impact	0	0	Negligible	--	275	2.0×10^{-1}	2.7×10^{-5}

Note 1: Heating rates based on a three foot nose radius.

Note 2: Radar altimeter not included.

II

An examination of the heating rates and temperature and pressure ranges associated with the four possible supersonic entries in tables 4.4-1 and -2 indicates the selection of operating ranges for the sensors will be governed primarily by the type of entry (direct vs. out-of-orbit) and not the atmospheric models. The occurrence of the 60 km design altitude near peak heating and acceleration for VM-9 entries poses no extraordinary problems, but forces careful selection of the accelerometer sampling rates to provide a density-altitude profile with accuracy close to the NASA/LRC goal of ±5 percent at altitude.

The next key event is the initiation of the mass spectrometer near Mach 5. The selection of this initiation point is governed by the known extreme difficulty in measuring ambient atmospheric composition during periods of significant ablation and outgassing. Such a situation should exist during all the entries of tables 4.4-1 and -2. To minimize the problem, initiation of Mach 5 was selected where the heating rates are well past their maximum values and heat shield outgassing should be minimal. Further reduction of the problem is possible through the use of non-ablative material near the inlet port of the mass spectrometer (see point design descriptions in Vol. IV).

The initiation of the water vapor detector at Mach 5 is also indicated for the present study. However, the low level heating that persists for direct entry may be sufficient to pose a contamination problem for the ultra-sensitive detector (1 ppb sensitivity). Its use at Mach 5 for direct entry missions may be prohibited therefore, but the decision requires further detailed study.

In summary, the initiation prior to entry of the supersonic measurements will meet the design goal of 60 km for all missions. However, the question of whether the accuracies can be met is discussed in Section 4.5.1. In addition, the initiation of the mass spectrometer and water detector at Mach 5 will almost meet the 50 km design goal for VM-9 entries but is 38 km lower than the goal for VM-8 entries. Solution to this problem does not appear to lie in direct measurements during entry.

4.4.1.2 Subsonic Entry

The start of the subsonic measurement regime of temperature and pressure can be considered to occur with parachute deployment in the vicinity of Mach 2, which can be indicated by g sensors and base pressure. As can be seen in tables 4.4-1 and -2, heating phenomena can be ignored at these velocities and the spread in in operating ranges required for the pressure sensors is approximately one order of magnitude and for the temperature sensors about $75°K$. The primary method of analysis will use the sensors' data and knowledge of the Capsule's dynamic properties to estimate Mach numbers for reading corrections, to determine the altitude-time profile and to provide calculated values for the mean molecular weight. The results of the experiment simulation analyses indicate that temperature and pressure should be sampled at least once per second to perform the latter tasks with acceptable accuracies.

The water detector will operate continuously during this phase of the descent to collect adequate statistical data for determining the atmospheric water vapor content.

Its data will support the mass spectrometer data which will also continue to operate during descent.

The only significant difference in the scientific aspects of the missions will occur in the subsonic regime with the addition of a radar altimeter to deploy the parachute at 6.1 km. The altitude and descent times will differ (see table 2.4-4) but modification of the sampling rates in table 4.4-3 is not believed necessary.

TABLE 4.4-3. ENTRY SCIENCE SAMPLING RATES

Measurement	Above Mach 5	Mach 5 to Mach 2	Below Mach
1. Stagnation Temperature-1	1 sample/sec	1 sample/sec	N/A*
2. Stagnation Pressures – 4 (each sensor)	1 sampel/sec	1 sample/sec	N/A
3. Base Pressure	1 sample/sec	1 sample/sec	1 sample/sec
4. Triaxial Accelerometers (each axis)	10 sample/secs	10 sample/secs	10 sample/secs
5. Composition	N/A	1 sample/10 sec	1 sample/10 sec
6. Base Temperature	N/A	1 sample/sec	1 sample/sec
7. Water Vapor	N/A	1 sample/15 sec	1 sample/15 sec

*N/A – Not applicable

4.4.2 MINIMUM LANDED SCIENCE

4.4.2.1 Metereological

The objective of the landed science package is to obtain scientific information about the nature of the planet on, under, and above the planet's surface. After the impact of the Lander and the deployment of various instrumentation has occurred, the experiments can begin. The majority of the information is obtained from transducers that are in equilibrium with the parameter they are measuring. At certain intervals of time these instruments are interrogated and the readings obtained are stored and later transmitted back to Earth. Table 4.4-4, outlines the sequence of the sampling times. A description of the reasons for choosing these times are given below.

TABLE 4.4.4. METEROLOGICAL DATA SEQUENCE

Instrument	Sample Rate	Comment
Pressure Transducer	3 per hour	Based on maximum rate of pressure change.
Temperature Transducer	3 per hour	Based on rate of change around sunrise and sunset.
Moisture Detector	3 per hour	Related to temperature changes.
Wind Velocity-Transducer	3 per hour	Chosen to conform with other sample rates.
Clinometer	3 per hour	Chosen to conform with other sample rates.

TABLE 4.4.5. BACK SCATTER SEQUENCE

Event	Time	Comment
1. All power switched on and checked	$T = 0$	
2. Calibrate 3. Monitor Background 4. Calibrate 5. Deploy	2 hrs < T < 4 hrs.	Variability function of background count.
6. Calibrate 7. Monitor Surface 8. Calibrate	20 < T < 22 hrs.	Maximum time possible for count.

Sampling Sequence:

The instrument data stored will be sampled once every three hours. Calibration background and surface data will be stored.

The pressure transducer monitors the ambient pressure; this instrument is sampled three times per hour throughout the 24.6 hour period. Under normal circumstances this frequency is not necessary but, as a result of the lower atmospheric pressure on Mars, the time constant for atmospheric changes may be faster than on Earth and so, in the event of a pressure change accompanying or preceding a sudden large atmospheric event, a sample rate geared to the anticipated most rapid change was chosen.

The temperature transducer monitors the ambient temperature in the vicinity of the Lander. Apart from interest in the maximum and minimum temperatures, great interest is centered upon the maximum rate of change following sunrise and sunset; three samples per hour was chosen as a suitable time interval.

The moisture detector sequence is also sampled at the rate of three times per hour because of its anticipated dependence on the atmospheric temperature. The water content-temperature behavior on Mars may be similar to that on Earth with the exception that a greater proportion of the atmospheric moisture may be driven out of the soil by action of the Sun during the day; conversely it may condense during the setting of the Sun and through the night.

The wind velocity sensor's sampling requirement is more of an unknown quantity since so little is known about the surface winds. If more information becomes available it may be necessary to increase its frequency of sampling; alternatively in order to present unnecessarily excessive use of the storage and telemetry systems, a logic system controlling the sampling rate may be necessary. The system could increase sampling rate as a function of rate of change of the parameter. However, in the presently proposed system, in order to retain uniformity of the switching sequence, three samples per hour is the current preferred rate.

The latter reasoning has also been applied to the sequencing of the clinometer. Because of the Lander's anticipated stability at rest on the ground, three samples per hour would appear to be unnecessarily high. However, if the unexpected does occur, and the Lander is unstable in high winds, then the sample rate, again chosen to conform to the other instruments, will prove to be of great value.

The alpha-scattering equipment and the photoimaging program are the two cases that differ considerably from those above, and will be described separately.

4.4.2.2 The Alpha Back-Scatter Equipment

The instrument to be used on Mars is expected to be a redesigned version of the Surveyor instrument. The redesign is anticipated to result in this instrument being included in the minimum payload, minimum lifetime concept for Point Designs 1 and 2. In order to accomplish this, the rate at which the data is accrued must be higher than on Surveyor, otherwise a sufficient statistical count cannot be obtained in the 24.6 hour period. The proposed sequence of the Mars mode is shown in table 4.4-5, and a few explanatory comments are necessary. In comparison with the Surveyor sequence, it will be noticed that the stowed calibration phase is missing. This is because in the Mars concept the sensor's head is deployed from the lower center

of the Lander onto the surface below. It is therefore not possible to have an "open" background count and a stowed background count that differ substantially; as a result of the pressing need for a maximum counting time on the surface the stowed phase was eliminated. The period allotted to the background count may be insufficient which may preclude the consideration of the instrument on the minimum lifetime mission.

The confidence of the alpha back-scatter experimental results obtained may be substantially lower than those of Surveyor for these reasons:

1. The time available for pulse counting is limited - this will be more significant for low abundance constituents.

2. The inclination of the sensor head may not be parallel to the local surface, leading to an erroneous geometrical configuration.

3. Clumps of surface materials or small rocks of 1/2-inch to 1-inch diameter intercepting the alpha beam will give rise to the same error as in (2) above.

The latter two are significantly affected by the absence of a command facility that enables a visual selection of a suitable site for the back-scatter instrument. In addition to selecting a suitable site the visual link allows appropriate correction via terrestrial simulation for any misalignment of the instrument on deployment, thereby improving the overall accuracy and confidence in the experiment.

4.4.2.3 Photoimaging

The photoimaging sequence is programmed to take four low resolution pictures in a format containing 1.75×10^5 resolution elements; the frame limits are variable, the present extremes are $70^\circ \times 25^\circ$ and $60^\circ \times 29^\circ$. Each of the low resolution frames has nested within it a high resolution frame of $5^\circ \times 5^\circ$ and containing 2.5×10^5 resolution elements. The four frames are taken in four directions that are mutually at right angles. The combination of the aforementioned resolution elements of 1.75×10^5 (low resolution) and 2.5×10^5 (high resolution), four frames, and a 6-bit gray level results in a total imaging data load of 1.02×10^7 bits.

As has been previously discussed, the Lander imaging data is relayed in real time to the Orbiter. For the nominal relay link data rate under consideration for the out-of-orbit case, 1.6×10^5 bits per sec the time required to transmit the imagery data is therefore 63.8 seconds.

To ensure the collection of the imaging data, the camera sequence is initiated at the start of Lander-to-Orbiter transmission and recycled several times during the available transmission period. One of the main areas for concern regarding the design and development the cameras will be its ability to respond to this requirement for rapid camera cycling after having experienced the landing 'g' impact load.

TABLE 4.4.6. REPRESENTATIVE CAMERA SEQUENCE FOR TWO CAMERAS;
WITH HIGH RESOLUTION AND LOW RESOLTUION CAPABILITIES

Event	Time	Comment
1. Cameras Deployed	T = 0	
2. Camera Sequence begins	T = 36 secs	The 36 secs are required for other switching sequences
3. 1st Low Resolution Picture on Camera 1, Position 1	T = 42.625 secs	Picture 1 1 L
4. 2nd Low Resolution Picture on Camera 2, Position 1	T = 49.25 secs	Picture 2 1 L - Camera resets for high resolution frame
5. 1st High Resolution Picture on Camera 1, Position 1	T = 58.575 secs	Picture 1 1 H - Camera 2 resets for high resolution frame
6. 2nd High Resolution Picture on Camera 2, Position 1	T = 67.89 secs	Picture 2 1 H - Camera 1 moves to position 2. Resets for low resolution
7. 3rd Low Resolution Picture on Camera 1, Position 2	T = 74.515 secs	Picture 1 2 L - Camera 2 moves to position 2. Resets for low resolution
8. 4th Low Resolution Picture on Camera 2, Position 2	T = 81.140 secs	Picture 2 2 L - Camera 1 resets for high resolution
9. 3rd High Resolution Picture on Camera 1, Position 2	T = 90.465 secs	Picture 1 2 H - Camera 2 resets for high resolution
10. 4th High Resolution Picture on Camera 2, Position 2	T = 99.790 secs	Picture 2 2 H

The relaying of the photoimaging data imposes the requirement on the cameras and on the sequencing of the cameras that they present a continuous data stream to the telemetry transmitter. Thus, in accordance with the 1.6×10^5 bits per sec the low resolution format for a 6 bit gray level must complete one frame in 6.625 seconds and the high resolution frame in 9.325 seconds. The total time for the full photoimaging sequence assuming no camera switching intervals is 63.8 seconds as quoted above. The full camera sequence is expected to follow the outline given in table 4.4-6.

4.4.3 EXTENDED LIFETIME MISSIONS

With Point Designs 3 and 4, extended lifetimes of the order of 90 days or more are available for the surface science experiments. In the case of the surface meteorology, this ability to examine long-term climatic changes is of extreme interest. As for the alpha back-scatter experiment, due to the desire to minimize the Lander's interval volume requirements, the experiment's deployment system is designed so as to limit surface examination to one site. For this reason it is presently planned to only conduct surface composition tests during the first day of the landed mission. It may be of interest, however, to extend that period even though the same site would be continually examined since during the 24.6 hour period, the nighttime background level can be different than the daytime level and, therefore, an extended period of measurements may improve the accuracy of the results. A further thought with regard to the alpha back-scatter equipment is to consider the trade-off of providing for a relocatable sensor (i.e., deployable to more than one site) versus the resultant complexity in Lander design. A relocatable sensor, in conjunction with the command capability of Point Designs 3 and 4, would permit the collection and comparison of soil composition from several sites. This would tend to avoid the possible examination of just one sample site wherein the site had been contaminated by some Lander-introduced material, such as phenolic glass honeycomb crush-up material.

The photoimaging data collection and relay rate to the Orbiter will be unchanged during the first three days. In preference to imaging the same part of the planet on each occasion, it would be desirable to move the relative positions of the cameras so that they take, for example, adjacent formats at each imaging opportunity. By this means of full $360°$ panoramic scene could be obtained by the end of the three days.

4.4.4 EXPANDED PAYLOAD

The expanded payload considered for Point Designs 5 and 6 introduce a new factor into the sequencing arrangements. This factor is caused by the inclusion of two instruments that are not sequenced sequentially, but obtain a singular result which is sampled once, stored, and no further sampling ensues. These two instruments are the Subsurface Water Detector and the Large Molecule Detector. These instruments derive their results from a soil sample obtained by a subsurface boring device. The whole experiment covers a period of two hours and the selection of this period for the experiment within the whole mission lifetime is quite arbitrary.

The only real restraints on the choice of time is the time of the transmission for the transfer of its data back to Earth, and a suitable time lapse after the harder impact. Based on these criteria a proposed sequence for the instruments is shown in table 4.4-7. The remaining instruments may be sampled on a sequential basis: these are the Airborne Dust Detector and the Ultra Violet Radiometer. The former instrument counts the number of impacts it receives from small dust particles; these are counted throughout the day and the total count over four hour intervals is sampled. The sequence for this instrument can be started as soon as the checkout and deployment procedures have finished. The Ultra Violet Radiometer only works during the day and the amplitude of its output is sampled once each hour in each of the daylight hours; initiation of the experiment can coincide with the of the Dust Detector; the sequence for these instruments is shown in table 4.4-7.

TABLE 4.4.7. SEQUENCE FOR SOIL MOISTURE SENSOR AND LARGE MOLECULE DETECTOR

T Impact plus one hour, up to, T data transmission minus three hours

The full landed sequence is as follows:-

Event	Time	Experiment	Sample Rate
1. Impact	T = 0		
2. Deployment and Checkout Complete	T = 2.5 min	Airborne Dust Det.	1 per 4 hrs
		U. V. Radiometer	1 per hr
3. Time Gate Opens for Large Molecule Detector and Sub-Surface Soil Moisture	T = 2.5 min+1 hr	Large Molecule Detector; Sub-Surface Moisture Sensor	
4. Time Gate for Large Molecule Detector and Sub-Surface Moisture Sensor ends	T = Transmission −3 hrs		Once only during time interval
5. Data Transmission	T = Transmit		

The combination of command capability for Point Designs 5 and 6, together with a low total bit imagery capability during the direct link transmission phase enables particular items seen on the surface in the earlier imagery program (during the first three days when the relay link was used) to be examined in more detail. This imposes a requirement on the cameras that may only be realized by using a more sophisticated and therefore heavier model of camera than has been considered for use in the main photoimaging mission. An alternative imaging mission for the expanded payload might be to use a separate, light camera for the combined purpose of assuming the alpha back scatter sensor and the surrounding region beneath the Lander.

The uncertainty in the expanded payload obviates the formation of a definite sequence but with a command capability, flexibility is the main feature so that a rigid sequence is not necessarily required.

4.5 ANTICIPATED MEASUREMENT ACCURACIES

4.5.1 ATMOSPHERIC PROFILE

Measurement accuracies during entry are affected by not only the usual sensor and subsystem inaccuracies but also by the uncertainty in predicting the effects caused by the Capsule passage through the atmosphere. A full evaluation of the anticipated accuracies involves, therefore, considerable preflight studies into the perturbation phenomena and their associated data analysis procedures. In addition, the overall accuracy in the results can be affected by the data analysis methods, particularly when key parameters are not measured (such as altitude or density) but must be extracted from the data. The analysis of the experiment's accuracy must include the consideration of: (1) errors due to discrepancies between local and ambient values (resulting from flow effects, etc.), (2) instrument errors, (3) telemetry errors, and (4) data analysis errors inherent in the methods.

Table 4.5-1 shows the basic accuracy guidelines supplied by NASA/LRC at the beginning of this study and the results of analyses performed during the study.

4.5.1.1 Temperature

In the case of ambient temperature, direct measurements during hypersonic flight are impossible and the determination of local ambient conditions must rely on post-flight analysis. Detailed studies into the analysis difficulties are not as yet available and represent a key activity in the future phases of the Lander development. Present indications, based on Earth flight experience, are that measurements made in the stagnation region can be most reliably analyzed for ambient values and that the results should be good to about ± 5 to 10 percent (table 4.5-1). Such accuracies are anticipated provided there is adequate data on ratio of specific heats, angle-of-attack, and velocity. Careful evaluations of the manner in which the accuracies worsen as the required auxiliary data loses quality are beyond the scope of the current study.

Ambient temperature measurements during subsonic flight are subjected to less severe perturbations and as a result should show significant improvement in accuracy. Without the benefit of detailed subsonic data for temperature measurements made at the Capsule base, estimates of the accuracies are in the area of ± 2 percent if flow heating effects can be ignored.

The evaluation of the anticipated accuracies in subsonic temperature measurements are made using the Experiment Simulation Techniques described in Section 4.2.2. The final results shown in fig. 4.5-1 are based on the matrix of simulated missions shown in table 4.5-2. The use of a ballistic coefficient of 0.39 dictates that sampling intervals of less than 6 seconds should provide temperatures with about a ± 2 percent accuracy at all subsonic altitudes.
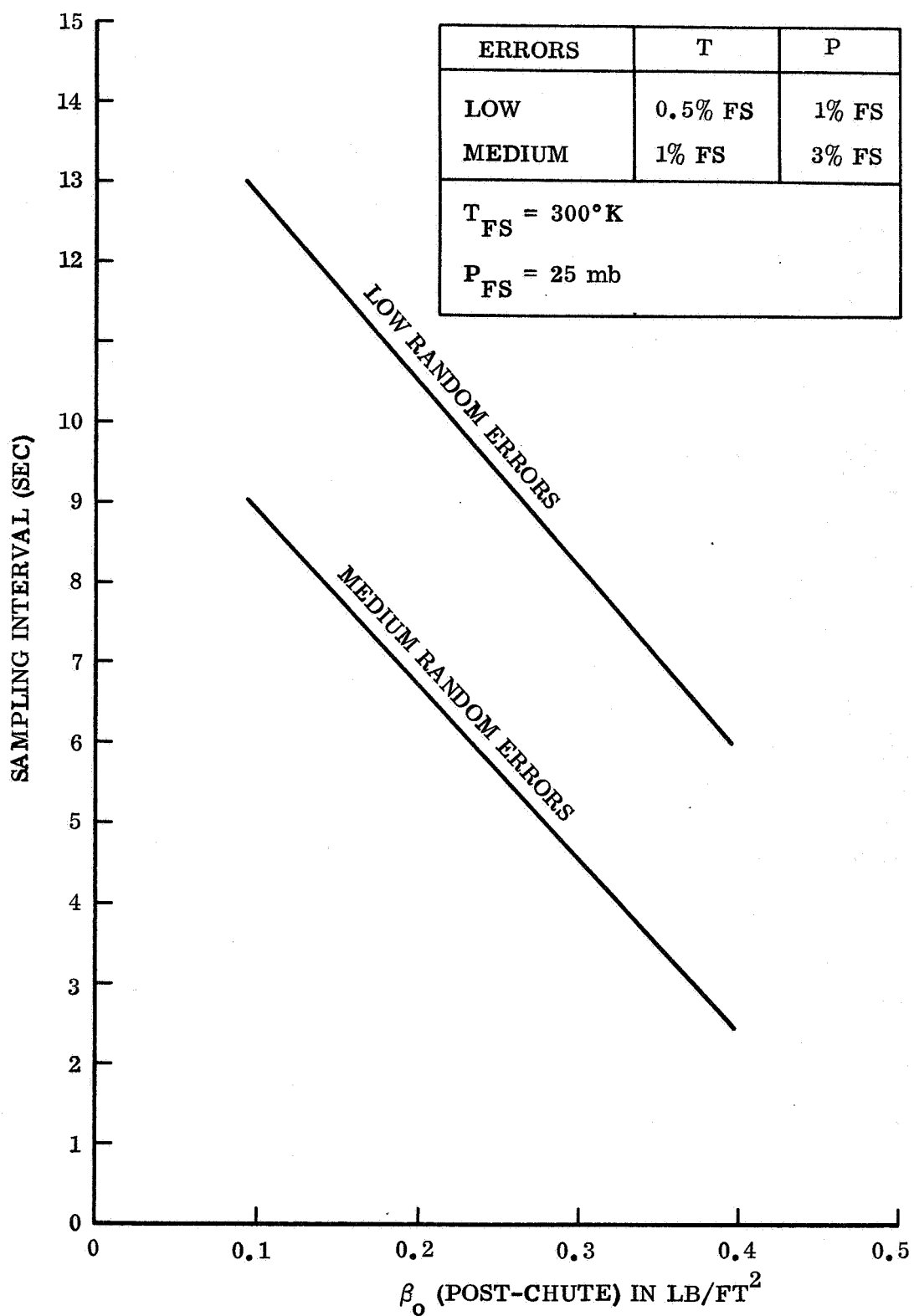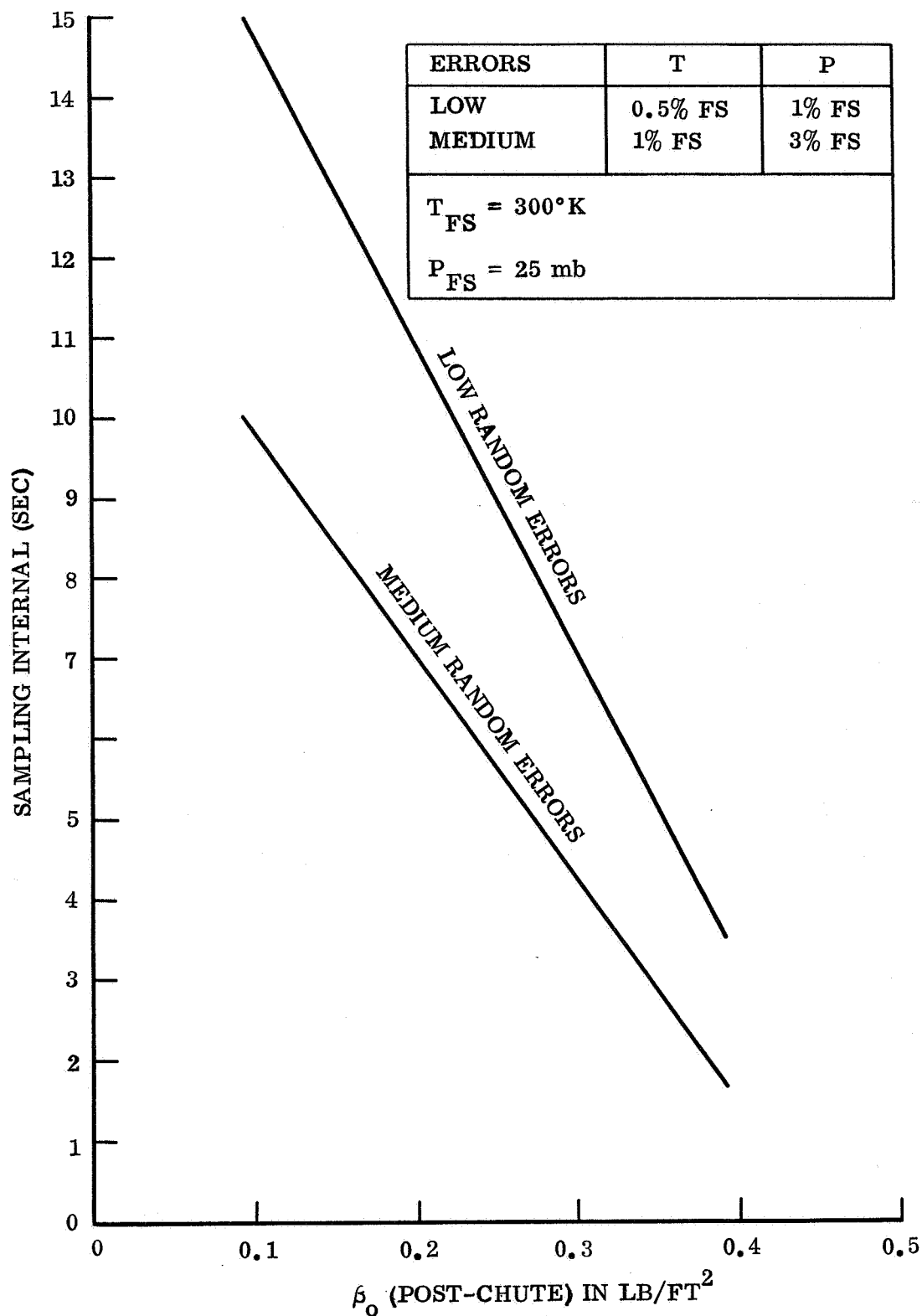
Figure 4.5-1. Sampling Interval – Ballistic Coefficient Relations for Achieving 2 Percent Measurement Accuracy of Temperature-Altitude Profile

TABLE 4.5-1. ACCURACY OF ATMOSPHERIC MEASUREMENTS

Parameter	NASA/LRC Accuracy Objective	NASA/LRC Altitude Range	Hard Lander Accuracy Capability Prediction		Comments
			Supersonic	Subsonic	
Pressure Profile	±5%	0-60 Km	±10%	<+5%	Supersonic measurements will be difficult to improve over 10% accuracy. Subsonic measurements can improve to ±2% if an altimeter is used to provide an altitude base.
			Supersonic	Subsonic	
Temperature Profile	±2%	0-60 Km	±10%	<±2%	Error predictions are based upon analytical relationships being identified that remove raw heating of sensor and angle of attack effects. Analysis techniques may be aided by pre-flight simulation testing of prototype vehicles.
			Pre Chute	Post Chute	
Density Profile	±5%	0-60 Km	±5%	<±5%	Predictions based upon results of Experiment Simulation Techniques.
Atmospheric Composition	±10%	50 Km	<±10%		Detection of minor constituents down to 10^{-11} torr partial pressure is expected. Mass resolution of 1 AMU for continuous scan system from 10-60 AMU is possible. Amplitude resolution of each mass number should be 1-2%.

TABLE 4.5-1. ACCURACY OF ATMOSPHERIC MEASUREMENTS (Continued)

Parameter	LRC Accuracy Objective	LRC Altitude Range	Hard Lander Accuracy Capability Prediction	Comments
Magnitude of Wind Velocity	±5 M/Sec	Surface	~ 1 M/Sec	Accuracy will be strongly dependent upon Reynolds number and location of sensor relative to local perturbations on atmosphere motion. Accuracy of time measurements is limiting item in electronics. See Section 4.5.2.
Wind Direction	±10°	Surface	$< \pm 10°$	Accuracy will depend upon wind direction and have finest values when wind is aligned to one axis of sensor. See Section 4.5.2.
Atmospheric Moisture	None	< 50 KM	±5% for concentration > 1 ppm	Accuracy is a function of pumping system and time available for counting.

TABLE 4.5-2. CASES CONSIDERED IN PARAMETRIC STUDY

Case	Atmosphere	Trajectory	Total Random Errors
1	VM-8	Direct	Low
2	VM-8	Direct	Medium
3	VM-8	Direct	High
4	VM-8	Out of Orbit	Low
5	VM-8	Out of Orbit	Medium
6	VM-8	Out of Orbit	High
7	VM-9	Direct	Low
8	VM-9	Direct	Medium
9	VM-9	Direct	High
10	VM-9	Out of Orbit	Low
11	VM-9	Out of Orbit	Medium
12	VM-9	Out of Orbit	High

Note:

1. All cases were run for two values of post-chute ballistic coefficient β_o, and three sampling intervals.

	β_o (lb/ft^2)
Nominal	0.393
Low	0.0982

Sampling Intervals (sec)	Nominal β	Low β
1	.5	1
2	1	2
3	2	4

2. The trajectory parameters are as follows:

	Entry Velocity (km/sec)	Entry Angle
Direct	6.34	25°
Out of Orbit	4.66	16°

3. The total random errors are identified as follows (in % of full scale, one sigma value):

Errors (%)	Pressure	Temperature
Low	1	0.5
Medium	3	1
High	5	2

4. The nominal β, out-of-orbit case corresponds to Point Design 1, while the nominal β, direct entry case corresponds to Point Design 2.

5. Normal β corresponds to parachute configuration for terminal velocity of 150 fps; Low β corresponds to configuration for terminal velocity of 75 fps.

II

4.5.1.2 Pressure

The measurement of pressure involves the same situation on the perturbations during hypersonic flight and on the current ability to correct for these effects. A significant difference is that considerable Earth flight test data (ref. 4-16) indicates that base pressure readings can be useful at high Mach numbers for determining ambient pressures. However, until more ground test data is available the anticipated accuracies for both stagnation and base measurements is estimated to be ±10 to 15 percent if adequate knowledge of the entry atmosphere and flight conditions exists.

Base pressure for a given configuration in laminar flow is generally some fraction of free stream pressure and is primarily a function of Reynolds number (ReL) and Mach number (M_L) at zero angle-of-attack. However, once a turbulent boundary layer has been established, the Reynolds number dependence drops out, and base pressure is solely a function of Mach number and angle of attack. Angle-of-attack (α) effects on base pressure tend to perturbate the $\alpha = 0$ base pressure level. The free stream static pressure of a planet can be derived directly from the base pressure measurements from a probe if limited trajectory date (Mach number, altitude and attitude time histories) are available for the flight. The utilization of base pressure readings for this purpose appear most attractive since available Earth flight data indicates a reliable correction curve can be established for the supersonic flow effects. A curve of this type is shown in fig. 4.5-2 taken from ref. 4-17.

Base pressure readings during subsonic flight are also subject to the same type of corrections. Again the generation of reliable correction curves appears feasible with sufficient preflight testing. The accuracies in pressure altitude profiles that can be expected, if such curves are assumed to exist, have been established with the use of the Experiment Simulation Techniques. The summation of the results are shown in fig. 4.5-3 for achieving the design goal of ±5 percent of any altitude. The data indicates that for a design ballistic coefficient of 0.39 the sampling interval should be less than 4 seconds.

4.5.1.3 Density

In the supersonic (pre-chute) regime, density is to be obtained from triaxial accelerometer data. The experiment simulation computer code has been applied to this technique and on the basis of the results obtained, taking into account further refinements involving iterative methods, it is anticipated that accuracies of 5 per cent can be achieved (ref. 4-18). In the subsonic (post-chute) regime, density is to be derived from measured pressure and temperature data. Parametric studies again employing Experiment Simulation were conducted for this case, and the final results are shown in fig. 4.5-4. The results indicate that agreement with the true densities within ±5 percent can be achieved if sampling intervals below 2 seconds are used.
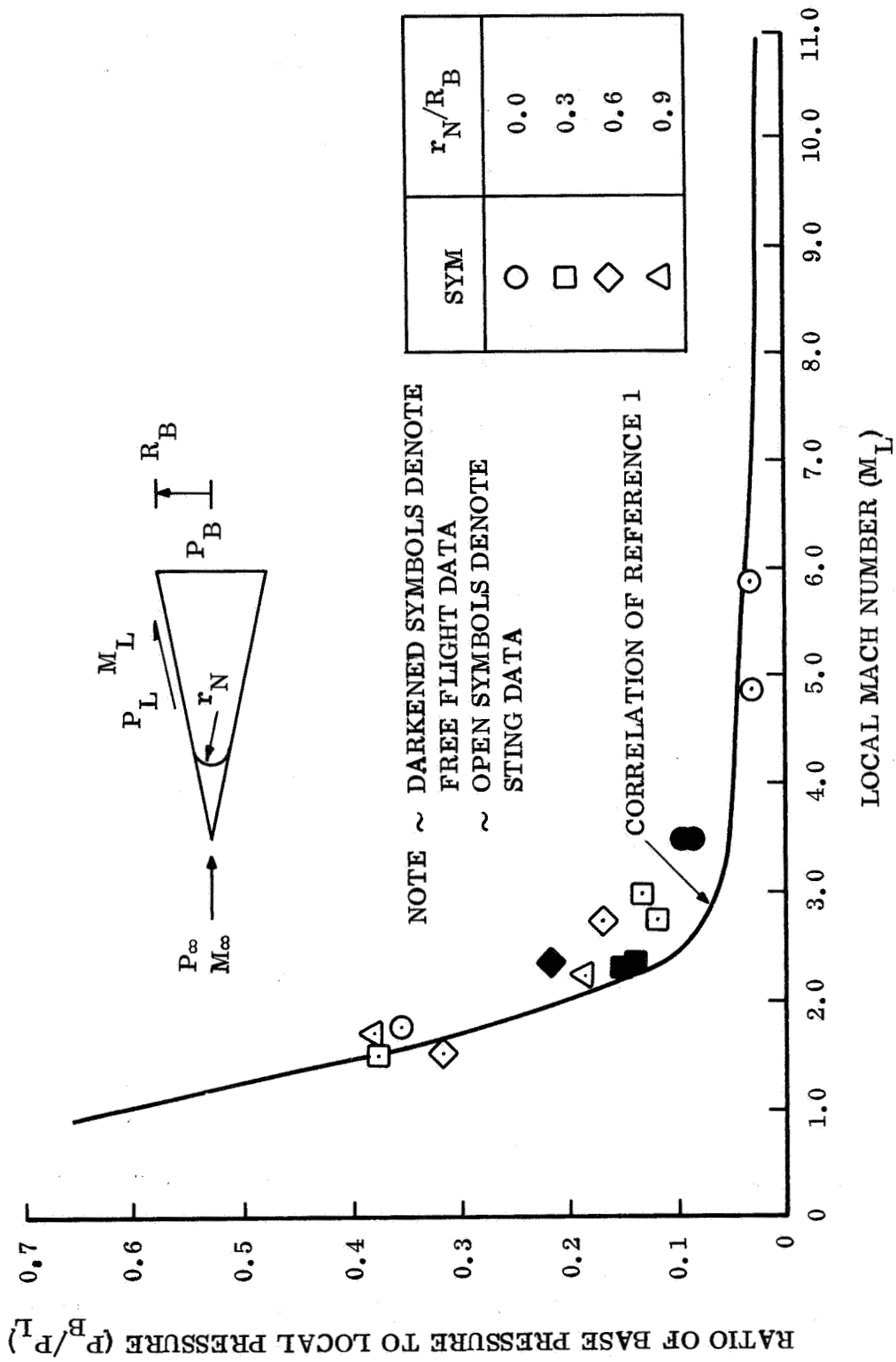
Figure 4.5-2. Turbulent Flow Base Pressure Correlation

Figure 4.5-3 Sampling Interval - Ballistic Coefficient Relations for
Achieving 5 percent Measurement Accuracy of
Pressure-Altitude Profile
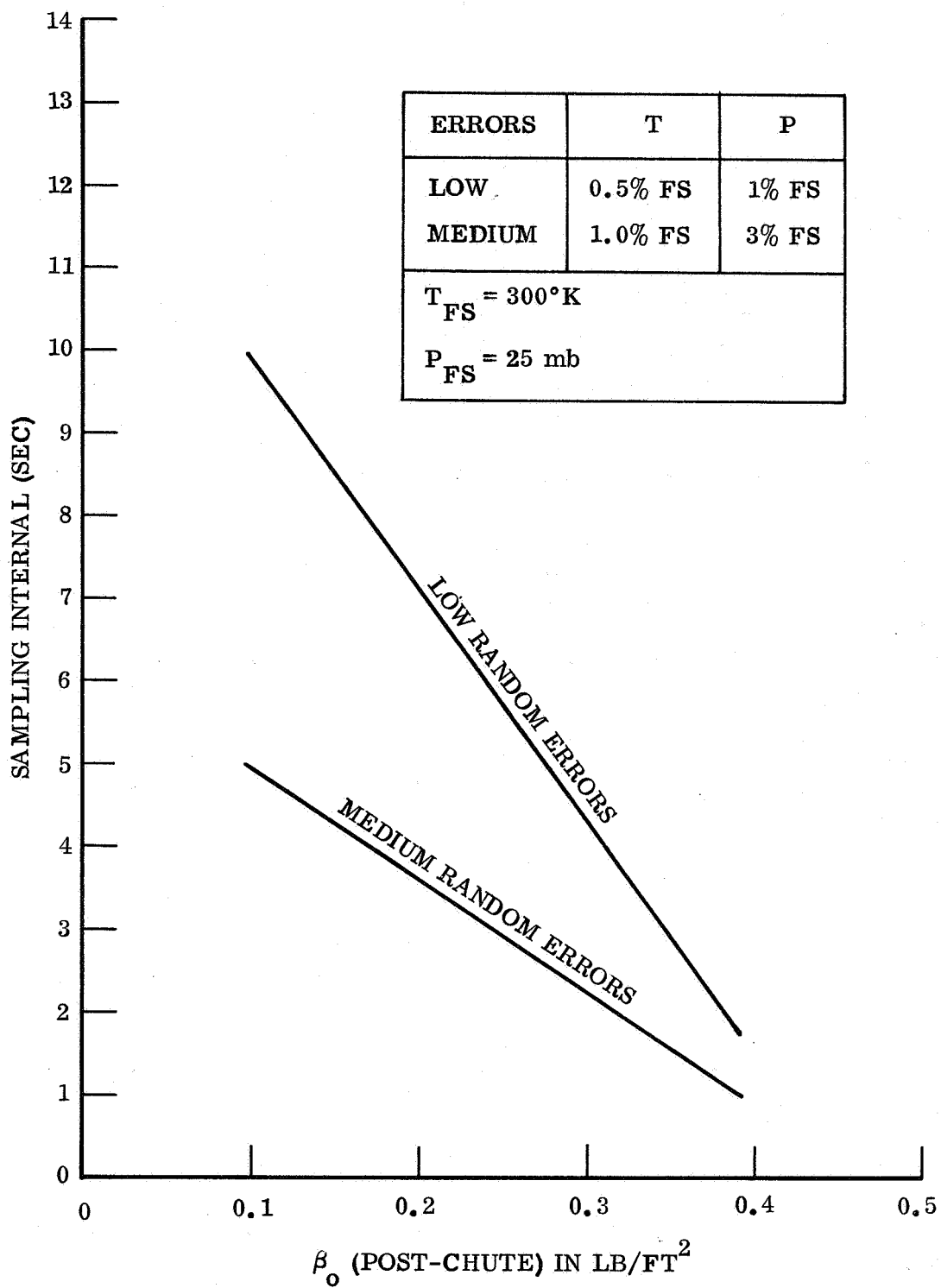
Figure 4.5-4. Sampling Interval – Ballistic Coefficient Relations for
Achieving 5 Percent Measurement Accuracy of
Density – Altitude Profile

The dependence of the density determination upon temperature and pressure data has produced the expected result that its measurement requirements are the most stringent. The selection of a design goal of 1 sample per second was based on this requirement and the intent to provide a reasonable margin in the sampling intervals for unaccounted-for uncertainties.

4.5.1.4 Composition

One of the most influential factors affecting the accuracy of the composition determination at a height above the planet, is the method used for sampling the gas. In the vented form of sampling, the gas is sampled throughout the whole of the scan period of the mass spectrometer which is of the order of 2 secs. During this time the ambient pressure can have reduced by about 40 percent for a steep angled entry if the vehicle is traveling at about Mach 5. The approach places great emphasis on post-flight analysis where the Capsule altitude profile and the ambient pressure and temperature altitude profiles must be used. Uncertainties in their values will be strongly reflected in the composition results. This error can be circumvented by using an alternative sampling technique that samples over a very short time, collects the gas in a reservoir, and bleeds the gas through a succession of valves into the ionization chamber.

The greatest accuracy is obtained with this approach since the final accuracy will primarily be only a function of the mass spectrometer resolution and the quantity of the constituent present in the sample. The accuracy of the percentage composition of each component will largely depend on this latter factor, since the signal/noise ratio is directly related to it. Current instruments are expected to be able to detect components of the sample giving rise to an ion current of 10^{-15} amps. corresponding to a partial pressure of 10^{-11} mm Hg. Mass resolution is of the order of 1 AMU for a continuous scan system for the range 10-60 AMU. This is adequate since isotopic resolution capability is not required. The amplitude resolution is of the order of 1-2 percent and is a function of the amplifying electronics.

As a back-up to the mass spectrometer, the mean molecular weight determinations by experiment simulation calculations will be available. The molecular weight is a direct output of the data anslysis methods used and is determined with accuracies comparable to the density values. The summary of results for the matrix of runs of table 4.5-2 is shown in fig. 4.5-5. It is noted that for a sampling interval of one second and a subsonic β of 0.39, one can expect about $\alpha \pm 5$ percent accuracy in the mean molecular weight in any atmosphere.

4.5.1.5 Water Vapor

Atmospheric water vapor detection is accomplished by the surface water vapor detection equipment discussed in paragraph 4.5.2.3 .

ERRORS	T	P
LOW	0.5% FS	1% FS
MEDIUM	1% FS	3% FS

$T_{FS} = 300°K$

$P_{FS} = 25$ mb

NOMINAL VALUES OF MOL. WT.

VM 8   44.0

VM 9   31.2
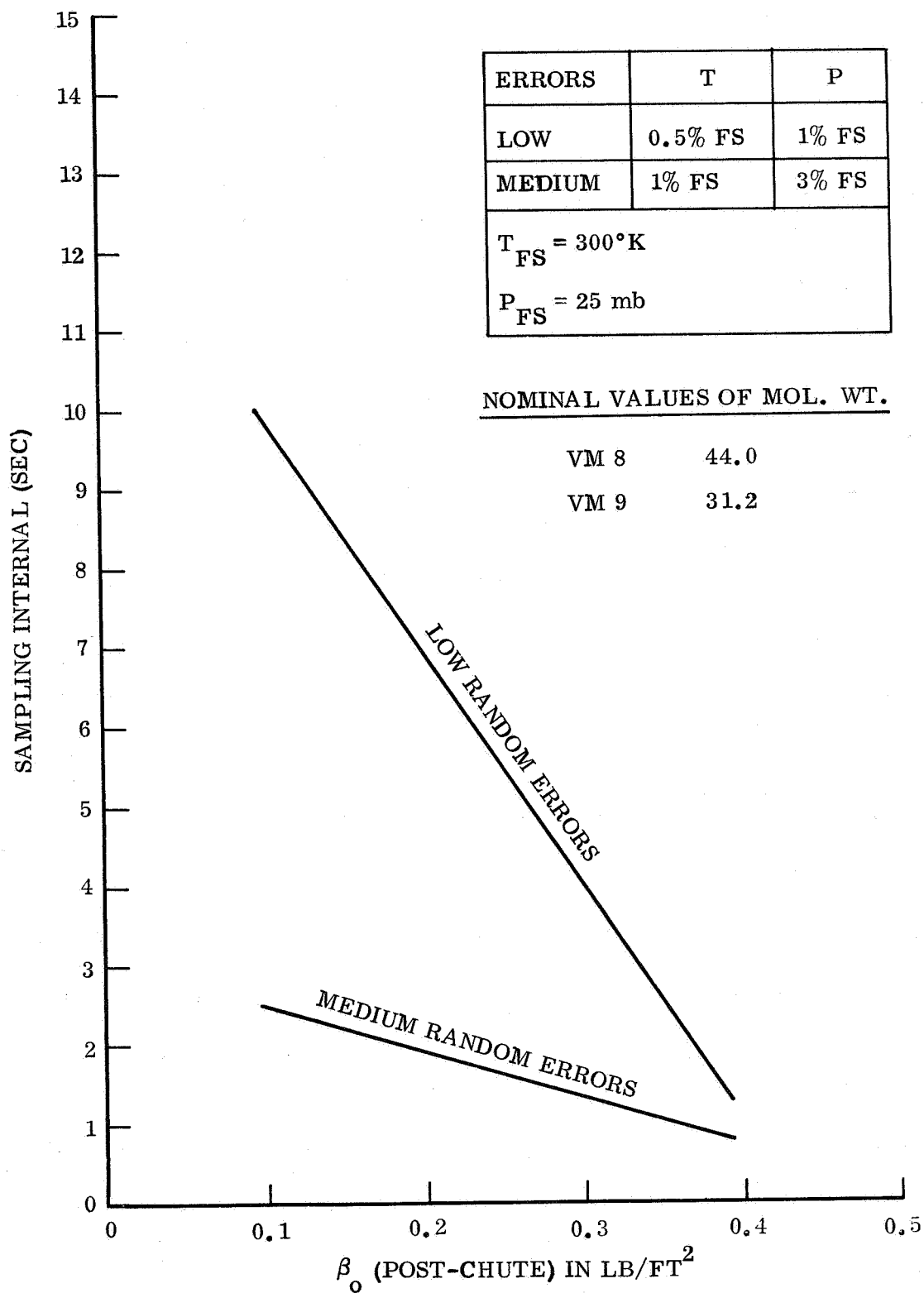
Figure 4.5-5. Sampling Interval – Ballistic Coefficient Relations for
Achieving 5 percent Measurement Accuracy of
Molecular Weight

4.5.2 SURFACE METEOROLOGY

4.5.2.1 Pressure

The accuracy to which the atmospheric pressure on the surface of Mars can be measured is dependent upon the following error sources:

1. Perturbation of the atmospheric flow over the Lander and the resultant deviation from the free stream pressure at the pressure sensor port.

2. Errors inherent in the pressure transducer itself.

3. Errors resulting from the digitization process in the telemetry system.

4. Drop-out of bits in the telemetry signal due to random processes associated with the detection system.

The first of these sources is impossible to predict at present due to the lack of information about the Martian atmosphere. Errors generated in the sensor itself can probably be kept below 0.25 percent following calibration to remove bias and non-linearity contributions. The random telemetry drop-outs can produce very significant errors if the number of statistical samples is small; however when the same function is measured many times in a short period of time (so as to minimize variation of the parameter during the sampling period) this error becomes negligible. The digitization error for the pressure transducer will be approximately 1 percent. Taking the root sum square of these errors it appears that a 2 percent measurement may be possible if the first error source can be kept below ~ 1.5 percent. Assuming the pressure transducer has a full scale of 25 mb, the best resolution possible will then be ≈ 0.25 mb (one digital level) and the accuracy will be ≈ 0.5 mb.

4.5.2.2 Temperature

As indicated in paragraph 4.2.3.2, the measurement of temperature on the surface of Mars will be a difficult task. Until the relationships between true atmospheric temperature and equilibrium temperature of the resistance element can be defined any attempts to evaluate the accuracy of this measurement must be directed at the ability of the system to measure the temperature of the transducer's sensitive element only and the predictions treated as optimistic.

Resistance thermometers can faithfully measure the temperature of their sensitive element to accuracies of 0.1 percent or better. The errors encountered in telemetering this data will swamp out this error and the result will be a system error equal to the digitization error. At best, the resolution of temperature to $\pm 3^{\circ}$ K will be possible with a telemetry system capable of 1 percent analog to digital conversions. The accuracy of this measurement cannot be defined at this time.

4.5.2.3 Water Vapor

The water vapor detection scheme carried on the 1973 Hard Lander will use a radioactive detector and event counter. The accuracy of transmission of the digital information provided by this sensor will depend upon the bit error probability of the telemetry system and the number of times the information is transmitted. Since the number of bits involved in this measurement is relatively small, repeated transmission of the data can be accomplished and thus the probability of error reduced to a negligible level.

The accuracy of the chemical/radiological water detection system is expected to be better than 5 percent for water vapor concentration levels of 1 part per million or greater. If interferences with the measurement originating in the sampling system can be controlled, extension to lower concentrations can be considered but longer sampling periods will be required to maintain reasonable precision in the measurement.

4.5.2.4 Surface Winds

The anticipation that Mars' atmosphere may indeed support steady-state winds of up to 200 fps leads to a wind velocity sensor with a full scale of 200 fps. The ability of acoustic propagation devices to measure wind velocities to a resolution of better than ± 1 m/sec has been established on Earth and thus the measurement of Martian winds ± 1 m/sec should be possible if local disturbances to the wind patterns can be avoided.

4.5.3 SURFACE CHARACTERISTICS

4.5.3.1 Imagery

4.5.3.1.1 Resolution Considerations

The facsimile cameras have a limiting angular resolution that is fixed by the design of the imaging optics. For this mission the two selected angular fields of view are $0.1°$ and $0.01°$. The linear resolution in the objective plane is simply the angle multiplied by the distance between the imaging lens and the optics. The Hard Lander can assume any one of a wide variety of landed positions on the planet, each of which can result in a different distance between the lens and nearest object (optical arm). The nearest object is selected because the greatest linear resolution is obtained at the minimum optical arm. Typical figures for the smallest linear element corresponding to the angular fields of view of $0.1°$ and $0.01°$ are 2.5 mm and 0.25 mm, respectively. This does not mean that an object with these linear dimensions will be resolved on playback of the recorded information. The digitization and telemetry of the imaging data results in a loss of information which typically increases the linear picture resolutions quoted above by a factor of 1.4 horizontally and 1.4 vertically. The identification of an object with these dimensions will depend on its shape; those that are long and thin, such that they are one linear resolution element in width and at least four such elements in length, will be resolved provided they are in strong enough contrast with the background. Objects that are square or

round shaped will not be resolved unless their linear dimensions are at least twice that of the minimum resolvable ground resolution.

Since the discussion above presupposed a clear optical path with subject lens distances in the region of a few feet even in a scattering atmosphere, the assumed linear resolutions of 2.5 mm and 0.25 mm are valid. However, the presence of a thick dust cloud could conceivably result in such a high degree of scattering that photographic resolution could be impaired both by motion of the scattering cloud and by a reduction in contrast.

A reduction in resolution may also occur at very low light levels, such as may occur in the shadow of the Lander. The data given above assumes a high contrast ratio in the subject. Details of the performance of the camera in low illumination situations are not available, but they will undoubtedly be affected by the speed at which the scanning is carried out. This type of data can be evaluated when the variable parameter camera becomes available.

Based on assumed clear conditions, it will be possible to resolve long thin objects that are at least 4 mm by 12 mm, or round or square shaped objects that are 8 mm in width or in diameter with a 0.1° IFOV, and objects of one tenth of these dimensions with a 0.01° IFOV.

4.5.3.1.2 Vibration Effects

Serious degradation of the image can occur through vibration induced into the optical system. The susceptibility of the facsimile imaging process is particularly acute due to the lack of correlation between line scans and each element of each line scan. Vibration can rise through two principle mechanisms – wind and mechanical motion. The mechanical motion of motors and gears within the camera assembly, through friction, gives rise to minute deflections of the camera. These in turn effectively deviate, possibly in synchronous manner, the optical line of sight from its intended direction. If the deflection of the line of sight is large enough this can either superimpose a modulation pattern onto the image or degrade it in contrast. By designing to reduce the induced vibration to less than one tenth of an IFOV, vibrational effects can be ignored.

More troublesome is wind-induced movement of the camera support and the Lander. These are, to a large degree, unknown factors that at best can only have rough probabilities assigned to them. The Lander may land in a very stable position so that it can be treated as a stable mass and only vibration of the camera support itself need be treated for induced vibration. Or, the whole Lander could be unstable. Design control can be exercised to reduce the vibration of the support to less than one tenth of the IFOV. The weight penalty resulting from meeting these requirements is discussed in Section 4.1.1 of Volume III.

4.5.3.2 Soil Composition

The accuracy expected from this instrument is difficult to estimate. Excluding the existing but low probability of error due to data transmission, the instrument accuracy is mainly affected by the temperature attained by the instrument on the planet, and, of greater importance, the background count. Provided the instrument temperature is monitored the effect of temperature variations can be corrected by techniques established in the laboratory. The greatest source of unknown error is the signal-to-noise ratio achieved at the various energy levels which is entirely dependent on the magnitude of the background radiation. If the signal-to-noise ratio remains greater then 10:1 then accuracy of percentage abundance can be expected to be similar to the Surveyor results. These varied from ± 50 percent for the low abundance constituents to about ± 8 percent for those of high abundance. The re-design for the Mars environment will tend to diminish these errors by increasing the source strength and diminishing the distance between sample and detector, however, this may not be enough to accommodate for a large increase in the background rate compared with that on the Moon.

No evidence exists for the effect on accuracy caused by irregularities of the surface in the region of the impact point of the alpha beam; these may be subsequently evaluated terrestrially. Another problem is associated with the deployment of the sensor head: the plane of the base of the instrument must lie parallel to the surface -- i.e., the instrument must be free to align itself with the gross surface inclination -- this may prove to be a difficult engineering problem in view of the g-load. Consequently until further studies are made, the Surveyor results must be taken as an indication of achievable accuracies.

4.5.3.3 Expanded Payloads

The assessment and establishment of measurement accuracies for experiments in the expanded payloads can be done only on a speculative basis without the aid of quantitative information. The instrumentation involved in each experiment is either in early development stages or has not been properly configured and fully tested for the Martian mission. As a result, reasonable estimates can be made on the sensor and circuitry performance but evaluation of the inaccuracies involved in data analysis and interpretation must await future development and testing. In the following sections, sensor performance only is discussed for the subsurface water detector, airborne dust detector, ultraviolet radiometer, and the large molecule detection system.

4.5.3.3.1 Subsurface Water Detector

The subsurface water detector is a combination of two instruments, the soil boring instrument and the water vapor detector. The presence of water vapor is detected in the latter; this has a current ability to detect 6×10^{13} molecules of water at standard atmospheric conditions. The flight version is expected to be able to detect 6×10^{11} molecules of water.

4.5.3.3.2 Airborne Dust Detector

Owing to uncertainties in the particle size distribution, nature of the particles and their velocities, a good assessment of the instrument accuracy cannot be made. However current particle detectors are available that have threshold impulse sensitivities of 10^{-3} to 10^{-5} dynes-seconds. This threshold may not be applicable to those instruments used in an atmospheric environment if wind impulses can generate noise within the bandpass of the instrument.

4.5.3.3.3 Ultraviolet Radiometer

This is a well established form of instrument and the accuracy it can achieve is of the order of 1 percent or less. The main causes of inaccuracies will be in the stability of electronic circuitry and telemetry. An overall accuracy of 1 percent in energy within a given optical band should be achieved.

4.5.3.3.4 The Gas Chromatograph - Mass Spectrometer

This instrument is capable of resolving between 20 and 30 components in a sample. The accuracy may be defined in terms of component resolution or in fractional content of the various components. The two parts of the instrument are complementary in that a deficiency of one part is compensated for by high efficiency in the other. The overall accuracy will clearly depend on the nature of the sample and the percentage composition of the components of the sample. A typical estimate for the instrumental sensitivity is 3×10^{-10} mole at standard atmospheric conditions.

4.6 REFERENCES

4-1.   Hess, D. S. and Pounder, E., "Voyager Environmental Predictions Document", SE-003-BB001-1B28, NASA-JPL, Oct., 1966.

4-2.   Vachon, D. N., "Final Report, Voyager Spacecraft, Phase B Task D, Volume IV, Mars Atmosphere Definition", DIN 67SD4379; GE; Oct., 1967.

4-3.   Weidner, D. K. and Hasseltine, C. L., "Natural Environment Design Criteria Guidelines for MSFC Voyager Spacecraft for Mars 1973 Mission", NASA-TM-X-53616, June, 1967.

4-4.   NASA/Langley Research Center, "Preliminary Draft-Mars Engineering Model Parameters for Mission and Design Studies - 1968", dated May, 1968.

4-5.   Hess, D. S. and Pounder, E., "Voyager Environmental Predictions Document", SE003BB001-1B28, NASA-JPL, Oct., 1966.

4-6.   Neubauer, F. M., "Thermal Convection in the Martian Atmosphere", Journal of Geophysical Research, Vol. 71, p. 2419, May 15, 1966.

4-7.   House, F. B., "The Seasonal Climatology of Mars"; Contributions to Planetary Meteorology GCA Technical Report No. 66-8-N, March, 1966.

4-8.   Ohring, G. and Mariano, J., "Seasonal and Latitudinal Variations of the Average Surface Temperature Profile of Mars", GCA Tech. Rpt. 67-5-N, March, 1967.

4-9.   Leovy, C., "Radiative-Convective Equilibrium Calculations for a Two Layer Mars Atmosphere", Rand Memo RM-5017, 1966.

4-10. Gifford, F., "The Surface - Temperature Climate of Mars", Ap. J., 123, 1956.

4-11. Leighton, R. B. and Murray, B. C., "Behaviour of CO_2 and Other Volatiles on Mars", Science, 153, p. 136, July, 1966.

4-12. Vachon, D., "Mars Atmosphere Definition", DIN 67SD4379, Oct., 1967, GE-MSD.

4-13. Galbraith, T. L., "Particle Transport in the Martian Atmosphere", GE-MSD, GE-TM-8126-4, May, 1966.

4-14. GE Re-entry Systems Organization Technical Brief "Correlation of Available Flight-Test, Base-Pressure Data for Application on Planetary Entry Configurations"

4-15. Vachon, Statistical Sampling of Winds on Mars, General Electric Co., TM 8126-7, July, 1966.

4-16. "Correlation of Available Flight Test Base Pressure Data", General Electric Company, Re-entry Systems, November 29, 1967.

4-17. "Evaluation of Base Pressure Characteristics for Planetary Entry Configurations", General Electric Company, Re-entry Systems, Technical Brief, November 10, 1967.

4-18. "Synthesis Techniques for Experiments in Planetary Atmospheres", S. O. Smith, P. DeVries, R. J. Homsey; AIAA Paper No. 68-155; January 22, 1968.

APPENDIX

REFERENCE MISSIONS — OUT-OF-ORBIT ENTRY AND DIRECT ENTRY — TYPE I TRANSIT TRAJECTORIES

APPENDIX

REFERENCE MISSIONS

- OUT-OF-ORBIT ENTRY AND DIRECT ENTRY -

TYPE I TRANSIT TRAJECTORIES

As noted in Section 3.1 (see tables 3.1-6 and 3.1-11), entry trajectory parameters were determined for both the out-of-orbit entry and direct entry modes for four VM atmospheres; namely, VM-3, -7, -8 and -9. The resultant curves are presented in Section 3.1 for the VM-3 case while this Appendix contains the corresponding figures for the VM-7, VM-8 and VM-9 cases.

PER = -14.4°   β EI = 14°
TEI = 400 sec   landing latitude = 10°
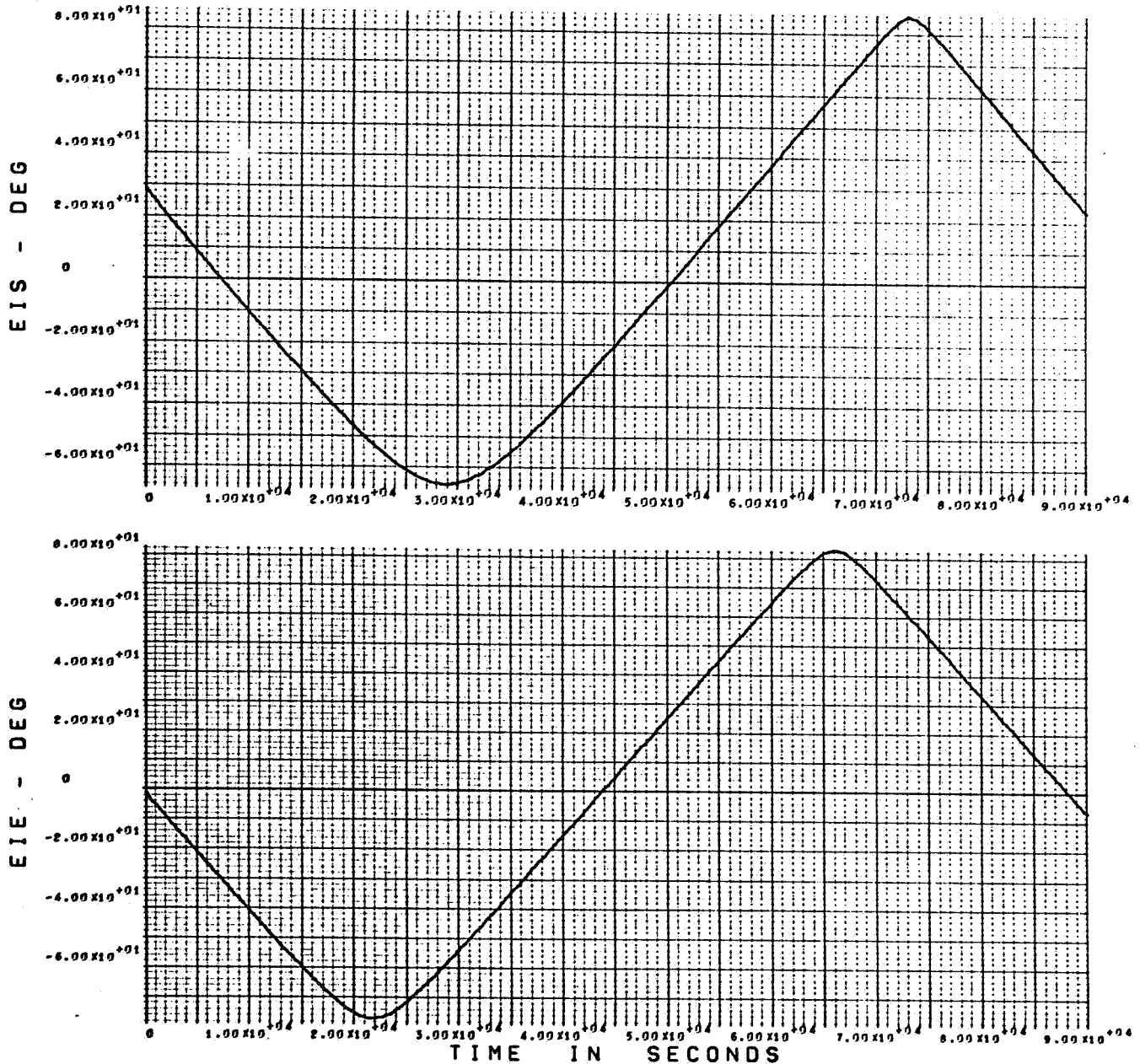
EIS = SUN ELEVATION ABOVE HORIZON
EIE = EARTH ELEVATION ABOVE HORIZON

Figure A-1. Earth and Sun Elevations at Landing Site During First Orbit After
Landing, Out-of-Orbit Entry

PER = −14.4°   𝒷 EI = 14°
TEI = 400 sec   landing latitude = 10°

EIB = S/C ELEVATION ABOVE HORIZON

Figure A-2. Relay Communication Range and S/C Elevation at Landing Site,
During First Orbit After Landing, Out-of-Orbit Entry

PER = -14.4°   ⊖   EI = 14°
TEI = 400 sec   landing latitude = 10°

COA = CONE ANGLE
CLA = CLOCK ANGLE

Figure A-3. Lander Clock and Cone Angle at S/C During First Orbit After
Landing Out-of-Orbit Entry

PER = -14.4° $\mathcal{C}$ EI = 14°

TEI =   400 sec   landing latitude = 20°

EIS = SUN ELEVATION ABOVE HORIZON
EIE = EARTH ELEVATION ABOVE HORIZON

Figure A-4. Earth and Sun Elevations at Landing Site During First Orbit After
Landing Out-of-Orbit Entry

PER = -14.4° θ EI = 14°
TEI = 400 sec   landing latitude = 20°

EIB = S/C ELEVATION ABOVE HORIZON

Figure A-5. Relay Communication Range and S/C Elevation at Landing Site
During First Orbit After Landing, Out-of-Orbit Entry

PER = -14.4°
TEI = 400 sec

e EI = 14°
landing latitude = 20°
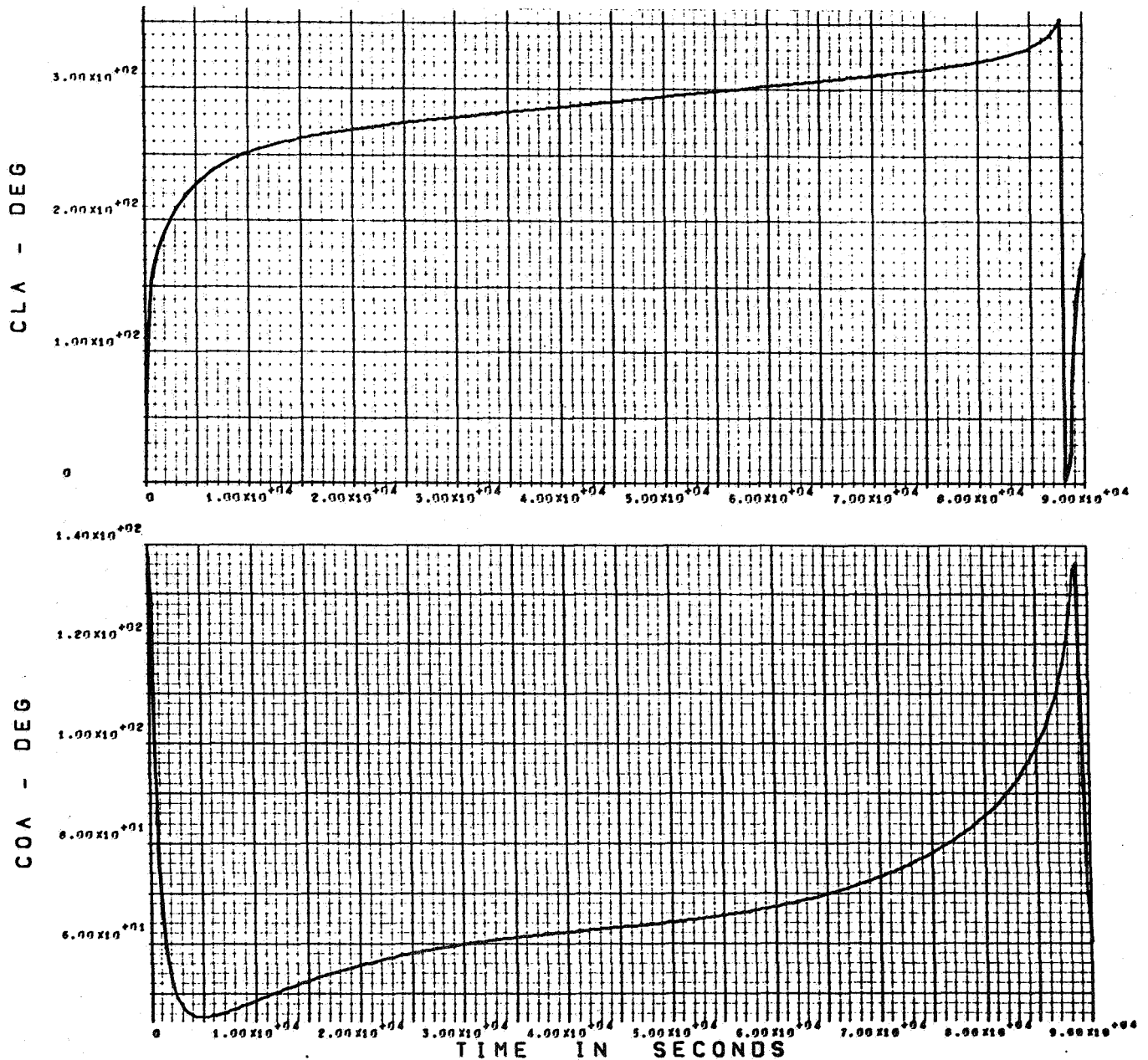
COA = CONE ANGLE
CLA = CLOCK ANGLE

Figure A-6. Lander Clock and Cone Angle at S/C During First Orbit After
Landing, Out-of-Orbit Entry

PER = -14.4°   ℮ EI = 14°
TEI = 1000 secs   landing latitude = 10°

EIS = SUN ELEVATION ABOVE HORIZON
EIE = EARTH ELEVATION ABOVE HORIZON

Figure A-7. Earth and Sun Elevations at Landing Site During First Orbit After
Landing, Out-of-Orbit Entry

#2

PER = −14.4°
TEI = 1000 secs

EI = 14°
landing latitude = 10°

EIB = S/C ELEVATION ABOVE HORIZON

Figure A-8. Relay Communication Range and S/C Elevation at Landing Site
During First Orbit After Landing, Out-of-Orbit Entry

PER = -14.4°   𝒫 EI = 14°
TEI = 1000 secs   landing latitude = 10°

COA = CONE ANGLE
CLA = CLOCK ANGLE

Figure A-9. Lander Clock and Cone Angle at S/C During First Orbit After
Landing, Out-of-Orbit Entry

PER = -14.4° β EI = 14°

TEI = 1000 secs   landing latitude = 20°

EIS = SUN ELEVATION ABOVE HORIZON

EIE = EARTH ELEVATION ABOVE HORIZON

Figure A-10.   Earth and Sun Elevations at Landing Site During First Orbit After
Landing, Out-of-Orbit Entry

PER = -14.4°
TEI = 1000 secs

EI = 14°
landing latitude = 20°
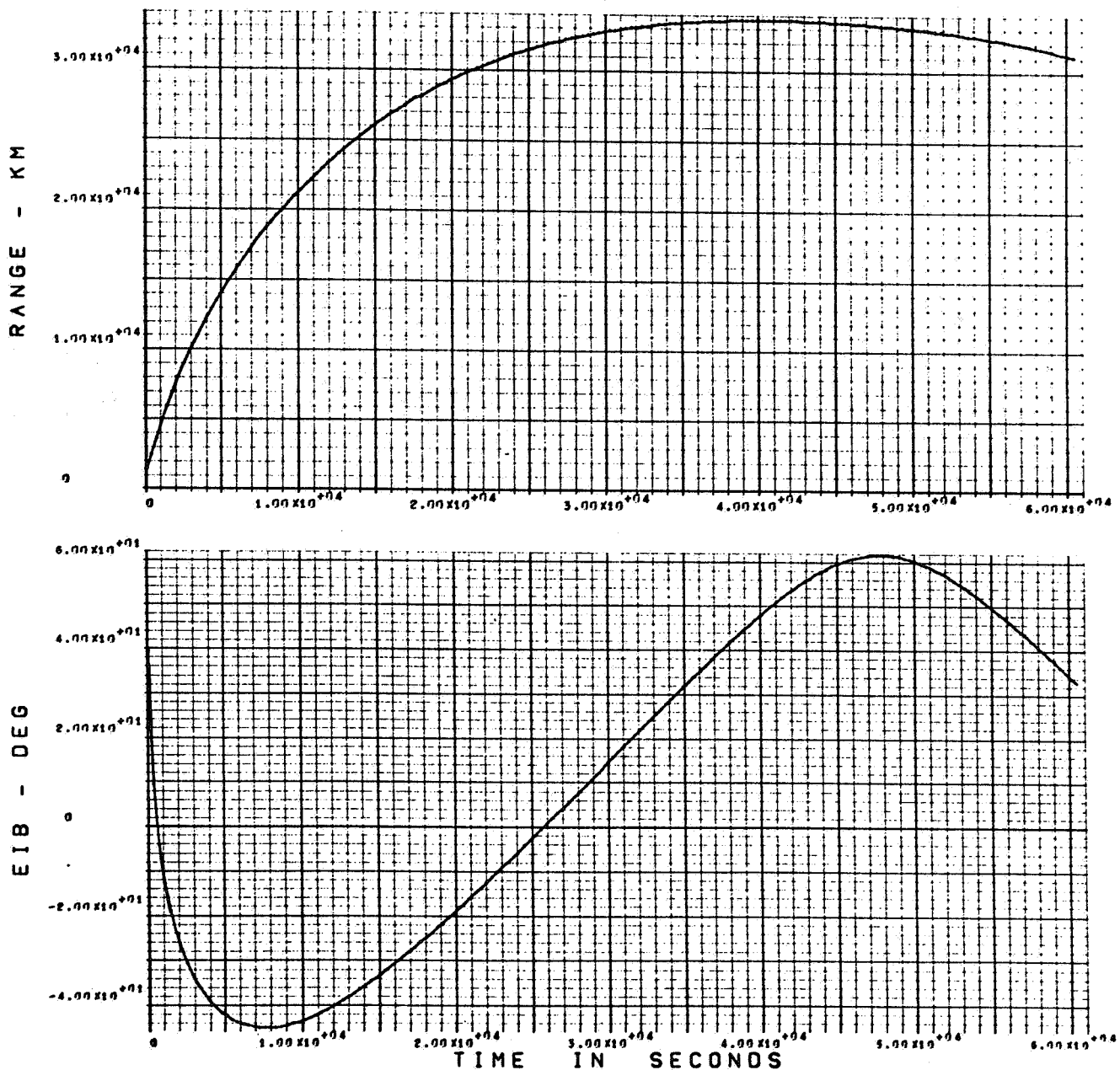
EIB = S/C ELEVATION ABOVE HORIZON

Figure A-11. Relay Communication Range and S/C Elevation at Landing Site
During First Orbit After Landing, Out-of-Orbit Entry
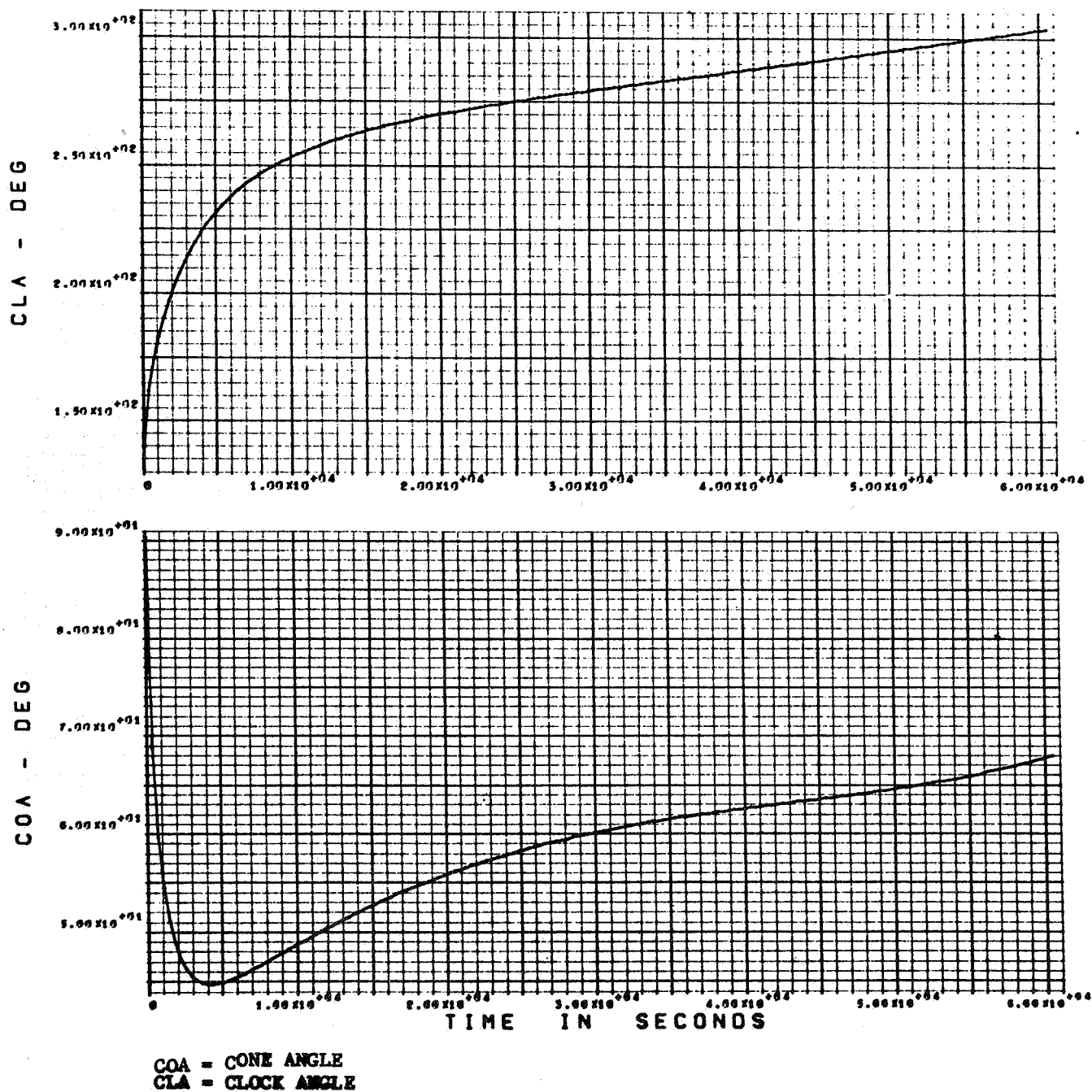
Figure A-12. Lander Clock and Cone Angle at S/C During First Orbit After
Landing, Out-of-Orbit Entry
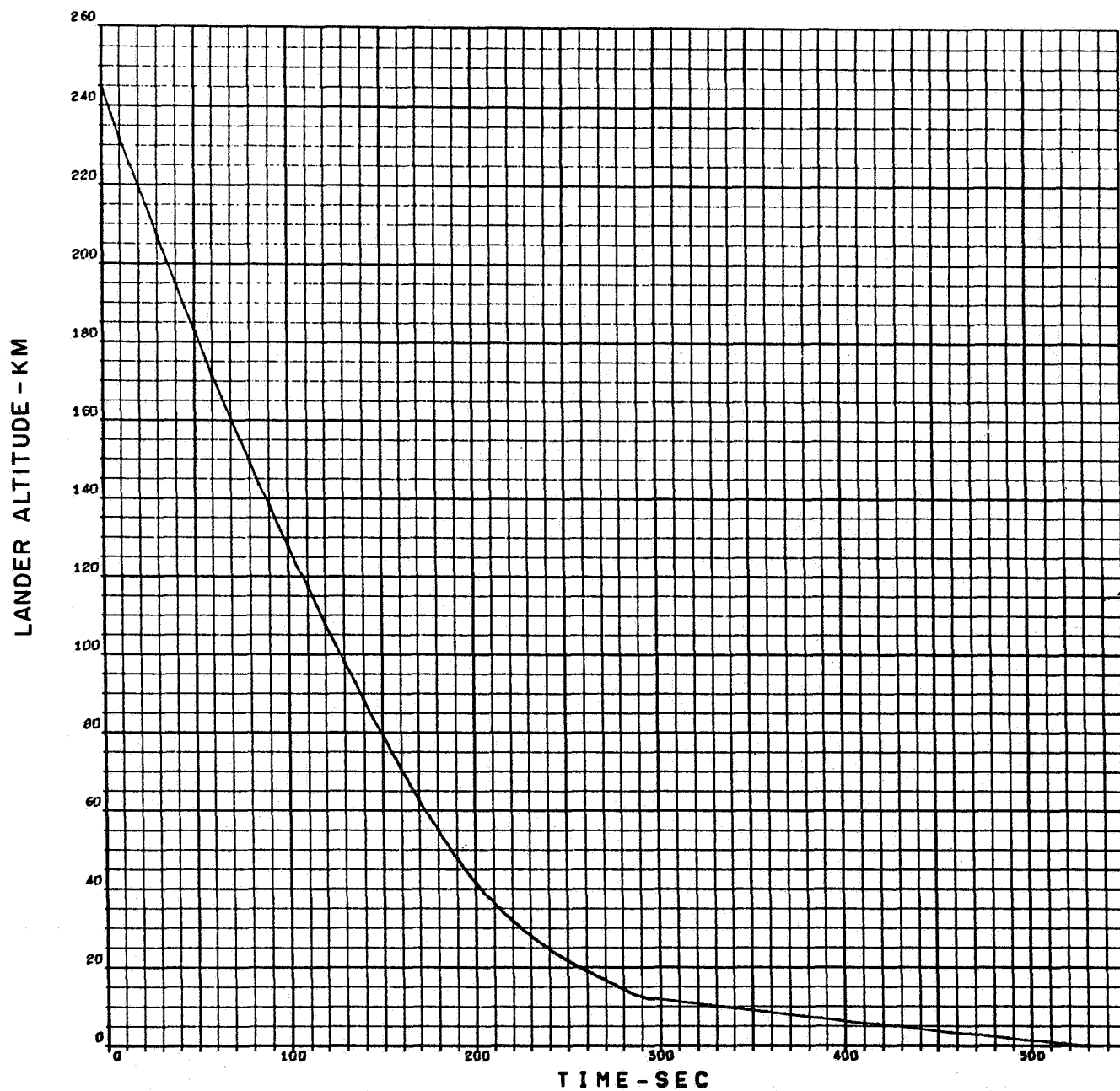
ENTRY VELOCITY   - 15,300 FT/SEC.
ENTRY PATH ANGLE - 16 DEG.
ENTRY ALTITUDE   - 244 KM
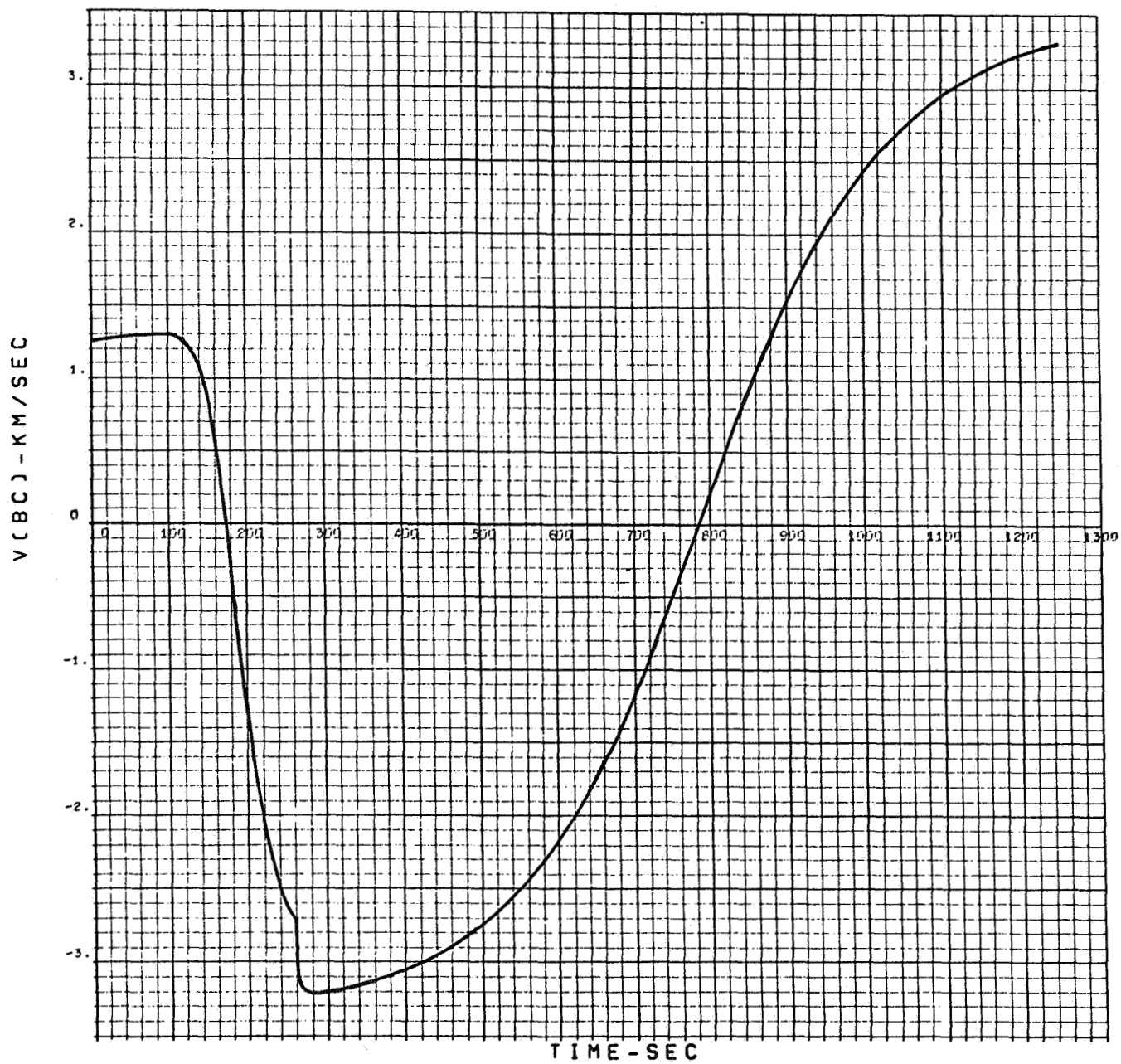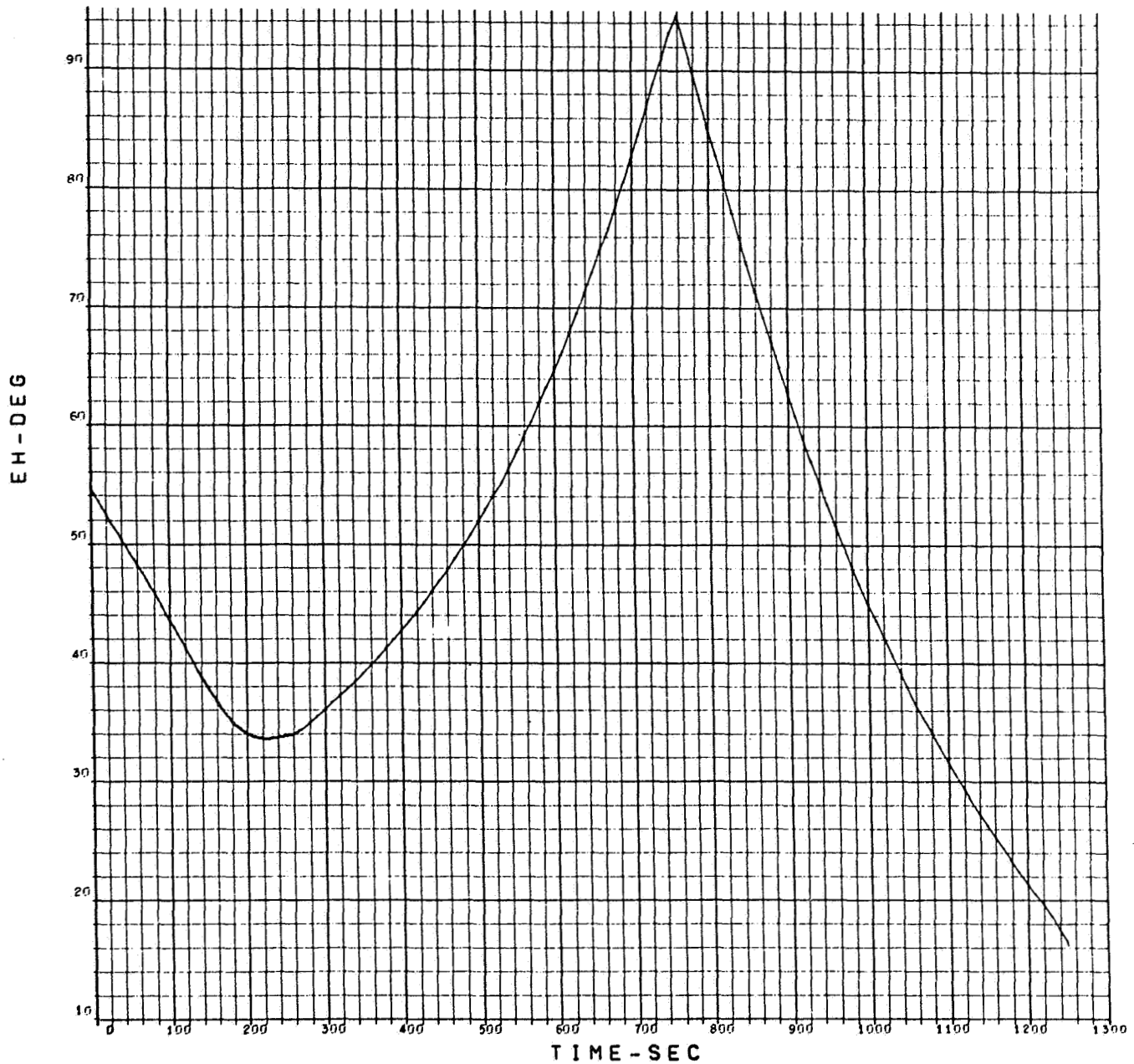DRAG, SEE FIGURE 3.1-20
VM-7

Figure A-13. Lander Altitude vs Time, VM-7, Out-of-Orbit Entry
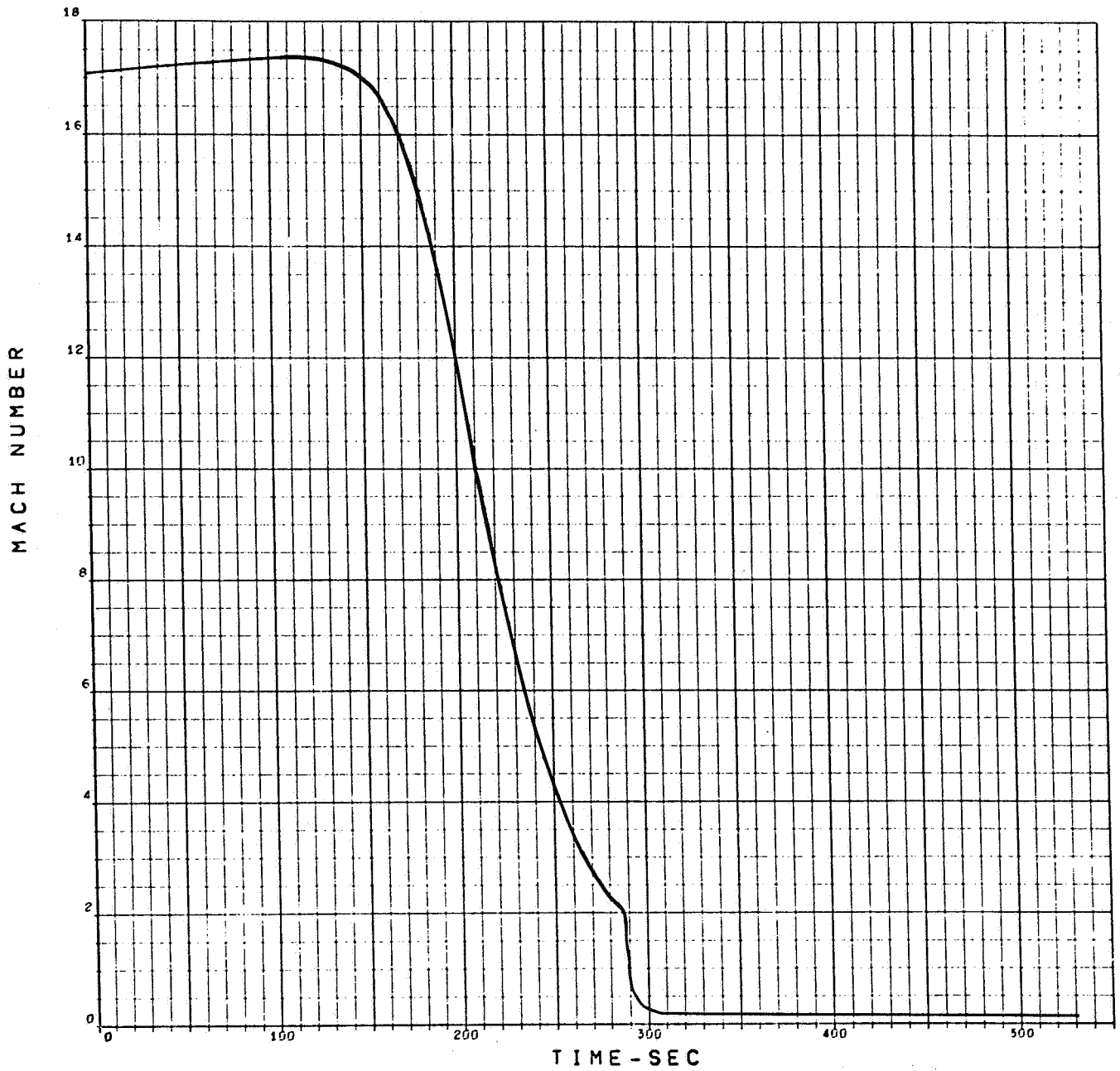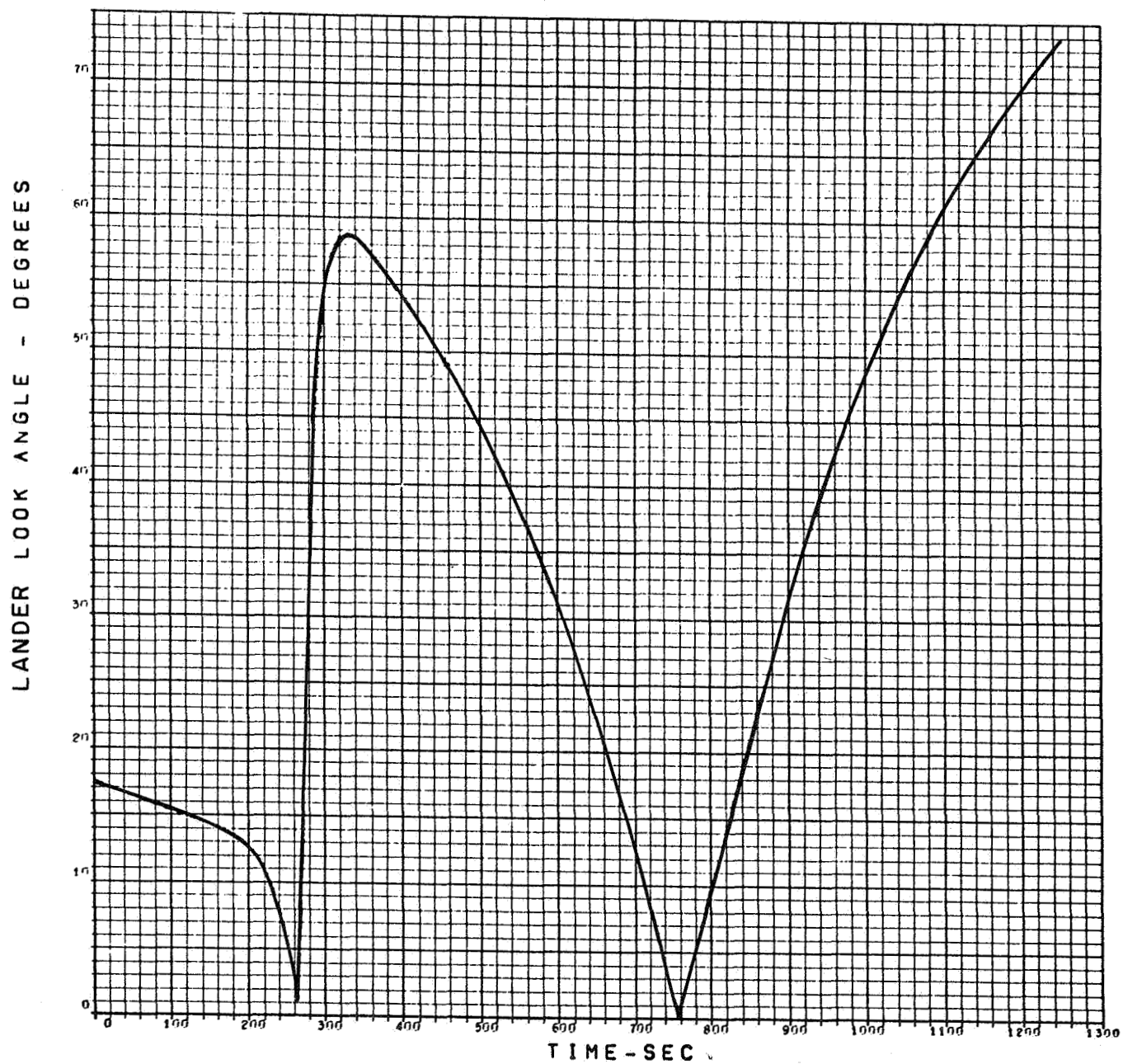
ENTRY VELOCITY   - 15,300 FT/SEC.
ENTRY PATH ANGLE - 16 DEG.
ENTRY ALTITUDE   - 244 KM
DRAG, SEE FIGURE 3.1-20
VM-7

Figure A-14. Mach Number vs Time, VM-7, Out-of-Orbit Entry
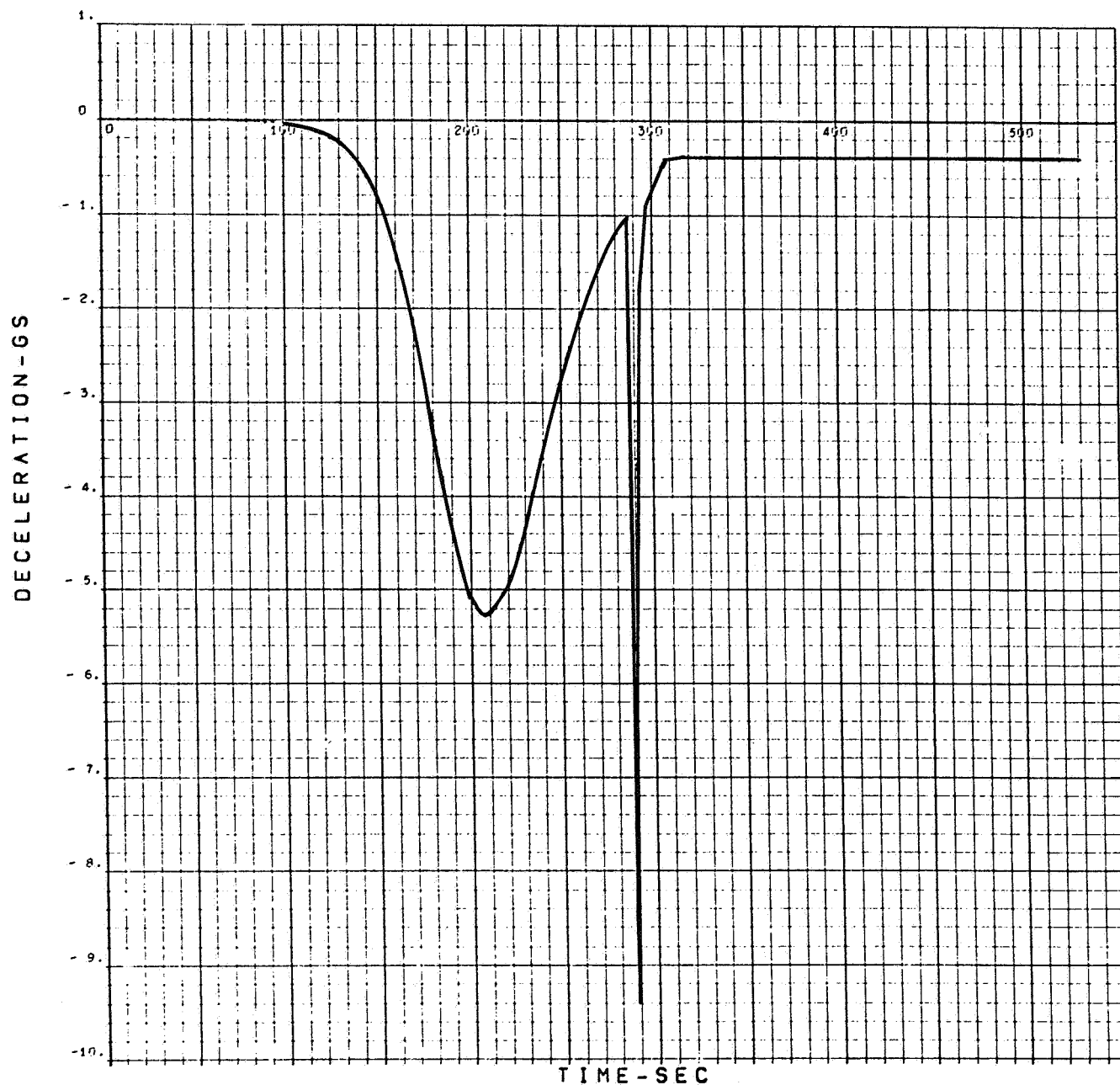
ENTRY VELOCITY   - 15,300 FT/SEC.
ENTRY PATH ANGLE - 16 DEG.
ENTRY ALTITUDE   - 244 KM
DRAG, SEE FIGURE 3.1-20
VM-7

Figure A-15. Lander Deceleration vs Time, VM-7, Out-of-Orbit Entry
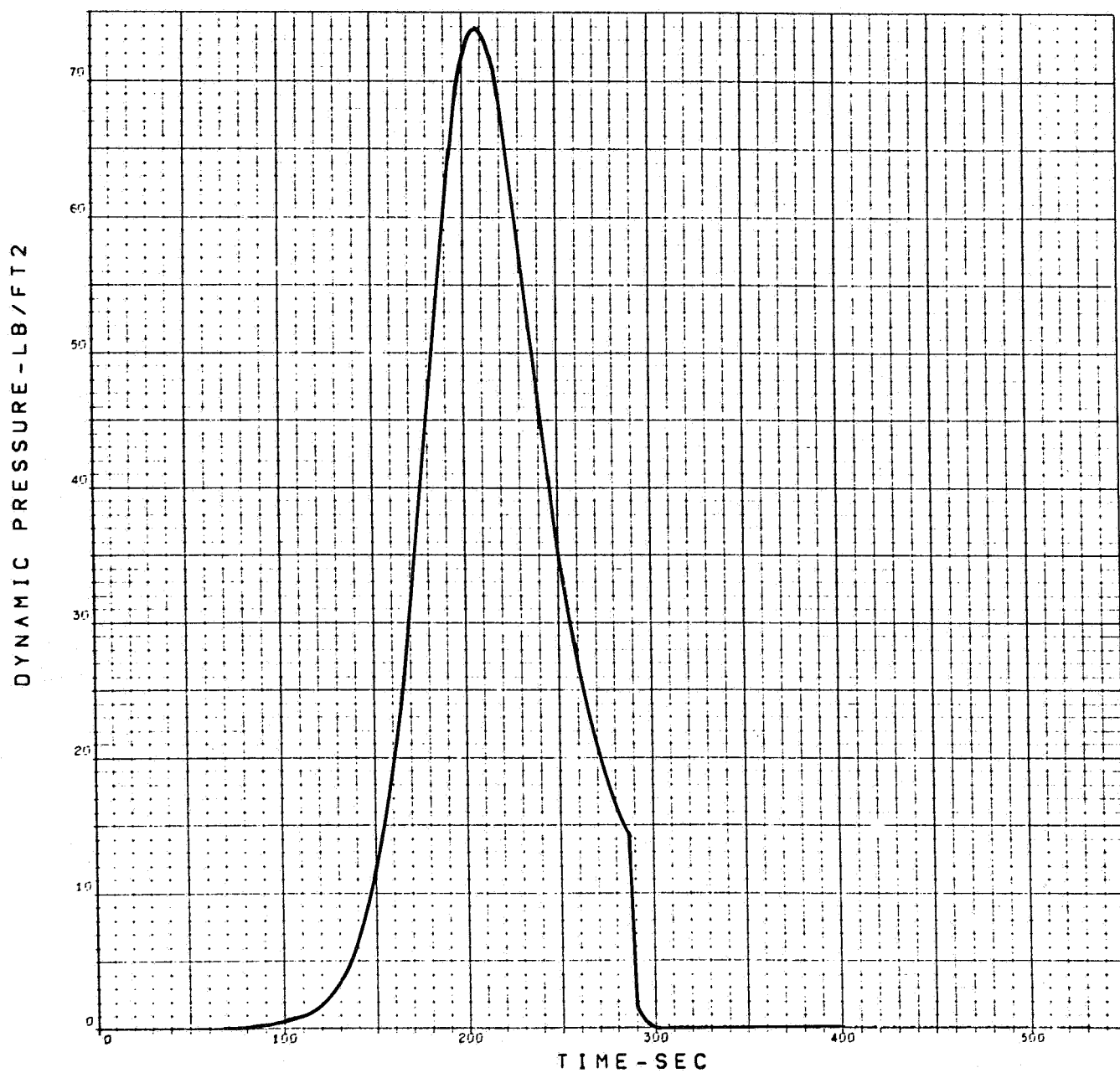
ENTRY VELOCITY   - 15,300 FT/SEC.
ENTRY PATH ANGLE   - 16 DEG.
ENTRY ALTITUDE   - 244 KM
DRAG, SEE FIGURE 3.1-20
VM-7

Figure A-16. Dynamic Pressure vs Time, VM-7, Out-of-Orbit Entry
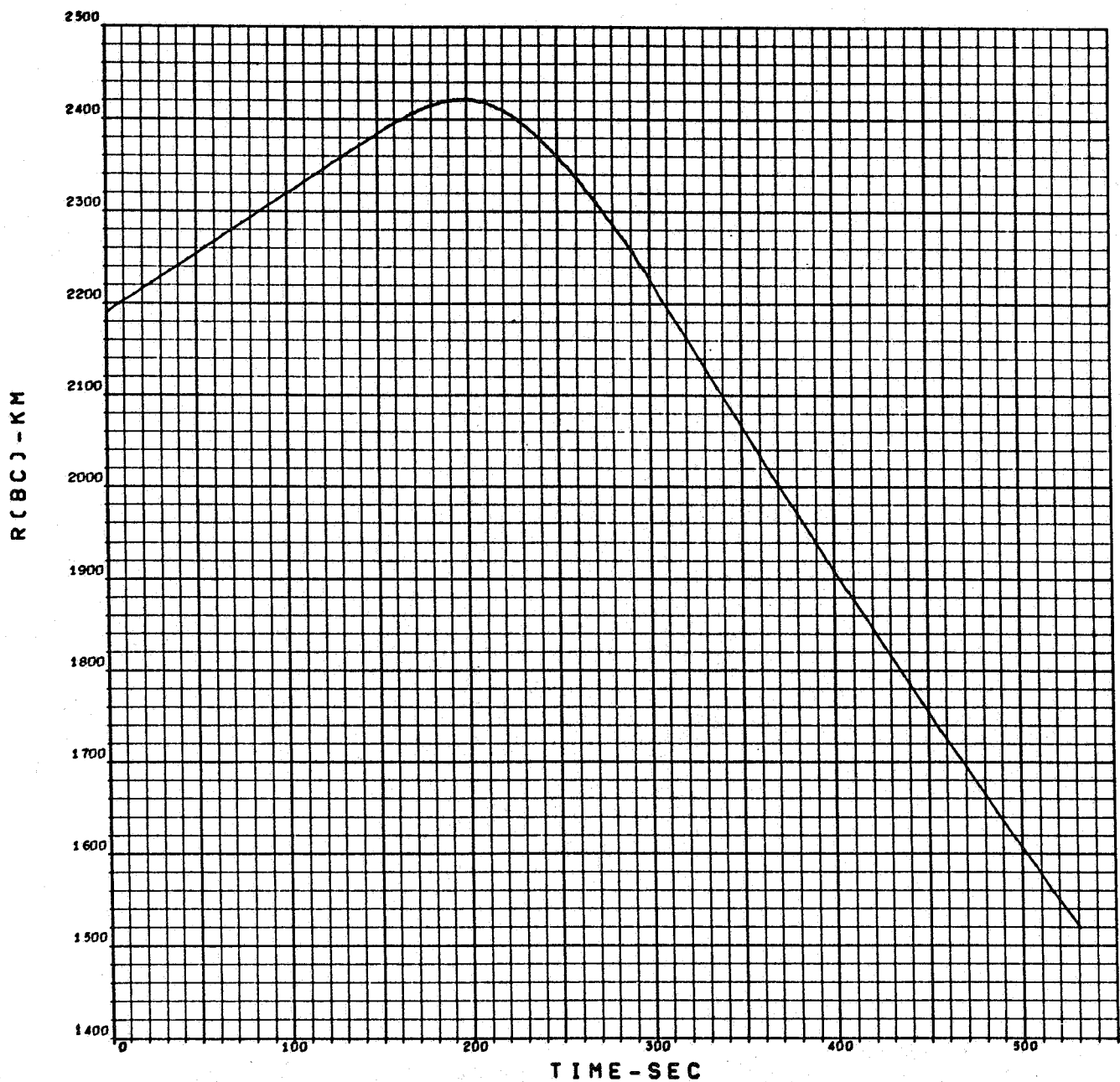
ENTRY VELOCITY   - 15,300FT/SEC.
ENTRY PATH ANGLE - 16 DEG.
ENTRY ALTITUDE   - 244 KM
DRAG, SEE FIGURE 3.1-20
VM-7

Figure A-17. Communication Distance R(BC) vs Time, VM-7, Out-of-Orbit Entry
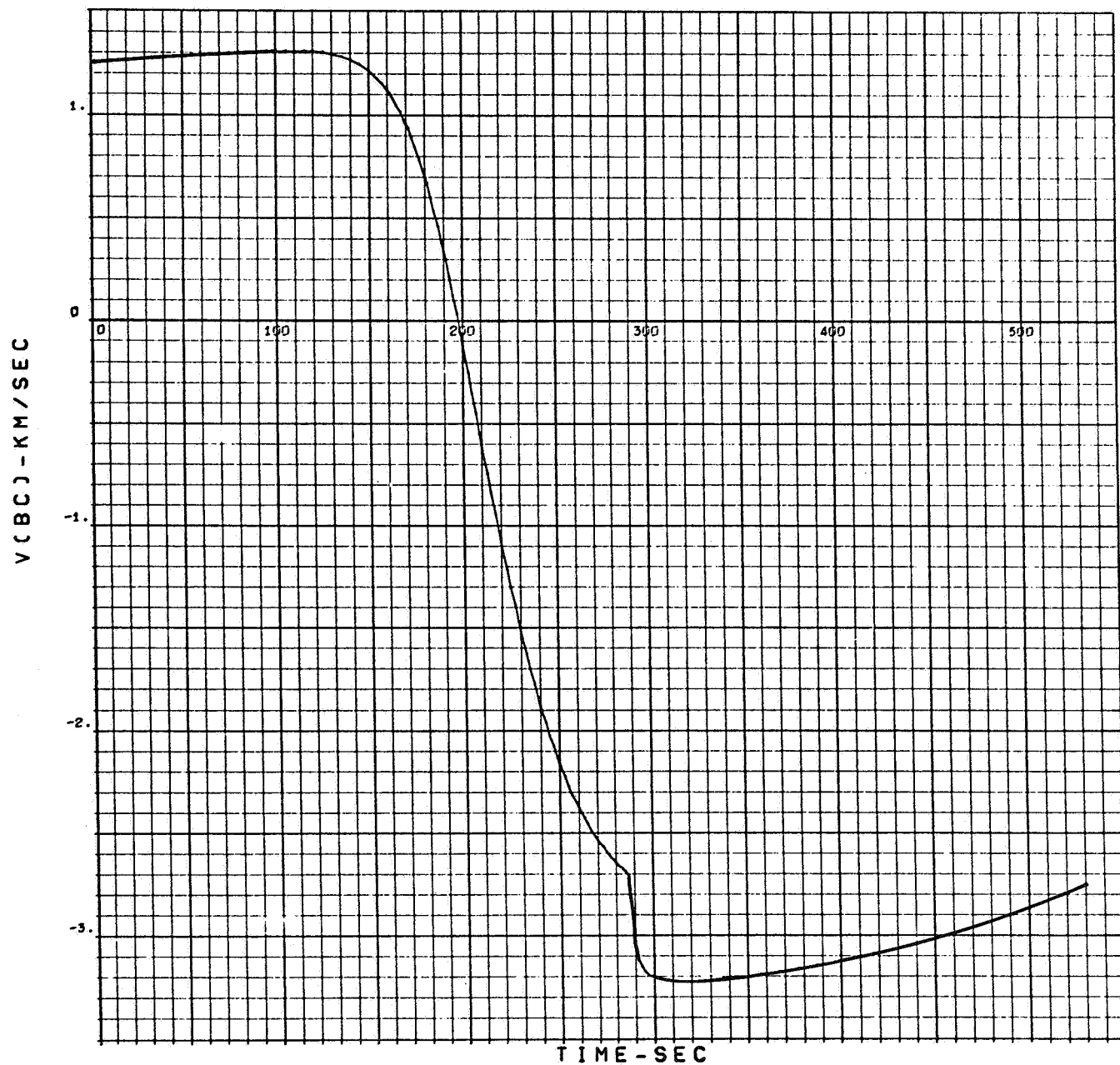
ENTRY VELOCITY   - 15,300 FT/SEC.
ENTRY PATH ANGLE   - 16 DEG.
ENTRY ALTITUDE   - 244 KM
DRAG, SEE FIGURE 3.1-20
VM-7

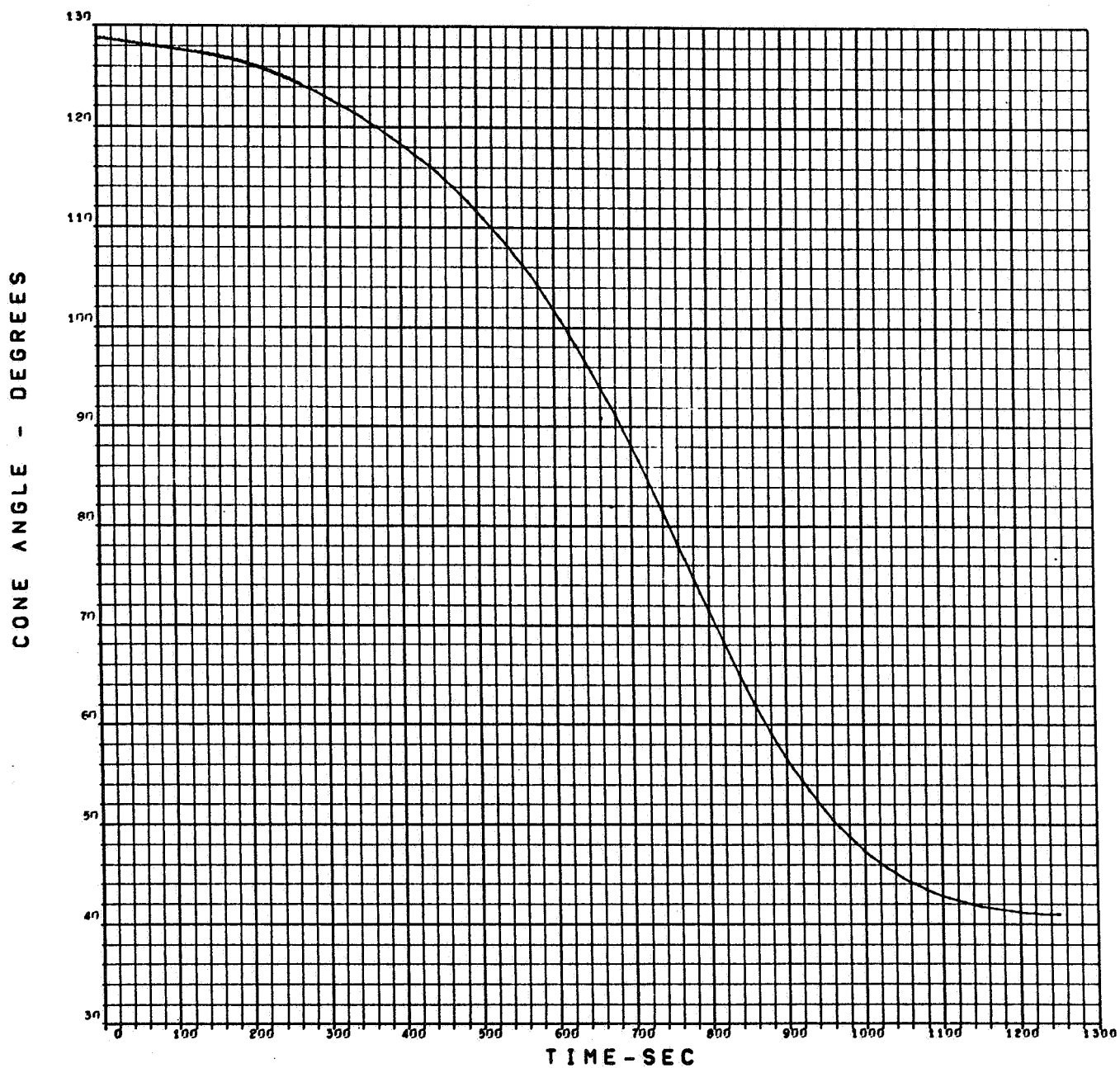Figure A-18. Range Rate vs Time, VM-7, Out-of-Orbit Entry
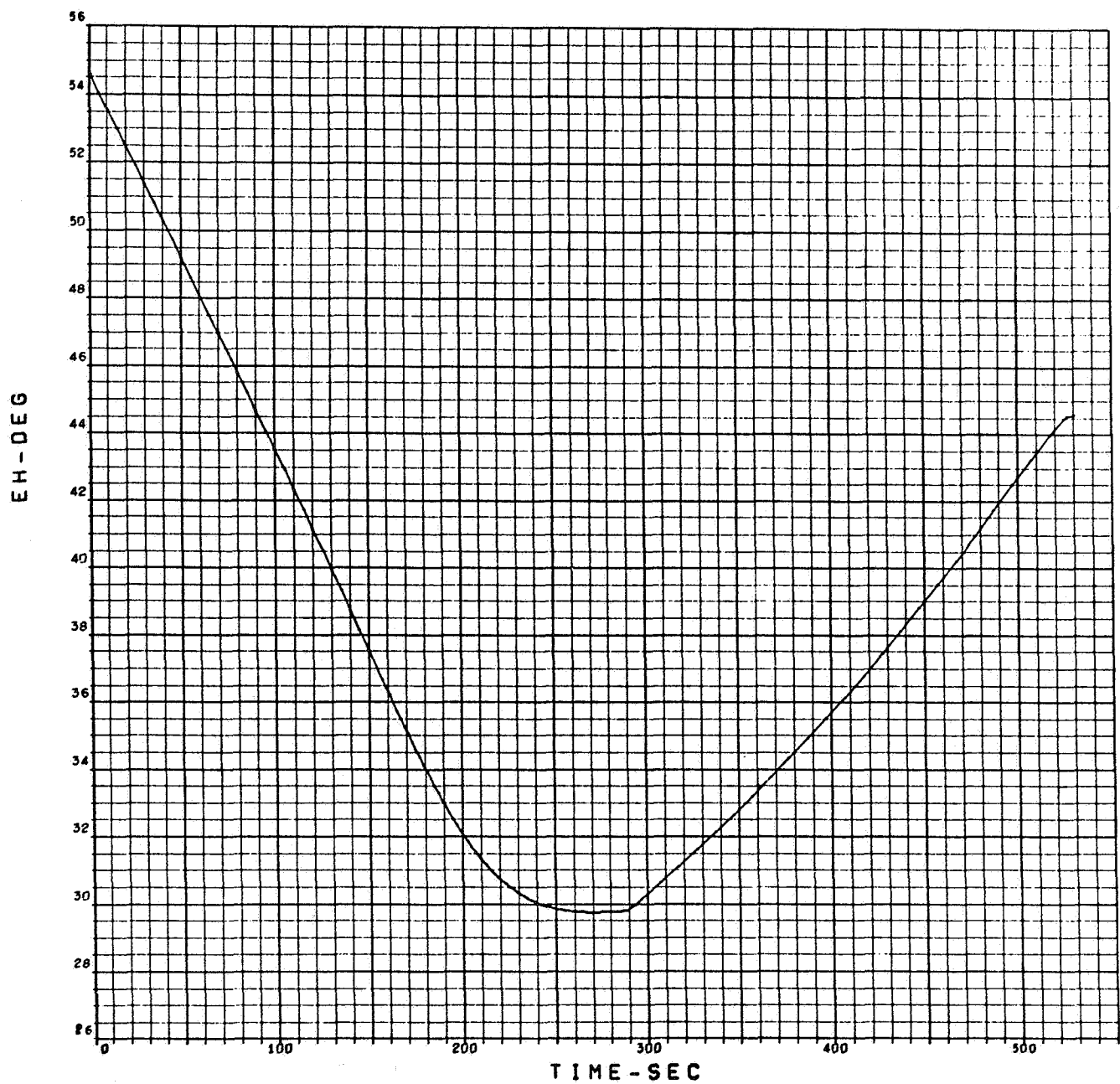
ENTRY VELOCITY - 15,300 FT/SEC.
ENTRY PATH ANGLE - 16 DEG.
ENTRY ALTITUDE - 244 KM
DRAG, SEE FIGURE 3.1-20
VM-7

Figure A-19. Angle at which Lander Sees Orbiter Above Horizon, VM-7,
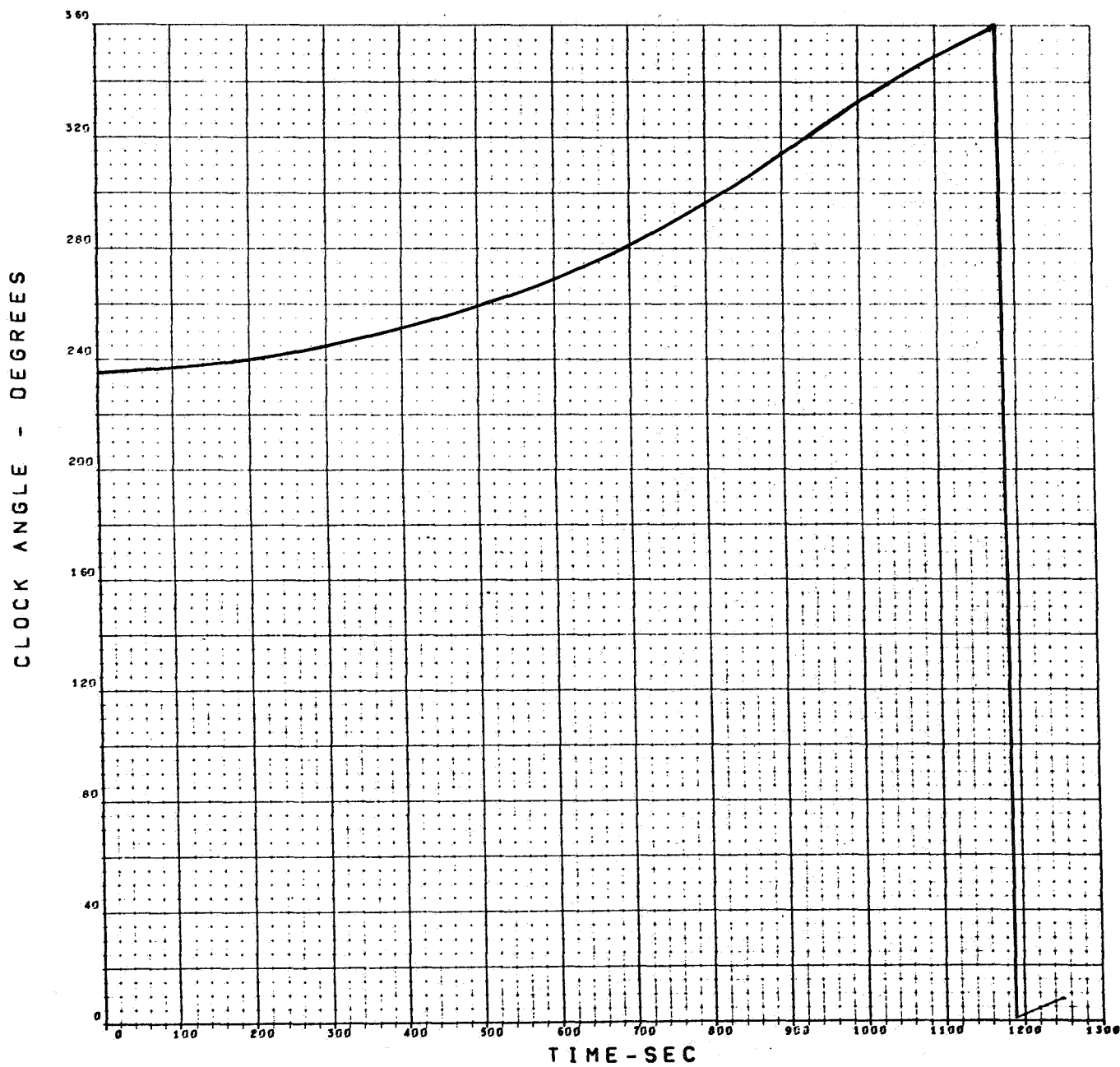Out-of-Orbit Entry

ENTRY VELOCITY   – 15,300 FT/SEC.
ENTRY PATH ANGLE   – 16 DEG.
ENTRY ALTITUDE   – 244 KM
DRAG, SEE FIGURE 3.1-20
VM-7
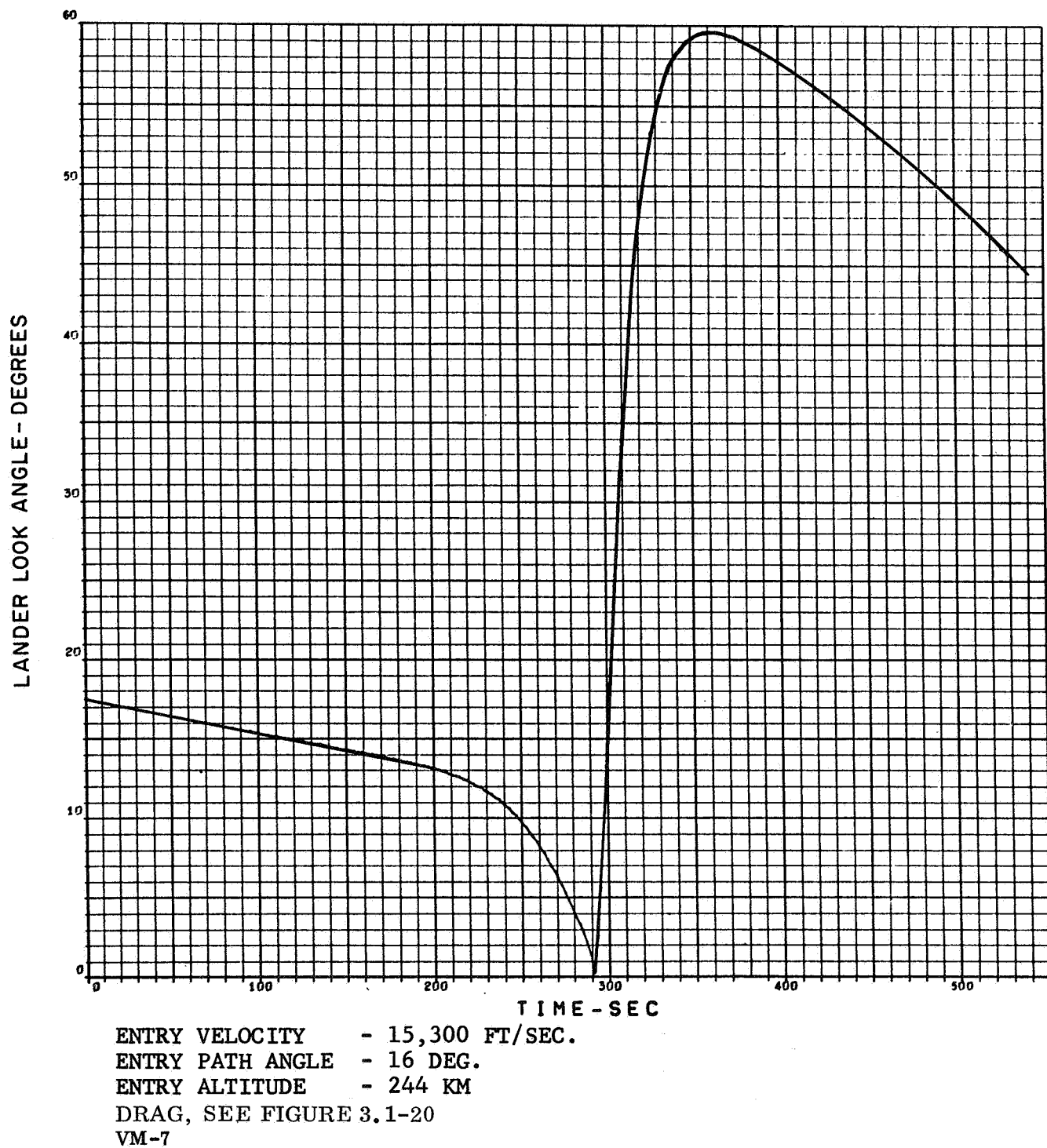
Figure A-20. Lander Look Angle vs Time, VM-7, Out-of-Orbit Entry
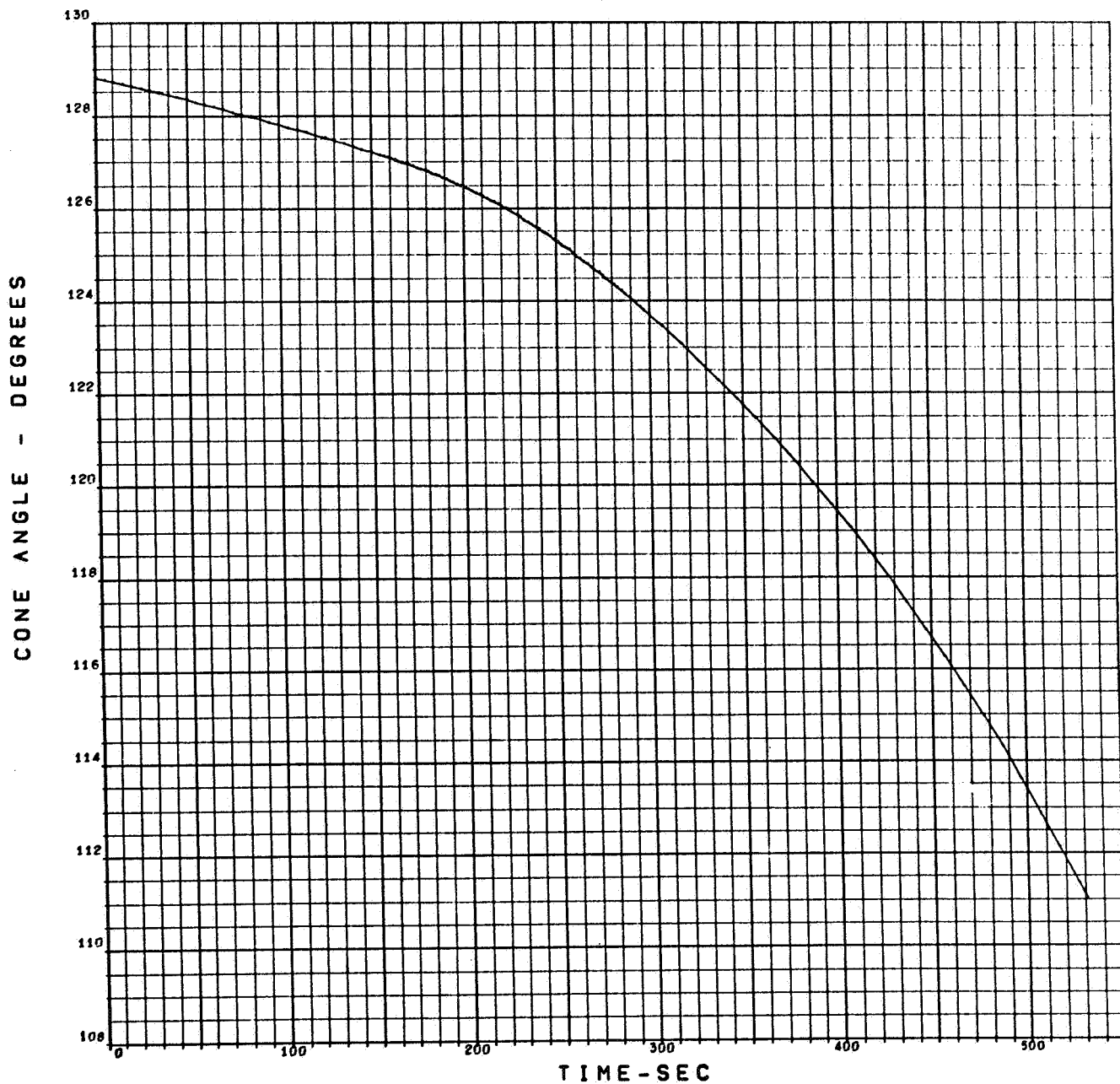
ENTRY VELOCITY   - 15,300 FT/SEC.
ENTRY PATH ANGLE - 16 DEG.
ENTRY ALTITUDE   - 244 KM
DRAG, SEE FIGURE 3.1-20
VM-7

Figure A-21. Cone Angle vs Time, VM-7, Out-of-Orbit Entry
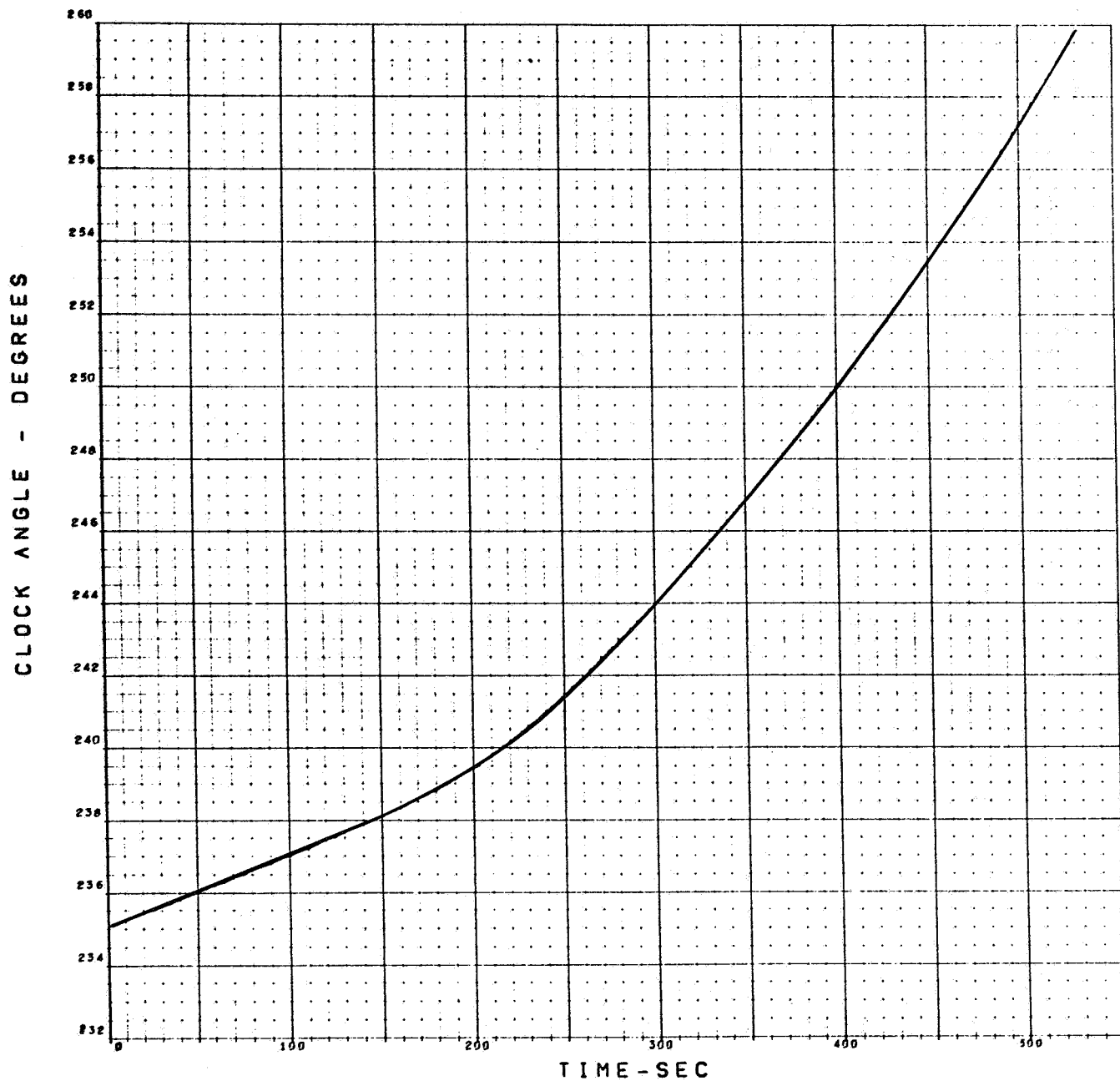
ENTRY VELOCITY   - 15,300 FT/SEC.
ENTRY PATH ANGLE - 16 DEG.
ENTRY ALTITUDE   - 244 KM
DRAG, SEE FIGURE 3.1-20
VM-7

Figure A-22.   Clock Angle vs Time, VM-7, Out-of-Orbit Entry
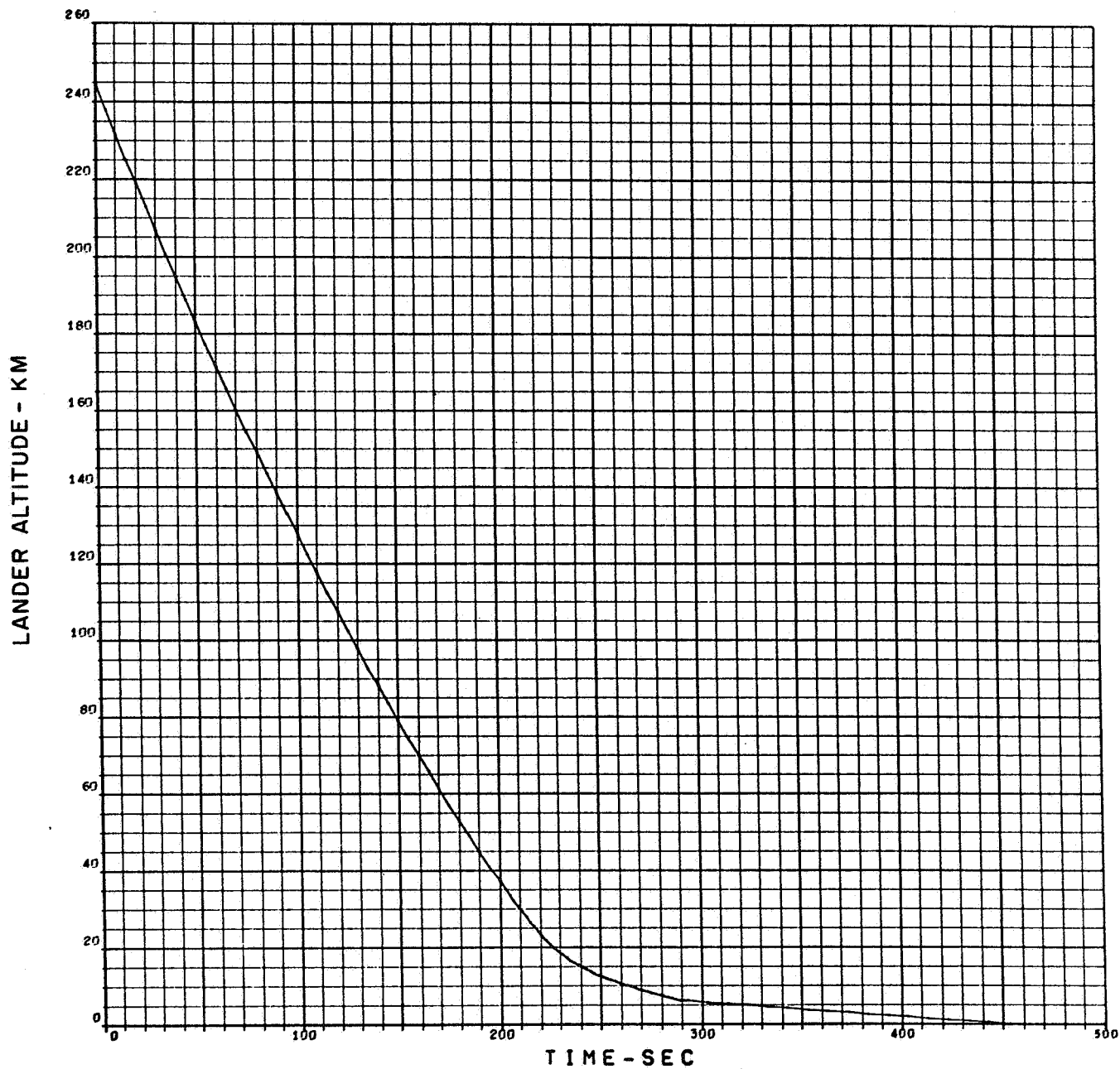
ENTRY VELOCITY   - 15,300 FT/SEC.
ENTRY PATH ANGLE - 16 DEG.
ENTRY ALTITUDE   - 244 KM
DRAG, SEE FIGURE 3.1-20
VM-8

Figure A-23. Lander Altitude vs Time, VM-8, Out-of-Orbit Entry
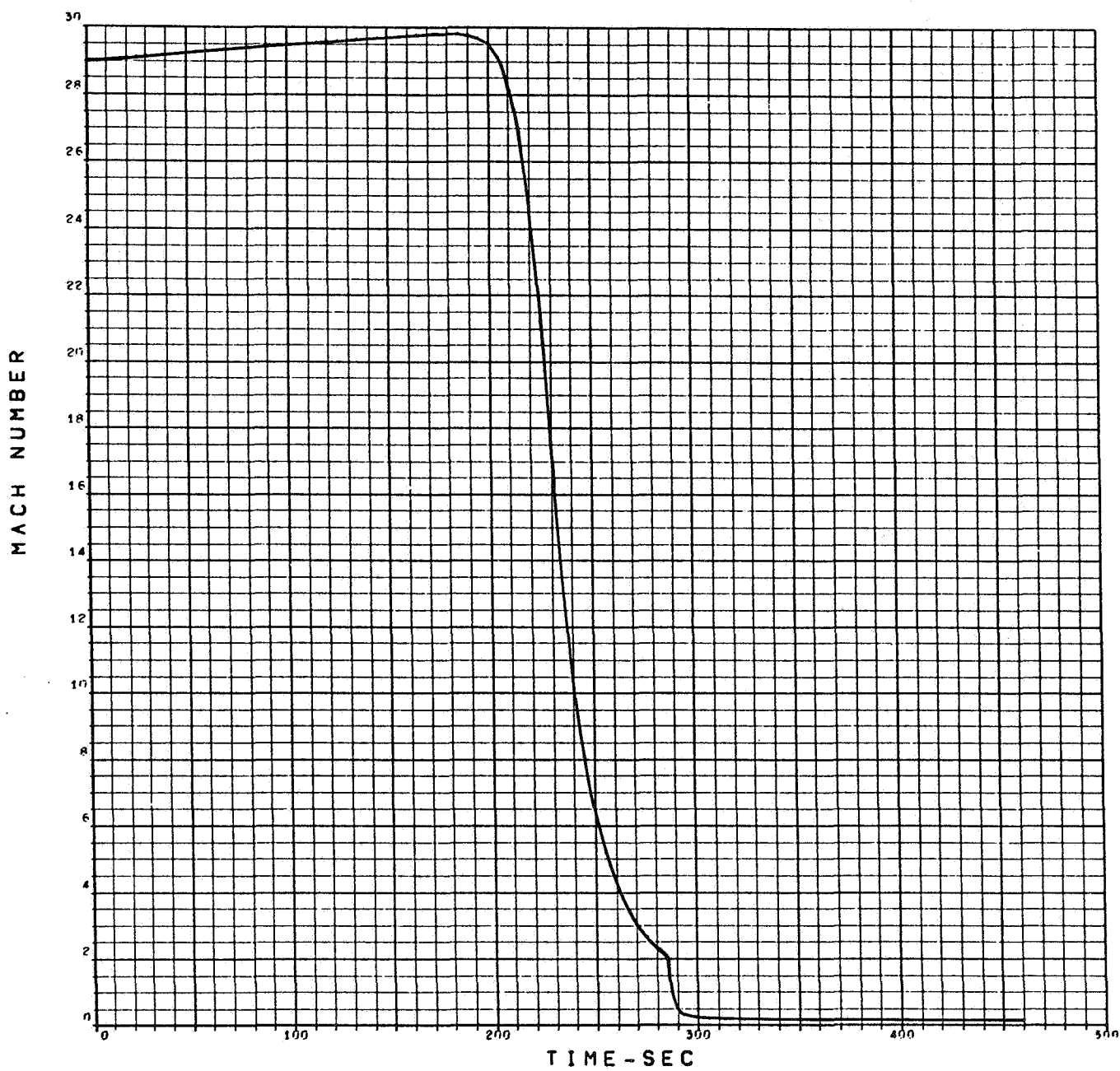
ENTRY VELOCITY   - 15,300 FT/SEC.
ENTRY PATH ANGLE   - 16 DEG.
ENTRY ALTITUDE   - 244 KM
DRAG, SEE FIGURE 3.1-20
VM-8

Figure A-24. Mach Number vs Time, VM-8, Out-of-Orbit Entry
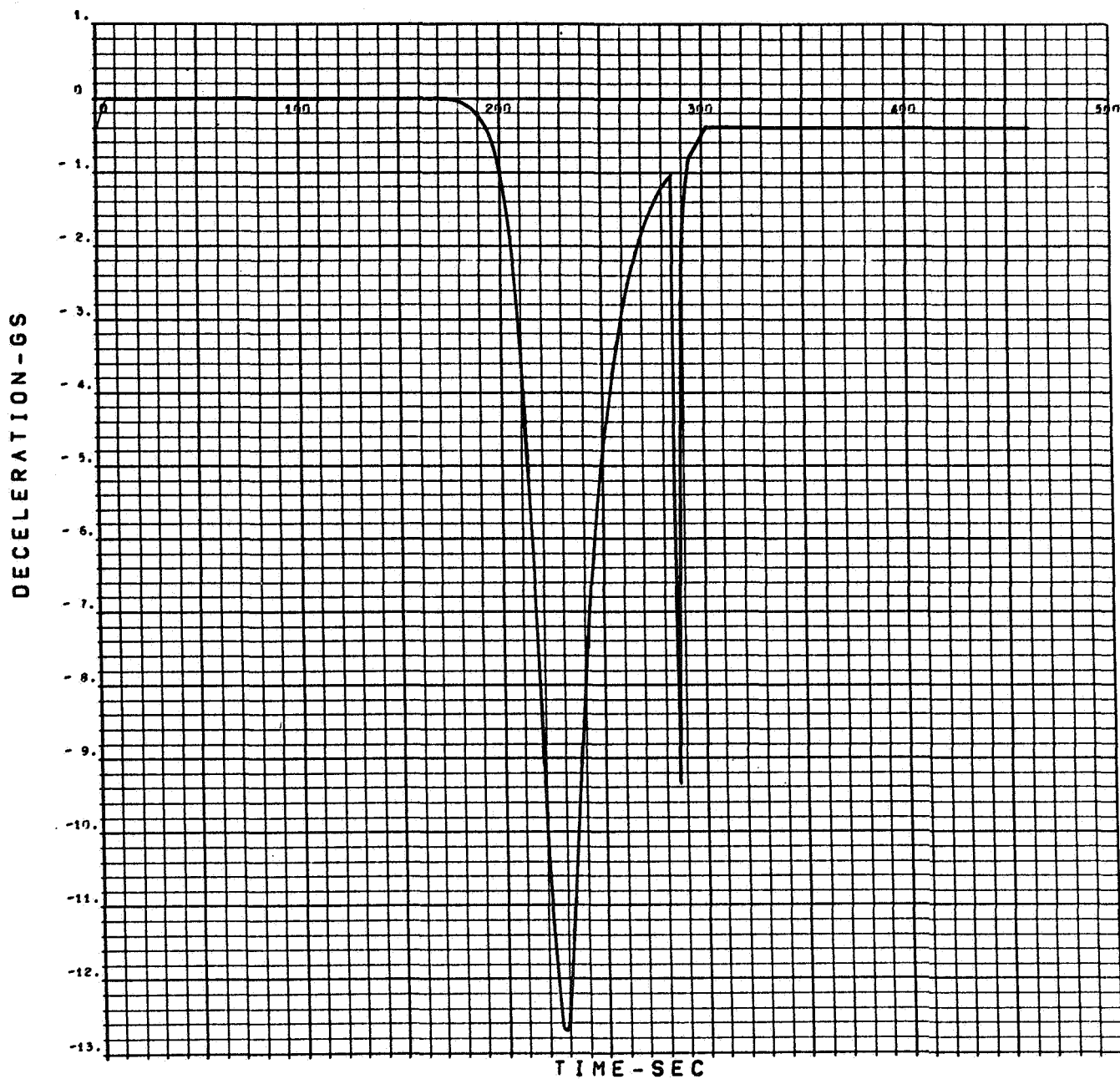
ENTRY VELOCITY   - 15,300 FT/SEC.
ENTRY PATH ANGLE - 16 DEG.
ENTRY ALTITUDE   - 244 KM
DRAG, SEE FIGURE 3.1-20
VM-8

Figure A-25. Lander Deceleration vs Time, VM-8, Out-of-Orbit Entry
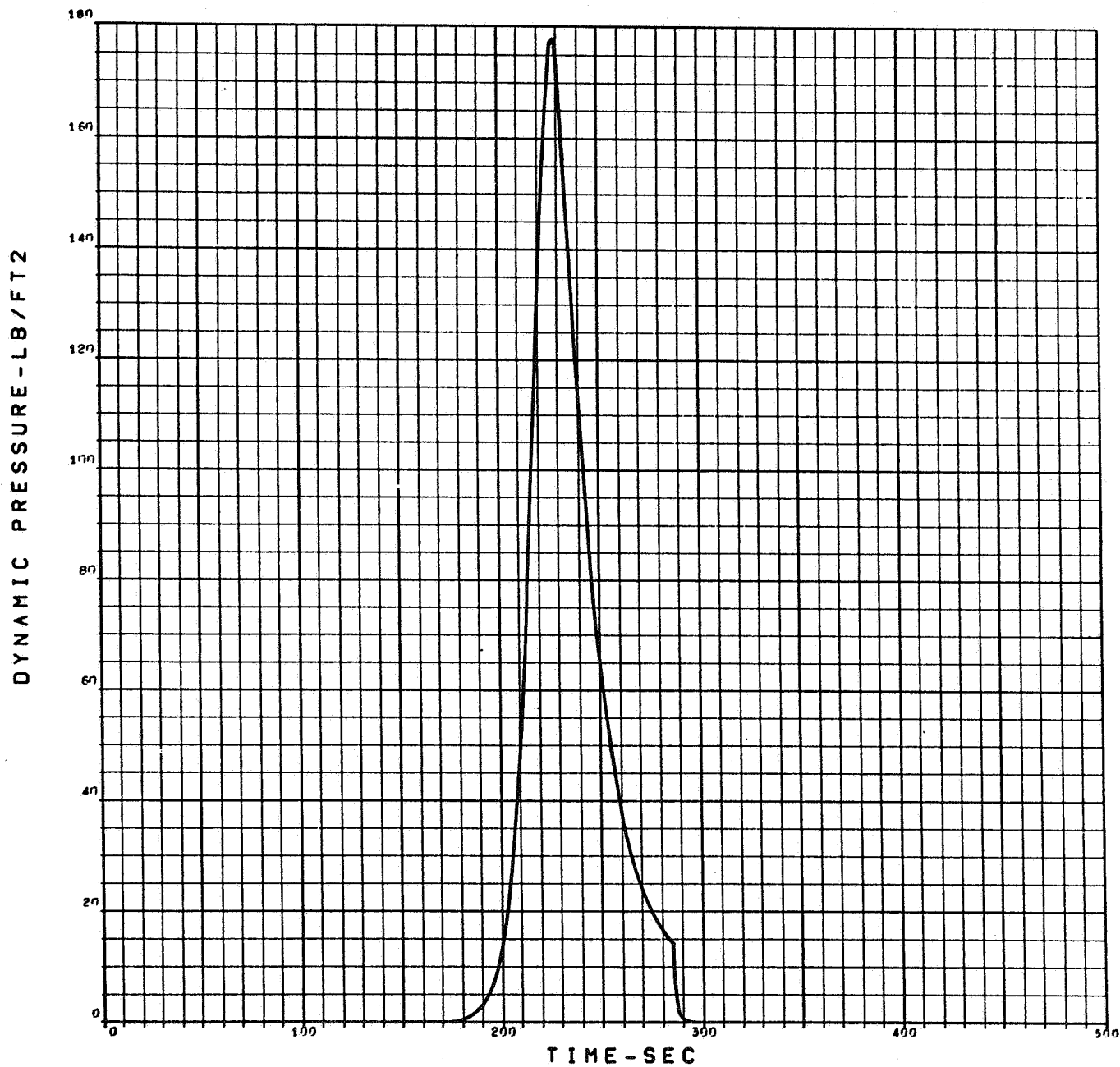
ENTRY VELOCITY   - 15,300 FT/SEC.
ENTRY PATH ANGLE   - 16 DEG.
ENTRY ALTITUDE   - 244 KM
DRAG, SEE FIGURE 3.1-20
VM-8

Figure A-26. Dynamic Pressure vs Time, VM-8, Out-of-Orbit Entry

ENTRY VELOCITY   - 15,300 FT/SEC.
ENTRY PATH ANGLE   - 16 DEG.
ENTRY ALTITUDE   - 244 KM
DRAG, SEE FIGURE 3.1-20
VM-8
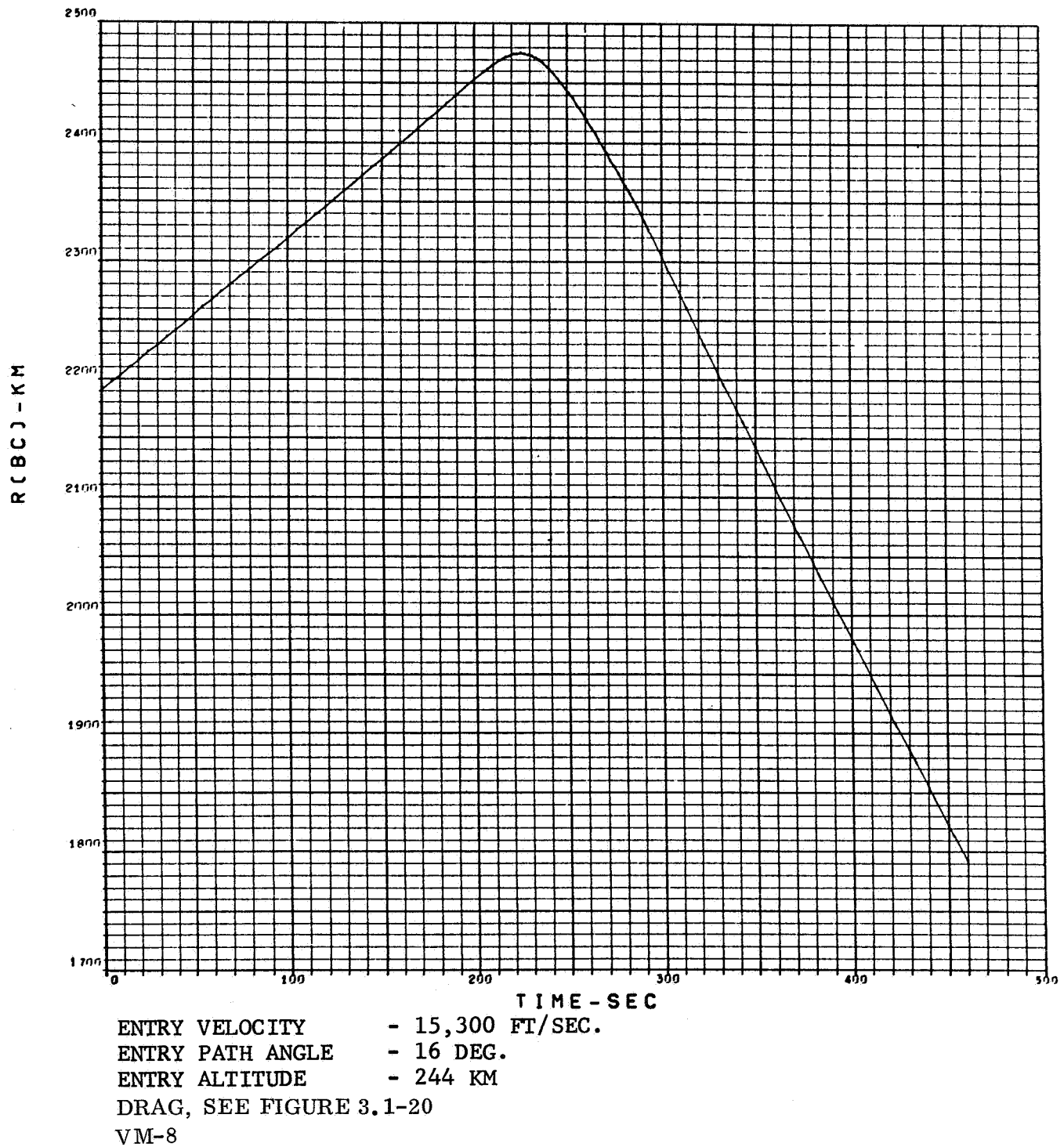
Figure A-27. Communication Distance R(BC) vs Time, VM-8, Out-of-Orbit Entry
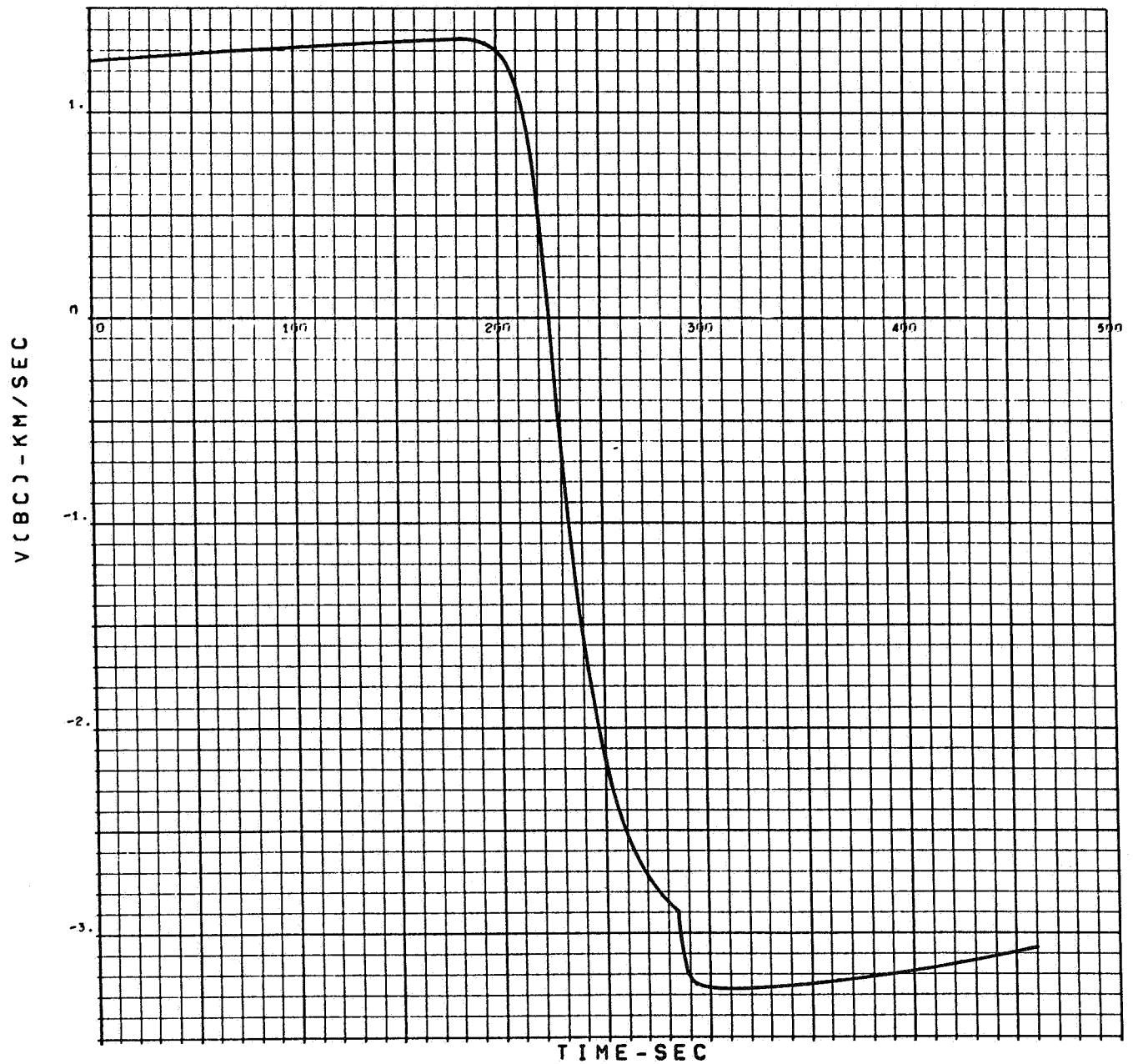
ENTRY VELOCITY   - 15,300 FT/SEC.
ENTRY PATH ANGLE   - 16 DEG.
ENTRY ALTITUDE   - 244 KM
DRAG, SEE FIGURE 3.1-20
VM-8

Figure A-28. Range Rate vs Time, VM-8, Out-of-Orbit Entry
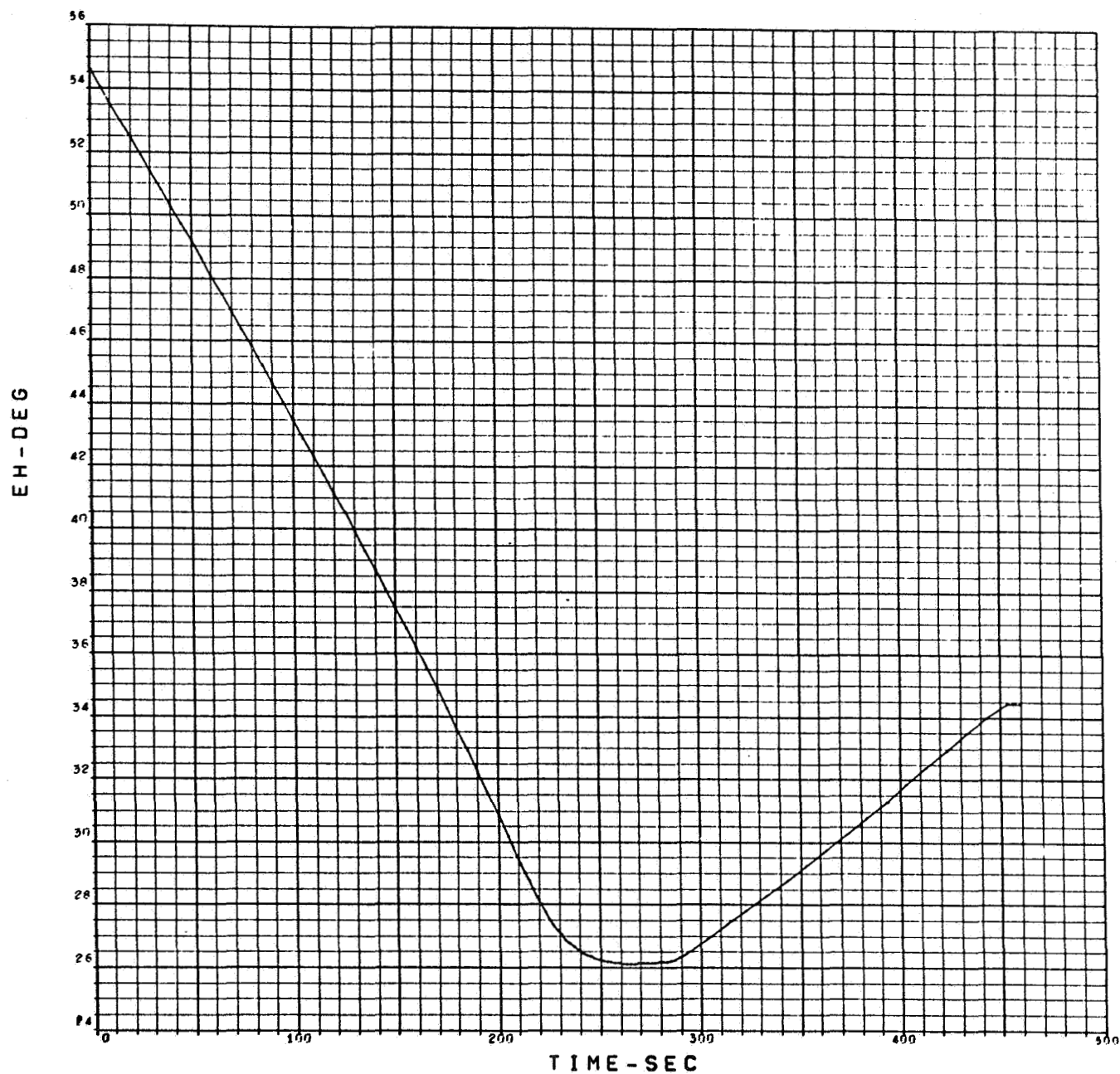
ENTRY VELOCITY   - 15,300 FT/SEC.
ENTRY PATH ANGLE   - 16 DEG.
ENTRY ALTITUDE   - 244 KM
DRAG, SEE FIGURE 3.1-20
VM-8

Figure A-29. Angle at which Lander Sees Orbiter Above Horizon, VM-8,
Out-of-Orbit Entry
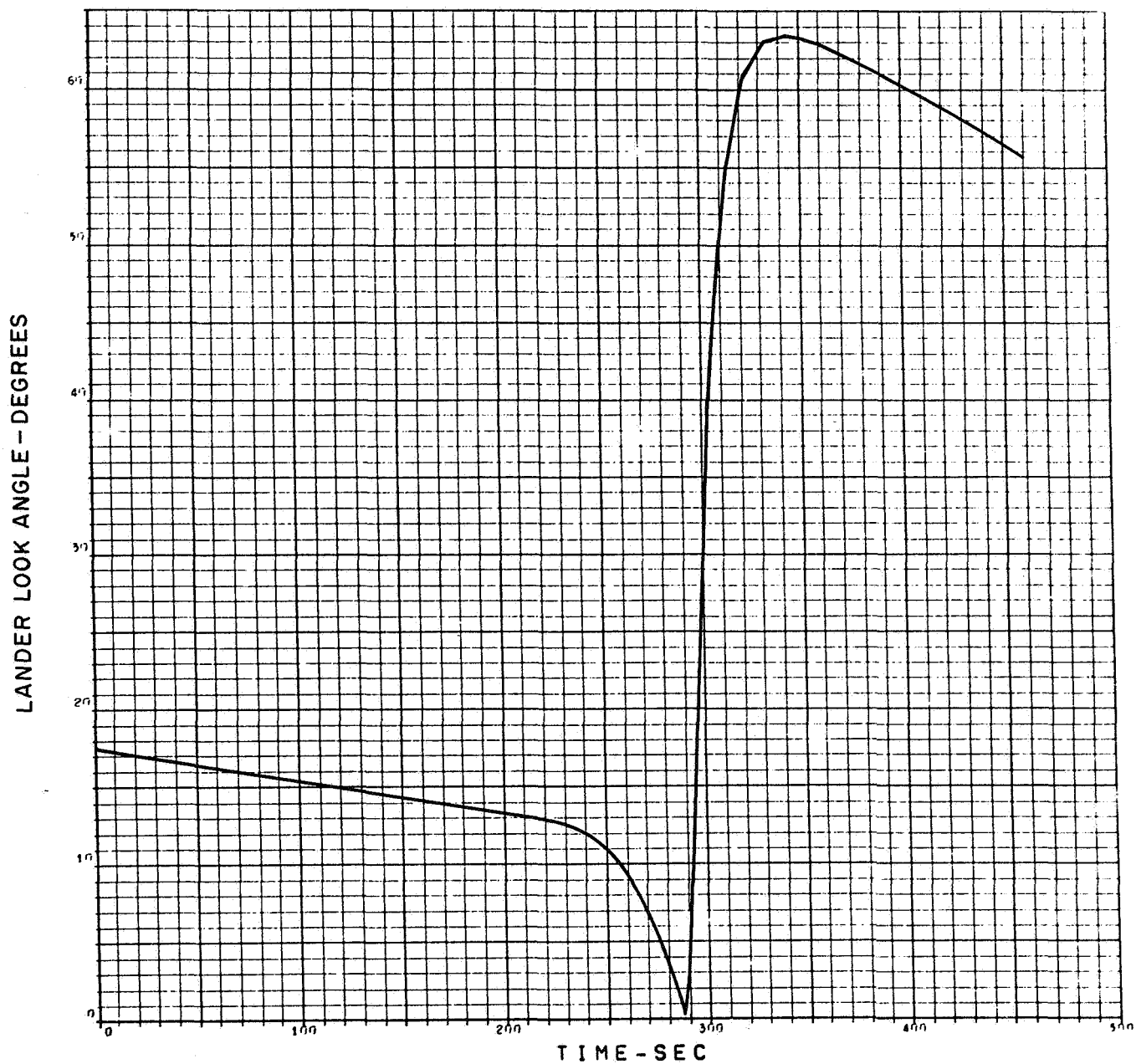
Y-axis: LANDER LOOK ANGLE – DEGREES

X-axis: TIME - SEC

ENTRY VELOCITY   - 15,300 FT/SEC.
ENTRY PATH ANGLE   - 16 DEG.
ENTRY ALTITUDE   - 244 KM
DRAG. SEE FIGURE 3.1-20
VM-8

Figure A-30. Lander Look Angle vs Time, VM-8, Out-of-Orbit Entry
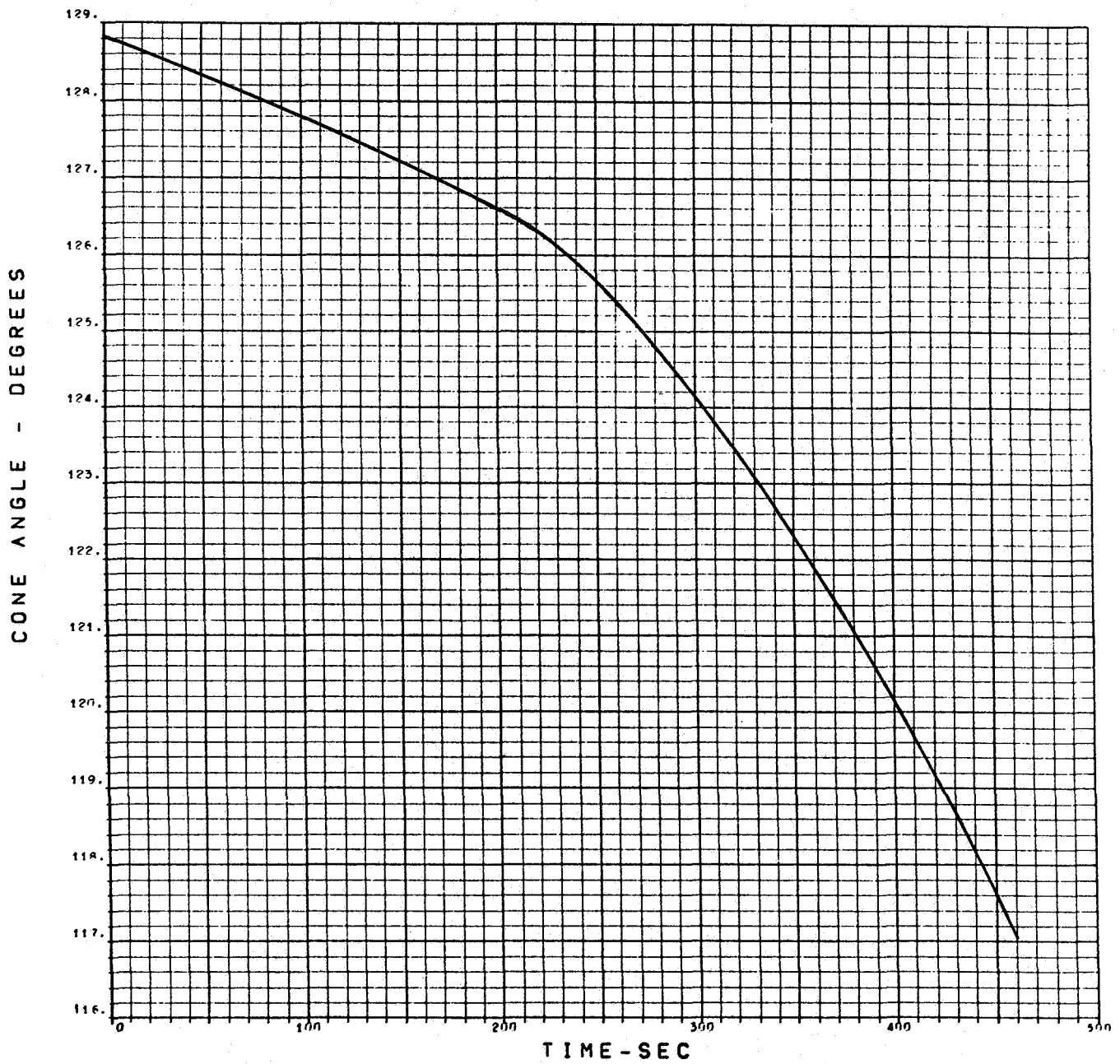
II

ENTRY VELOCITY   - 15,300 FT/SEC.
ENTRY PATH ANGLE   - 16 DEG.
ENTRY ALTITUDE   - 244 KM
DRAG, SEE FIGURE 3.1-20
VM-8

Figure A-31. Cone Angle vs Time, VM-8, Out-of-Orbit Entry
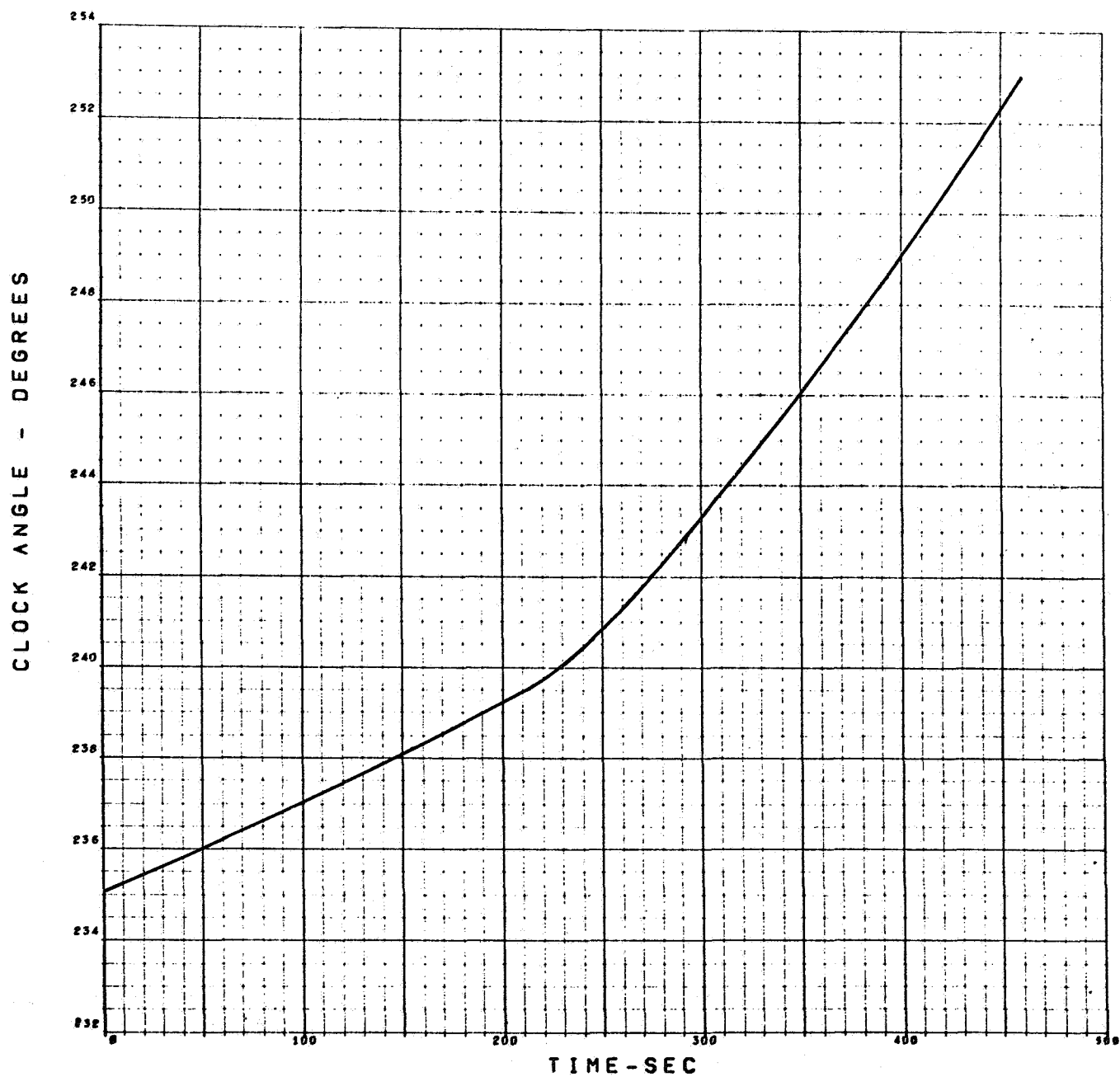
ENTRY VELOCITY   - 15,300 FT/SEC.
ENTRY PATH ANGLE   - 16 DEG.
ENTRY ALTITUDE   - 244 KM
DRAG, SEE FIGURE 3.1-20
VM-8

Figure A-32. Clock Angle vs Time, VM-9, Out-of-Orbit Entry
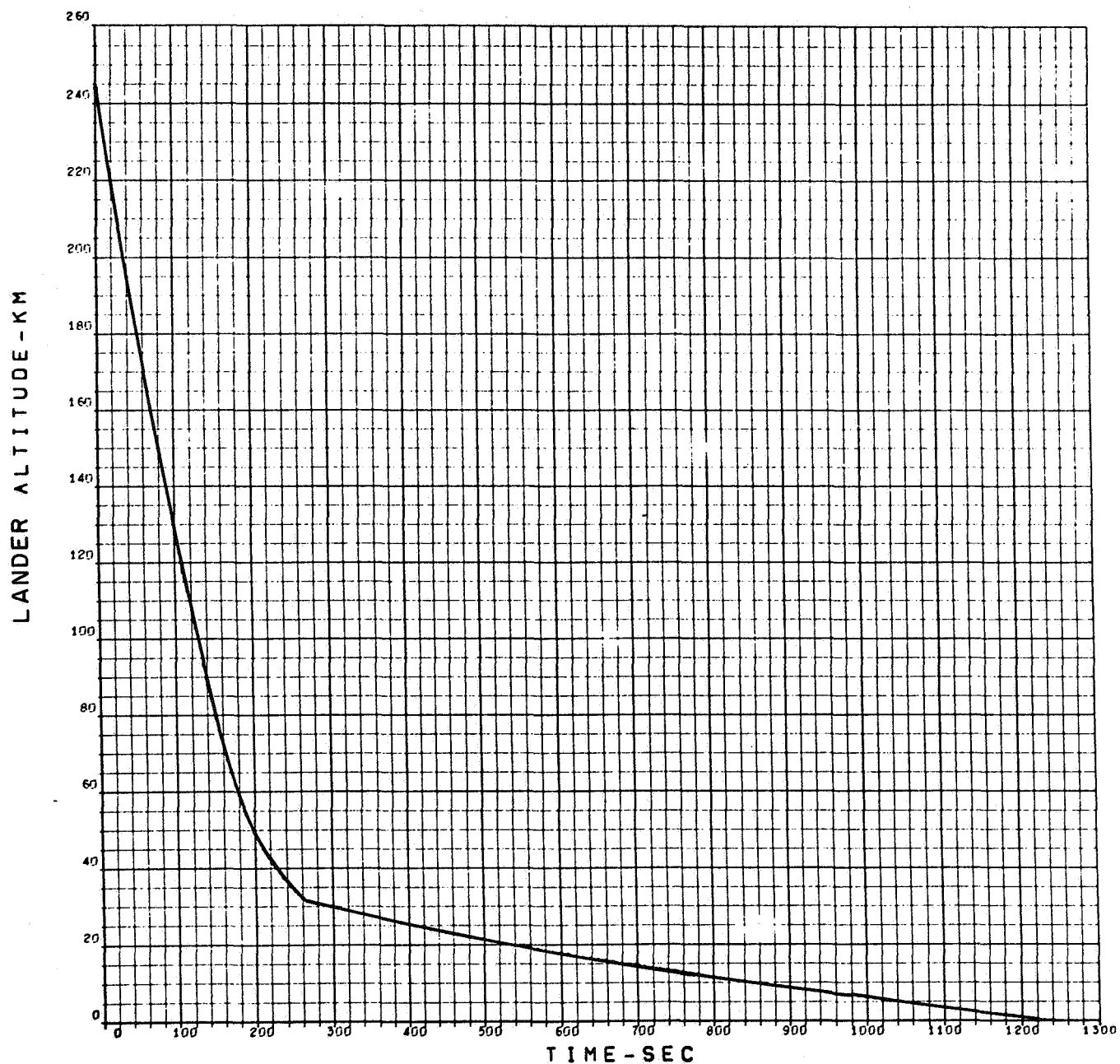
ENTRY VELOCITY   - 15,300 FT/SEC.
ENTRY PATH ANGLE   - 16 DEG.
ENTRY ALTITUDE   - 244 KM
DRAG, SEE FIGURE   3.1-20
VM-9

Figure A-33. Lander Altitude vs Time, VM-9, Out-of-Orbit Entry
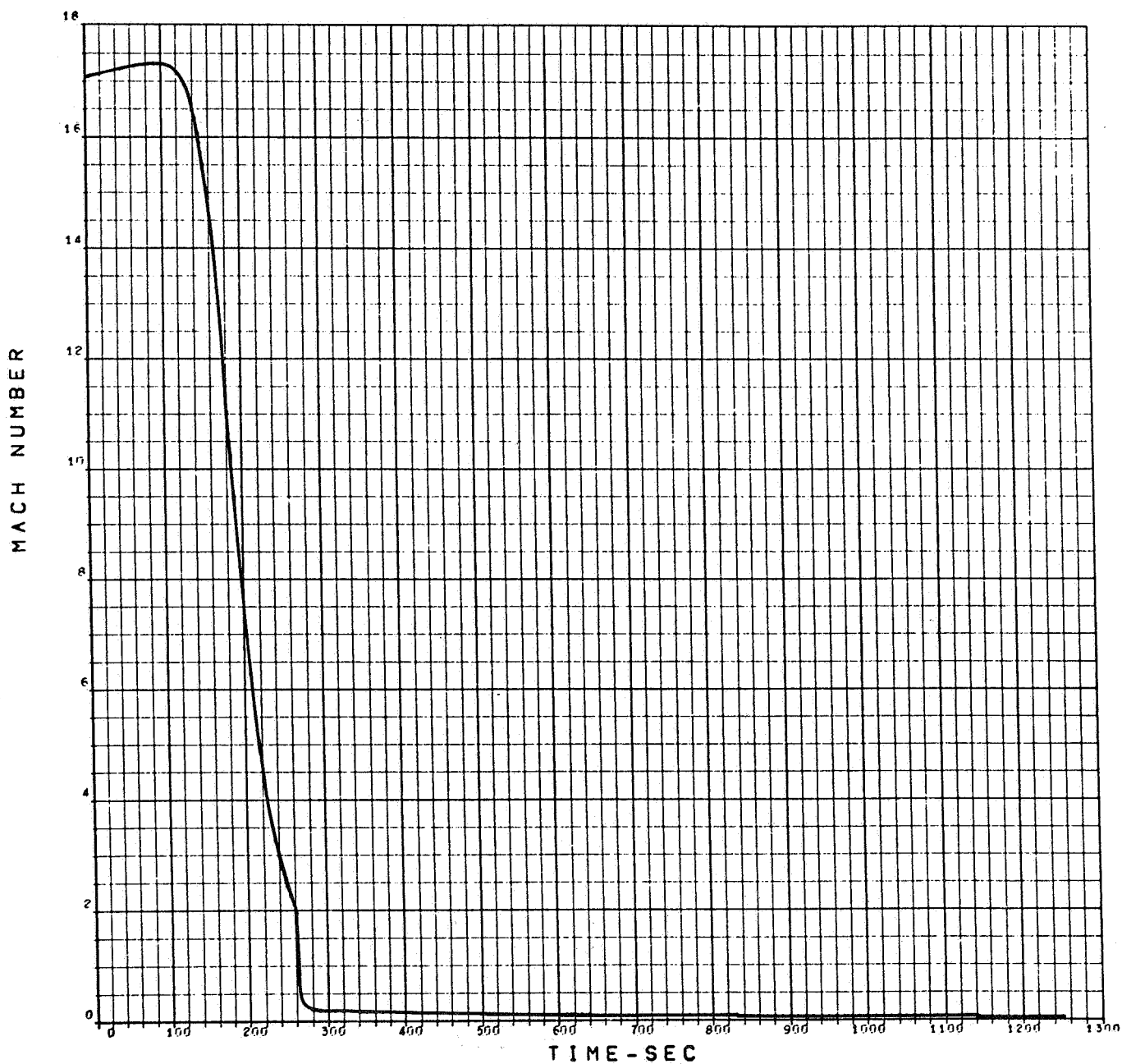
ENTRY VELOCITY   - 15,300 FT/SEC.
ENTRY PATH ANGLE   - 16 DEG.
ENTRY ALTITUDE   - 244 KM
DRAG, SEE FIGURE 3.1-20
VM-9

Figure A-34. Mach Number vs Time, VM-9, Out-of-Orbit Entry
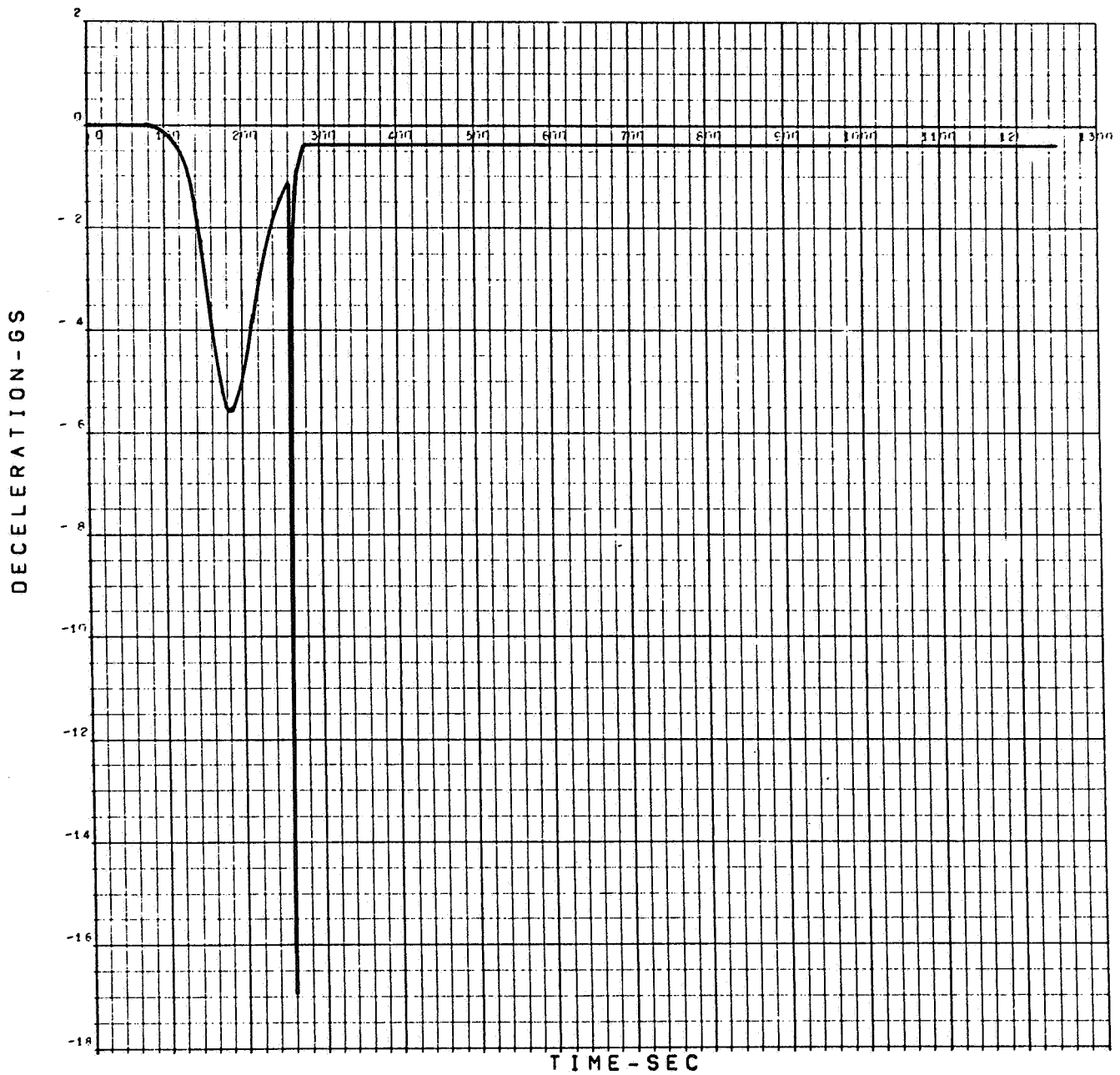
ENTRY VELOCITY   - 15,300 FT/SEC.
ENTRY PATH ANGLE   - 16 DEG.
ENTRY ALTITUDE   - 244 KM
DRAG, SEE FIGURE 3.1-20
VM-9

Figure A-35. Lander Deceleration vs Time, VM-9, Out-of-Orbit Entry

DYNAMIC PRESSURE - LB/FT2

TIME - SEC

ENTRY VELOCITY   - 15,300 FT/SEC.
ENTRY PATH ANGLE   - 16 DEG.
ENTRY ALTITUDE   - 244 KM
DRAG, SEE FIGURE 3.1-20
VM-9
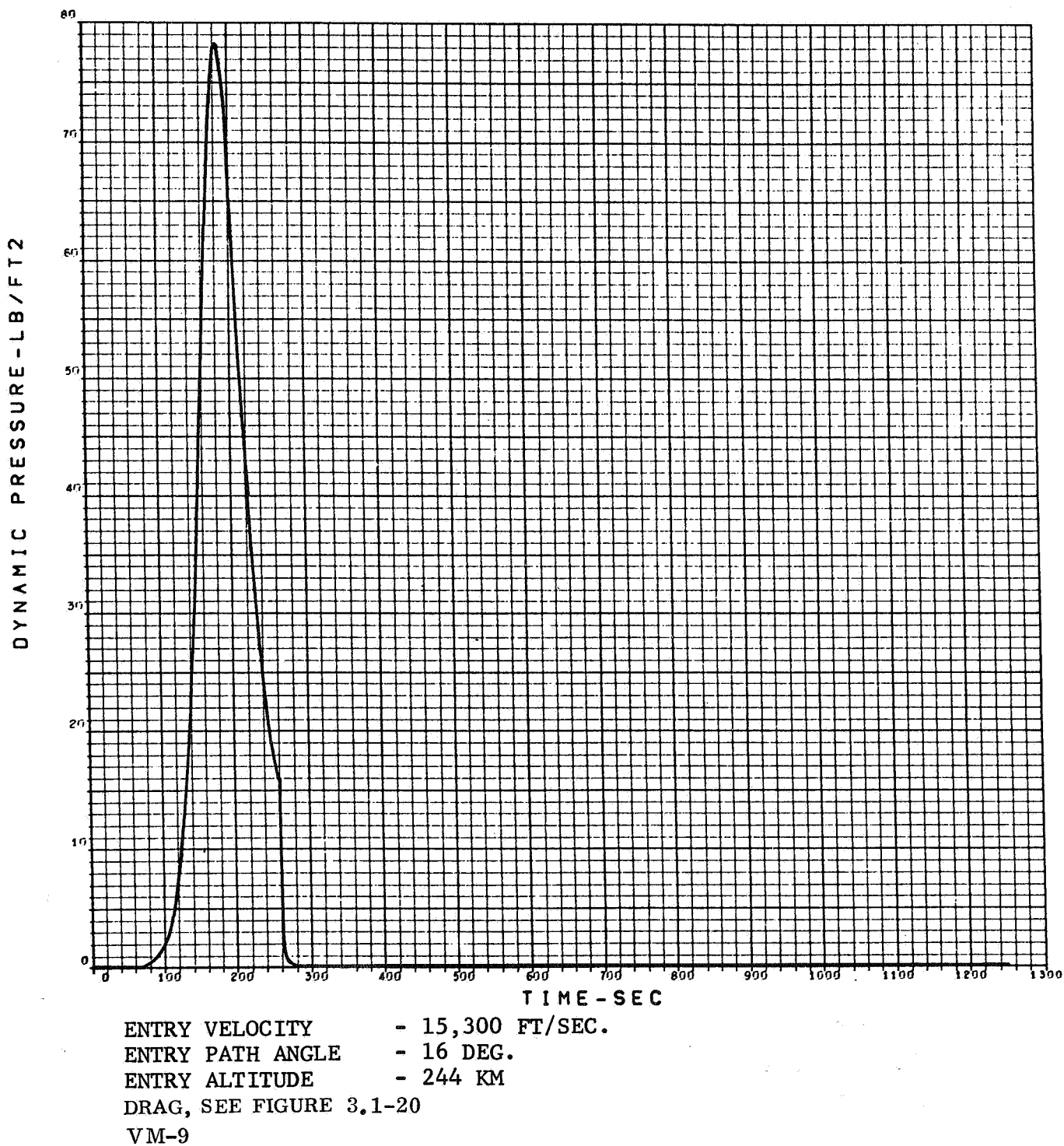
Figure A-36. Dynamic Pressure vs Time, VM-9, Out-of-Orbit Entry
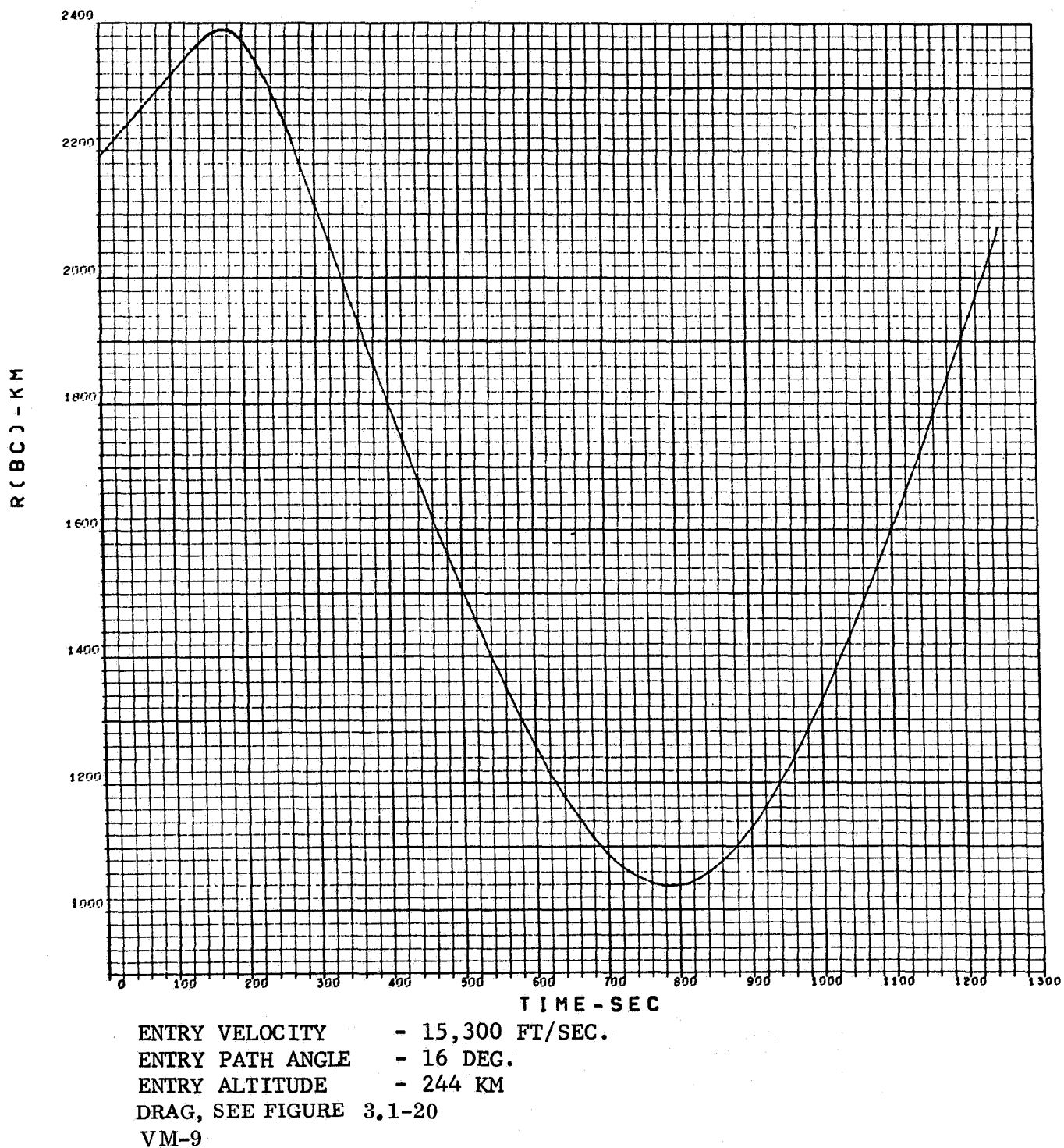
Figure A-37. Communication Distance R(BC) vs Time, VM-9, Out-of-Orbit Entry

The graph contains the following information:

Y-axis: R(BC) - KM, ranging from 1000 to 2400

X-axis: TIME-SEC, ranging from 0 to 1300

ENTRY VELOCITY   - 15,300 FT/SEC.
ENTRY PATH ANGLE   - 16 DEG.
ENTRY ALTITUDE   - 244 KM
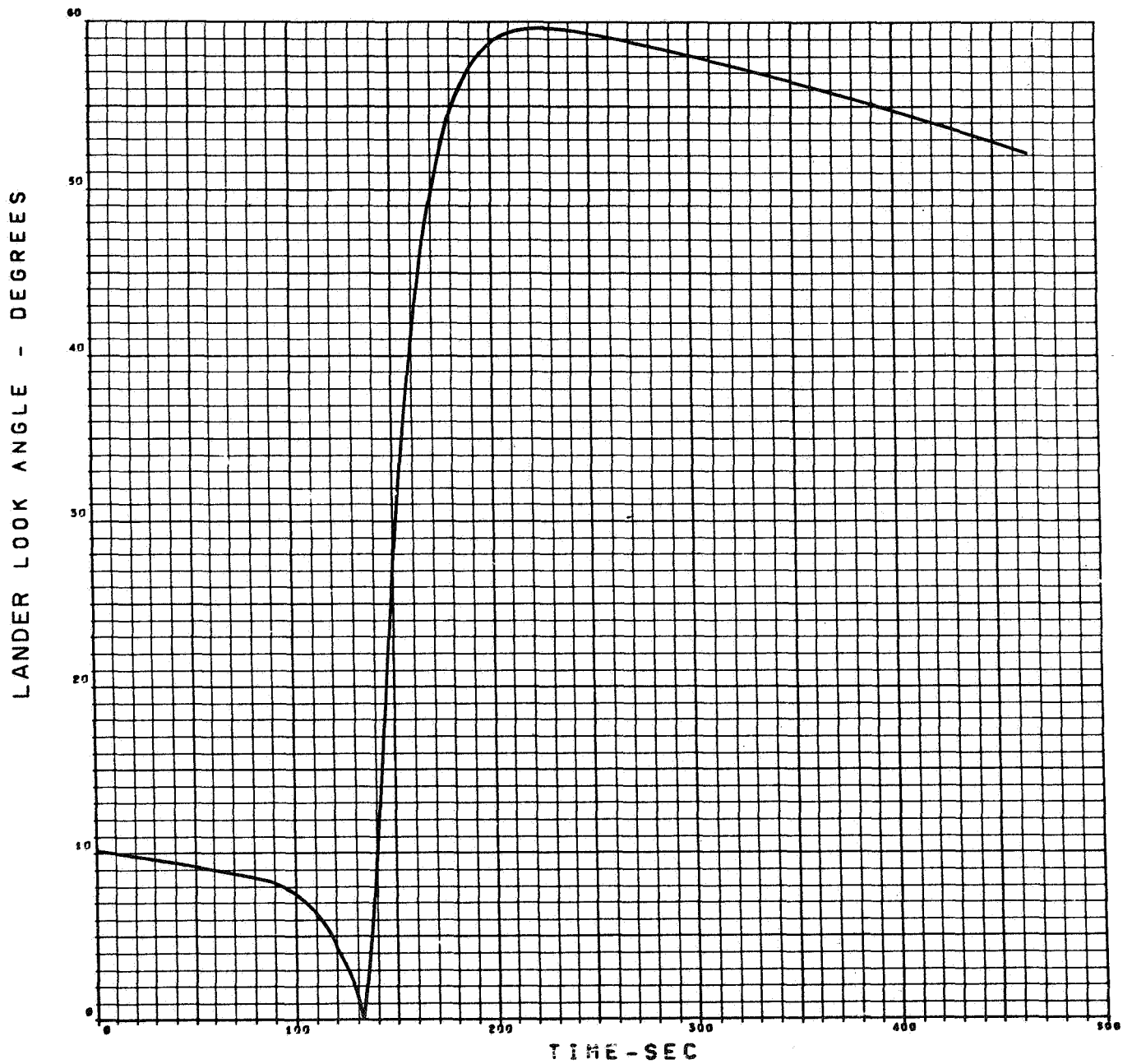DRAG, SEE FIGURE 3.1-20
VM-9

ENTRY VELOCITY   - 15,300 FT/SEC.
ENTRY PATH ANGLE   - 16 DEG.
ENTRY ALTITUDE   - 244 KM
DRAG, SEE FIGURE 3.1-20
VM-9

Figure A-38. Range Rate vs Time, VM-9, Out-of-Orbit Entry

ENTRY VELOCITY   - 15,300 FT/SEC.
ENTRY PATH ANGLE - 16 DEG.
ENTRY ALTITUDE   - 244 KM
DRAG, SEE FIGURE 3.1-20
VM-9

Figure A-39. Angle at which Lander Sees Orbiter Above Horizon, VM-9,
Out-of-Orbit Entry

ENTRY VELOCITY   - 15,300 FT/SEC.
ENTRY PATH ANGLE - 16 DEG.
ENTRY ALTITUDE   - 244 KM
DRAG, SEE FIGURE 3.1-20
VM-9

Figure A-40. Lander Look Angle vs Time, VM-9, Out-of-Orbit Entry

ENTRY VELOCITY   - 15,300 FT/SEC.
ENTRY PATH ANGLE - 16 DEG.
ENTRY ALTITUDE   - 244 KM
DRAG, SEE FIGURE 3.1-20
VM-9

Figure A-41. Cone Angle vs Time, VM-9, Out-of-Orbit Entry

ENTRY VELOCITY   - 15,300 FT/SEC.
ENTRY PATH ANGLE - 16 DEG.
ENTRY ALTITUDE   - 244 KM
DRAG, SEE FIGURE 3.1-20
VM-9

Figure A-42. Clock Angle vs Time, VM-9, Out-of-Orbit Entry

II

landing latitude = 10°
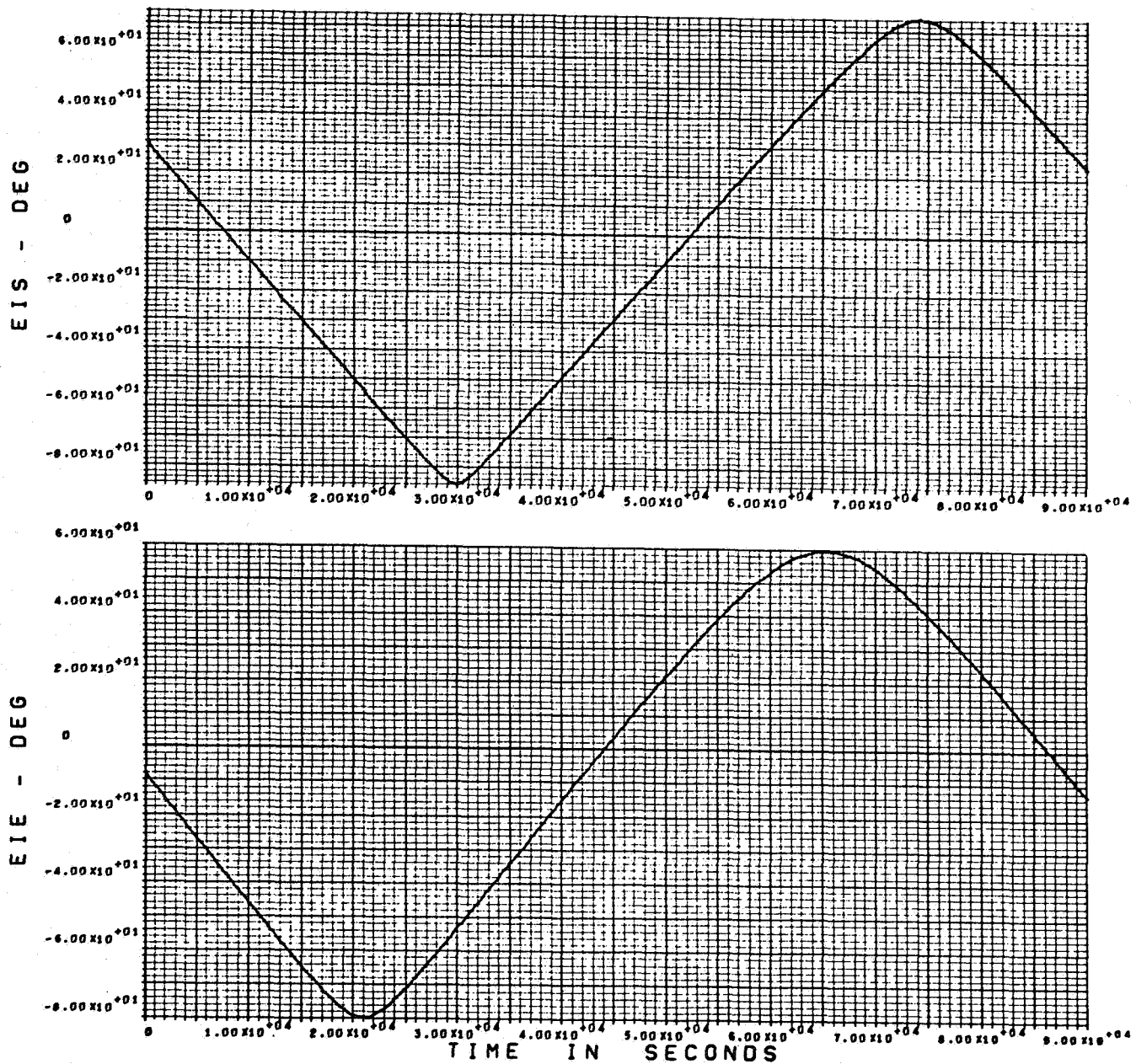
EIS = SUN ELEVATION ABOVE HORIZON
EIE = EARTH ELEVATION ABOVE HORIZON

Figure A-43. Earth and Sun Elevations at Landing Site During First Orbit After Landing, Direct Entry

landing latitude = 10°
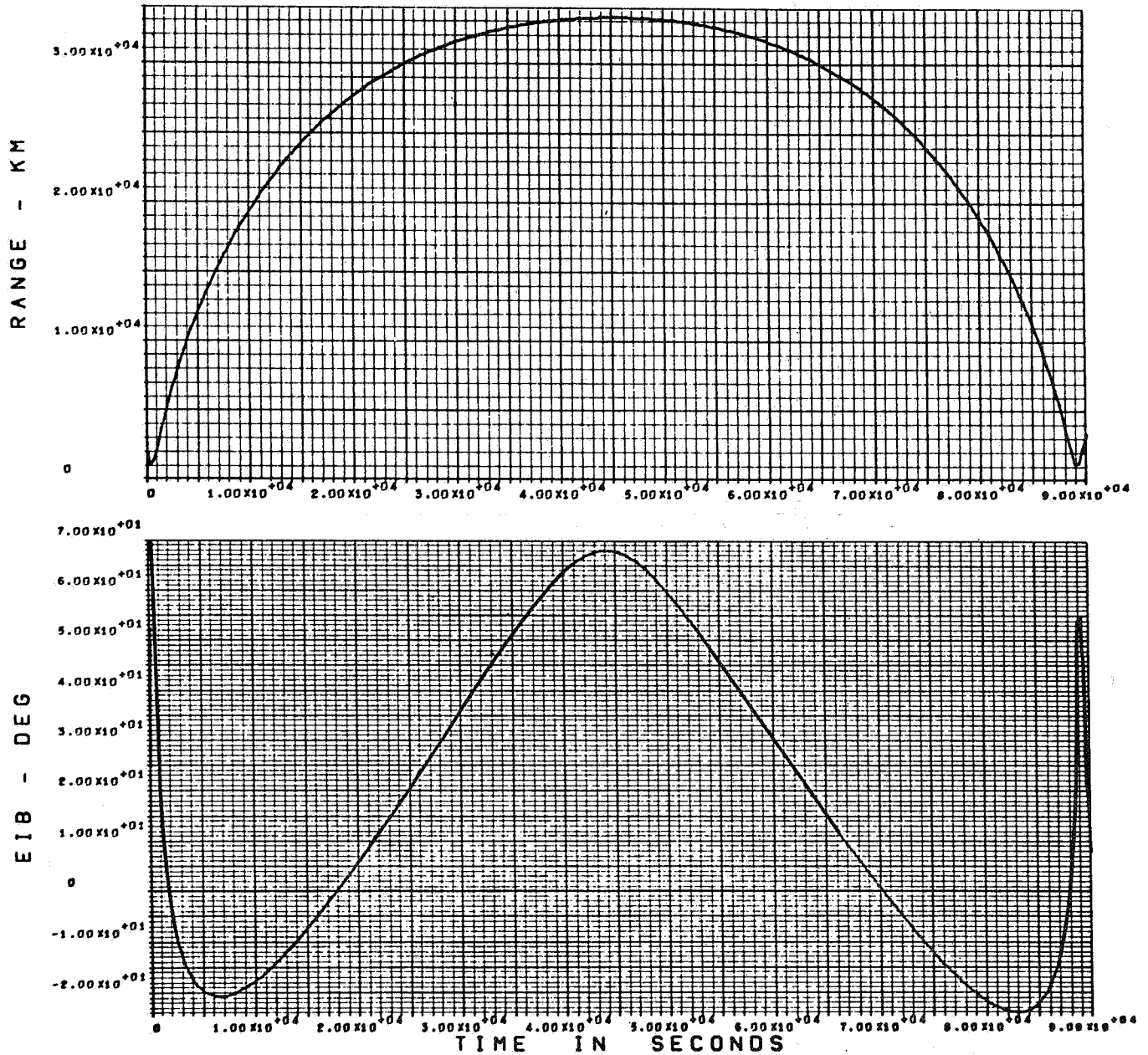
EIB = S/C ELEVATION ABOVE HORIZON

Figure A-44. Relay Communication Range and S/C Elevation at Landing Site During First Orbit After Landing, Direct Entry

landing latitude = 10°
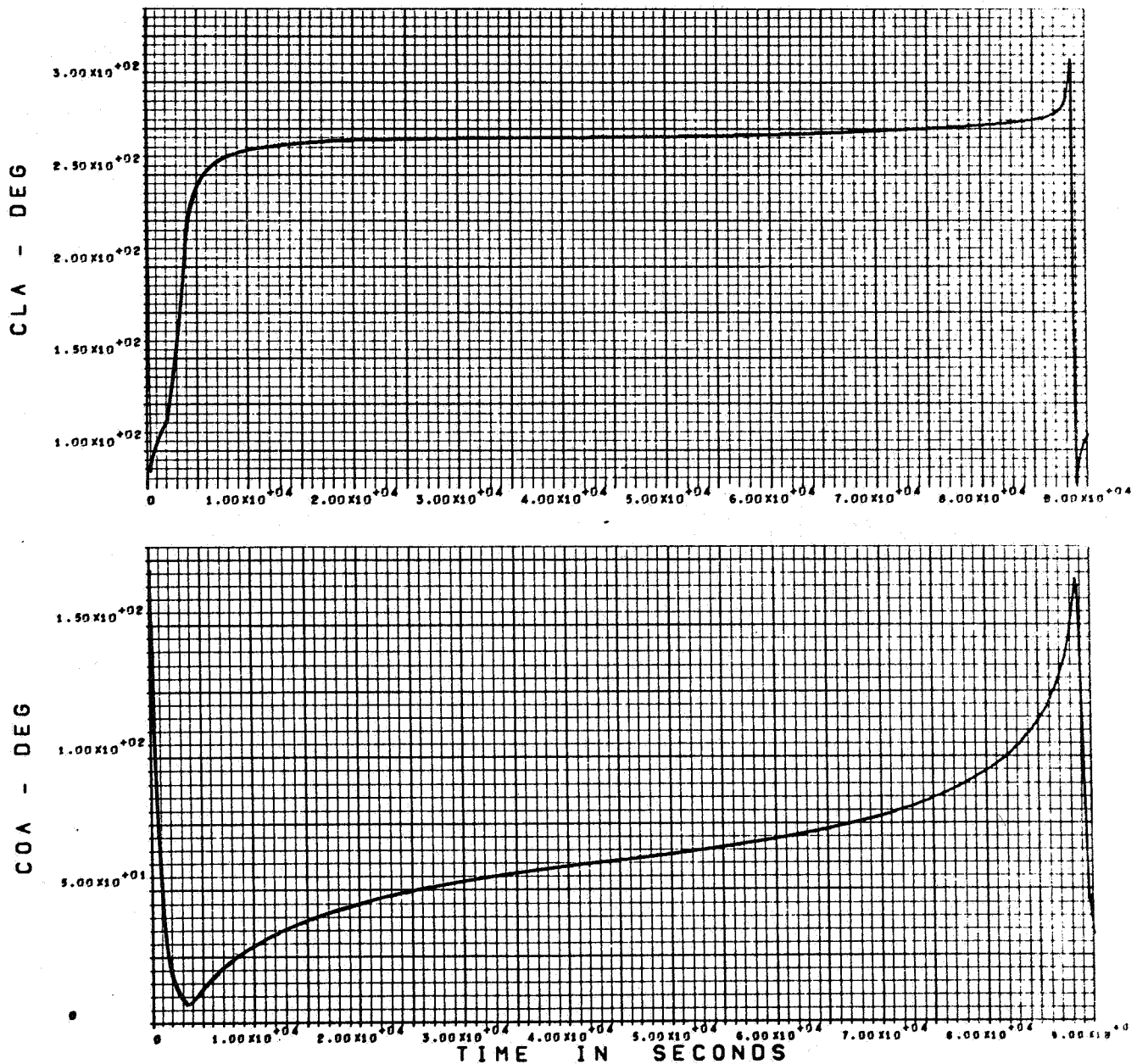
COA = CONE ANGLE
CLA = CLOCK ANGLE

Figure A-45. Lander Clock and Cone Angle at S/C During First Orbit After Landing,
Direct Entry

landing latitude = 10°
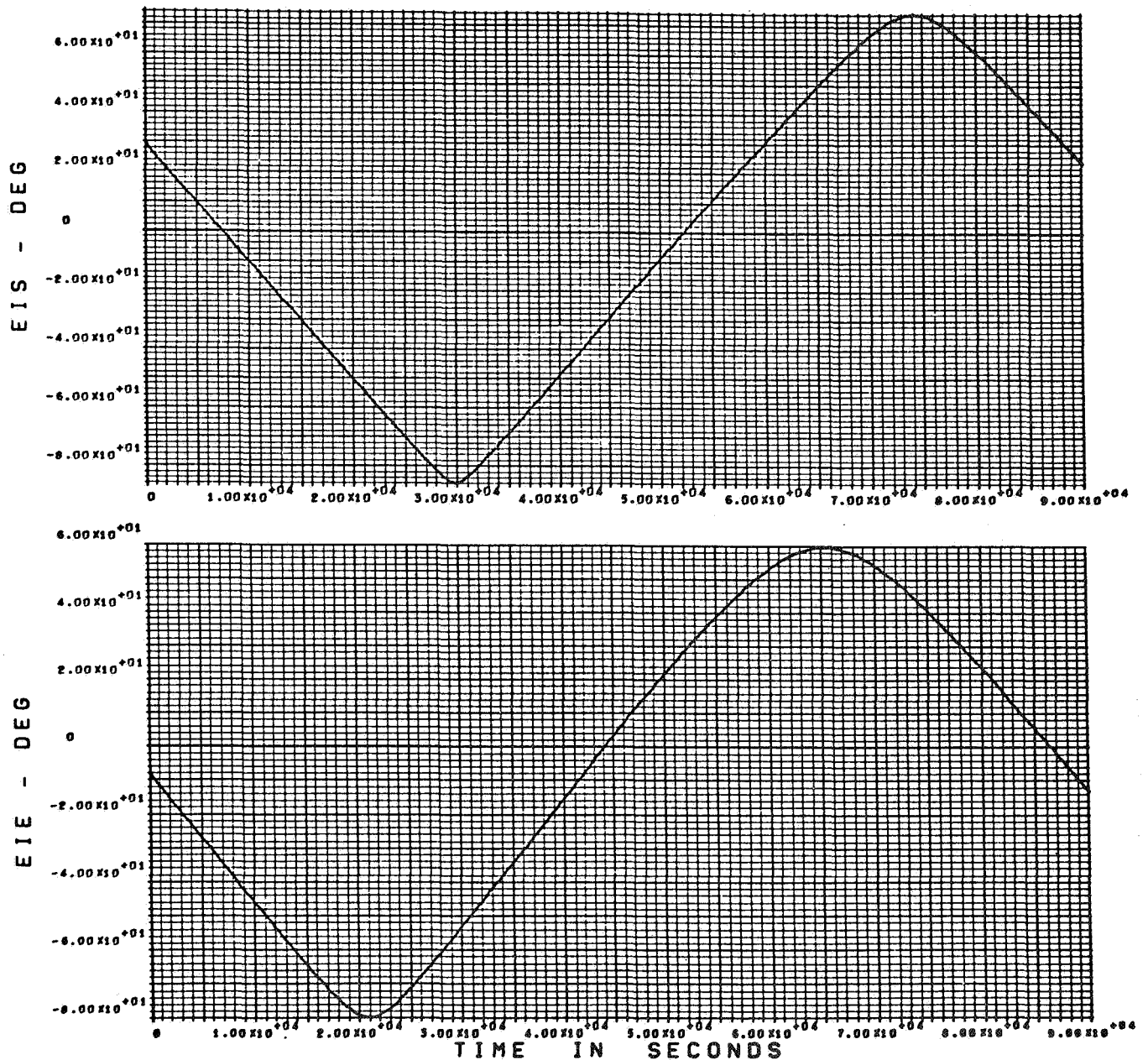
EIS = SUN ELEVATION ABOVE HORIZON
EIE = EARTH ELEVATION ABOVE HORIZON

Figure A-46. Earth and Sun Elevations at Landing Site During First Orbit After
Landing, Direct Entry

II

landing latitude = 10°
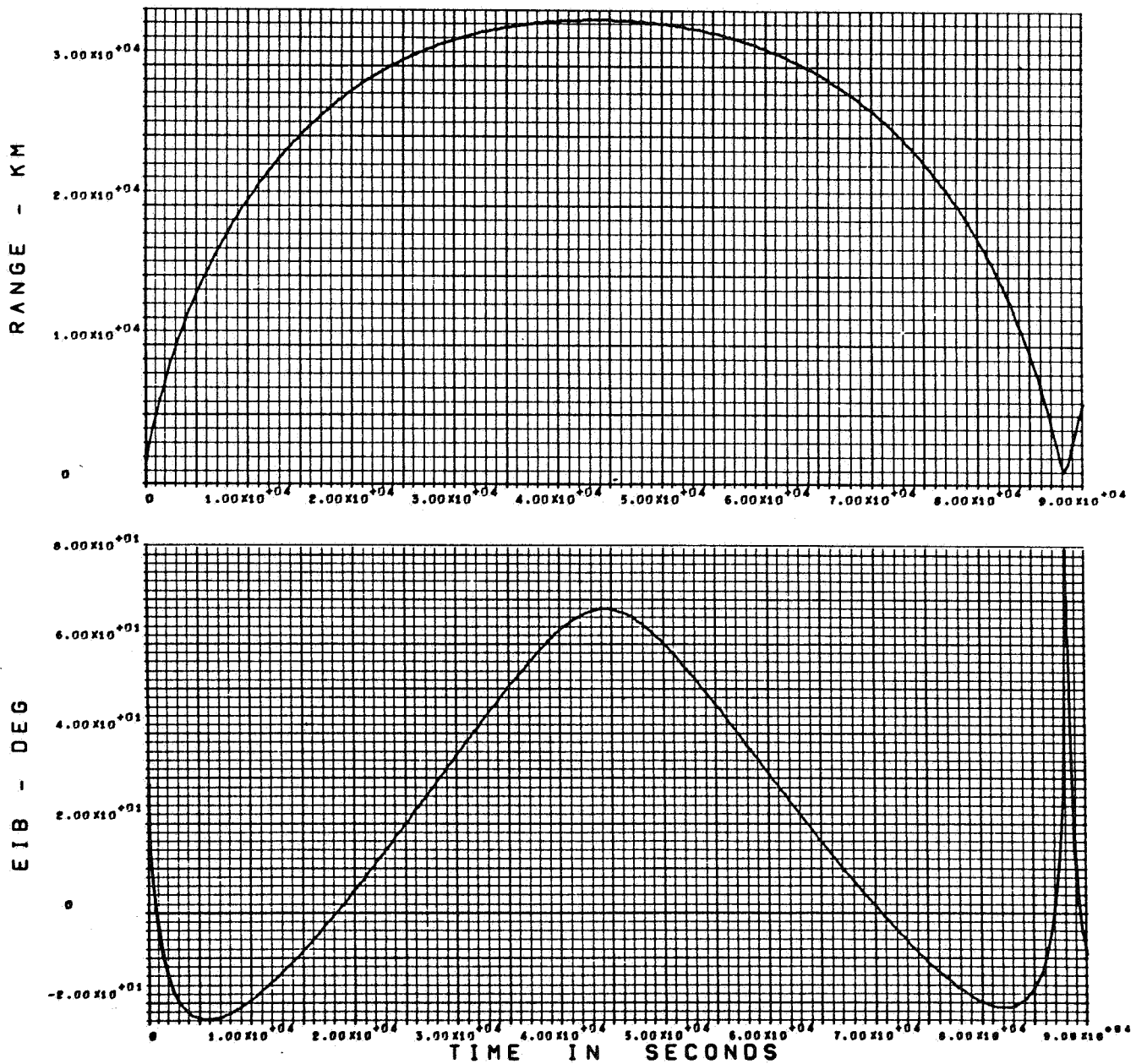
EIB = S/C ELEVATION ABOVE HORIZON

Figure A-47. Relay Communication Range and S/C Elevation at Landing Site During
First Orbit After Landing, Direct Entry

landing latitude = 10°

COA = CONE ANGLE
CLA = CLOCK ANGLE
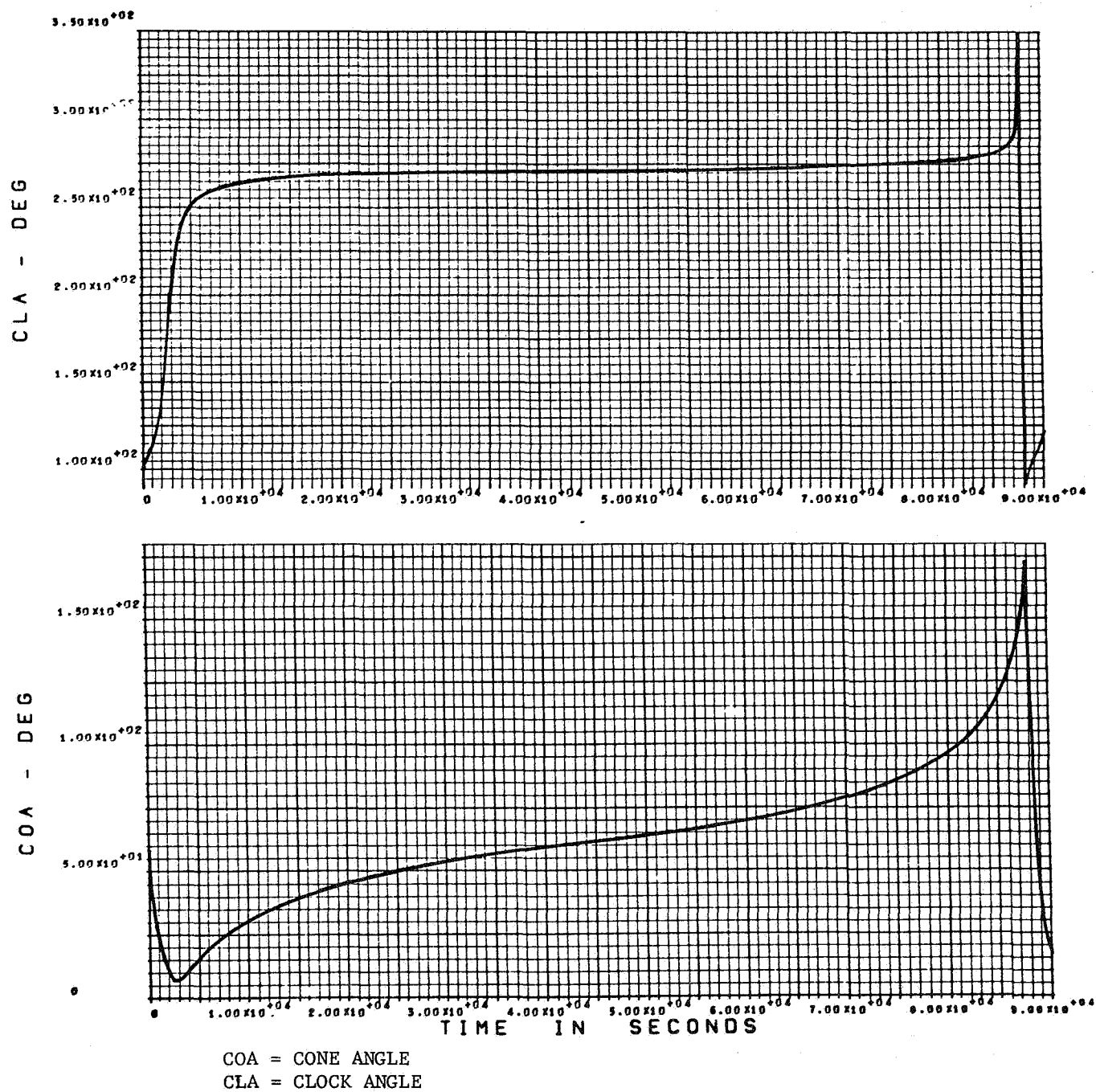
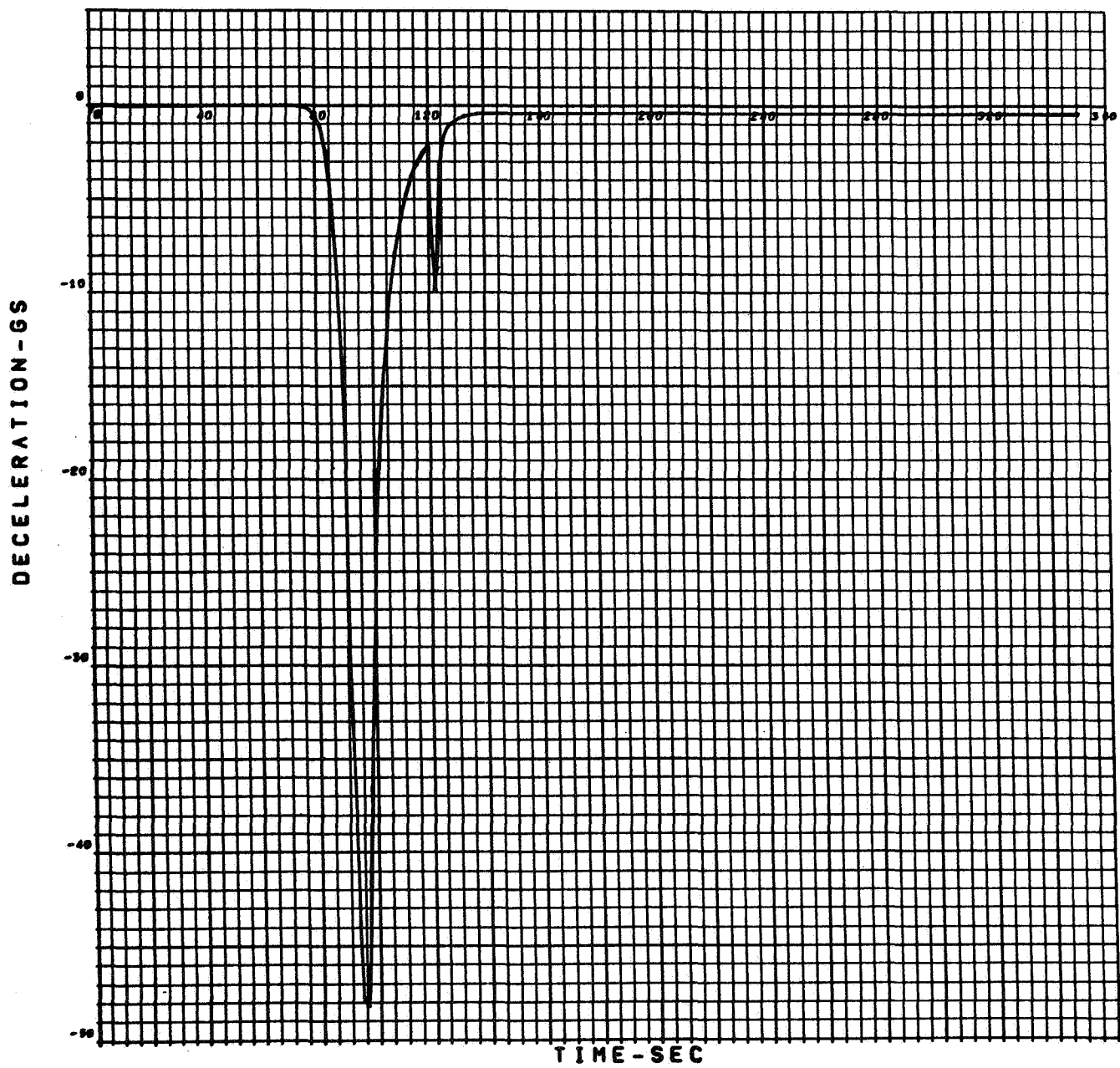Figure A-48. Lander Clock and Cone Angle at S/C During First Orbit After
Landing, Direct Entry
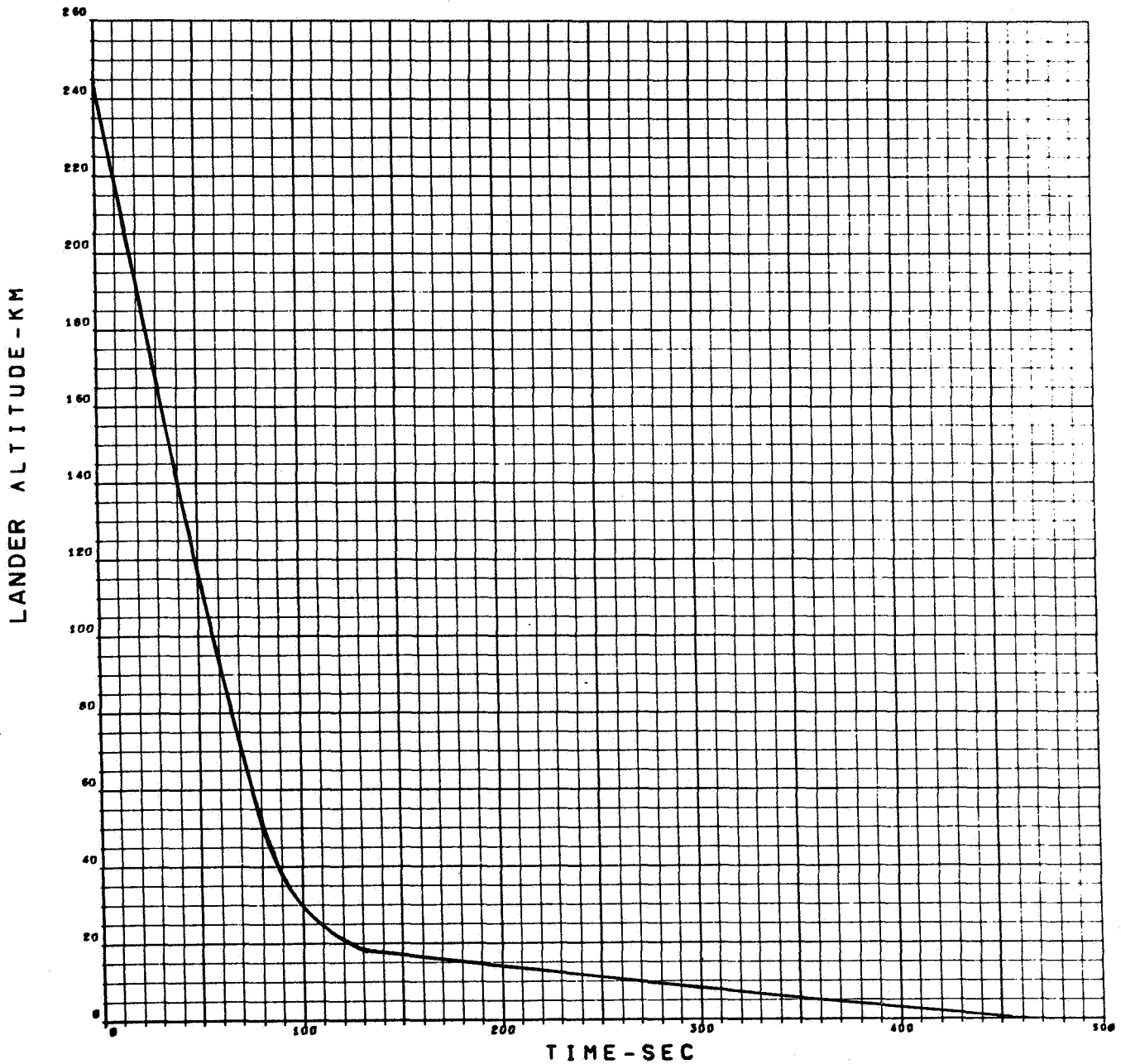
ENTRY VELOCITY   - 20,788 FT/SEC.
ENTRY PATH ANGLE   - 25°
ENTRY ALTITUDE   - 244 KM.
DRAG, SEE FIGURE 3.1-41
VM-7

Figure A-49. Lander Altitude vs Time, VM-7, Direct Entry
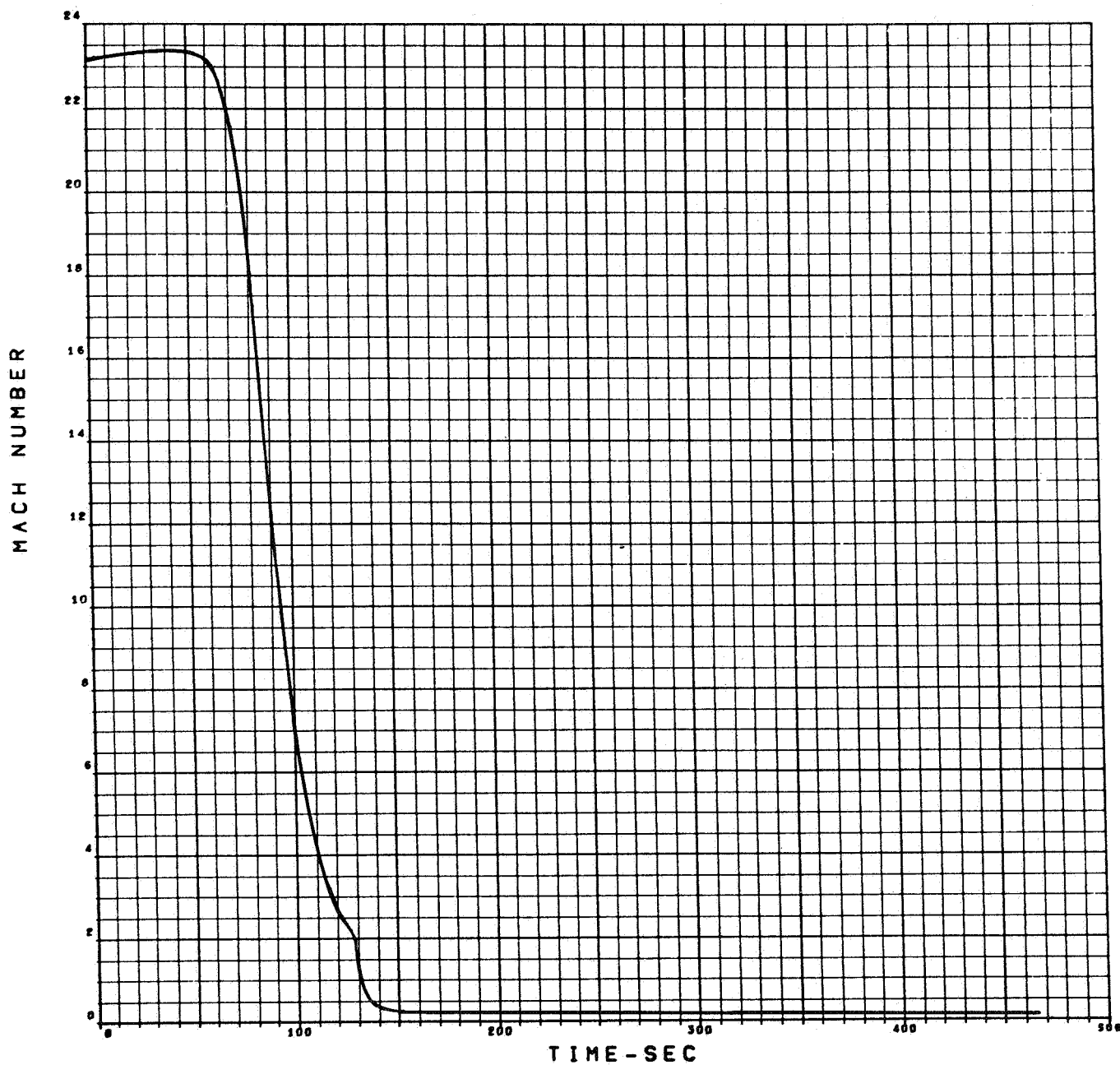
ENTRY VELOCITY   - 20,788 FT/SEC.
ENTRY PATH ANGLE   - 25°
ENTRY ALTITUDE   - 244 KM.
DRAG, SEE FIGURE 3.1-41
VM-7

Figure A-50. Mach Number vs Time, VM-7, Direct Entry

ENTRY VELOCITY   - 20,788 FT/SEC.
ENTRY PATH ANGLE   - 25°
ENTRY ALTITUDE   - 244 KM.
DRAG, SEE FIGURE 3.1-41
VM-7

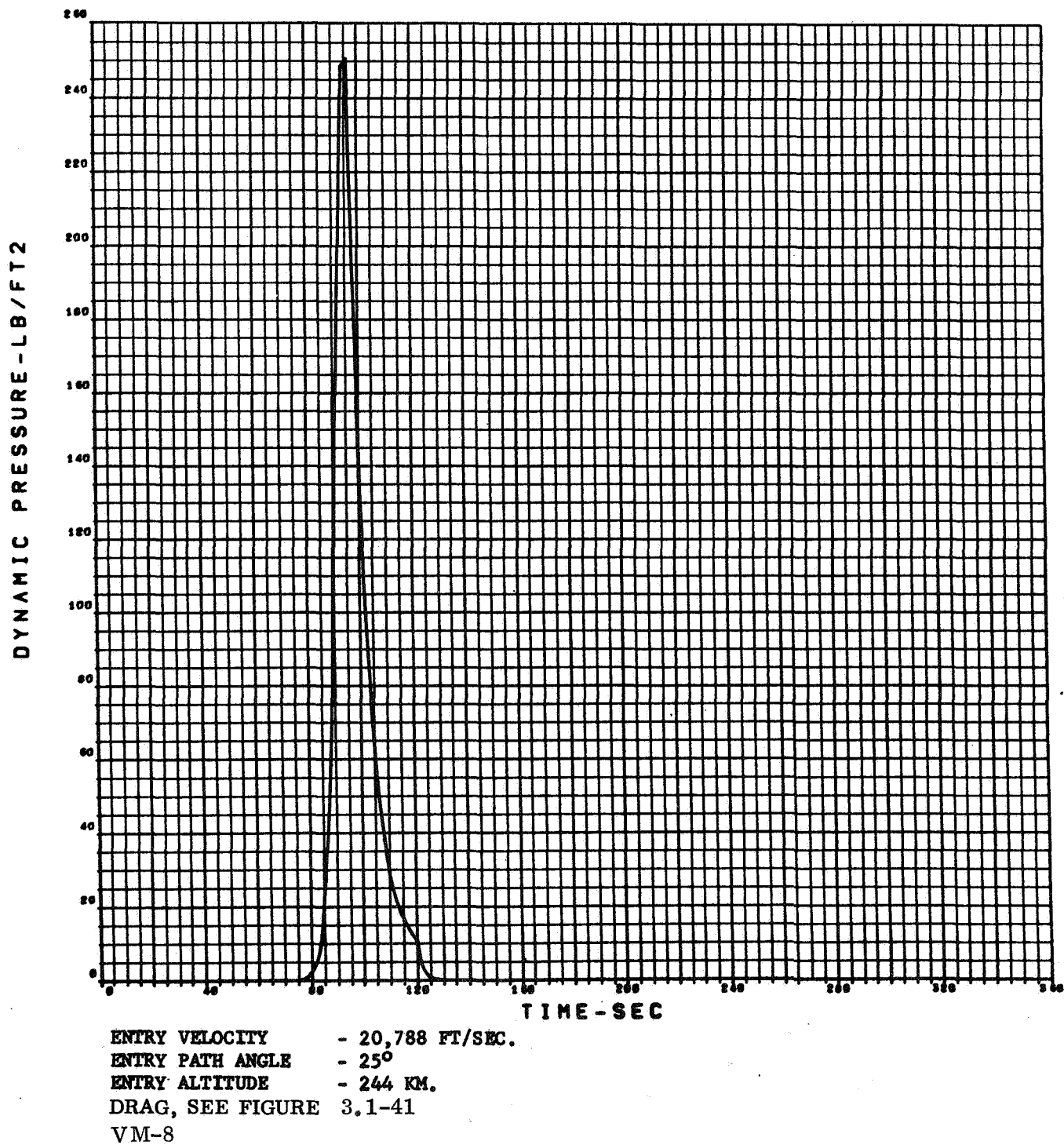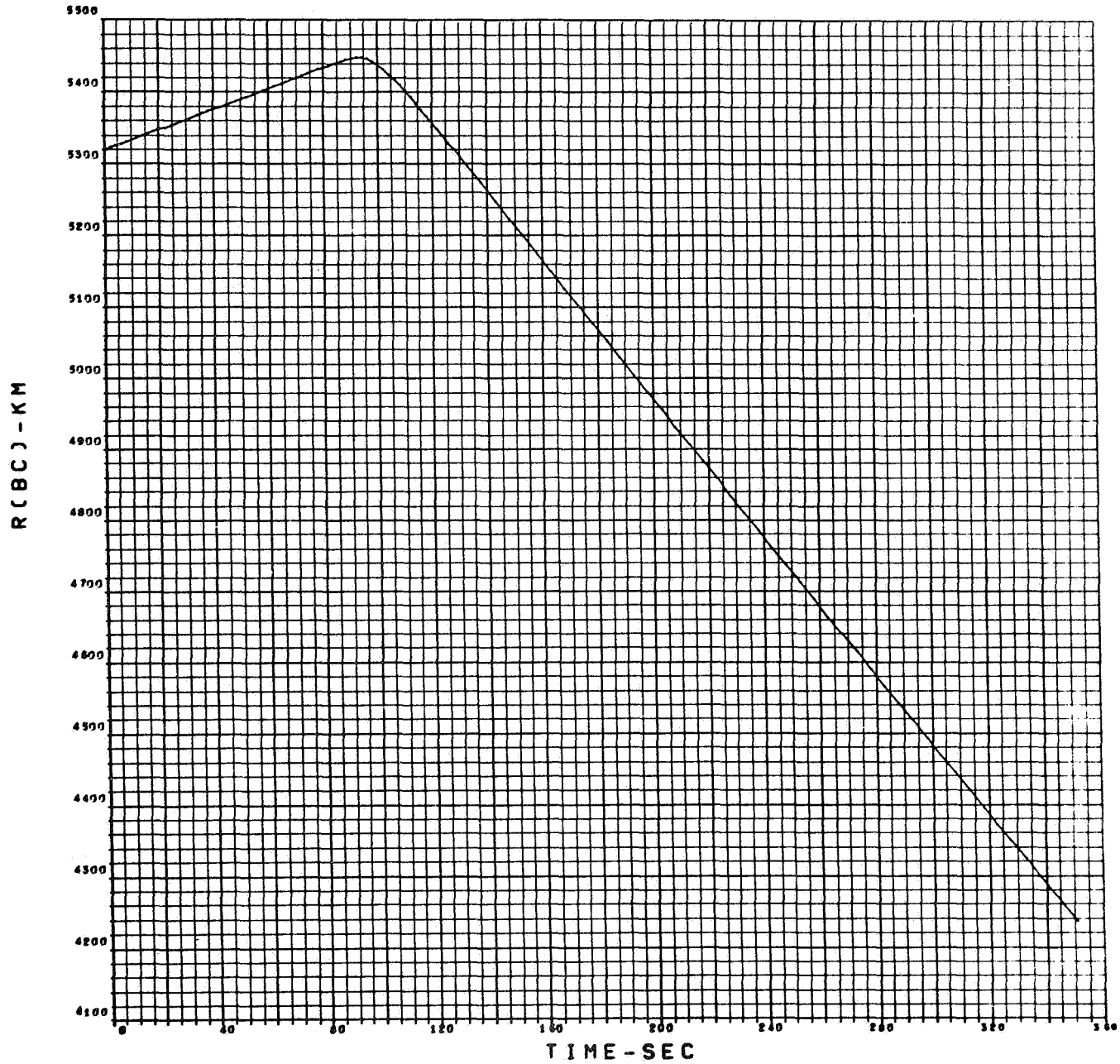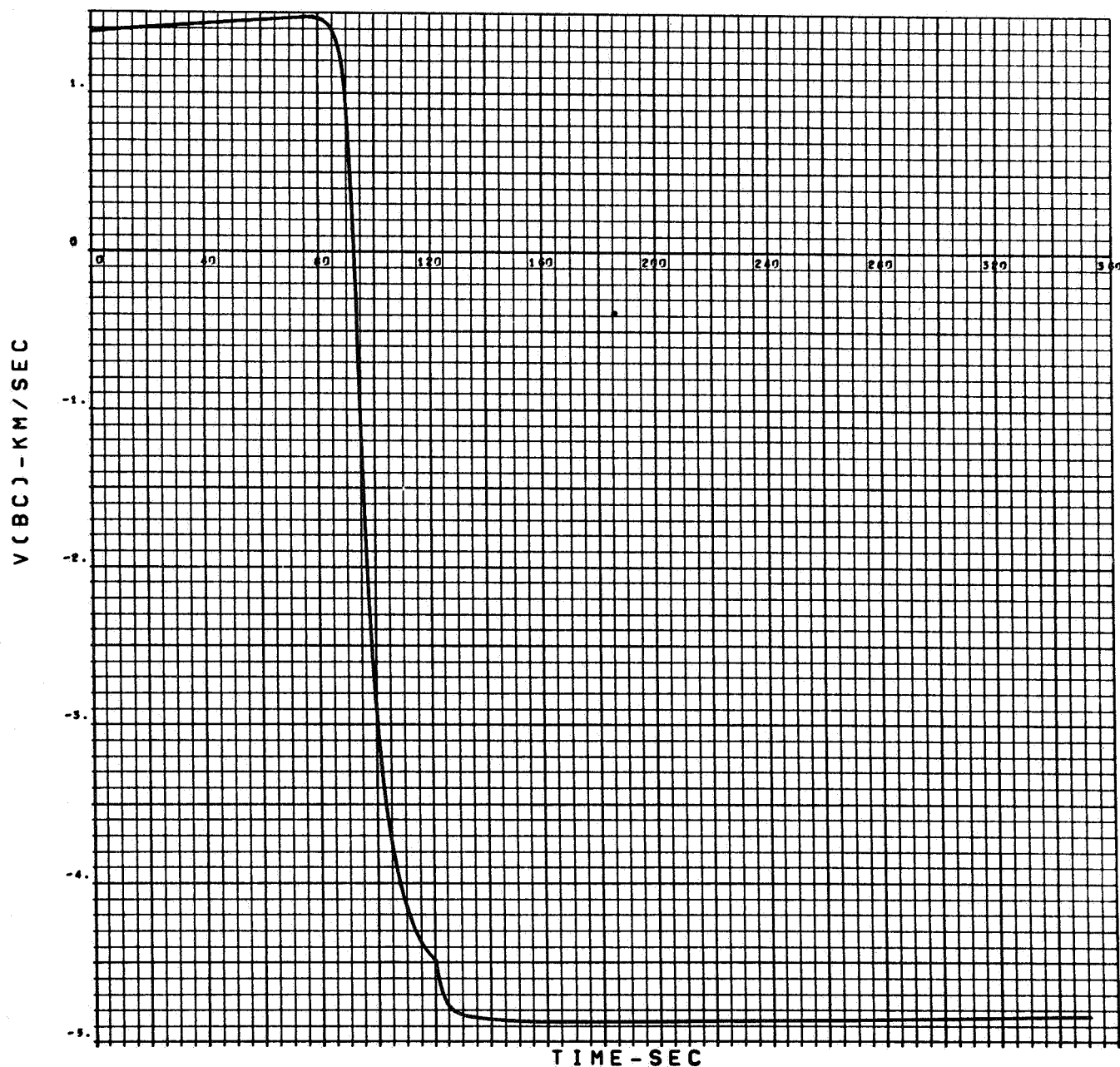Figure A-51. Lander Deceleration vs Time, VM-7, Direct Entry
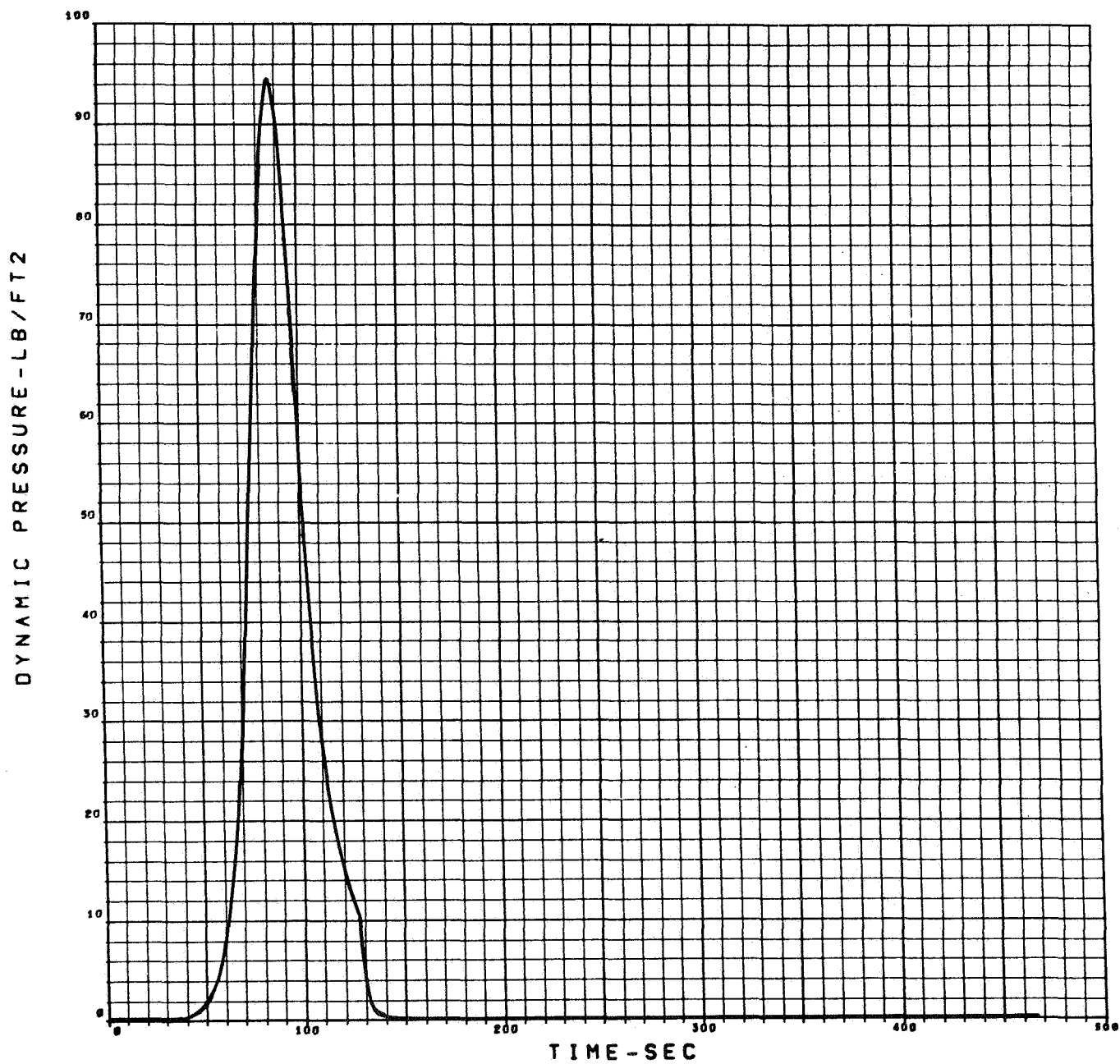
ENTRY VELOCITY   - 20,788 FT/SEC.
ENTRY PATH ANGLE   - 25°
ENTRY ALTITUDE   - 244 KM.
DRAG, SEE FIGURE 3.1-41
VM-7

Figure A-52. Dynamic Pressure vs Time, VM-7, Direct Entry
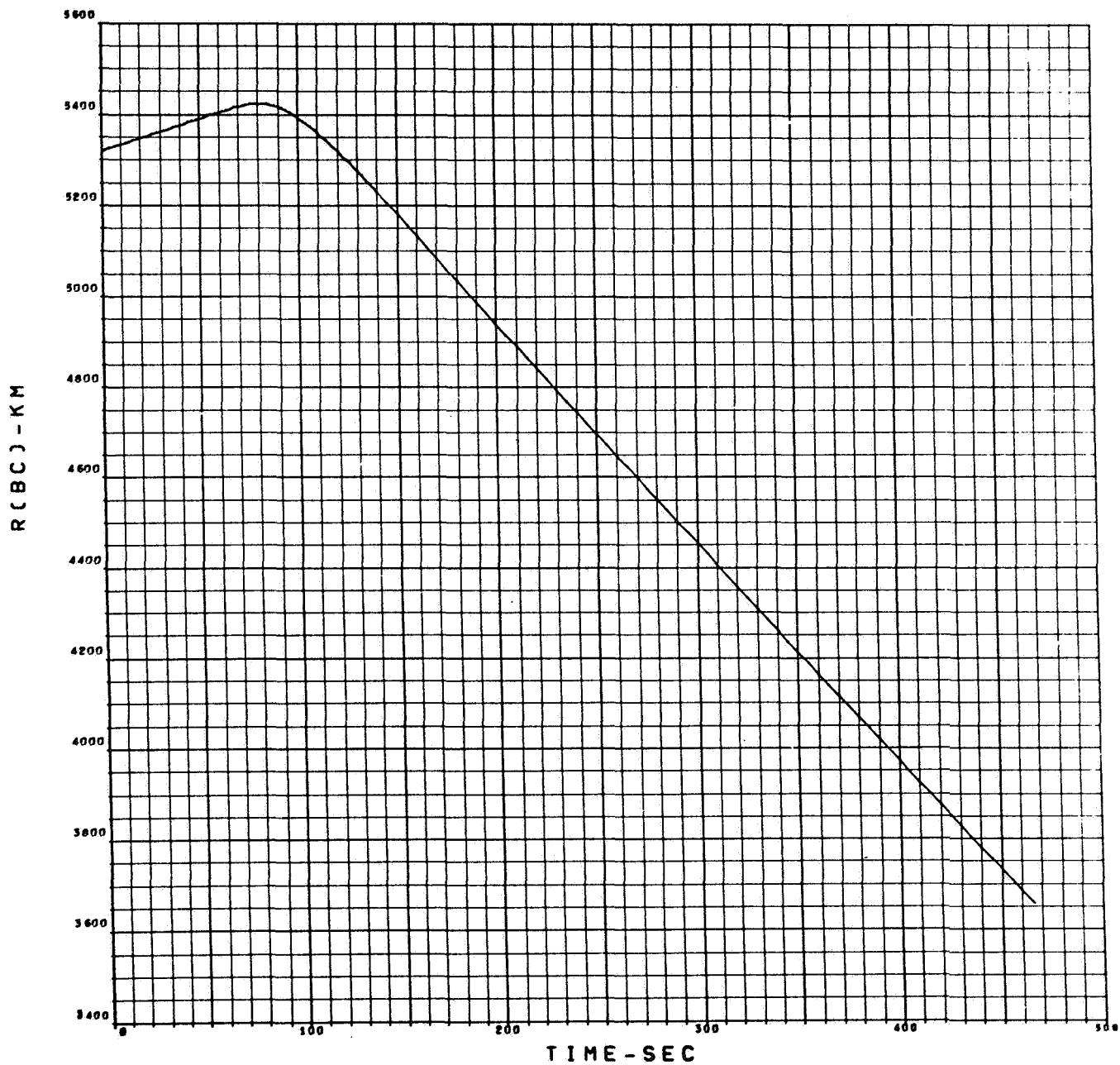
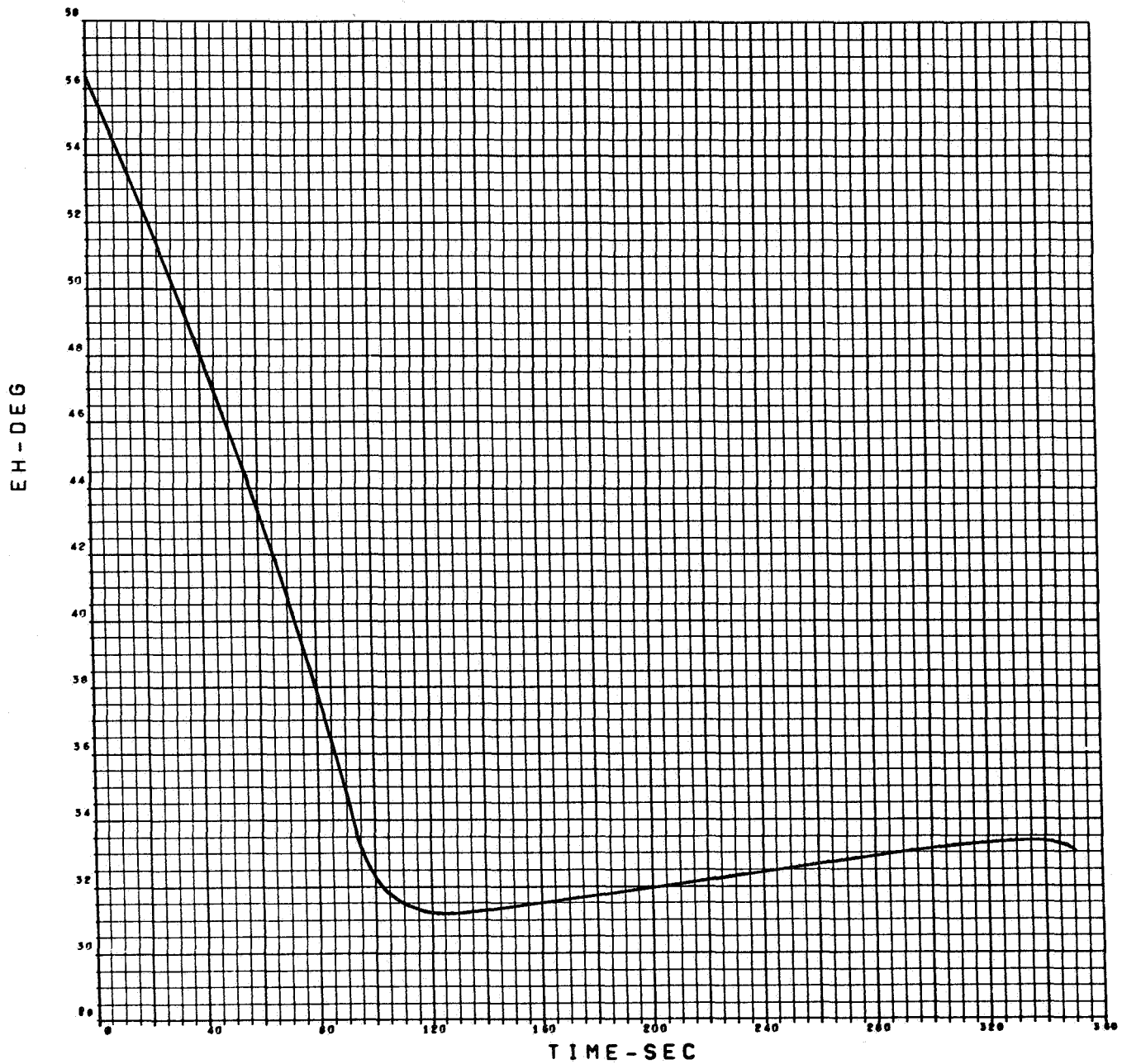Figure A-53. Communication Distance R(BC) vs Time, VM-7, Direct Entry
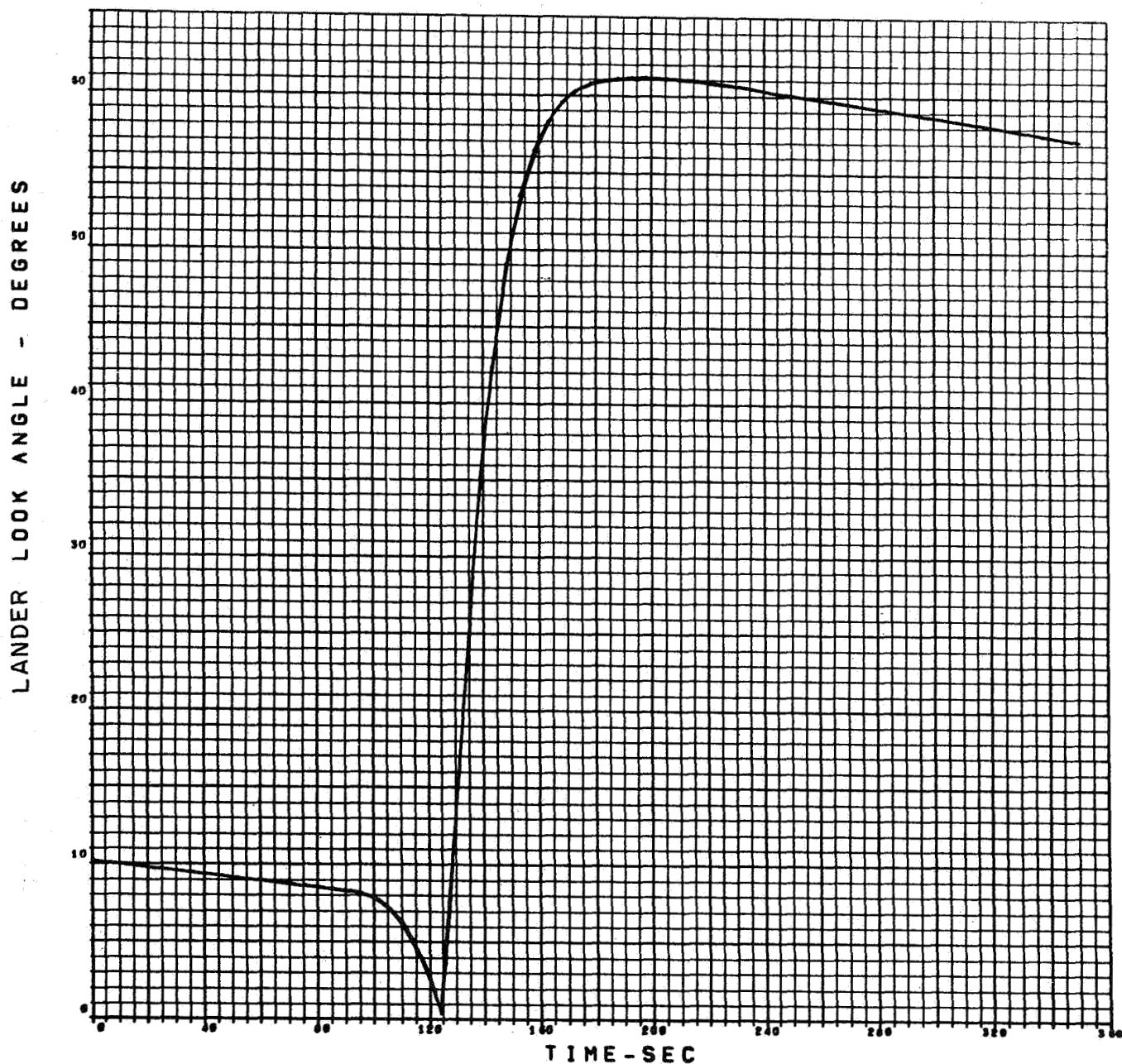
ENTRY VELOCITY   - 20,788 FT/SEC.
ENTRY PATH ANGLE   - 25°
ENTRY ALTITUDE   - 244 KM.
DRAG, SEE FIGURE 3.1-41
VM-7

Figure A-54. Range Rate vs Time, VM-7, Direct Entry
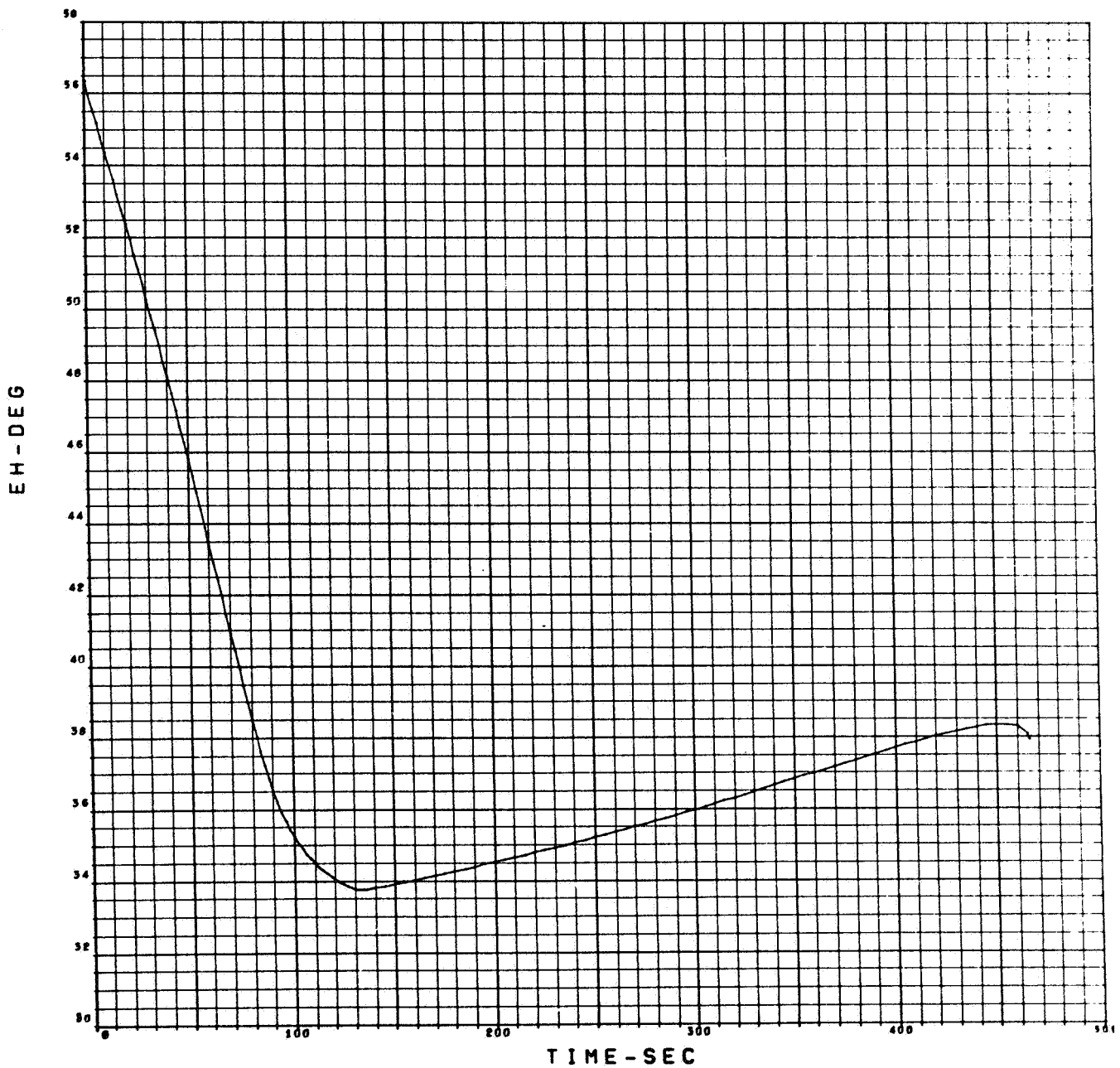
ENTRY VELOCITY   - 20,788 FT/SEC.
ENTRY PATH ANGLE - 25°
ENTRY ALTITUDE   - 244 KM.
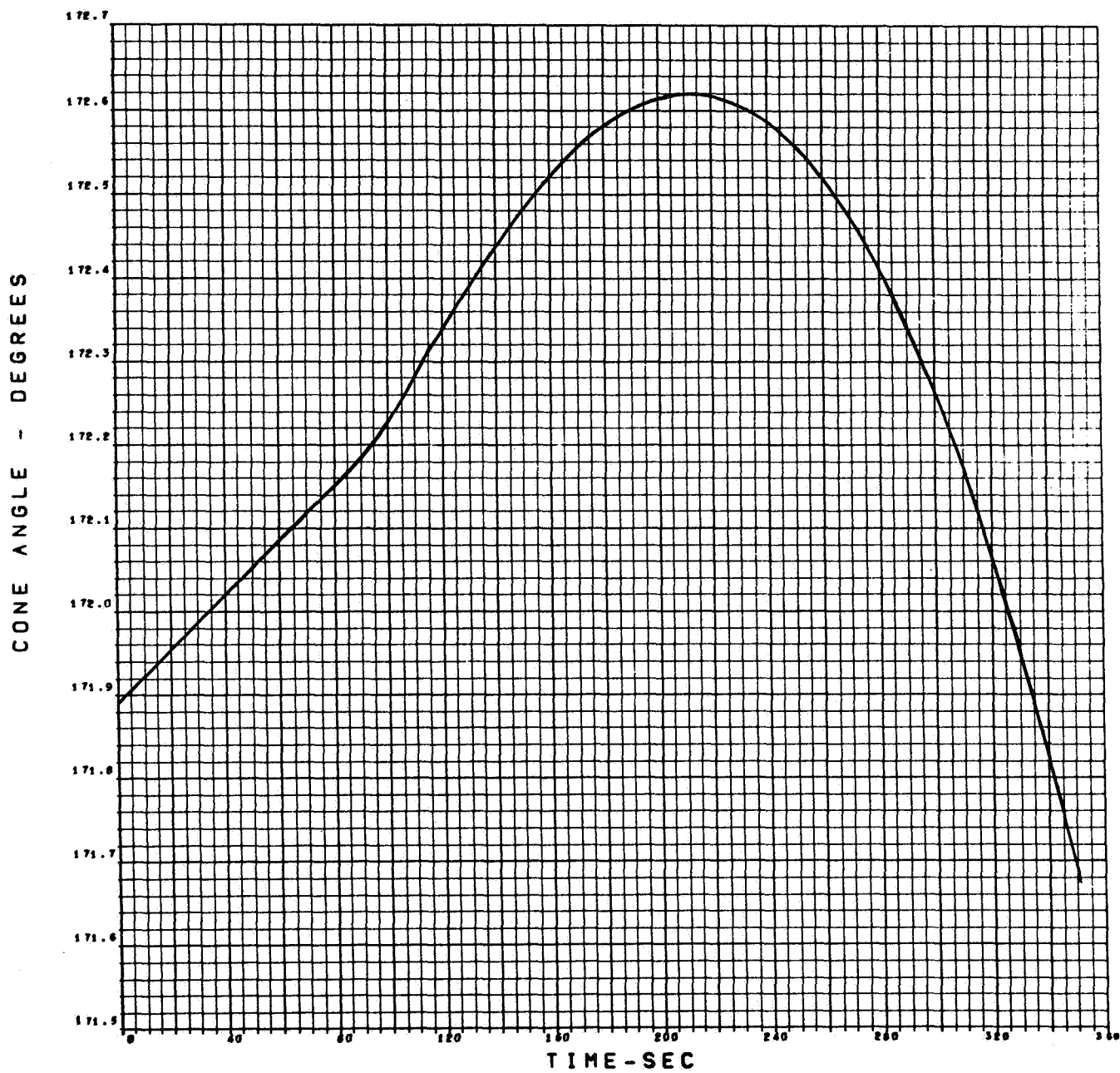DRAG, SEE FIGURE 3.1-41
VM-7

ENTRY VELOCITY   - 20,788 FT/SEC.
ENTRY PATH ANGLE   - 25°
ENTRY ALTITUDE   - 244 KM.
DRAG, SEE FIGURE 3.1-41
VM-7

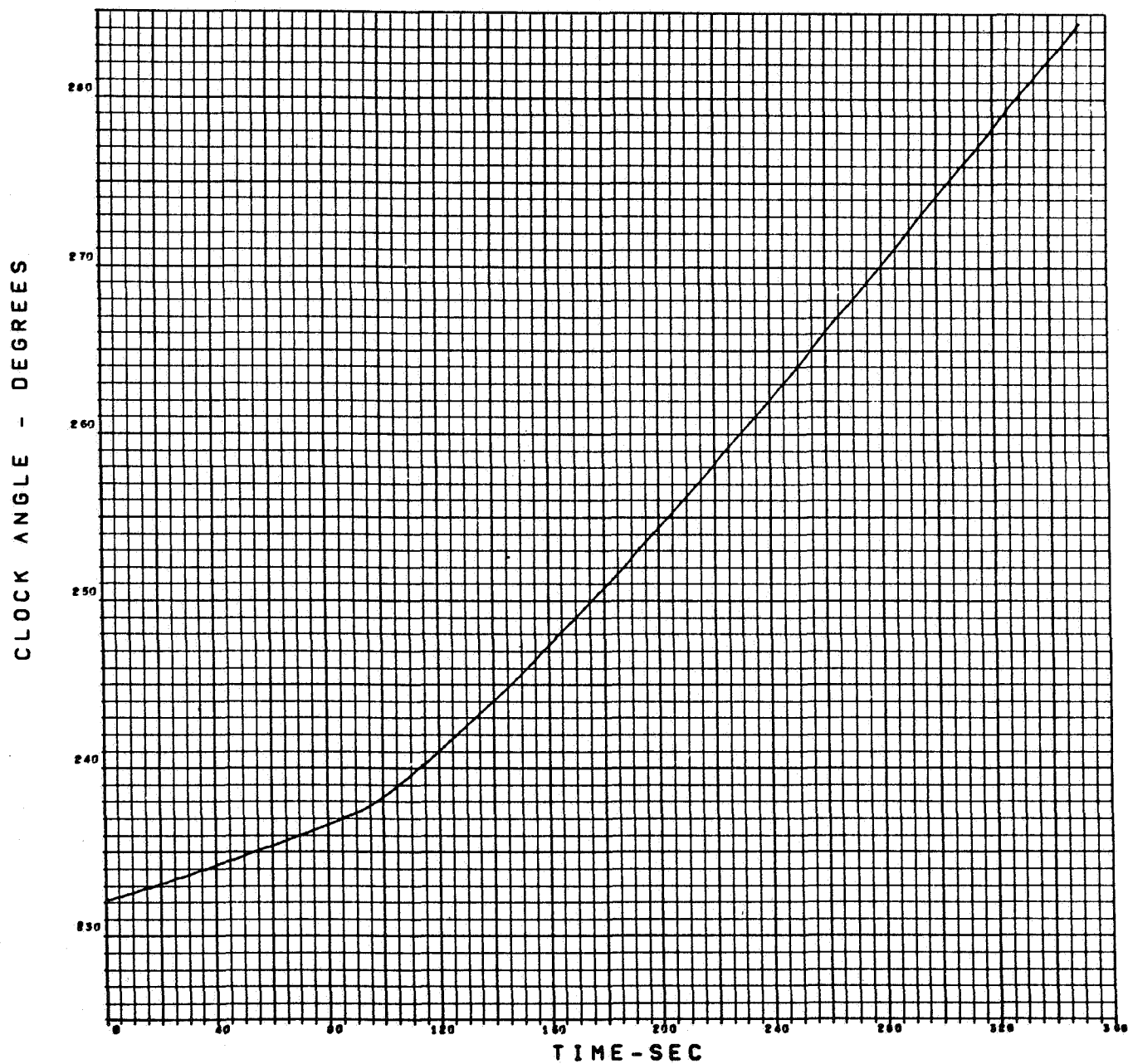Figure A-55. Angle at which Lander Sees Orbiter Above Horizon, VM-7, Direct Entry

ENTRY VELOCITY   - 20,788 FT/SEC.
ENTRY PATH ANGLE   - 25°
ENTRY ALTITUDE   - 244 KM.
DRAG, SEE FIGURE 3.1-41
VM-7

Figure A-56. Lander Look Angle vs Time, VM-7, Direct Entry
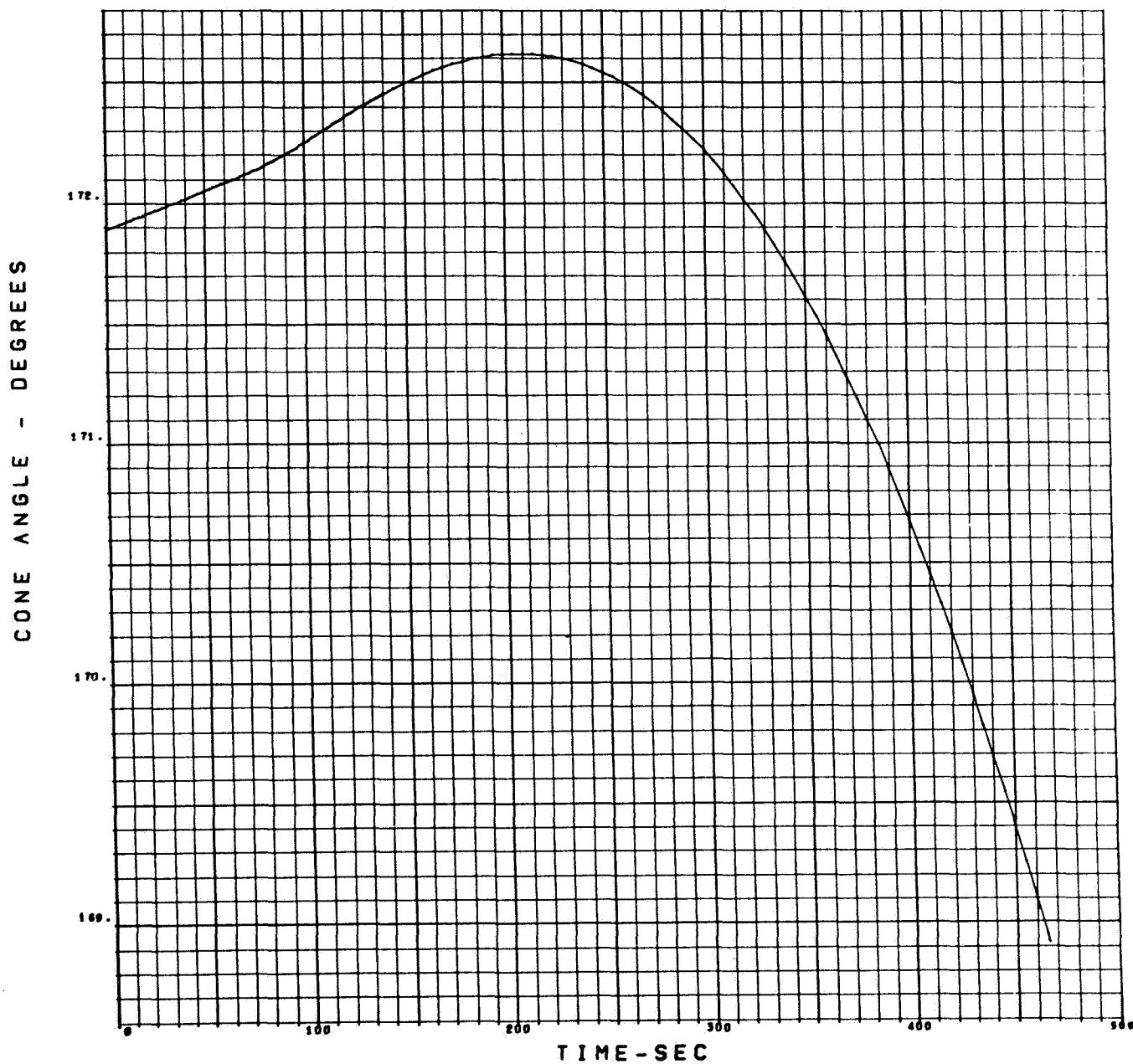
ENTRY VELOCITY   - 20,788 FT/SEC.
ENTRY PATH ANGLE   - 25°
ENTRY ALTITUDE   - 244 KM.
DRAG, SEE FIGURE 3.1-41
VM-7

Figure A-57. Cone Angle vs Time, VM-7, Direct Entry

ENTRY VELOCITY   - 20,788 FT/SEC.
ENTRY PATH ANGLE   - 25°
ENTRY ALTITUDE   - 244 KM.
DRAG, SEE FIGURE 3.1-41
VM-7
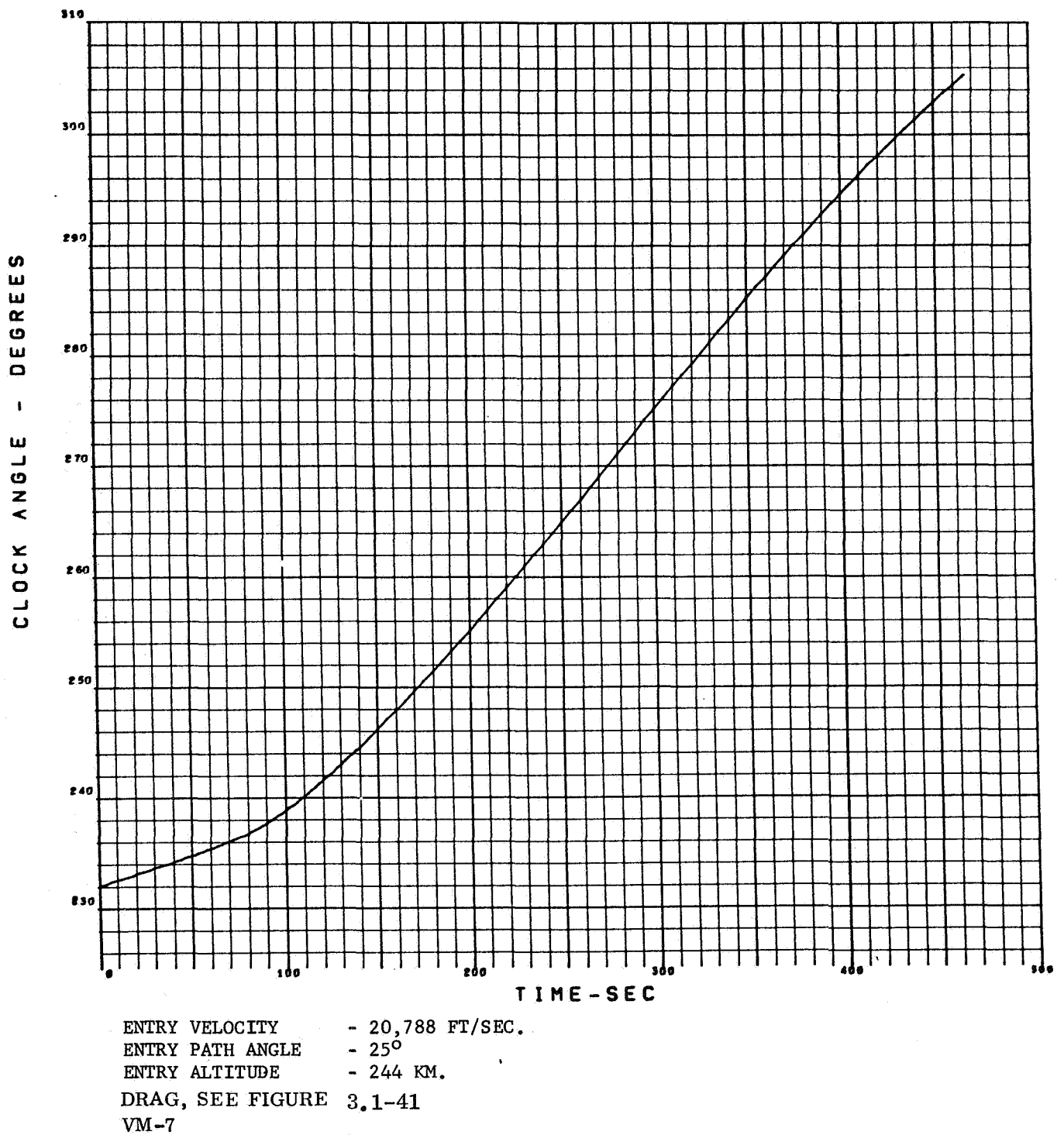
Figure A-58. Clock Angle vs Time, VM-7, Direct Entry
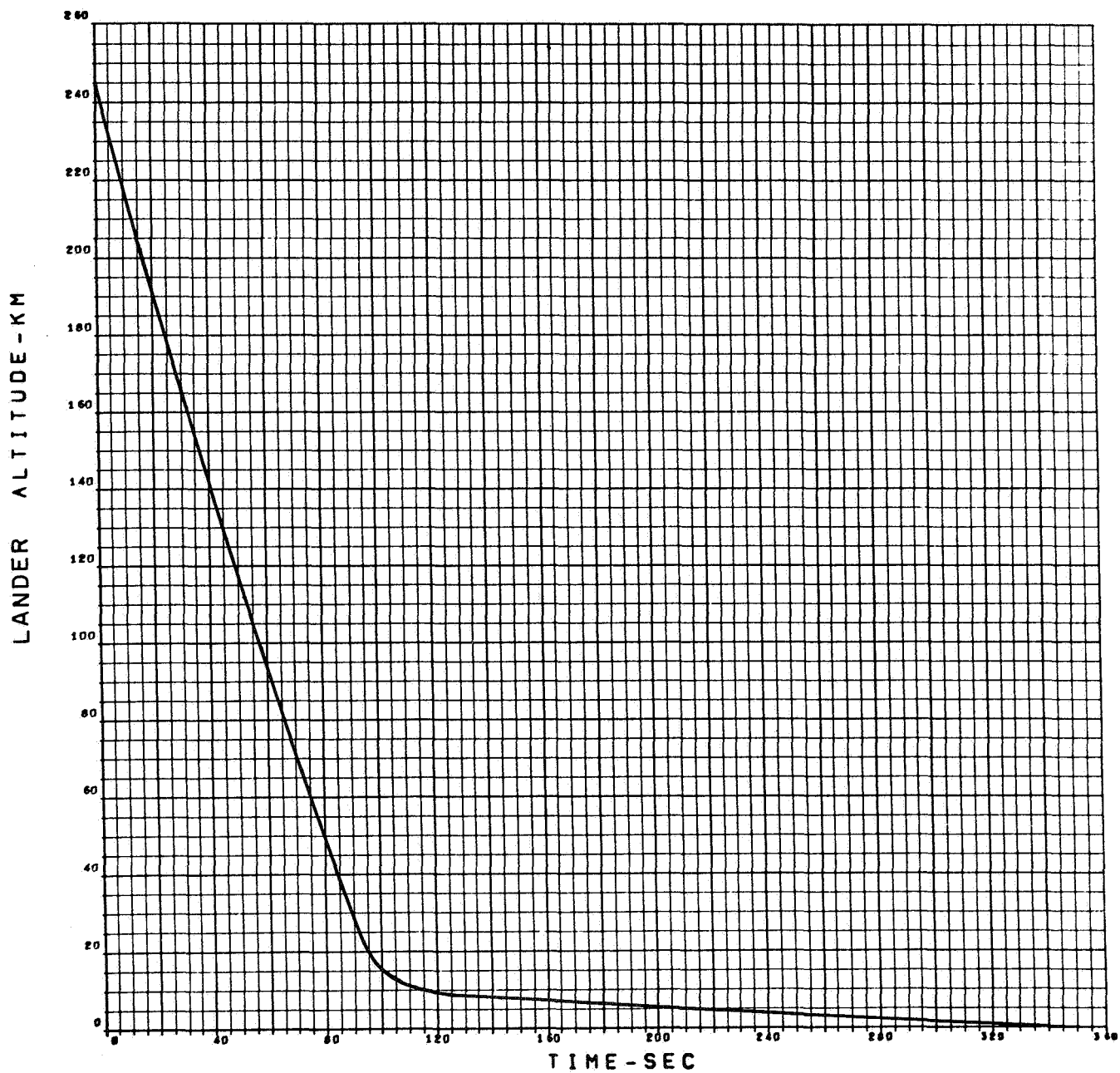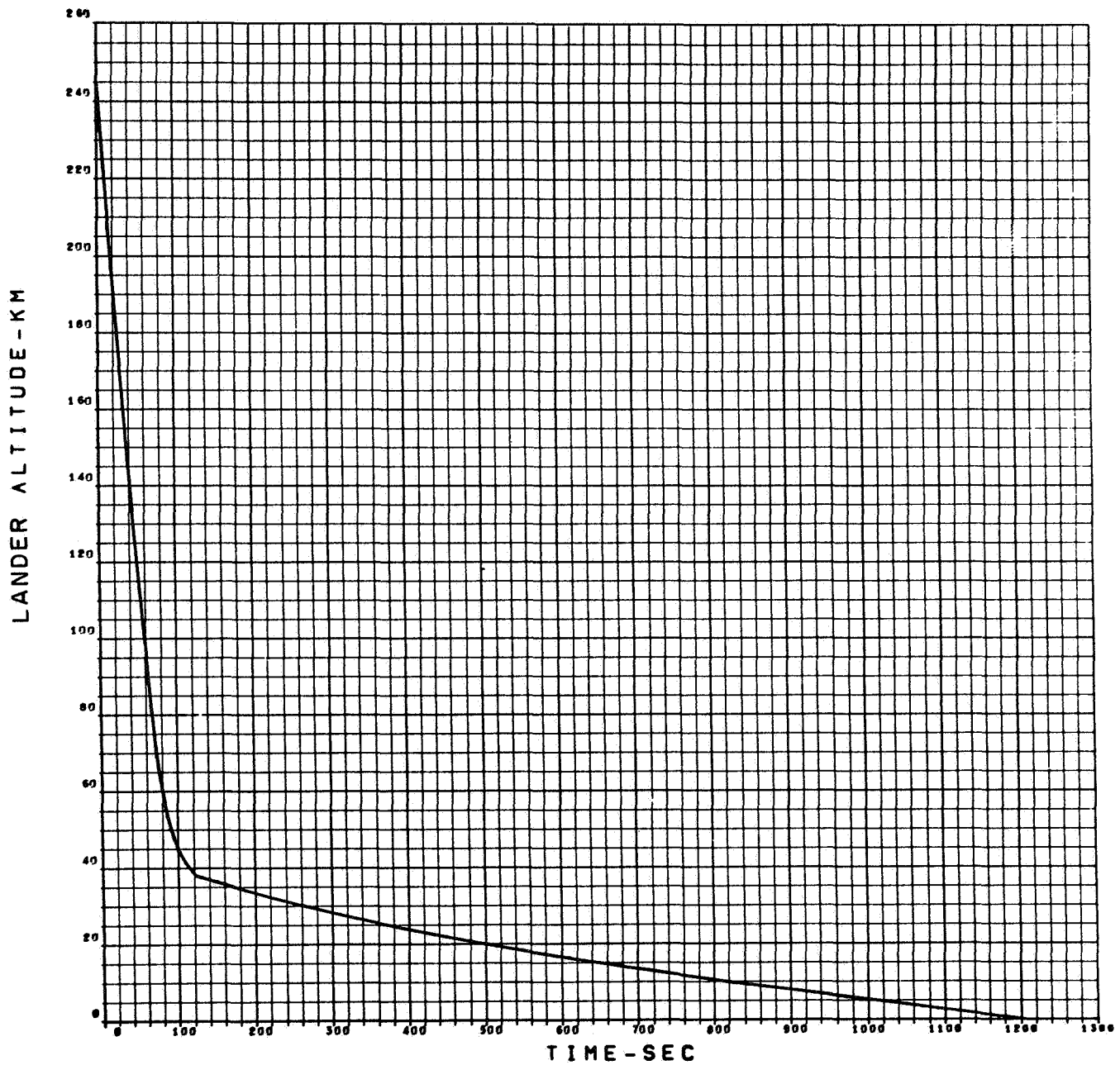
ENTRY VELOCITY   - 20,788 FT/SEC.
ENTRY PATH ANGLE   - 25°
ENTRY ALTITUDE   - 244 KM.
DRAG, SEE FIGURE 3.1-41
VM-8

Figure A-59. Lander Altitude vs Time, VM-8, Direct Entry
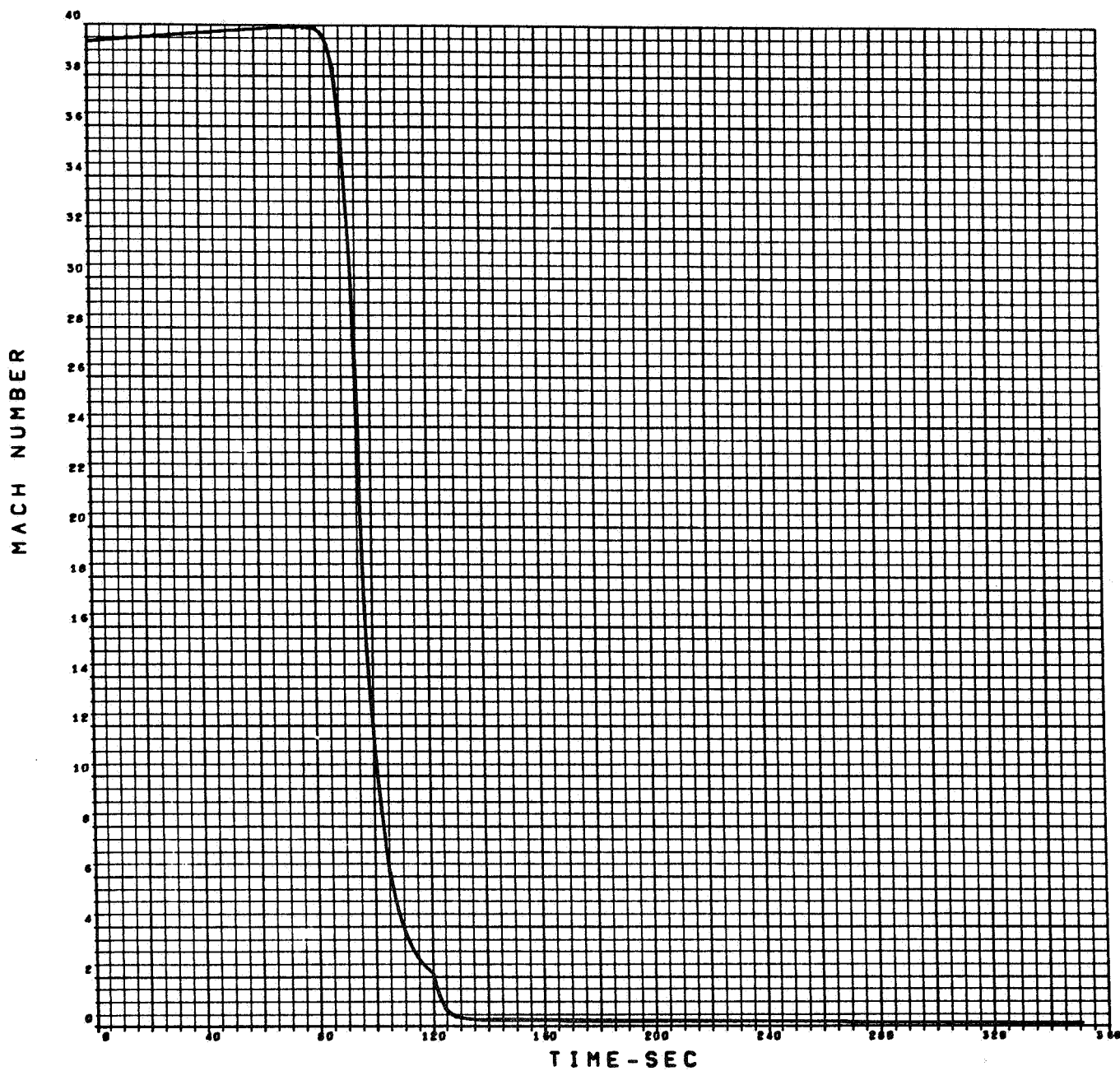
ENTRY VELOCITY — 20,788 FT/SEC.
ENTRY PATH ANGLE — 25°
ENTRY ALTITUDE — 244 KM.
DRAG, SEE FIGURE 3.1-41
VM-8

Figure A-60. Mach Number vs Time, VM-8, Direct Entry

Figure A-61. Lander Deceleration vs Time, VM-8, Direct Entry

ENTRY VELOCITY   - 20,788 FT/SEC.
ENTRY PATH ANGLE   - 25°
ENTRY ALTITUDE   - 244 KM.
DRAG, SEE FIGURE 3.1-41
VM-8

ENTRY VELOCITY   – 20,788 FT/SEC.
ENTRY PATH ANGLE   – 25°
ENTRY ALTITUDE   – 244 KM.
DRAG, SEE FIGURE 3.1-41
VM-8

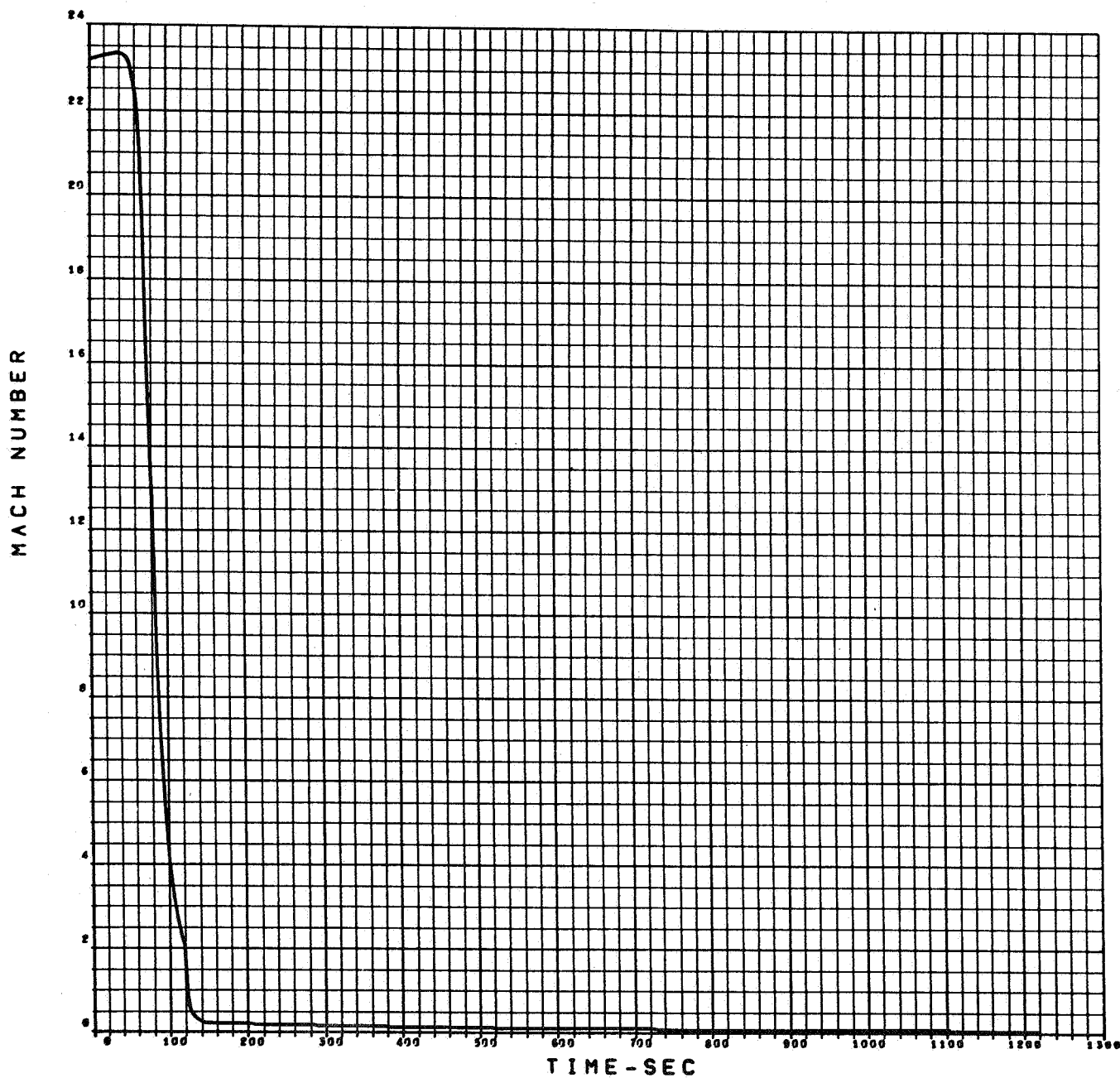Figure A-62. Dynamic Pressure vs Time, VM-8, Direct Entry

Figure A-63. Communication Distance R(BC) vs Time, VM-8, Direct Entry

ENTRY VELOCITY   - 20,788 FT/SEC.
ENTRY PATH ANGLE   - 25°
ENTRY ALTITUDE   - 244 KM.
DRAG, SEE FIGURE 3.1-41
VM-8

ENTRY VELOCITY   - 20,788 FT/SEC.
ENTRY PATH ANGLE   - 25°
ENTRY ALTITUDE   - 244 KM.
DRAG, SEE FIGURE 3.1-41
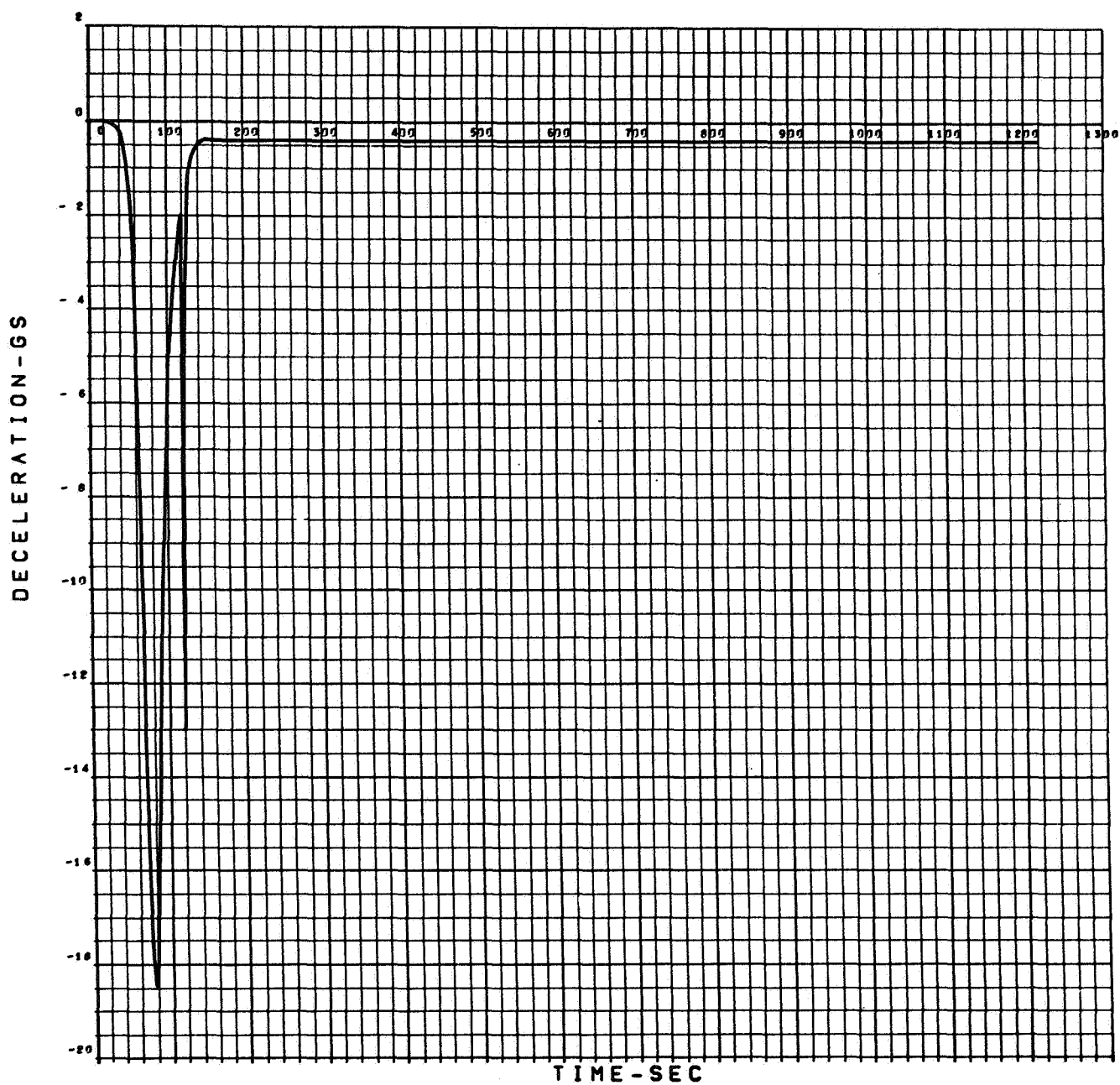VM-8

Figure A-64. Range Rate vs Time, VM-8, Direct Entry

ENTRY VELOCITY   - 20,788 FT/SEC.
ENTRY PATH ANGLE   - 25°
ENTRY ALTITUDE   - 244 KM.
DRAG, SEE FIGURE 3.1-41
VM-8

Figure A-65.   Angle at which Lander Sees Orbiter Above Horizon, VM-8,
Direct Entry

ENTRY VELOCITY   - 20,788 FT/SEC.
ENTRY PATH ANGLE   - 25°
ENTRY ALTITUDE   - 244 KM.
DRAG, SEE FIGURE 3.1-41
VM-8

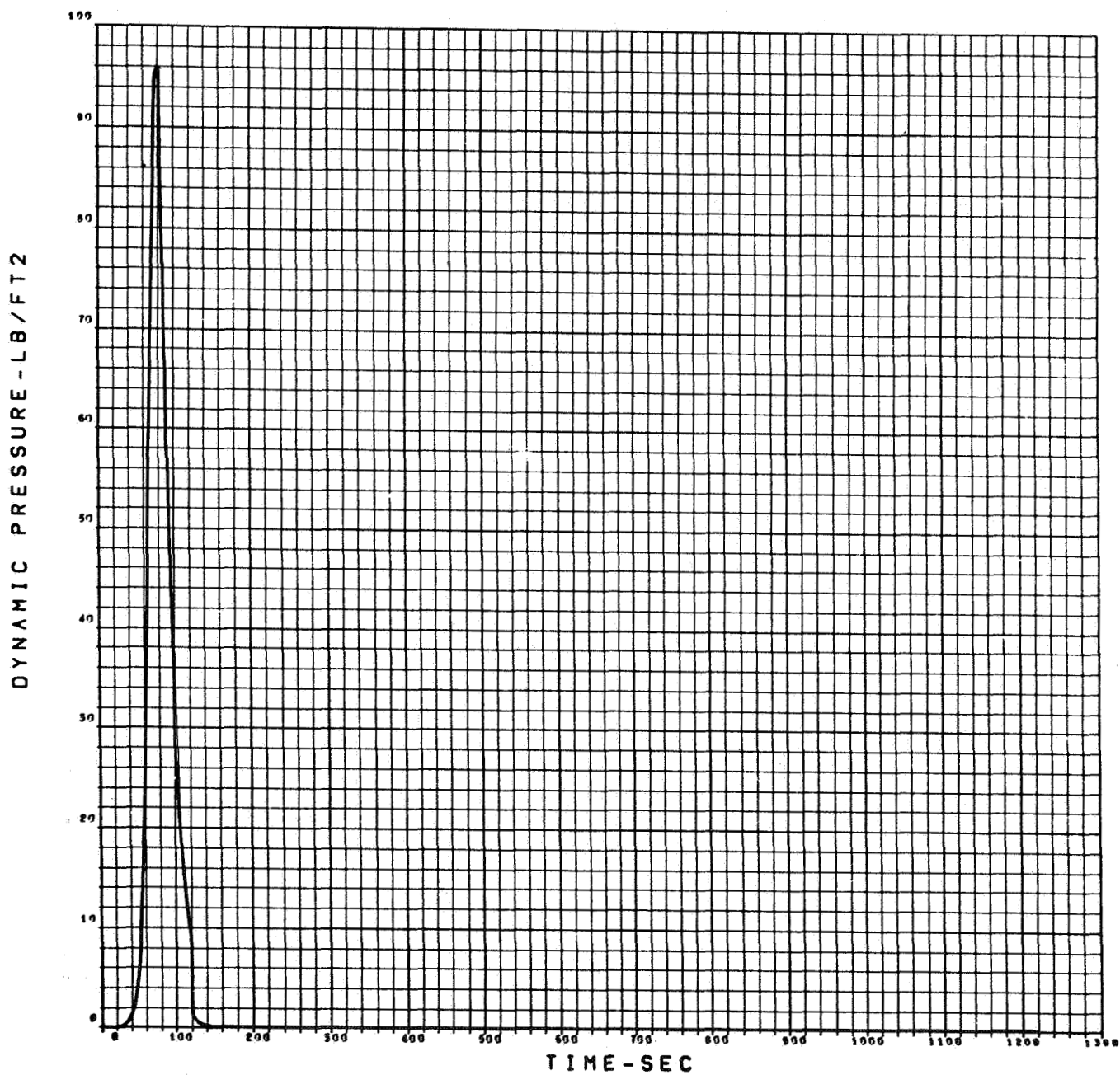Figure A-66. Lander Look Angle vs Time, VM-8, Direct Entry

II

ENTRY VELOCITY   - 20,788 FT/SEC.
ENTRY PATH ANGLE   - 25°
ENTRY ALTITUDE   - 244 KM.
DRAG, SEE FIGURE 3.1-41
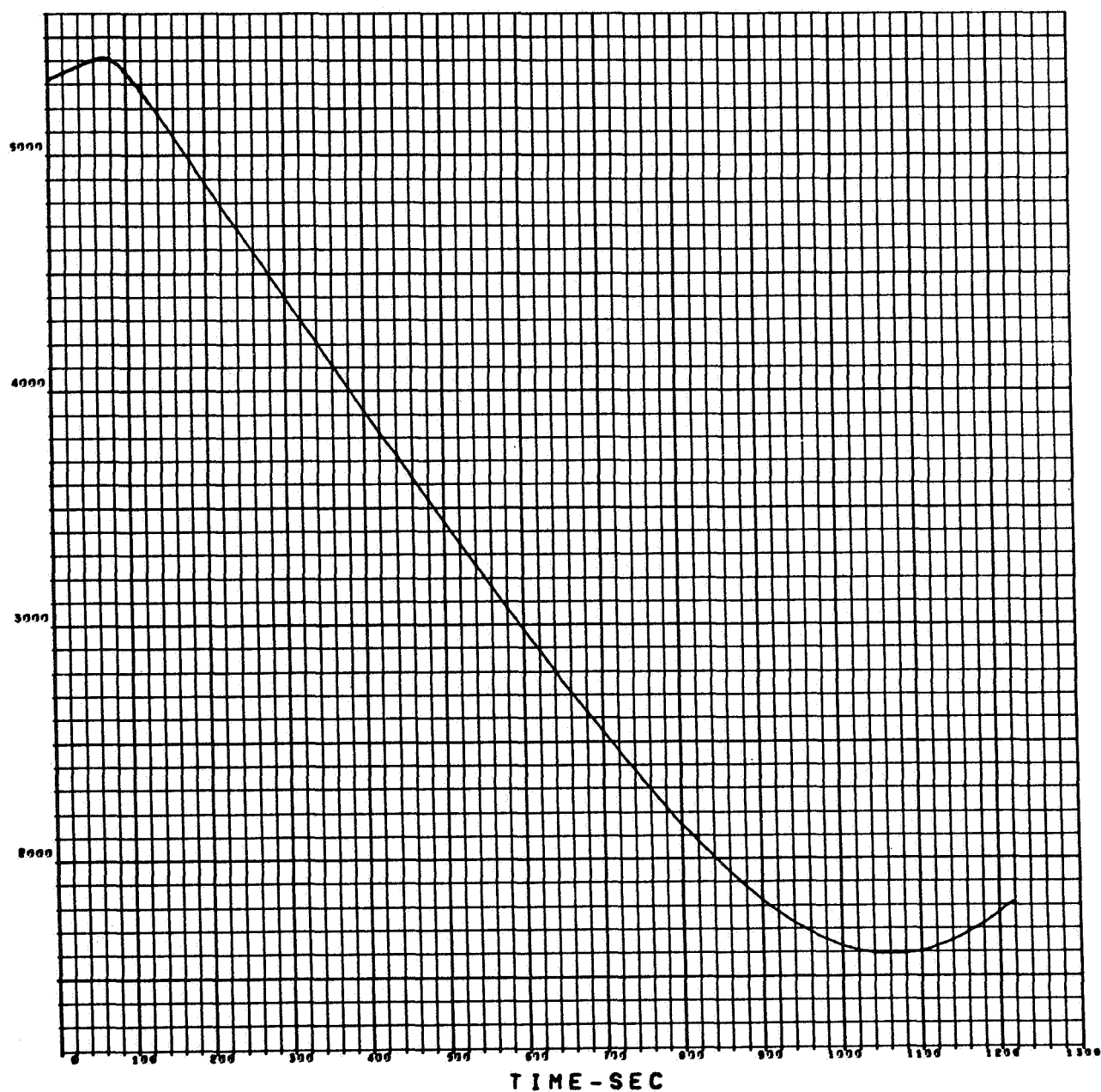VM-8

Figure A-67. Cone Angle vs Time, VM-8, Direct Entry

ENTRY VELOCITY   - 20,788 FT/SEC.
ENTRY PATH ANGLE   - 25°
ENTRY ALTITUDE   - 244 KM.
DRAG, SEE FIGURE 3.1-41
VM-8

Figure A-68. Clock Angle vs Time, VM-8, Direct Entry

Figure A-69. Lander Altitude vs Time, VM-9, Direct Entry

ENTRY VELOCITY   - 20,788 FT/SEC.
ENTRY PATH ANGLE   - 25°
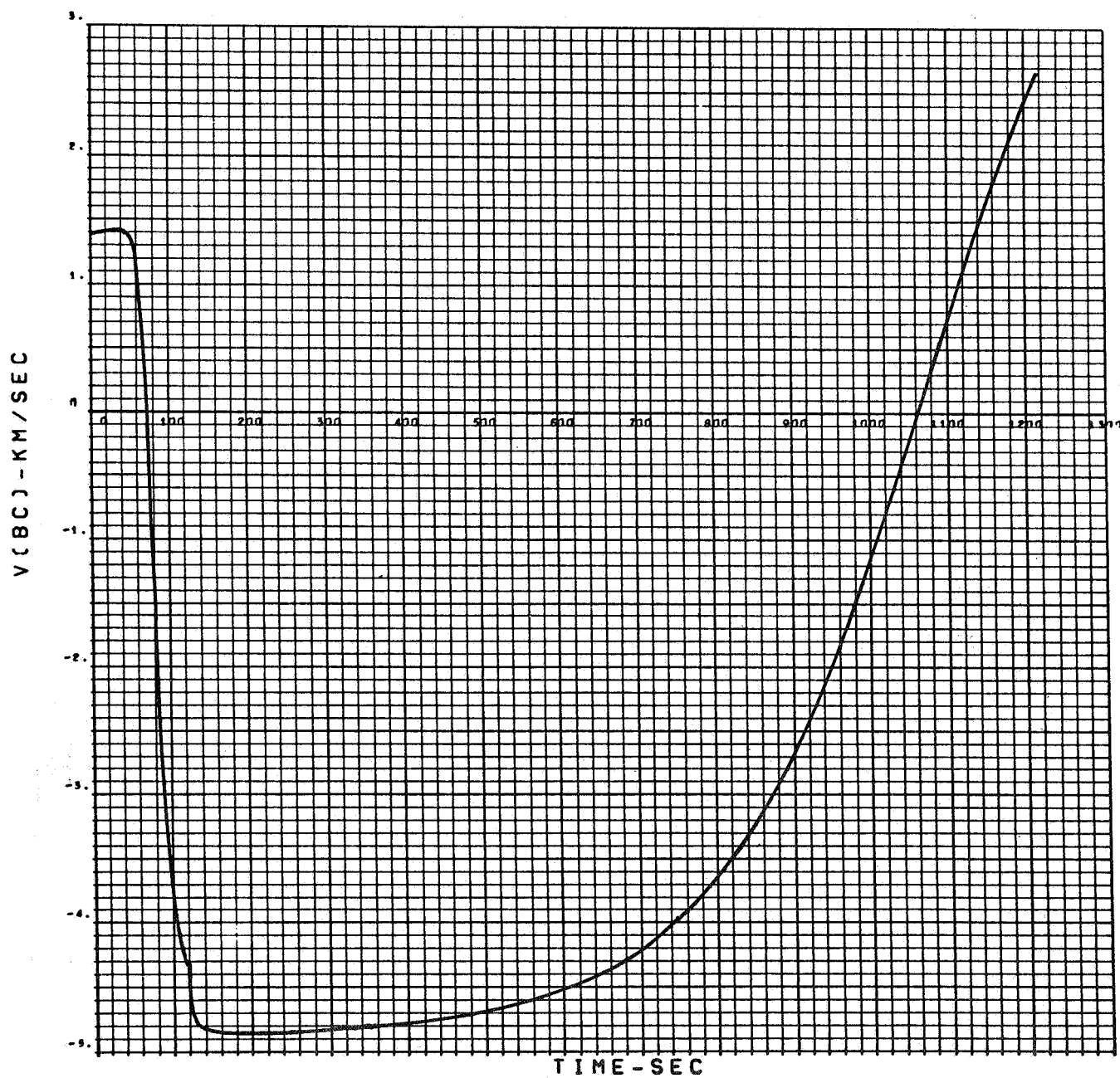ENTRY ALTITUDE   - 244 KM.
DRAG, SEE FIGURE 3.1-41
VM-9

ENTRY VELOCITY   - 20, 788 FT/SEC.
ENTRY PATH ANGLE   - 25°
ENTRY ALTITUDE   - 244 KM.
DRAG, SEE FIGURE 3.1-41
VM-9

Figure A-70. Mach Number vs Time, VM-9, Direct Entry

ENTRY VELOCITY — 20,788 FT/SEC.
ENTRY PATH ANGLE — 25°
ENTRY ALTITUDE — 244 KM.
DRAG, SEE FIGURE 3.1-41
VM-9

Figure A-71. Lander Deceleration vs Time, VM-9, Direct Entry

ENTRY VELOCITY   - 20,788 FT/SEC.
ENTRY PATH ANGLE   - 25°
ENTRY ALTITUDE   - 244 KM.
DRAG, SEE FIGURE 3.1-41
VM-9

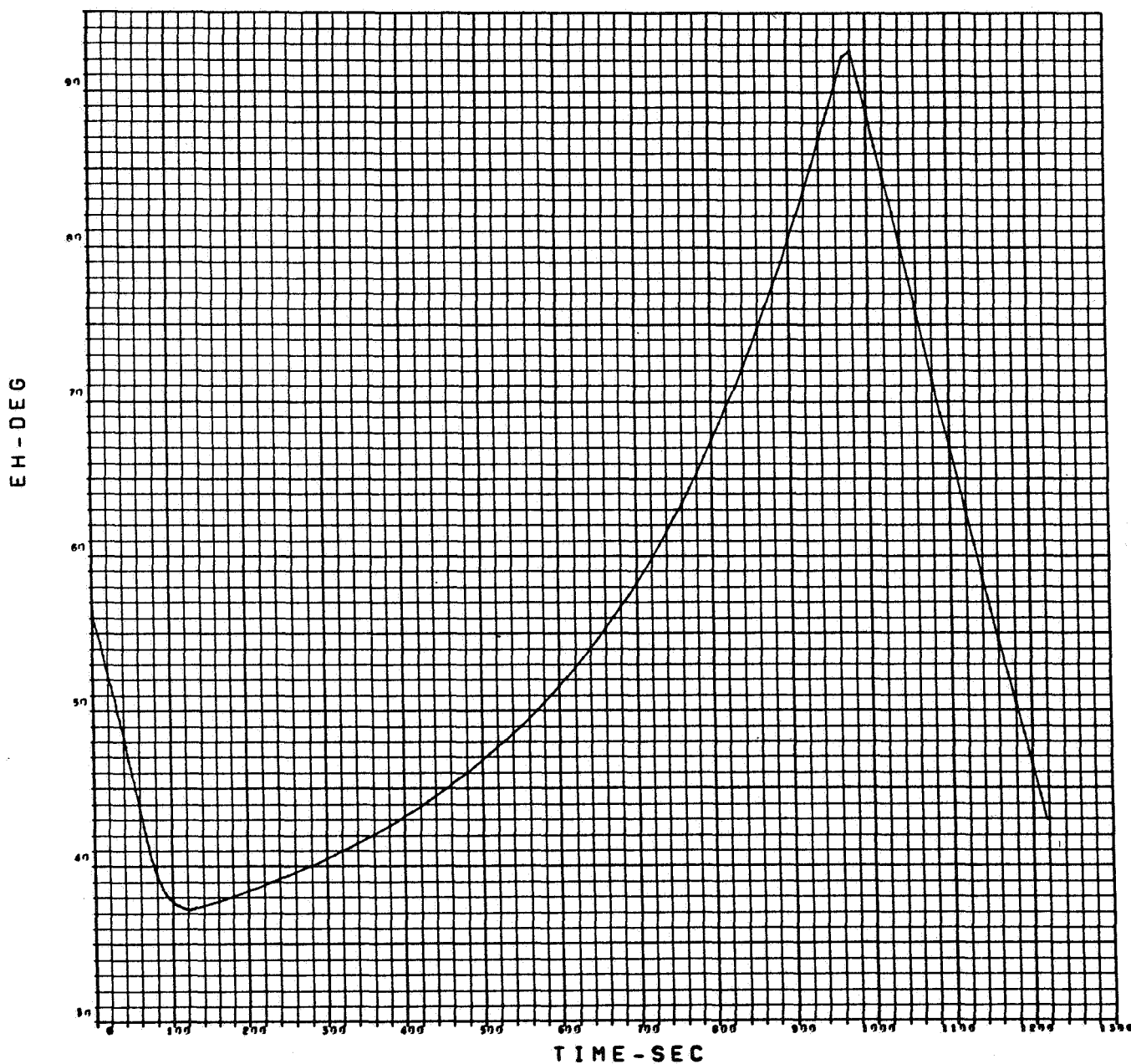Figure A-72. Dynamic Pressure vs Time, VM-9, Direct Entry

ENTRY VELOCITY   - 20,788 FT/SEC.
ENTRY PATH ANGLE   - 25°
ENTRY ALTITUDE   - 244 KM.
DRAG, SEE FIGURE 3.1-41
VM-9

Figure A-73. Communication Distance R(BC) vs Time, VM-9, Direct Entry
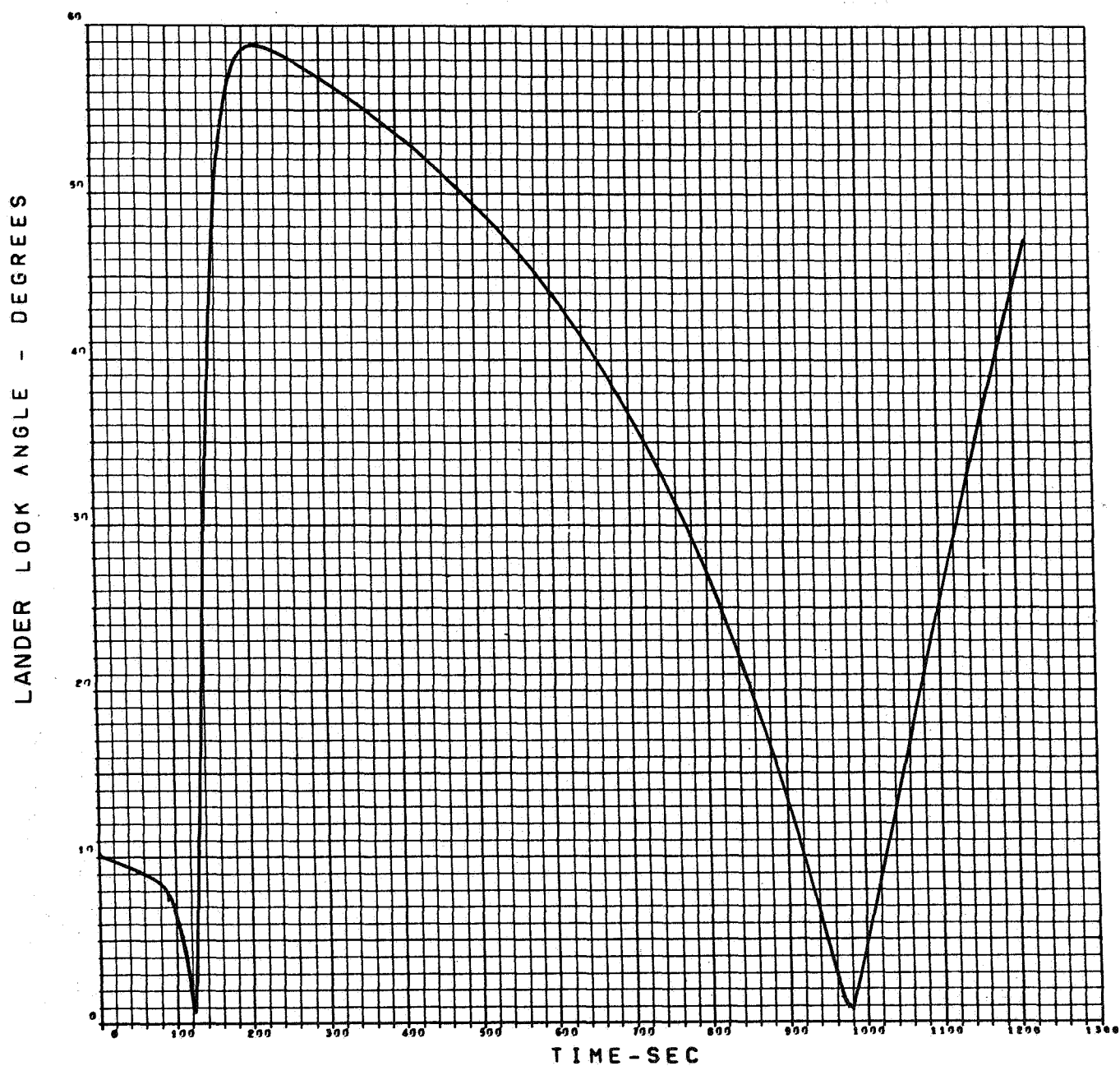
ENTRY VELOCITY   - 20,788 FT/SEC.
ENTRY PATH ANGLE   - 25°
ENTRY ALTITUDE   - 244 KM.
DRAG, SEE FIGURE 3.1-41

VM-9

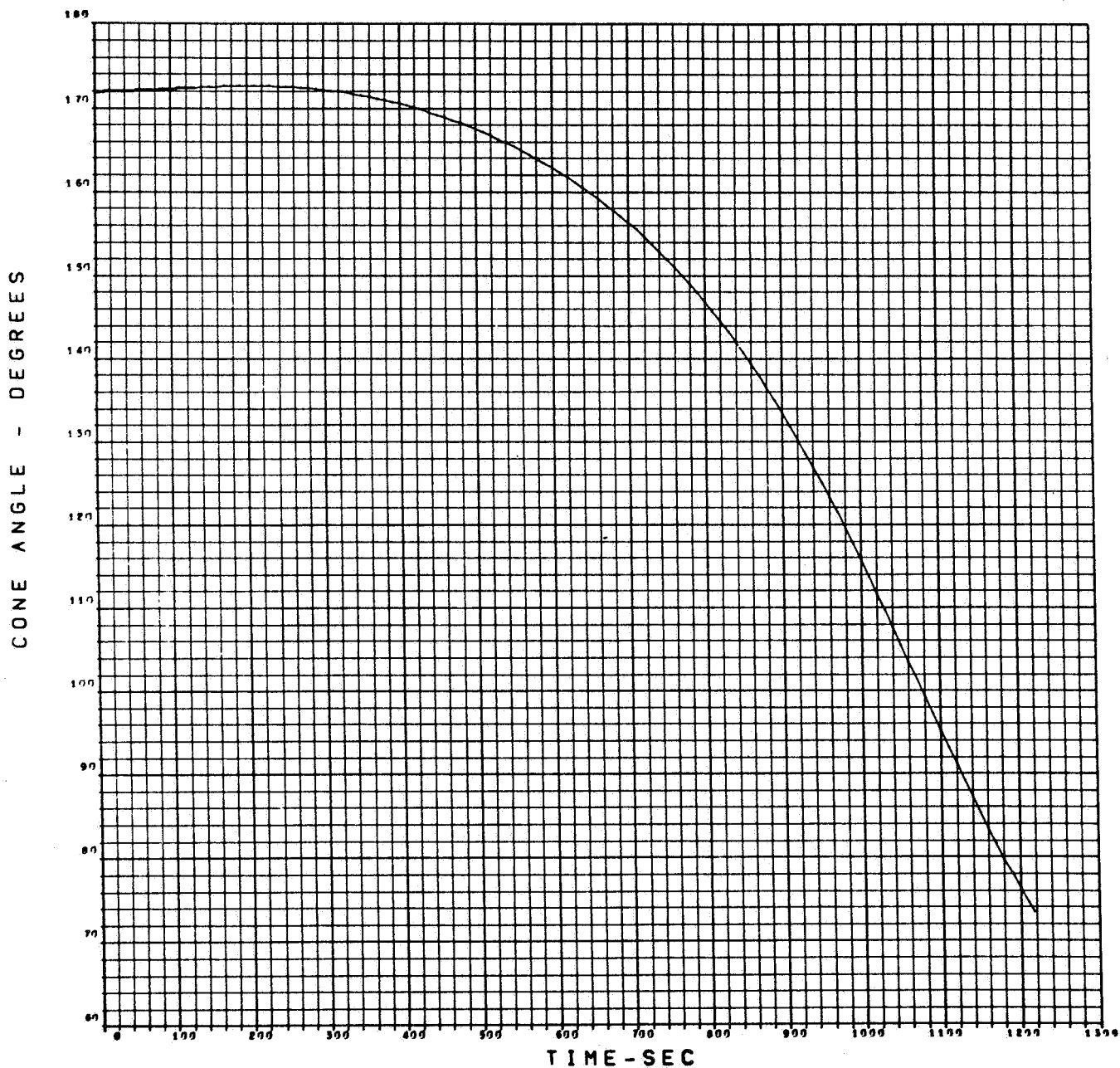Figure A-74.   Range Rate vs Time, VM-9, Direct Entry

ENTRY VELOCITY   - 20,788 FT/SEC.
ENTRY PATH ANGLE   - 25°
ENTRY ALTITUDE   - 244 KM.
DRAG, SEE FIGURE 3.1-41
VM-9

Figure A-75.   Angle at which Lander Sees Orbiter Above Horizon, VM-9,
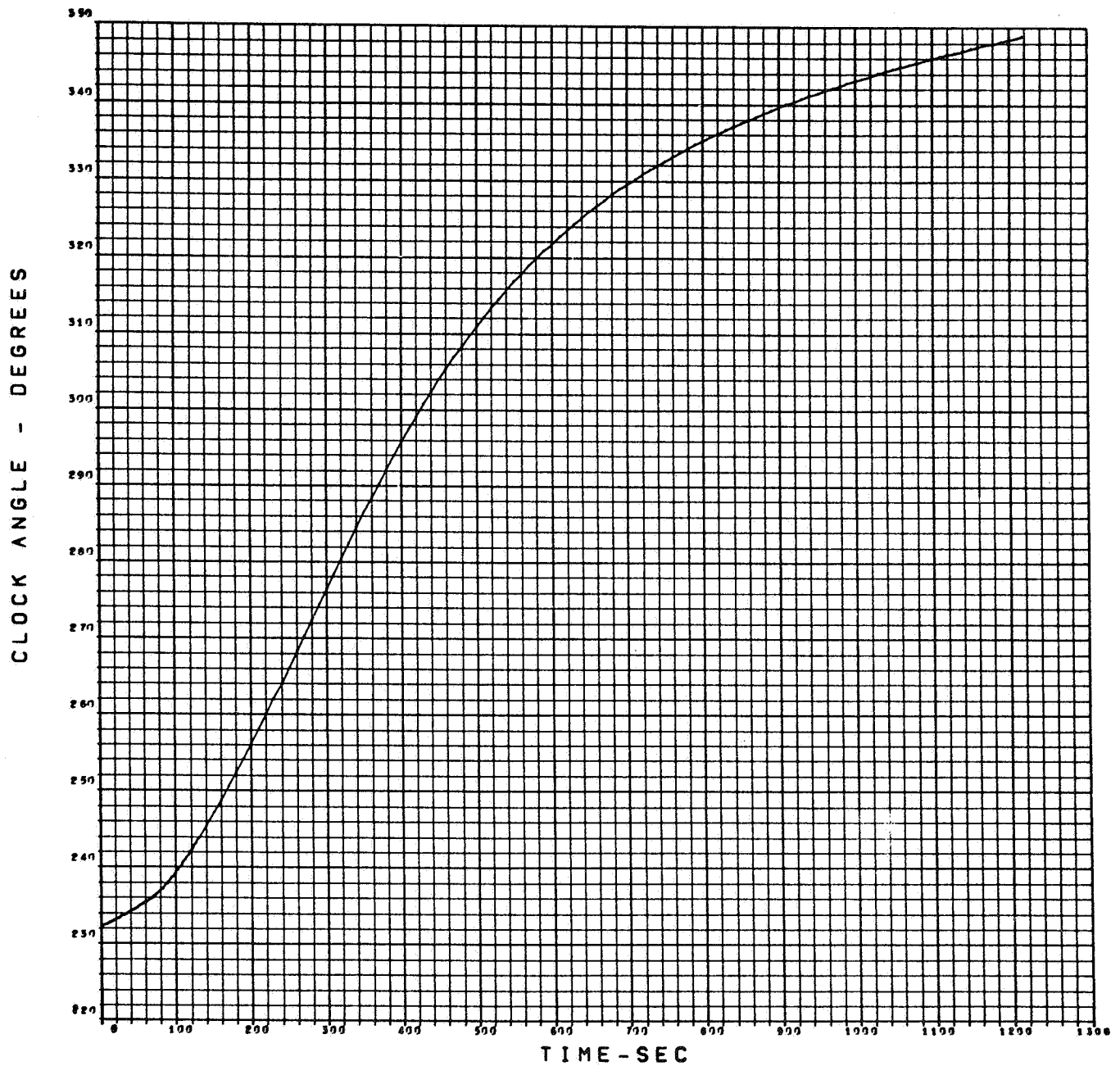Direct Entry

ENTRY VELOCITY   - 20,788 FT/SEC.
ENTRY PATH ANGLE   - 25°
ENTRY ALTITUDE   - 244 KM.
DRAG, SEE FIGURE   3.1-41
VM-9

Figure A-76. Lander Look Angle vs Time, VM-9, Direct Entry

Figure A-77. Cone Angle vs Time, VM-9, Direct Entry

ENTRY VELOCITY   - 20,788 FT/SEC.
ENTRY PATH ANGLE   - 25°
ENTRY ALTITUDE   - 244 KM.
DRAG, SEE FIGURE 3.1-41
VM-9

#6

ENTRY VELOCITY   - 20,788 FT/SEC.
ENTRY PATH ANGLE   - 25°
ENTRY ALTITUDE   - 244 KM.
DRAG, SEE FIGURE 3.1-41
VM-9

Figure A-78.   Clock Angle vs Time, VM-9, Direct Entry